Titre: Title:	Nouvelles techniques pratiques pour la modélisation du comportement dynamique des systèmes eau-structure
Auteur: Author:	Benjamin Miquel
Date:	2012
Type:	Mémoire ou thèse / Dissertation or Thesis
Référence: Citation:	Miquel, B. (2012). Nouvelles techniques pratiques pour la modélisation du comportement dynamique des systèmes eau-structure [Thèse de doctorat, École Polytechnique de Montréal]. PolyPublie. https://publications.polymtl.ca/845/

URL de PolyPublie: PolyPublie URL:	https://publications.polymtl.ca/845/
Directeurs de recherche: Advisors:	Najib Bouaanani
Programme: Program:	Génie civil

UNIVERSITÉ DE MONTRÉAL

NOUVELLES TECHNIQUES PRATIQUES POUR LA MODÉLISATION DU COMPORTEMENT DYNAMIQUE DES SYSTÈMES EAU-STRUCTURE

BENJAMIN MIQUEL
DÉPARTEMENT DES GÉNIES CIVIL, GÉOLOGIQUE ET DES MINES
ÉCOLE POLYTECHNIQUE DE MONTRÉAL

THÈSE PRÉSENTÉE EN VUE DE L'OBTENTION
DU DIPLÔME DE PHILOSOPHIÆ DOCTOR (Ph.D.)
(GÉNIE CIVIL)
AVRIL 2012

UNIVERSITÉ DE MONTRÉAL

ÉCOLE POLYTECHNIQUE DE MONTRÉAL

Cette thèse intitulée :

NOUVELLES TECHNIQUES PRATIQUES POUR LA MODÉLISATION DU COMPORTEMENT DYNAMIQUE DES SYSTÈMES EAU-STRUCTURE

présentée par : MIQUEL Benjamin
en vue de l'obtention du diplôme de : Philosophiæ Doctor
a été dûment acceptée par le jury d'examen constitué de :

M. LÉGER Pierre, Ph.D., président
M. BOUAANANI Najib, Ph.D., membre et directeur de recherche
M. MUREITHI Njuki W., Ph.D., membre
M. PROULX Jean, Ph.D., membre

DÉDICACE

À tout ceux qui ont su me faire grandir par leur amour, leur amitié, leur savoir et leurs différences

...

REMERCIEMENTS

Je tiens avant tout à remercier Najib Bouaanani, mon directeur de recherche, pour la qualité de son encadrement, sa disponibilité et surtout pour la confiance qu'il a su m'accorder tout au long de ces années. Ses connaissances scientifiques et sa rigueur ont permis de cadrer ma recherche. Je tiens aussi à lui exprimer mon admiration et ma reconnaissance pour ses grandes qualités humaines. Elles ont été source de motivation à travers toute cette thèse et ont fait de nos rencontres des moments fort agréables.

Ce fut un réel plaisir de travailler au sein du groupe de recherche en génie des structures de l'École Polytechnique de Montréal. L'entraide et la bonne ambiance qui existent entre étudiants, professeurs, ingénieurs, techniciens et secrétaire de ce groupe offrent un cadre idéal pour étudier et avancer dans sa recherche. Je tiens particulièrement à remercier les professeurs Najib Bouaanani, Jean-Philippe Charron, Sanda Koboevic, Pierre Léger, et Robert Tremblay pour la qualité de leurs enseignements. Je remercie également Anne Marie Goulet pour sa bonne humeur ainsi que mes collègues pour tous les bons moments que j'ai vécu avec eux et les conseils qu'ils ont pu me donner.

Je tiens aussi à souligner le support financier du Conseil de Recherches en Sciences Naturelles et Génie du Canada (CRSNG) tout comme celui du Fonds Québécois de la Recherche sur la Nature et les Technologies (FQRNT).

Cette thèse n'aurait jamais abouti sans les nombreux bars et cafés dans lesquels j'ai installé mon bureau. Je tiens donc à remercier le Café Rico, le bar Les Passages, le bar Vice & Versa et le dernier mais pas des moindres Café Ellefsen pour m'avoir accueilli pendant de longues heures de calculs et de rédaction. Votre staff et clientèle ont été sources d'inspiration et de réconforts tout au long de ces quatre dernières années.

Qui aurait pensé qu'un jour je finirais par remercier une personne pour son amour ? Il faut bien croire qu'une thèse transforme un individu. Merci Cécile pour ton amour inconditionnel malgré ces longues soirées passées seule pendant que je regardais des chiffres défiler sur mon ordinateur, malgré mes sautes d'humeur et tous les plans que j'ai annulés pour travailler ou dormir. Je te promets un avenir bien plus funky.

Finalement, je tiens à remercier du fond du coeur le Québec et ses habitants pour leur accueil chaleureux, et l'opportunité incroyable qu'ils m'ont offerts en me laissant m'établir dans ce pays splendide pour y poursuivre mes études. Après de nombreuses années à vadrouiller à travers la planète, votre générosité, votre sincérité et votre simplicité ne me laissent que le choix de poser bagages.

RÉSUMÉ

L'étude des comportements dynamique et sismique des ouvrages hydrauliques est, comme pour les structures conventionnelles, primordiale afin d'assurer la protection des vies humaines. Elle a aussi pour objectif de limiter les dommages structuraux que peut engendrer un tremblement de terre et d'éviter le cas de rupture ou d'effondrement. Ces structures particulières subissent non seulement les déplacements imposées par les secousses sismiques, mais aussi ceux induits par les forces hydrodynamiques générées par l'interaction fluide-structure. Cette thèse passe en revue les différentes méthodes complexes et simplifiées existantes permettant l'analyse dynamique d'ouvrages hydrauliques. En ce qui concerne les méthodes complexes, une attention particulière est consacrée aux difficultés liées à leur utilisation. Parmi celles-ci, nous insisterons sur la modélisation des conditions aux frontières transmettantes permettant de simuler numériquement l'effet de la géométrie semi-infinie du réservoir. En développant une procédure pour estimer l'erreur qu'induisent les conditions existantes, nous montrons que celles-ci peuvent avoir un effet très important sur le comportement dynamique des structures en contact avec de l'eau.

Pour les besoins des ingénieurs-praticiens, des méthodes simplifiées sont nécessaires afin de vérifier le comportement dynamique des ouvrages en contact avec de l'eau. La revue des méthodes simplifiées existantes montre que celles-ci sont basées sur de nombreuses simplifications qui peuvent affecter la qualité des résultats. L'un des objectifs de cette thèse a été de développer des méthodes simplifiées plus performantes que celles existantes. Une première méthode a été mise au point pour la réalisation d'une analyse spectrale de ces ouvrages. Pour son développement, il a été nécessaire de proposer une méthodologie pour le calcul précis de la période fondamental d'un système eau-structure. Nous montrons que cette nouvelle procédure est facilement programmable, avec un temps de calcul instantané, et que celle-ci donne d'excellents résultats lorsque comparée à des méthodes complexes.

Les analyses spectrales ne tiennent pas compte de la nature oscillatoire et transitoire des vibrations. Lorsqu'une analyse spectrale démontre que des zones de l'ouvrage excèdent les contraintes admissibles, il est nécessaire de réaliser une analyse dynamique plus détaillée pour examiner la durée du dépassement des contraintes admissibles et de l'étendue de ces zones concernées. Par ailleurs, la méthode spectrale proposée et celle existante effectuent une correction statique pour la prise en compte des modes supérieurs. Bien que pour les barrages cela soit généralement suffisant, pour les structures plus flexibles l'effet dynamique doit être pris en compte. Pour cela, différentes méthodes ont été mises au point pour tenir compte de l'effet de l'interaction fluide-structure et de la flexibilité du sol. La première permet l'étude de

structure vibrant en contact avec de l'eau d'un ou des deux côtés. Cette nouvelle technique permet de tenir compte de la flexibilité de la structure et du sol, des modes de vibrations supérieurs, des niveaux d'eau variables, et de différentes conditions aux frontières pour les domaines d'eau. Une méthodologie a été développée pour calculer les fréquences naturelles de chaque mode de vibration du système eau-structure. Cette nouvelle technique a ensuite été étendue pour le calcul de poutres en contact avec de l'eau. Cette méthode originale étend les solutions analytiques existantes pour le calcul des modes de vibrations et période naturelle des poutres à une solution intégrant l'effet d'interaction fluide-structure. Elle permet une très bonne estimation dynamique du comportement d'un système poutre-fluide ou bien d'une structure ayant un comportement similaire. Finalement, une Méthode d'Accélérogramme Modifiée (MAM) a été développée. Celle-ci consiste à transformer l'accélérogramme de dimensionnement ou d'analyse en un nouvel accélérogramme intégrant l'effet de l'interaction fluide-structure. Ce dernier peut alors être appliqué directement à la structure sèche (i.e. sans eau) afin d'obtenir la réponse dynamique de la structure en contact avec de l'eau. Cette nouvelle technique intègre dans sa formulation de nombreux paramètres ayant de l'influence sur le comportement dynamique et permet de traiter l'effet de l'interaction fluide-structure analytiquement tout en gardant les avantages de la modélisation par éléments finis.

ABSTRACT

The dynamic or seismic behavior of hydraulic structures is, as for conventional structures, essential to assure protection of human lives. These types of analyses also aim at limiting structural damage caused by an earthquake to prevent rupture or collapse of the structure. The particularity of these hydraulic structures is that not only the internal displacements are caused by the earthquake, but also by the hydrodynamic loads resulting from fluid-structure interaction. This thesis reviews the existing complex and simplified methods to perform such dynamic analysis for hydraulic structures. For the complex existing methods, attention is placed on the difficulties arising from their use. Particularly, interest is given in this work on the use of transmitting boundary conditions to simulate the semi infinity of reservoirs. A procedure has been developed to estimate the error that these boundary conditions can introduce in finite element dynamic analysis. Depending on their formulation and location, we showed that they can considerably affect the response of such fluid-structure systems.

For practical engineering applications, simplified procedures are still needed to evaluate the dynamic behavior of structures in contact with water. A review of the existing simplified procedures showed that these methods are based on numerous simplifications that can affect the prediction of the dynamic behavior of such systems. One of the main objectives of this thesis has been to develop new simplified methods that are more accurate than those existing. First, a new spectral analysis method has been proposed. Expressions for the fundamental frequency of fluid-structure systems, key parameter of spectral analysis, have been developed. We show that this new technique can easily be implemented in a spreadsheet or program, and that its calculation time is near instantaneous. When compared to more complex analytical or numerical method, this new procedure yields excellent prediction of the dynamic behavior of fluid-structure systems.

Spectral analyses ignore the transient and oscillatory nature of vibrations. When such dynamic analyses show that some areas of the studied structure undergo excessive stresses, time history analyses allow a better estimate of the extent of these zones as well as a time notion of these excessive stresses. Furthermore, the existing spectral analyses methods for fluid-structure systems account only for the static effect of higher modes. Thought this can generally be sufficient for dams, for flexible structures the dynamic effect of these modes should be accounted for. New methods have been developed for fluid-structure systems to account for these observations as well as the flexibility of foundations. A first method was developed to study structures in contact with one or two finite or infinite water domains. This new technique includes flexibility of structures and foundations as well as the dynamic effect

of higher vibration modes and variations of the levels of the water domains. Extension of this method was performed to study beam structures in contact with fluids. These new developments have also allowed extending existing analytical formulations of the dynamic properties of a dry beam to a new formulation that includes effect of fluid-structure interaction. The method yields a very good estimate of the dynamic behavior of beam-fluid systems or beam like structures in contact with fluid. Finally, a Modified Accelerogram Method (MAM) has been developed to modify the design earthquake into a new accelerogram that directly accounts for the effect of fluid-structure interaction. This new accelerogram can therefore be applied directly to the dry structure (i.e. without water) in order to calculate the dynamic response of the fluid-structure system. This original technique can include numerous parameters that influence the dynamic response of such systems and allows to treat analytically the fluid-structure interaction while keeping the advantages of finite element modeling.

TABLE DES MATIÈRES

DÉDICACE iii

REMERCIEMENTS iv

RÉSUMÉ v

ABSTRACT vii

TABLE DES MATIÈRES ix

LISTE DES TABLEAUX xiv

LISTE DES FIGURES xv

LISTE DES ANNEXES xviii

LISTE DES SIGLES ET ABRÉVIATIONS xix

CHAPITRE 1 INTRODUCTION 1
- 1.1 Contexte 1
- 1.2 Problématique 2
- 1.3 Cadre et objectifs de la recherche 3
- 1.4 Méthodologie 4
  - 1.4.1 Estimation de l'erreur associée à l'utilisation de conditions aux frontières transmettantes 4
  - 1.4.2 Formulation simplifiée pour le calcul de la période fondamentale de système eau-structure et développement d'une méthode pseudo-dynamique 4
  - 1.4.3 Développement d'une méthode simplifiée d'analyse dynamique des systèmes eau-structure 5
  - 1.4.4 Prise en compte simplifiée de l'effet de l'interaction fluide-structure dans un modèle éléments finis 5
- 1.5 Portée et contributions originales 5
- 1.6 Contenu de la thèse 6

CHAPITRE 2 REVUE DE LITTÉRATURE 8
- 2.1 Introduction 8

2.2 Méthodes complexes de modélisation des systèmes eau-structure 9
2.2.1 Méthodes analytiques avancées 9
2.2.2 Méthodes des Éléments Finis 11
2.2.3 Méthode des Équations Intégrales 17
2.2.4 Modélisation de la fondation 17
2.3 Méthodes simplifiés de modélisation des systèmes fondations-barrage-réservoir 19
2.3.1 Méthode pseudo-statique ou méthode des masses-ajoutées 19
2.3.2 Méthode pseudo-dynamique 20
2.3.3 Analyse dynamique temporelle 22
2.3.4 Autres formulations simplifiées 23

CHAPITRE 3 Article 1 : Simplified evaluation of the vibration period and seismic response of gravity dam-water systems 28
3.1 Introduction 31
3.2 Analytical formulation for vibrating dam-reservoir systems 32
3.2.1 Basic assumptions 32
3.2.2 Coupling hydrodynamic pressure and dam structural response 33
3.3 Simplified formulation 36
3.3.1 Fundamental mode response analysis 36
3.3.2 Simplified formulation of dam-reservoir interaction assuming incompressible water 39
3.3.3 Simplified formulation of dam-reservoir interaction considering water compressibility 42
3.3.4 Application to the simplified earthquake analysis of gravity dams . . . 47
3.4 Dam models, analyses and results 49
3.4.1 Analyses conducted 49
3.4.2 Validation of the proposed simplified formulation 53
3.5 Concluding remarks 57

CHAPITRE 4 Article 2 : Practical dynamic analysis of structures laterally vibrating in contact with water 65
4.1 Introduction 66
4.2 Analytical formulation 66
4.2.1 Geometry of the structure-water systems, basic assumptions and notation 66
4.2.2 Frequency-domain dynamic response of the structure 67
4.2.3 Frequency-domain dynamic response of the water domains 69

4.2.4 Coupled frequency and time-domain response of the structure-water system . . . 71
4.3 Simplified procedure . . . 74
4.3.1 Simplified generalized coordinates . . . 75
4.3.2 Evaluation of the vibration periods of a structure-water system . . . 78
4.4 Effects of water domain boundary conditions . . . 79
4.5 Case studies and results . . . 82
4.5.1 Studied structure-water systems, models and analysis types . . . 82
4.5.2 Vibration periods of the structure-water systems . . . 85
4.5.3 Hydrodynamic pressure . . . 87
4.5.4 Seismic response of the structure-water systems . . . 89
4.6 Conclusions . . . 91

CHAPITRE 5 Article 3 : Efficient Earthquake Modal Analysis of Flexible Beam-Fluid Systems . . . 101
5.1 Introduction . . . 102
5.2 Modal dynamic response of a beam interacting with a fluid . . . 103
5.2.1 Basic assumptions and notation . . . 103
5.2.2 Governing equations . . . 103
5.2.3 Frequency to time response solutions . . . 106
5.2.4 Evaluation of the natural frequencies of coupled beam-fluid systems . . . 111
5.3 Illustrative numerical examples . . . 113
5.3.1 Beam-fluid systems studied . . . 113
5.3.2 Earthquake time-history response of the beam-water systems . . . 113
5.3.3 Coupled frequencies of beam-water systems . . . 118
5.4 Conclusions . . . 120

CHAPITRE 6 Article 4 : Accounting for Earthquake-induced Dam-reservoir Interaction using Modified Accelerograms . . . 127
6.1 Introduction . . . 128
6.2 Formulations of the proposed Modified Accelerogram Method . . . 129
6.2.1 Description of the studied dam-reservoir system, basic notation and assumptions . . . 129
6.2.2 Exact formulation of the proposed Modified Accelerogram Method . . . 129
6.2.3 Simplified formulation of the proposed Modified Accelerogram Method 132
6.3 Numerical examples . . . 137
6.3.1 Frequency response of gravity dams on rigid foundations . . . 137

6.3.2 Time-history response of gravity dams on rigid foundations 138
6.3.3 Time-history response of a gravity dam including the effects of foundation flexibility and reservoir bottom wave absorption 143
6.4 Conclusions 143

CHAPITRE 7 Discussion générale 152
7.1 Introduction 152
7.2 Description des méthodes étudiées 152
7.2.1 Méthodes de références 153
7.2.2 Description des méthodes simplifiées existantes 156
7.3 Description et discussion des propriétés utilisées pour l'analyse paramétrique . 160
7.3.1 Description du modèle utilisé 160
7.3.2 Type d'analyse effectuée 160
7.3.3 Analyse paramétrique et programme développé 161
7.3.4 Discussion sur l'amortissement 162
7.4 Résultats 167
7.4.1 Validité de la méthode des masses ajoutées de Westergaard [9] 167
7.4.2 Validité de la méthode simplifiée de Fenves et Chopra [5] 169
7.4.3 Validité de la méthode simplifiée développée au cours de cette thèse . . 172
7.4.4 Exemple 172
7.4.5 Effet de la compressibilité 175
7.4.6 Effet des modes supérieurs 177
7.5 Conclusion 178

CHAPITRE 8 Conclusions et recommandations 181
8.1 Conclusions 181
8.1.1 Développement d'une formulation simplifiée pour le calcul de la période fondamentale d'un système eau-structure 182
8.1.2 Développement d'une méthode spectrale simplifiée pour l'étude d'un système eau-structure 182
8.1.3 Développement de méthodes numériques pour l'analyse dynamique des structures en contact avec de l'eau 182
8.1.4 Développement de la méthode de l'accélérogramme modifiée 184
8.1.5 Développement d'un test d'erreur associée à l'utilisation de conditions aux frontières transmettantes 184
8.1.6 Conclusions générales 185
8.2 Recommandations 186

8.2.1 Accélération verticale 186
8.2.2 Généralisation de ces méthodes à d'autres systèmes 186
8.2.3 Analyse non-linéaire 186
8.2.4 Prise en compte de l'effet de l'interaction sol-structure 187
8.2.5 Étude des systèmes tridimensionnels 187

BIBLIOGRAPHIE 188

ANNEXES 197

LISTE DES TABLEAUX

Table 3.1 Coefficients $\widehat{\gamma}_i$ and γ_i, $i = 1, \ldots, 6$. 41
Table 3.2 Coefficients $\widehat{\zeta}_i$ and ζ_i, $i = 1, 2, 3$. 42
Table 3.3 Pine Flat dam fundamental mode shapes used. 53
Table 3.4 Summary of analysis types conducted. 57
Table 4.1 Coefficients C_r and $D_{r,k}$ for $r = 1 \ldots 6$ and $k = 0 \ldots N_{\boldsymbol{\psi}_j} = 11$. 82
Table 4.2 CPU times for analysis types I to IV. 91
Table 5.1 Modal parameters for Clamped-Free beam configuration 109
Table 5.2 Modal parameters for Clamped-Pinned beam configuration. 109
Table 5.3 Modal parameters for Pinned-Clamped beam configuration 109
Table 5.4 Modal parameters for Clamped-Sliding beam configuration. 110
Table 5.5 Modal parameters for Sliding-Clamped beam configuration. 110
Table 5.6 Modal parameters for Clamped-Clamped beam configuration 110
Table 5.7 Modal parameters for Pinned-Pinned beam configuration 111
Table 5.8 Frequency ratios for concrete beam-water system. 119
Table 5.9 Frequency ratios for steel beam-water system. 121
Table 5.A1 Equations to determine σ_j and β_j for modes $j = 1 \ldots N_{\mathrm{s}}$. 126
Table 6.A1 Coefficients $A_{k,s} \times 10^3$ and $B_k \times 10^3$ evaluated for $k, s = 0 \ldots 8$. 145
Table A1 Error estimation of hydrodynamic force coefficients. 230

LISTE DES FIGURES

Figure 2.1 Système Barrage-réservoir-fondation 10
Figure 2.2 Système Barrage-réservoir et condition aux frontière utilisées 12
Figure 2.3 Modèle éléments finis d'un système barrage-réservoir. 12
Figure 2.4 Interaction fluide-structure 13
Figure 2.5 Système Barrage-réservoir et conditions aux frontières utilisés 15
Figure 2.6 Pression hydrodynamique simplifiée et masses ajoutées de Westergaard. 20
Figure 3.1 Dam-reservoir system. 33
Figure 3.2 Approximation of the fundamental mode shape of a gravity dam. . . . 38
Figure 3.3 Variation of Φ and $\widehat{\varphi}$ 40
Figure 3.4 Variation of the terms $4\rho_{\mathrm{r}}H_{\mathrm{s}}^2\,\varphi(\eta)$ and $(B_1 - B_{1,1})$ 45
Figure 3.5 Dam-reservoir geometry and analysis types. 50
Figure 3.6 Variation of period ratio T_{r}/T_1 assuming incompressible water. 54
Figure 3.7 Variation of period ratio T_{r}/T_1 considering water compressibility. 55
Figure 3.8 Geometry and finite element models of gravity dam cross-sections . . . 56
Figure 3.9 Variation of period ratio T_{r}/T_1 58
Figure 3.10 Variation of the damping ratio $\widetilde{\xi}_1$ 59
Figure 3.11 Normalized equivalent lateral earthquake forces 60
Figure 4.1 Examples of structure-water systems studied. 67
Figure 4.2 Structure-water systems, boundary conditions and notation 68
Figure 4.3 Approximation of structural mode shapes by polynomial functions. . . 76
Figure 4.4 Effects of water domain boundary conditions. 81
Figure 4.5 Studied structure-water systems 83
Figure 4.6 Models and types of analysis used 86
Figure 4.7 Estimation of vibration periods of the three systems studied 87
Figure 4.8 Hydrodynamic pressure distributions for system B 88
Figure 4.9 Ground motions considered. 90
Figure 4.10 Time-history of relative displacement under El Centro earthquake. . . . 93
Figure 4.11 Time-history of relative displacement under Saguenay earthquake. . . . 94
Figure 5.1 Slender beam vibrating in contact with a fluid 104
Figure 5.2 Studied beams-fluid configurations 106
Figure 5.3 Horizontal acceleration component of Imperial Valley earthquake 113
Figure 5.4 Time-history responses of the concrete beam-fluid system. 114
Figure 5.5 Time-history responses of the steel beam-fluid system. 115

Figure 5.6 Time-history responses of the concrete dry beam and beam-fluid system 116
Figure 5.7 Time-history responses of the steel dry beam and beam-fluid system . . 117
Figure 6.1 Studied systems 130
Figure 6.2 Approximation of the mode shapes of a gravity dam-foundation system. 135
Figure 6.3 Dimensions of studied gravity dam monoliths. 138
Figure 6.4 Displacement frequency response under unit harmonic ground motion. . 139
Figure 6.5 Input accelerograms 140
Figure 6.6 Crest displacements. 141
Figure 6.7 Maximum principal stress at maximum displacement. 142
Figure 6.8 Crest displacement. 144
Figure 7.1 Valeur de $C_{\mathrm{e},n}$ 158
Figure 7.2 Section de Pine Flat et transformations géométriques. 160
Figure 7.3 Effet de l'amortissement : eau incompressible 165
Figure 7.4 Effet de l'amortissement : eau compressible 166
Figure 7.5 y_{g} : méthode des masses ajoutées de Westergaard 168
Figure 7.6 $\mathcal{V}$: méthode des masses ajoutées de Westergaard 168
Figure 7.7 $\mathcal{V}$: méthode des masses ajoutées de Westergaard 169
Figure 7.8 y_{g} : méthode simplifiée de Fenves et Chopra [5] 170
Figure 7.9 $\mathcal{V}$: méthode simplifiée de Fenves et Chopra [5] 170
Figure 7.10 y_{g} : méthode simplifiée de Fenves et Chopra [5] 171
Figure 7.11 $\mathcal{V}$: méthode simplifiée de Fenves et Chopra [5] 172
Figure 7.12 y_{g} : méthode développée dans cette thèse 173
Figure 7.13 $\mathcal{V}$: méthode développée dans cette thèse 173
Figure 7.14 y_{g} méthode développée dans cette thèse 174
Figure 7.15 $\mathcal{V}$: méthode développée dans cette thèse 174
Figure 7.16 Enregistrement d'Imperial Valley 175
Figure 7.17 Force de cisaillement à la base du barrage $\mathcal{V}$ 176
Figure 7.18 $\mathcal{V}$: effet de la compressibilité 176
Figure 7.19 $\mathcal{V}$: Effet des modes supérieurs 178
Figure A.1 Dam-reservoir systems considered for the analytical formulation 202
Figure A.2 Dam-reservoir systems studied and boundary conditions used 206
Figure A.3 Variation of the parameter $H_{\mathrm{r}}\left|\theta_0^{(L_{\mathrm{r}})}\right|$ for a rigid dam 214
Figure A.4 Variation of the parameter $H_{\mathrm{r}}\left|\theta^{(L_{\mathrm{r}})}\right|$ for a flexible dam$E_{\mathrm{s}} = 35\,\mathrm{GPa}$ . . 216
Figure A.5 Variation of the parameter $H_{\mathrm{r}}\left|\theta^{(L_{\mathrm{r}})}\right|$ for a flexible dam $E_{\mathrm{s}} = 25\,\mathrm{GPa}$ . . 217
Figure A.6 Variation of the parameter $H_{\mathrm{r}}\left|\theta^{(L_{\mathrm{r}})}\right|$ for $\omega = 0.8\omega_0$ 219
Figure A.7 Variation of the parameter $H_{\mathrm{r}}\left|\theta^{(L_{\mathrm{r}})}\right|$ for $\omega = 1.2\omega_0$ 220

Figure A.8 Variation of the parameter $H_{\mathrm{r}}\left|\theta^{(L_{\mathrm{r}})}\right|$ for $\omega = 2\omega_0$ 221
Figure A.9 Variation of the parameter $H_{\mathrm{r}}\left|\theta^{(L_{\mathrm{r}})}\right|$ for $\omega = 4\omega_0$ 222
Figure A.10 FRFs for normalized hydrodynamic forces 224
Figure A.11 Heightwise distributions of normalized hydrodynamic pressures 225
Figure A.12 FRFs for normalized hydrodynamic forces 226
Figure A.13 FRFs for normalized hydrodynamic forces 232
Figure A.14 FRFs for normalized hydrodynamic forces 233
Figure A.15 FRFs for normalized hydrodynamic forces 234
Figure A.16 Hydrodynamic force error for a truncation length $L_{\mathrm{r}} = 0.1H_{\mathrm{r}}$ 235
Figure A.17 Hydrodynamic force error for a truncation length $L_{\mathrm{r}} = 0.5H_{\mathrm{r}}$ 236
Figure A.18 Hydrodynamic force error for a truncation length $L_{\mathrm{r}} = H_{\mathrm{r}}$ 237
Figure A.19 Hydrodynamic force error for a truncation length $L_{\mathrm{r}} = 2H_{\mathrm{r}}$ 238
Figure C.1 General geometry 254
Figure C.2 Geometry of the studied geometrically asymmetric wall-water system. . 261
Figure C.3 Geometry of the studied geometrically asymmetric wall-water system. . 262
Figure C.4 Mode shapes, frequencies and effective modal masses of the walls. . . . 263
Figure C.5 Nondimensionalized hydrodynamic pressures and displacements 264
Figure C.6 Nondimensionalized hydrodynamic pressure profiles on the walls 265
Figure C.7 Horizontal acceleration component of Imperial Valley earthquake (1940).265
Figure C.8 Time-history response of the geometrically asymmetric wall-water system266
Figure C.9 Geometry of the studied materially asymmetric tank-reservoir system. . 266
Figure C.10 Finite elements models. 267
Figure C.11 Mode shapes, frequencies and effective modal masses of the tank. . . . 267
Figure C.12 Nondimensionalized hydrodynamic pressures and displacements 268
Figure C.13 Nondimensionalized hydrodynamic pressure profiles on the walls 269
Figure C.14 Time-history response of the materially asymmetric tank-reservoir system270

LISTE DES ANNEXES

Annexe A	A new formulation and error analysis for vibrating dam-reservoir systems with upstream transmitting boundary conditions	197
Annexe B	Étapes de calcul pour la méthode pseudo-dynamique	247
Annexe C	Seismic response of asymmetric rectangular liquid containing structures	252

LISTE DES SIGLES ET ABRÉVIATIONS

Abréviations

CC	Clamped-Clamped
CFT	Condition aux frontières transmettantes
CF	Clamped-Free
CP	Clamped-Pinned
CS	Clamped-Sliding
ESDOF	Equivalent single degree of freedom
FE	Finite elements
FRF	Fonctions de Réponses en Fréquences
MAM	Méthode de l'Accélérogramme Modifié
NM	Nouvelle Méthode
PP	Pinned-Pinned

Symbols romains

A_1, A_2, A_3, A_4	coefficients donnés par les équations (3.59) à (3.63)
$A_{k,s}$	paramètre hydrodynamique calculé par les équations (4.B.16) ou (4.B.17)
$a_{j,k}$	coefficients utilisés pour l'approximation polynomiale des modes
$a_{\mathrm{g}}, \bar{a}_{\mathrm{g}}$	accélérogramme modifié exact et simplifié respectivement
b_{s}	largeur de la structure
B_k	coefficients calculés par les équations (4.B.21) ou (4.B.22) ou (4.B.23)
B_0, B_1	paramètres hydrodynamiques donnés par les équations (3.22) et (3.23)
B_{0n}, B_{1n}	paramètres hydrodynamiques donnés par les équations (3.24) et (3.25)
$\widehat{B}_{0n}, \widehat{B}_{1n}$	paramètres hydrodynamiques donnés par les équations (3.32) et (3.33)
$B_j^{(0)}, B_j^{(1)}$	paramètres donnés par les équations (4.A.1) et (4.A.2)
C_e	correction pour la compressibilité
$C_n, \widetilde{C}_n$	$n^{\text{ième}}$ amortissement généralisé de la structure et système eau-structure
C_{r}	vitesse des ondes de pressions dans le domaine d'eau
$C_r, D_{r,k}$	coefficients donnés dans le tableau 4.1
D_1, D_2	coefficients donnés par l'équation (3.65)

E_{s}	module d'élasticité de la structure
f_k	coefficients définis dans l'équation (4.47)
$f_{\mathrm{x}}, f_{\mathrm{y}}$	facteurs de transformation géométrique
F_{st}	force hydrostatique totale s'exerçant sur la face amont de la structure
F_n, G_n	fonctions données par l'équation (3.34)
$\overline{\mathbf{F}}^{(1)}, \overline{\mathbf{F}}^{(2)}$	vecteur de forces hydrodynamiques dues au domaine d'eau gauche/droit
f_1	force équivalente latérale donnée par l'équation (3.80)
f_{sc}	force équivalente dû aux modes supérieurs donnés par l'équation (3.83)
$\mathcal{G}$	constante de Catalan
$H_{\mathrm{r}}, H_{\mathrm{w}}$	hauteur du domaine d'eau
H_{s}, H	hauteur de la structure
I_{jn}	intégrale donnée par l'équation (3.8)
I	moment d'inertie
K_1	rigidité généralisée du mode fondamental de la structure
ℓ	côté du domaine d'eau
$L_n, \widetilde{L}_n$	$n^{\text{ième}}$ forces généralisées de la structure et du système eau-structure
L_j^*	coefficients donnés dans les tableaux 5.1 à 5.6
$L_{\mathrm{r}}, L_t extw$	longueur du domaine d'eau
$\mathbf{M}$	matrice de masse de la structure
M_{s}	masse totale de la structure
m_i	masse ajoutée au noeud i du modèle éléments finis de la structure
$M_n, \widetilde{M_n}$	$n^{\text{ième}}$ masses généralisées de la structure et système eau-structure
M_j^*	coefficients donnés dans les tableaux 5.1 à 5.6
$\mathcal{M}$	moment de flexion
$\mathcal{M}_{\mathrm{st}}$	moment de flexion du aux forces hydrostatique
$N_{\mathrm{r}}, N_{\mathrm{f}}$	nombre de modes acoustiques considérés dans l'analyse
N_{s}	nombre de modes structuraux considérés dans l'analyse
$N_{\boldsymbol{\psi}_j}$	ordre de l'approximation polynomiale de mode
q	coefficient pour l'absorption d'énergie due au dépôt de sédiments
$\bar{\mathbf{Q}}$, $\bar{Q}_n$	vecteur de l'équation (3.11) et ses éléments donnés par l'équation (3.13)
$p, \bar{p}$	pression hydrodynamique et les FRFs correspondantes
$\bar{p}_0, \bar{p}_j$	FRFs des pressions hydrodynamiques données par l'équation (3.3)
$\bar{p}_{0n}, \bar{p}_{jn}$	FRFs des pressions hydrodynamiques données par (3.4) et (3.5)
$\widehat{\bar{p}}_0$	pression hydrodynamique purement réelle donnée par l'équation (3.84)
R_1, R_{r}	ratios de fréquences définis par respectivement ω_1/ω_0 et $\omega_{\mathrm{r}}/\omega_0$
$\bar{\mathbf{S}}, \bar{S}_{nj}$	matrice de l'équation (3.11) et ses éléments donnés par l'équation (3.12)

$\tilde{S}_{n,j}$	éléments donnés par les équations (4.48) à (4.50)
S_{a}	pseuso-accélération du spectre de dimmenssionement
t	temps
T_1	période fondamentale de la structure
T_{r}	période fondamentale du système eau-structue
$\widetilde{T}_j$	$j^{\text{ième}}$ période naturelle du système eau-structue
U	coefficient donné par l'équation (3.67)
$\bar{u}, \bar{\bar{u}}$	FRFs de déplacements et accélérations horizontaux
$\bar{u}^{\mathrm{e}}$	FRFs de déplacements pour la structure sèche
V	coefficient donné par l'équation(3.67)
V_i	volume d'eau tributaire du noeud i
V_j	paramètres hydrodynamiques définis par les équations (4.A.8) à (4.A.13)
$\bar{v}, \bar{\bar{v}}$	FRFs de déplacements et accélérations verticaux
$\mathcal{V}$	force de cisaillement
$\mathcal{V}_{\mathrm{st}}$	force de cisaillement due aux forces hydrostatiques
u_{st}	déplacement dû aux forces hydrostatiques
$\ddot{x}_{\mathrm{g}}, \bar{\bar{u}}_{\mathrm{g}}$	accélération du sol
$\ddot{x}_{\mathrm{g}}^{(\max)}$	accélération de pointe au sol
$X, \widehat{X}$	coefficients définis par l'équation (4.12)
y_{g}	position de la résultante des forces hydrodynamiques
y_i	hauteur du noeud i du modèle éléments-finis de la structure
$\bar{y}$	hauteur normalisée, i.e. y/H_{s}
$\bar{\mathbf{Z}}, \bar{Z}_j$	vecteur de coordonnée généralisée et $j^{\text{ième}}$ coordonnée généralisée
$\bar{Z}_j^{\mathrm{e}}$	$j^{\text{ième}}$ coordonnée généralisée de la structure sèche

Symbols Grecque

α	coefficient de réflexion des ondes dû au dépôt de sédiments
α_j	coefficient défini par l'équation (4.56)
β_j	coefficient défini par l'équation (4.56) ou donné dans le tableau (5.A1)
$\gamma_i, \widehat{\gamma}_i$	coefficients définis dans le tableau 3.1 pour $i = 1 \ldots 6$
γ_m	coefficients donnés par l'équation (4.26)
$\gamma_{j,m}^*$	coefficients donnés par l'équation (6.43)
Γ	variable donnée par l'équation (3.65)
Γ_m	variables données par l'équation (4.23)

$\Gamma_1, \Gamma_2, \Gamma_3, \Gamma_4$	solutions analytiques de l'équation (3.64)
Γ^*	solution réelle de l'équation (3.64)
Γ^*_m	constantes données dans les tableaux 5.1 à 5.6
Δ	déterminant de l'équation (3.64)
δ_{nj}	symbol de Kronecker
ε	erreur
$\zeta_i, \widehat{\zeta}_i$	coefficients donnés dans le tableau 3.2 pour $i = 1 \dots 3$
η	ratio des hauteurs du domaine d'eau et de la structure, i.e. $H_\mathrm{r}/H_\mathrm{s}$
$\eta^{(\mathrm{FE})}, \eta^{(\mathrm{NM})}$	ratios de fréquences définis dans l'équation (5.36)
$\theta, \widehat{\theta}, \Theta$	paramètres donnés par les équations (3.76), (3.43) et (3.42)
$\theta_0, \theta_0, \theta_j$	CFT
$\theta_{j,m}$	coefficients donnés par l'équation (4.25)
$\theta^*_{j,m}$	constantes données dans les tableaux 5.1 à 5.6 ou par l'équation (6.44)
$\vartheta_{j,m}$	variables données par l'équation (4.23)
κ_n	fonction définie dans l'équation (3.7)
κ_j	coefficients définis par l'équation (4.56)
λ_n	$n^{\text{ième}}$ valeur propre du domaine d'eau
Λ_f	côté du domaine d'eau
μ	facteur d'amortissement hystérétique
μ_s	masse de la structure par unité de hauteur
ν	coefficient de Poisson pour le béton de la structure
ξ_n	$n^{\text{ième}}$ ratio d'amortissement critique de la structure
$\widetilde{\xi}_\mathrm{r}$	ratio d'amortissement équivalent du système eau-structure
$\rho_\mathrm{r}, \rho_\mathrm{w}, \rho_\mathrm{f}$	masse volumique de l'eau
ρ_s	masse volumique de la structure
τ	coefficient défini par l'équation (3.67)
$\varphi, \widehat{\varphi}, \Phi$	coefficients définis par les équations(3.57), (3.39) et (3.38)
χ	paramètre défini par R^2_r
$\chi_j^{(\min)}, \chi_j^{(\max)}$	racines minimale et maximale du polynôme de l'équation (4.55)
$\boldsymbol{\psi}_n, \psi_n^{(x)}$	$n^{\text{ième}}$ mode structural de vibration et sa composante selon x
ω	fréquence d'excitation
ω_0	période fondamentale de vibration du domaine d'eau
ω_n	$n^{\text{ième}}$ fréquences naturelles de la structure
ω_r	fréquence fondamentale du système eau-structure
$\widetilde{\omega}_j$	$j^{\text{ième}}$ fréquences naturelles du système eau-structure

CHAPITRE 1

INTRODUCTION

Le but de ce chapitre est d'introduire le sujet de cette thèse en décrivant le contexte dans lequel elle s'inscrit ainsi que la problématique à laquelle elle répond. Les objectifs de la recherche ainsi qu'un descriptif de la méthodologie employée sont présentés. Les portées et contributions originales du projet de recherche sont également décrites. De plus, la structure du document est présentée à la fin du chapitre.

1.1 Contexte

La rupture ou l'effondrement d'une structure hydraulique, telle qu'un barrage, peut entraîner des pertes humaines et matérielles catastrophiques. De même, la dégradation de ces structures peut engendrer un coût économique très important. Pour ces raisons, beaucoup d'efforts ont été consacrés à assurer une grande fiabilité de ces ouvrages sous l'effet des sollicitations statique et dynamiques. Lors d'un tremblement de terre, ces structures particulières subissent non seulement les déplacements imposés par les secousses sismiques, mais aussi ceux induits par les forces hydrodynamiques générées par l'interaction fluide-structure.

À travers le monde, de nombreuses structures hydrauliques sont construites dans des régions à forte sismicité. Afin d'assurer la fiabilité sismique de ces ouvrages, les forces hydrodynamiques doivent être prises en considération lors de leur conception ou de l'évaluation de leur comportement sécuritaire. Au Québec, le règlement sur la sureté des barrages, qui est entré en vigueur le 11 avril 2002 (Art. 28 à 29), impose aux propriétaires de concevoir ou de vérifier le comportement structural de leurs barrages en tenant compte des charges sismiques auxquelles ils peuvent être soumis. Cette réglementation s'applique aussi bien aux barrages neufs ou existants. L'évaluation de sureté d'un barrage doit être effectuée au plus tard dix ans après sa mise en exploitation initiale et répétée tous les dix ans. Pour répondre à ce règlement, les propriétaires de ces ouvrages, tel que Hydro-Québec, doivent valider leur stabilité structurale en utilisant des méthodes plus ou moins complexes selon la zone sismique où se situe l'ouvrage et selon la vulnérabilité et les conséquences d'une éventuelle rupture. D'autres structures hydrauliques telles que des pontons, des digues, ou des écluses peuvent aussi être vulnérables à un tremblement de terre. Pour celles-ci, il n'existe quasiment aucune réglementation concernant la validation de leur comportement lors d'un tel évènement.

1.2 Problématique

Pour vérifier qu'une structure hydraulique existante ou en cours de conception peut résister aux charges sismiques anticipées, des méthodes de calculs rigoureuses doivent être mises à la disposition des ingénieurs-praticiens. En se basant sur certaines hypothèses simplificatrices, ces méthodes devraient permettre de modéliser numériquement ou analytiquement le système étudié et tenir compte des effets de l'interaction fluide-structure qui rendent le problème souvent très complexe.

Parmi les méthodes numériques utilisées pour étudier le comportement dynamique des systèmes eau-structure, on retrouve la Méthode des Éléments Finis ainsi que la Méthode des Éléments de Frontières aussi connue sous le nom de Méthode des Équations Intégrales. Bien que celles-ci nécessitent une grande expertise, ces méthodes permettent de tenir compte d'un grand nombre de paramètres influençant le comportement d'un système eau-structure, tels que la flexibilité de la structure, la compressibilité de l'eau ou encore l'interaction fluide-structure. De par la longueur quasi infinie de la retenue d'eau, ces méthodes nécessitent cependant de couper virtuellement le domaine d'eau à une certaine distance de la structure. Une condition aux frontières appropriée doit alors être appliquée pour éviter la réflexion des ondes au droit de la section de coupe du réservoir. Par ailleurs, pour diminuer le temps de calcul, il est intéressant de diminuer au maximum cette distance de coupe. Cependant, ces conditions aux frontières doivent être définies avec précision au risque de fausser considérablement la prédiction du comportement dynamique du système étudié. Comme l'utilisation de la méthode des éléments finis ou de frontières est de plus en plus courante pour modéliser autant la structure que le domaine d'eau, il est primordial d'étudier le comportement des conditions aux frontières transmettantes couramment employées afin d'anticiper l'erreur induite.

Pour les besoins des ingénieurs-praticiens, des méthodes simplifiées sont nécessaires pour valider des résultats obtenus avec des méthodes plus avancées, mais aussi pour la conception préliminaire ainsi que l'évaluation de la sûreté des structures hydraulique existantes. Dans la pratique, les méthodes simplifiées sont par ailleurs souvent utilisées pour calculer les charges hydrodynamiques engendrées par à l'interaction fluide-structure. Ces charges sont ensuite introduites dans des modèles éléments finis créés au stade du dimensionnement final afin de simuler l'effet hydrodynamique de l'eau. Par conséquent, ces méthodes nécessitent de prendre en compte de manière appropriée l'interaction fluide-structure afin de ne pas fausser la réponse dynamique du système eau-structure étudié. Les méthodes simplifiées existantes découlent

pour la plupart de formulations analytiques où plusieurs hypothèses simplificatrices ont été adoptées afin de simplifier la complexité de la prise en compte de l'interaction fluide-structure. Il a été montré que plusieurs de ces simplifications peuvent avoir un impact sur la prédiction du comportement structural. Des méthodes simplifiées robustes sont donc encore requises pour les besoins de la pratique. Nous avons vu précédemment que selon la zone sismique où l'ouvrage est situé, des critères de vulnérabilité et de conséquences d'une éventuelle rupture, une analyse dynamique plus ou moins complexe est requise. Comme cela sera présenté plus tard, les méthodes simplifiées existantes se limitent à des analyses pseudo-statiques ou pseudo-dynamiques, et ne permettent pas d'effectuer une analyse dynamique temporelle.

1.3 Cadre et objectifs de la recherche

La présente thèse de doctorat a pour but principal d'étudier le comportement dynamique et sismique des systèmes eau-structure tels que les systèmes barrage-réservoir-fondation. Elle vise notamment à : (i) apporter des outils nécessaires à la modélisation numérique de tels systèmes ; (ii) répondre à un grand besoin des ingénieurs-praticiens d'avoir des méthodes simplifiées pour prendre en compte de manière efficace le phénomène complexe qu'est l'interaction fluide-structure. À cet égard, plusieurs objectifs spécifiques ont motivé ce projet de recherche :

- Développer un test numérique permettant d'estimer l'erreur introduite dans un modèle d'éléments finis lors de l'utilisation de conditions aux frontières transmettantes pour représenter le comportement dynamique d'une structure retenant un domaine d'eau quasi infini.
- Développer une formulation simplifiée pour le calcul de la période fondamentale d'un système eau-structure, une information importante lors de l'évaluation du comportement dynamique.
- Développer une méthode analytique simplifiée pour l'étude dynamique d'un système eau-structure prenant en compte un maximum de phénomènes ayant une grande influence sur le comportement dynamique, tel que la géométrie de structure, l'effet des modes supérieurs et la compressibilité de l'eau.
- Développer une méthode numérique pour effectuer l'analyse dynamique temporelle d'un système eau-structure en incluant directement l'effet de l'interaction fluide-structure au modèle éléments finis de la structure seule, i.e. sans eau.

1.4 Méthodologie

Dans cette section, la méthodologie adoptée pour mener à bien cette recherche est décrite.

1.4.1 Estimation de l'erreur associée à l'utilisation de conditions aux frontières transmettantes

Bien que la littérature contient plusieurs formulations des conditions aux frontières transmettantes (CFT), il n'existe aucune technique pour estimer l'erreur qu'elles induisent lorsqu'elles sont introduites dans un modèle d'éléments finis. Par conséquent, l'utilisateur est souvent amené à augmenter la distance de troncature du domaine d'eau jusqu'à obtenir la convergence des résultats par tâtonnement. Ce processus est long et ne garantit pas forcément la convergence.

L'enjeu de ce premier objectif spécifique a donc été de développer une nouvelle formulation analytique exacte des conditions aux frontières transmettantes. Cette formulation a ensuite permis de comprendre le fonctionnement des CFT mais aussi de tester des conditions aux frontières existantes dans la littérature et/ou programmées dans les logiciels d'éléments finis. Ces analyses ont conduit à la définition d'un test d'erreur permettant de justifier le choix des CFT afin d'assurer la convergence des modèles éléments finis des systèmes eau-structure avec réservoir semi-infini. Par ailleurs, ces premiers développements nous ont permis de nous assurer de la validité de nos modèles éléments finis afin de pouvoir utiliser cette méthode comme référence dans le reste de la recherche.

1.4.2 Formulation simplifiée pour le calcul de la période fondamentale de système eau-structure et développement d'une méthode pseudo-dynamique

Un des paramètres clefs de toute analyse dynamique est la période fondamentale du système étudié. Contrairement aux bâtiments, la littérature ne contient que de très rares références traitant de la période de vibration d'un système barrage-poids et son réservoir. Non seulement l'interaction fluide-structure rend le problème très compliqué, mais négliger l'effet du réservoir sur cette fréquence peut entraîner une grande imprécision. En se basant sur une méthode analytique, une telle formulation simplifiée a été développée considérant une hypothèse d'eau incompressible ou compressible. Les résultats obtenus ont été comparés à ceux de la méthode des éléments finis et à ceux d'une méthode analytique avancée, et cela, pour différentes géométries et propriétés des barrages-poids étudiés. En utilisant ces développements dans la formulation de la force statique équivalente, une nouvelle méthode pseudo-dynamique a été développée.

1.4.3 Développement d'une méthode simplifiée d'analyse dynamique des systèmes eau-structure

Il est souvent nécessaire de réaliser une analyse dynamique de structures en contact avec de l'eau. En effet, les analyses pseudo-dynamiques ne tiennent pas compte exactement de l'effet des modes supérieurs et surtout ignorent la nature oscillatoire et transitoire des oscillations. Par conséquent, lorsqu'une analyse spectrale démontre que des zones de l'ouvrage excèdent les contraintes admissibles, il est nécessaire de réaliser une analyse dynamique pour juger de la durée et de l'étendue de ces zones. Actuellement, seules des méthodes numériques ou analytiques complexes tenant compte de l'interaction fluide-structure peuvent permettre ce type d'analyse. Dans cette partie de la recherche, une généralisation de la formulation pseudo-dynamique a été réalisée. Elle tient compte de l'effet des modes supérieur sur la réponse dynamique des systèmes eau-structures. Sa facilité d'implantation et sa rapidité de calcul apportent un avantage significatif par rapport aux méthodes complexes. Elle fut aussi développée pour prendre en compte deux domaines d'eau et différentes conditions aux frontières à l'extrémité de ces domaines.

1.4.4 Prise en compte simplifiée de l'effet de l'interaction fluide-structure dans un modèle éléments finis

L'utilisation des logiciels d'éléments finis devient de plus en plus courante pour l'étude des structures en contact avec de l'eau. En effet, ceux-ci permettent non seulement de visualiser le comportement des structures, mais aussi de facilement obtenir les efforts internes. Cependant, le recours à la technique des masses ajoutées est encore très populaire parce que l'interaction fluide-structure est souvent complexe à modéliser, qu'elle augmente énormément le temps de calcul et/ou que relativement peu de logiciels accessibles sur le marché permettent de la prendre en compte. Afin de rendre ce type d'analyses plus accessible, une nouvelle méthode numérique a été développée dans le cadre de cette thèse. Cette technique est un artifice de calcul qui modifie l'accélérogramme de dimensionnement pour obtenir un séisme qui tient compte de l'effet de l'interaction fluide-structure. Ce nouveau séisme peut alors être directement appliqué à la structure et peut tenir compte de la compressibilité de l'eau, de l'absorption d'énergie occasionnée par le dépôt de sédiments au fond du réservoir, ainsi que de la flexibilité de la fondation.

1.5 Portée et contributions originales

Les contributions originales de cette recherche sont multiples.

Tout d'abord, l'étude des conditions aux frontières transmettantes a permis de mieux comprendre leur fonctionnement, mais aussi de tester de nouvelles formulations. Cette étude et le test d'erreur proposé serviront aussi à sensibiliser les utilisateurs de la méthode d'éléments finis ou des éléments de frontières à l'importance de ces conditions et des erreurs qu'elles peuvent introduire.

Les développements concernant la période fondamentale des systèmes eau-structure sont uniques. Ils répondent à un besoin réel d'estimer ce paramètre clef dans l'évaluation dynamique des systèmes eau-structure. Grâce à cette nouvelle formulation couplée à de nouveaux développements, une nouvelle méthode pseudo-dynamique plus générale que les techniques existantes a été développée et mise à disposition des ingénieurs-praticiens. L'extension de cette méthode à une méthode dynamique simplifiée offre la possibilité de déterminer la réponse temporelle ou fréquentielle d'une structure en contact avec de l'eau. Elle tient compte des modes supérieurs, d'un ou deux domaines d'eau, et de différentes conditions aux frontières. Elle permet de répondre au besoin d'effectuer des analyses plus poussées.

La formulation de la Méthode de l'Accélérogramme Modifié (MAM) est également originale et peut s'avérer très intéressante : (i) pour simplifier la modélisation par éléments finis des ouvrages hydrauliques en s'affranchissant du domaine d'eau, mais aussi (ii) pour réaliser des essais dynamiques sur table vibrante de modèles de barrages réduits ou d'éléments de structures hydrauliques pour lesquels il est inconcevable de construire un bassin d'eau. Grâce à cette formulation, les propriétés dynamiques de la section étudiée permettent de déterminer directement l'accélérogramme modifié. Celui-ci peut alors être appliqué au modèle numérique de la structure seule ou bien comme accélération à imposer à la table vibrante supportant le spécimen étudié.

Cette recherche a permis de répondre au besoin de mieux estimer l'effet de l'interaction fluide-structure pour s'assurer d'une conception sécuritaire des systèmes eau-structure. Les méthodes proposées sont simples, précises, facilement programmables, et donneront ainsi lieu au développement d'outils numériques dédiés à l'usage des ingénieurs-praticiens.

1.6 Contenu de la thèse

À la suite de cette introduction, une revue de littérature permet de mettre à jour l'état des connaissances sur les différents sujets abordés dans cette thèse. Dans les chapitres 3 à 6, nous présentons les méthodes simplifiées développées au cours de ce doctorat pour l'étude du com-

portement dynamique des structures en contact avec de l'eau. Ces chapitres correspondent à quatre articles publiés ou soumis à des revues scientifiques. Le chapitre 8 propose une analyse paramétrique pour étudier la robustesse des méthodes pseudo-dynamiques existantes et met en relief certaines difficultés et considérations dont il faut tenir compte. La conclusion de ce document propose une synthèse des différents développements réalisés à travers cette thèse, et présente des futurs axes possibles de recherche. Enfin, le document se conclut avec les annexes A à C qui présentent deux articles publiés et des compléments du texte.

CHAPITRE 2

REVUE DE LITTÉRATURE

2.1 Introduction

La menace que peut représenter la rupture d'une structure hydraulique sur la population est à l'origine de la création d'organismes fédéraux ou provinciaux à travers le monde ayant comme mandat d'assurer la construction et l'exploitation sécuritaires de ces ouvrages. Au Canada, les provinces sont responsables de la gestion des barrages. Plusieurs d'entre elles ont adopté des mesures législatives réglementant la sécurité des barrages comme c'est le cas pour le Québec depuis avril 2002. Parallèlement à ces réglementations, des organismes ministériels ont été mis en place afin d'assurer l'application et le respect de ces lois et réglementations tel qu'étudié par Côté (2008). Par exemple, au Québec, le centre d'expertise hydrique de Québec (CEHQ) assure la conformité des ouvrages aux normes de sécurité. Aux États-Unis, le "Federal Emergency Management Agency (FEMA)" a pour objectif de réduire les risques de rupture d'un barrage américain. Pour assister ces organismes ainsi que les propriétaires des ouvrages, plusieurs guides ont été rédigés (ACB, 2007 ; FEMA, 2004 ; FERC, 2004 ; Hydro-Québec, 2000 ; CSB , 2003 ; USBR, 1987) afin de statuer sur la sécurité d'un ouvrage. Ces guides se basent notamment sur les résultats de la recherche.

Les tremblements de terre pouvant causer la rupture d'un ouvrage hydraulique, énormément de recherches ont été consacrées à la compréhension du comportement dynamique des systèmes eau-structure, et ce, depuis les années 30. Des méthodes analytiques ou numériques, fréquentielles ou temporelles, ont été développées afin de prendre en compte la flexibilité de la structure, la compressibilité de l'eau ainsi que la dissipation d'énergie due au dépôt des sédiments au fond du domaine d'eau. Certaines d'entre elles ont été validées par des tests de vibration forcée in situ (Proulx et Paultre, 1997) ou par simulation en laboratoire (Javanmardi et al., 2005). Il va s'en dire que le comportement sismique de telles structures peut être affecté par certaines non-linéarités. De nombreux phénomènes non-linéaires ont été étudiés par plusieurs chercheurs entre autres l'effet de la fissuration lors d'un tremblement de terre (Stefan, 2011 ; Christopoulos et al., 2003), la variation de sous-pressions dans les fissures sismiques (Léger et al., 2005) mais aussi la cavitation causée par la pression hydrodynamique s'exerçant sur l'ouvrage (Fenves et Luis, 1988, Noble, 2010). La littérature abonde donc de publications et d'ouvrages traitant de l'étude de tels systèmes, seuls seront abordés dans ce chapitre les aspects les plus pertinents pour les besoins des études présentées dans les

chapitres suivants.

Ce chapitre commence par la présentation des méthodes avancées de modélisation, incluant une revue des recherches sur les conditions aux frontières transmettantes requises lors de la modélisation par éléments finis ou éléments de frontières. Ensuite, une revue des méthodes simplifiées existantes sera présentée.

2.2 Méthodes complexes de modélisation des systèmes eau-structure

Les méthodes analytiques ou numériques complexes n'ont quasiment aucune limites sur la complexité du modèle à l'étude. Cependant, elles nécessitent une grande expertise et des équipements de calcul très performants. Une des méthodes analytiques les plus courantes sera décrite en premier, pour ensuite s'intéresser aux méthodes numériques. Une dernière partie traitera de la modélisation numérique ou analytique des fondations.

2.2.1 Méthodes analytiques avancées

Les méthodes analytiques sont généralement restreintes par la complexité de la géométrie et des équations régissant le comportement du domaine d'étude. Cela explique notamment pourquoi ces méthodes se limitent généralement à une étude bidimensionnelle (2D) de ces systèmes. Cette hypothèse est néanmoins justifiée lorsque les dimensions du problème et son comportement obéissent aux conditions de contraintes planes ou de déformations planes. La première méthode analytique a été développée par Westergaard (1933), qui a considéré explicitement l'effet de la pression hydrodynamique s'exerçant sur un barrage soumis à un séisme. Sa recherche a conduit entre autre au concept de masses ajoutées, une méthode simplifiée populaire qui sera revue en détail plus loin dans ce chapitre. Depuis lors, une importante quantité de travaux ont été réalisés pour tenir compte d'autres paramètres affectant la pression hydrodynamique et donc la réponse dynamique d'un barrage. Parmi ces techniques, la méthode analytique proposée par Chopra et ses collaborateurs (Chakrabarti et Chopra, 1973, Chopra, 1970, 1978, Fenves et Chopra, 1984) a marqué un grand pas dans la compréhension de la contribution de l'interaction fluide-structure au comportement sismique des barrages. Cette approche est basée sur une technique de sous-structuration, impliquant que les différents domaines de l'étude interagissent uniquement à l'interface d'interaction barrage-réservoir ou barrage-fondation. Elle permet de rendre compte de la flexibilité du barrage, de la compressibilité de l'eau, de l'interaction barrage-fondation, et de l'absorption des ondes au fond du réservoir tel qu'illustré dans la figure 2.1. La prise en compte de la flexibilité du sol des fondations se fait à travers l'utilisation de matrices d'impédance dépendantes de

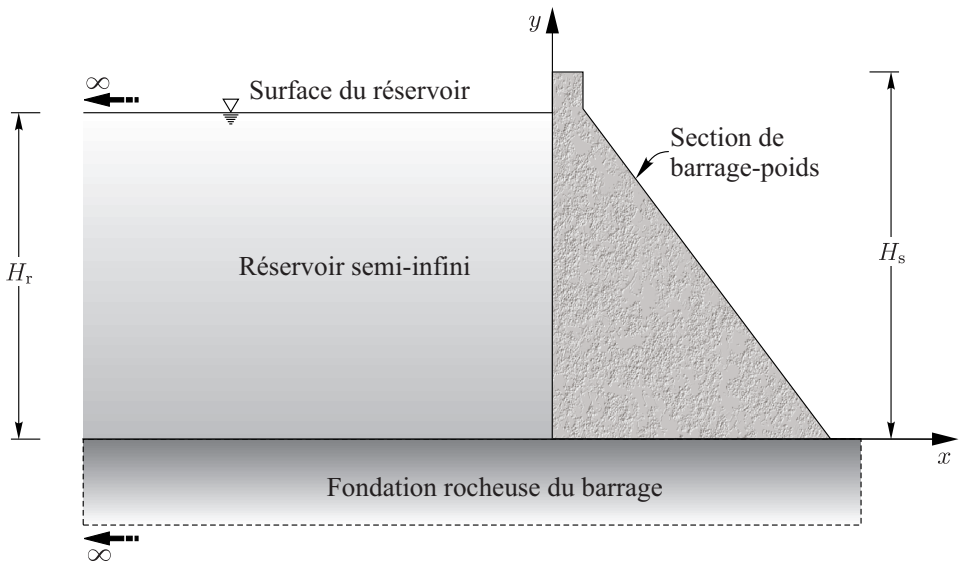

Figure 2.1 Système Barrage-réservoir-fondation

la fréquence d'excitation, dont le développement sera décrit plus tard dans ce chapitre. Les équations régissant le comportement du système barrage-fondation sont obtenues en écrivant l'équilibre des forces et la compatibilité des déplacements à l'interface. Pour réduire le nombre de degrés de liberté, et donc le nombre d'équations à résoudre, l'approche basée sur le concept de Ritz est utilisée. Celle-ci consiste à exprimer le déplacement u d'un nœud de la structure par

$$u(x, y, t) = \sum_{j=1}^{N_s} \psi_j^{(x)}(x, y)\, Z_j(t) \tag{2.1}$$

où Z_j et $\psi_j^{(x)}(x, y)$ sont respectivement la coordonnée généralisée et la fonction de forme du système barrage-fondation pour le mode j, et où N_s est le nombre de modes inclus dans l'analyse. Afin de déterminer les fonctions de formes modales où les vecteurs propres ainsi que les fréquences naturelles du système barrage-fondation, la résolution du problème aux valeurs propres est simplifiée en tenant compte seulement de la valeur statique de la matrice de rigidité de la fondation.

Pour le réservoir, la pression hydrodynamique $p(x, y, t)$ est régie par l'équation des ondes

$$\nabla^2 p = \frac{1}{C_r^2} \frac{\partial^2 p}{\partial t^2} \tag{2.2}$$

où C_r est la vitesse de propagation des ondes dans l'eau et ∇^2 le Laplacien. Sous l'effet d'une

accélération harmonique unitaire, les déplacements et les pressions hydrodynamiques peuvent être exprimés en terme de leurs Fonctions de Réponse en Fréquence (FRF) complexes $\bar{u}$ et $\bar{p}$: $u(x,y,t) = \bar{u}(x,y,\omega)\,\mathrm{e}^{\mathrm{i}\omega t}$ et $p(x,y,t) = \bar{p}(x,y,\omega)\,\mathrm{e}^{\mathrm{i}\omega t}$. En introduisant cette transformation dans l'équation (2.2), on obtient l'équation de Helmholtz

$$\nabla^2 \bar{p} + \frac{\omega^2}{C_\mathrm{r}^2}\,\bar{p} = 0 \tag{2.3}$$

Une des originalités de cette méthode analytique est le couplage de la pression hydrodynamique $\bar{p}(x,y,\omega)$ aux coordonnées généralisées $\bar{Z}_j(\omega)$, $j = 1 \ldots N_\mathrm{s}$

$$\bar{p}(x,y,\omega) = \bar{p}_0(x,y,\omega) - \omega^2 \sum_{j=1}^{N_\mathrm{s}} \bar{Z}_j(\omega)\,\bar{p}_j(x,y,\omega) \tag{2.4}$$

où $\bar{p}_0(x,y,\omega)$ peut être interprétée comme étant respectivement la fonction de réponse fréquentielle de la pression hydrodynamique due au mouvement de corps rigide du barrage, et $\bar{p}_j(x,y,\omega)$ la fonction de réponse fréquentielle de la pression hydrodynamique due à l'accélération horizontale $\psi_j^{(x)}(y) = \psi_j^{(x)}(0,y)$ de la face amont de la structure. Les conditions aux frontières illustrées dans la figure 2.2 sont utilisées pour la résolution de l'équation de Helmholtz permettant d'obtenir les expressions des pressions $\bar{p}_0$ et $\bar{p}_j$. Au fond du réservoir, un coefficient q est introduit pour prendre en compte l'absorption d'énergie due au dépôt de sédiments. La résolution de l'équation de la dynamique permet alors d'obtenir l'expression de la coordonnée généralisée et donc les FRF de la pression hydrodynamique ou du déplacement. Une transformée de Fourier peut alors être utilisée pour obtenir la réponse temporelle du système eau-structure soumis à un séisme.

Chopra et ses collaborateurs ont démontré que la compressibilité de l'eau doit être incluse si le ratio de la fréquence de résonance du réservoir, donnée par $\omega_0 = \pi\,C_\mathrm{r}/2\,H_\mathrm{r}$ ou H_r est la hauteur du réservoir, sur la fréquence de résonance du la structure seule est supérieur à 2. Cette situation est souvent obtenue dans le cas pour des barrages. Ceci a d'ailleurs été confirmé par Proulx et Paultre (1997) en comparant les résultats d'essais en vibrations forcées in situ aux prédictions de la méthode analytique décrite ici. Proulx et Paultre (1997) ont aussi validé la nécessité de prendre en compte l'absorption d'énergie due au dépôt des sédiments au fond du réservoir.

2.2.2 Méthodes des Éléments Finis

La méthode des éléments finis est devenue très populaire en particulier pour la modélisation des systèmes eau-réservoir-fondation. Les différentes sous-structures sont discrétisées

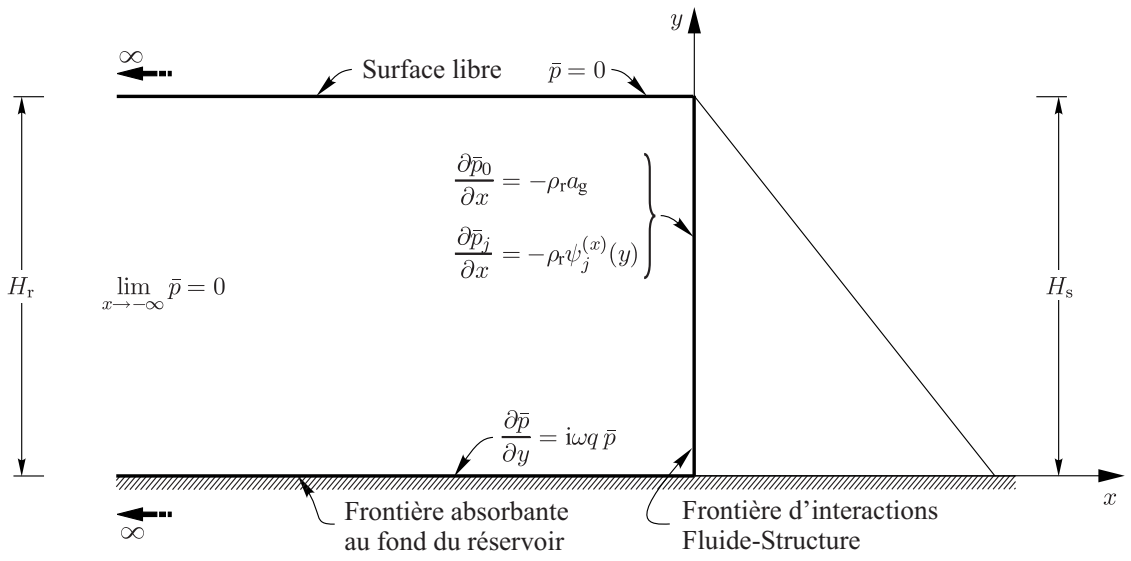

Figure 2.2 Système Barrage-réservoir et condition aux frontière utilisées

en éléments finis solides ou fluides, et des interfaces d'interaction sont placées entre ces domaines. La figure 2.3 illustre un tel modèle pour un système barrage-réservoir tenant compte de l'absorption d'énergie au fond du réservoir. Une description des différentes méthodes exis-

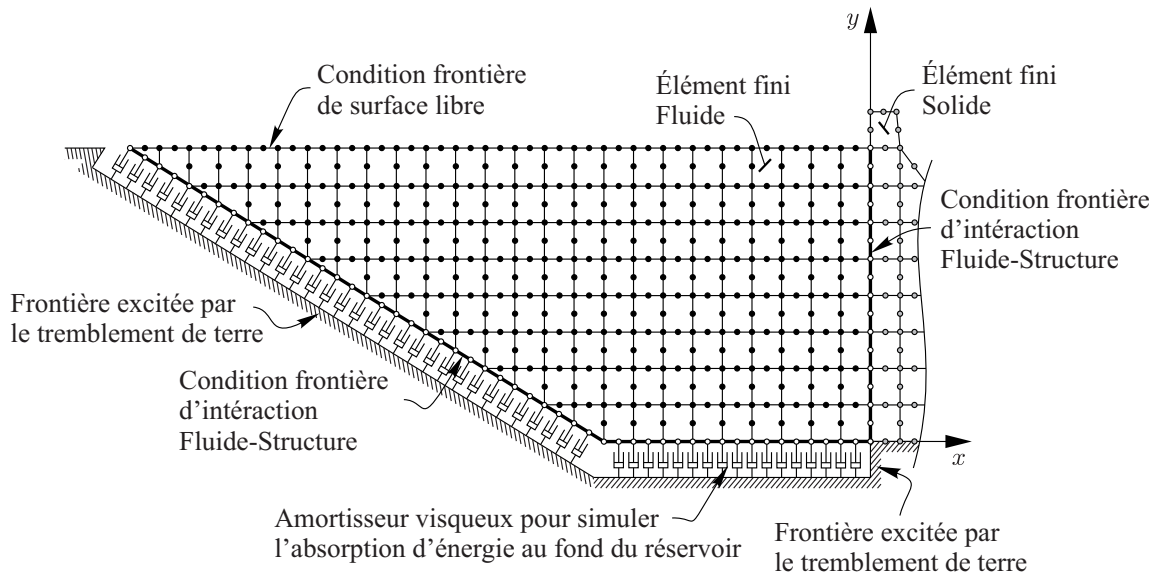

Figure 2.3 Modèle éléments finis d'un système barrage-réservoir. Extrait de Bouaanani et Lu, 2009

tantes de modélisation d'interaction fluide-structure et sols-structure en utilisant la Méthode

des Éléments Finis, peut être trouvée dans la thèse de Noble (2010). Seuls certains aspects seront traités ici.

Éléments finis fluides

Une importante quantité de travaux a été dédiée à la formulation d'éléments finis fluides, et on distingue entre autres les approches Lagrangienne et Eulérienne. La première est une extension de la formulation classique en déplacement des éléments finis développée pour des solides, c'est-à-dire que les degrés de liberté pour le fluide sont les mêmes que ceux des solides : les déplacements nodaux. Les fonctions de formes des éléments finis solide et fluide sont les mêmes. Cependant, mais les éléments fluides sont caractérisés par un module d'élasticité volumétrique égal à celui du module de compressibilité du fluide, et une résistance au cisaillement nulle pour simuler un écoulement non visqueux. La compatibilité à l'interface fluide-structure est simplement réalisée en imposant les mêmes déplacements normaux aux nœuds du fluide et du solide superposés à l'interface. La formulation Eulérienne (Lamb, 1945), aussi connue sous le nom de formulation basée sur le potentiel ou sur la pression, permet d'avoir un seul degré de liberté par élément (pression, potentiel de déplacement, ou bien potentiel de vitesse) offrant ainsi une diminution significative du nombre de degrés de liberté du modèle. Cependant, des éléments interfaces sont nécessaires pour assurer des conditions de compatibilité et d'équilibre à l'interface fluide-structure tels qu'illustrées figure 2.4. Ces

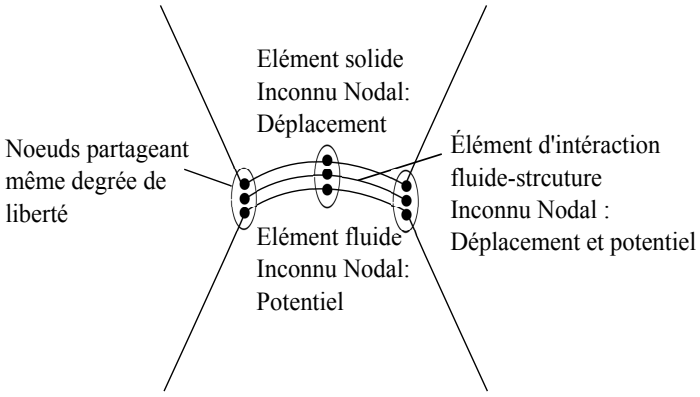

Figure 2.4 Interaction fluide-structure par formulation Eulerienne des éléments fluides

éléments permettent de connecter les éléments fluides aux éléments solides adjacents. Chaque nœuds de ces éléments comporte un degré de liberté potentiel ainsi que les degrés de libertés de déplacements. La formulation Lagrangienne a démontré son efficacité dans plusieurs domaines (Bathe et Hahn, 1979 ; Wilson et Khalvati, 1983) mais entraine l'apparition de modes parasites dans les analyses fréquentielles lorsque le fluide est quasi incompressible. Par

ailleurs, contrairement à la formulation basée sur la pression, les conditions aux frontières à utiliser sont bien moins évidentes. Par conséquent, et de par sa rapidité, la formulation Eulérienne est plus attractive pour ce domaine d'étude. Sa précision a par ailleurs été validée par Bouaanani et Lu (2009) qui ont comparé les résultats obtenus du logiciel ADINA (2006) utilisant la formulation Eulérienne, avec ceux de la méthode développée par Chopra et collaborateur décrite précédemment.

Conditions aux Frontières Transmettantes

Quelque soit la formulation utilisée pour les éléments fluides, la méthode des éléments finis nécessite que, de par la longueur quasi infinie du réservoir, celui-ci soit virtuellement tronqué à une distance finie de la paroi amont du barrage afin de permettre sa modélisation. Une Condition aux Frontières Transmettantes (CFT) doit alors être appliquée à une telle distance L_{r} pour simuler l'infinité du réservoir comme illustré dans la figure 2.5. Le système d'axe dans cette figure sera utilisé dans toute cette section. Ces conditions aux frontières permettent d'empêcher la réflexion des ondes parasites vers le barrage. En pratique, il est très avantageux de minimiser cette distance de troncature afin de limiter le nombre d'éléments dans le modèle d'éléments finis et par conséquent augmenter la vitesse de calcul. Cependant, selon la performance de la CFT, une distance de troncature trop courte pourrait entrainer une erreur considérable dans les résultats. Ces CFT, ici noté θ, sont généralement définies mathématiquement par la relation qui lie la pression hydrodynamique à son gradient normal pris à la frontière de troncature. En utilisant l'équation (2.4), on peut écrire

$$\frac{\partial \bar{p}_0^{(\infty)}}{\partial x}(-L_{\mathrm{r}}, y, \omega) = \theta_0^{(L_{\mathrm{r}})}(y, \omega)\, \bar{p}_0^{(\infty)}(-L_{\mathrm{r}}, y, \omega) \tag{2.5}$$

$$\frac{\partial \bar{p}_j^{(\infty)}}{\partial x}(-L_{\mathrm{r}}, y, \omega) = \theta_j^{(L_{\mathrm{r}})}(y, \omega)\, \bar{p}_j^{(\infty)}(-L_{\mathrm{r}}, y, \omega) \tag{2.6}$$

où $\theta_0^{(L_{\mathrm{r}})}$ et $\theta_j^{(L_{\mathrm{r}})}$ peuvent être interprétés comme les CFT liées respectivement au mouvement rigide et flexible du barrage. Parmi les nombreuses CFT existante dans la littérature, la condition aux frontières de Sommerfeld (1949) est souvent employée et définie, par

$$\theta_0^{(L_{\mathrm{r}})}(\omega) = \theta_j^{(L_{\mathrm{r}})}(\omega) = \frac{\mathrm{i}\,\omega}{C_{\mathrm{r}}} \tag{2.7}$$

Elle peut être très facilement implémentée dans un programme d'éléments finis comme illustré par Bouaanani et Lu (2009) et donne de bons résultats à condition qu'elle soit placée à une grande distance du barrage.

Humar et Roufaiel (1983) ont développé une condition aux frontières, sous l'hypothèse d'un

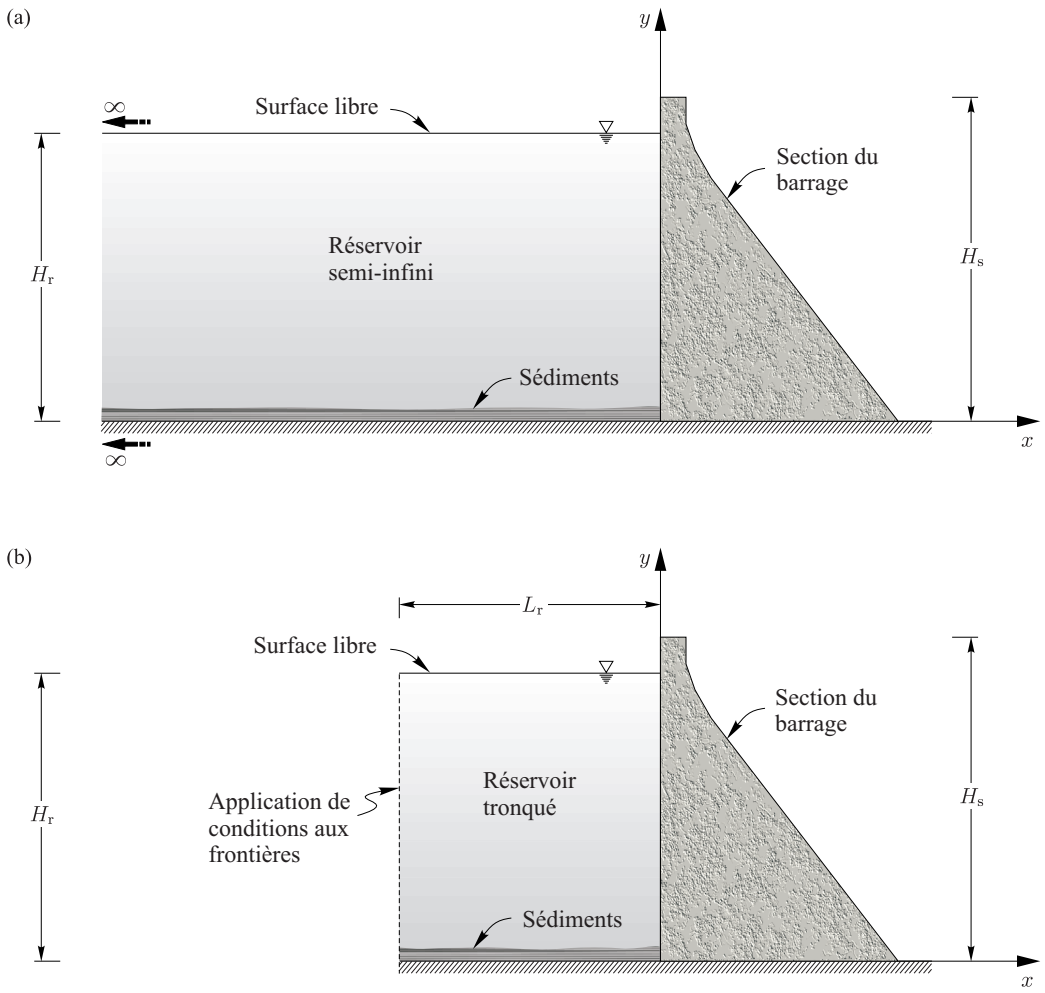

Figure 2.5 Système Barrage-réservoir et conditions aux frontières utilisés : (a) Barrage retenant un réservoir semi-infini ; (b) Barrage retenant un réservoir de longueur tronquée.

barrage infiniment rigide, correspondant à une modification de celle de Sommerfeld qu'ils ont programmé dans un logiciel d'éléments finis. Selon la fréquence d'excitation, l'expression de leur CFT est différente :

- pour $\omega = 0 \ldots \omega_0$; $\theta_0^{(L_r)} = 0$: leur condition est équivalente à placer un mur rigide à la frontière de troncature, ou peut aussi être vue comme la condition de Sommerfeld pour laquelle la compressibilité de l'eau est négligée.
- pour $\omega = \omega_0 \ldots 3\,\omega_0$; $\theta_0^{(L_r)} = \dfrac{\mathrm{i}\,\omega}{C_r}\sqrt{1 - \dfrac{\omega_0^2}{\omega}}$
- pour $\omega > 3\,\omega_0$; $\theta_0^{(L_r)} = \dfrac{\mathrm{i}\,\omega}{C_r}$: condition de Sommerfeld

Humar et Roufaiel (1983) ont montré que leur condition donne de meilleurs résultats que celle de Sommerfeld pour des fréquences d'excitation comprises entre la première et deuxième fréquence naturelle du réservoir. Dans leur étude, l'effet de l'absorption des ondes aux fonds du réservoir fut négligé. En négligeant la compressibilité de l'eau, Sharan (1985a) à développé une condition basée sur l'expression analytique de la pression hydrodynamique dans un réservoir en contact avec un barrage rigide et propose une méthode pour l'implémenter dans un logiciel d'éléments finis. Cette condition est la suivante

$$\theta_0^{(L_\mathrm{r})} = \frac{\pi}{2\,H_\mathrm{r}} \tag{2.8}$$

Il démontre alors que celle-ci donne des résultats acceptables même pour des distances de troncature très petite. Sharan (1985b) améliore alors sa CFT pour inclure la compressibilité de l'eau, mais négligeant encore l'absorption des ondes au fond du réservoir. Il conclut que ca CFT est une généralisation de celle proposée par Sommerfeld ainsi que celle développée par Humar et Roufaiel (1983). Il confirme que la condition de Sommerfeld donne de bon résultats seulement si celle-ci est placée très loin de la paroi du barrage et si les fréquences d'excitation n'excédent pas la première fréquence naturelle du réservoir. Sharan (1987) étend l'utilisation de sa CFT à un barrage flexible en séparant le réservoir en une partie proche du barrage pouvant avoir une géométrie quelconque et une partie éloignée de forme rectangulaire. Le barrage et le réservoir sont modélisés par des éléments finis, et sa CFT, développée pour un barrage rigide, est appliquée à l'extrémité du réservoir. Finalement, Sharan (1992) inclut l'effet d'absorption des ondes au fond du réservoir et démontre que sa nouvelle CFT donne de très bons résultats pour des faibles distances de troncature ainsi qu'un grand intervalle de fréquences sauf lorsque celles-ci sont proches de la deuxième et troisième fréquence naturelle du réservoir. L'expression de cette CFT n'est pas d'écrite ici, mais elle sera revue à travers la recherche.

Toutes les conditions précédentes négligent la flexibilité du barrage et par conséquent ne dépendent pas de la hauteur. Maity et Bhattacharyya (1999) ont récemment proposé une CFT qui prend en compte cette flexibilité et donc qui est fonction de la hauteur. Celle-ci considère le fond du réservoir comme étant entièrement réflectif et fut insérée dans un logiciel d'éléments finis. Cette formulation fut améliorée par Gogoi et Maity (2006) pour prendre en compte la dissipation d'énergie au fond du réservoir en se basant sur une méthode analytique simplifiée développée par Bouaanani et Paultre (2003) et revue ci-dessous. Cette CFT fut aussi implantée dans un logiciel d'éléments finis, et s'avère donner de bons résultats pour une large gamme de fréquences. Les CFT sont donc généralement basées sur de nombreuses

approximations et n'absorbent qu'une certaine partie des ondes parasites, introduisant donc une erreur dans la réponse dynamique du système. Cette erreur doit être minimisée basée sur l'expérience et le jugement de l'analyste. Plusieurs essais doivent être alors réalisés pour s'assurer de la convergence de la solution d'éléments finis. La solution est souvent validée par une comparaison avec la solution exacte d'un modèle mathématique décrivant le système barrage-réservoir avec CFT. Il n'existe cependant aucun modèle mathématique permettant de prendre en compte une CFT qui dépend de la hauteur et ainsi qui tient compte de la flexibilité du barrage.

2.2.3 Méthode des Équations Intégrales

Une autre technique pour modéliser efficacement des domaines continus de grande dimension est d'avoir recours à la méthode des éléments de frontières aussi connue sous le nom de méthode des équations intégrales. Celle-ci consiste à transformer le problème mathématique régi par des équations différentielles en équations dites d'intégrales de frontières. Cette méthode est une alternative à la méthode des éléments finis en particulier lorsque le domaine à l'étude est infini, car seules la surface (3D) ou périphérie (2D) de la frontière du domaine doit être discrétisée. Contrairement à la méthode des éléments finis, on n'a donc pas besoin de mailler tout le domaine de propagation. Elle permet directement de satisfaire la condition à l'infini. Cependant, pour réduire le temps de calcul, un domaine de longueur infinie est souvent divisé en : (i) un domaine fini proche discrétisé en utilisant la méthode des éléments finis ; (ii) un domaine infini lointain modélisé comme un domaine infini continu où bien par des éléments finis infinis. De même que pour la méthode des éléments finis des CFT sont aussi nécessaires et doivent être placées entre les deux domaines. Nous ne l'utiliserons pas dans cette recherche car peu de logiciels sur le marché utilisent ce type de formulation.

2.2.4 Modélisation de la fondation

L'interaction barrage-fondation introduit : (i) de la flexibilité à la base de la structure ; (ii) de l'amortissement additionnel sous forme d'amortissement lié aux matériaux et d'amortissement par radiation. Par conséquent, des fondations flexibles ont pour effet d'augmenter la période de vibration ainsi que l'amortissement global du système barrage-réservoir-fondation. L'effet de ce type d'interaction se traduit par la présence de forces d'interactions qui dépendent de la fréquence d'excitation du système. La matrice de rigidité des fondations, aussi appelée matrice d'impédance, dépend donc aussi de la fréquence. Dans cette sous-section les différentes façons numériques ou analytiques de modéliser les fondations sont décrites.

Modélisation par la Méthodes des Élements Finis

L'interaction barrage-fondation peut être représentée en incluant dans le modèle éléments finis le domaine de la fondation pour lequel tout les degrés de libertés en bas de ce domaine sont bloqués tels que proposé par l'U.S. Army Corps of Engineers (2003). Le domaine modélisé doit être de longueur et profondeur suffisante afin d'obtenir convergence des déformations, contraintes et fréquences naturelles. Cela peut donc se traduire par la nécessité d'un modèle des fondations énorme et donc d'un temps de calcul très long. Comme pour le fluide, des conditions aux frontières visqueuses ou absorbantes peuvent être employées pour diminuer la taille du modèle des fondations. La plus commune est celle développée par Lysmer et Kuhlemeyer (1969) pour un demi-plan élastique, qui consiste tout simplement à insérer des amortisseurs le long des frontières du domaine des fondations. Celle-ci est déjà programmée dans de nombreux logiciels, dont Adina. Une quantité exhaustive de conditions aux frontières est présentée par Feltrin (1997). Un des problèmes liés à cette méthode est que le signal sismique est modifié à l'intérieur des fondations. Par conséquent, le séisme qui doit être appliqué à la base du domaine des fondations, n'est pas celui provenant d'un enregistrement à la surface du sol, mais une modification de celui-ci.

Pour remédier à ces différents problèmes de modélisation, il est commun de modéliser les fondations par des éléments auxquels on attribue une masse nulle. Dans ce cas, seul l'effet de flexibilité des fondations est pris en compte alors que l'inertie est négligée. Il est convenu qu'une fondation excédant la hauteur du barrage dans chaque direction (amont, aval, et en profondeur) est suffisante pour obtenir la convergence des résultats. Par ailleurs, contrairement au modèle proposé précédemment en négligeant la masse, le signal sismique n'est pas modifié, et donc le tremblement de terre enregistré à la surface du sol peut directement être appliqué à la base de la fondation. D'après l'U.S. Army Corps of Engineers (2003), les degrés de liberté de translation verticale et horizontale doivent être bloqués pour les nœuds situés à la base de la fondation. Pour les noeuds aux extrémités amont et aval de la fondation, seul le degré de translation verticale doit être bloqué pour une excitation horizontale et inversement pour une excitation verticale.

Modélisation visco-élastique

Dans cette méthode, la rigidité et l'amortissement caractéristique de l'interaction barrage-fondation pour un modèle de demi-plan viscoélastique sont caractérisés par leur fonction d'impédance. Celle-ci est une matrice qui permet de relier les forces à la base de la structure aux déplacements et rotations relatifs de la fondation. Les termes de cette matrice d'impédance

sont complexes et dépendent de la fréquence. La partie réelle représente les termes d'inertie et de rigidité de la fondation, alors que la partie imaginaire caractérise l'amortissement par radiation ou matériel. La matrice d'impédance, noté $S_{\mathrm{f}}(\omega)$ peut être évaluée en utilisant la méthode développée par Dasgupta et Chopra (1979). Ce type de modèle n'est applicable que pour modéliser un domaine homogène donc sans changement de matériaux. Si les fondations sont constituées de différent type de roches, elles doivent alors être analysées par éléments finis.

2.3 Méthodes simplifiés de modélisation des systèmes fondations-barrage-réservoir

Bien que la plupart de ces méthodes numériques ou analytiques permettent de prendre en compte efficacement plusieurs aspects liés à l'interaction fluide-structures, leur utilisation nécessite une grande expertise et des logiciels spécialisés. Pour des applications pratiques, il reste donc nécessaire de développer des méthodes simplifiées.

2.3.1 Méthode pseudo-statique ou méthode des masses-ajoutées

En simplifiant sa formulation développée, Westergaard (1933) développa la méthode connue sous le nom de masses ajoutées. Pour cela, il développa une formule simplifiée pour le calcul de la pression hydrodynamique maximale, qui, en supposant une accélération unitaire, est donnée par :

$$\bar{p}(y) = \frac{7}{8}\rho_{\mathrm{r}}\sqrt{H_{\mathrm{r}}\,(H_{\mathrm{r}} - y)} \tag{2.9}$$

où ρ_{r} est la masse volumique de l'eau. Il proposa alors une technique pour transformer l'effet de cette pression en masses m que l'on vient directement appliquer aux nœuds situés sur la face amont du modèle de l'ouvrage à l'étude donnée par

$$m(y_i) = \frac{7}{8}\rho_{\mathrm{r}}\,V_i\sqrt{H_{\mathrm{r}}\,(H_{\mathrm{r}} - y)} \tag{2.10}$$

où V_i est est le volume tributaire d'eau au nœuds i. Il est important de noter que si des éléments solides ayant plus de deux nœuds sur chaque face sont choisis pour modéliser le barrage, ces masses doivent être rendues consistantes. La technique est illustrée dans la figure 2.6. L'équation (2.10) peut être modifiée pour apporter une correction due à la compressibilité de l'eau

$$m_i = \frac{7}{8}\,C_{\mathrm{e}}\,V_i\,\rho_{\mathrm{r}}\sqrt{H_{\mathrm{r}}(H_{\mathrm{r}} - y_i)} \tag{2.11}$$

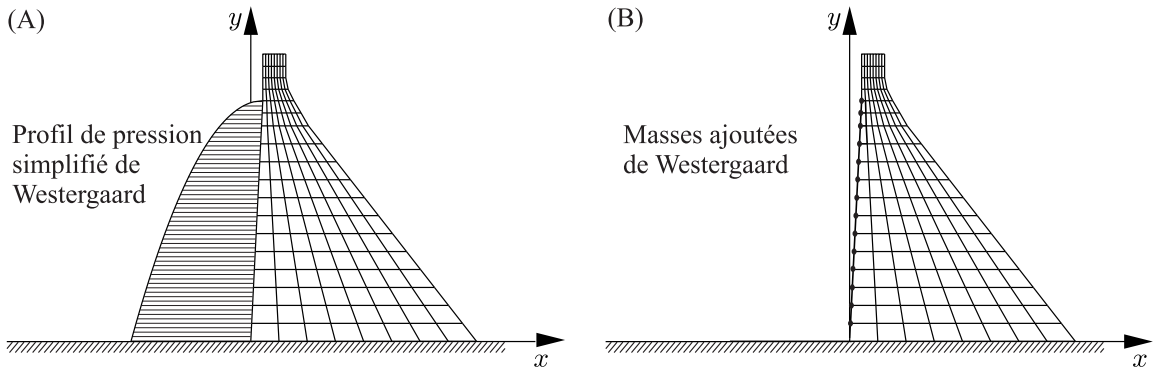

Figure 2.6 (A) Pression hydrodynamique simplifiée de Westergaard ; (B) Masses ajoutées de Westergaard.

où C_{e} est le coefficient de correction pour la compressibilité et est donné par

$$C_{\mathrm{e}} = \left[(1 - 7.75 \left(\frac{H_{\mathrm{r}}}{1000\,T} \right)^2 \right]^{-0.5} \tag{2.12}$$

Dans cette équation, T est la période d'excitation. Un des grands avantages de la méthode des masses ajoutées est que celles-ci sont indépendantes de la période de vibration. C'est pour cela que lorsque l'on apporte la correction pour la compressibilité de l'eau, la valeur de T est fixée à celle de la période moyenne de l'accélérogramme de dimensionnement. Celle-ci peut être obtenue par une transformée de Fourrier du signal. Dans l'ouest du Canada où les tremblements de terre ont un contenu fréquentiel bas, une valeur de $T = 0.5\,\mathrm{s}$ est utilisée alors que pour l'est du Canada on utilisera plutôt une valeur de $T = 0.1\,\mathrm{s}$ car le contenu fréquentiel est plus élevé. L'effet de cette simplification sera étudié plus tard.

Bien que ces développements soient basés sur des hypothèses très simplificatrices, cette méthode reste fortement utilisée de par sa simplicité. Plusieurs chercheurs ont par ailleurs proposé d'autre facteurs correcteurs permettant de tenir compte approximativement de la compressibilité de l'eau (Corns et al., 1988) ainsi que de tenir compte d'un fruit non nul de la face amont du barrage.

2.3.2 Méthode pseudo-dynamique

Dans le cas d'une structure infiniment rigide, la méthode précédente peut s'avérer suffisante. Néanmoins, pour une grande majorité des ouvrages, la flexibilité de la structure a pour conséquences d'amplifier les forces d'inertie. Il est alors nécessaire de réaliser une analyse qui

tient compte de cette flexibilité.

Fenves et Chopra (1985, 1987) ont analysé plusieurs sections de barrages triangulaires sur fondations rigides pour déterminer une approximation du mode fondamental de vibration d'un barrage type ainsi que sa fréquence ω_1 ou période T_1 fondamentale de vibration donnée par

$$\omega_1 = \frac{2\pi\sqrt{E_\mathrm{s}}}{0.38\,H_\mathrm{s}}\,; \qquad\qquad T_1 = \frac{0.38\,H_\mathrm{s}}{\sqrt{E_\mathrm{s}}} \tag{2.13}$$

où E_s est le module d'élasticité du béton. Ils ont alors implanté ce mode "type" dans leur méthode analytique (Fenves et Chopra, 1984) pour créer une méthode pseudo-dynamique basée sur une analyse modale du mode fondamental. L'effet d'utiliser un mode type quelque soit le barrage à l'étude sera étudié dans se qui suit.
En observant numériquement qu'une séparation des effets d'interaction réservoir-barrage et barrage-fondation n'affecte pas considérablement les résultats, ils montrent que l'interaction fluide-structure et l'effet des fondations modifient indépendamment la période de vibration et l'amortissement du barrage sur fondation rigide.

$$\widetilde{T}_1 = R_\mathrm{r}\,R_\mathrm{f}\,T_1\,; \qquad\qquad \widetilde{\xi}_1 = \frac{1}{R_\mathrm{r}}\frac{1}{R_\mathrm{f}^3}\,\xi_1 + \xi_\mathrm{r} + \xi_\mathrm{f} \tag{2.14}$$

où $\widetilde{T}_1$ et $\widetilde{\xi}_1$ sont respectivement la période fondamentale et le ratio d'amortissement du système barrage-réservoir-fondation, ξ_1, ξ_f et ξ_r, les ratios d'amortissement du barrage, des fondations, et le ratio d'amortissement ajouté du à l'interaction fluide-structure. R_r est un facteur dépendant des propriétés du barrage, de la hauteur d'eau, et de l'absorption d'énergie du au sédiments, R_f est un facteur dépendant des propriétés du barrage et des fondation. Les forces statiques équivalentes peuvent alors être calculées :

$$f_1(y) = \frac{\widetilde{L}_1}{\widetilde{M}_1}\,S_\mathrm{a}\big(\widetilde{T}_1, \widetilde{\xi}_1\big)\,\Big\{\mu_\mathrm{s}(y)\,\psi_1^{(x)}(0,y) - \bar{p}_1(0,y,T_\mathrm{r})\Big\} \tag{2.15}$$

où $\widetilde{L}_1$, $\widetilde{M}_1$, et T_r sont respectivement la force, masse généralisée et période fondamentale du système barrage-réservoir. $S_\mathrm{a}\big(\widetilde{T}_1, \widetilde{\xi}_1\big)$ est la pseudo accélération obtenue par le spectre de dimensionnement pour la période fondamentale et le coefficient d'amortissement du système barrage-réservoir-fondation. $\mu_\mathrm{s}(y)$ est la masse linéique du barrage, $\psi_1^{(x)}$ est le mode de vibration fondamentale du barrage sec sur sa fondation, et $\bar{p}_1$ est la FRF pour la pression due à la déformation du barrage. Une correction pour les modes supérieurs est aussi proposée. Celle-ci est développée en négligeant l'effet de la fondation sur les modes supérieurs. Par ailleurs comme les modes supérieurs ont des périodes de vibration très courte, les termes d'inertie

dans l'équation de la dynamique sont négligés. Ainsi, l'équation suivante est proposée

$$f_{\mathrm{sc}}(y) = \ddot{x}_{\mathrm{g}}^{(\max)} \left\{ \mu_{\mathrm{s}}(y) \left[1 - \frac{L_1}{M_1}\, \psi_1^{(x)}(0,y) \right] - \left[\widehat{\bar{p}}_0(0,y) + \frac{\mu_{\mathrm{s}}(y)}{M_1}\, \psi_1^{(x)}(0,y) \int_0^{H_{\mathrm{r}}} \widehat{\bar{p}}_0(0,y)\, \psi_1^{(x)}(0,y)\, \mathrm{d}y \right] \right\} \tag{2.16}$$

où L_1 et M_1 sont les forces et masses généralisées du barrage, et $\widehat{\bar{p}}$ est la FRF pour la pression du au mouvement de corps rigide du barrage. Sa méthode ne permet donc pas de tenir en compte de la géométrie exacte du barrage et donc induit une erreur directement dans le mode et la période fondamentale du barrage. Par conséquent, l'erreur est répétée dans l'estimation de la période fondamentale du système barrage-réservoir-fondation, paramètre clef de toutes analyses dynamiques ou sismiques. Cette méthode a été programmée dans CADAM, logiciel développé par Leclerc et al. (2003).

2.3.3 Analyse dynamique temporelle

Les analyses pseudo-dynamiques ne permettent pas de tenir compte de la nature oscillatoire du comportement dynamique des ouvrages. Dans le cas ou une analyse pseudo-dynamique démontre que certaines zones de la structure sont susceptibles d'être soumises à des efforts internes supérieurs aux contraintes admissibles, il est recommandé d'effectuer une analyse dynamique afin de juger de la durée et de l'étendue de ces zones. Par ailleurs, l'analyse pseudo-dynamique existante ne permet pas de tenir compte de l'effet dynamique des modes supérieurs. Bien que pour les barrages cela peut être suffisant, pour des structures plus souples, ces modes supérieurs doivent être correctement pris en compte. Finalement, lors d'une analyse pseudo-dynamique, la direction des efforts dus à chaque mode est ignorée. La réponse du mode fondamental et celle due aux modes supérieurs sont combinées par des techniques de combinaisons modales (CQC, SRSS) pour calculer la réponse totale. Ceci engendre une certaine erreur.

Une analyse dynamique temporelle permet de répondre à ces faiblesses et correspond donc à un niveau de raffinement supérieur. Dans la littérature, il n'existe aucune méthode simplifiée existante développée pour permettre une telle analyse. Dans la pratique, les masses ajoutées de Westergaard sont utilisées pour réaliser ce type d'analyse. Cette pratique peut entraîner une erreur importante dans les résultats, car, comme il a été mentionné précédemment, ces masses ont été développées en ignorant la compressibilité de l'eau et la flexibilité de la structure. On doit noter que les types d'analyses qui ont été présentées jusqu'ici (mé-

thode pseudo-statique, méthode pseudo-dynamique et méthode dynamique) correspondent chronologiquement aux analyses qui peuvent être réalisées afin de conclure sur le comportement dynamique d'un ouvrage. Par conséquent, l'utilisation de ces masses ajoutées pour une analyse de niveau supérieur ne semble pas être justifiée.

2.3.4 Autres formulations simplifiées

Il existe dans la littérature plusieurs autres méthodes simplifiées notamment pour le calcul de différents paramètres hydrodynamiques. Malgré l'importance de la période fondamentale des systèmes eau-structure, peu de techniques sont proposées dans la littérature pour l'estimer. Hatanaka (1960) a développé des expressions simplifiées pour estimer la fréquence fondamentale d'un barrage avec un réservoir vide. Pour cela, la géométrie du barrage fut approximée par un triangle symétrique et différentes formulations furent développées pour traiter les cas où les déformations en flexion ou en cisaillement furent prédominantes dans la réponse dynamique du barrage. En considérant l'analogie avec la théorie des poutres, Okamoto (1984) proposa une méthode simplifiée pour estimer la période fondamentale d'un système barrage-réservoir.

Pour ce qui est de méthodes simplifiées pour le calcul des pressions hydrodynamiques, Bouaanani et Perrault (2010) ont proposé une équation qui relie directement la pression hydrodynamique due au mouvement de corps rigide du barrage à celle due au mouvement de flexion du barrage. Par ailleurs, dans ce même travail, une expression approximative a été développée pour estimer les valeurs propres d'un réservoir avec un fond absorbant. Ceci offre un avantage considérable, car les calculer exactement ne peut se faire que par itération en utilisant des méthodes telles que Newton-Raphson.

RÉFÉRENCES

ADINA Theory and Modeling Guide. Report ARD 06-7. ADINA R & D, Inc., 2006.

ACB/CDA, (2007). Dam Safety Guidelines, Canadian Dam Association, Edmonton

Engineering and Design - Time-History Dynamic Analysis of Concrete Hydraulic Structures . Report No. EM 1110-2-6051, 2003.

Bathe KJ, Hahn W. On transient analysis of fluid–structure systems. *Journal of Computers and Structures* 1979 ; **10** : 383–91.

Bouaanani N, Lu F.Y. Assessment of potential-based fluid finite elements for seismic analysis of dam-reservoir systems. *Journal of Computers and Structures* 2009 ; **87** : 206-224.

Bouaanani N, Paultre P. A closed-form formulation for earthquake-induced hydrodynamic pressure on gravity dams. *Journal of Sound and Vibration* 2003 ; **261** : 573-582.

Bouaanani N, Perrault C. Practical Formulas for Frequency Domain Analysis of Earthquake-Induced Dam-Reservoir Interaction.*Journal of Engineering Mechanics*(ASCE) 2010 ; **136** : 107-119.

Chakrabarti P, Chopra AK. Earthquake analysis of gravity dams including hydrodynamic interaction. *Earthquake Engineering and Structural Dynamics* 1973 ; **2** : 143-160.

Chopra AK. Earthquake response of concrete gravity dams. Report No. UCB/EERC-70/01, University of California, Berkeley, 1970.

Chopra AK. Earthquake resistant design of concrete gravity dams. *Journal of the Structural Division*(ASCE) 1978 ; **104** : 953-971.

Chopra A.K, Chakrabarti P, Gupta S. Earthquake response of concrete gravity dams including hydrodynamic and foundation interaction effects. Report No. UCB/EERC-80/01, University of California, Berkeley, California, 1980.

Christopoulos, C., Léger, P., Filliatraut, A. Sliding response of gravity dams including vertical seismic accelerations. *Earthquake Engineering and Engineering vibration* 2003 ; **2** : 89-200.

Corns C.F, Schrader E.K, Tarbox G.S. Gravity dam design and analysis. Advanced Dam Engineering For Design, Construction and Rehabilitation. Chapter 16, edited by R.B Jansen, Van Nostrand Reinhold, 1988.

Coté, M. Revue critique sur la nouvelle Loi sur la securite des barrages L.R.Q., chapitre S-3.1.01. Mémoire. Université de Sherbrooke, 2008, 330 pages.

CSB (Comite Suisse des Barrages). Methods of analysis for the prediction and the verification of dam behaviour, Wasser Energie Luft, Baden, Suisse, p. 74-110 ; 2003.

Dasgupta G, Chopra A.K. Dynamic stifness Matrices for viscoelastic half planes. *Journal of the engineering mechanics division* 1979 ; **105** : 729-745.

Fenves G, Chopra A.K. Earthquake analysis and response of concrete gravity dams. Report No. UCB/EERC-84/10, University of California, Berkeley, California, 1984.

Fenves G, Chopra AK. Simplified analysis for earthquake resistant design of concrete gravity dams. Report No. UCB/EERC-85/10, University of California, Berkeley, 1985.

Fenves G, Chopra AK. Simplified earthquake analysis of concrete gravity dams. *Journal of Structural Engineering* 1987 ; **113**(8) : 1688-1708.

Fenves G, Luis M. V. Nonlinear Dynamic Analysis of Fluid-Structure Systems *J. Eng. Mech* 1988 ; **114** : 219-241.

Feltrin G. Absorbing Boundaries for the Time-Domain Analysis of Dam-Reservoir-Foundation Systems. Institute of Structural Engineering Swiss Federal Institute of Technology Zurich 1997.

Federal Guidelines for Dam Safety, U.S. Department of Homeland Security, Federal Emergency Management Agency, United States, 50 p ; 2004.

FERC (Federal Energy Regulatory Commission). Engineering guidelines for evaluation of hydropower projects - Chapter III Gravity Dams. Federal Energy Regulatory Commission, Office of Hydropower Licensing. Report No. FERC 0119-2, Washington D.C.,USA ; 1991.

Gogoi I, Maity D. A non-reflecting boundary condition for the finite element modeling of infinite reservoir with layered sediment. *Advances in Water Resources* 2006 ; **29** : 1515-1527.

Hatanaka M. Study on the earthquake-resistant design of gravity type dams. *Proceedings of the Second World Conference on Earthquake Engineering*, Tokyo and Kyoto, Japan, 1960 ; **II** : 82.1–82.16.

Humar J, Roufaiel M. Finite element analysis of reservoir vibration. *Journal of Engineering Mechanics*(ASCE) 1983 ; **109** : 215-230.

Hydro-Québec. Guide devaluation de la securite sismique des barrages, Hydro-Québec, Québec ; 2000.

Javanmardi, F., Léger, P., Tinawi R. Seismic Water Pressure in Cracked Concrete Gravity Dams : Experimental Study and Theoretical Modeling. *Journal of Structural Engineering* 2005 ; **131** : 139-150.

Lamb, H. Hydrodynamics. 6th ed. New York : Dover ; 1945.

Leclerc, M., Léger, P., Tinawi, R.Computer Aided Stability Analysis of Gravity Dams - CADAM. *International Journal Advances in Engineering Software* 2003 ; **34** : 403-420.

Léger, P., Javanmardi, F., Tinawi, R. (2005). Variations des sous-pressions dans les fissures sismiques des barrages en béton - modélisation numérique. 7iemes Colloque National de calcul en structures, v. 2, p. 507-512.

Lysmer J, Kuhlemeyer RL. Finite dynamic model for infinite media. *J Eng Mech Div* (ASCE) 1969 ; **95** :859–77.

Maity D, Bhattacharyya S.K. Time-domain analysis of infinite reservoir by finite element method using a novel far-boundary condition. *Finite Elements in Analysis and Design* 1999 ; **32** : 85-96.

Noble, CR. Finite element techniques for realistically simulating the seismic response of concrete dams. Ph.D. Thesis, University of California, Davis, 2007, 231 pages.

Okamoto S. *Introduction to earthquake engineering*. 2nd edition, University of Tokyo Press : Tokyo, 1984.

Proulx J, Paultre P. An experimental investigation of water level effects on the dynamic behaviour of a large arch dam.*Canadian Journal of Civil Engineering* 1996 ; **24** : 90-105.

Proulx J, Paultre P. Experimental and numerical investigation of dam-reservoir-foundation for a large gravity dam.*Canadian Journal of Civil Engineering* 1997 ; **24** : 90-105.

Sharan S.K. Finite element analysis of unbounded and incompressible fluid domains. *International Journal of Numerical Methods in Engineering* 1985 ; **21** : 1659-1669.

Sharan S.K. Finite element modelling of infinite reservoirs. *Journal of Engineering Mechanics*(ASCE) 1985 ; **111** : 1457-1469.

Sharan S.K. A non-reflecting boundary in fluid-structure interaction. *Journal of Computers and Structures* 1987 ; **26** : 841-846.

Sharan S.K. Efficient finite element analysis of hydrodynamic pressure on dams. *Journal of Computers and Structures* 1992 ; **42** : 713-723.

Sommerfeld A. Partial differential equations in physics. Academic Press, New York, 1949.

Stefan C. L. Modèle constitutif hydromécanique tridimensionnel pour l'analyse de stabilité des piliers d'évacuateur de crues. Thèse de doctorat, École Polytechnique de Montréal, Montréal, 2011, 199 pages.

USBR (United States Bureau of Reclamation). Design of small dams. Denver, Colorado ; 1987.

Westergaard HM. Water pressures on dams during earthquakes. *Transactions*(ASCE) 1933 ; **98** : 418-472.

Wilson EL, Khalvati M. Finite elements for the dynamics analysis of fluid–solid systems. *Int J Numer Methods Eng* 1983 ; **19** : 1657–68.

CHAPITRE 3

Article 1 : Simplified evaluation of the vibration period and seismic response of gravity dam-water systems

Benjamin Miquel [1] **and Najib Bouaanani** [2]

Paper published in *Journal of Engineering Structures*, Volume 32, Issue 8, August 2010, Pages 2488-2502. Doi :10.1016/j.engstruct.2010.04.025

Submitted 30 May 2009. Accepted 12 April 2010.

This paper proposes a practical procedure for a simplified evaluation of the fundamental vibration period of dam-water systems, and corresponding added damping, force and mass, all key parameters to assess the seismic behavior. The proposed technique includes the effects of dam geometry and flexibility, dam-reservoir interaction, water compressibility and varying reservoir level. The mathematical derivations of the method are provided considering both incompressible and compressible water assumptions. In the former case, we propose a closed-form expression for the fundamental vibration period of a dam-reservoir system. When water compressibility is included, we show that the fundamental vibration period can be obtained by simply solving a cubic equation. The proposed procedure is validated against classical Westergaard added mass formulation as well as other more advanced analytical and finite element techniques. Gravity dam monoliths with various geometries and rigidities impounding reservoirs with different heights are investigated. The new approach yields results in excellent agreement with those obtained when the reservoir is modeled analytically, or numerically using potential-based finite elements. The analytical expressions developed and the procedure steps are presented in a manner so that calculations can be easily implemented in a spreadsheet or program for simplified and practical seismic analysis of gravity dams.

1. Graduate Research Assistant, Department of Civil, Geological and Mining Engineering, École Polytechnique de Montréal, Montréal, QC H3C 3A7, Canada.

2. Associate Professor, Department of Civil, Geological and Mining Engineering, École Polytechnique de Montréal, Montréal, QC H3C 3A7, Canada
Corresponding author. E-mail : najib.bouaanani@polymtl.ca

Nomenclature

Abbreviations

ESDOF	Equivalent single degree of freedom
FRF	Frequency response function

Roman symbols

$A_1,\ A_2,\ A_3,\ A_4$	coefficients given by Eqs. (3.59) to (3.63)
a_1, a_2, a_3	coefficients used for cubic approximation of structural mode shapes
B_0, B_1	hydrodynamic parameters given by Eqs. (3.22) and (3.23), respectively
B_{0n}, B_{1n}	hydrodynamic parameters given by Eqs. (3.24) and (3.25), respectively
$\widehat{B}_{0n}, \widehat{B}_{1n}$	hydrodynamic parameters given by Eqs. (3.32) and (3.33), respectively
$C_n, \widetilde{C}_n$	n^{th} generalized damping of the dam and dam-reservoir system, respectively
C_r	velocity of pressure waves in the reservoir
D_1, D_2	coefficients given by Eq. (3.65)
E_s	modulus of elasticity of the dam
F_st	total hydrostatic force exerted on dam upstream face
F_n, G_n	functions given by Eq. (3.34)
f_1	equivalent lateral force given by Eq. (3.80)
f_sc	equivalent lateral force including higher mode effects as given by Eq. (3.83)
H_r, H_s	reservoir and dam heights, respectively
I_{jn}	integral given by Eq. (3.8)
K_1	generalized stiffness of the dam at fundamental vibration mode
$L_n, \widetilde{L}_n$	n^{th} generalized forces of the dam and dam-reservoir system, respectively
$\mathbf{M}$	mass matrix of the dam monolith
M_s	total mass of the dam monolith
m_i	Westergaard added mass at node i of the dam finite element mesh
$M_n, \widetilde{M_n}$	n^{th} generalized masses of the dam and dam-reservoir system, respectively
N_r, N_s	number of considered reservoir and structural modes, respectively
$\bar{\mathbf{Q}}$, $\bar{Q}_n$	vector in Eq. (3.11) and its elements given by Eq. (3.13), respectively
$p, \bar{p}$	hydrodynamic pressure and corresponding FRF, respectively
$\bar{p}_0, \bar{p}_j$	hydrodynamic pressure FRFs given by Eq. (3.3)
$\bar{p}_{0n}, \bar{p}_{jn}$	hydrodynamic pressure FRFs given by Eqs. (3.4) and (3.5), respectively
$\widehat{\bar{p}}_0$	real-valued hydrodynamic pressure given by Eq. (3.84)
R_1, R_r	frequency ratios given by ω_1/ω_0 and ω_r/ω_0, respectively
$\bar{\mathbf{S}}, \bar{S}_{nj}$	matrix in Eq. (3.11) and its elements given by Eq. (3.12), respectively

S_a	pseudo-acceleration ordinate of the earthquake design spectrum
t	time
T_1, T_r	fundamental periods of the dam and dam-reservoir system, respectively
U	coefficient given by Eq. (3.67)
$\bar{u}, \bar{\ddot{u}}$	FRFs for horizontal displacement and acceleration, respectively
V	coefficient given by Eq. (3.67)
V_i	volume of water tributary to node i of the dam finite element mesh
$\bar{v}, \bar{\ddot{v}}$	FRFs for vertical displacement and acceleration, respectively
$\ddot{x}_\mathrm{g}, \ddot{x}_\mathrm{g}^{(\max)}$	ground acceleration time history and peak ground acceleration, respectively
y_i	height of node i of the dam finite element mesh
$\bar{\mathbf{Z}}, \bar{Z}_j$	vector of generalized coordinates and j^th generalized coordinate, respectively

Greek symbols

$\gamma_i, \widehat{\gamma}_i$	coefficients given in Table 3.1 for $i = 1 \ldots 6$
Γ	variable given by Eq. (3.65)
$\Gamma_1, \Gamma_2, \Gamma_3, \Gamma_4$	analytical solutions of Eq. (3.64) as given by Eq. (3.66)
Γ^*	real solution of Eq. (3.64)
Δ	discriminant of Eq. (3.64)
δ_{nj}	Kronecker symbol
ε	error estimator
$\zeta_i, \widehat{\zeta}_i$	coefficients given in Table 3.2 for $i = 1 \ldots 3$
η	ratio of reservoir level to dam height, i.e. $H_\mathrm{r}/H_\mathrm{s}$
$\theta, \widehat{\theta}, \Theta$	parameters given by Eqs. (3.76), (3.43) and (3.42), respectively
κ_n	function given by Eq. (3.7)
λ_n	n^th reservoir eigenvalue
μ_s	mass of the dam per unit height
ν	Poisson's ratio of dam concrete
ξ_n	n^th fraction of critical damping of the dam
$\widetilde{\xi}_\mathrm{r}$	equivalent damping ratio of the dam-reservoir ESDOF system
$\rho_\mathrm{r}, \rho_\mathrm{s}$	mass densities of water and dam concrete, respectively
τ	coefficient given by Eq. (3.67)
$\varphi, \widehat{\varphi}, \Phi$	parameters given by Eqs. (3.57), (3.39) and (3.38), respectively
χ	frequency parameter defined by R_r^2
$\boldsymbol{\psi}_n, \psi_j^{(x)}$	n^th structural mode shape and x–component of the j^th structural mode shape
ω	exciting frequency
ω_0	fundamental vibration frequency of the full reservoir
ω_n	n^th vibration frequency of the dam
ω_r	fundamental vibration frequency of the dam-reservoir system

3.1 Introduction

Considering the effects of fluid-structure dynamic interactions is important for the design and safety evaluation of earthquake-excited gravity dams. Significant research has been devoted to this subject since the pioneering work of Westergaard [1] who modeled hydrodynamic loads as an added-mass attached to the dam upstream face. Although Wesregaard's analytical formulation was developed assuming a rigid dam impounding incompressible water, it has been widely used for many decades to design earthquake-resistant concrete dams because of its simplicity. During the last four decades, several researchers developed advanced analytical and numerical approaches to account for dam deformability and water compressibility in the seismic response of concrete dams [2, 3, 4, 5, 6, 7, 8, 9, 10, 11, 12]. Most of these methods are based on a coupled field solution through sub-structuring of the dam-reservoir system, making use of analytical formulations, finite elements, boundary elements or a mix of these techniques. In the approach proposed by Chopra and collaborators [2, 3, 4, 7], the reservoir is modeled analytically as a continuum fluid region extending towards infinity in the upstream direction. When finite or boundary elements are used, the reservoir has to be truncated at a finite distance and appropriate transmitting boundary conditions have to be applied at the cutting boundaries to prevent reflection of spurious waves as discussed by the authors in a previous work [13]. Some procedures were implemented in numerical codes specialized in two- and three-dimensional analyses of concrete dams [9, 14], and some were validated against experimental findings from in-situ forced-vibration tests [15, 16, 17, 18]. Although such sophisticated techniques were proven to efficiently handle many aspects of dam-reservoir interactions, their use requires appropriate expertise and specialized software. For practical engineering applications, simplified procedures are still needed to globally evaluate the seismic response of gravity dams, namely for preliminary design or safety evaluation purposes [19, 20, 21].

The fundamental vibration period of dam-reservoir systems is a key factor in the assessment of their dynamic or seismic behavior. Most seismic provisions and simplified procedures use the fundamental vibration period as an input parameter to determine seismic design accelerations and forces from a site-specific earthquake response spectrum. It is therefore crucial to dispose of accurate and yet practical expressions to evaluate the fundamental period of gravity dams dynamically interacting with their impounded reservoirs. Hatanaka [22] developed simplified expressions to estimate the fundamental vibration period of dams with empty reservoirs. He approximated the dam geometry as a symmetrical triangle and distinguished the cases where bending or shear effects are predominant in the dynamic response of the dam. Considering analogy with beam theory, Okamoto [23] proposed simplified for-

mulas to estimate the fundamental vibration periods of dams with empty and full reservoirs. Chopra [2, 4] analyzed several idealized triangular dam cross-sections to obtain an approximate fundamental vibration period and corresponding mode shape of typical gravity dams with an empty reservoir. These standard dynamic properties and related quantities were implemented in simplified earthquake response analyses of gravity dams [19, 20]. To determine the fundamental vibration period of a dam including impounded water effects, Chopra and collaborators [2, 3, 4, 7, 15] first obtained the frequency response curves characterizing dam-reservoir vibrations, and then identified the fundamental vibration frequency as the one corresponding to the first resonance on the curves. The authors found that hydrodynamic effects lengthen the fundamental vibration period of gravity dams and the results obtained for standard dam cross-sections were presented in figures and tables [19].

As mentioned above, although significant work has been devoted to investigate the effects of dam-water interaction on the dynamic response of gravity dams, there is no available practical closed-form technique to accurately estimate the fundamental vibration period of a gravity dam including hydrodynamic effects. In this work, we propose simplified analytical expressions and a systematic procedure to rigourously determine the fundamental period of vibrating dam-reservoir systems and corresponding added damping, force and mass. The method includes the effects of dam geometry and flexibility, water compressibility and varying reservoir level. Formulations assuming either incompressible or compressible impounded water are developed. To assess the efficiency and accuracy of the proposed procedure, we validate it against classical Westergaard added mass formulation as well as other advanced analytical and finite element techniques. We finally illustrate how the proposed technique can be efficiently implemented in a simplified and practical earthquake analysis of dam-reservoir systems.

3.2 Analytical formulation for vibrating dam-reservoir systems

3.2.1 Basic assumptions

The formulation described in this section was originally developed by Fenves and Chopra [7] to investigate earthquake excited gravity dams impounding semi-infinite rectangular-shape reservoirs. The approach is based on a sub-structuring technique, where the dam is modeled using finite elements and reservoir effects are accounted for analytically through hydrodynamic loads applied at dam upstream face. The hydrodynamic pressures are obtained by first determining mode shapes of the dam with an empty reservoir and then applying these mode shapes as boundary conditions to the solution of Helmholtz equation that governs reservoir motion in the frequency domain. Bouaanani and Lu [24] showed that this procedure to include dam-reservoir interaction yields excellent results when compared to techniques

where the reservoir is modeled numerically using potential-based fluid finite elements. The basic equations of the formulation are reviewed in this section considering compressible and incompressible water assumptions.

To illustrate the dynamics of dam-reservoir systems, we consider a 2D gravity dam cross-section shown in Fig. 3.1. The dam has a total height H_{s} and it impounds a semi-infinite reservoir of constant depth H_{r}. A Cartesian coordinate system with axes x and y with origin at the heel of the structure is adopted and the following main assumptions are made : (i) the dam and water are assumed to have a linear elastic behavior ; (ii) the dam foundation is assumed rigid ; (iii) the water in the reservoir is assumed inviscid, with its motion irrotational and limited to small amplitudes ; and (iv) gravity surface waves are neglected.

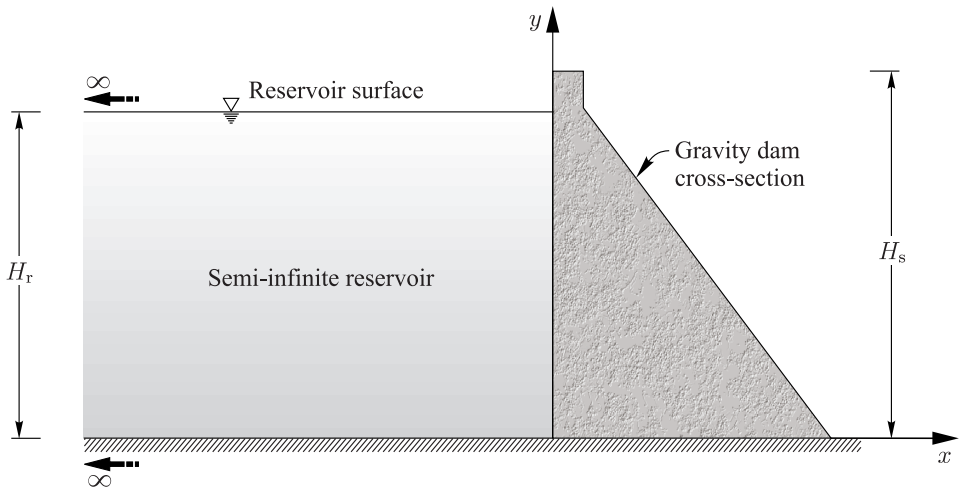

Figure 3.1 Dam-reservoir system.

3.2.2 Coupling hydrodynamic pressure and dam structural response

Considering a unit horizontal and harmonic exciting free-field ground motion $\ddot{x}_{\mathrm{g}}(t) = \mathrm{e}^{\mathrm{i}\omega t}$, the hydrodynamic pressure in the reservoir can be expressed in the frequency domain as $p(x, y, t) = \bar{p}(x, y, \omega)\, \mathrm{e}^{\mathrm{i}\omega t}$, where ω denotes the exciting frequency, and $\bar{p}(x, y, \omega)$ a complex-valued frequency response function (FRF) obeying the classical Helmholtz equation

$$\frac{\partial^2 \bar{p}}{\partial x^2} + \frac{\partial^2 \bar{p}}{\partial y^2} + \frac{\omega^2}{C_{\mathrm{r}}^2}\, \bar{p} = 0 \tag{3.1}$$

where C_r is the velocity of pressure waves in water. Fenves and Chopra [7] showed that hydrodynamic pressure FRF $\bar{p}$ can be decomposed as

$$\bar{p}(x,y,\omega) = \bar{p}_0(x,y,\omega) - \omega^2 \sum_{j=1}^{N_\mathrm{s}} \bar{Z}_j(\omega)\, \bar{p}_j(x,y,\omega) \tag{3.2}$$

in which $\bar{p}_0$ is the FRF for hydrodynamic pressure at rigid dam upstream face due to ground acceleration, $\bar{p}_j$ the FRF for hydrodynamic pressure due to horizontal acceleration $\psi_j^{(x)}(0,y)$ of the dam upstream face where $\psi_j^{(x)}$ is the x–components of the $j^{\,\mathrm{th}}$ structural mode shape $\boldsymbol{\psi}_j$, $\bar{Z}_j$ the corresponding generalized coordinate and N_s the total number of mode shapes included in the analysis.

The complex FRFs $\bar{p}_0$ and $\bar{p}_j$ can be expressed as the summation of N_r FRFs $\bar{p}_{0n}$ and $\bar{p}_{jn}$ corresponding each to a reservoir mode n

$$\bar{p}_0(x,y,\omega) = \sum_{n=1}^{N_\mathrm{r}} \bar{p}_{0n}(x,y,\omega)\,; \qquad\qquad \bar{p}_j(x,y,\omega) = \sum_{n=1}^{N_\mathrm{r}} \bar{p}_{jn}(x,y,\omega) \tag{3.3}$$

FRFs $\bar{p}_{0n}$ and $\bar{p}_{jn}$ are given by

$$\bar{p}_{0n}(x,y,\omega) = \frac{4\rho_\mathrm{r}}{\pi}\, \frac{(-1)^n}{(2n-1)}\, \frac{\mathrm{e}^{\kappa_n(\omega)x}}{\kappa_n(\omega)}\, \cos\left(\lambda_n\, y\right) \tag{3.4}$$

$$\bar{p}_{jn}(x,y,\omega) = -2\rho_\mathrm{r}\, I_{jn}\, \frac{\mathrm{e}^{\kappa_n(\omega)x}}{\kappa_n(\omega)}\, \cos\left(\lambda_n\, y\right) \tag{3.5}$$

where ρ_r denotes water mass density and where the frequency-independent eigenvalues λ_n and terms κ_n and I_{jn} are given by

$$\lambda_n = \frac{(2n-1)\,\pi}{2H_\mathrm{r}} \tag{3.6}$$

$$\kappa_n(\omega) = \sqrt{\lambda_n^2(\omega) - \frac{\omega^2}{C_\mathrm{r}^2}} \tag{3.7}$$

$$I_{jn} = \frac{1}{H_\mathrm{r}} \int_0^{H_\mathrm{r}} \psi_j^{(x)}(0,y)\, \cos\left(\lambda_n\, y\right) \mathrm{d}y \tag{3.8}$$

When water compressibility is neglected, i.e. $C_\mathrm{r} \to +\infty$, Eq. (3.7) yields the frequency-

independent term $\kappa_n = \lambda_n$. Eqs. (3.4) and (3.5) simplify then to

$$\bar{p}_{0n}(x,y) = \frac{8\rho_\mathrm{r} H_\mathrm{r}}{\pi^2} \frac{(-1)^n}{(2n-1)^2} \mathrm{e}^{\lambda_n x} \cos(\lambda_n y) \tag{3.9}$$

$$\bar{p}_{jn}(x,y) = -\frac{4\rho_\mathrm{r} H_\mathrm{r}}{\pi} \frac{I_{jn}}{(2n-1)} \mathrm{e}^{\lambda_n x} \cos(\lambda_n y) \tag{3.10}$$

Using modal superposition and mode shapes orthogonality, we show that the vector $\bar{\mathbf{Z}}$ of frequency-dependent generalized coordinates $\bar{Z}_j$, $j = 1 \ldots N_\mathrm{s}$, can be obtained by solving the system of equations

$$\bar{\mathbf{S}}\,\bar{\mathbf{Z}} = \bar{\mathbf{Q}} \tag{3.11}$$

in which, for $n = 1 \ldots N_\mathrm{s}$ and $j = 1 \ldots N_\mathrm{s}$

$$\bar{S}_{nj}(\omega) = \left(\omega_n^2 - \omega^2 + 2\,\mathrm{i}\,\omega\,\omega_n\,\xi_n\right) M_n\,\delta_{nj} + \omega^2 \int_0^{H_\mathrm{r}} \bar{p}_j(0,y,\omega)\,\psi_n^{(x)}(0,y)\,\mathrm{d}y \tag{3.12}$$

$$\bar{Q}_n(\omega) = -L_n + \int_0^{H_\mathrm{r}} \bar{p}_0(0,y,\omega)\,\psi_n^{(x)}(0,y)\,\mathrm{d}y \tag{3.13}$$

with

$$M_n = \boldsymbol{\psi}_n^\mathrm{T}\,\mathbf{M}\,\boldsymbol{\psi}_n\,; \qquad\qquad L_n = \boldsymbol{\psi}_n^\mathrm{T}\,\mathbf{M}\,\mathbf{1} \tag{3.14}$$

and where δ_{nj} is the Kronecker symbol, $\mathbf{1}$ is a column vector with ones when a horizontal translational degree of freedom corresponds to the direction of earthquake excitation, and zero otherwise, $\mathbf{M}$ is the dam mass matrix, ω_n is the vibration frequency along mode shape $\boldsymbol{\psi}_n$, and ξ_n, M_n and L_n are the corresponding modal damping ratio, generalized mass and force, respectively. When mode shapes are also mass-normalized, the generalized masses have unit values $M_n = 1$ for $n = 1 \ldots N_\mathrm{s}$. Eq. (3.2) can then be applied to find FRFs for hydrodynamic pressure, and those for dam displacements and accelerations can be expressed as

$$\bar{u}(x,y,\omega) = \sum_{j=1}^{N_\mathrm{s}} \psi_j^{(x)}(x,y)\,\bar{Z}_j(\omega)\,; \qquad \bar{\ddot{u}}(x,y,\omega) = -\omega^2 \sum_{j=1}^{N_\mathrm{s}} \psi_j^{(x)}(x,y)\,\bar{Z}_j(\omega) \tag{3.15}$$

$$\bar{v}(x,y,\omega) = \sum_{j=1}^{N_\mathrm{s}} \psi_j^{(y)}(x,y)\,\bar{Z}_j(\omega)\,; \qquad \bar{\ddot{v}}(x,y,\omega) = -\omega^2 \sum_{j=1}^{N_\mathrm{s}} \psi_j^{(y)}(x,y)\,\bar{Z}_j(\omega) \tag{3.16}$$

where $\bar{u}$ and $\bar{v}$ denote the horizontal and vertical displacements, respectively, $\bar{\ddot{u}}$ and $\bar{\ddot{v}}$ the horizontal and vertical accelerations, respectively, $\psi_j^{(x)}$ and $\psi_j^{(y)}$ the x– and y–components of structural mode shape $\boldsymbol{\psi}_j$, and N_s the number of structural mode shapes included in the

analysis.

3.3 Simplified formulation

3.3.1 Fundamental mode response analysis

As described in the previous section, a rigorous analysis of a dam-reservoir system requires the determination of several structural mode shapes of the dam with an empty reservoir. To investigate most significant factors influencing dam seismic behavior, simplified procedures using only fundamental vibration mode response have been developed and proven efficient for preliminary dam design and safety evaluation [20]. Considering only the fundamental mode response, Eqs. (3.11) to (3.13) simplify to

$$\bar{Z}_1(\omega) = \frac{-L_1 - B_0(\omega)}{-\omega^2\Big(M_1 + \mathrm{Re}\big[B_1(\omega)\big]\Big) + \mathrm{i}\omega\Big(C_1 - \omega\,\mathrm{Im}\big[B_1(\omega)\big]\Big) + K_1} \tag{3.17}$$

where the generalized earthquake force coefficient L_1, generalized mass M_1, generalized damping C_1, and generalized stiffness K_1 of the Equivalent Single Degree of Freedom (ESDOF) system of the dam with an empty reservoir are given by

$$L_1 = \boldsymbol{\psi}_1^{\mathrm{T}}\,\mathbf{M}\,\mathbf{1}\,; \qquad M_1 = \boldsymbol{\psi}_1^{\mathrm{T}}\,\mathbf{M}\,\boldsymbol{\psi}_1\,; \qquad C_1 = 2\xi_1\omega_1 M_1\,; \qquad K_1 = \omega_1^2 M_1 \tag{3.18}$$

in which ξ_1 is the fraction of critical damping at the fundamental vibration mode $\boldsymbol{\psi}_1$ of the dam with an empty reservoir, and ω_1 its fundamental vibration frequency. A finite element analysis can be conducted to obtain the generalized force L_1 and generalized mass M_1 from their discretized forms according to Eq. (3.18). The following analytical expressions can also be used

$$L_1 = \iint \rho_{\mathrm{s}}(x,y)\,\psi_1^{(x)}(x,y)\,\mathrm{d}x\mathrm{d}y \tag{3.19}$$

$$M_1 = \iint \rho_{\mathrm{s}}(x,y)\left[\psi_1^{(x)}(x,y)\right]^2 \mathrm{d}x\,\mathrm{d}y + \iint \rho_{\mathrm{s}}(x,y)\left[\psi_1^{(y)}(x,y)\right]^2 \mathrm{d}x\,\mathrm{d}y \tag{3.20}$$

in which ρ_{s} is the mass density of the dam concrete. These equations can be simplified by approximating the integration over the area of the dam by integration over its height [20] as

$$L_1 = \int_0^{H_{\mathrm{s}}} \mu_{\mathrm{s}}(y)\,\psi_1^{(x)}(0,y)\,\mathrm{d}y\,; \qquad M_1 = \int_0^{H_{\mathrm{s}}} \mu_{\mathrm{s}}(y)\left[\psi_1^{(x)}(0,y)\right]^2 \mathrm{d}y \tag{3.21}$$

where μ_{s} is the mass of the dam per unit height.

The complex-valued hydrodynamic terms B_0 and B_1 in Eq. (3.17) can be expressed as

$$B_0(\omega) = -\int_0^{H_\mathrm{r}} \bar{p}_0(0,y,\omega)\,\psi_1^{(x)}(0,y)\,\mathrm{d}y = \sum_{n=1}^{N_\mathrm{r}} B_{0n}(\omega) \tag{3.22}$$

$$B_1(\omega) = -\int_0^{H_\mathrm{r}} \bar{p}_1(0,y,\omega)\,\psi_1^{(x)}(0,y)\,\mathrm{d}y = \sum_{n=1}^{N_\mathrm{r}} B_{1n}(\omega) \tag{3.23}$$

in which

$$B_{0n}(\omega) = -\int_0^{H_\mathrm{r}} \bar{p}_{0n}(0,y,\omega)\,\psi_1^{(x)}(0,y)\,\mathrm{d}y \tag{3.24}$$

$$B_{1n}(\omega) = -\int_0^{H_\mathrm{r}} \bar{p}_{1n}(0,y,\omega)\,\psi_1^{(x)}(0,y)\,\mathrm{d}y \tag{3.25}$$

These parameters account for the effects of dam-reservoir interaction. As can be seen from Eq. (3.17), the term B_0 can be interpreted as an added force, the real part of B_1 as an added mass and the imaginary part of B_1 as an added damping. Accordingly, Fenves and Chopra [7] showed that the seismic response of a dam-reservoir system can be approximated by evaluating the generalized coordinate $\bar{Z}_1$ at the natural vibration frequency ω_r of the dam-reservoir system. At this frequency, hydrodynamic pressures $\bar{p}_0$, $\bar{p}_1$ and consequently hydrodynamic terms B_0 and B_1 are real, yielding from Eq. (3.17)

$$\bar{Z}_1(\omega_\mathrm{r}) = \frac{-\widetilde{L}_1}{-\omega_\mathrm{r}^2\widetilde{M}_1 + \mathrm{i}\,\omega_\mathrm{r}\widetilde{C}_1 + \omega_1^2 M_1} \tag{3.26}$$

where the generalized force $\widetilde{L}_1$, generalized mass $\widetilde{M}_1$ and generalized damping $\widetilde{C}_1$ of the dam-reservoir ESDOF system are obtained by modifying the parameters of the ESDOF system of the dam with an empty reservoir as follows

$$\widetilde{L}_1 = L_1 + B_0(\omega_\mathrm{r}) \tag{3.27}$$

$$\widetilde{M}_1 = M_1 + \mathrm{Re}\big[B_1(\omega_\mathrm{r})\big] = M_1 + B_1(\omega_\mathrm{r}) \tag{3.28}$$

$$\widetilde{C}_1 = C_1 - \omega_\mathrm{r}\,\mathrm{Im}\big[B_1(\omega_\mathrm{r})\big] = C_1 \tag{3.29}$$

From Eq. (3.29), we may deduce the equivalent damping ratio $\widetilde{\xi}_\mathrm{r}$ of the dam-reservoir ESDOF system as

$$\widetilde{\xi}_\mathrm{r} = \frac{\widetilde{C}_1}{2\omega_\mathrm{r}\widetilde{M}_1} \tag{3.30}$$

To develop analytical expressions for determining the fundamental vibration period of the dam including the effects of impounded water, we assume that the x–component of the dam fundamental mode shape $\boldsymbol{\psi}_1$ can be approximated as a cubic polynomial function

$$\psi_1^{(x)}(0,y) = a_1\frac{y}{H_\mathrm{s}} + a_2\left(\frac{y}{H_\mathrm{s}}\right)^2 + a_3\left(\frac{y}{H_\mathrm{s}}\right)^3 \tag{3.31}$$

where y is a coordinate varying along the height of the structure measured from its base. The coefficients a_1, a_2 and a_3 can be determined based on a finite element analysis of the dam monolith as illustrated in Fig. 3.2, or using the fundamental mode shape of a standard gravity dam section proposed by Fenves and Chopra [19] as will be shown later.

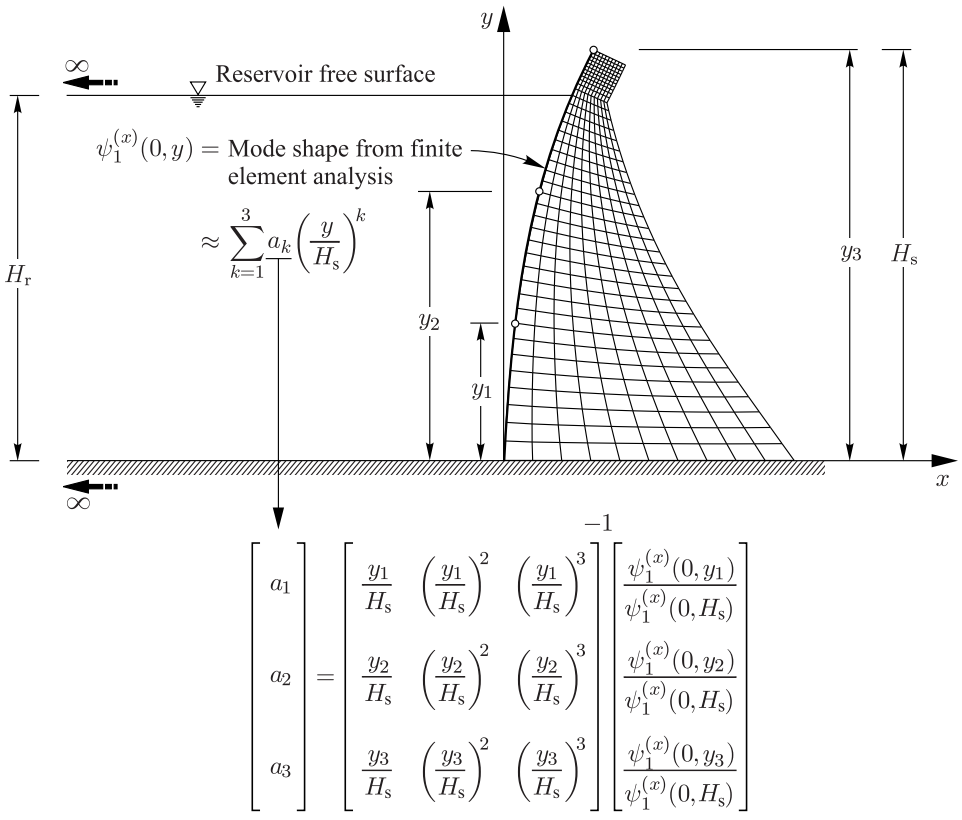

Figure 3.2 Approximation of the fundamental mode shape of a gravity dam.

3.3.2 Simplified formulation of dam-reservoir interaction assuming incompressible water

Introducing Eqs. (3.6), (3.9), (3.10) and (3.31) into Eqs. (3.22) and (3.23), we show that hydrodynamic terms B_{0n} and B_{1n} are real-valued and frequency-independent. They can be expressed as

$$\widehat{B}_{0n} = 8\rho_{\mathrm{r}}\eta^2 H_{\mathrm{s}}^2 \, \frac{(-1)^n \left[2\times(-1)^n F_n(\eta) - (2n-1)\,\pi\, G_n(\eta)\right]}{(2n-1)^3\,\pi^3} \tag{3.32}$$

$$\widehat{B}_{1n} = 4\rho_{\mathrm{r}}\eta^2 H_{\mathrm{s}}^2 \, \frac{\left[2\times(-1)^n F_n(\eta) - (2n-1)\,\pi\, G_n(\eta)\right]^2}{(2n-1)^3\,\pi^3} \tag{3.33}$$

where the hat sign indicates quantities corresponding to the incompressible water case, $\eta = H_{\mathrm{r}}/H_{\mathrm{s}}$ denotes the ratio of reservoir level to dam height, and where functions F_n and G_n are given by

$$\begin{aligned} F_n(\eta) &= \eta a_1 + \left[1 - \frac{8}{(2n-1)^2\,\pi^2}\right]\eta^2 a_2 + \left[1 - \frac{24}{(2n-1)^2\,\pi^2}\right]\eta^3 a_3 \\ G_n(\eta) &= -\frac{4\eta}{(2n-1)^2\,\pi^2}\left[a_1 - \frac{24\eta^2}{(2n-1)^2\,\pi^2}\, a_3\right] \end{aligned} \tag{3.34}$$

Eq. (3.17) simplifies then to

$$\bar{Z}_1(\omega) = \frac{-L_1 - \widehat{B}_0}{-\omega^2\big(M_1 + \widehat{B}_1\big) + \mathrm{i}\omega C_1 + K_1} \tag{3.35}$$

It can be shown numerically that the generalized damping C_1 has little effect on the fundamental vibration frequency ω_{r} of the dam-reservoir system. Consequently, ω_{r} can be approximated as the excitation frequency corresponding to the resonance of the generalized coordinate $\bar{Z}_1$ in Eq. (3.35) with $C_1 = 0$, yielding

$$\omega_{\mathrm{r}}^2\big(M_1 + \widehat{B}_1\big) - K_1 = 0 \tag{3.36}$$

where

$$\widehat{B}_1 = \sum_{n=1}^{N_{\mathrm{r}}} \widehat{B}_{1n} = 4\rho_{\mathrm{r}} H_{\mathrm{s}}^2\, \Phi(\eta, N_{\mathrm{r}}) \tag{3.37}$$

in which the function $\Phi(\eta, N_\mathrm{r})$ is defined by

$$\Phi(\eta, N_\mathrm{r}) = \eta^2 \sum_{n=1}^{N_\mathrm{r}} \frac{\left[2\times(-1)^n F_n(\eta) - (2n-1)\,\pi\, G_n(\eta)\right]^2}{(2n-1)^3\,\pi^3} \tag{3.38}$$

A sufficient number N_r of reservoir modes should be included to determine the sum Φ in Eq. (3.38). Figure 3.3 illustrates the variation of Φ as a function of reservoir height ratio η and number of included reservoir modes N_r. We show numerically that the sum Φ converges towards a function $\widehat{\varphi}$ depending only on reservoir height ratio η

$$\begin{aligned}\lim_{N_\mathrm{r}\to+\infty} \Phi(\eta, N_\mathrm{r}) &= \eta^4\left[\widehat{\gamma}_1 a_1^2 + \widehat{\gamma}_2 a_1 a_2 \eta + \left(\widehat{\gamma}_3 a_2^2 + \widehat{\gamma}_4 a_1 a_3\right)\eta^2 + \widehat{\gamma}_5 a_2 a_3 \eta^3 + \widehat{\gamma}_6 a_3^2\,\eta^4\right] \\ &= \widehat{\varphi}(\eta)\end{aligned} \tag{3.39}$$

where coefficients $\widehat{\gamma}_1$ to $\widehat{\gamma}_6$ are given in Table 3.1.

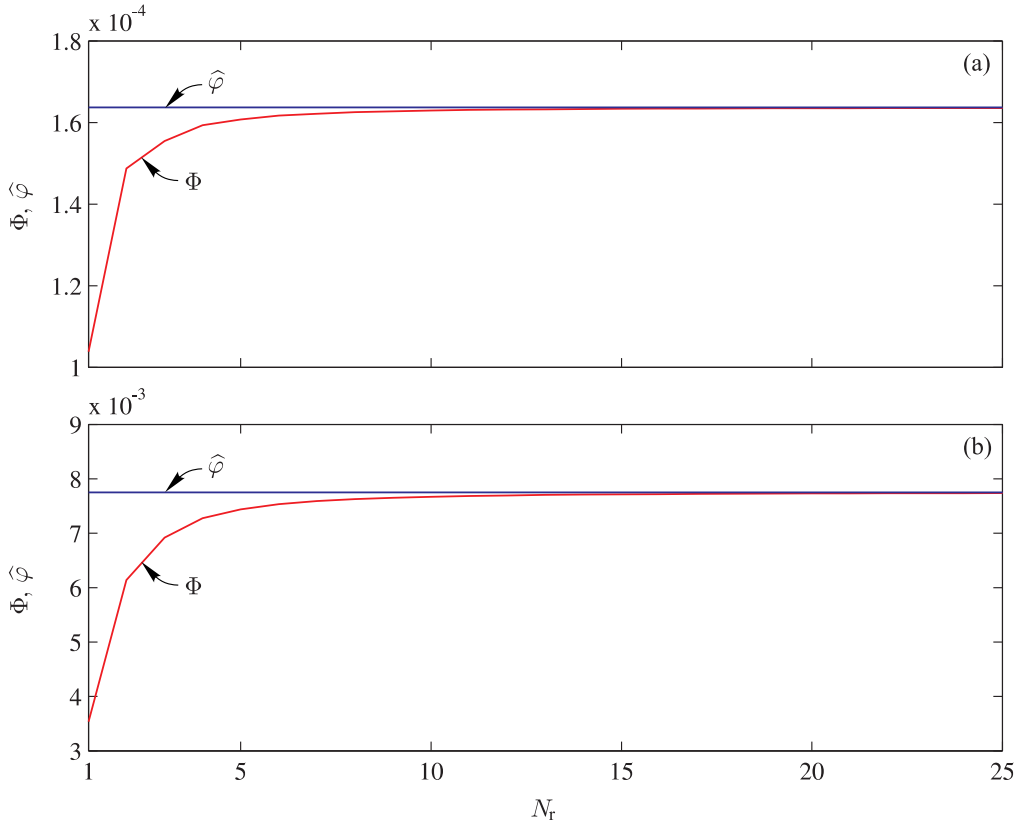

Figure 3.3 Variation of Φ and $\widehat{\varphi}$ as a function of reservoir height ratio η and number of included reservoir modes N_r : (a) $\eta = 0.50$ and (b) $\eta = 1.00$.

The limit $\widehat{\varphi}$ is also shown in Fig. 3.3. Replacing into Eq. (3.36) yields the fundamental

resonant frequency and period of a dam-reservoir system with water compressibility neglected

$$\omega_{\mathrm{r}} = \frac{\omega_1}{\sqrt{1 + \dfrac{4\rho_{\mathrm{r}} H_{\mathrm{s}}^2\, \widehat{\varphi}(\eta)}{M_1}}}\,; \qquad\qquad T_{\mathrm{r}} = T_1 \sqrt{1 + \frac{4\rho_{\mathrm{r}} H_{\mathrm{s}}^2\, \widehat{\varphi}(\eta)}{M_1}} \tag{3.40}$$

where T_1 denotes the fundamental vibration period of the dam with an empty reservoir.

Table 3.1 Coefficients $\widehat{\gamma}_i$ and γ_i, $i = 1, \ldots, 6$.

Incompressible water	Compressible water
$\widehat{\gamma}_1 = 25.769 \times 10^{-3}$	$\gamma_1 = \ \ 8.735 \times 10^{-3}$
$\widehat{\gamma}_2 = 31.820 \times 10^{-3}$	$\gamma_2 = 14.059 \times 10^{-3}$
$\widehat{\gamma}_3 = 10.405 \times 10^{-3}$	$\gamma_3 = \ \ 5.776 \times 10^{-3}$
$\widehat{\gamma}_4 = 22.082 \times 10^{-3}$	$\gamma_4 = 11.172 \times 10^{-3}$
$\widehat{\gamma}_5 = 15.031 \times 10^{-3}$	$\gamma_5 = \ \ 9.343 \times 10^{-3}$
$\widehat{\gamma}_6 = \ \ 5.587 \times 10^{-3}$	$\gamma_6 = \ \ 3.840 \times 10^{-3}$

To obtain a simplified expression of the generalized coordinate $\bar{Z}_1$ of the dam-reservoir system at resonant frequency ω_{r}, a simplified expression of the hydrodynamic term $\widehat{B}_0$ has to be found. When water compressibility is neglected, we have according to Eq. (3.32)

$$\widehat{B}_0 = \sum_{n=1}^{N_{\mathrm{r}}} \widehat{B}_{0n} = 8\rho_{\mathrm{r}} H_{\mathrm{s}}^2\, \Theta(\eta, N_{\mathrm{r}}) \tag{3.41}$$

where the function $\Theta(\eta, N_{\mathrm{r}})$ is given by

$$\Theta(\eta, N_{\mathrm{r}}) = \eta^2 \sum_{n=1}^{N_{\mathrm{r}}} \frac{(-1)^{n-1} \left[2 \times (-1)^{n-1} F_n(\eta) + (2n-1)\, \pi\, G_n(\eta)\right]}{(2n-1)^3\, \pi^3} \tag{3.42}$$

As for the function Φ, we show numerically that the sum Θ converges towards a function $\widehat{\theta}$ depending only on reservoir height ratio η

$$\lim_{N_{\mathrm{r}} \to +\infty} \Theta(\eta, N_{\mathrm{r}}) = \eta^3 \big(\widehat{\zeta}_1 a_1 + \widehat{\zeta}_2 a_2 \eta + \widehat{\zeta}_3 a_3 \eta^2\big) = \widehat{\theta}(\eta) \tag{3.43}$$

where the coefficients $\widehat{\zeta}_1$ to $\widehat{\zeta}_3$ are given in Table 3.2. The hydrodynamic term $\widehat{B}_0$ can then be approximated as

$$\widehat{B}_0 = 8\rho_{\mathrm{r}} H_{\mathrm{s}}^2\, \widehat{\theta}(\eta) \tag{3.44}$$

Table 3.2 Coefficients $\widehat{\zeta}_i$ and ζ_i, $i = 1, 2, 3$.

Incompressible water	Compressible water
$\widehat{\zeta}_1 = 27.234 \times 10^{-3}$	$\zeta_1 = 3.795 \times 10^{-3}$
$\widehat{\zeta}_2 = 15.323 \times 10^{-3}$	$\zeta_2 = 3.105 \times 10^{-3}$
$\widehat{\zeta}_3 = 10.006 \times 10^{-3}$	$\zeta_3 = 2.500 \times 10^{-3}$

Neglecting the influence of damping on the fundamental vibration frequency ω_r of the dam-reservoir system and using the analytical expressions developed above, the properties given in Eqs. (3.27), (3.28) and (3.30) to characterize the dam-reservoir ESDOF system can now be obtained as

$$\widetilde{L}_1 = L_1 + 8\rho_\mathrm{r} H_\mathrm{s}^2\, \widehat{\theta}(\eta) \tag{3.45}$$

$$\widetilde{M}_1 = M_1 + 4\rho_\mathrm{r} H_\mathrm{s}^2\, \widehat{\varphi}(\eta) = \frac{\omega_1^2}{\omega_\mathrm{r}^2}\, M_1 \tag{3.46}$$

$$\widetilde{\xi}_1 = \frac{C_1}{2\omega_\mathrm{r}\widetilde{M}_1} = \frac{\omega_\mathrm{r}}{\omega_1}\, \xi_1 \tag{3.47}$$

3.3.3 Simplified formulation of dam-reservoir interaction considering water compressibility

Introducing Eqs. (3.4) to (3.6) and Eq. (3.31) into Eqs. (3.22) and (3.23), we show that the hydrodynamic terms B_{0n} and B_{1n} are now complex-valued and frequency-dependent, and that they can be expressed as

$$B_{0n}(\omega) = 4\rho_\mathrm{r}\eta H_\mathrm{s}\, \frac{(-1)^n \left[2\times(-1)^n F_n(\eta) - (2n-1)\,\pi\, G_n(\eta)\right]}{(2n-1)^2\,\pi^2 \sqrt{\dfrac{(2n-1)^2\pi^2}{4\eta^2 H_\mathrm{s}^2} - \dfrac{\omega^2}{C_\mathrm{r}^2}}} \tag{3.48}$$

$$B_{1n}(\omega) = 2\rho_\mathrm{r}\eta H_\mathrm{s}\, \frac{\left[2\times(-1)^n F_n(\eta) - (2n-1)\,\pi\, G_n(\eta)\right]^2}{(2n-1)^2\,\pi^2 \sqrt{\dfrac{(2n-1)^2\pi^2}{4\eta^2 H_\mathrm{s}^2} - \dfrac{\omega^2}{C_\mathrm{r}^2}}} \tag{3.49}$$

As mentioned previously, the fundamental vibration frequency ω_r of the dam-reservoir system can be approximated as the frequency corresponding to the resonance of the generalized

coordinate $\bar{Z}_1$ in Eq. (3.17) with $C_1 = 0$, yielding in this case

$$\omega_{\mathrm{r}}^2 \big[M_1 + B_1(\omega_{\mathrm{r}}) \big] - K_1 = 0 \tag{3.50}$$

Eq. (3.50) is more difficult to solve than Eq. (3.36) obtained assuming incompressible water, since the term B_1 is now frequency-dependent. To circumvent this difficulty, we show that we can approximate the value of hydrodynamic term B_1 at the resonant frequency ω_{r} as

$$B_1(\omega_{\mathrm{r}}) = B_{1,1}(\omega_{\mathrm{r}}) + \sum_{n=2}^{N_{\mathrm{r}}} B_{1n}(0) \tag{3.51}$$

where $B_{1,1}(\omega_{\mathrm{r}})$ is given by

$$B_{1,1}(\omega_{\mathrm{r}}) = 4\rho_{\mathrm{r}}\eta^2 H_{\mathrm{s}}^2 \, \frac{\big[2F_1(\eta) + \pi \, G_1(\eta) \big]^2}{\pi^3 \sqrt{1 - \dfrac{\omega_{\mathrm{r}}^2}{\omega_0^2}}} \tag{3.52}$$

in which $\omega_0 = \pi C_{\mathrm{r}}/(2H_{\mathrm{r}})$ denotes the fundamental vibration frequency of the full reservoir, and where F_1 and G_1 can be obtained from Eq. (3.34) with $n = 1$

$$\begin{aligned} F_1(\eta) &= \eta a_1 + \left(1 - \frac{8}{\pi^2} \right) \eta^2 a_2 + \left(1 - \frac{24}{\pi^2} \right) \eta^3 a_3 \\ G_1(\eta) &= -\frac{4\eta}{\pi^2} \left(a_1 - \frac{24\eta^2}{\pi^2} \, a_3 \right) \end{aligned} \tag{3.53}$$

The value of B_{1n} at $\omega = 0$ is given by Eq. (3.49)

$$B_{1n}(0) = 4\rho_{\mathrm{r}}\eta^2 H_{\mathrm{s}}^2 \, \frac{\big[2 \times (-1)^n F_n(\eta) - (2n-1) \, \pi \, G_n(\eta) \big]^2}{(2n-1)^3 \, \pi^3} \tag{3.54}$$

Eq. (3.51) can then be rewritten as

$$B_1(\omega_{\mathrm{r}}) = B_{1,1}(\omega_{\mathrm{r}}) + 4\rho_{\mathrm{r}} H_{\mathrm{s}}^2 \left\{ \Phi(\eta, N_{\mathrm{r}}) - \frac{\eta^2}{\pi^3} \Big[2F_1(\eta) + \pi \, G_1(\eta) \Big]^2 \right\} \tag{3.55}$$

where $\Phi(\eta, N_{\mathrm{r}})$ is given by Eq. (3.38). Considering the limit as $N_{\mathrm{r}} \to +\infty$, we find that

$$B_1(\omega_{\mathrm{r}}) = B_{1,1}(\omega_{\mathrm{r}}) + 4\rho_{\mathrm{r}} H_{\mathrm{s}}^2 \, \varphi(\eta) \tag{3.56}$$

in which

$$\begin{aligned}\varphi(\eta) &= \lim_{N_\mathrm{r}\to+\infty} \Phi(\eta, N_\mathrm{r}) - \frac{\eta^2}{\pi^3}\Big[2F_1(\eta) + \pi\, G_1(\eta)\Big]^2 \\ &= \widehat{\varphi}(\eta) - \frac{\eta^2}{\pi^3}\Big[2F_1(\eta) + \pi\, G_1(\eta)\Big]^2 \\ &= \eta^4\Big[\gamma_1 a_1^2 + \gamma_2 a_1 a_2 \eta + \big(\gamma_3 a_2^2 + \gamma_4 a_1 a_3\big)\,\eta^2 + \gamma_5 a_2 a_3 \eta^3 + \gamma_6 a_3^2 \eta^4\Big]\end{aligned} \tag{3.57}$$

We note that $\varphi(\eta)$ has the same expression as $\widehat{\varphi}(\eta)$ in Eq. (3.39), but with coefficients γ_1 to γ_6 corresponding to the compressible water case as indicated in Table 3.1. To validate Eq. (3.56), Fig. 3.4 compares the term $4\rho_\mathrm{r} H_\mathrm{s}^2\,\varphi(\eta)$ to the real and imaginary parts of the hydrodynamic term $(B_1 - B_{1,1})$ determined at frequency ratios ω/ω_0 varying from 0 to 4. As can be seen, the approximation in Eq. (3.56) is valid for frequency ratios ω/ω_0 up to 1, and a fortiori for the dam-reservoir fundamental frequency ω_r, since $\omega_\mathrm{r}/\omega_0 < 1$. Substituting Eq. (3.56) into Eq. (3.50) and introducing the frequency ratios $R_\mathrm{r} = \omega_\mathrm{r}/\omega_0$ and $R_1 = \omega_1/\omega_0$, we show that Eq. (3.50) can be rewritten under the form of a cubic equation to be solved for $\chi = R_\mathrm{r}^2$

$$A_1\,\chi^3 + A_2\,\chi^2 + A_3\,\chi + A_4 = 0 \tag{3.58}$$

where

$$A_0 = 1 + \frac{4\rho_\mathrm{r} H_\mathrm{s}^2\,\varphi(\eta)}{M_1} \tag{3.59}$$

$$A_1 = A_0^2 \tag{3.60}$$

$$A_2 = -A_0\left(A_0 + 2R_1^2\right) + \left\{\frac{4\rho_\mathrm{r}\eta^2 H_\mathrm{s}^2}{M_1\pi^3}\Big[2F_1(\eta) + \pi\, G_1(\eta)\Big]^2\right\}^2 \tag{3.61}$$

$$A_3 = R_1^2\left(2A_0 + R_1^2\right) \tag{3.62}$$

$$A_4 = -R_1^4 \tag{3.63}$$

The fundamental vibration frequency $\omega_\mathrm{r} = \omega_0 R_\mathrm{r}$ and period $T_\mathrm{r} = 2\pi/\omega_\mathrm{r}$ of the dam-reservoir system can then be obtained by solving Eq. (3.58) numerically or analytically using Cardano's formula. In the latter case, Eq. (3.58) can be first reduced to

$$\Gamma^3 + D_1\,\Gamma + D_2 = 0 \tag{3.64}$$

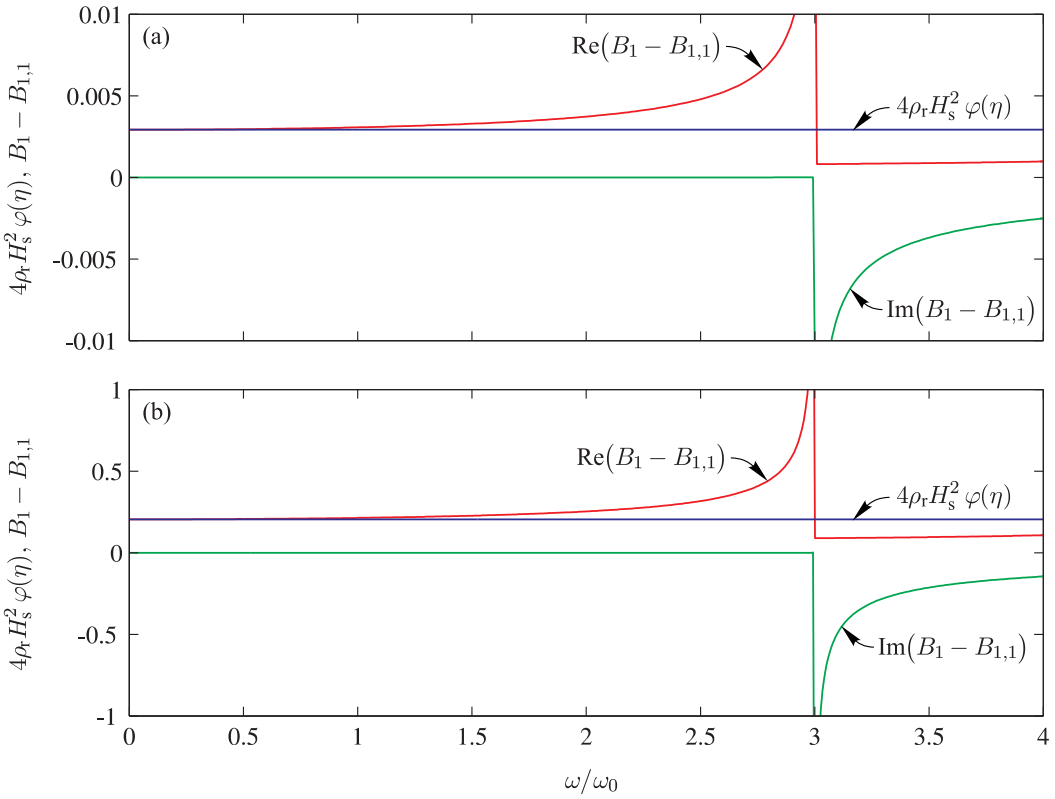

Figure 3.4 Variation of the terms $4\rho_r H_s^2\,\varphi(\eta)$ and $(B_1 - B_{1,1})$ as a function of frequency ratio ω/ω_0 and reservoir height ratio η : (a) $\eta = 0.50$ and (b) $\eta = 1.00$.

where

$$\Gamma = \chi + \frac{1}{3}\frac{A_2}{A_1}\,; \qquad D_1 = \frac{A_3}{A_1} - \frac{1}{3}\left(\frac{A_2}{A_1}\right)^2; \qquad D_2 = \frac{2}{27}\left(\frac{A_2}{A_1}\right)^3 - \frac{A_2 A_3}{3A_1^2} + \frac{A_4}{A_1} \tag{3.65}$$

Eq. (3.64) has three solutions Γ_1, Γ_2 and Γ_3 that can be expressed as [25]

$$\Gamma_1 = U + V\,; \qquad \Gamma_2 = \tau\,U + \tau^2\,V\,; \qquad \Gamma_3 = \tau^2\,U + \tau\,V \tag{3.66}$$

where

$$U = \left(-\frac{D_2}{2} + \sqrt{\Delta}\right)^{1/3}; \qquad V = -\frac{1}{3}\frac{D_1}{U}\,; \qquad \tau = -\frac{1}{2} + \mathrm{i}\,\frac{\sqrt{3}}{2} \tag{3.67}$$

and where Δ denotes the discriminant

$$\Delta = \left(\frac{D_1}{3}\right)^3 + \left(\frac{D_2}{2}\right)^2 \tag{3.68}$$

We denote as Γ^* the only real solution among Γ_1, Γ_2 and Γ_3 that satisfies

$$\frac{A_2}{3A_1} \leqslant \Gamma^* \leqslant R_1^2 + \frac{A_2}{3A_1} \tag{3.69}$$

The frequency ratio R_r and fundamental vibration period T_r of the dam-reservoir system are then given by

$$R_\mathrm{r} = \frac{\omega_\mathrm{r}}{\omega_0} = \sqrt{\Gamma^* - \frac{A_2}{3A_1}}\,; \qquad\qquad T_\mathrm{r} = \frac{2\pi}{\omega_0\sqrt{\Gamma^* - \dfrac{A_2}{3A_1}}} \tag{3.70}$$

Once the vibration frequency ω_r is known, we can determine the properties of the dam-reservoir ESDOF system as described in the previous section for the case of incompressible water. When water compressibility is included, we show that the hydrodynamic term $B_0(\omega_\mathrm{r})$ can be expressed as

$$B_0(\omega_\mathrm{r}) = B_{0,1}(\omega_\mathrm{r}) + \sum_{n=2}^{N_\mathrm{r}} B_{0n}(0) \tag{3.71}$$

where $B_{0,1}(\omega_\mathrm{r})$ is given by

$$B_{0,1}(\omega_\mathrm{r}) = 8\rho_\mathrm{r}\eta^2 H_\mathrm{s}^2\,\frac{\big[2F_1(\eta) + \pi\,G_1(\eta)\big]}{\pi^3\,\sqrt{1-R_\mathrm{r}^2}} \tag{3.72}$$

and where the value of B_{0n} at $\omega = 0$ is obtained from Eq. (3.48)

$$B_{0n}(0) = 8\rho_\mathrm{r}\eta^2 H_\mathrm{s}^2\,\frac{\big[2\times(-1)^{n-1}F_n(\eta) + (2n-1)\,\pi\,G_n(\eta)\big]}{(2n-1)^3\,\pi^3} \tag{3.73}$$

Eq. (3.71) can then be rewritten as

$$B_0(\omega_\mathrm{r}) = B_{0,1}(\omega_\mathrm{r}) + 8\rho_\mathrm{r}H_\mathrm{s}^2\left\{\Theta(\eta, N_\mathrm{r}) - \frac{\eta^2}{\pi^3}\Big[2F_1(\eta) + \pi\,G_1(\eta)\Big]\right\} \tag{3.74}$$

where $\Theta(\eta, N_\mathrm{r})$ is given by Eq. (3.42). Considering the limit as $N_\mathrm{r} \to +\infty$, we find that

$$B_0(\omega_\mathrm{r}) = B_{0,1}(\omega_\mathrm{r}) + 8\rho_\mathrm{r}H_\mathrm{s}^2\,\theta(\eta) \tag{3.75}$$

in which

$$\begin{aligned}\theta(\eta) &= \lim_{N_\mathrm{r}\to+\infty}\Theta(\eta,N_\mathrm{r}) - \frac{\eta^2}{\pi^3}\Big[2F_1(\eta)+\pi\,G_1(\eta)\Big]\\ &= \widehat{\theta}(\eta) - \frac{\eta^2}{\pi^3}\Big[2F_1(\eta)+\pi\,G_1(\eta)\Big]\\ &= \eta^3\big(\zeta_1 a_1 + \zeta_2 a_2\eta + \zeta_3 a_3\eta^2\big)\end{aligned} \tag{3.76}$$

where coefficients ζ_1 to ζ_3 are given in Table 3.2. Neglecting the influence of damping on the fundamental vibration frequency of the dam-reservoir system and using the analytical expressions developed above, Eqs. (3.27), (3.28) and (3.30) become when water compressibility is included

$$\widetilde{L}_1 = L_1 + 8\rho_\mathrm{r}H_\mathrm{s}^2\left\{\theta(\eta) + \eta^2\frac{\big[2F_1(\eta)+\pi\,G_1(\eta)\big]}{\pi^3\sqrt{1-R_\mathrm{r}^2}}\right\} \tag{3.77}$$

$$\widetilde{M}_1 = M_1 + 4\rho_\mathrm{r}H_\mathrm{s}^2\left\{\varphi(\eta) + \eta^2\frac{\big[2F_1(\eta)+\pi\,G_1(\eta)\big]^2}{\pi^3\sqrt{1-R_\mathrm{r}^2}}\right\} = \frac{\omega_1^2}{\omega_\mathrm{r}^2}\,M_1 \tag{3.78}$$

$$\widetilde{\xi}_1 = \frac{\omega_\mathrm{r}}{\omega_1}\,\xi_1 \tag{3.79}$$

3.3.4 Application to the simplified earthquake analysis of gravity dams

The maximum response of a dam-reservoir ESDOF system to a horizontal earthquake ground motion can be approximated by its static response under the effect of equivalent lateral forces f_1 applied at the dam upstream face and expressed per unit dam height as [20, 26]

$$\begin{aligned}f_1(y) &= \frac{\widetilde{L}_1}{\widetilde{M}_1}\,S_\mathrm{a}\big(T_\mathrm{r},\widetilde{\xi}_1\big)\Big\{\mu_\mathrm{s}(y)\,\psi_1^{(x)}(0,y) - \bar{p}_1(0,y,\omega_\mathrm{r})\Big\}\\ &= \frac{\widetilde{L}_1}{\widetilde{M}_1}\,S_\mathrm{a}\big(T_\mathrm{r},\widetilde{\xi}_1\big)\left[\mu_\mathrm{s}(y)\left(a_1\frac{y}{H_\mathrm{s}} + a_2\frac{y^2}{H_\mathrm{s}^2} + a_3\frac{y^3}{H_\mathrm{s}^3}\right) - \bar{p}_1(0,y,\omega_\mathrm{r})\right]\end{aligned} \tag{3.80}$$

where $S_\mathrm{a}\big(T_\mathrm{r},\widetilde{\xi}_1\big)$ is the pseudo-acceleration ordinate of the earthquake design spectrum at vibration period T_r and for damping ratio $\widetilde{\xi}_1$ of the dam-reservoir ESDOF system described previously, and where the hydrodynamic pressure $\bar{p}_1(0,y,\omega_\mathrm{r})$ can be expressed using a cubic

mode shape approximation as

$$\bar{p}_1(0,y,\omega_\mathrm{r}) = 2\rho_\mathrm{r}\sum_{n=1}^{N_\mathrm{r}} \frac{2\times(-1)^n F_n(\eta) - (2n-1)\,\pi\, G_n(\eta)}{(2n-1)\,\pi\sqrt{\dfrac{(2n-1)^2\,\pi^2}{4\eta^2 H_\mathrm{s}^2} - \dfrac{\omega_\mathrm{r}^2}{C_\mathrm{r}^2}}}\,\cos\left[\frac{(2n-1)\,\pi}{2H_\mathrm{r}}\,y\right] \tag{3.81}$$

in which F_n and G_n are given by Eq. (3.34), and the ratio of generalized force $\widetilde{L}_1$ to generalized mass $\widetilde{M}_1$ is obtained from Eqs. (3.77) and (3.78). If water compressibility is neglected, Eq. (3.81) simplifies to

$$\bar{p}_1(0,y,\omega_\mathrm{r}) = 4\rho_\mathrm{r}\eta H_\mathrm{s}\sum_{n=1}^{N_\mathrm{r}} \frac{2\times(-1)^n F_n(\eta) - (2n-1)\,\pi\, G_n(\eta)}{(2n-1)^2\,\pi^2}\,\cos\left[\frac{(2n-1)\,\pi}{2H_\mathrm{r}}\,y\right] \tag{3.82}$$

with $\widetilde{L}_1$ and $\widetilde{M}_1$ to be determined using Eqs. (3.45) and (3.46). We note that the minus sign in Eq. (3.80) corresponds to the orientation of the system of axes shown in Fig. 3.5. We also assume that the fundamental mode shape component $\psi_1^{(x)}$ is positive as indicated on the same Figure.

Fenves and Chopra [19, 20] discussed the effects of higher vibration modes on dam earthquake response. Using a static correction technique, this effect can be accounted for approximately by evaluating the static response of the dam-reservoir ESDOF subjected to the lateral forces f_sc applied at the dam upstream face and expressed per unit dam height as

$$\begin{aligned} f_\mathrm{sc}(y) = \ddot{x}_\mathrm{g}^{(\max)} \Bigg\{ & \mu_\mathrm{s}(y)\left[1 - \frac{L_1}{M_1}\,\psi_1^{(x)}(0,y)\right] \\ & - \left[\widehat{\bar{p}}_0(0,y) + \frac{\mu_\mathrm{s}(y)}{M_1}\,\psi_1^{(x)}(0,y)\int_0^{H_\mathrm{r}} \widehat{\bar{p}}_0(0,y)\,\psi_1^{(x)}(0,y)\,\mathrm{d}y\right]\Bigg\} \end{aligned} \tag{3.83}$$

where $\ddot{x}_\mathrm{g}^{(\max)}$ denotes the maximum ground acceleration, and $\widehat{\bar{p}}_0(0,y)$ the real-valued, frequency-independent hydrodynamic pressure applied on a rigid dam subjected to a unit ground acceleration and impounding an incompressible water reservoir given by

$$\widehat{\bar{p}}_0(0,y) = \frac{8\rho_\mathrm{r}\eta H_\mathrm{s}}{\pi^2}\sum_{n=1}^{N_\mathrm{r}} \frac{(-1)^n}{(2n-1)^2}\,\cos\left[\frac{(2n-1)\,\pi}{2\eta H_\mathrm{s}}\,y\right] \tag{3.84}$$

Assuming a cubic mode approximation, we show that Eq.(3.83) can be rewritten as

$$f_{\mathrm{sc}}(y) = \ddot{x}_{\mathrm{g}}^{(\max)} \left\{ \mu_{\mathrm{s}}(y) \left(1 - \left[\frac{L_1}{M_1} + 8\rho_{\mathrm{r}} H_{\mathrm{s}}^2 \frac{\widehat{\theta}(\eta)}{M_1} \right] \left[a_1 \frac{y}{H_{\mathrm{s}}} + a_2 \frac{y^2}{H_{\mathrm{s}}^2} + a_3 \frac{y^3}{H_{\mathrm{s}}^3} \right] \right) - \widehat{\widehat{p}}_0(0, y) \right\} \quad (3.85)$$

The total earthquake response of the dam can then be determined by applying the SRSS rule to combine response quantities associated with the fundamental and higher vibration modes [19, 20].

3.4 Dam models, analyses and results

3.4.1 Analyses conducted

In this section, we assess the effectiveness of the equations developed above in determining the fundamental mode response of gravity dams. To illustrate the analysis types conducted, we consider a dam section with dimensions inspired from the tallest non-overflow monolith of Pine Flat dam [15]. The dam cross-section is shown in Fig. 3.5 (a).

The following six types of analysis are conducted to determine the fundamental vibration frequency of the dam-reservoir system :

- Analysis type I : a finite element analysis where both the dam and the reservoir are modeled using finite elements. The software ADINA [27] is used to discretize the dam monolith into 9-node plane stress finite elements. The reservoir is truncated at a large distance of $20H_{\mathrm{r}}$ from the dam upstream face to eliminate reflection of waves at the far reservoir upstream end. The 9-node potential-based finite elements programmed in ADINA [27] are used to model the reservoir. Fluid-structure interaction is accounted for through special interface elements also included in the software. A finite element model of the dam-reservoir system is shown in Fig. 3.5 (d). The performance of the potential-based formulation and the fluid-structure interface elements was assessed in a previous work [24]. The method can accurately account for fluid-structure interaction in dam-reservoir systems with a general geometry, including when the dam upstream face is not vertical, which is for example the case of the slightly inclined upstream face of the Pine Flat dam section. The results of this analysis will serve as our reference solution in the rest of the paper.
- Analysis type II : the analytical solution originally developed by Fenves and Chopra [7] and reviewed in section 3.2. The same 9-node plane stress finite element model built for Type I analysis is used as illustrated in Fig. 3.5 (c). The structural frequency response of the dam including hydrodynamic effects is then determined using Eqs. (3.2) to (3.16). The fundamental frequency is identified next as that corresponding to the first resonant

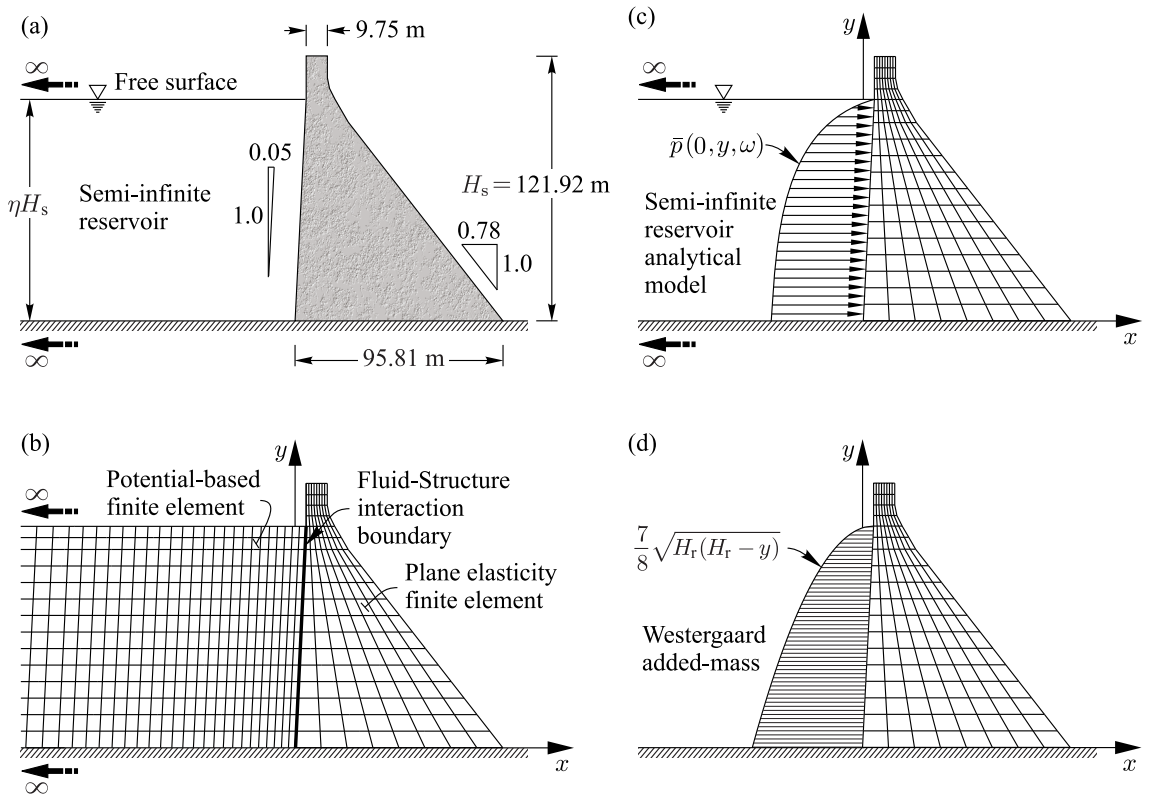

Figure 3.5 (a) Dam-reservoir system geometry ; (b) Analysis type I : Finite element model ; (c) Analysis type II : analytical solution ; (d) Analysis type III : Westergaard added mass formulation.

structural response.

– Analysis type III : a finite element analysis of the Pine Flat dam where the reservoir hydrodynamic loading is modeled approximately using Westergaard added mass formulation, assuming a rigid dam with a vertical upstream face, impounding incompressible water [1]. The effect of the reservoir is equivalent in this case to inertia forces generated by a body of water of parabolic shape moving back and forth with the vibrating dam. The finite element model of the dam and the body of water are shown in Fig. 3.5 (d). The added masse m_i to be attached to a node i belonging to dam-reservoir interface can be written as

$$m_i = \frac{7}{8}\,\rho_r\,V_i\,\sqrt{H_r(H_r - y_i)} \tag{3.86}$$

where y_i denotes the height of node i above the dam base and V_i the volume of water tributary to node i. As previously, the software ADINA [27] is used to discretize the dam monolith into 9-node plane stress finite elements.

– Analysis type IV : the new procedure proposed in this paper is applied using approxi-

mate parameters L_1, M_1, ω_1 and $\psi_1^{(x)}$ proposed by Fenves and Chopra [19, 20]. The authors analyzed several standard dam cross-sections and obtained the following conservative approximations for preliminary design purposes : $L_1 = 0.13\, M_\mathrm{s}$ and $M_1 = 0.043\, M_\mathrm{s}$, where M_s is the total mass of the dam monolith. Fenves and Chopra [19, 20] also proposed to estimate the fundamental vibration frequency ω_1 and period T_1 of the dam with an empty reservoir as

$$\omega_1 = \frac{2\pi\sqrt{E_\mathrm{s}}}{0.38\, H_\mathrm{s}}\,; \qquad\qquad T_1 = \frac{0.38\, H_\mathrm{s}}{\sqrt{E_\mathrm{s}}} \tag{3.87}$$

where the dam concrete modulus of elasticity E_s is expressed in MPa and H_s in meters to yield ω_1 in rad/s and T_1 in seconds. To develop a simplified earthquake analysis procedure, Fenves and Chopra [19, 20] used the standard fundamental mode shape given in Table 3.3. Applying the procedure illustrated in Fig. 3.2, this standard mode shape can be approximated using three points at elevations $y_1 = H_\mathrm{s}/3$, $y_2 = 2H_\mathrm{s}/3$ and $y_3 = H_\mathrm{s}$, yielding the coefficients $a_1 = 0.3535$, $a_2 = -0.5455$ and $a_3 = 1.1920$. Eq. (3.31) becomes then

$$\psi_1^{(x)}(0, y) = 0.3535\, \frac{y}{H_\mathrm{s}} - 0.5455 \left(\frac{y}{H_\mathrm{s}}\right)^2 + 1.1920 \left(\frac{y}{H_\mathrm{s}}\right)^3 \tag{3.88}$$

The resulting cubic interpolation is shown in Table 3.3. When water compressibility is neglected, Eq. (3.39) simplifies to

$$\widehat{\varphi}(\eta) = \eta^4 \left[7.938\, \eta^4 - 9.774\, \eta^3 + 12.400\, \eta^2 - 6.136\, \eta + 3.220\right] \times 10^{-3} \tag{3.89}$$

after replacing the coefficients a_1 to a_3 by their values. Introducing $M_1 = 0.043\, M_\mathrm{s}$ and substituting Eqs. (3.87) and (3.89) into Eq. (3.40) yields the dam-reservoir fundamental vibration frequency ω_r and period T_r when water compressibility is neglected. For example, considering a full reservoir, i.e. $\eta = 1$, we obtain

$$\omega_\mathrm{r} = \frac{\omega_1}{\sqrt{1 + \dfrac{711.6 H_\mathrm{s}^2}{M_\mathrm{s}}}}\,; \qquad\qquad T_\mathrm{r} = T_1 \sqrt{1 + \frac{711.6 H_\mathrm{s}^2}{M_\mathrm{s}}} \tag{3.90}$$

When water compressibility is included, replacing the coefficients a_1 to a_3 by their

values into Eqs. (3.53) and (3.57) yields

$$\varphi(\eta) = \eta^4 \left[5.456\,\eta^4 - 6.075\,\eta^3 + 6.426\,\eta^2 - 2.711\,\eta + 1.091 \right] \times 10^{-3} \tag{3.91}$$

$$F_1(\eta) = 0.3535\,\eta - 0.1033\,\eta^2 - 1.7065\,\eta^3 \tag{3.92}$$

$$G_1(\eta) = -0.1433\,\eta + 1.1748\,\eta^3 \tag{3.93}$$

The frequency ratio R_1 can be approximated as

$$R_1 = \frac{\omega_1}{\omega_0} = \frac{4\eta\sqrt{E_s}}{0.38\,C_r} \tag{3.94}$$

Coefficients A_0 to A_4 can be obtained using $M_1 = 0.043\,M_s$ and substituting Eqs. (3.91) to (3.94) into Eqs. (3.59) to (3.63). Eq. (3.58) is then solved for $\chi = R_r^2$ to obtain the fundamental vibration frequency $\omega_r = \omega_0 R_r$ and period $T_r = 2\pi/\omega_r$ of the dam-reservoir system.

– Analysis type V : the new procedure proposed in this paper is applied using the approximate parameters L_1, M_1 and $\psi_1^{(x)}$ proposed by Fenves and Chopra [19, 20], but with the natural frequency ω_1 obtained from a finite element analysis. All the equations described in the previous analysis Type IV apply except for the frequency ratio R_1 which now results from finite element analysis.

– Analysis type VI : the new procedure proposed in this paper is applied using parameters L_1, M_1, $\psi_1^{(x)}$ and ω_1 obtained from a finite element analysis of the dam section with an empty reservoir. A fundamental mode shape normalized with respect to the mass of the dam can be used, yielding a generalized mass $M_1 = 1$. Applying the procedure illustrated in Fig. 3.2, the fundamental mode shape evaluated at dam upstream face is interpolated using three points at elevations $y_1 = H_s/3$, $y_2 = 2H_s/3$ and $y_3 = H_s$ to find the coefficients a_1 to a_3 in Eq. (3.31). Table 3.3 contains the original mode shape resulting from finite element analysis of Pine Flat dam section as well as the cubic interpolation used. When water compressibility is neglected, the resulting coefficients are introduced into Eq. (3.39) to obtain $\widehat{\varphi}(\eta)$ and then the dam-reservoir vibration frequency ω_r using the generalized mass M_1 and the fundamental vibration frequency ω_1 obtained from finite element analysis of the dam with an empty reservoir. When water compressibility is included, coefficients a_1 to a_3 are introduced into Eqs. (3.57) and (3.53) to obtain the parameters $\varphi(\eta)$, $F_1(\eta)$ and $G_1(\eta)$. Coefficients A_0 to A_4 are determined next and Eq. (3.58) is then solved for $\chi = R_r^2$ to obtain the vibration frequency of the dam-reservoir system as described in section 3.3.

Table 3.3 Pine Flat dam fundamental mode shapes used.

	Normalized mode shape $\psi_1^{(x)}(0,y)/\psi_1^{(x)}(0,H_s)$			
	Fenves and Chopra [19]		Finite element analysis	
y/H_s	Original mode shape	Cubic interpolation	Original mode shape	Cubic interpolation
1.00	1.000	1.000	1.000	1.000
0.95	0.866	0.866	0.875	0.871
0.90	0.735	0.745	0.752	0.755
0.85	0.619	0.638	0.640	0.650
0.80	0.530	0.544	0.543	0.556
0.75	0.455	0.461	0.461	0.472
0.70	0.389	0.389	0.391	0.398
0.65	0.334	0.327	0.331	0.333
0.60	0.284	0.273	0.279	0.277
0.55	0.240	0.228	0.233	0.228
0.50	0.200	0.189	0.194	0.186
0.45	0.165	0.157	0.159	0.150
0.40	0.135	0.130	0.129	0.120
0.35	0.108	0.108	0.102	0.094
0.30	0.084	0.089	0.080	0.073
0.25	0.065	0.073	0.060	0.056
0.20	0.047	0.058	0.044	0.042
0.15	0.034	0.045	0.030	0.030
0.10	0.021	0.031	0.019	0.019
0.05	0.010	0.016	0.010	0.009
0.00	0.000	0.000	0.000	0.000

3.4.2 Validation of the proposed simplified formulation

The six analysis types described in the previous section are carried out to assess the effectiveness of the method proposed in this paper. The Pine Flat dam section described previously is studied first. A mass density $\rho_s = 2400$ kg/m^3 and a Poisson's ratio $\nu = 0.2$ are assumed as concrete material properties. To examine the influence of dam stiffness, two moduli of elasticity $E_s = 25$ GPa and $E_s = 35$ GPa are considered. A water mass density $\rho_r = 1000$ kg/m^3 is adopted. Both compressible and incompressible water assumptions are investigated, with a pressure wave velocity of $C_r = 1440$ m/s in the former case. We compute the period ratios T_r/T_1 where T_r is the fundamental vibration period of the dam-reservoir system obtained using any of the six analysis types described previously, and T_1 is the reference fundamental vibration period determined using a finite element analysis of the dam with an empty reservoir. Fi-

gures 3.6 and 3.7 illustrate the period ratios T_r/T_1 obtained considering incompressible and compressible water assumptions, respectively. Results for reservoir height ratios from $\eta = 0.5$ to 1.0 and two moduli of elasticity $E_s = 25$ GPa and $E_s = 35$ GPa are given. Figures 3.6 and 3.7 also show bar charts representing the following error estimator

$$\varepsilon = \frac{T_r - T_r^{(FE)}}{T_r^{(FE)}} \tag{3.95}$$

where $T_r^{(FE)}$ denotes the reference fundamental vibration period obtained using a finite element analysis of the dam-reservoir system, i.e. analysis type I.

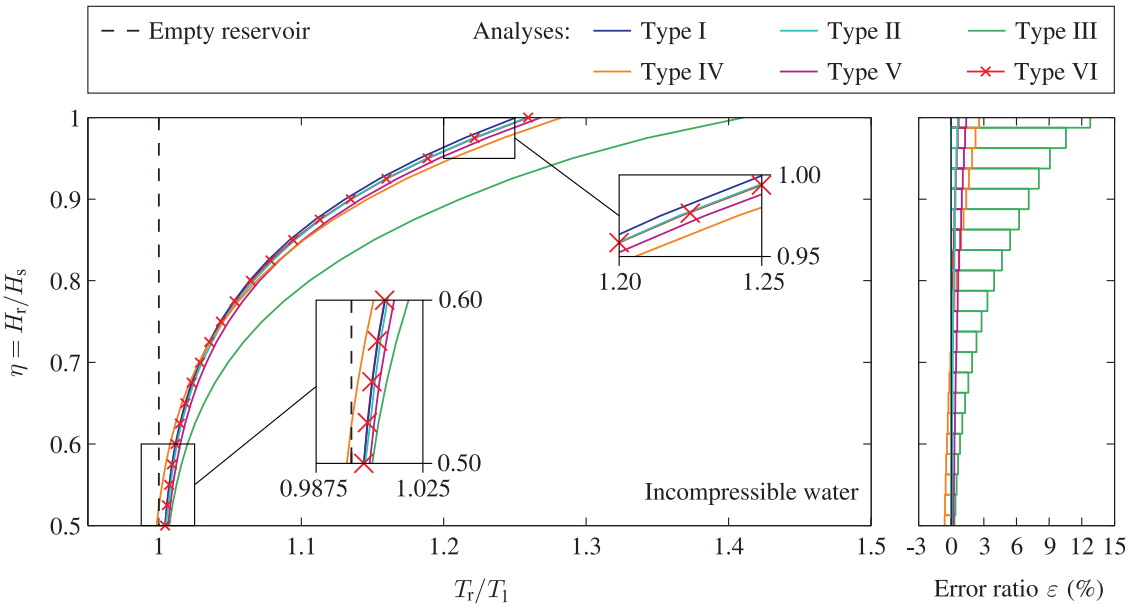

Figure 3.6 Variation of period ratio T_r/T_1 as a function of reservoir height ratio η assuming incompressible water.

First, it is apparent from the curves that the fundamental period predicted using finite elements, i.e. analysis type I, and the analytical formulation proposed by Fenves and Chopra [7], i.e. analysis type II, are very close for all height ratios and regardless of whether water is considered compressible or not. This observation confirms the effectiveness of the analytical formulation even for dams with a slightly inclined upstream face. When water compressibility is neglected, Eq. (3.40) shows that the elasticity modulus of the dam has no effet on the ratio T_r/T_1, a result that we confirmed numerically and analytically, i.e. using analysis types I and II. Therefore, period ratios T_r/T_1 for incompressible water are illustrated independently of the dam elasticity modulus. Fig. 3.6 shows that analysis type III using Westergaard added mass predicts the fundamental frequency of the dam-reservoir system with a an error of about

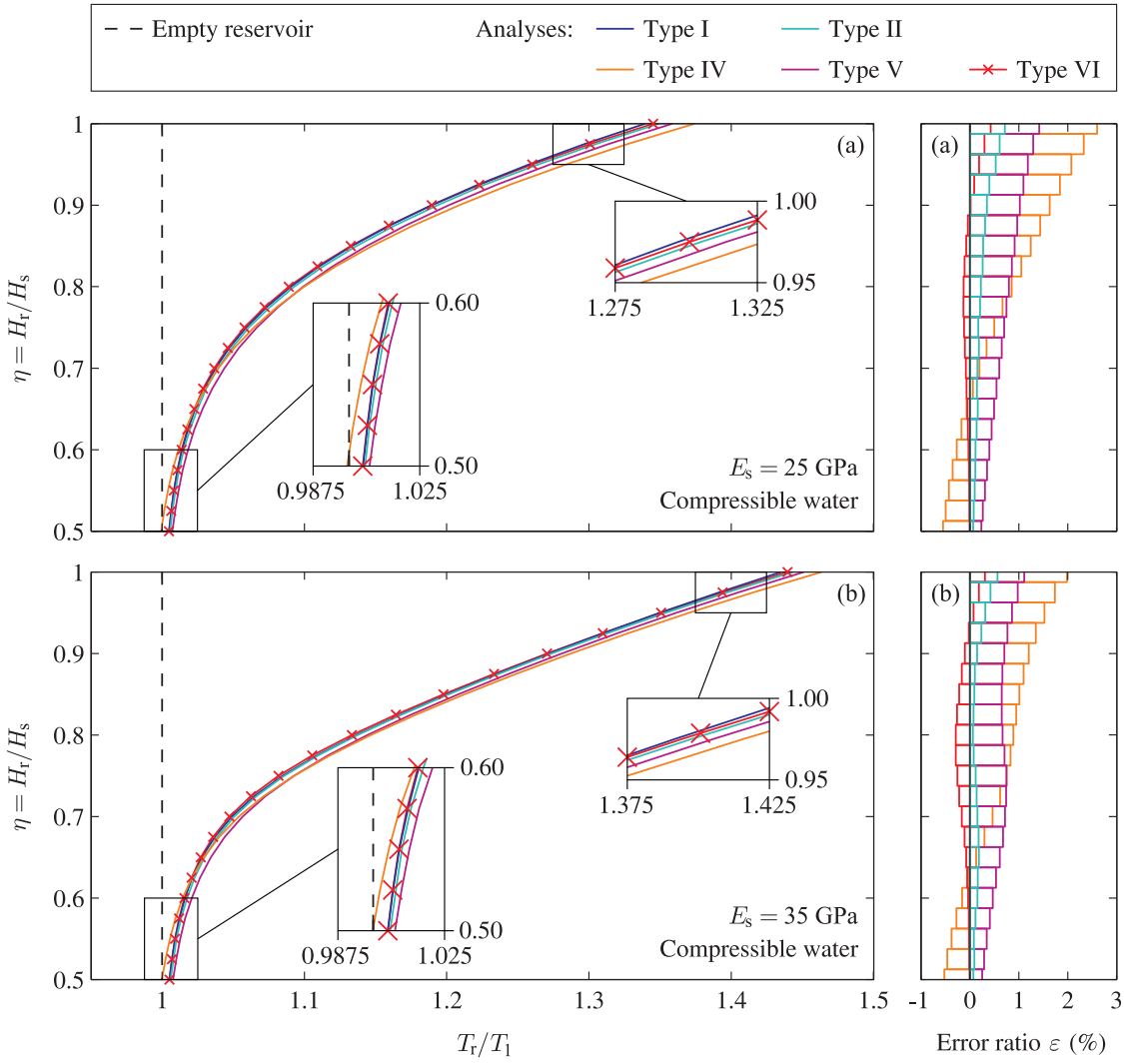

Figure 3.7 Variation of period ratio T_r/T_1 as a function of reservoir height ratio η considering water compressibility : (a) $E_s = 25$ GPa and (b) $E_s = 35$ GPa.

12 per cent for a full reservoir in the case of Pine Flat dam. Figs. 3.6 and 3.7 also clearly indicate that our simplified procedure, i.e. analysis type VI, yields excellent results regardless of dam stiffness and compressible or incompressible water assumptions. The results of the new simplified procedure remain in very good agreement when approximate parameters are used instead of those obtained from finite element analysis of the dam section, i.e. analysis types IV and V.

To investigate the influence of gravity dam cross-section geometry and dam stiffness on the accuracy of the simplified procedure proposed in this paper, we analyse three typical gravity dam cross-sections with heights varying from 90 m to 35 m as illustrated in Fig. 3.8.

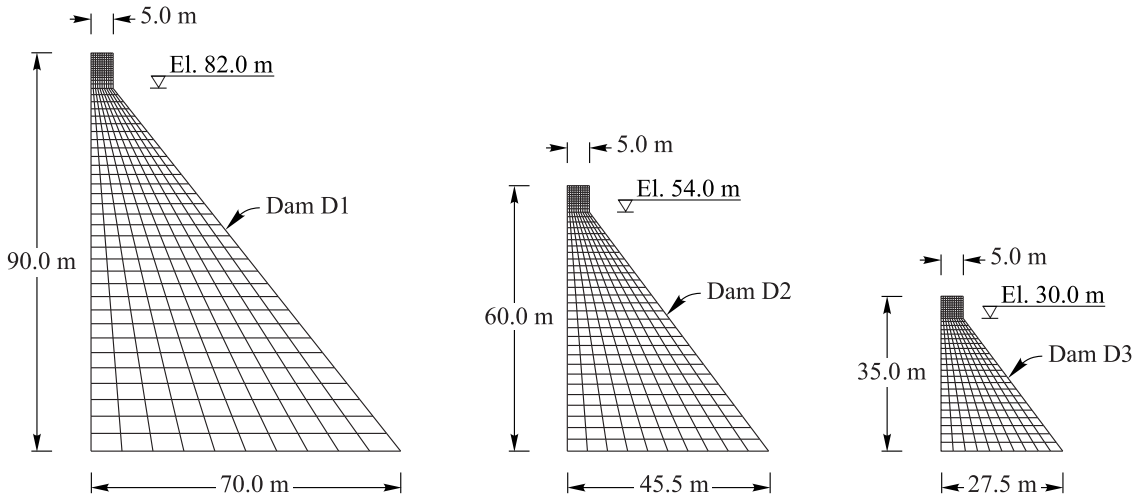

Figure 3.8 Geometry and finite element models of gravity dam cross-sections D1, D2 and D3.

The three dams are denoted D1 to D3 from the highest to the lowest. Finite element models of the dam sections and corresponding dam-reservoir systems are built using the software ADINA [27]. The new simplified method is then applied using approximate parameters, i.e. analysis types IV to V, as well as parameters resulting from finite element analyses of each of the dam sections with an empty reservoir, i.e. analysis type VI. The period ratios T_r/T_1 obtained are illustrated in Fig. 3.9 considering reservoir height ratios from $\eta = 0.5$ to 1.0 and two moduli of elasticity $E_s = 25$ GPa and $E_s = 35$ GPa. The different analyses are summarized in Table 3.4 for clarity purposes.

We first observe that the results of analysis types I and VI are almost identical for all the studied dam sections independently of water compressibility or incompressibility assumptions, dam geometry and stiffness. Analysis types IV and V yield satisfactory results for the 90-m high dam section D1. They are less accurate however when applied to smaller dam sections D2 and D3. Analysis type IV introduces large discrepancies because it uses approximate fundamental generalized force, generalized mass, mode shape and vibration period that were mainly calibrated using higher standard dam sections [19, 20]. We note that the fundamental period predictions are improved when an input fundamental vibration period obtained from a finite element analysis of the dam with empty reservoir is used instead of Eq. (3.87), i.e. analysis type V.

Based on the previous findings, we recommend to use the proposed simplified method according to scheme of analysis type VI. The other schemes would provide appropriate results for high gravity dams, while an increasing error is introduced for smaller dams. To asses the

Table 3.4 Summary of analysis types conducted.

		Gravity dam							
		$E_s = 25$ GPa				$E_s = 35$ GPa			
Water assumption	Analysis	Pine Flat	D1	D2	D3	Pine Flat	D1	D2	D3
Incompressible	Type I	x	x	x	x	x	x	x	x
	Type II	x	-	-	-	x	-	-	-
	Type III	x	-	-	-	x	-	-	-
	Type IV	x	x	x	x	x	x	x	x
	Type V	x	x	x	x	x	x	x	x
	Type VI	x	x	x	x	x	x	x	x
Compressible	Type I	x	x	x	x	x	x	x	x
	Type II	x	-	-	-	x	-	-	-
	Type III	-	-	-	-	-	-	-	-
	Type IV	x	x	x	x	x	x	x	x
	Type V	x	x	x	x	x	x	x	x
	Type VI	x	x	x	x	x	x	x	x

accuracy of the proposed method in determining the damping ratio $\widetilde{\xi}_1$ of the dam-reservoir system ESDOF, Fig. 3.10 illustrates the variation of this parameter as a function of reservoir height ratio $\eta \geqslant 0.5$ considering water compressibility, two moduli of elasticity $E_s = 25$ GPa and $E_s = 35$ GPa and the four gravity dam cross-sections described previously. In this figure, the results determined by applying the proposed method following the scheme of analysis type VI are compared to those obtained using the classical method developed by Fenves and Chopra [7] and reviewed in section 3.2. The curves clearly show that both techniques yield identical damping ratios for the four dam monoliths.

Finally, denoting $F_{st} = \rho_r g H_r^2/2$ the total hydrostatic force exerted on dam upstream face, we determine the normalized equivalent lateral forces $H_s f_1(y)/F_{st}$ considering a unit ordinate of pseudo-acceleration spectrum, water compressibility, a full reservoir, i.e. $\eta = 1$, two moduli of elasticity and the four dams cross-sections as before. Again, the resulting force distributions obtained using the classical and proposed methods are practically coincident for the four dam monoliths studied as illustrated in Fig. 3.11.

3.5 Concluding remarks

This paper proposed an original practical method to evaluate the seismic response of gravity dams. We first developed a simplified but yet a rigorous and practical formulation to determine the fundamental period of vibrating dam-reservoir systems and corresponding

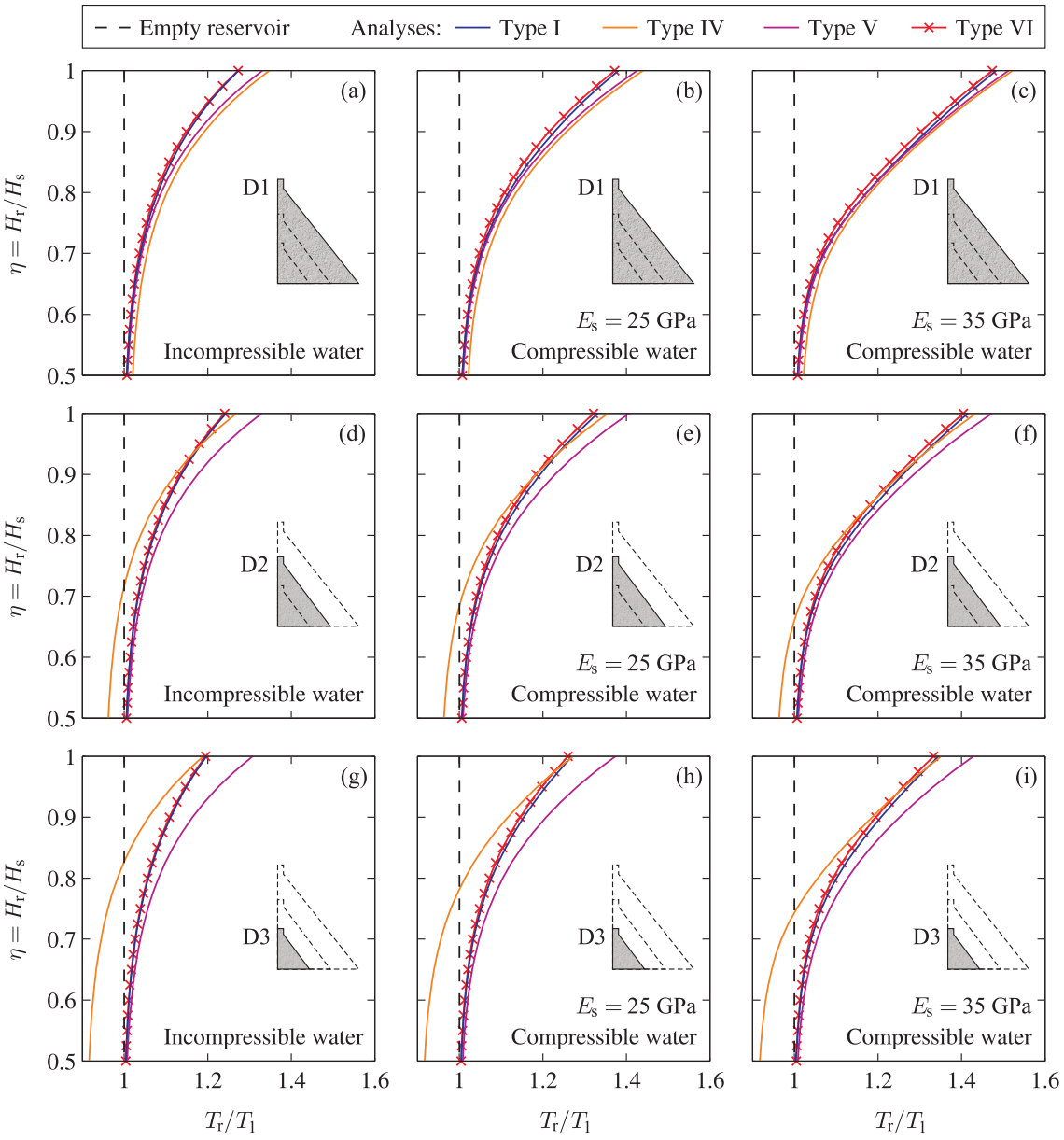

Figure 3.9 Variation of period ratio T_r/T_1 as a function of reservoir height ratio η considering water compressibility : (a) to (c) Dam D1 ; (d) to (f) Dam D2 ; and (g) to (i) Dam D3.

added damping, force and mass. The new formulation includes the effects of dam geometry and flexibility, water compressibility and varying reservoir level. The mathematical derivations of the method were provided considering both incompressible and compressible water assumptions. In the former case, we proposed a closed-form expression to determine the fundamental vibration period of a dam-reservoir system. When water compressibility is considered, we showed that the fundamental vibration period of a dam-reservoir system can be obtained

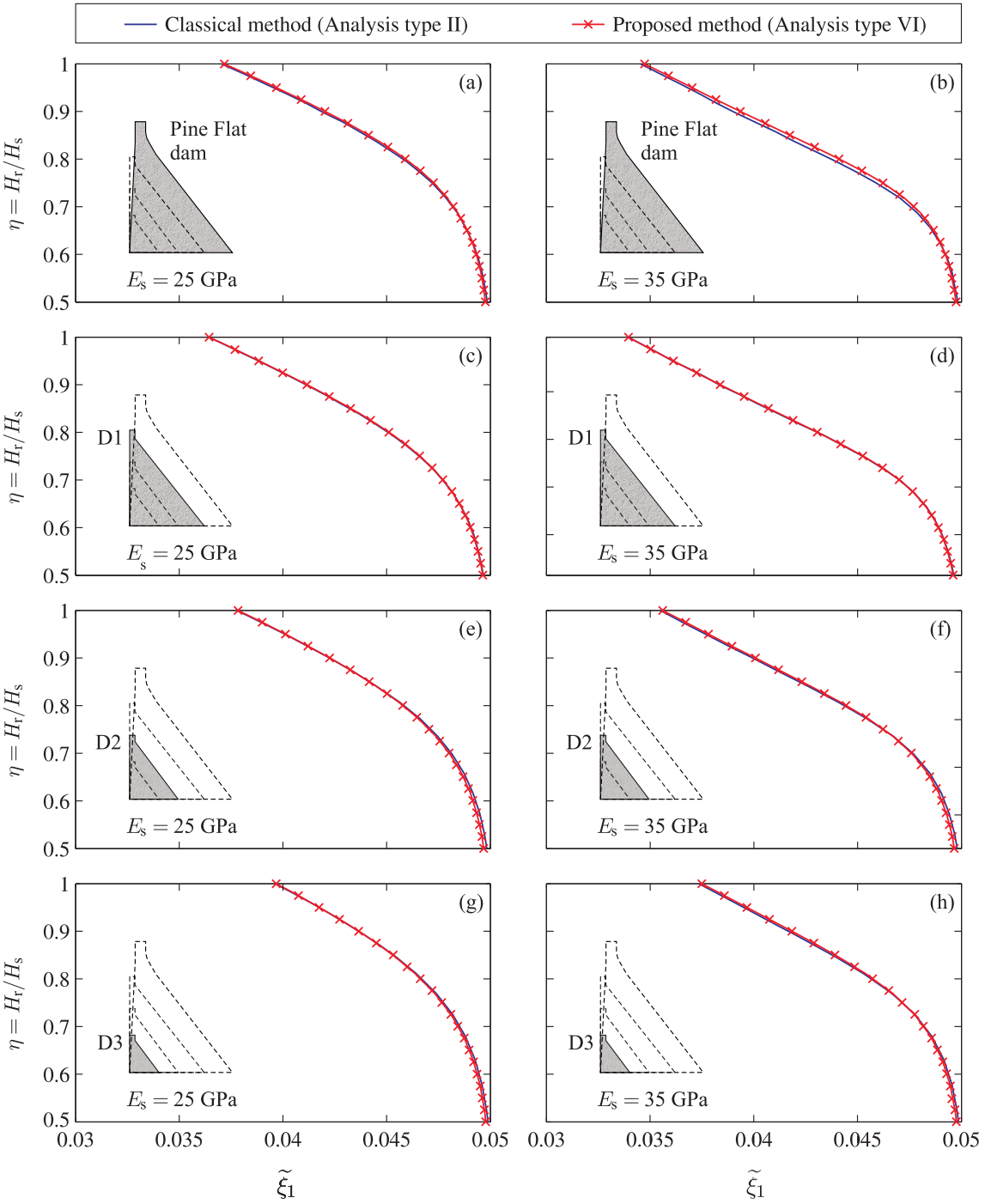

Figure 3.10 Variation of the damping ratio $\widetilde{\xi}_1$ as a function of reservoir height ratio η considering water compressibility : (a) and (b) Pine Flat dam ; (c) and (d) Dam D1 ; (e) and (f) Dam D2 ; and (g) and (h) Dam D3.

by simply solving a cubic equation. Simplified expressions to compute the equivalent lateral

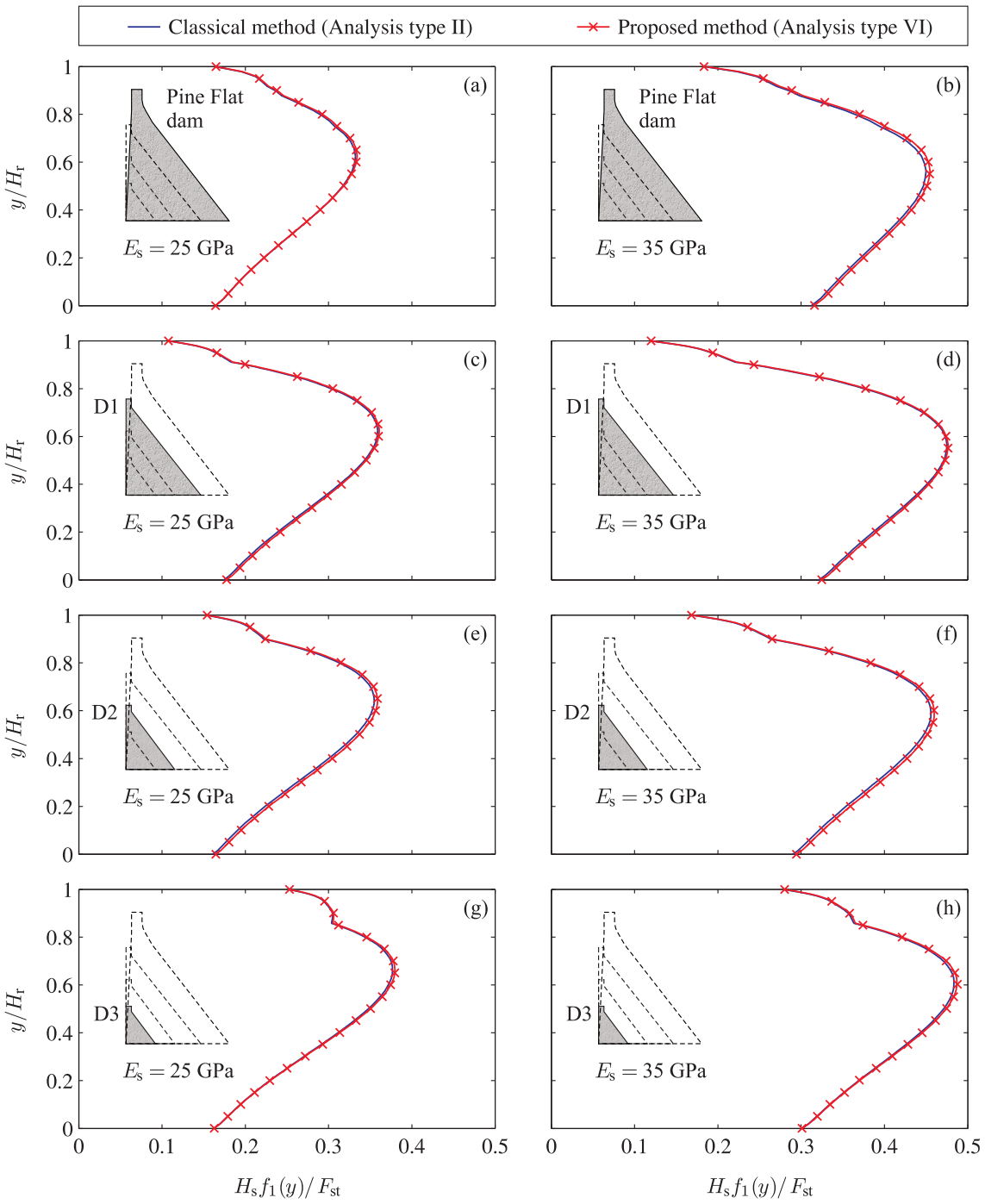

Figure 3.11 Normalized equivalent lateral earthquake forces corresponding to dam fundamental mode response considering water compressibility : (a) and (b) Pine Flat dam ; (c) and (d) Dam D1 ; (e) and (f) Dam D2 ; and (g) and (h) Dam D3.

earthquake forces and the static correction forces are proposed. These forces are to be applied at the dam upstream face to determine response quantities of interest, such as the stresses

throughout the dam cross-section. To assess the efficiency and accuracy of the proposed technique, several analysis types were applied to dam cross-sections with various geometries and rigidities impounding reservoirs with different levels.

The following conclusions could be drawn from the comparison of the period predictions obtained from the different analyses : (i) the analytical formulation of hydrodynamic effects yields accurate predictions when compared to numerical results obtained by modeling the reservoir using potential-based finite elements, (ii) the proposed simplified procedure gives excellent results when the fundamental generalized earthquake force coefficient, generalized mass, mode shape and vibration period are directly obtained from a finite element analysis of the dam with an empty reservoir, and (iii) the fundamental period predictions of the simplified procedure remain satisfactory for large dams while larger discrepancies are observed for smaller ones when approximate parameters are used instead of those obtained from finite element analysis. We also showed that the new procedure yields an excellent estimation of the equivalent damping ratio and equivalent earthquake lateral forces. The proposed technique presents a significant advantage over conventional Westergaard added-mass formulation, namely because it can directly account for dam flexibility and water compressibility, while Westergaard's solution assumes that the dam is rigid and water is incompressible. The analytical expressions developed and the procedure steps were presented in a manner such that calculations could be easily implemented in a spreadsheet or program for practical dynamic analysis of gravity dams. We clearly showed that the proposed procedure can be used effectively for simplified evaluation of the vibration period and seismic response of gravity dams irrespective of their geometry and stiffness.

Acknowledgements

The authors would like to acknowledge the financial support of the Natural Sciences and Engineering Research Council of Canada (NSERC) and the Quebec Fund for Research on Nature and Technology (FQRNT).

References

[1] Westergaard HM. Water pressures on dams during earthquakes. *Transactions*(ASCE) 1933 ; **98** : 418-472.

[2] Chopra AK. Earthquake response of concrete gravity dams. Report No. UCB/EERC-70/01, University of California, Berkeley, 1970.

[3] Chakrabarti P, Chopra AK. Earthquake analysis of gravity dams including hydrodynamic interaction. *Earthquake Engineering and Structural Dynamics* 1973 ; **2** : 143-160.

[4] Chopra AK. Earthquake resistant design of concrete gravity dams. *Journal of the Structural Division*(ASCE) 1978 ; **104** : 953-971.

[5] Saini SS, Bettess P, Zienkiewicz OC. Coupled hydrodynamic response of concrete gravity dams using finite and infinite elements. *Earthquake Engineering and Structural Dynamics* 1978 ; **6** : 363-374.

[6] Hall JF, Chopra AK. Two-dimensional dynamic analysis of concrete gravity and embankment dams including hydrodynamic effects. *Earthquake Engineering and Structural Dynamics* 1982 ; **10** : 305-332.

[7] G. Fenves, A.K. Chopra, Earthquake analysis and response of concrete gravity dams. Report No. UCB/EERC-84/10, University of California, Berkeley, California, 1984.

[8] Liu PH, Cheng A. Boundary solutions for fluid-structure interaction. *Journal of Hydraulic Engineering*(ASCE) 1984 ; **110**(1) : 51-64.

[9] Fok KL, Hall JF, Chopra AK. EACD-3D, a computer program for three-dimensional earthquake analysis of concrete dams. Report No UCB/EERC-86/09, University of California, Berkeley, California, 1986.

[10] Tsai CS, Lee GC. Arch dam-fluid interactions : by FEM-BEM and substructure concept. *International Journal of Numerical Methods in Engineering* 1987 ; **24** : 2367-2388.

[11] Humar JL, Jablonski AM. Boundary element reservoir model for seismic analysis of gravity dams. *Earthquake Engineering and Structural Dynamics* 1988 ; **16** : 1129-1156.

[12] Maeso O, Aznarez JJ, Dominguez J. Three-dimensional models of reservoir sediment and effects on the seismic response of arch dams. *Earthquake Engineering and Structural Dynamics* 2004 ; **33** : 1103-1123.

[13] Bouaanani N, Miquel B. A new formulation and error analysis for vibrating dam–reservoir systems with upstream transmitting boundary conditions. *Journal of Sound and Vibration* 2010 ; **329** : 1924-1953.

[14] Fenves G, Chopra AK. EAGD-84, a computer program for earthquake analysis of concrete gravity dams. Report No UCB/EERC-84/11, University of California, Berkeley, California, 1984.

[15] Rea D, Liaw CY, Chopra, AK. Dynamic properties of Pine Flat dam. Report UCB/EERC-72/07, University of California, Berkeley, California, 1972.

[16] Duron Z, Hall J. Experimental and finite element studies of the forced vibration response of Morrow Point Dam. *Earthquake Engineering and Structural Dynamics* 1988 ; **16** : 1021–1039.

[17] Proulx J, Paultre P, Rheault J, Robert Y. An experimental investigation of water level effects on the dynamic behaviour of a large arch dam. *Earthquake Engineering and Structural Dynamics* 2001 ; **30** : 1147-1166.

[18] Bouaanani N, Paultre P, Proulx J. Two-dimensional modelling of ice-cover effects for the dynamic analysis of concrete gravity dams. *Earthquake Engineering and Structural Dynamics* 2002 ; **31** : 2083-2102.

[19] Fenves G, Chopra AK. Simplified analysis for earthquake resistant design of concrete gravity dams. Report No. UCB/EERC-85/10, University of California, Berkeley, 1985.

[20] Fenves G, Chopra AK. Simplified earthquake analysis of concrete gravity dams. *Journal of Structural Engineering* 1987 ; **113**(8) : 1688-1708.

[21] Bouaanani N, Paultre P, Proulx J. A closed-form formulation for earthquake-induced hydrodynamic pressure on gravity dams. *Journal of Sound and Vibration* 2003 ; **261** : 573-582.

[22] Hatanaka M. Study on the earthquake-resistant design of gravity type dams. *Proceedings of the Second World Conference on Earthquake Engineering*, Tokyo and Kyoto, Japan, 1960 ; **II** : 82.1–82.16.

[23] Okamoto S. *Introduction to earthquake engineering*. 2nd edition, University of Tokyo Press : Tokyo, 1984.

[24] Bouaanani N, Lu FY. Assessment of potential-based fluid finite elements for seismic analysis of dam–reservoir systems. *Journal of Computers and Structures* 2009; **87** : 206-224.

[25] Reinhardt F, Soeder H. *dtv-Atlas zur Mathematik*. Deutscher Taschenbuch Verlag : Munich, 2001.

[26] Clough RW, Penzien J. Dynamics of Structures, McGraw-Hill, Inc., New York, 1975.

[27] ADINA Theory and Modeling Guide. Report ARD 06-7. ADINA R & D, Inc., 2006.

CHAPITRE 4

Article 2 : Practical dynamic analysis of structures laterally vibrating in contact with water

Benjamin Miquel [1] **and Najib Bouaanani** [2]

Paper published in *Computers and Structures* Volume 89, Issue 23-24, December 2011, Pages 2195-221, doi :10.1016/j.compstruc.2011.08.017

Submitted 7 February 2011. Accepted 24 August 2011.

This paper proposes a practical formulation to investigate the dynamic response of structures laterally vibrating in contact with water on one or both sides. The proposed technique accounts for structure's flexibility, soil flexibility, varying water levels and various boundary conditions. Simplified procedures are developed for practical assessment of the vibration periods, hydrodynamic loads and seismic response of structure-water systems including higher mode effects. The efficiency of the proposed techniques is validated through examples of structure-water systems with different configurations. We show that the proposed methods give excellent results when compared to more advanced finite element solutions including fluid-structure interaction capabilities.

1. Graduate Research Assistant, Department of Civil, Geological and Mining Engineering, École Polytechnique de Montréal, Montréal, QC H3C 3A7, Canada.

2. Associate Professor, Department of Civil, Geological and Mining Engineering, École Polytechnique de Montréal, Montréal, QC H3C 3A7, Canada
Corresponding author. E-mail : najib.bouaanani@polymtl.ca

4.1 Introduction

Appropriate account of fluid-structure dynamic interactions has been shown an important factor in the design and safety evaluation of earthquake-excited civil engineering structures vibrating in contact with water. The pioneering work of Westergaard [1] consisted of taking account of hydrodynamic loads as an added-mass attached to the a structure's face in contact with water. The added-masses are determined assuming a rigid structure and a semi-infinite water domain. This method has been widely used and suggested by several codes of practice due to its simplicity [2, 3, 4, 5, 6]. Several researchers developed simplified to more complex analytical and numerical approaches to account for fluid-structure interactions in various civil engineering applications including dam-reservoir systems, water storages, breakwaters and navigation locks. Most of these approaches are based on coupled fluid-structure solutions through finite elements, boundary elements, finite differences or a mix of these techniques [7, 8, 9, 10, 11, 12, 13, 14, 15, 16, 17, 18, 19, 20].

In this paper, we focus on the developing original analytical and simplified solutions for structures vibrating in contact with water as schematically illustrated in Fig. 4.1. Under dynamic excitation, the response of such systems involves the interaction between the structure and water on both sides. The surrounding water domain could be semi-infinite as in Fig. 4.1 (a) or of finite extent as in Fig. 4.1 (b). The methods developed will investigate the linear dynamic and seismic behavior of such systems using a sub-structuring technique where structural and hydrodynamic responses are coupled through interface forces. The vibration periods of structure-water systems are key factors in the assessment of their dynamic or seismic behavior, and are required by most seismic provisions and codes of practice. Although significant work has been devoted to investigate the effects of hydrodynamic loads, there is no available practical analytical technique to evaluate the vibration periods and dynamics of structure-water systems including higher mode effects. This need is also addressed in the present work by developing practical analytical expressions for vibration periods as well as a simplified method including the effects of fluid-structure interaction, structure's geometry and flexibility, higher vibration modes, varying water levels and soil flexibility.

4.2 Analytical formulation

4.2.1 Geometry of the structure-water systems, basic assumptions and notation

Fig. 4.2 shows a symmetrical structure of height H_{s} and thickness $2b_{\mathrm{s}}$ vibrating in contact with water on both sides. We adopt a Cartesian coordinate system with origin at the base of the structure, a horizontal axis x and a vertical axis y belonging to the plane of symmetry

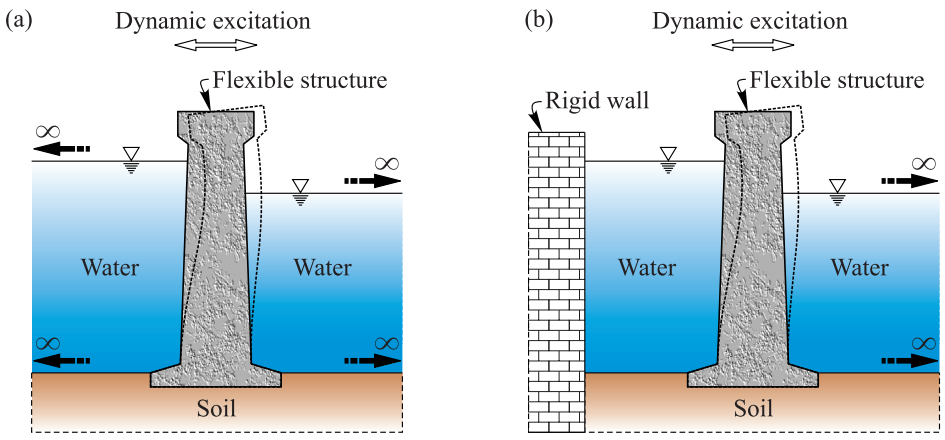

Figure 4.1 Examples of structure-water systems studied : (a) Structure vibrating in contact with semi-infinite water domains on both sides ; (b) Structure vibrating in contact with water domain of limited extent on one side and semi-infinite on the other side.

of the structure. We denote by side 1 and side 2 the left and right water domains extending from the structure towards negative and positive x directions, respectively. To alleviate the notation, an index $\ell = 1$ or $\ell = 2$ will be used to refer to parameters corresponding to water domains on the left and right sides of the structure, respectively. The interfaces between the structure and the left and right water domains are located at $x_1 = -b_s$ and $x_2 = b_s$, and are designated as the structure's left and right faces, respectively. The left and right water domains have a rectangular geometry with constant heights $H_w^{(1)}$ and $H_w^{(2)}$, respectively. The left (resp. right) water domain could either : (i) be delimited by a rigid quay wall located at a distance $L_w^{(1)}$ (resp. $L_w^{(2)}$) from the left (resp. right) face ; or (ii) extend to infinity along the negative (resp. positive) x direction. Figs. 4.2 (a) to (c) show three typical configurations illustrating these boundary conditions. We also assume that : (i) the longitudinal dimension of the structure-water system is sufficiently large compared to cross-sectional dimensions so that the system can be modeled as a two-dimensional plane-strain elasticity problem ; (ii) the structure has a linear elastic behavior ; (iii) water, of mass density ρ_w, is incompressible and inviscid, with its motion irrotational and limited to small amplitudes ; and (iv) the structure may lie on a rigid or massless flexible soil foundation.

4.2.2 Frequency-domain dynamic response of the structure

The structure's cross-section is first modeled using plane-strain finite elements. Assuming a unit harmonic free-field horizontal ground motion $\ddot{x}_g(t) = e^{i\omega t}$, the dynamic equilibrium of

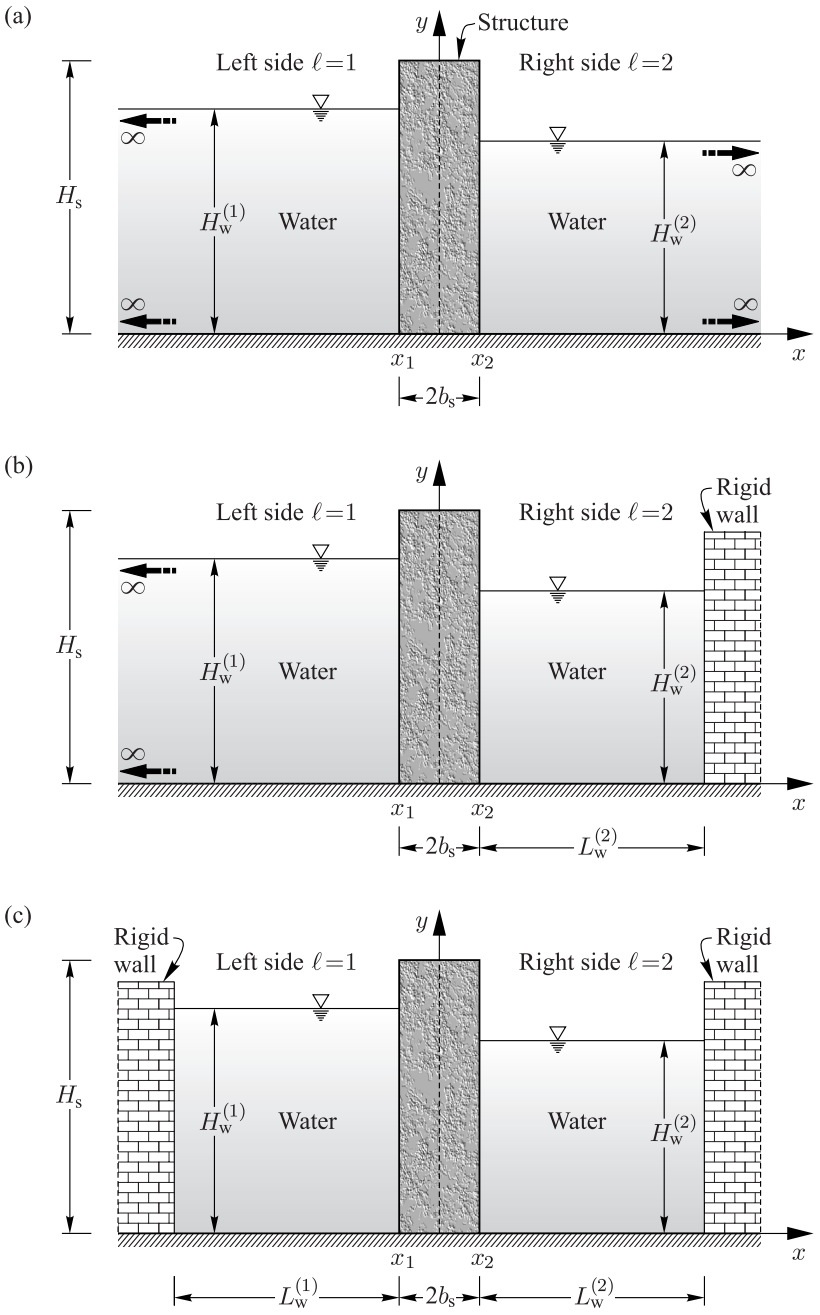

Figure 4.2 Structure-water systems, boundary conditions and notation : (a) Structure surrounded by semi-infinite water domains on both sides; (b) Structure surrounded by water domain of limited extent on one side and semi-infinite on the other side; (c) Structure surrounded by water domains of limited extent on both sides.

the structure-water systems described above can be expressed in the frequency domain as

$$\left[-\omega^2\,\mathbf{M} + (1+\mathrm{i}\,\mu)\,\mathbf{K}\right]\overline{\mathbf{U}}(\omega) = -\mathbf{M}\,\mathbf{1} + \overline{\mathbf{F}}^{(1)}(\omega) - \overline{\mathbf{F}}^{(2)}(\omega) \tag{4.1}$$

where $\overline{\mathbf{U}}$ is a column-vector containing the frequency response functions of the structure nodal displacements relative to the ground, $\mathbf{M}$ is the mass matrix of the structure, $\mathbf{K}$ is the stiffness matrix of the structure including the effect of a massless soil foundation when considered in the analysis, $\mathbf{1}$ is a column-vector with the same dimension as the vector of nodal relative displacements containing zeros except along horizontal degrees of freedom which correspond to the direction of earthquake excitation, μ is a hysteretic damping factor assumed constant and assigned to the structure including the effect of the massless soil foundation when considered in the analysis, and $\overline{\mathbf{F}}^{(1)}$ and $\overline{\mathbf{F}}^{(2)}$ are column-vectors containing the frequency response functions of hydrodynamic loads exerted on the structure by the left and right water domains, respectively. We note that the special case of a structure in contact with water on only one side ℓ can be analyzed by considering $H_{\mathrm{w}}^{(\ell)} = 0$ and $\overline{\mathbf{F}}^{(\ell)} = \mathbf{0}$.

4.2.3 Frequency-domain dynamic response of the water domains

Considering the above assumptions and based on previous studies [10, 11], frequency response functions $\bar{p}^{(\ell)}(x, y, \omega)$ can be decomposed as

$$\bar{p}^{(\ell)}(x, y, \omega) = \bar{p}_0^{(\ell)}(x, y) - \omega^2 \sum_{j=1}^{N_{\mathrm{s}}} \bar{Z}_j(\omega)\, \bar{p}_j^{(\ell)}(x, y) \tag{4.2}$$

in which $\bar{p}_0^{(\ell)}$ is the frequency-independent response function for hydrodynamic pressure within water domain on side ℓ due to rigid body motion of the structure, $\bar{p}_j^{(\ell)}$ is the frequency-independent response function corresponding to hydrodynamic pressure due to horizontal acceleration $\psi_j^{(x)}(x_\ell, y)$ of the structure's face at $x = x_\ell$, where $\psi_j^{(x)}$ denotes the x–component of the j th structural mode shape including the effect of a massless soil foundation when considered in the analysis, $\bar{Z}_j$ is a generalized coordinate to be discussed later and N_{s} is the total number of structural mode shapes included in the analysis.

The hydrodynamic pressure within water domains depends on the applied boundary conditions, including :

– A compatibility-based boundary condition at water-structure interface

$$\frac{\partial \bar{p}_0^{(\ell)}}{\partial x}(x_\ell, y) = (-1)^\ell \rho_{\mathrm{w}}\,; \qquad \frac{\partial \bar{p}_j^{(\ell)}}{\partial x}(x_\ell, y) = (-1)^\ell \rho_{\mathrm{w}}\, \psi_j^{(x)}(x_\ell, y) \tag{4.3}$$

– A rigid boundary condition at water domain bottom

$$\frac{\partial \bar{p}_0^{(\ell)}}{\partial y}(x, 0) = \frac{\partial \bar{p}_j^{(\ell)}}{\partial y}(x, 0) = 0 \tag{4.4}$$

– A boundary condition neglecting the effect of gravity waves at water surface

$$\frac{\partial \bar{p}_0^{(\ell)}}{\partial y}(x, H_{\mathrm{w}}^{(\ell)}) = \frac{\partial \bar{p}_j^{(\ell)}}{\partial y}(x, H_{\mathrm{w}}^{(\ell)}) = 0 \tag{4.5}$$

In this work, we investigate the effects of the following boundary conditions :

– BC-I : A rigid wall located at a distance $L_{\mathrm{w}}^{(\ell)}$ from the structure's face on side ℓ and moving at the same ground acceleration as the structure

$$\frac{\partial \bar{p}_0^{(\ell)}}{\partial x}(L_{\mathrm{w}}^{(\ell)}, y) = (-1)^{\ell}\, \rho_{\mathrm{w}}\,; \qquad\qquad \frac{\partial \bar{p}_j^{(\ell)}}{\partial x}(L_{\mathrm{w}}^{(\ell)}, y) = 0 \tag{4.6}$$

This condition will be referred to as the moving rigid wall boundary condition in what follows.

– BC-II : A non-disturbed boundary condition at the far end of water domain on side ℓ to study infinite water domains

$$\lim_{x\to-\infty} \bar{p}_0^{(\ell)}\,(x, y) = \lim_{x\to-\infty} \bar{p}_j^{(\ell)}\,(x, y) = 0 \qquad \text{if } \ell = 1 \tag{4.7}$$

$$\lim_{x\to+\infty} \bar{p}_0^{(\ell)}\,(x, y) = \lim_{x\to+\infty} \bar{p}_j^{(\ell)}\,(x, y) = 0 \qquad \text{if } \ell = 2 \tag{4.8}$$

– BC-III : A rigid boundary condition located at a distance $L_{\mathrm{w}}^{(\ell)}$ from the structure's face on side ℓ

$$\frac{\partial \bar{p}_0^{(\ell)}}{\partial x}(L_{\mathrm{w}}^{(\ell)}, y) = \frac{\partial \bar{p}_j^{(\ell)}}{\partial x}(L_{\mathrm{w}}^{(\ell)}, y) = 0 \tag{4.9}$$

This boundary condition is introduced to study the extent of water domain that should be taken into account to obtain the same results as the non-disturbed boundary condition BC-II. It will be referred to as the fixed rigid wall boundary condition in the rest of the paper.

Using the above-mentioned boundary conditions, we show that frequency response functions $\bar{p}_0^{(\ell)}$ and $\bar{p}_j^{(\ell)}$ corresponding to hydrodynamic pressure within water domain on side ℓ can be expressed as

$$\bar{p}_0^{(\ell)}(x, y) = -\frac{8\times(-1)^{\ell}}{\pi^2}\, \rho_{\mathrm{w}} H_{\mathrm{w}}^{(\ell)} \sum_{n=1}^{N_{\mathrm{w}}} \frac{(-1)^n}{(2n-1)^2}\, X_n^{(\ell)}(x)\, \cos\big[y\, \lambda_n^{(\ell)}\big] \tag{4.10}$$

$$\bar{p}_j^{(\ell)}(x, y) = \frac{4\times(-1)^{\ell}}{\pi}\, \rho_{\mathrm{w}} H_{\mathrm{w}}^{(\ell)} \sum_{n=1}^{N_{\mathrm{w}}} \frac{I_{j,n}^{(\ell)}}{(2n-1)}\, \widehat{X}_n^{(\ell)}(x)\, \cos\big[y\, \lambda_n^{(\ell)}\big] \tag{4.11}$$

where N_{w} is the number of water modes included in the analysis, and where $X_n^{(\ell)}$ and $\widehat{X}_n^{(\ell)}$ are given by

$$\begin{aligned} X_n^{(\ell)}(x) &= \frac{\cosh\left\{\left[(-1)^\ell\,(x_\ell - x) + L_{\mathrm{w}}^{(\ell)}\right]\lambda_n^{(\ell)}\right\} - \cosh\left[(-1)^\ell\,(x_\ell - x)\,\lambda_n^{(\ell)}\right]}{\sinh\left[L_{\mathrm{w}}^{(\ell)}\lambda_n^{(\ell)}\right]} \\ \widehat{X}_n^{(\ell)}(x) &= \frac{\cosh\left\{\left[(-1)^\ell\,(x_\ell - x) + L_{\mathrm{w}}^{(\ell)}\right]\lambda_n^{(\ell)}\right\}}{\sinh\left[\lambda_n^{(\ell)}L_{\mathrm{w}}^{(\ell)}\right]} \end{aligned} \tag{4.12}$$

for a rigid boundary condition BC-I, and

$$X_n^{(\ell)}(x) = \widehat{X}_n^{(\ell)}(x) = \mathrm{e}^{(-1)^\ell(x_\ell - x)\lambda_n^{(\ell)}} \tag{4.13}$$

for a non-disturbed boundary condition BC-II at the far end of water domain, and

$$X_n^{(\ell)}(x) = \widehat{X}_n^{(\ell)}(x) = \frac{\cosh\left\{\left[(-1)^\ell\,(x_\ell - x) + L_{\mathrm{w}}^{(\ell)}\right]\lambda_n^{(\ell)}\right\}}{\sinh\left[\lambda_n^{(\ell)}L_{\mathrm{w}}^{(\ell)}\right]} \tag{4.14}$$

for a rigid boundary condition BC-III. In Eqs. (4.10) to (4.14), the eigenvalues $\lambda_n^{(\ell)}$ and parameters $I_{j,n}^{(\ell)}$ are given for each water mode n by

$$\lambda_n^{(\ell)} = \frac{(2n-1)\,\pi}{2H_{\mathrm{w}}^{(\ell)}} \tag{4.15}$$

$$I_{j,n}^{(\ell)} = \frac{1}{H_{\mathrm{w}}^{(\ell)}}\int_0^{H_{\mathrm{w}}^{(\ell)}} \psi_j^{(x)}(x_\ell, y)\,\cos\left[y\,\lambda_n^{(\ell)}\right]\mathrm{d}y \tag{4.16}$$

4.2.4 Coupled frequency and time-domain response of the structure-water system

Using modal superposition and mode shapes orthogonality, we show that the vector $\bar{\mathbf{Z}}$ of frequency-dependent generalized coordinates $\bar{Z}_j$, $j = 1 \ldots N_{\mathrm{s}}$, can be obtained by solving the system of equations

$$\bar{\mathbf{S}}\,\bar{\mathbf{Z}} = \bar{\mathbf{Q}} \tag{4.17}$$

in which, for $j = 1 \ldots N_\mathrm{s}$ and $m = 1 \ldots N_\mathrm{s}$,

$$\bar{S}_{j,m}(\omega) = \left[-\omega^2 + (1 + \mathrm{i}\,\mu)\,\omega_j^2 \right] M_j\,\delta_{j,m} + \omega^2 \left[\int_0^{H_\mathrm{w}^{(1)}} \bar{p}_j^{(1)}(x_1, y)\,\psi_m^{(x)}(x_1, y)\,\mathrm{d}y - \int_0^{H_\mathrm{w}^{(2)}} \bar{p}_j^{(2)}(x_2, y)\,\psi_m^{(x)}(x_2, y)\,\mathrm{d}y \right] \tag{4.18}$$

and

$$\bar{Q}_m = -L_m + \int_0^{H_\mathrm{w}^{(1)}} \bar{p}_0^{(1)}(x_1, y)\,\psi_m^{(x)}(x_1, y)\,\mathrm{d}y - \int_0^{H_\mathrm{w}^{(2)}} \bar{p}_0^{(2)}(x_2, y)\,\psi_m^{(x)}(x_2, y)\,\mathrm{d}y \tag{4.19}$$

with

$$M_j = \boldsymbol{\psi}_m^\mathrm{T}\,\mathbf{M}\,\boldsymbol{\psi}_j\,; \qquad\qquad L_m = \boldsymbol{\psi}_m^\mathrm{T}\,\mathbf{M}\,\mathbf{1} \tag{4.20}$$

and where $\delta_{j,m}$ is the Kronecker symbol, ω_j is the vibration frequency along mode shape $\boldsymbol{\psi}_j$, and M_j and L_m the corresponding generalized mass and force, respectively. When mode shapes are also mass-normalized, the generalized masses have unit values $M_j = 1$, $j = 1 \ldots N_\mathrm{s}$. The dynamic properties ω_j and $\boldsymbol{\psi}_j$ can be obtained using closed-form expressions available for simple geometries such as in Ref. [21], or from finite element modal analysis for complex structures. When the effect of soil flexibility is to be included, the properties ω_j and $\boldsymbol{\psi}_j$ of the massless-soil-structure system should be used. To alleviate the text, these properties will be referred to as structural parameters in the rest of the paper.

Substituting the frequency-independent hydrodynamic pressures given in Eqs. (4.10) and (4.11) into the system of equations (4.17), and introducing the non-dimensional height ratio $\eta_\ell = H_\mathrm{w}^{(\ell)}/H_\mathrm{s}$ for $\ell = 1, 2$, we show that Eqs. (4.18) and (4.19) can be rewritten under a more compact form

$$\bar{S}_{j,m}(\omega) = \left[-\omega^2 + (1 + \mathrm{i}\,\mu)\,\omega_j^2 \right] M_j\,\delta_{j,m} - \omega^2\,\vartheta_{j,m}(\eta_1, \eta_2) \tag{4.21}$$

$$\bar{Q}_m = -L_m + \Gamma_m(\eta_1, \eta_2) \tag{4.22}$$

where

$$\vartheta_{j,m}(\eta_1, \eta_2) = \theta_{j,m}(\eta_1) + \theta_{j,m}(\eta_2)\,; \qquad\qquad \Gamma_m(\eta_1, \eta_2) = \gamma_m(\eta_1) + \gamma_m(\eta_2) \tag{4.23}$$

in which, for $\ell = 1, 2$

$$\theta_{j,j}(\eta_\ell) = \frac{4\rho_{\mathrm{w}}}{\pi}\,\eta_\ell^2\,H_{\mathrm{s}}^2 \sum_{n=1}^{N_{\mathrm{w}}} \frac{\widehat{X}_n^{(\ell)}(x_\ell)}{(2n-1)} \left[I_{j,n}^{(\ell)}\right]^2 \tag{4.24}$$

$$\begin{aligned}\theta_{j,m}(\eta_\ell) &= \theta_{m,j}(\eta_\ell) \\ &= \frac{4\rho_{\mathrm{w}}}{\pi}\,\eta_\ell^2\,H_{\mathrm{s}}^2 \sum_{n=1}^{N_{\mathrm{w}}} \frac{\widehat{X}_n^{(\ell)}(x_\ell)}{(2n-1)}\, I_{j,n}^{(\ell)}\, I_{m,n}^{(\ell)}\end{aligned} \tag{4.25}$$

$$\gamma_m(\eta_\ell) = \frac{8\rho_{\mathrm{w}}}{\pi^2}\,\eta_\ell^2\,H_{\mathrm{s}}^2 \sum_{n=1}^{N_{\mathrm{w}}} \frac{(-1)^n\, X_n^{(\ell)}(x_\ell)}{(2n-1)^2}\, I_{m,n}^{(\ell)} \tag{4.26}$$

where $I_{j,n}^{(\ell)}$ and $I_{m,n}^{(\ell)}$ are given by Eq. (4.16) for $m,\, j = 1 \ldots N_{\mathrm{s}}$ and $n = 1 \ldots N_{\mathrm{w}}$ and where $\widehat{X}_n^{(\ell)}(x_\ell)$ and $X_n^{(\ell)}(x_\ell)$ simplify to

$$\widehat{X}_n^{(\ell)}(x_\ell) = \coth\left[\frac{(2n-1)\,\pi\,L_{\mathrm{w}}^{(\ell)}}{2H_{\mathrm{w}}^{(\ell)}}\right]; \qquad X_n^{(\ell)}(x_\ell) = \widehat{X}_n^{(\ell)}(x_\ell) - \sinh\left[\frac{(2n-1)\,\pi\,L_{\mathrm{w}}^{(\ell)}}{2H_{\mathrm{w}}^{(\ell)}}\right]^{-1} \tag{4.27}$$

for boundary condition BC-I,

$$\widehat{X}_n^{(\ell)}(x_\ell) = X_n^{(\ell)}(x_\ell) = 1 \tag{4.28}$$

for boundary condition BC-II, and

$$\widehat{X}_n^{(\ell)}(x_\ell) = X_n^{(\ell)}(x_\ell) = \coth\left[\frac{(2n-1)\,\pi\,L_{\mathrm{w}}^{(\ell)}}{2H_{\mathrm{w}}^{(\ell)}}\right] \tag{4.29}$$

for boundary condition BC-III. If the structure is symmetrical and if water levels and boundary conditions are the same for water domains on both sides, we show from Eqs. (4.24) to (4.26) that Eq. (4.23) simplifies to

$$\vartheta_{j,m}(\eta_1, \eta_2) = 2\,\theta_{j,m}(\eta_\ell)\,; \qquad \Gamma_m(\eta_1, \eta_2) = 2\,\gamma_m(\eta_\ell) \tag{4.30}$$

If only one face ℓ of the structure is in contact with water, Eqs. (4.23) simplifies to

$$\vartheta_{j,m}(\eta_\ell, 0) = \theta_{j,m}(\eta_\ell)\,; \qquad \Gamma_m(\eta_\ell, 0) = \gamma_m(\eta_\ell) \tag{4.31}$$

The vector $\bar{\mathbf{Z}}$ of complex-valued frequency response functions is first determined from Eq. (4.17) for frequencies in the range of interest. Eq. (4.2) is then applied to obtain frequency response functions for hydrodynamic pressure, and those for structural displacements and

accelerations can be expressed as

$$\bar{u}(x,y,\omega) = \sum_{j=1}^{N_\mathrm{s}} \psi_j^{(x)}(x,y)\,\bar{Z}_j(\omega)\,; \qquad \bar{\ddot{u}}(x,y,\omega) = -\omega^2 \sum_{j=1}^{N_\mathrm{s}} \psi_j^{(x)}(x,y)\,\bar{Z}_j(\omega) \tag{4.32}$$

$$\bar{v}(x,y,\omega) = \sum_{j=1}^{N_\mathrm{s}} \psi_j^{(y)}(x,y)\,\bar{Z}_j(\omega)\,; \qquad \bar{\ddot{v}}(x,y,\omega) = -\omega^2 \sum_{j=1}^{N_\mathrm{s}} \psi_j^{(y)}(x,y)\,\bar{Z}_j(\omega) \tag{4.33}$$

where $\bar{u}$ and $\bar{v}$ denote the horizontal and vertical displacements, respectively, $\bar{\ddot{u}}$ and $\bar{\ddot{v}}$ the horizontal and vertical accelerations, respectively, and $\psi_j^{(x)}$ and $\psi_j^{(y)}$ the x– and y–components of structural mode shape $\boldsymbol{\psi}_j$.

The structural displacement and acceleration time-history responses to a ground acceleration $\ddot{u}_\mathrm{g}(t)$ can be obtained as

$$u(x,y,t) = \sum_{j=1}^{N_\mathrm{s}} \psi_j^{(x)}(x,y)\,Z_j(t)\,; \qquad \ddot{u}(x,y,t) = \sum_{j=1}^{N_\mathrm{s}} \psi_j^{(x)}(x,y)\,\ddot{Z}_j(t) \tag{4.34}$$

$$v(x,y,t) = \sum_{j=1}^{N_\mathrm{s}} \psi_j^{(y)}(x,y)\,Z_j(t)\,; \qquad \ddot{v}(x,y,t) = \sum_{j=1}^{N_\mathrm{s}} \psi_j^{(y)}(x,y)\,\ddot{Z}_j(t) \tag{4.35}$$

where the time-domain generalized coordinates Z_j are given by the Fourier integrals

$$Z_j(t) = \frac{1}{2\pi}\int_{-\infty}^{\infty} \bar{Z}_j(\omega)\,\bar{\ddot{u}}_\mathrm{g}(\omega)\,\mathrm{e}^{\mathrm{i}\omega t}\,\mathrm{d}\omega\,; \qquad \ddot{Z}_j(t) = -\frac{1}{2\pi}\int_{-\infty}^{\infty} \omega^2\,\bar{Z}_j(\omega)\,\bar{\ddot{u}}_\mathrm{g}(\omega)\,\mathrm{e}^{\mathrm{i}\omega t}\,\mathrm{d}\omega \tag{4.36}$$

in which $\bar{\ddot{u}}_\mathrm{g}(\omega)$ is the Fourier transform of the ground acceleration $\ddot{u}_\mathrm{g}(t)$

$$\bar{\ddot{u}}_\mathrm{g}(\omega) = \int_0^{t_a} \ddot{u}_\mathrm{g}(t)\,\mathrm{e}^{-\mathrm{i}\omega t}\,\mathrm{d}t \tag{4.37}$$

in which t_a is the time duration of the applied accelerogram.

4.3 Simplified procedure

The analytical formulation presented above is used in this section to develop a simplified method for practical assessment of the dynamic response of structure-water systems and the evaluation of coupled vibration periods.

4.3.1 Simplified generalized coordinates

The system of equations (4.17) has to be solved numerically for generalized coordinates $\bar{Z}_j$, $j=1\ldots N_\mathrm{s}$, to obtain frequency response functions corresponding to hydrodynamic pressures, displacements and accelerations as described previously. Here, we propose a simplified method to obtain the generalized coordinates $\bar{Z}_j$, $j=1\ldots N_\mathrm{s}$, instead of solving Eq. (4.17) using a matrix analysis numerical solution scheme. In a fundamental mode analysis, i.e. $N_\mathrm{s}=1$, the only generalized coordinate $\bar{Z}_1$ is given by

$$\bar{Z}_1(\omega) = \frac{\bar{Q}_1}{\bar{S}_{1,1}(\omega)} \tag{4.38}$$

If two structural modes are to be included, the generalized coordinates can be obtained as

$$\bar{Z}_1(\omega) = \frac{\bar{S}_{2,2}(\omega)\,\bar{Q}_1 - \bar{S}_{1,2}(\omega)\,\bar{Q}_2}{\bar{S}_{1,1}(\omega)\bar{S}_{2,2}(\omega) - \bar{S}^2_{1,2}(\omega)} \tag{4.39}$$

$$\bar{Z}_2(\omega) = \frac{\bar{S}_{1,1}(\omega)\,\bar{Q}_2 - \bar{S}_{1,2}(\omega)\,\bar{Q}_1}{\bar{S}_{1,1}(\omega)\bar{S}_{2,2}(\omega) - \bar{S}^2_{1,2}(\omega)} \tag{4.40}$$

Finally, if higher mode effects are to be included in the analysis, i.e. $N_\mathrm{s} \geqslant 3$, we show that the generalized coordinates can be approximated by decoupling the system of equations (4.17) as follows

$$\bar{Z}_1(\omega) \approx \frac{\bar{S}_{2,2}(\omega)\,\bar{Q}_1 - \bar{S}_{1,2}(\omega)\,\bar{Q}_2}{\bar{S}_{1,1}(\omega)\bar{S}_{2,2}(\omega) - \bar{S}^2_{1,2}(\omega)} \tag{4.41}$$

$$\bar{Z}_j(\omega) \approx \frac{\bar{S}_{j-1,j-1}(\omega)\,\bar{Q}_j - \bar{S}_{j-1,j}(\omega)\,\bar{Q}_{j-1}}{\bar{S}_{j-1,j-1}(\omega)\bar{S}_{j,j}(\omega) - \bar{S}^2_{j-1,j}(\omega)} \qquad \text{for } j=2\ldots N_\mathrm{s} \tag{4.42}$$

where the parameters $\bar{S}_{j,m}$ and $\bar{Q}_m$ for $j=1\ldots N_\mathrm{s}$ and $m=1\ldots N_\mathrm{s}$ are given by Eqs. (4.21) and (4.22), respectively.

A simplified procedure to estimate these coefficients is developed next based on the approach proposed in Ref. [22]. This technique consists of approximating the x–component of a structural mode shape $\boldsymbol{\psi}_j$ by a polynomial function of order $N_{\boldsymbol{\psi}_j}$ and coefficients $a_{j,k}$ as illustrated in Fig. 4.3 for mode shapes 1 to 4.Such modal shape approximations can also be obtained using classical interpolation methods commonly built-in spreadsheet or numerical packages such as MATLAB ® [23].

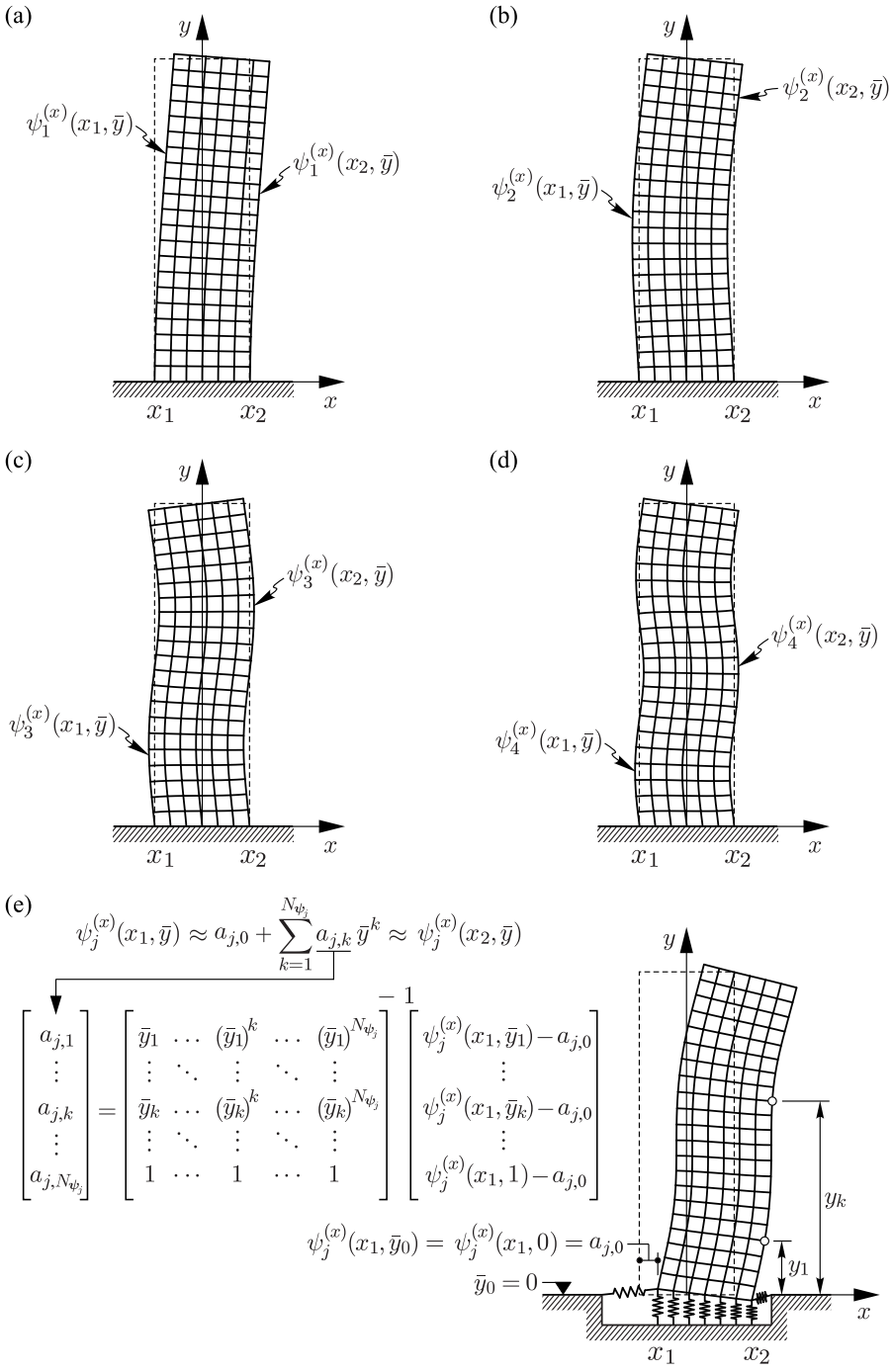

Figure 4.3 Approximation of the x–component of structural mode shapes by polynomial functions : (a) Mode shape 1 : $\psi_1^{(x)}(x_1,\bar{y}) \approx \psi_1^{(x)}(x_2,\bar{y}) \approx \sum_{k=0}^{N_{\boldsymbol{\psi}_1}} a_{1,k}\bar{y}^k$; (b) Mode shape 2 : $\psi_2^{(x)}(x_1,\bar{y}) \approx \psi_2^{(x)}(x_2,\bar{y}) \approx \sum_{k=0}^{N_{\boldsymbol{\psi}_2}} a_{2,k}\bar{y}^k$; (c) Mode shape 3 : $\psi_3^{(x)}(x_1,\bar{y}) \approx \psi_3^{(x)}(x_2,\bar{y}) \approx \sum_{k=0}^{N_{\boldsymbol{\psi}_3}} a_{3,k}\bar{y}^k$; (d) Mode shape 4 : $\psi_4^{(x)}(x_1,\bar{y}) \approx \psi_4^{(x)}(x_2,\bar{y}) \approx \sum_{k=0}^{N_{\boldsymbol{\psi}_4}} a_{4,k}\bar{y}^k$; (e) Polynomial approximation of the mode shapes.

If the structure is symmetrical, the mode shapes at the structure-water interface on each side can be assumed equal, yielding

$$\psi_j^{(x)}(x_1, \bar{y}) \approx \psi_j^{(x)}(x_2, \bar{y}) \approx \sum_{k=0}^{N_{\psi_j}} a_{j,k}\, \bar{y}^k \tag{4.43}$$

where $\bar{y} = y/H_\mathrm{s}$. Coefficients $a_{j,0}$ take account of translations due to soil flexibility. We note that if the structure is clamped at its base, then $a_{j,0} = 0$. Substituting Eq. (4.43) into Eqs. (4.24) to (4.26) and proceeding with a change of variable $\bar{y} = y/H_\mathrm{s}$, we show that the parameters $\theta_{j,j}$ and γ_j for $j = 1 \ldots N_\mathrm{s}$, and $\theta_{j,j-1}$ for $j = 2 \ldots N_\mathrm{s}$ can be obtained as

$$\theta_{j,j-1}(\eta_\ell) = \frac{4\rho_\mathrm{w} H_\mathrm{s}^2}{\pi} \sum_{n=1}^{N_\mathrm{w}} \frac{\widehat{X}_n^{(\ell)}(x_\ell)}{(2n-1)} \left[\sum_{k=0}^{N_{\psi_j}} a_{j-1,k}\, \eta_\ell^{k+1}\, f_k(n)\right] \left[\sum_{k=0}^{N_{\psi_j}} a_{j,k}\, \eta_\ell^{k+1}\, f_k(n)\right] \tag{4.44}$$

$$\theta_{j,j}(\eta_\ell) = \frac{4\rho_\mathrm{w} H_\mathrm{s}^2}{\pi} \sum_{n=1}^{N_\mathrm{w}} \frac{\widehat{X}_n^{(\ell)}(x_\ell)}{(2n-1)} \left[\sum_{k=0}^{N_{\psi_j}} a_{j,k}\, \eta_\ell^{k+1}\, f_k(n)\right]^2 \tag{4.45}$$

$$\gamma_j(\eta_\ell) = \frac{8\rho_\mathrm{w}}{\pi^2}\, \eta_\ell\, H_\mathrm{s}^2 \sum_{n=1}^{N_\mathrm{w}} \frac{(-1)^n\, X_n^{(\ell)}(x_\ell)}{(2n-1)^2} \left[\sum_{k=0}^{N_{\psi_j}} a_{j,k}\, \eta_\ell^{k}\, f_k(n)\right] \tag{4.46}$$

where the function $f_k(n)$ is shown to depend only on the reservoir mode n and is given by

$$f_k(n) = \frac{1}{\eta_\ell^{k+1}} \int_0^{\eta_\ell} \bar{y}^k \cos\left[\frac{(2n-1)\,\pi\,\bar{y}}{2\eta_\ell}\right] \mathrm{d}\bar{y} \tag{4.47}$$

The generalized coordinates can be obtained from Eqs. (4.38) to (4.40) for $N_\mathrm{s} \leqslant 2$, or Eqs. (4.41) and (4.42) for $N_\mathrm{s} \geqslant 3$, after applying Eqs. (4.21) to (4.23) and Eqs. (4.44) to (4.46) combined with Eq. (4.27) for boundary condition BC-I, Eq. (4.28) for boundary condition BC-II, and Eq. (4.29) for boundary condition BC-III. For practical programming into a spreadsheet, we propose expressions of the real and imaginary parts of generalized coordinates in Appendix A. Once generalized coordinates are determined, Eqs. (4.32) to (4.37) can be used to obtain the structural response in frequency or time domains.

4.3.2 Evaluation of the vibration periods of a structure-water system

We define the frequency-dependent parameters $\tilde{S}_{j-1,\,j-1}$, $\tilde{S}_{j,\,j}$ and $\tilde{S}_{j-1,\,j}$, $j = 2 \ldots N_\mathrm{s}$, obtained from Eq. (4.21) with damping being neglected as

$$\tilde{S}_{j-1,\,j-1} = \left(\omega_{j-1}^2 - \omega^2\right) M_{j-1} - \omega^2\, \vartheta_{j-1,j-1}(\eta_1, \eta_2) \tag{4.48}$$

$$\tilde{S}_{j,j} = \left(\omega_{j}^2 - \omega^2\right) M_{j} - \omega^2\, \vartheta_{j,j}(\eta_1, \eta_2) \tag{4.49}$$

$$\tilde{S}_{j-1,j} = -\omega^2\, \vartheta_{j-1,j}(\eta_1, \eta_2) \tag{4.50}$$

The resonant frequencies of a structure-water system can be approximated by the frequencies $\widetilde{\omega}_j$, $j = 1 \ldots N_\mathrm{s}$, that make the generalized coordinates $\bar{Z}_j$ infinite. Therefore, according to Eq. (4.38), the frequency $\widetilde{\omega}_1$ in a fundamental mode analysis can be obtained by solving

$$\tilde{S}_{1,1}(\widetilde{\omega}_1) = 0 \tag{4.51}$$

yielding

$$\widetilde{\omega}_1 = \frac{\omega_1}{\sqrt{1 + \dfrac{\vartheta_{1,1}(\eta_1, \eta_2)}{M_1}}} \tag{4.52}$$

When higher modes are included in the analysis, using Eqs. (4.41) and (4.42) yields

$$\tilde{S}_{1,1}(\widetilde{\omega}_1)\, \tilde{S}_{2,2}(\widetilde{\omega}_1) - \tilde{S}_{1,2}^2(\widetilde{\omega}_1) = 0 \tag{4.53}$$

for the fundamental mode, and

$$\tilde{S}_{j-1,j-1}(\widetilde{\omega}_j)\, \tilde{S}_{j,j}(\widetilde{\omega}_j) - \tilde{S}_{j-1,j}^2(\widetilde{\omega}_j) = 0 \qquad \text{for } j = 2 \ldots N_\mathrm{s} \tag{4.54}$$

for higher modes. Using $j = 2$ in Eq. (4.54) and comparing it to Eq. (4.53) shows that both $\widetilde{\omega}_1$ and $\widetilde{\omega}_2$ are roots of the same equation. As a consequence, solving only Eq. (4.54) will lead to all N_s first vibration frequencies. Replacing Eqs. (4.48) to (4.50) into Eq. (4.54) yields the following simple second order equation to be solved for χ_j

$$\alpha_j\, \chi_j^2 - \beta_j\, \chi_j + \kappa_j = 0 \qquad \text{for } j = 2 \ldots N_\mathrm{s} \tag{4.55}$$

in which

$$\begin{aligned}
\alpha_j &= M_{j-1}M_j + M_{j-1}\,\vartheta_{j,j}(\eta_1,\eta_2) + M_j\,\vartheta_{j-1,j-1}(\eta_1,\eta_2) \\
&\quad + \vartheta_{j-1,j-1}(\eta_1,\eta_2)\,\vartheta_{j,j}(\eta_1,\eta_2) - \vartheta^2_{j-1,j}(\eta_1,\eta_2) \\
\beta_j &= M_{j-1}M_j\left(\omega^2_{j-1}+\omega^2_j\right) + \omega^2_{j-1}M_{j-1}\,\vartheta_{j,j}(\eta_1,\eta_2) + \omega^2_j M_j\,\vartheta_{j-1,j-1} \\
\kappa_j &= M_{j-1}M_j\,\omega^2_{j-1}\,\omega^2_j
\end{aligned} \tag{4.56}$$

For each mode j, Eq. (4.55) has two real positive solutions $\chi_j^{(\min)}$ and $\chi_j^{(\max)}$ corresponding to the smallest and largest roots of the polynomial, respectively. We show that the resonant frequencies $\widetilde{\omega}_j$, $j=1\ldots N_{\rm s}$, can be approximated as

$$\widetilde{\omega}_1 = \sqrt{\chi_2^{(\min)}} \tag{4.57}$$

$$\widetilde{\omega}_j = \sqrt{\chi_j^{(\max)}} \qquad \text{for } j = 2\ldots N_{\rm s} \tag{4.58}$$

Although the previous equations were derived assuming a symmetrical structure, the procedure can be easily adapted to investigate non-symmetrical structures vibrating in contact with two water domains. In this latter case, mode shapes have to be approximated by polynomial functions along each face of the structure

$$\psi_j^{(x)}(x_\ell\,,\bar{y}) \approx \sum_{k=0}^{N_{\boldsymbol{\psi}_j}} a_{j,k}^{(\ell)}\,\bar{y}^k \tag{4.59}$$

where two different sets of coefficients $a_{j,k}^{(\ell)}$ are obtained for each mode shape $\psi_j^{(x)}(x_\ell\,,\bar{y})$, $\ell=1,2$. Eqs. (4.44) to (4.46) have then to be determined for both sides considering the new coefficients $a_{j,k}^{(\ell)}$.

4.4 Effects of water domain boundary conditions

The objective of this section is to investigate the effect of boundary conditions on the dynamic response of structure-water systems. For that purpose, we first show in Appendix B that Eqs. (4.44) to (4.46) can be rewritten as Eqs. (4.B.15), (4.B.18) and (4.B.20), respectively. The resulting expressions contain the effect of boundary conditions into the coefficients $A_{k,s}^{(\ell)}$ and $B_k^{(\ell)}$, given for $k=0\ldots N_{\boldsymbol{\psi}_j}$ and $s=0\ldots N_{\boldsymbol{\psi}_j}$ by Eqs. (4.B.16) and (4.B.21) for a moving rigid wall boundary condition BC-I, Eqs. (4.B.17) and (4.B.22) for a non-disturbed boundary condition BC-II, and Eqs. (4.B.16) and (4.B.23) for a fixed rigid wall boundary condition BC-III. When a boundary condition BC-I or BC-III is applied at a distance $L_{\rm w}^{(\ell)}$ from the

structure, it is seen that Eqs. (4.B.16), (4.B.21) and (4.B.23) depend only on water modes and distance $L_{\rm w}^{(\ell)}$. According to Eqs. (4.27) and (4.29), we have for both boundary conditions BC-I and BC-III

$$\lim_{L_{\rm w}^{(\ell)}\to+\infty} X_n^{(\ell)}(x_\ell) = \lim_{L_{\rm w}^{(\ell)}\to+\infty} \widehat{X}_n^{(\ell)}(x_\ell) = 1 \tag{4.60}$$

Therefore, as the ratio $L_{\rm w}^{(\ell)}/H_{\rm w}^{(\ell)}$ increases, the coefficients $A_{k,s}^{(\ell)}$ and $B_k^{(\ell)}$ obtained from Eqs. (4.B.16) and (4.B.21) or (4.B.23), converge towards coefficients $A_{k,s}$ and B_k given by Eqs. (4.B.17) and (4.B.22) for a non-disturbed boundary condition BC-II. To examine further this observation, we define the ratios

$$\varepsilon_A^{(\ell)}(k,s) = \frac{A_{k,s}^{(\ell)}\ \text{(Determined for BC-I/BC-III)}}{A_{k,s}\ \text{(Determined for BC-II)}} \tag{4.61}$$

and

$$\varepsilon_B^{(\ell)}(k) = \frac{B_k^{(\ell)}\ \text{(Determined for BC-I/BC-III)}}{B_k\ \text{(Determined for BC-II)}} \tag{4.62}$$

Fig. 4.4 illustrates the variations of the ratios $\varepsilon_A^{(\ell)}$and $\varepsilon_B^{(\ell)}$ as a function of $L_{\rm w}^{(\ell)}/H_{\rm w}^{(\ell)}$ for $k,\, s = 0 \ldots N_{\psi_j} = 11$. For boundary conditions BC-I and BC-III, the $A_{k,s}$ coefficients are equal, thus producing identical ratios $\varepsilon_A^{(\ell)}$. We clearly see that the boundary conditions BC-III and BC-II yield approximately similar ratios for $L_{\rm w}^{(\ell)} \geqslant 2H_{\rm w}^{(\ell)}$. This result implies that the dynamic response of a structure in contact with an infinite incompressible water domain can be simulated by applying a fixed rigid wall boundary condition at a distance $L_{\rm w}^{(\ell)} \geqslant 2H_{\rm w}^{(\ell)}$. Comparing BC-I and BC-II, we obtain similar ratios for $L_{\rm w}^{(\ell)} \geqslant 3H_{\rm w}^{(\ell)}$, which represents the minimum distance where an applied moving rigid wall boundary condition affects the dynamic response of a structure-water system. Introducing polynomial modal shape approximations into Eqs. (4.10) and (4.11), yields hydrodynamic pressures

$$\bar{p}_0^{(\ell)}(x,y) = -\frac{8\times(-1)^\ell}{\pi^2}\,\rho_{\rm w} H_{\rm w}^{(\ell)} \sum_{n=1}^{N_{\rm w}} \frac{(-1)^n}{(2n-1)^2}\; X_n^{(\ell)}(x)\, \cos\left[\frac{(2n-1)\,\pi\, y}{2H_{\rm w}^{(\ell)}}\right] \tag{4.63}$$

$$\bar{p}_j^{(\ell)}(x,y) = \frac{4\times(-1)^\ell}{\pi}\,\rho_{\rm w} H_{\rm w}^{(\ell)} \sum_{k=0}^{N_{\psi_j}} \left\{ a_{j,k}\,\eta_\ell^k \sum_{n=1}^{N_{\rm w}} \frac{f_k(n)}{(2n-1)}\; \widehat{X}_n^{(\ell)}(x)\, \cos\left[\frac{(2n-1)\,\pi\, y}{2H_{\rm w}^{(\ell)}}\right] \right\} \tag{4.64}$$

For a semi-infinite water domain, or if boundary condition BC-I is used with $L_{\rm w}^{(\ell)} \geqslant 3H_{\rm w}^{(\ell)}$, we show that Eqs. (4.63) and (4.64) can be simplified further by polynomial functions to yield

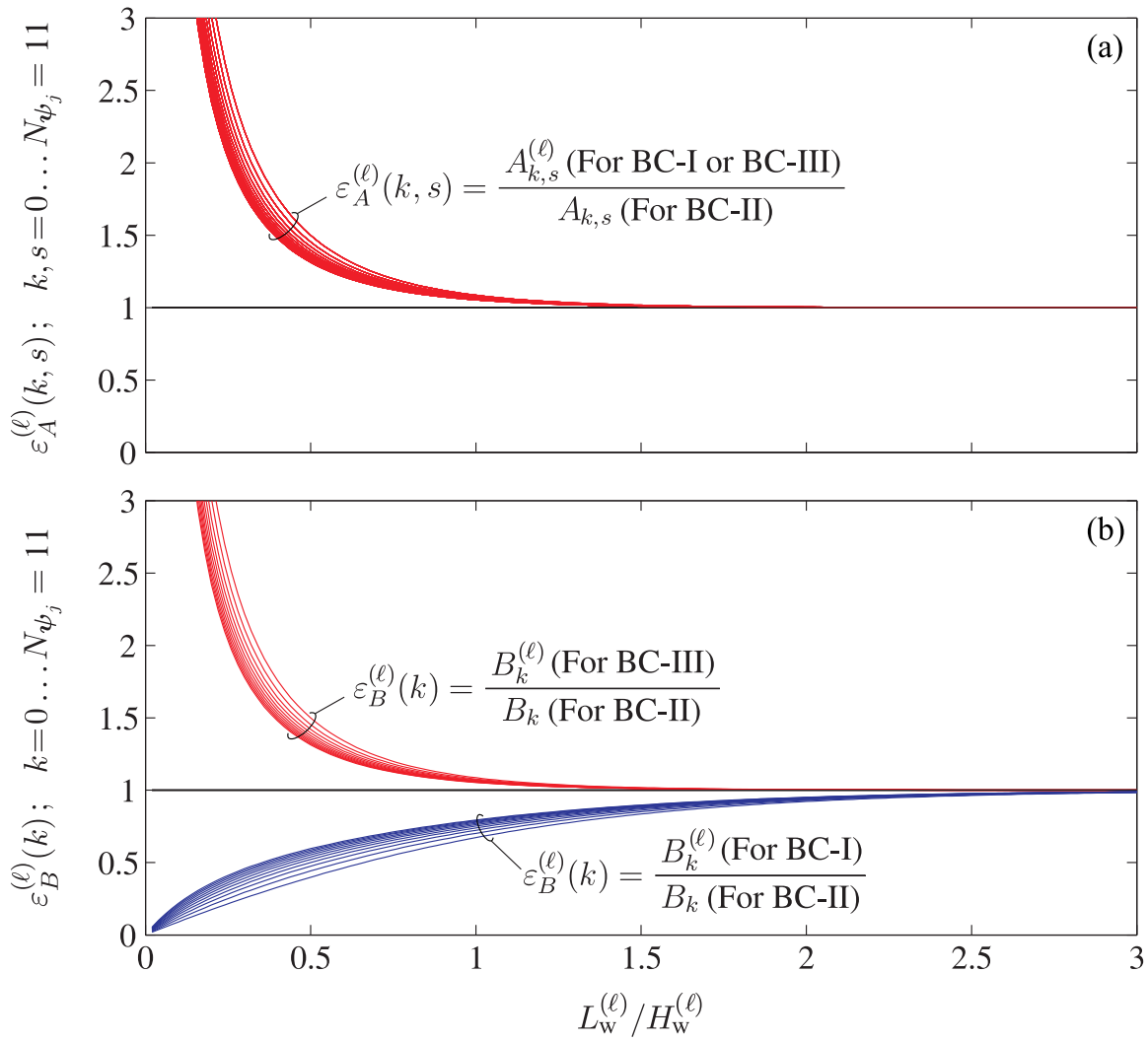

Figure 4.4 Effects of water domain boundary conditions : (a) Variation of ratio $\varepsilon_A^{(\ell)}$ as a function of truncation ratio $L_{\mathrm{w}}^{(\ell)}/H_{\mathrm{w}}^{(\ell)}$; (b) Variation of ratio $\varepsilon_B^{(\ell)}$ as a function of truncation ratio $L_{\mathrm{w}}^{(\ell)}/H_{\mathrm{w}}^{(\ell)}$.

hydrodynamic pressures exerted at the structure's left and right faces

$$\bar{p}_0^{(\ell)}(x_\ell, y) = -\frac{8\times(-1)^\ell}{\pi^2}\,\rho_{\mathrm{w}} H_{\mathrm{w}}^{(\ell)} \sum_{r=0}^{6} C_r \left(\frac{y}{H_{\mathrm{w}}^{(\ell)}}\right)^r \tag{4.65}$$

$$\bar{p}_j^{(\ell)}(x_\ell, y) = \frac{4\times(-1)^\ell}{\pi}\,\rho_{\mathrm{w}} H_{\mathrm{w}}^{(\ell)} \sum_{k=0}^{N_{\psi_j}} \left[a_{j,k}\,\eta_\ell^k \sum_{r=0}^{6} D_{r,k} \left(\frac{y}{H_{\mathrm{w}}^{(\ell)}}\right)^r \right] \tag{4.66}$$

where the coefficients C_r and $D_{r,k}$ are given in Table 4.1 for $r=0\ldots6$ and $k=0\ldots N_{\psi_j}=11$.

The validity of Eqs. (4.65) and (4.66) will be illustrated later in Section 4.5.3. It is important to note that Eqs. (4.65) and (4.66) are valid only when a moving rigid wall is located at a distance $L_{\mathrm{w}}^{(\ell)}$ larger than $3H_{\mathrm{w}}^{(\ell)}$ or when a semi-infinite water domain is to be modeled, otherwise, Eqs. (4.63) and (4.64) must be used instead.

Table 4.1 Coefficients C_r and $D_{r,k}$ for $r = 1 \ldots 6$ and $k = 0 \ldots N_{\psi_j} = 11$.

$r =$	0	1	2	3	4	5	6
$C_r =$	-0.9137	-0.1307	2.2041	-7.4868	16.4673	-16.6579	6.5055
				$D_{r,k}$			
$k = 0$	0.5817	0.0832	-1.4032	4.7663	-10.4834	10.6047	-4.1415
$k = 1$	0.1552	0.1042	-0.4812	3.6282	-9.30417	9.83994	-3.9344
$k = 2$	0.0713	0.0837	-0.8263	4.7976	-10.6220	10.6861	-4.1826
$k = 3$	0.0407	0.0851	-0.9581	4.9205	-10.5643	10.7293	-4.2452
$k = 4$	0.0260	0.0863	-1.0058	4.9634	-10.7550	11.1210	-4.4281
$k = 5$	0.0177	0.0893	-1.0600	5.1666	-11.3266	11.7970	-4.6760
$k = 6$	0.0128	0.0935	-1.1226	5.4394	-11.9824	12.4549	-4.8876
$k = 7$	0.0095	0.0976	-1.1784	5.6801	-12.5042	12.9150	-5.0114
$k = 8$	0.0071	0.1006	-1.2175	5.8367	-12.8031	13.1227	-5.0380
$k = 9$	0.0055	0.1022	-1.2367	5.8960	-12.8721	13.0928	-4.9791
$k = 10$	0.0042	0.1025	-1.2370	5.8659	-12.7420	12.8685	-4.8534
$k = 11$	0.0033	0.1014	-1.2213	5.7625	-12.4555	12.4982	-4.6798

4.5 Case studies and results

4.5.1 Studied structure-water systems, models and analysis types

The proposed analytical and simplified methods described in Sections 4.2 and 4.3 were programmed using MATLAB [23]. In this section, we assess the effectiveness of these formulations in determining the dynamic response of a structure in contact with water. The irregular structure with cross-section illustrated in Fig. 4.5 (a) is considered. The properties of this illustrative example were selected to validate the proposed methods and namely to assess their ability to account for complex geometry and higher mode effects. The structure consists of two parts : (i) a lower 50 m high wall, with thickness varying from 10 m at the base to 5 m at the top, and (ii) an upper concentrated mass of rectangular cross-section 10 m wide and 5 m high. A mass density $\rho_{\mathrm{s}}^{(1)} = 2400$ kg/m^3, a Poisson's ratio $\nu^{(1)} = 0.2$ and a modulus of elasticity $E_{\mathrm{s}}^{(1)} = 25$ GPa are assumed as material properties for the lower structure. The upper part has a mass density $\rho_{\mathrm{s}}^{(2)} = 7200$ kg/m^3, a Poisson's ratio $\nu^{(2)} = 0.2$ and a modulus of elasticity $E_{\mathrm{s}}^{(2)} = 60$ GPa. A constant hysteretic damping factor $\mu = 0.1$ is assigned to the

structure including the massless soil foundation when considered in the analysis. A water mass density $\rho_w = 1000$ kg/m^3 is considered. The two structure-water systems illustrated in

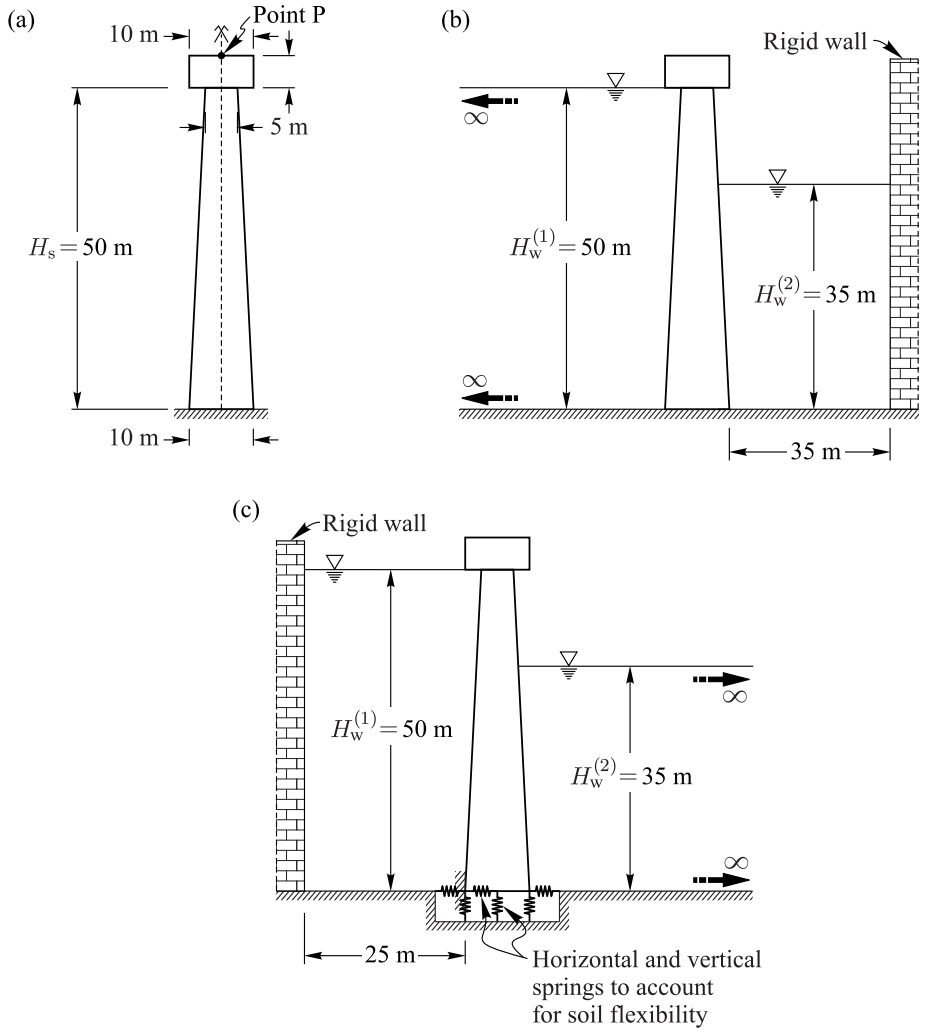

Figure 4.5 Studied structure-water systems : (a) Structure dimensions; (b) System A; (c) System B.

Figs. 4.5 (b) and (c) are investigated :

- System A [Fig. 4.5 (b)] : The structure lies on a rigid soil and is in contact with two water domains of heights $H_w^{(1)} = 50$ m ($\eta_1 = 1$) and $H_w^{(2)} = 35$ m ($\eta_2 = 0.7$). The boundary conditions are selected as infinite for the left water domain (i.e. BC-II) and moving rigid wall (i.e. BC-I) at a distance $L_w^{(2)} = H_w^{(2)}$ for the right water domain.
- System B [Fig. 4.5 (c)] : The structure lies on a flexible soil modeled by uniformly distributed springs with stiffness $K_H = 1.0 \times 10^8$ N/m along the horizontal direction

and $K_{\mathrm{V}} = 5.0 \times 10^8$ N/m along the vertical direction. The structure is in contact with two water domains of heights $H_{\mathrm{w}}^{(1)} = 50\,\mathrm{m}$ ($\eta_1 = 1$) and $H_{\mathrm{w}}^{(2)} = 35\,\mathrm{m}$ ($\eta_2 = 0.7$). The boundary conditions are assumed as non-disturbed for the right water domain (i.e. BC-II) and moving rigid wall (i.e. BC-I) at a distance $L_{\mathrm{w}}^{(2)} = 0.5\, H_{\mathrm{w}}^{(1)}$ for the left water domain.

The structure-water systems A and B are studied using the following four analysis types :

– Analysis type I : a finite element analysis where both the structure and the water domains are modeled using finite elements as shown in Fig. 4.6 (b). The software ADINA [24] is used to discretize the structure into 9-node plane-strain finite elements and refinement of the model was performed until convergence of the results. The 9-node potential-based finite elements programmed in ADINA [24] are used to model the water domains. Fluid-structure interaction is accounted for through special interface elements also included in the software. The performance of the potential-based formulation and the fluid-structure interface elements was assessed in a previous work [11]. The semi-infinite water domain is simulated by a $20H_{\mathrm{w}}^{(\ell)}$ length water domain with a fixed rigid wall boundary condition applied at the far end. The method can accurately account for fluid-structure interaction in systems with a general geometry, including non-vertical fluid-structure interfaces. The results of this analysis will serve as our reference solution in the rest of the paper. The same type of analysis is also performed considering a shorter water domain truncation length with a fixed rigid wall boundary condition applied at a distance $2H_{\mathrm{w}}^{(\ell)}$ from structure's face.

– Analysis type II : a finite element analysis of the structure where hydrodynamic loading is modeled approximately using Westergaard added mass formulation [1] as illustrated in Fig. 4.6 (b). The added mass m_i to be attached to a node i belonging to structure-water interface can be written as

$$m_i = \frac{7}{8}\,\rho_{\mathrm{w}}\, S_i \sqrt{H_{\mathrm{w}}^{(\ell)} \left(H_{\mathrm{w}}^{(\ell)} - y_i \right)} \tag{4.67}$$

where y_i denotes the height of node i above the structure's base and S_i the transverse surface area associated to node i, considering a unit-thick slice of the structure. As previously, the software ADINA [24] is used to discretize the structure into 9-node finite elements, and a consistent formulation is used to determine the added masses. This process is illustrated in Fig. 4.6 (b) for a three-node edge side of a 9-node finite element belonging to the water-structure interface.

– Analysis type III : the analytical method proposed in section 4.2 is applied to determine hydrodynamic pressure distributions as illustrated in Fig. 4.6 (c). The mode shapes

along structure's face and its vibration frequencies are determined by a finite element analysis as described in analysis type I, but where only the structure or soil-structure system are modeled, i.e. without water domains.

– Analysis type IV : the simplified procedure proposed in Section 4.3 is applied to determine hydrodynamic pressure distributions as illustrated in Fig. 4.6 (c). The mode shapes along the right face of the structure and its vibration frequencies are determined by a finite element analysis as described in analysis type I, where only the structure or soil-structure system are modeled, i.e. without water domains. The j th mode shape is then approximated by a polynomial function of order $N_{\psi_j} = j + 3$.

To assess the effect of boundary conditions, we also evaluate both analysis types III and IV by replacing the rigid moving wall boundary condition BC-I by a non disturbed boundary condition BC-II. For the sake of brevity, these analyses will be denoted as types III* and IV*.

4.5.2 Vibration periods of the structure-water systems

We first investigate the ability of the proposed methods to estimate the 8 first vibration periods of the two structure-water systems described above. Such periods can be obtained using Analysis types I, II and IV. The results are normalized by the vibration period of the dry structure obtained through reference analysis type I. For systems A and B, analysis type IV* is also carried out. The following error estimators are computed to better illustrate the comparison with the finite element solution

$$\varepsilon^{(\mathrm{II})} = \frac{\widetilde{T}_j^{(\mathrm{II})} - \widetilde{T}_j^{(\mathrm{I})}}{\widetilde{T}_j^{(\mathrm{I})}}\,; \qquad \varepsilon^{(\mathrm{IV})} = \frac{\widetilde{T}_j^{(\mathrm{IV})} - \widetilde{T}_j^{(\mathrm{I})}}{\widetilde{T}_j^{(\mathrm{I})}}\,; \qquad \varepsilon^{(\mathrm{IV}^*)} = \frac{\widetilde{T}_j^{(\mathrm{IV}^*)} - \widetilde{T}_j^{(\mathrm{I})}}{\widetilde{T}_j^{(\mathrm{I})}} \tag{4.68}$$

where $\widetilde{T}_j^{(\mathrm{I})}$, $\widetilde{T}_j^{(\mathrm{II})}$, $\widetilde{T}_j^{(\mathrm{IV})}$ and $\widetilde{T}_j^{(\mathrm{IV}^*)}$ denote the vibration periods at mode j evaluated using analysis types I, II, IV, and IV*, respectively. The obtained results are illustrated in Fig. 4.7 along with errors given in percentage. First, we clearly see that, independently of the system studied, vibration period predictions by the proposed analytical and simplified methods are in excellent agreement with finite element solutions. Westergaard's added mass formulation yields satisfactory results for the first mode, while the error with respect to Finite Element predictions increases for higher modes. This result is expected since Westergaard's solution assumes a rigid body motion, which implies a decreasing accuracy of the method as the vibrating structure is more flexible. Fig. 4.7 also reveals that for structure-water system A, using a non-disturbed boundary condition BC-II instead of the moving rigid boundary condition BC-I has very little effect on the evaluation of the vibration periods. This effect is more pronounced for structure-water system B although not significant. This result can be interpreted

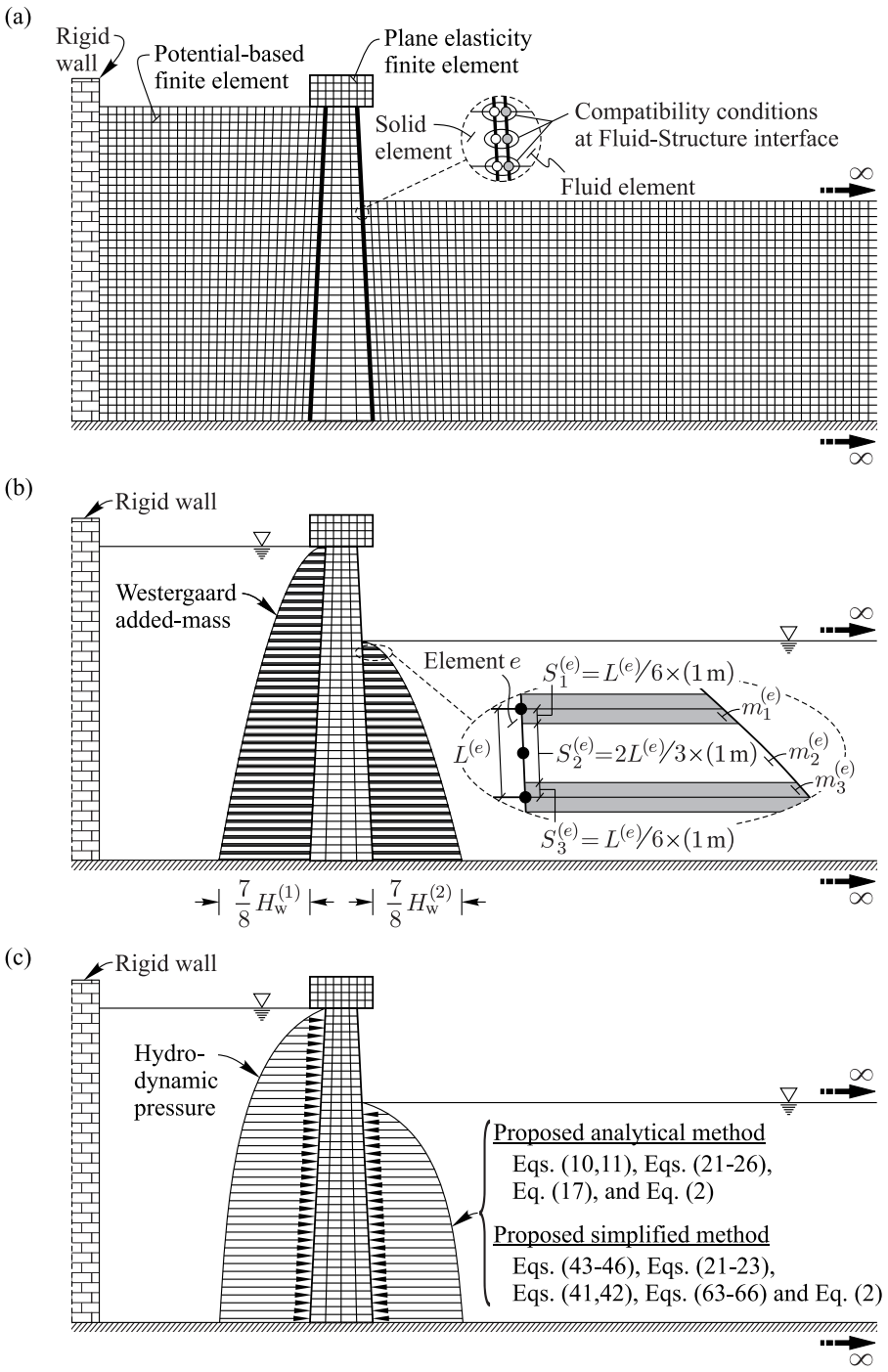

Figure 4.6 Models and types of analysis used : (a) Finite Element model including Fluid-Structure interaction - Analysis type I; (b) Finite element model and applied Westergaard added mass - Analysis type II; (c) Finite element model and applied hydrodynamic loads - Analysis types III and IV.

based on the ratios presented previously in Fig. 4.4. It can be seen that for $L_{\mathrm{w}}^{(\ell)} = H_{\mathrm{w}}^{(\ell)}$, which is the case of system A, using non-disturbed boundary condition BC-II instead of rigid BC-I does not introduce a significant error in the evaluation of hydrodynamic parameters, while this error becomes important when $L_{\mathrm{w}}^{(1)} = 0.5\, H_{\mathrm{w}}^{(1)}$, which is the case system B.

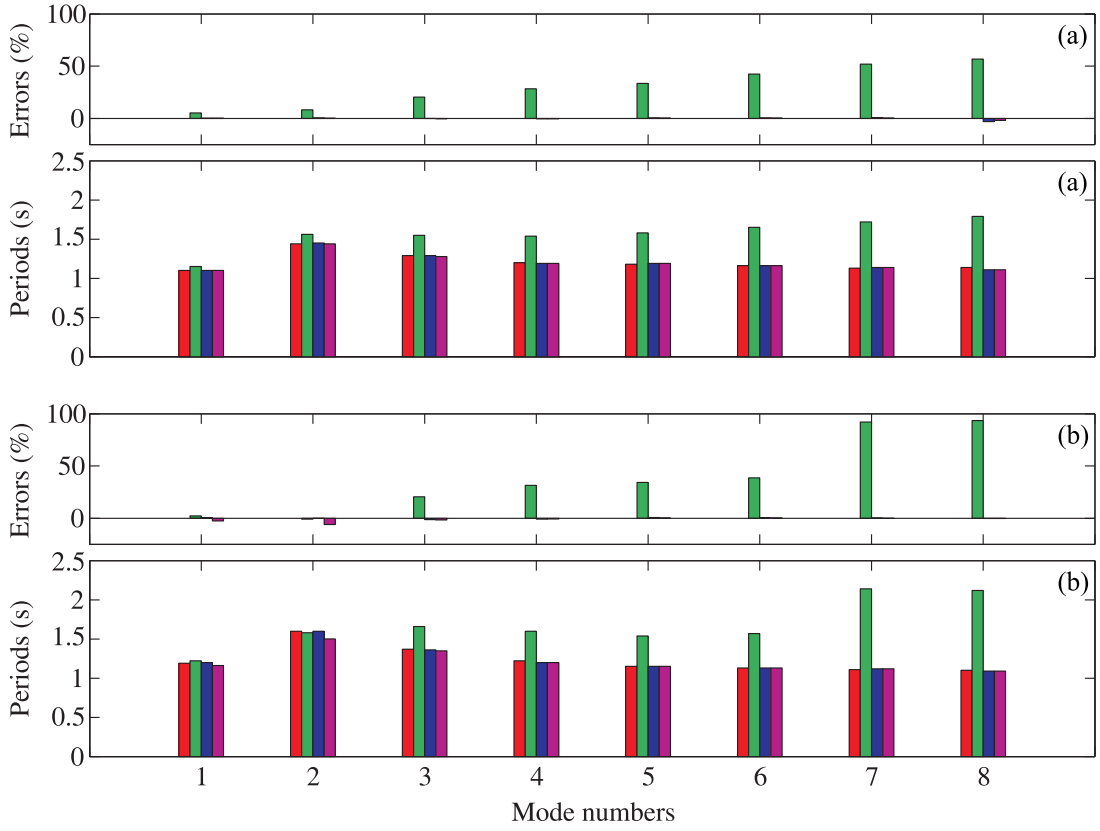

Figure 4.7 Estimation of vibration periods of the three systems studied using four analysis types I, II, IV and IV* : (a) System A ; (b) System B. Analysis type I ; Analysis type II ; Analysis type IV ; Analysis type IV*.

4.5.3 Hydrodynamic pressure

In this section, the techniques described previously are applied to determine hydrodynamic pressure profiles corresponding to different vibration periods. For the sake of brevity, only the results of system B are illustrated in Fig. 4.8. The hydrodynamic pressure $\bar{p}_0^{(\ell)}$ due to rigid body motion of the structure is first determined and shown in Fig. 4.8 (a).

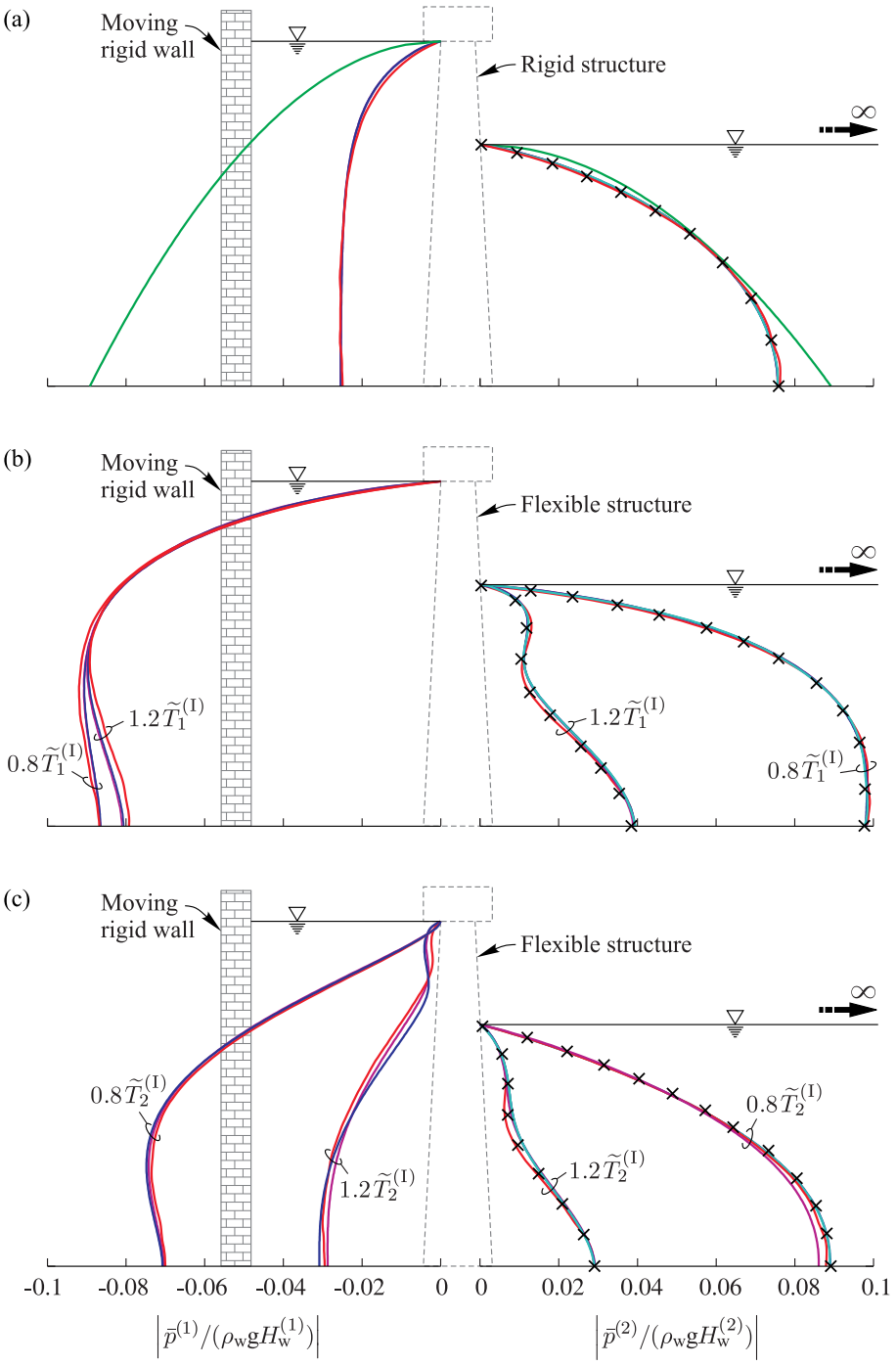

Figure 4.8 Hydrodynamic pressure distributions for system B : (a) Hydrodynamic pressure $\bar{p}_0^{(\ell)}$; (b) and (c) Hydrodynamic pressure $\bar{p}^{(\ell)}$; — Analysis type I ; — Analysis type II ; — Analysis type III ; — Analysis type IV ; — Simplified expressions [Eqs. (4.65) and (4.66)] ; × Analysis Type I with semi-infinite water domain truncated by a fixed rigid wall boundary condition applied at a distance $2H_{\mathrm{w}}^{(\ell)}$ from structure's face.

We observe an excellent agreement between FE solutions (analysis type I), and the proposed methods (analysis types III and IV). Westergaard added mass formulation gives satisfactory results for the semi-infinite domain, while it predicts higher hydrodynamic pressure within the finite water domain of less than $3H_{\mathrm{w}}^{(1)}$ length. The proposed closed-form expression in Eq. (4.65) is also applied to obtain hydrodynamic pressure $\bar{p}_0^{(\ell)}$ within the semi-infinite water domain, which yields excellent results as illustrated in Fig. 4.8 (a). The total hydrodynamic pressure $\bar{p}^{(\ell)}$ is determined next for different coupled vibration periods of the structure-water system. Hydrodynamic pressure profiles at periods $0.8\,\widetilde{T}_1^{(\mathrm{I})}$ and $1.2\,\widetilde{T}_1^{(\mathrm{I})}$ are shown in Fig. 4.8 (b), while those at periods $0.8\,\widetilde{T}_2^{(\mathrm{I})}$ and $1.2\,\widetilde{T}_2^{(\mathrm{I})}$ are given in Fig. 4.8 (c). These figures confirm that the three analysis types I, III, and IV yield almost identical results. The excellent prediction of hydrodynamic pressure profiles close to the second vibrating period $\widetilde{T}_2^{(\mathrm{I})}$ of the water-structure system also confirms that the proposed simplified method accounts appropriately for higher modes effects. These results also validate the closed-form expression for flexible hydrodynamic pressure given in Eq. (4.66) for a semi-infinite water domain or a water domain with length larger than $3H_{\mathrm{w}}^{(\ell)}$. These results also reveal that the effect of an incompressible semi-infinite water domain can be modeled appropriately using a finite water domain with a fixed rigid wall boundary condition applied at a distance $2H_{\mathrm{w}}^{(\ell)}$ from structure's face, which corroborates the discussions under Section 4.4. Finally, comparing hydrodynamic pressures obtained assuming a rigid structure, i.e. Fig. 4.8 (a), to those obtained including structural flexibility, i.e. Fig. 4.8 (b) and (c), we conclude that flexibility effects may result in higher hydrodynamic pressures and significantly affect hydrodynamic load distribution over structure's height. This observation confirms the shortcomings of Westergaard's added masses solution which assumes a rigid structure.

4.5.4 Seismic response of the structure-water systems

In this section, the four analysis types are conducted to assess the seismic response of the structure-water systems described in the previous section, subjected to two ground motions from Imperial Valley earthquake (1940) and Saguenay earthquake (1988), characterized by low and high frequency contents, respectively. Fig. 4.9 illustrates the horizontal acceleration components at El Centro and at La Malbaie selected to conduct the analyses. The time-history displacements of point P indicated in Fig. 4.5 (a) are shown in Figs. 4.10 and 4.11. For the two structure-water systems A and B, the proposed analytical and simplified methods, i.e. types III and IV, yield excellent results when compared to FE results. Westergaard added mass solution, i.e. analysis type II, is shown to be less accurate in predicting the dynamic response of both structure-water systems. Figs. 4.10 and 4.11 also show that for system A, analysis type IV* accurately predicts the response of the structure even though a moving

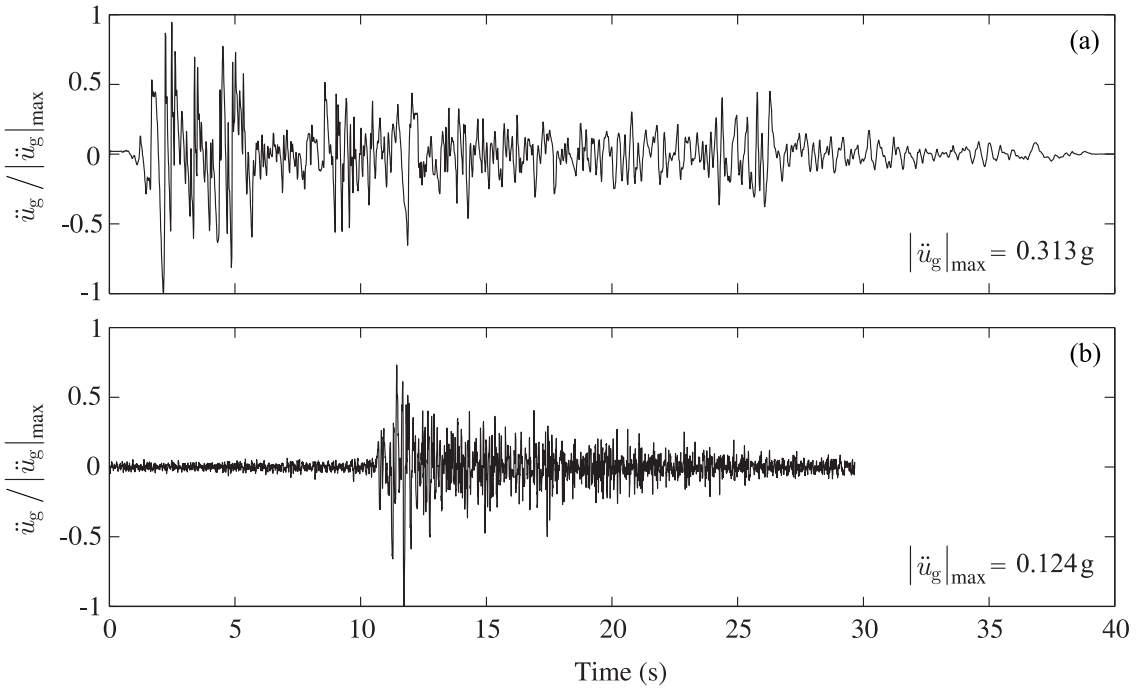

Figure 4.9 Ground motions considered : (a) Horizontal acceleration component of Imperial Valley earthquake (1940) at El Centro ; (b) Horizontal acceleration component of Saguenay earthquake (1988) at La Malbaie.

rigid wall is located at a distance less than $3H_{\mathrm{w}}^{(2)}$. We observe that the dynamic response of system B is however affected when the moving rigid wall boundary condition located at a distance $L_{\mathrm{w}}^{(1)} = 0.5\,H_{\mathrm{w}}^{(1)}$ is replaced by a non-disturbed boundary condition.

For analysis types I to IV, the CPU times that were required to compute time-history displacements at point P of system B under El Centro earthquake are compared for illustration purposes. The same time step of 0.005 s was used and 8 horizontal structural modes were included in the response. Only the time-history displacements at point P were saved for maximum execution speed. The CPU times were obtained using one core of a 2.0 GHz Intel® Core™ 2 Duo Processor T6400. Computations were performed under the following considerations :

- For analysis types I and II : Modeling and post-processing are ignored in the CPU time, as well as the added mass computations for Analysis type II.
- For analysis type III and IV : Modeling and post-processing of the modal analysis of the structure are ignored in the CPU time, while the finite element modal analysis needed to retrieve dynamic properties of the structure are included. MATLAB [23] was used to run analysis types III and IV.

The obtained CPU times are presented in Table 4.2. We clearly see the effectiveness of simplified procedures such as analysis type II and IV with almost instantaneous execution times. The proposed simplified method, i.e. analysis type IV, is shown to be even faster than the Westergaard added mass solution, i.e. analysis type II. Furthermore, the new simplified approach allows a more refined prediction of the dynamic response of structure-water systems as it accounts for structural and soil flexibility, which are neglected parameters in Westergaard's formulation.

Table 4.2 also shows that the proposed analytical formulation, i.e. analysis type III, is less CPU time consuming than the finite element method, i.e. analysis type I. This new analytical formulation constitutes then an interesting practical alternative considering the high expertise required and fluid-structure modeling complexities generally involved when using advanced finite element software.

Table 4.2 CPU times for analysis types I to IV.

Analysis type	I	II	III	IV
CPU Time (s)	1114.6	36.6	748.8	4.5

4.6 Conclusions

In this paper, we developed and validated an original analytical formulation to study wall-type structures with vertical or slightly inclined faces, vibrating in contact with water on one or both sides. The proposed method accounts for structure's flexibility, soil flexibility, varying water levels and boundary conditions corresponding to : (i) semi-infinite water domains, or (ii) finite water domains delimited by rigid walls. The proposed analytical formulation was then used to develop a simplified procedure for practical assessment of the vibration periods and seismic response of structure-water systems including higher mode effects. We first proved that the vibration frequencies of a structure-water system can be obtained by solving a simple second order polynomial equation. We also investigated the effect of boundary conditions at the end water domains, and we showed that : (i) for a structure-water system in contact with a semi-infinite incompressible water domain, only a finite water domain truncated by a fixed wall boundary condition at twice water domain height needs to be modeled, thus allowing a considerable gain of time when using finite elements ; (ii) for a structure-water system in contact with a finite incompressible water domain with a length less than three times its height, the effect of the end moving rigid boundary condition should be taken into account. If a structure in contact with a semi-infinite water domain or a finite water domain of

length longer than tree times its height, closed-form expressions were provided to determine hydrodynamic pressure distributions exerted on the structure. To assess the efficiency and accuracy of the proposed techniques, several analysis types were applied to structure-water systems with different configurations, including the effect of massless flexible soil foundation. The methods were validated against classical Westergaard added mass formulation as well as more advanced finite element techniques. The proposed approach presents a significant advantage over conventional Westergaard's added-mass formulation, namely because it can directly account for the flexibility of the structure and its soil foundation, as well as a finite extent of water domain, while Westergaard's solution assumes that both the structure and its foundation are rigid and that the water domain is semi-infinite. The following conclusions could be drawn from the comparison of the period ratios and hydrodynamic pressure profiles obtained from the different analyses : (i) the proposed simplified procedure give excellent period predictions for the first and higher vibration modes, (ii) an excellent agreement is obtained when comparing hydrodynamic profiles obtained using the proposed analytical and simplified methods to those from advanced finite elements, (iii) the proposed analytical and simplified techniques account appropriately for structure and soil flexibility as well as higher mode effects, all parameters that were shown to affect significantly the magnitude and distribution of hydrodynamic loads in a manner that generally differs from classical added-mass solutions. The seismic response of the structure-water systems subjected to typical low and high frequency earthquakes was also examined, and the proposed analytical and simplified methods gave an excellent agreement when compared to finite element solutions including fluid-structure interaction capabilities. In addition, the proposed methods performed within low execution times, namely the simplified procedure. Finally, we illustrated throughout the paper that the proposed techniques constitute interesting alternatives to conventional methods, and that they can be efficiently implemented in simplified and practical earthquake analysis of the structure-water systems.

Acknowledgements

The authors would like to acknowledge the financial support of the Natural Sciences and Engineering Research Council of Canada (NSERC) and the Quebec Fund for Research on Nature and Technology (FQRNT).

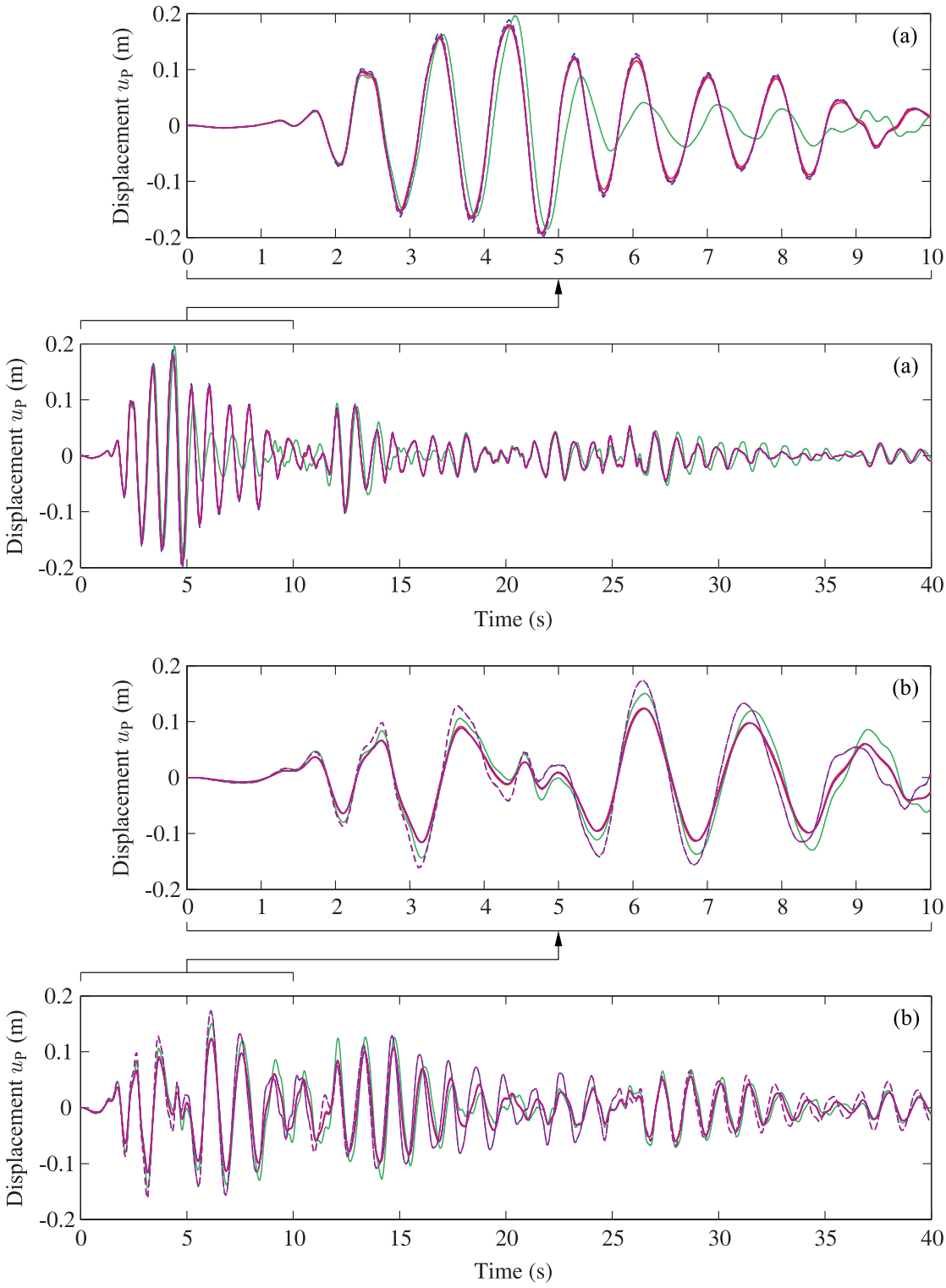

Figure 4.10 Time-history of relative displacement at point P under El Centro earthquake : (a) System A ; (b) System B. Continuous lines : — Analysis type I ; — Analysis type II ; — Analysis type III ; — Analysis type IV. Dotted lines : – – Analysis type III* ; – – Analysis type IV*.

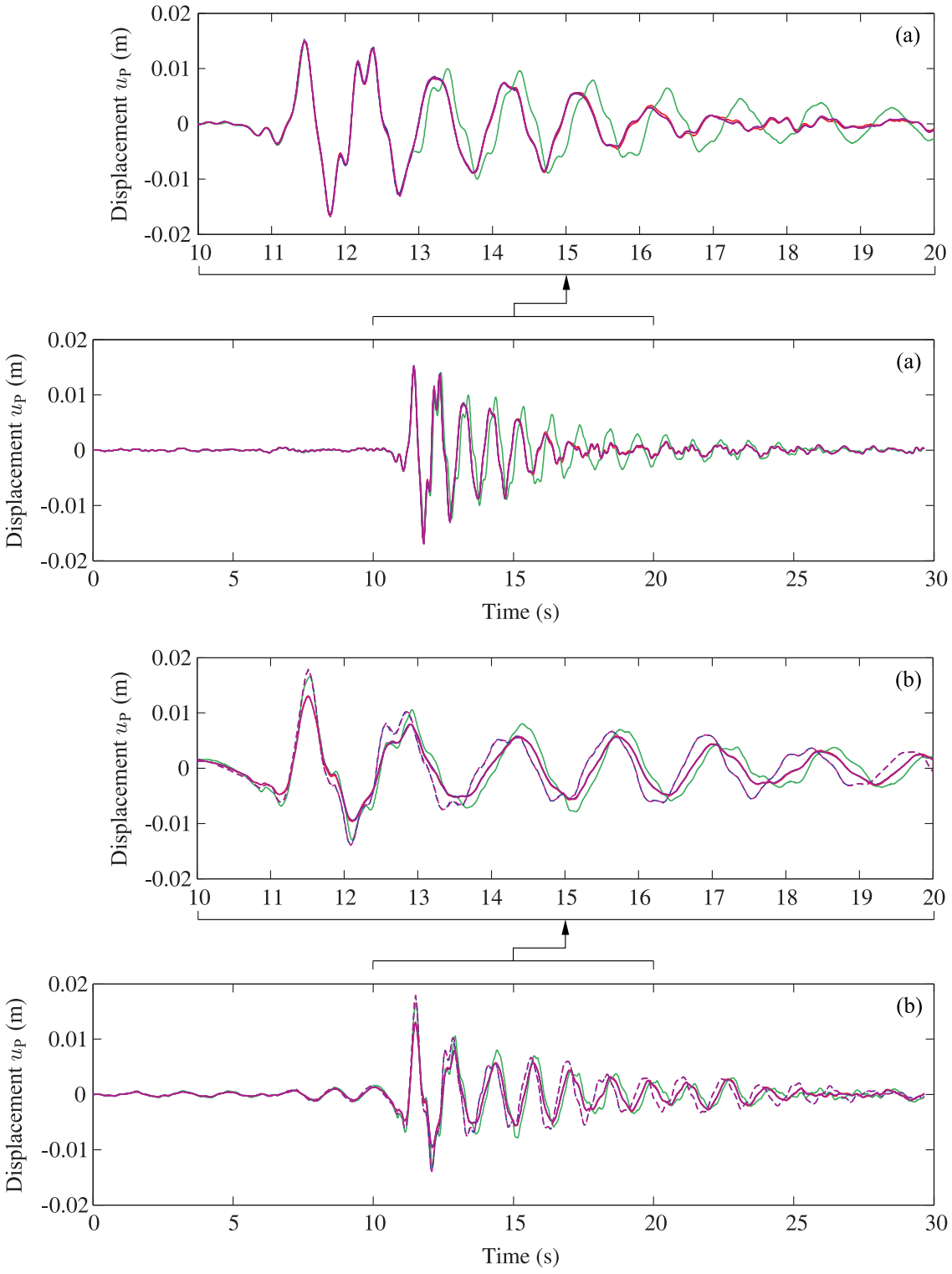

Figure 4.11 Time-history of relative displacement at point P under Saguenay earthquake : (a) System A ; (b) System B. Continuous lines : — Analysis type I ; — Analysis type II ; — Analysis type III ; — Analysis type IV. Dotted lines : – – Analysis type III* ; – – Analysis type IV*.

References

[1] H.M. Westergaard, Water pressures on dams during earthquakes, Transactions, ASCE 98 (1933) 418–472.

[2] US Army corps of Engineers. Engineering and Design - Gravity Dam Design. Report No. EM 1110-2-2200, 1995.

[3] US Army corps of Engineers.Engineering and Design - Time-History Dynamic Analysis of Concrete Hydraulic Structures. Report No. EM 1110-2-6051, 2003.

[4] FERC (Federal Energy Regulatory Commission). Engineering guidelines for evaluation of hydropower projects – Draft Chapter III Gravity Dams. Federal Energy Regulatory Commission, Office of Energy Projects, Division of Dam Safety and Inspections, Washington DC, USA ; 2000.

[5] Canadian Dam Association (CDA). Dam safety guidelines. Edmonton, Alberta ; 1999.

[6] USBR (United States Bureau of Reclamation). Design of small dams. Denver, Colorado ; 1987.

[7] A.K. Chopra, Earthquake response of concrete gravity dams. Report No. UCB/EERC-70/01, University of California, Berkeley, California, 1970.

[8] B.F. Chen, The significance of earthquake-induced dynamic forces in coastal structures design, Ocean Engineering 22 (1995) 47–65.

[9] B.F. Chen, Dynamic responses of coastal structures during earthquakes including sediment-sea-structure interaction, Soil Dynamics and Earthquake Engineering 20 (2000) 445–467.

[10] G. Fenves, A.K. Chopra, Earthquake analysis and response of concrete gravity dams. Report No. UCB/EERC-84/10, University of California, Berkeley, California, 1984.

[11] N. Bouaanani, F.Y. Lu, Assessment of potential-based fluid finite elements for seismic analysis of dam–reservoir systems, Journal of Computers and Structures 87 (2009) 206–224.

[12] P.H. Liu, A. Cheng, Boundary solutions for fluid-structure interaction, Journal of Hydraulic Engineering, ASCE 110 (1984) 51–64.

[13] K.L. Fok, J.F. Hall, A.K. Chopra, EACD-3D, a computer program for three-dimensional earthquake analysis of concrete dams. Report No. UCB/EERC-86/09, University of California, Berkeley, California, 1986.

[14] C.S. Tsai, G.C. Lee, Arch dam-fluid interactions : by FEM-BEM and substructure concept, International Journal of Numerical Methods in Engineering 24 (1987) 2367–2388.

[15] J.L. Humar, A.M. Jablonski, Boundary element reservoir model for seismic analysis of gravity dams, Earthquake Engineering and Structural Dynamics 16 (1988) 1129–1156.

[16] O. Maeso, J.J. Aznarez, J. Dominguez, Three-dimensional models of reservoir sediment and effects on the seismic response of arch dams, Earthquake Engineering and Structural Dynamics 33 (2004) 1103–1123.

[17] J.S. Wu, C.T. Chen, An exact solution for the natural frequencies and mode shapes of an immersed elastically restrained wedge beam carrying an eccentric tip mass with mass moment of inertia, Journal of Sound and Vibration 286 (2005) 549–568.

[18] J.T. Xing, Natural vibration of two-dimensional slender structure–water interaction systems subject to Sommerfeld radiation condition, Journal of Sound and Vibration 308 (2007) 67–79.

[19] B. Miquel, N. Bouaanani, Simplified evaluation of the vibration period and seismic response of gravity dam-water systems, Journal of Engineering Structures 32 (2010) 2488–2502.

[20] S.S. Saini, P. Bettess, O.C. Zienkiewicz, Coupled hydrodynamic response of concrete gravity dams using finite and infinite elements, Earthquake Engineering and Structural Dynamics 6 (1978) 363–374.

[21] R.D. Blevins, Formulas for natural frequency and mode shape, Kriger publishing Company, Florida, 1984.

[22] N. Bouaanani, C. Perrault, Practical formulas for frequency domain analysis of earthquake-induced dam-reservoir interaction, ASCE Journal of Engineering Mechanics 136 (2010) 107–119.

[23] MATLAB ®. The Mathworks, Inc., Natick, MA, USA, 2011.

[24] ADINA Theory and Modeling Guide. Report ARD 10-7. ADINA R & D, Inc., 2010.

Appendix A

For practical programming, this appendix proposes expressions to separate the real and imaginary parts of the frequency dependent generalized coordinates $\tilde{Z}_j$, $j=1\ldots N_\mathrm{s}$. Introducing the following notation

$$B_j^{(0)} = -L_j + \Gamma_j(\eta_1,\eta_2) \tag{4.A.1}$$

$$B_j^{(1)} = M_j + \vartheta_{j,\,j}(\eta_1,\eta_2) \tag{4.A.2}$$

the generalized coordinate for a fundamental mode analysis given by Eq. (4.38) can be decomposed as

$$\bar{Z}_1(\omega) = \frac{B_1^{(0)}\left(\omega_1^2\,M_1 - \omega^2\,B_1^{(1)}\right)}{\left(\omega_1^2\,M_1 - \omega^2\,B_1^{(1)}\right)^2 + \left(\mu\,\omega_1^2\,M_1\right)^2} - \mathrm{i}\frac{\mu\,\omega_1^2\,B_1^{(0)}\,M_1}{\left(\omega_1^2\,M_1 - \omega^2\,B_1^{(1)}\right)^2 + \left(\mu\,\omega_1^2\,M_1\right)^2} \tag{4.A.3}$$

If $N_\mathrm{s}=2$, the generalized coordinates defined in Eqs. (4.39) and (4.40) can be expressed as

$$\bar{Z}_1(\omega) = \left\{\frac{V_2^{(1)}(\omega)V_2^{(2)}(\omega) - V_2^{(3)}V_2^{(4)}(\omega)}{\left[V_2^{(2)}(\omega)\right]^2 + \left[V_2^{(4)}(\omega)\right]^2}\right\} - \mathrm{i}\left\{\frac{V_2^{(1)}(\omega)V_2^{(4)}(\omega) + V_2^{(3)}V_2^{(2)}(\omega)}{\left[V_2^{(2)}(\omega)\right]^2 + \left[V_2^{(4)}(\omega)\right]^2}\right\} \tag{4.A.4}$$

$$\bar{Z}_2(\omega) = -\left\{\frac{V_2^{(2)}(\omega)V_2^{(5)}(\omega) + V_2^{(6)}V_2^{(4)}(\omega)}{\left[V_2^{(2)}(\omega)\right]^2 + \left[V_2^{(4)}(\omega)\right]^2}\right\} + \mathrm{i}\left\{\frac{V_2^{(4)}(\omega)V_2^{(5)}(\omega) - V_2^{(6)}V_2^{(2)}(\omega)}{\left[V_2^{(2)}(\omega)\right]^2 + \left[V_2^{(4)}(\omega)\right]^2}\right\} \tag{4.A.5}$$

Finally, if $N_\mathrm{s}>2$, the simplified formulation for generalized coordinates given by Eqs. (4.41) and (4.42) can be expressed as

$$\tilde{Z}_1(\omega) = \left\{\frac{V_2^{(1)}(\omega)V_2^{(2)}(\omega) - V_2^{(3)}V_2^{(4)}(\omega)}{\left[V_2^{(2)}(\omega)\right]^2 + \left[V_2^{(4)}(\omega)\right]^2}\right\} - \mathrm{i}\left\{\frac{V_2^{(1)}(\omega)V_2^{(4)}(\omega) + V_2^{(3)}V_2^{(2)}(\omega)}{\left[V_2^{(2)}(\omega)\right]^2 + \left[V_2^{(4)}(\omega)\right]^2}\right\} \tag{4.A.6}$$

$$\tilde{Z}_j(\omega) = -\left\{\frac{V_j^{(2)}(\omega)V_j^{(5)}(\omega) + V_j^{(6)}V_j^{(4)}(\omega)}{\left[V_j^{(2)}(\omega)\right]^2 + \left[V_j^{(4)}(\omega)\right]^2}\right\} + \mathrm{i}\left\{\frac{V_j^{(4)}(\omega)V_j^{(5)}(\omega) - V_j^{(6)}V_j^{(2)}(\omega)}{\left[V_j^{(2)}(\omega)\right]^2 + \left[V_j^{(4)}(\omega)\right]^2}\right\}$$

$$\text{for } j = 2\ldots N_\mathrm{s} \tag{4.A.7}$$

in which

$$V_j^{(1)}(\omega) = \omega^2 \left[B_{j-1}^{(0)} \, B_j^{(1)} - B_j^{(0)} \, \vartheta_{j-1,j}(\eta_1, \eta_2) \right] - B_{j-1}^{(0)} \, {\omega_j}^2 \, M_j \tag{4.A.8}$$

$$V_j^{(2)} = M_{j-1} \, M_j \, {\omega_{j-1}}^2 \, {\omega_j}^2 \left(\mu^2 - 1 \right) + \omega^2 \left[{\omega_{j-1}}^2 \, M_{j-1} \, B_j^{(1)} + {\omega_j}^2 \, M_j \, B_{j-1}^{(1)} \right] + \omega^4 \left[{\vartheta_{1-1,j}}^2(\eta_1, \eta_2) - B_j^{(1)} \, B_{j-1}^{(1)} \right] \tag{4.A.9}$$

$$V_j^{(3)}(\omega) = \mu \, M_j \, {\omega_j}^2 \, B_{j-1}^{(0)} \tag{4.A.10}$$

$$V_j^{(4)}(\omega) = \mu \left[\omega^2 \left({\omega_j}^2 \, B_{j-1}^{(1)} \, M_j + {\omega_{j-1}}^2 \, B_j^{(1)} \, M_{j-1} \right) - 2 \, M_{j-1} \, M_j \, {\omega_{j-1}}^2 \, \omega_j^2 \right] \tag{4.A.11}$$

$$V_j^{(5)}(\omega) = \omega^2 \left[B_{j-1}^{(0)} \, \vartheta_{j-1,j}(\eta_1, \eta_2) - B_j^{(0)} \, B_{j-1}^{(1)} \right] + B_j^{(0)} \, {\omega_{j-1}}^2 \, M_{j-1} \tag{4.A.12}$$

$$V_j^{(6)} = \mu \, M_{j-1} \, {\omega_{j-1}}^2 \, B_j^{(0)} \tag{4.A.13}$$

Appendix B

In this appendix, we rewrite Eqs. (4.44) to (4.46) in a manner to isolate the effects of boundary conditions. Rearranging the sums in Eq. (4.44) yields

$$\theta_{j,j-1}(\eta_\ell) = \frac{4\rho_{\rm w}}{\pi}\,\eta_\ell^2 H_{\rm s}^2 \sum_{k=0}^{N_{\boldsymbol{\psi}_j}} \Bigg\{ \sum_{s=k}^{N_{\boldsymbol{\psi}_j}} \Bigg[(a_{j,k}\,a_{j-1,s} + a_{j-1,k}\,a_{j,s})\,\eta_\ell^k\,\eta_\ell^s \sum_{n=1}^{N_{\rm w}} \frac{f_k(n)\,f_s(n)}{(2n-1)}\widehat{X}_n^{(\ell)}(x_\ell) \Bigg] - a_{j,k}\,a_{j-1,k}\,\eta_\ell^{2k} \sum_{n=1}^{N_{\rm w}} \frac{f_k(n)^2}{(2n-1)}\widehat{X}_n^{(\ell)}(x_\ell) \Bigg\} \tag{4.B.14}$$

We show numerically that the sums from $n=1$ to $N_{\rm w}$ are convergent, and therefore Eq. (4.B.14) can be rewritten as

$$\theta_{j,j-1}(\eta_\ell) = \frac{4\rho_{\rm w}}{\pi}\,\eta_\ell^2 H_{\rm s}^2 \sum_{k=0}^{N_{\boldsymbol{\psi}_j}} \Bigg\{ \sum_{s=k}^{N_{\boldsymbol{\psi}_j}} \Big[(a_{j,k}\,a_{j-1,s} + a_{j-1,k}\,a_{j,s})\,\eta_\ell^k\,\eta_\ell^s\,A_{k,s}^{(\ell)} \Big] - a_{j,k}\,a_{j-1,k}\,\eta_\ell^{2k}\,A_{k,k}^{(\ell)} \Bigg\} \tag{4.B.15}$$

where $A_{k,s}^{(\ell)}$ is given by

$$A_{k,s}^{(\ell)} = \sum_{n=1}^{N_{\rm w}} \frac{f_k(n)\,f_s(n)}{(2n-1)} \coth\left[\frac{(2n-1)\,\pi\,L_{\rm w}^{(\ell)}}{2H_{\rm w}^{(\ell)}} \right] \tag{4.B.16}$$

for boundary conditions BC-I and BC-III, and

$$A_{k,s} = \sum_{n=1}^{N_{\rm w}} \frac{f_k(n)\,f_s(n)}{(2n-1)} \tag{4.B.17}$$

for a non-disturbed boundary condition BC-II. In a similar manner, we show that Eq. (4.45) can be rewritten as

$$\theta_{j,j}(\eta_\ell) = \frac{4\rho_{\rm w}}{\pi}\,\eta_\ell^2 H_{\rm s}^2 \sum_{k=0}^{N_{\boldsymbol{\psi}_j}} \left[2 \sum_{s=k}^{N_{\boldsymbol{\psi}_j}} \Big(a_{j,k}\,a_{j,s}\,A_{k,s}^{(\ell)}\,\eta_\ell^k\,\eta_\ell^s \Big) - a_{j,k}^2\,A_{k,k}^{(\ell)}\,\eta_\ell^{2k} \right] \tag{4.B.18}$$

Finally, we obtain by rearranging the sums in Eq. (4.46)

$$\gamma_j(\eta_\ell) = \frac{8\rho_{\rm w}}{\pi^2}\,\eta_\ell\,H_{\rm s}^2 \sum_{k=0}^{N_{\boldsymbol{\psi}_j}} a_{j,k}\,\eta_\ell^k \sum_{n=1}^{N_{\rm w}} \frac{(-1)^n\,f_k(n)}{(2n-1)^2} X_n^{(\ell)}(x_\ell) \tag{4.B.19}$$

We show numerically that the sum from $n=1$ to Nw is convergent, and therefore Eq. (4.B.19) can be simplified to

$$\gamma_j(\eta_\ell) = \frac{8\rho_{\mathrm{w}}}{\pi^2}\,\eta_\ell\,H_{\mathrm{s}}^2 \sum_{k=0}^{N_{\boldsymbol{\psi}_j}} a_{j,k}\,\eta_\ell^k\,B_k^{(\ell)} \tag{4.B.20}$$

where the coefficients $B_k^{(\ell)}$ are given by

$$B_k^{(\ell)} = \sum_{n=1}^{N_{\mathrm{w}}} \frac{(-1)^n\,f_k(n)}{(2n-1)^2} \left\{ \coth\left[\frac{(2n-1)\,\pi\,L_{\mathrm{w}}^{(\ell)}}{2H_{\mathrm{w}}^{(\ell)}}\right] - \sinh\left[\frac{(2n-1)\,\pi\,L_{\mathrm{w}}^{(\ell)}}{2H_{\mathrm{w}}^{(\ell)}}\right]^{-1} \right\} \tag{4.B.21}$$

for boundary condition BC-I,

$$B_k = \sum_{n=1}^{N_{\mathrm{w}}} \frac{(-1)^n\,f_k(n)}{(2n-1)^2} \tag{4.B.22}$$

for boundary condition BC-II, and

$$B_k^{(\ell)} = \sum_{n=1}^{N_{\mathrm{w}}} \frac{(-1)^n\,f_k(n)}{(2n-1)^2} \coth\left[\frac{(2n-1)\,\pi\,L_{\mathrm{w}}^{(\ell)}}{2H_{\mathrm{w}}^{(\ell)}}\right] \tag{4.B.23}$$

for boundary condition BC-III.

CHAPITRE 5

Article 3 : Efficient Earthquake Modal Analysis of Flexible Beam-Fluid Systems

Benjamin Miquel [1] **and Najib Bouaanani** [2]

Paper submitted to *Journal of Applied Mathematical Modelling*

Submitted 13 November 2011.

This paper proposes an efficient simplified method to determine the modal dynamic and earthquake response of coupled flexible beam-fluid systems and to evaluate their natural vibration frequencies. The methodology developed extends available analytical solutions for mode shapes and natural vibration frequencies of slender beams with various boundary conditions to include the effects of fluid-structure interaction. Simplified formulations are developed for various beam boundary conditions considering transverse interaction with one or two semi-infinite fluid domains. We show that the simplified procedure yields excellent results when compared to more advanced finite element analysis, independently of the number of modes, beam boundary conditions, and number of fluid domains. The numerical results obtained confirm the importance of accounting for fluid-structure interaction effects which could reduce by more than twice the fundamental vibration frequency of the dry beam. The proposed simplified method can be easily implemented in day-to-day practice, and the methodology proposed can be extended to other types of structures for which natural vibration frequencies and mode shapes can be evaluated using closed-form mathematical expressions.

1. Graduate Research Assistant, Department of Civil, Geological and Mining Engineering, École Polytechnique de Montréal, Montréal, QC H3C 3A7, Canada.

2. Associate Professor, Department of Civil, Geological and Mining Engineering, École Polytechnique de Montréal, Montréal, QC H3C 3A7, Canada
Corresponding author. E-mail : najib.bouaanani@polymtl.ca

5.1 Introduction

Several civil engineering and industrial applications involve the vibrations of beam-like structures in contact with water or fluid domains, including dams, navigation locks, quay walls, break-waters, offshore platforms, drilling risers, liquid storages, nuclear reactors, oil refineries, petrochemical plants, fuel storage racks, etc. This popular topic has attracted many researchers over the last decades and various approaches were proposed, varying from simplified to more complex analytical and numerical formulations. Neglecting structural flexibility, Westergaard [1] introduced the hydrodynamic added-mass concept and applied it to a dam-reservoir system, and later Jacobsen [2] and Rao [3] generalized the added-mass formulation to evaluate hydrodynamic effects on rigid circular and rectangular piers vibrating in water. Goto and Toki [4] and Kotsubo [5] evaluated the hydrodynamic pressures induced by harmonic motions on circular or elliptical cross-section cylindrical towers along rigid body and deformed mode shapes. Chopra [6, 7] showed that a dam's flexibility influences significantly its interaction with the impounded reservoir, and consequently the overall dynamic and seismic response. Other studies also confirmed the importance of accounting for structural flexibility and fluid-structure interaction [8, 9, 10, 11]. Han and Xu [12] developed an analytical model to compute the modal properties of a slender flexible cylinder vibrating in water, and proposed a simplified added-mass formula to compute its natural frequencies. Other researchers studied the sensitivity of the hydrodynamic response of cantilever structures to various factors, such as : (i) a tip mass or inertia concentrated at one end [13, 14, 15, 16], (ii) a restrained boundary condition at the base of the beam [16, 17, 18], and (iii) non-uniformity of beam cross-section [16, 17, 19].

Most of the previous studies focused on cantilever structures surrounded by fluid. Work on beam-like structures interacting with 2D semi-infinite fluid domains was mainly related to dam monoliths impounding water reservoirs, while fewer researchers investigated the behavior of slender beams subjected to hydrodynamic loading of the latter type. Xing et al. [20], Zhao et al. [21] and Xing [22] developed analytical formulations to examine the dynamic response of a cantilever flexible beam interacting with a 2D semi-infinite water domain, and discussed the effects of various boundary conditions of the fluid domain. Nasserzare et al. [23] proposed a procedure to extract the natural frequencies and modes of a dry structure from vibrational data containing fluid-structure interaction effects, and they applied the methodology to a beam-water system. De Souza and Pedroso [24] developed a finite element procedure to determine the coupled dynamic response of a Bernoulli beam interacting with a 2D acoustical cavity, and they validated the vibration frequencies and modes obtained by comparing to other finite element and analytical solutions.

The present paper is motivated by the need to develop simplified analytical expressions extending results from classical vibration beam theory to include the effects of 2D hydrodynamic forces on one or both sides of a vibrating beam. The majority of the previous work and other relevant literature addressed hydrodynamic effects on cantilever beams, fully clamped or partially restrained at the base, and little attention has been given to other boundary conditions such as pinned or sliding supports. Most of the previous studies also focused on the determination of the modal properties of a vibrating beam interacting with a fluid, while less concern has been devoted to the time evolution of beam's earthquake response indexes such as displacements, shear forces, and bending moments. These restrictions will be addressed in this paper.

5.2 Modal dynamic response of a beam interacting with a fluid

5.2.1 Basic assumptions and notation

Fig. 5.1 shows a slender beam of height H vibrating in contact with fluid on one or both sides. We adopt a Cartesian coordinate system with origin at the base of the beam, a horizontal axis x and a vertical axis y coincident with the axis of symmetry of the beam. The infinite fluid domains have a rectangular geometry with constant height equal to that of the beam. We denote by Λ_{f} the number of fluid domains in contact with the beam, and by left and right side fluid domains those extending from the beam towards negative and positive x directions, respectively. Both configurations illustrated in Figs. 5.1 (a) and (b) will be investigated here, i.e. $\Lambda_{\mathrm{f}} = 1$ and $\Lambda_{\mathrm{f}} = 2$, respectively. The boundary conditions of the beam can be Clamped-Free (CF) as shown in Fig. 5.1 or Clamped-Pinned (CP), Clamped-Sliding (CS), Clamped-Clamped (CC) or Pinned-Pinned (PP) as illustrated in Fig. 5.2. We also assume that : (i) the beam is slender so that only flexural deformations are considered ; (ii) the beam is made of a linear, homogenous, and isotropic elastic material ; (iii), only deflections normal to the undeformed beam axis are included ; (iii) the fluid is considered incompressible and inviscid, with its motion irrotational and limited to small amplitudes, and (iv) gravity surface waves and non-convective effects are neglected.

5.2.2 Governing equations

We assume that the beam-fluid system is subjected to a unit harmonic free-field horizontal ground motion $\ddot{u}_{\mathrm{g}}(t) = \mathrm{e}^{\mathrm{i}\omega t}$. Based on previous studies [25, 26, 27] and considering N_{s} beam mode shapes, we show that the coupling between beam vibrations and fluid hydrodynamic

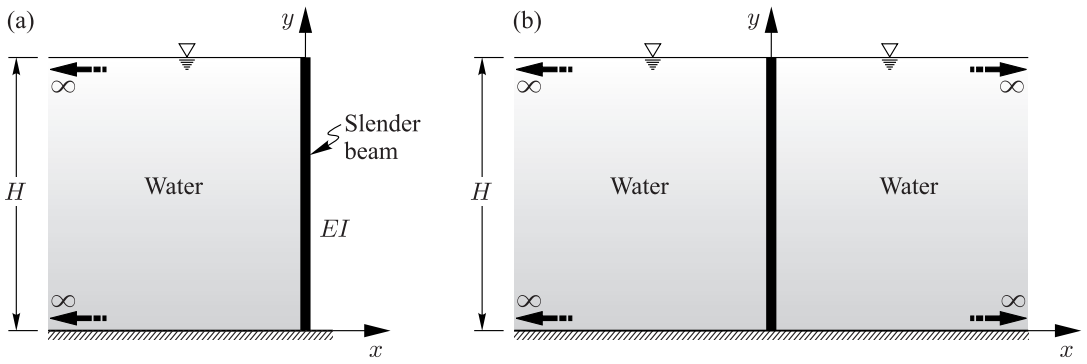

Figure 5.1 Slender beam vibrating in contact with a fluid acting on : (a) one side, (b) both sides.

pressure yields to a system of equations

$$\bar{\mathbf{S}}\,\bar{\mathbf{Z}} = \bar{\mathbf{Q}} \tag{5.1}$$

where $\bar{\mathbf{Z}}$ is a vector of generalized coordinates $\bar{Z}_j(\omega)$, $j=1\ldots N_\mathrm{s}$, and where the elements of matrix $\bar{\mathbf{S}}$ and vector $\bar{\mathbf{Q}}$ are obtained for $j=1\ldots N_\mathrm{s}$ and $m=1\ldots N_\mathrm{s}$ as

$$\bar{S}_{j,m}(\omega) = \big[-\omega^2 + (1+\mathrm{i}\,\eta_\mathrm{s})\,\omega_j^2\big]\,M_j\,\delta_{j,m} - \Lambda_\mathrm{f}\,\omega^2 \int_0^H \bar{p}_j(y,\omega)\,\psi_m(y)\,\mathrm{d}y \tag{5.2}$$

and

$$\bar{Q}_m = -L_m - \Lambda_\mathrm{f} \int_0^H \bar{p}_0(y,\omega)\,\psi_m(y)\,\mathrm{d}y \tag{5.3}$$

in which

- $\bar{p}_0$ is the FRF for hydrodynamic pressure exerted on the left side of the beam due to its rigid body motion ;
- $\bar{p}_j$ is the FRF for hydrodynamic pressure exerted on the left side of the beam due to its horizontal acceleration $\psi_j(y)$ with ψ_j being the x–component of the $j^{\,\mathrm{th}}$ vibration mode shape $\boldsymbol{\psi}_j$ of the beam without the fluid domain, i.e. $\Lambda_\mathrm{f}=0$;
- ω_j is the natural frequency corresponding to the $j^{\,\mathrm{th}}$ beam vibration mode shape $\boldsymbol{\psi}_j$;
- η_s is an assumed constant hysteretic damping ratio ;

– M_j and L_m are respectively the generalized mass and force given by

$$M_j = \mu_\mathrm{s} \int_0^H \left[\psi_j(y)\right]^2 \mathrm{d}y = \mu_\mathrm{s}\, H \int_0^1 \left[\bar{\psi}_j(\bar{y})\right]^2 \mathrm{d}\bar{y} = \mu_\mathrm{s}\, H\, M_j^* \tag{5.4}$$

$$L_m = \mu_\mathrm{s} \int_0^H \psi_m(y)\, \mathrm{d}y = \mu_\mathrm{s}\, H \int_0^1 \bar{\psi}_m(\bar{y})\, \mathrm{d}\bar{y} = \mu_\mathrm{s}\, H\, L_m^* \tag{5.5}$$

in which μ_s is the beam's mass per unit height and $\bar{\psi}$ is a function resulting from the introduction of the change of variable $\bar{y}=y/H$ into ψ_j.

Performing a change of integration variable as in Eqs. (5.4) and (5.5), and expressing hydrodynamic pressures as in [26, 27], we show that the integrals in Eqs. (5.2) and (5.3), which represent the effects of beam-fluid dynamic interaction, can be expressed as the sum of N_f terms corresponding each to a fluid domain mode n

$$\int_0^H \bar{p}_j(y)\, \psi_j(y)\, \mathrm{d}y = \frac{4\rho_\mathrm{f}}{\pi}\, H^2 \sum_{n=1}^{N_\mathrm{f}} \frac{\left(I_{j,n}\right)^2}{(2n-1)} = \frac{4\rho_\mathrm{f}}{\pi}\, H^2\, \theta_{j,j}^* \tag{5.6}$$

$$\int_0^H \bar{p}_j(y)\, \psi_m(y)\, \mathrm{d}y = \frac{4\rho_\mathrm{f}}{\pi}\, H^2 \sum_{n=1}^{N_\mathrm{f}} \frac{I_{j,n}\, I_{m,n}}{(2n-1)} = \frac{4\rho_\mathrm{f}}{\pi}\, H^2\, \theta_{j,m}^* \tag{5.7}$$

$$\int_0^H \bar{p}_0(y)\, \psi_m(y)\, \mathrm{d}y = -\frac{8\rho_\mathrm{f}}{\pi^2}\, H^2 \sum_{n=1}^{N_\mathrm{f}} \frac{(-1)^n I_{m,n}}{(2n-1)^2} = -\frac{8\rho_\mathrm{f}}{\pi^2}\, H^2\, \Gamma_m^* \tag{5.8}$$

where the parameters $I_{\ell,n}$ are obtained for $\ell=1\ldots N_\mathrm{s}$ and $n=1\ldots N_\mathrm{f}$ as

$$I_{\ell,n} = \int_0^1 \bar{\psi}_\ell(\bar{y})\, \cos\left[\frac{(2n-1)\,\pi}{2}\, \bar{y}\right]\, \mathrm{d}\bar{y} \tag{5.9}$$

Substituting the frequency independent hydrodynamic pressures given in Eqs. (5.6) to (5.8) into the system of equations (5.1), we show that Eqs. (5.2) and (5.3) can be rewritten under a more compact form

$$\bar{S}_{j,m}(\omega) = \left[-\omega^2 + (1+\mathrm{i}\,\eta_\mathrm{s})\,\omega_j^2\right] M_j\, \delta_{j,m} - \frac{4\rho_\mathrm{f}}{\pi}\, \Lambda_\mathrm{f}\, \omega^2\, H^2\, \theta_{j,m}^* \tag{5.10}$$

$$\bar{Q}_m = -L_m + \frac{8\rho_\mathrm{f}}{\pi^2}\, \Lambda_\mathrm{f}\, H^2\, \Gamma_m^* \tag{5.11}$$

We clearly see that the ingredients of the system of equations (5.1) require the availability of beam mode shapes. Such mode shapes are available for slender beams [28] and are reviewed

in Appendix A as a function of the various boundary conditions illustrated in Fig. 5.2. Using these beam mode shapes, we show that the integrals in Eqs. (5.6) to (5.8) and corresponding series are convergent.

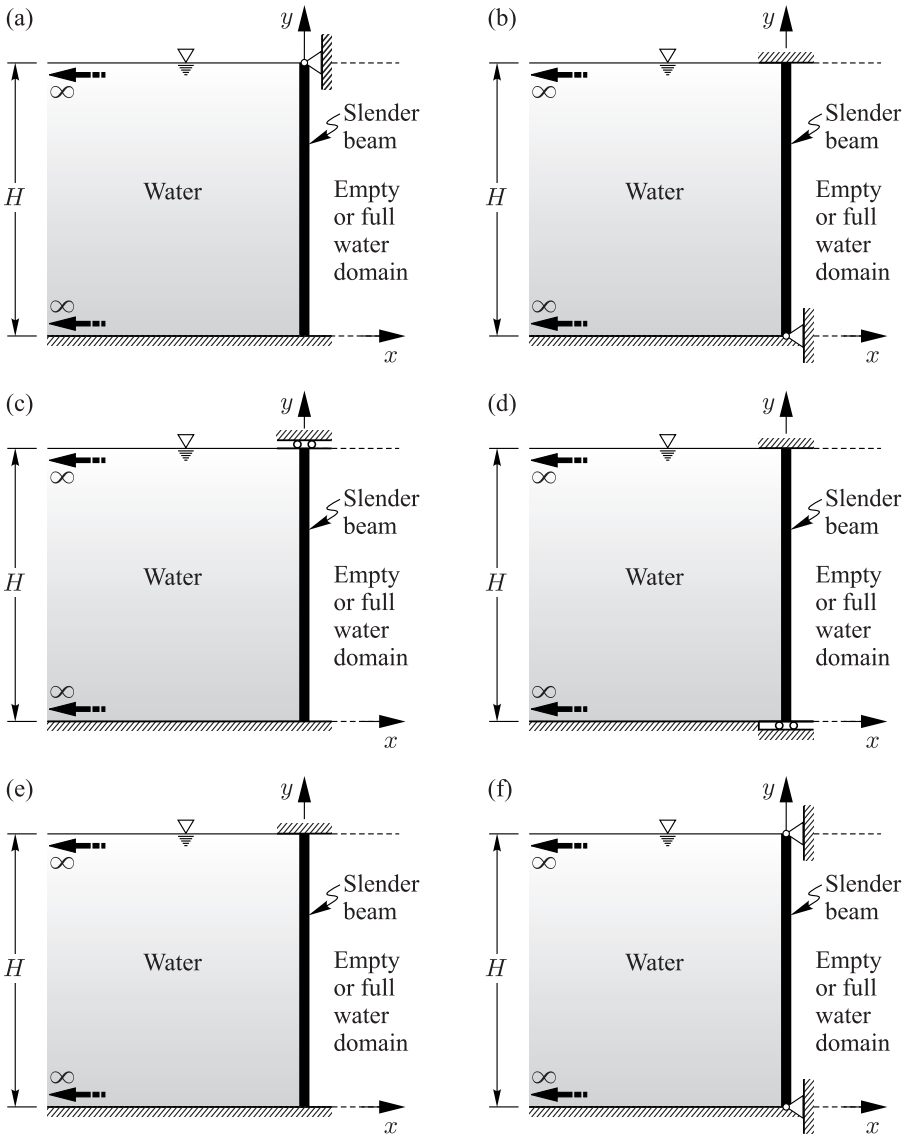

Figure 5.2 Studied beams-fluid configurations : (a) Clamped-Pinned ; (b) Pinned-Clamped ; (c) Clamped-Sliding ; (d) Sliding-Clamped ; (e) Clamped-Clamped ; (f) Pinned-Pinned.

5.2.3 Frequency to time response solutions

To obtain the dynamic frequency response of the studied beam-fluid systems, the system of analytical equations (5.1) has first to be solved for the vector $\bar{\mathbf{Z}}$ of complex-valued genera-

lized coordinates considering frequencies ω in the range of interest. Standard matrix analysis numerical schemes could be used for that purpose. Instead, a practical simplified procedure is proposed hereafter to expedite the solution process. We show that if only one beam mode is included in the analysis, i.e. fundamental mode analysis, the generalized coordinate $\bar{Z}_1$ is given by

$$\bar{Z}_1(\omega) = \frac{\bar{Q}_1}{\bar{S}_{1,1}(\omega)} \tag{5.12}$$

If two beam modes are to be included, the generalized coordinates can be obtained as

$$\bar{Z}_1(\omega) = \frac{\bar{S}_{2,2}(\omega)\,\bar{Q}_1 - \bar{S}_{1,2}(\omega)\,\bar{Q}_2}{\bar{S}_{1,1}(\omega)\bar{S}_{2,2}(\omega) - \bar{S}^2_{1,2}(\omega)} \tag{5.13}$$

$$\bar{Z}_2(\omega) = \frac{\bar{S}_{1,1}(\omega)\,\bar{Q}_2 - \bar{S}_{1,2}(\omega)\,\bar{Q}_1}{\bar{S}_{1,1}(\omega)\bar{S}_{2,2}(\omega) - \bar{S}^2_{1,2}(\omega)} \tag{5.14}$$

If higher mode effects are to be included in the analysis, i.e. $N_\mathrm{s} \geqslant 3$, we show that the generalized coordinates can be approximated by uncoupling the system of equations (5.1) as follows

$$\bar{Z}_1(\omega) \approx \frac{\bar{S}_{2,2}(\omega)\,\bar{Q}_1 - \bar{S}_{1,2}(\omega)\,\bar{Q}_2}{\bar{S}_{1,1}(\omega)\bar{S}_{2,2}(\omega) - \bar{S}^2_{1,2}(\omega)} \tag{5.15}$$

$$\bar{Z}_j(\omega) \approx \frac{\bar{S}_{j-1,j-1}(\omega)\,\bar{Q}_j - \bar{S}_{j-1,j}(\omega)\,\bar{Q}_{j-1}}{\bar{S}_{j-1,j-1}(\omega)\bar{S}_{j,j}(\omega) - \bar{S}^2_{j-1,j}(\omega)} \qquad \text{for } j = 2 \ldots N_\mathrm{s} \tag{5.16}$$

It can be seen from Eqs. (5.13) to (5.16) that the determination of the generalized coordinates $\bar{Z}_j$ for $j = 1 \ldots N_\mathrm{s}$ requires the computation of natural frequencies ω_j and parameters M^*_j, L^*_j, Γ^*_j, $\theta^*_{j,j}$ and $\theta^*_{j,j+1}$ as defined in Eqs. (5.4) to (5.8). For each of beam configurations CF, CP, CS, and CC, the values of parameters β_j provided in Table 5.A1 are computed using high precision arithmetic for the first ten beam modes, $j = 1 \ldots 10$, and are given in Tables 5.1 to 5.6. The natural frequencies ω_j can then be obtained as [28]

$$\omega_j = \frac{\beta_j^2}{H^2}\sqrt{\frac{EI}{\mu_\mathrm{s}}} \qquad \text{for } j = 1 \ldots N_\mathrm{s} \tag{5.17}$$

where E is the modulus of elasticity of the beam and I the area moment of inertia of the beam about the neutral axis of bending. The obtained values of β_j, $j = 1 \ldots 10$, are also used to compute parameters M^*_j, L^*_j, Γ^*_j, $\theta^*_{j,j}$ and $\theta^*_{j,j+1}$ and the results are also shown Tables 5.1 to 5.6 for boundary conditions CF, CP, CS, and CC, respectively. For beam configuration

PP, we show that these parameters can be expressed for $j=1\ldots N_{\rm s}$ as

$$\beta_j = \pi j\,; \qquad M_j^* = \frac{1}{2}\,; \qquad L_j^* = -\frac{(-1)^j-1}{\pi j} \tag{5.18}$$

$$\Gamma_j^* = -\frac{1}{\pi j}\left\{\mathcal{G} + \sum_{q=0}^{\infty}\frac{(-1)^q}{\left[4j^2-(1+2q)^2\right]}\right\} \tag{5.19}$$

$$\theta_{j,j}^* = \frac{1}{8\pi^2 j^2}\left\{\pi^2 j + 8\sum_{q=1}^{j}\frac{1}{(2q-1)} - 8j\sum_{q=0}^{\infty}\frac{1}{\left[1+2\,(j+q)\,\right]^2}\right\} \tag{5.20}$$

$$\theta_{j,j+1}^* = -\frac{1}{\pi^2 j\,(j+1)}\left[\frac{j^2}{(2j+1)^2} - \sum_{q=1}^{j}\frac{1}{(2q-1)}\right] \tag{5.21}$$

where $\mathcal{G}=0.915965...$ is the Catalan's constant [29]. The numerical values of these parameters are included in Table 5.7 for the first ten beam modes along beam configuration PP.

We note that for all beam configurations, special care should be exercised when computing these parameters for modes higher than ten. Such computations may indeed be affected by numerical cancelation, a phenomenon that can be circumvented by using a precision higher than the commonly used double precision [30]. For accurate results, higher precision should also be used to compute the parameters $\beta_j,\ j>10$ as was done in Tables 5.1 to 5.7 for the first ten beam modes.

As can be seen from Tables 5.1 to 5.7, the generalized mass parameter M_j^* is independent of the mode number j, therefore the subscript j can be omitted for simplicity and Eq. (5.4) can be rewritten as

$$M = \mu_{\rm s}\, H\, M^* \tag{5.22}$$

for all the modes $j=1\ldots N_{\rm s}$.

Once the generalized coordinates $\bar{Z}_j(\omega)$, $j=1\ldots N_{\rm s}$, are determined using the simplified method described above, the time-history responses along beam's height of transverse displacement u, transverse acceleration $\ddot{u}$, bending moment $\mathcal{M}$ and shear force $\mathcal{V}$ under the effect of an arbitrary ground acceleration $\ddot{u}_{\rm g}(t)$ of duration t_a, i.e. $0\leqslant t\leqslant t_a$, can be obtained as

$$u(y,t) = \sum_{j=1}^{N_{\rm s}}\psi_j(y)\,Z_j(t)\,; \qquad \ddot{u}(y,t) = \sum_{j=1}^{N_{\rm s}}\psi_j(y)\,\ddot{Z}_j(t) \tag{5.23}$$

$$\mathcal{M}(y,t) = EI\sum_{j=1}^{N_{\rm s}}Z_j(t)\frac{\partial^2\psi_j(y)}{\partial y^2}\,; \qquad \mathcal{V}(y,t) = EI\sum_{j=1}^{N_{\rm s}}Z_j(t)\frac{\partial^3\psi_j(y)}{\partial y^3} \tag{5.24}$$

Table 5.1 Modal parameters for Clamped-Free beam configuration and modes $j=1\ldots N_{\mathrm{s}}$.

Mode	β_j	M_j^*	L_j^*	Γ_j^*	$\theta_{j,j}^*$	$\theta_{j,j+1}^*=\theta_{j+1,j}^*$
$j=1$	1.87510407	1.0	0.78299176	-0.37664404	0.18737387	0.13892005
$j=2$	4.69409113	1.0	0.43393590	-0.45319253	0.25471037	0.10086234
$j=3$	7.85475744	1.0	0.25442530	-0.21267463	0.14743392	0.05443977
$j=4$	10.99554073	1.0	0.18189802	-0.17682233	0.10091027	0.03428706
$j=5$	14.13716839	1.0	0.14147084	-0.12338220	0.07599194	0.02378338
$j=6$	17.27875953	1.0	0.11574906	-0.11015798	0.06045054	0.01753889
$j=7$	20.42035225	1.0	0.09794150	-0.08674672	0.05001112	0.01352467
$j=8$	23.56194490	1.0	0.08488264	-0.07997338	0.04251850	0.01077358
$j=9$	26.70353756	1.0	0.07489644	-0.06687086	0.03690987	0.00893450
$j=10$	29.84513021	1.0	0.06701261	-0.06278742	0.03292094	–

Table 5.2 Modal parameters for Clamped-Pinned beam configuration and modes $j=1\ldots N_{\mathrm{s}}$.

Mode	β_j	M_j^*	L_j^*	Γ_j^*	$\theta_{j,j}^*$	$\theta_{j,j+1}^*=\theta_{j+1,j}^*$
$j=1$	3.92660231	1.0	0.86000091	-0.57463863	0.34894675	0.09636523
$j=2$	7.06858275	1.0	0.08263119	-0.22387192	0.18069842	0.05207102
$j=3$	10.21017612	1.0	0.33438600	-0.19610132	0.11733903	0.03252944
$j=4$	13.35176878	1.0	0.04387308	-0.12740364	0.08546839	0.02239573
$j=5$	16.49336143	1.0	0.20700531	-0.11747947	0.06663395	0.01644885
$j=6$	19.63495408	1.0	0.02983386	-0.08877191	0.05432145	0.01264531
$j=7$	22.77654674	1.0	0.14990040	-0.08379277	0.04569814	0.01005606
$j=8$	25.91813939	1.0	0.02260141	-0.06808364	0.03934902	0.00820841
$j=9$	29.05973205	1.0	0.11748951	-0.06510595	0.03449382	0.00684054
$j=10$	32.20132470	1.0	0.01819138	-0.05520717	0.03066917	–

Table 5.3 Modal parameters for Pinned-Clamped beam configuration and modes $j=1\ldots N_{\mathrm{s}}$.

Mode	β_j	M_j^*	L_j^*	Γ_j^*	$\theta_{j,j}^*$	$\theta_{j,j+1}^*=\theta_{j+1,j}^*$
$j=1$	3.92660231	1.0	0.86000091	-0.65008940	0.42517390	-0.05350698
$j=2$	7.06858275	1.0	0.08263119	0.07630378	0.16093621	-0.02220990
$j=3$	10.21017612	1.0	0.33438600	-0.18764735	0.11404365	-0.01510174
$j=4$	13.35176878	1.0	0.04387308	0.06077168	0.07776274	-0.01002847
$j=5$	16.49336143	1.0	0.20700531	-0.10437260	0.06298601	-0.00757148
$j=6$	19.63495408	1.0	0.02983386	0.04753510	0.05001431	-0.00575587
$j=7$	22.77654674	1.0	0.14990040	-0.07134176	0.04301687	-0.00464037
$j=8$	25.91813939	1.0	0.02260141	0.03871677	0.03654159	-0.00376960
$j=9$	29.05973205	1.0	0.11748951	-0.05389831	0.03250732	-0.00316737
$j=10$	32.20132470	1.0	0.01819138	0.03258968	0.02867225	–

Table 5.4 Modal parameters for Clamped-Sliding beam configuration and modes $j=1\ldots N_{\mathrm{s}}$.

Mode	β_j	M_j^*	L_j^*	Γ_j^*	$\theta_{j,j}^*$	$\theta_{j,j+1}^*=\theta_{j+1,j}^*$
$j=1$	2.36502037	1.0	0.83086152	-0.43286636	0.22689237	0.14212399
$j=2$	5.49780392	1.0	0.36376941	-0.42564792	0.25076544	0.08206427
$j=3$	8.63937983	1.0	0.23149808	-0.16756711	0.12952877	0.04471813
$j=4$	11.78097245	1.0	0.16976527	-0.18178679	0.09818120	0.02975177
$j=5$	14.92256510	1.0	0.13402522	-0.10517937	0.07140046	0.02081033
$j=6$	18.06415776	1.0	0.11071648	-0.11405107	0.05910757	0.01569606
$j=7$	21.20575041	1.0	0.09431404	-0.07681828	0.04808430	0.01217325
$j=8$	24.34734307	1.0	0.08214446	-0.08275794	0.04176228	0.00981897
$j=9$	27.48893572	1.0	0.07275727	-0.06056682	0.03589467	0.00805830
$j=10$	30.63052837	1.0	0.06531788	-0.06482811	0.03209558	–

Table 5.5 Modal parameters for Sliding-Clamped beam configuration and modes $j=1\ldots N_{\mathrm{s}}$.

Mode	β_j	M_j^*	L_j^*	Γ_j^*	$\theta_{j,j}^*$	$\theta_{j,j+1}^*=\theta_{j+1,j}^*$
$j=1$	2.36502037	1.0	0.83086152	-0.68350770	0.49079872	0.04802871
$j=2$	5.49780392	1.0	0.36376941	-0.17189508	0.16975665	0.01534789
$j=3$	8.63937983	1.0	0.23149808	-0.07913826	0.10157987	0.00743933
$j=4$	11.78097245	1.0	0.16976527	-0.04607007	0.07236825	0.00437216
$j=5$	14.92256510	1.0	0.13402522	-0.03038167	0.05617515	0.00287253
$j=6$	18.06415776	1.0	0.11071648	-0.02165278	0.04589287	0.00202983
$j=7$	21.20575041	1.0	0.09431404	-0.01627248	0.03878766	0.00150988
$j=8$	24.34734307	1.0	0.08214446	-0.01271013	0.03358532	0.00116674
$j=9$	27.48893572	1.0	0.07275727	-0.01022325	0.02961225	0.00092850
$j=10$	30.63052837	1.0	0.06531788	-0.00841489	0.02647907	–

Table 5.6 Modal parameters for Clamped-Clamped beam configuration and modes $j=1\ldots N_{\mathrm{s}}$.

Mode	β_j	M_j^*	L_j^*	Γ_j^*	$\theta_{j,j}^*$	$\theta_{j,j+1}^*=\theta_{j+1,j}^*$
$j=1$	4.73004074	1.0	0.83086152	-0.59868962	0.37372242	0.06778702
$j=2$	7.85320462	1.0	0.00000000	-0.13987318	0.15976063	0.03574881
$j=3$	10.99560784	1.0	0.36376941	-0.21855053	0.11879885	0.02488654
$j=4$	14.13716549	1.0	0.00000000	-0.09614570	0.08161727	0.01729534
$j=5$	17.27875966	1.0	0.23149808	-0.12945024	0.06695049	0.01322241
$j=6$	20.42035225	1.0	0.00000000	-0.07230322	0.05304073	0.01024567
$j=7$	23.56194490	1.0	0.16976531	-0.09122753	0.04583308	0.00832457
$j=8$	26.70353756	1.0	0.00000000	-0.05783192	0.03879983	0.00677682
$j=9$	29.84513021	1.0	0.13404389	-0.07018907	0.03439606	-0.00078197
$j=10$	32.98672286	1.0	0.00000000	-0.04927199	0.01919082	–

Table 5.7 Modal parameters for Pinned-Pinned beam configuration and modes $j=1\ldots N_\mathrm{s}$.

Mode	β_j	M_j^*	L_j^*	Γ_j^*	$\theta_{j,j}^*$	$\theta_{j,j+1}^*=\theta_{j+1,j}^*$
$j=1$	π	0.5	$-2/\pi$	-0.45071585	0.20264262	0.04503164
$j=2$	$2\,\pi$	0.5	0.00	-0.11925463	0.09006340	0.01981392
$j=3$	$3\,\pi$	0.5	$-2/(3\pi)$	-0.11251300	0.05613953	0.01139576
$j=4$	$4\,\pi$	0.5	0.00	-0.06569036	0.04028959	0.00749098
$j=5$	$5\,\pi$	0.5	$-2/(5\pi)$	-0.06362745	0.03123383	0.00533858
$j=6$	$6\,\pi$	0.5	0.00	-0.04530423	0.02541755	0.00401713
$j=7$	$7\,\pi$	0.5	$-2/(7\pi)$	-0.04431800	0.02138389	0.00314341
$j=8$	$8\,\pi$	0.5	0.00	-0.03456940	0.01843056	0.00253352
$j=9$	$9\,\pi$	0.5	$-2/(9\pi)$	-0.03399328	0.01617913	0.00208975
$j=10$	$10\,\pi$	0.5	0.00	-0.02794578	0.01440837	–

in which the second and third derivatives of mode shapes ψ_j, $j=1\ldots N_\mathrm{s}$, are given in Appendix A, and where the time-domain generalized coordinates Z_j are given by the Fourier integrals

$$Z_j(t)=\frac{1}{2\pi}\int_{-\infty}^{\infty}\bar{Z}_j(\omega)\,\bar{\ddot{u}}_\mathrm{g}(\omega)\,\mathrm{e}^{\mathrm{i}\omega t}\,\mathrm{d}\omega\,;\qquad \ddot{Z}_j(t)=-\frac{1}{2\pi}\int_{-\infty}^{\infty}\omega^2\bar{Z}_j(\omega)\,\bar{\ddot{u}}_\mathrm{g}(\omega)\,\mathrm{e}^{\mathrm{i}\omega t}\,\mathrm{d}\omega \tag{5.25}$$

with $\bar{\ddot{u}}_\mathrm{g}(\omega)$ denoting the Fourier transform of the ground acceleration $\ddot{u}_\mathrm{g}(t)$, given by

$$\bar{\ddot{u}}_\mathrm{g}(\omega)=\int_0^{t_a}\ddot{u}_\mathrm{g}(t)\,\mathrm{e}^{-\mathrm{i}\omega t}\,\mathrm{d}t \tag{5.26}$$

5.2.4 Evaluation of the natural frequencies of coupled beam-fluid systems

The resonant frequencies of a vibrating beam-fluid system an another important feature characterizing its dynamic behavior. These frequencies can be approximated by the frequencies $\widetilde{\omega}_j$, $j=1\ldots N_\mathrm{s}$, that make the generalized coordinates $\bar{Z}_j$ infinite. Therefore, according to Eq. (5.12), the frequency $\widetilde{\omega}_1$ in a fundamental mode analysis can be obtained by solving

$$S_{1,1}(\widetilde{\omega}_1)=0 \tag{5.27}$$

Using Eq. (5.10) with null damping yields

$$\widetilde{\omega}_1^2=\frac{\pi\,\omega_1^2\,M}{\pi M+4\rho_\mathrm{f}\,\Lambda_\mathrm{f}\,H^2\,\theta_{1,1}^*} \tag{5.28}$$

or according to Eqs. (5.22) and (5.17)

$$\widetilde{\omega}_1^2 = \frac{\pi\,\beta_1^4\,EIM^*}{H^4\left(\pi\,\mu_\mathrm{s}\,M^* + 4\rho_\mathrm{f}\,\Lambda_\mathrm{f}\,H\,\theta_{1,1}^*\right)} \tag{5.29}$$

When higher modes are included in the analysis, Eqs. (5.15) and (5.16) show that the frequency of the fundamental mode can be obtained by solving

$$S_{1,1}(\widetilde{\omega}_1)\,S_{2,2}(\widetilde{\omega}_1) - S_{1,2}^2(\widetilde{\omega}_1) = 0 \tag{5.30}$$

and those for higher modes by solving

$$S_{j-1,j-1}(\widetilde{\omega}_j)\,S_{j,j}(\widetilde{\omega}_j) - S_{j-1,j}^2(\widetilde{\omega}_j) = 0 \qquad \text{for } j = 2\ldots N_\mathrm{s} \tag{5.31}$$

Using $j = 2$ in Eq. (5.31) and comparing it to Eq. (5.30) shows that both $\widetilde{\omega}_1$ and $\widetilde{\omega}_2$ are roots of the same equation. As a consequence, solving only Eq. (5.31) will lead to all N_s first vibration frequencies. Substituting Eq. (5.10) with null damping into Eq. (5.31), we show that the beam natural frequencies can be computed first by solving the following simple second order equation for χ_j

$$A_j\,\chi_j^2 - B_j\,\chi_j + C_j = 0 \qquad \text{for } j = 2\ldots N_\mathrm{s} \tag{5.32}$$

in which

$$\begin{aligned}
A_j &= \left(\mu_\mathrm{s}\,H\,M^*\right)^2 + \frac{4\rho_\mathrm{f}}{\pi}\,\mu_\mathrm{s}\,H^3\,M^*\left(\theta_{j,j}^* + \theta_{j-1,j-1}^*\right) + \frac{16\rho_\mathrm{f}^2}{\pi^2}\,H^4\left[\theta_{j-1,j-1}^*\,\theta_{j,j}^* - \left(\theta_{j-1,j}^*\right)^2\right] \\
B_j &= \left(\mu_\mathrm{s}\,H\,M^*\right)^2\left(\omega_{j-1}^2 + \omega_j^2\right) + \frac{4\rho_\mathrm{f}}{\pi}\,\mu_\mathrm{s}\,H\,M^*\,H^2\left(\omega_{j-1}^2\,\theta_{j,j}^* + \omega_j^2\,\theta_{j-1,j-1}^*\right) \\
C_j &= \left(\mu_\mathrm{s}\,H\,M^*\right)^2\omega_{j-1}^2\,\omega_j^2
\end{aligned} \tag{5.33}$$

For each mode j, Eq. (5.32) has two real positive solutions $\chi_j^{(\mathrm{min})}$ and $\chi_j^{(\mathrm{max})}$ corresponding to the smallest and largest roots of the polynomial, respectively. We then show that the frequencies $\widetilde{\omega}_j$, $j{=}1\ldots N_\mathrm{s}$, can be approximated as

$$\widetilde{\omega}_1 = \sqrt{\chi_2^{(\mathrm{min})}} \tag{5.34}$$

$$\widetilde{\omega}_j = \sqrt{\chi_j^{(\mathrm{max})}} \qquad \text{for } j = 2\ldots N_\mathrm{s} \tag{5.35}$$

5.3 Illustrative numerical examples

5.3.1 Beam-fluid systems studied

In this section, we assess the effectiveness of the proposed formulation in determining the dynamic response of beam-fluid systems. For illustration purposes, we consider a beam-water system where the beam has a height of 10 m and a unit cross-section of $1\,\mathrm{m}^2$. We assume that the beam can be subjected to the CF, CP, CS, CC or PP boundary conditions illustrated in Figs. 5.1 and 5.2. Two beam materials are considered : (i) Concrete with a mass density $\rho_\mathrm{s} = 2440\,\mathrm{kg/m}^3$ and a modulus of elasticity $E = 25\,\mathrm{GPa}$; and (ii) Steel with a mass density $\rho_\mathrm{s} = 7850\,\mathrm{kg/m}^3$ and a modulus of elasticity $E = 200\,\mathrm{GPa}$. A water mass density $\rho_\mathrm{f} = 1000\,\mathrm{kg/m}^3$ is used and the effects of one and two water domains, i.e. $\Lambda_\mathrm{f} = 1$ and 2, are investigated. The proposed simplified technique presented in Section 5.2 is programmed and applied to the concrete and steel beam-water systems. For comparison purposes, finite element analyses of the beam-water systems are also conducted using the software ADINA [31], where the beam and water domain(s) are discterized into 2-nodes beam finite elements and 4-node potential-based finite elements, respectively. In these finite element analyses, fluid-structure interaction is accounted for through special interface elements also included in the software. The performance of the potential-based formulation and the fluid-structure interface elements was assessed in a previous work [26]. In each case, a semi-infinite water domain is simulated by a finite water domain with a rigid boundary condition applied at a far distance until convergence of the results.

5.3.2 Earthquake time-history response of the beam-water systems

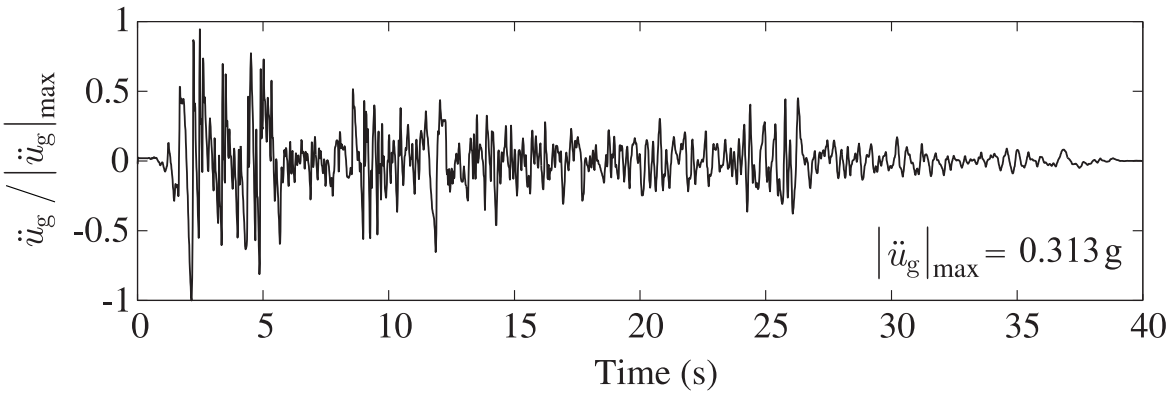

Figure 5.3 Horizontal acceleration component of Imperial Valley earthquake (1940) at El Centro.

We first validate the ability of the proposed formulation to evaluate the time-history response for displacements, accelerations, shear forces and bending moments. For brevity, the results are shown only for the beam-water systems with a Clamped-Free configuration and subjected to the horizontal acceleration component of Imperial Valley earthquake (1940) at El Centro illustrated in Fig. 5.3. Ten structural modes are included in the dynamic analysis of the concrete and steel beam-water systems and a constant hysteretic damping ratio $\eta_s = 0.1$ is used. The results obtained using the proposed simplified technique and the finite element method are illustrated in Figs. 5.4 to 5.7.

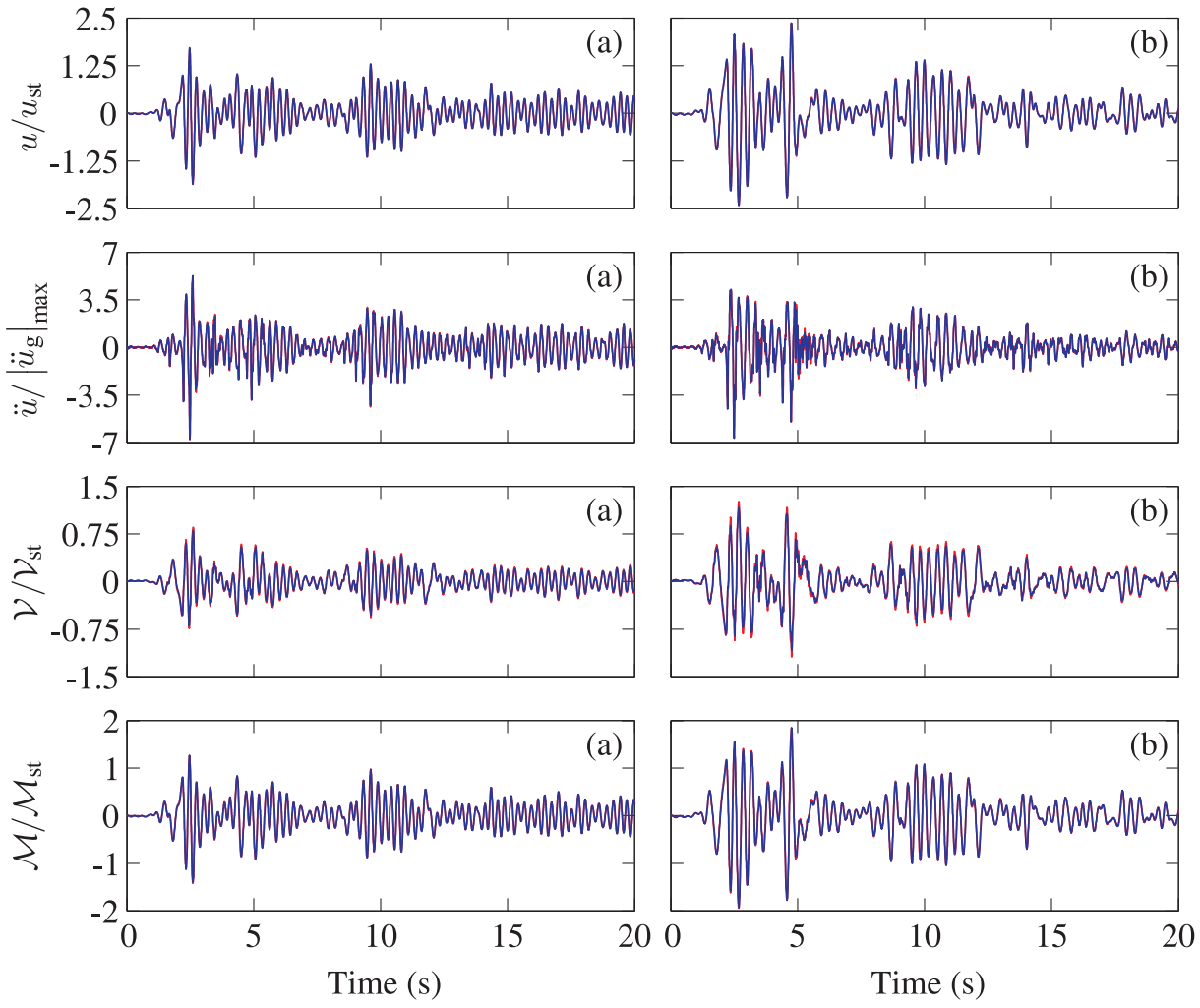

Figure 5.4 Time-history responses for displacements, accelerations, shear forces, and overturning bending moments of the concrete beam-fluid system : (a) beam in contact with water on one side ; (b) beam in contact with water on two sides. — Finite elements (Wet beam) ; — Proposed simplified method (Wet beam).

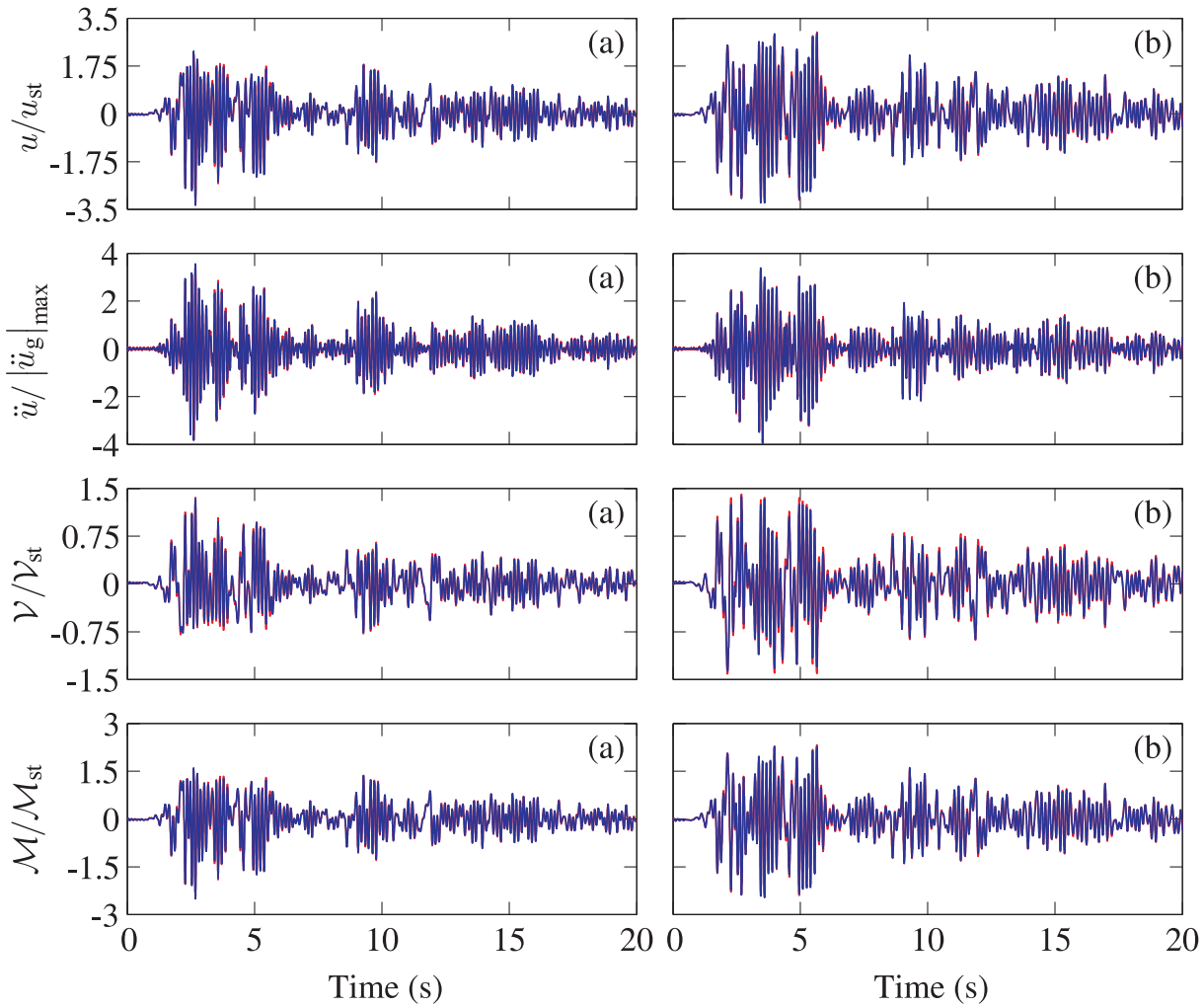

Figure 5.5 Time-history responses for displacements, accelerations, shear forces, and overturning bending moments of the steel beam-fluid system : (a) beam in contact with water on one side ; (b) beam in contact with water on two sides. — Finite elements (Wet beam) ; — Proposed simplified method (Wet beam).

In these figures, time-history responses for displacement u and acceleration $\ddot{u}$ at the beam-s's free end, as well as shear force $\mathcal{V}$, and overturning bending moment $\mathcal{M}$ at the base are nondimensionalized by the values $u_{st} = (\rho_f g H^5)/(30EI)$, peak ground acceleration $|\ddot{u}_g|_{max}$, $\mathcal{V}_{st} = (\rho_f g H^2)/2$ and $\mathcal{M}_{st} = (\rho_f g H^3)/6$, respectively. As can be seen from Figs. 5.4 and 5.5 illustrating the responses over the first 20 seconds of the earthquake, the results of the proposed simplified method and the advanced finite element technique are in excellent agrement for both concrete and steel beam-fluid systems. We can see that the extreme values of a given response quantity are obtained at different time instants depending on the number of water domains. For a better assessment of the quality of the predictions, Figs. 5.6 and 5.7

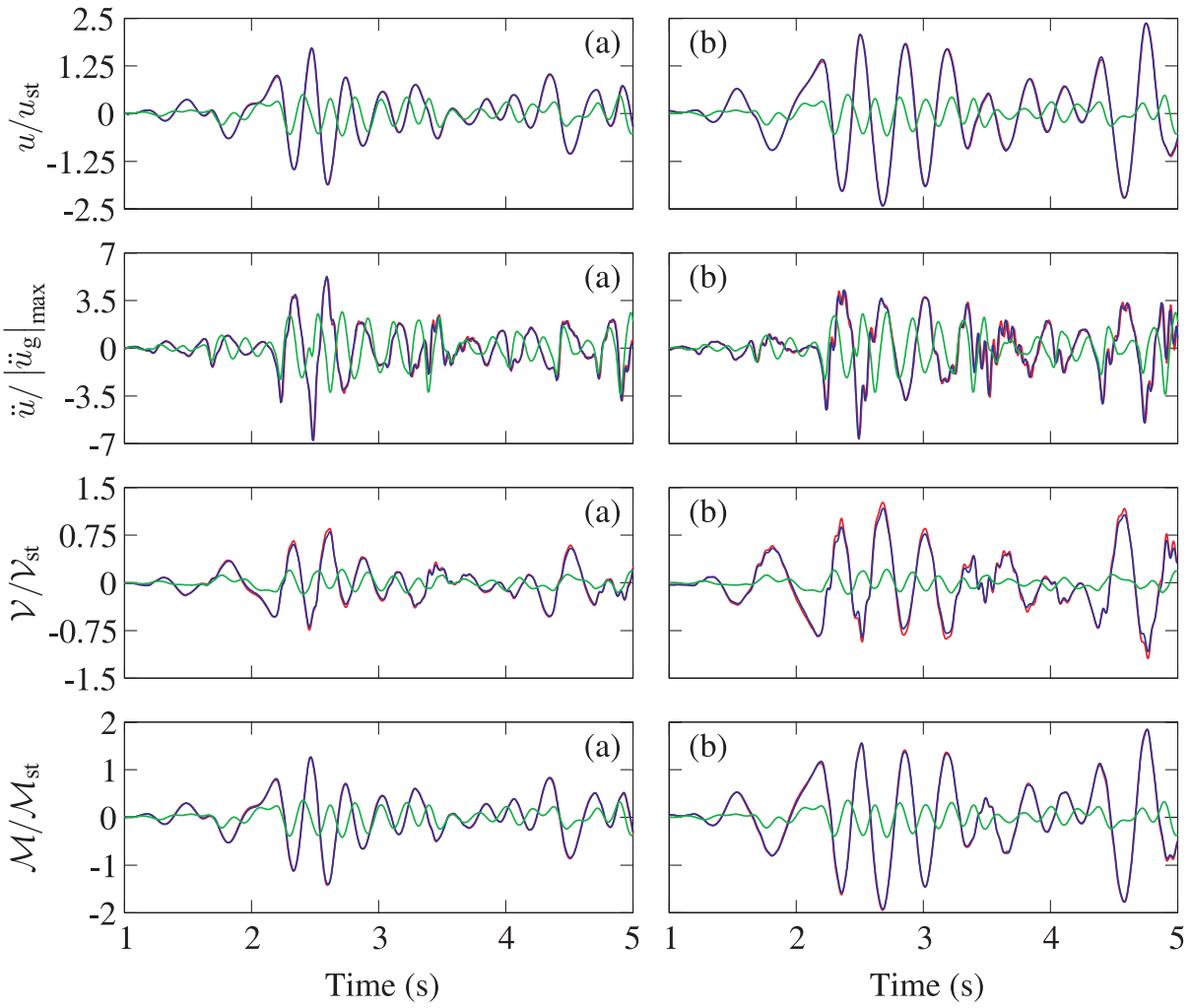

Figure 5.6 Time-history responses for displacements, accelerations, shear forces, and overturning bending moments of the concrete beam-fluid system and the dry beam : (a) beam in contact with water on one side ; (b) beam in contact with water on two sides. — Finite elements (Wet beam) ; — Proposed simplified method (Wet beam) ; — Proposed simplified method (Dry beam).

provide close up views of the responses of the concrete and steel beam-fluid systems over a short time interval between 1 and 5 s, respectively. For comparison purposes, the time-history responses of the dry concrete and steel beams are also superposed to the previous results. These close up views confirm that the proposed simplified method and the advanced finite element technique yield practically identical results for both concrete and steel beam-fluid systems. They also show that the earthquake response of the beams is clearly affected by the fluid-structure interaction and the number of water domains in contact with the beam. When comparing the seismic behavior of the dry and wet beams, we clearly observe the amplifi-

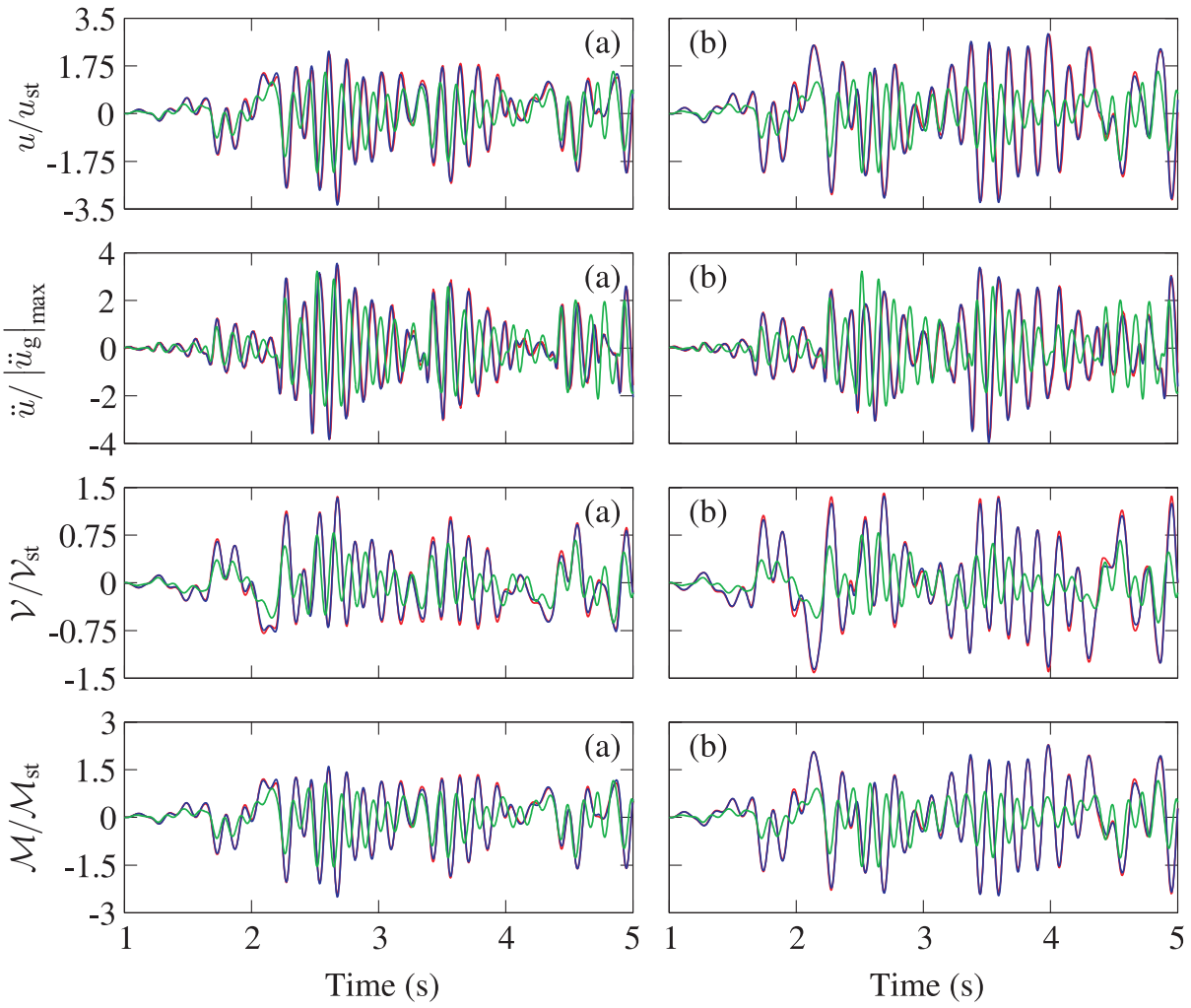

Figure 5.7 Time-history responses for displacements, accelerations, shear forces, and overturning bending moments of the steel beam-fluid system and the dry beam : (a) beam in contact with water on one side ; (b) beam in contact with water on two sides. — Finite elements (Wet beam) ; — Proposed simplified method (Wet beam) ; — Proposed simplified method (Dry beam).

cation of the amplitudes of all the response quantities studied, which emphasizes the need to include fluid-structure interaction effects for such applications. The results also confirm that fluid-structure interaction modifies the natural vibration frequencies of the beam-fluid systems, a phenomena that will investigated further in the next section.

5.3.3 Coupled frequencies of beam-water systems

Next, we determine the first ten natural frequencies of the above described beam-water systems using the proposed simplified procedure and the finite element method. The natural frequencies are determined for all the above-described beam configurations and the results are expressed for $j = 1 \ldots 10$ in terms of the frequency ratios

$$\eta^{(\mathrm{FE})} = \frac{\widetilde{\omega}_j^{(\mathrm{FE})}}{\omega_j}\,; \qquad\qquad \eta^{(\mathrm{NM})} = \frac{\widetilde{\omega}_j^{(\mathrm{NM})}}{\omega_j} \tag{5.36}$$

in which ω_j is the natural frequency of the dry beam computed using Eq. (5.17), and where $\widetilde{\omega}_j^{(\mathrm{FE})}$ and $\widetilde{\omega}_j^{(\mathrm{NM})}$ denote the natural frequencies of the beam-water systems determined using finite elements (FE) and the new method (NM) developed in section 5.2.4, respectively. Tables 5.8 and 5.9 contain the obtained ratios for concrete and steel beam-water systems, respectively. We clearly see that a very good agreement is obtained between the results of the proposed simplified method and those of finite elements independently of the mode number and beam boundary conditions.

The computed frequency ratios also emphasize the importance of beam-water interaction effects on the natural frequencies and consequently the dynamic response of the system. For example, in the case of the Sliding-Clamped (SC) beam configuration with water on both sides, the ratio of the natural frequency of the dry beam on the wet beam reaches 0.40 and 0.62 for the concrete and steel beam-water systems, respectively. For a given mode, the frequency ratios generally depend on the beam boundary conditions and the number of water domains in contact with the beam. When comparing frequency ratios obtained for the concrete and steel beam-water systems, we see that the effect of fluid-structure interaction decreases with larger beam stiffness. We also observe that the frequency ratios tend towards unity for higher modes, implying that hydrodynamic effects on the natural frequencies diminish as a function of increasing vibration modes.

Table 5.8 Frequency ratios for concrete beam-water system.

Configuration	Λ_f	Ratio	Vibration mode number									
			1	2	3	4	5	6	7	8	9	10
CF	1	$\eta^{(FE)}$	0.71	0.69	0.78	0.83	0.86	0.88	0.90	0.91	0.92	0.93
		$\eta^{(NM)}$	0.71	0.69	0.78	0.82	0.85	0.88	0.89	0.91	0.92	0.93
	2	$\eta^{(FE)}$	0.58	0.58	0.67	0.73	0.77	0.81	0.83	0.85	0.86	0.88
		$\eta^{(NM)}$	0.58	0.58	0.67	0.72	0.76	0.79	0.82	0.84	0.85	0.87
CP	1	$\eta^{(FE)}$	0.59	0.73	0.80	0.85	0.87	0.89	0.91	0.92	0.93	0.93
		$\eta^{(NM)}$	0.59	0.73	0.80	0.84	0.86	0.88	0.90	0.91	0.92	0.93
	2	$\eta^{(FE)}$	0.46	0.61	0.69	0.75	0.79	0.82	0.84	0.86	0.87	0.88
		$\eta^{(NM)}$	0.46	0.61	0.69	0.74	0.78	0.80	0.83	0.85	0.86	0.87
PC	1	$\eta^{(FE)}$	0.55	0.74	0.81	0.85	0.88	0.90	0.91	0.92	0.93	0.94
		$\eta^{(NM)}$	0.55	0.74	0.79	0.84	0.87	0.89	0.90	0.92	0.92	0.93
	2	$\eta^{(FE)}$	0.43	0.61	0.70	0.75	0.79	0.82	0.84	0.86	0.87	0.88
		$\eta^{(NM)}$	0.43	0.61	0.68	0.74	0.78	0.81	0.83	0.85	0.86	0.88
CS	1	$\eta^{(FE)}$	0.67	0.69	0.79	0.83	0.87	0.89	0.90	0.91	0.92	0.93
		$\eta^{(NM)}$	0.67	0.70	0.79	0.82	0.86	0.88	0.90	0.91	0.92	0.93
	2	$\eta^{(FE)}$	0.54	0.58	0.68	0.74	0.78	0.81	0.83	0.85	0.87	0.88
		$\eta^{(NM)}$	0.54	0.58	0.68	0.72	0.77	0.80	0.82	0.84	0.86	0.87
SC	1	$\eta^{(FE)}$	0.53	0.73	0.81	0.85	0.88	0.90	0.91	0.92	0.93	0.94
		$\eta^{(NM)}$	0.53	0.73	0.81	0.85	0.88	0.90	0.91	0.92	0.93	0.94
	2	$\eta^{(FE)}$	0.40	0.60	0.70	0.75	0.79	0.82	0.84	0.86	0.87	0.89
		$\eta^{(NM)}$	0.40	0.60	0.70	0.75	0.79	0.82	0.84	0.86	0.87	0.88
CC	1	$\eta^{(FE)}$	0.58	0.74	0.80	0.85	0.87	0.89	0.91	0.92	0.93	0.93
		$\eta^{(NM)}$	0.58	0.75	0.79	0.84	0.86	0.89	0.90	0.91	0.92	0.95
	2	$\eta^{(FE)}$	0.45	0.62	0.70	0.75	0.79	0.82	0.84	0.86	0.87	0.88
		$\eta^{(NM)}$	0.45	0.62	0.68	0.74	0.77	0.81	0.82	0.85	0.86	0.91
PP	1	$\eta^{(FE)}$	0.56	0.73	0.80	0.85	0.88	0.89	0.91	0.92	0.93	0.94
		$\eta^{(NM)}$	0.56	0.72	0.79	0.84	0.87	0.89	0.90	0.92	0.92	0.93
	2	$\eta^{(FE)}$	0.43	0.60	0.69	0.75	0.79	0.82	0.84	0.86	0.87	0.88
		$\eta^{(NM)}$	0.43	0.59	0.68	0.74	0.78	0.81	0.83	0.85	0.86	0.88

5.4 Conclusions

A simplified formulation was proposed to study the modal dynamic and earthquake response of flexible beam-type structures vibrating in contact with one or two fluid domains. The methodology developed extends available analytical solutions for mode shapes and natural vibration frequencies of slender beams with various boundary conditions to include the effects of fluid-structure interaction. Simplified expressions are then developed to determine the earthquake response of coupled beam-fluid systems and predict their natural vibration frequencies. Two beam-fluid systems were selected and numerical tests were performed to validate the results of the proposed simplified method against advanced finite element results. We showed that the simplified procedure gives an excellent assessment of (i) the earthquake response of coupled beam-fluid systems, and (ii) the natural vibration frequencies independently of the mode number and beam boundary conditions. The numerical results confirmed the importance of accounting for fluid-structure interaction effects which may reduce by more than twice the fundamental vibration frequency of the dry beam and amplify its response quantities. From a practical standpoint, the proposed simplified technique offers an obvious advantage when compared to advanced fluid-structure interaction capable finite element analysis. In the latter case indeed, the complexity of constructing finite element model of the beam-fluid system is added to the need to satisfy convergence criteria related to the number of elements or nodes in the beam model as well as the truncation length of the fluid domain. The proposed simplified expressions can be easily implemented in day-to-day practice, and can be used efficiently either to predict the modal dynamic properties of beam-fluid systems for design purposes, evaluate such properties for existing beam-fluid systems, or extract properties of a dry beam based on available modal data of a beam-fluid system. Finally, the methodology proposed can be extended to other types of structures for which mode shapes and natural vibration frequencies can be evaluated or approximated using closed-form expressions.

Acknowledgements

The authors would like to acknowledge the financial support of the Natural Sciences and Engineering Research Council of Canada (NSERC) and the Quebec Fund for Research on Nature and Technology (FQRNT).

Table 5.9 Frequency ratios for steel beam-water system.

Configuration	Λ_f	Ratio	Vibration mode number									
			1	2	3	4	5	6	7	8	9	10
CF	1	$\eta^{(FE)}$	0.88	0.85	0.91	0.93	0.95	0.96	0.96	0.97	0.97	0.98
		$\eta^{(NM)}$	0.88	0.85	0.91	0.93	0.95	0.96	0.96	0.97	0.97	0.97
	2	$\eta^{(FE)}$	0.79	0.77	0.84	0.88	0.91	0.92	0.93	0.94	0.95	0.96
		$\eta^{(NM)}$	0.79	0.77	0.84	0.88	0.90	0.92	0.93	0.94	0.95	0.95
CP	1	$\eta^{(FE)}$	0.80	0.88	0.92	0.94	0.95	0.96	0.97	0.97	0.98	0.98
		$\eta^{(NM)}$	0.80	0.89	0.92	0.94	0.95	0.96	0.97	0.97	0.97	0.98
	2	$\eta^{(FE)}$	0.68	0.81	0.86	0.89	0.91	0.93	0.94	0.95	0.95	0.96
		$\eta^{(NM)}$	0.68	0.81	0.86	0.89	0.91	0.92	0.93	0.94	0.95	0.95
PC	1	$\eta^{(FE)}$	0.77	0.89	0.92	0.94	0.96	0.96	0.97	0.97	0.98	0.98
		$\eta^{(NM)}$	0.77	0.89	0.92	0.94	0.95	0.96	0.97	0.97	0.97	0.98
	2	$\eta^{(FE)}$	0.65	0.81	0.86	0.90	0.92	0.93	0.94	0.95	0.95	0.96
		$\eta^{(NM)}$	0.65	0.81	0.86	0.89	0.91	0.93	0.94	0.95	0.95	0.96
CS	1	$\eta^{(FE)}$	0.86	0.85	0.91	0.93	0.95	0.96	0.97	0.97	0.97	0.98
		$\eta^{(NM)}$	0.85	0.86	0.91	0.93	0.95	0.96	0.96	0.97	0.97	0.98
	2	$\eta^{(FE)}$	0.76	0.77	0.85	0.88	0.91	0.92	0.94	0.94	0.95	0.96
		$\eta^{(NM)}$	0.76	0.77	0.85	0.88	0.91	0.92	0.93	0.94	0.95	0.95
SC	1	$\eta^{(FE)}$	0.75	0.89	0.93	0.95	0.96	0.97	0.97	0.97	0.98	0.98
		$\eta^{(NM)}$	0.75	0.89	0.93	0.95	0.96	0.96	0.97	0.97	0.98	0.98
	2	$\eta^{(FE)}$	0.62	0.81	0.87	0.90	0.92	0.93	0.94	0.95	0.96	0.96
		$\eta^{(NM)}$	0.62	0.81	0.87	0.90	0.92	0.93	0.94	0.95	0.96	0.96
CC	1	$\eta^{(FE)}$	0.79	0.89	0.92	0.94	0.95	0.96	0.97	0.97	0.98	0.98
		$\eta^{(NM)}$	0.79	0.89	0.92	0.94	0.95	0.96	0.97	0.97	0.97	0.98
	2	$\eta^{(FE)}$	0.67	0.82	0.86	0.90	0.92	0.93	0.94	0.95	0.95	0.96
		$\eta^{(NM)}$	0.67	0.82	0.85	0.89	0.91	0.92	0.93	0.94	0.95	0.97
PP	1	$\eta^{(FE)}$	0.78	0.88	0.92	0.94	0.96	0.96	0.97	0.97	0.98	0.98
		$\eta^{(NM)}$	0.78	0.88	0.92	0.94	0.95	0.96	0.97	0.97	0.97	0.98
	2	$\eta^{(FE)}$	0.66	0.80	0.86	0.90	0.92	0.93	0.94	0.95	0.95	0.96
		$\eta^{(NM)}$	0.66	0.80	0.86	0.89	0.91	0.93	0.94	0.95	0.95	0.96

References

[1] H.M. Westergaard, Water pressures on dams during earthquakes. Transactions, ASCE 98 (1933) 418–472.

[2] L.S. Jacobsen, Impulsive hydrodynamics of fluid inside a cylindrical tank and of fluid surrounding a cylindrical pier. Bulletin of the Seismological Society of America 39 (1949) 189–1949.

[3] P.V. Rao, Calculation of added mass of circular and rectangular piers oscillating in water. Proceedingd of the Fifth Symposium of Earthquake Engineering (1974) 97.

[4] H. Goto, K. Toki, Vibrational characteristics and aseismic design of submerged bridge piers. Proceedings of the Third World Conference on Earthguake Engineering, Vol. II, New Zealand, 1965 pp. 107–122.

[5] S. Kotsubo, Seismic force effect on submerged bridge piers with elliptic cross-sections. Proceedings of the Third World Conference on Earthguake Engineering, Vol. II, New Zealand, 1965 pp. 342–356.

[6] A. K. Chopra, Earthquake behavior of reservoir-dam systems. Journal of the Engineering Mechanics Division, ASCE, 94, No. EM6, (1968) 1475–1500.

[7] A. K. Chopra, Earthquake response of concrete gravity dams. Journal of the Engineering Mechanics Division, ASCE, 96, No. EM4, (1970) 443–454.

[8] O.C. Zienkiewicz, R.E. Newton, Coupled vibration of a structure submerged in a compressible fluid. Proceedings of the International Symposium of Finite Element Techniques, Vol. 15, 1969, pp. 1-–15.

[9] A.R. Chardrasekaran, S.S. Saini, M.M. Malhotra, Hydrodynamic pressure on circular cylindrical cantilever structures surrounded by water. Fourth Symposium on Earthquake Engineering, Roorkee, India, 1970, pp. 161–171.

[10] C.Y. Liaw, A.K. Chopra, Dynamics of towers surrounded by water. International Journal Earthquake Engineering and Structural Dynamics 3 (1974), no. 1, 33—49.

[11] Y. Tanaka, R. T. Hudspeth, Restoring forces on vertical circular cylinders forced by earthquakes. International Journal Earthquake Engineering and Structural Dynamics 16 (1988), no. 1, 99—119.

[12] Han, R.P.S., Xu, H, Simple and accurate added mass model for hydrodynamic fluid-structure interaction analysis. Journal of the Franklin Institute 333B (1996), no. 6, 929–945.

[13] K. Nagaya, Transient response in flexure to general uni-directional loads of variable cross-section beam with concentrated tip inertias immersed in a fluid. Journal of Sound and Vibration 99 (1985), no. 3, 361-–378.

[14] A. Uscilowska, J.A. Kolodziej, Free vibration of immersed column carrying a tip mass. Journal of Sound and Vibration 216 (1998), n0. 1, 147-–157.

[15] H.R. Oz, Natural frequenciesof an immersed beam carrying a tip mass with rotatory inertia. Journal of Sound and Vibration 266 (2003) 1099-–1108.

[16] J.S. Wu, S.-H. Hsu, A unified approach for the free vibration analysis of an elastically supported immersed uniform beam carrying an eccentric tip mass with rotary inertia. Journal of Sound and Vibration 291 (2006) 1122–1147.

[17] J.S. Wu, K.-W. Chen, An alternative approach to the structural motion analysis of wedge-beam offshore structures supporting a load. Ocean Engineering 30 (2003), no. 14, 1791–1806.

[18] Chang, J.Y., Liu, W.H, Some studies on the natural frequencies of immersed restrained column. Journal of Sound and Vibration, 130 (1989), no. 3, 516–524.

[19] Nagaya, K., Hai, Y., Seismic response of underwater members of variable cross section. Journal of Sound Vibration 103 (1985) 119–138.

[20] Xing, J.T., Price, W.G., Pomfret, M. J., Yam, L.H, Natural vibration of a beam-water interaction system. Journal of Sound and Vibration, 199 (1997), no. 3, 491–512.

[21] S. Zhao, J.T. Xing, W.G. Price, Natural vibration of a flexible beam–water coupled system with a concentrated mass attached at the free end of the beam. Proceedings of the Institution of Mechanical Engineers, Part M : Journal of Engineering for the Maritime Environment, Vol. 216, no. 2, 2002, pp. 145–154.

[22] J.T. Xing, Natural vibration of two-dimensional slender structure–water interaction systems subject to Sommerfeld radiation condition. Journal of Sound and Vibration 308 (2007) 67-–79.

[23] J. Nasserzare, Y. Lei, S. Eskandari-Shiri, Computation of natural frequencies and mode shapes of arch dams as an inverse problem. Advances in Engineering Software 31 (2000), no.11, 827–836

[24] S.M. de Souza, L.J. Pedroso, Study of flexible wall acoustic cavities using Beam Finite Element. Mechanics of Solids in Brazil, Brazilian Society of Mechanical Sciences and Engineering, H.S. da Costa Mattos & Marcílio Alves (Editors), 2009, pp. 223–237.

[25] G. Fenves, A.K. Chopra, Earthquake analysis and response of concrete gravity dams. Report No. UCB/EERC-84/10, University of California, Berkeley, California, 1984.

[26] N. Bouaanani, F.Y. Lu, Assessment of potential-based fluid finite elements for seismic analysis of dam–reservoir systems Journal of Computers and Structures 87 (2009) 206–224.

[27] B. Miquel, N. Bouaanani, Simplified evaluation of the vibration period and seismic response of gravity dam-water systems Journal of Engineering Structures 32 (2010) 2488–2502.

[28] Blevins RD. Formulas for natural frequency and mode shape. , Kriger publishing Company, Florida (1984) 296–297.

[29] S.R. Finch, Mathematical constants. Cambridge University Press, 2003.

[30] Higham, N. J, Accuracy and stability of numerical algorithms (second ed.) SIAM, 2002.

[31] ADINA Theory and Modeling Guide. Report ARD 10-7. ADINA R & D, Inc., 2010.

Appendix A

This appendix reviews the mode shapes ψ_j, $j = 1 \ldots N_s$, of a slender beam and its derivatives as a function of the various boundary conditions illustrated in Fig. 5.2 [28] :

– For Clamped-Free (CF), Clamped-Pinned (CP), Clamped-Sliding (CS) and Clamped-

Clamped (CC) boundary conditions

$$\psi_j^{(x)}(y) = \cosh\left(\frac{\beta_j\, y}{H}\right) - \cos\left(\frac{\beta_j\, y}{H}\right) - \sigma_j \left[\sinh\left(\frac{\beta_j\, y}{H}\right) - \sin\left(\frac{\beta_j\, y}{H}\right)\right] \tag{5.A.1}$$

$$\frac{\partial^2 \psi_j^{(x)}(y)}{\partial y^2} = \frac{\beta_j^2}{H^2}\left\{\cosh\left(\frac{\beta_j\, y}{H}\right) + \cos\left(\frac{\beta_j\, y}{H}\right) - \sigma_j \left[\sinh\left(\frac{\beta_j\, y}{H}\right) + \sin\left(\frac{\beta_j\, y}{H}\right)\right]\right\} \tag{5.A.2}$$

$$\frac{\partial^3 \psi_j^{(x)}(y)}{\partial y^3} = \frac{\beta_j^3}{H^3}\left\{\sinh\left(\frac{\beta_j\, y}{H}\right) - \sin\left(\frac{\beta_j\, y}{H}\right) - \sigma_j \left[\cosh\left(\frac{\beta_j\, y}{H}\right) + \cos\left(\frac{\beta_j\, y}{H}\right)\right]\right\} \tag{5.A.3}$$

where the parameters β_j and σ_j are given in Table 5.A1 for the different boundary conditions.

– For Pinned-Pinned (PP) boundary conditions

$$\psi_j^{(x)}(y) = \sin\left(\frac{\beta_j\, y}{H}\right) \tag{5.A.4}$$

$$\frac{\partial^2 \psi_j^{(x)}(y)}{\partial y^2} = -\frac{\beta_j^2}{H^2}\sin\left(\frac{\beta_j\, y}{H}\right) \tag{5.A.5}$$

$$\frac{\partial^3 \psi_j^{(x)}(y)}{\partial y^3} = -\frac{\beta_j^3}{H^3}\cos\left(\frac{\beta_j\, y}{H}\right) \tag{5.A.6}$$

where the parameters β_j are given in Table 5.A1.

The corresponding functions $\bar{\psi}_j$, $j = 1 \ldots N_\mathrm{s}$ in Eqs. (5.4), (5.5) and (5.9) are given by

– For Clamped-Free (CF), Clamped-Pinned (CP), Clamped-Sliding (CS) and Clamped-Clamped (CC) boundary conditions

$$\bar{\psi}_j(\bar{y}) = \cosh\left(\beta_j\, \bar{y}\right) - \cos\left(\beta_j\, \bar{y}\right) - \sigma_j \left[\sinh\left(\beta_j\, \bar{y}\right) - \sin\left(\beta_j\, \bar{y}\right)\right] \tag{5.A.7}$$

– For Pinned-Pinned (PP) boundary conditions

$$\bar{\psi}_j(\bar{y}) = \sin\left(\beta_j\, \bar{y}\right) \tag{5.A.8}$$

Table 5.A1 Equations to determine σ_j and β_j for modes $j = 1 \ldots N_s$.

Boundary conditions	σ_j	β_j is solution for :
Clamped-Free (CF)	$\frac{\sinh(\beta_j) - \sin(\beta_j)}{\cosh(\beta_j) + \cos(\beta_j)}$	$\cos(\beta_j)\cosh(\beta_j) + 1 = 0$
Clamped-Pinned (CP)	$\frac{\cosh(\beta_j) - \cos(\beta_j)}{\sinh(\beta_j) - \sin(\beta_j)}$	$\tan(\beta_j) - \tanh(\beta_j) = 0$
Clamped-Sliding (CS)	$\frac{\sinh(\beta_j) - \sin(\beta_j)}{\cosh(\beta_j) + \cos(\beta_j)}$	$\tan(\beta_j) + \tanh(\beta_j) = 0$
Clamped-Clamped (CC)	$\frac{\cosh(\beta_j) - \cos(\beta_j)}{\sinh(\beta_j) - \sin(\beta_j)}$	$\cos(\beta_j)\cosh(\beta_j) - 1 = 0$
Pinned-Pinned (PP)	–	$\beta_j = j\,\pi$

CHAPITRE 6

Article 4 : Accounting for Earthquake-induced Dam-reservoir Interaction using Modified Accelerograms

Benjamin Miquel [1] **and Najib Bouaanani** [2]

Paper submitted to *Journal of Structural Engineering* (ASCE)

Submitted 3 February 2012.

This paper proposes a new practical and efficient procedure to investigate the seismic response of gravity dams that : (i) avoids the finite or boundary element discretization of the reservoir ; (ii) can be applied using standard finite element software not necessarily including fluid-structure interaction capabilities ; and (iii) accounts for dam and foundation flexibility, water compressibility, and reservoir bottom wave absorption. The proposed technique consists of modifying the original input ground acceleration to obtain a new accelerogram that directly accounts for the complex effects of fluid-structure interaction. This new accelerogram can then be applied to a dam or dam-foundation system without the impounded reservoir. The exact and simplified formulations of the proposed method are developed, and its efficiency validated through examples of dam-reservoir systems with different geometries. Very satisfactory agreement is obtained when comparing the results to more advanced finite element solutions including fluid-structure interaction capabilities. The new procedure enhances the efficiency of seismic assessment of gravity dams by reducing the modeling and computational burden associated with reservoir discretization, while keeping the main advantages of conventional solid finite element software in conducting dynamic analyses and providing the resulting stresses, strains, or other dam response indicators.

1. Ph.D. Candidate, Department of Civil, Geological and Mining Engineering, École Polytechnique de Montréal, Montréal, QC H3C 3A7, Canada.

2. Professor, Department of Civil, Geological and Mining Engineering, École Polytechnique de Montréal, Montréal, QC H3C 3A7, Canada
Corresponding author. E-mail : najib.bouaanani@polymtl.ca

6.1 Introduction

Investigating the dynamic behavior of gravity dams and evaluating their seismic safety has been a major research and engineering concern for the last several decades. The significance of including structural deformability, water compressibility and energy dissipation at reservoir bottom in the seismic analysis of gravity dams has been highlighted by several researchers (Chopra, 1970, Chakrabarti and Chopra, 1973, Chopra, 1978, Saini et al., 1978, Hall and Chopra, 1982, Fenves and Chopra, 1984a, Liu and Cheng, 1984, Fok et al., 1986, Tsai and Lee, 1987, Humar and Jablonski, 1988, Maeso et al., 2004, Miquel and Bouaanani, 2010). Most available procedures accounting for these parameters are based on a coupled field solution through sub-structuring of the studied dam-reservoir system, making use of analytical formulations, finite elements, boundary elements or a combination of these techniques.

In the analytical studies, the hydrodynamic forces at the dam-reservoir interface are determined analytically by solving the classical Helmholtz equation under specified boundary conditions applied at the boundaries of an assumed rectangular shape reservoir extending to infinity in the upstream direction (Fenves and Chopra, 1984a, Bouaanani and Miquel, 2010). By doing so, the effects of water compressibility and reservoir bottom wave absorption can be included directly in the analysis. The overall dynamic response of the dam-reservoir-foundation system is then determined by coupling the effects of the three substructures by means of interface forces (Fenves and Chopra, 1984a, Fenves and Chopra, 1984b). A common feature to finite and boundary element methods is that they require the discretization of the water domain and the modeling of fluid-structure interaction forces and compatibility at the dam-reservoir interface, as well as energy absorption due to sedimentation at reservoir bottom (Hall and Chopra, 1982, Humar and Jablonski, 1988, Bouaanani and Lu, 2009). Due to the large extent of the reservoir, these methods also require its virtual truncation at a finite distance from dam face and application of appropriate transmitting boundary conditions at the upstream end to ensure adequate energy radiation at infinity (Sommerfeld, 1949, Zienkiewicz, 1969, Sharan, 1985, Maity, 2005, Bouaanani and Miquel, 2010).

To apply the previously described analytical and numerical procedures, specialized software or advanced programming, combined with appropriate user's expertise, are needed to obtain valid results. The main motivation of the present work is to provide engineering practice with a procedure to analyse earthquake-excited gravity dams that : (i) avoids the finite or boundary element discretization of the fluid domain and direct modeling of related fluid-structure interaction forces and boundary conditions ; (ii) can be applied using standard finite element software that includes only classical solid finite elements and not necessarily fluid-structure interaction capabilities ; and (iii) accounts for dam and foundation flexibility, water

compressibility, and reservoir bottom wave absorption. These objectives will be achieved by transforming the original input earthquake into a new accelerogram, modified to include fluid-structure interaction effects, and which can be applied directly to a dam monolith without the impounded reservoir. For brevity, the developed technique will be referred to as the Modified Accelerogram Method (MAM) in what follows. The new procedure enhances the efficiency of seismic assessment of gravity dams by reducing the modeling and computational burden associated with fluid domain discretization, while keeping the main advantages of conventional solid finite element software in conducting frequency- or time-domain dynamic analyses and providing the resulting stresses, strains, or other dam response indicators.

6.2 Formulations of the proposed Modified Accelerogram Method

6.2.1 Description of the studied dam-reservoir system, basic notation and assumptions

The 2D gravity dam cross-section shown in Fig. 6.1 (a) is considered here to illustrate the dynamics of dam-reservoir systems. The dam has a total height H_s and it impounds a semi-infinite reservoir of constant depth H_r. A Cartesian coordinate system with axes x and y with origin at the heel of the structure is adopted and the following main assumptions are made : (i) the dam has a linear elastic behavior ; (ii) the dam foundation is massless and can be rigid or flexible ; (iii) foundation radiation damping is neglected ; (iv) the water in the reservoir, of mass density ρ_r, is assumed inviscid, with its motion irrotational and limited to small amplitudes ; (v) gravity surface waves and compulsive effects are neglected ; (vi) effects of sediments that may be deposited at reservoir bottom are considered. For clarity and brevity of the text, the dam with an empty reservoir will be referred to as the dry structure, while the wet structure will refer to the dam-reservoir system.

6.2.2 Exact formulation of the proposed Modified Accelerogram Method

Considering unit horizontal harmonic ground acceleration $\ddot{u}_\mathrm{g}(t) = \mathrm{e}^{\mathrm{i}\omega t}$, assuming viscous damping ξ, and using modal superposition and mode shape orthogonality, the dynamic response of the dry dam structure can be obtained as the superposition of N_s responses of Equivalent Single Degree Of Freedom (ESDOF) systems with generalized coordinates $\bar{Z}_j^{(\mathrm{e})}$, $j = 1 \ldots N_\mathrm{s}$, satisfying (Fenves and Chopra, 1984a, Miquel and Bouaanani, 2010)

$$\bar{Z}_j^{(\mathrm{e})}(\omega) = \frac{-L_j}{-\omega^2 M_j + 2\,\mathrm{i}\,\xi\,\omega\,\omega_j\,M_j + \omega_j^2\,M_j} \tag{6.1}$$

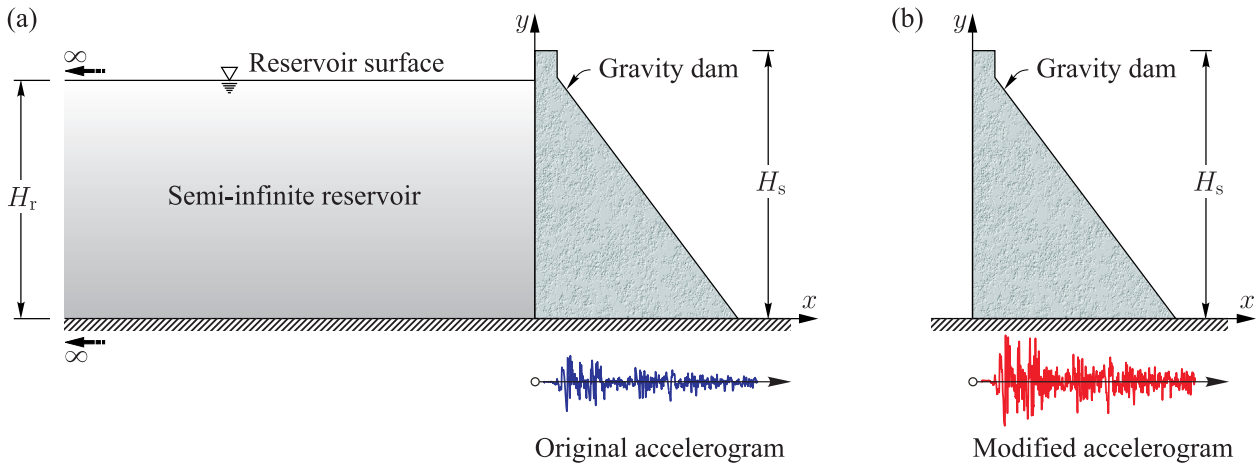

Figure 6.1 Studied systems : (a) Gravity dam-reservoir system or wet structure ; (b) Gravity dam without reservoir or dry structure.

with

$$M_j = \boldsymbol{\psi}_j^{\mathrm{T}}\,\mathbf{M}\,\boldsymbol{\psi}_j\,; \qquad\qquad L_j = \boldsymbol{\psi}_j^{\mathrm{T}}\,\mathbf{M}\,\mathbf{1} \tag{6.2}$$

and where $\mathbf{M}$ is the mass matrix of the structure, ω_j is the vibration frequency corresponding to structural mode shape $\boldsymbol{\psi}_j$, and M_j and L_j the corresponding generalized mass and force, respectively. When mode shapes are also mass-normalized, the generalized masses have unit values $M_j = 1$, $j = 1 \ldots N_{\mathrm{s}}$, otherwise, L_j and M_j can be determined as follows

$$L_j = \iint \rho_{\mathrm{s}}(x,y)\,\psi_j^{(x)}(x,y)\,\mathrm{d}x\mathrm{d}y \simeq \mu_{\mathrm{s}} \int_0^{H_{\mathrm{s}}} \psi_j^{(x)}(0,y)\,\mathrm{d}y \tag{6.3}$$

$$M_j = \iint \rho_{\mathrm{s}}(x,y) \left\{ \left[\psi_j^{(x)}(x,y)\right]^2 + \left[\psi_j^{(y)}(x,y)\right]^2 \right\} \mathrm{d}x\,\mathrm{d}y \simeq \mu_{\mathrm{s}} \int_0^{H_{\mathrm{s}}} \left[\psi_j^{(x)}(0,y)\right]^2 \mathrm{d}y \tag{6.4}$$

where ρ_{s} and μ_{s} are respectively the density and mass per unit height of the structure.

When fluid-structure interaction is included, the vector $\bar{\mathbf{Z}}$ of frequency-dependent generalized coordinates $\bar{Z}_j$, $j = 1 \ldots N_{\mathrm{s}}$, can be obtained by solving the system of equations (Fenves and Chopra, 1984a, Miquel and Bouaanani, 2010)

$$\bar{\mathbf{S}}\,\bar{\mathbf{Z}} = \bar{\mathbf{Q}} \tag{6.5}$$

in which, for $m = 1 \dots N_\mathrm{s}$ and $j = 1 \dots N_\mathrm{s}$,

$$\bar{S}_{j,m}(\omega) = \left[-\omega^2 + 2\,\mathrm{i}\,\xi\,\omega\,\omega_j + \omega_j^2 \right] M_j\,\delta_{j,m} - \omega^2\,\vartheta_{j,m}(\omega) \tag{6.6}$$

$$\bar{Q}_m = -L_m + \Gamma_m(\omega) \tag{6.7}$$

where $\delta_{j,m}$ is the Kronecker symbol and where

$$\vartheta_{j,m}(\omega) = -\int_0^{H_\mathrm{r}} \bar{p}_j(0,y,\omega)\,\psi_m^{(x)}(0,y)\,\mathrm{d}y \tag{6.8}$$

$$\Gamma_m(\omega) = \int_0^{H_\mathrm{r}} \bar{p}_0(0,y,\omega)\,\psi_m^{(x)}(0,y)\,\mathrm{d}y \tag{6.9}$$

with $\bar{p}_0$ and $\bar{p}_j$ denoting, respectively, the hydrodynamic pressures due to the rigid and flexible motions of the dam as defined in Appendix A for convenient reference.

The previous equations were developed for a unit horizontal harmonic ground acceleration $\ddot{u}_\mathrm{g}(t) = \mathrm{e}^{\mathrm{i}\omega t}$. In the general case, the Fourier transform of a given ground acceleration $\ddot{u}_\mathrm{g}(t)$ can be determined as

$$\ddot{u}_\mathrm{g}(\omega) = \int_0^{t_a} \ddot{u}_\mathrm{g}(t)\,\mathrm{e}^{-\mathrm{i}\omega t}\,\mathrm{d}t \tag{6.10}$$

in which t_a is the time duration of the applied accelerogram. For each mode $j = 1 \dots N_\mathrm{s}$, ground acceleration $\ddot{u}_\mathrm{g}$ produces the following modal displacements $\bar{u}_j^{(\mathrm{e})}$, $\bar{u}_j$ and accelerations $\bar{\ddot{u}}_j^{(\mathrm{e})}$ and $\bar{\ddot{u}}_j$ of the dry and wet structures, respectively

$$\bar{u}_j^{(\mathrm{e})}(x,y,\omega) = \ddot{u}_\mathrm{g}(\omega)\,\bar{Z}_j^{(\mathrm{e})}(\omega)\,\psi_j(x,y)\,; \qquad \bar{\ddot{u}}_j^{(\mathrm{e})}(x,y,\omega) = -\ddot{u}_\mathrm{g}(\omega)\,\omega^2\bar{Z}_j^{(\mathrm{e})}(\omega)\,\psi_j(x,y) \tag{6.11}$$

$$\bar{u}_j(x,y,\omega) = \ddot{u}_\mathrm{g}(\omega)\,\bar{Z}_j(\omega)\,\psi_j(x,y)\,; \qquad \bar{\ddot{u}}_j(x,y,\omega) = -\ddot{u}_\mathrm{g}(\omega)\,\omega^2\bar{Z}_j(\omega)\,\psi_j(x,y) \tag{6.12}$$

Let us define a mode- and frequency-dependent ground acceleration $a_\mathrm{g}^{(j)}$ so that

$$a_\mathrm{g}^{(j)}(\omega)\,\bar{Z}_j^{(\mathrm{e})}(\omega)\,\psi_j(x,y) = \ddot{u}_\mathrm{g}(\omega)\,\bar{Z}_j(\omega)\,\psi_j(x,y) \tag{6.13}$$

yielding to

$$a_\mathrm{g}^{(j)}(\omega) = \ddot{u}_\mathrm{g}(\omega)\,\frac{\bar{Z}_j(\omega)}{\bar{Z}_j^{(\mathrm{e})}(\omega)} \tag{6.14}$$

Applying Fourier inverse to this modal acceleration, we obtain N_s accelerograms each given by

$$a_\mathrm{g}^{(j)}(t) = \frac{1}{2\pi}\int_{-\infty}^{\infty} a_\mathrm{g}^{(j)}(\omega)\,\mathrm{e}^{\mathrm{i}\omega t}\,\mathrm{d}\omega \tag{6.15}$$

Executing N_s finite element modal analyses for every mode $j = 1 \ldots N_s$ of the dry structure subjected to respective ground motions $a_g^{(j)}$ and adding up the solutions leads to the response of the wet structure. As can be seen, this new formulation converts the analysis of the wet structure subjected to a ground acceleration $\ddot{u}_g$ into N_s analyses of the dry structure subjected to ground accelerations $a_g^{(j)}$, $j = 1 \ldots N_s$, obtained through modification of the original ground acceleration $\ddot{u}_g$. This process justifies the designation *Modified Accelerogram Method (MAM)* given to this technique. The formulation can be used to include the complex effects of fluid-structure interaction through a finite element analysis of the dry structure as illustrated in Fig. 6.1 (b). As will be shown later, the MAM requires only a few structural modes to obtain convergence. The formulation presented in this section is referred to as *exact* as it yields *exactly* the same results as the sub-structuring method proposed by Fenves and Chopra (1984a). In the next section, we propose a *simplified* formulation of the MAM, where the modified accelerogram is mode-independent.

6.2.3 Simplified formulation of the proposed Modified Accelerogram Method

In the previous section, we showed that the exact formulation of the MAM requires the execution of N_s dynamic analyses of the dry structure with each analysis using a mode-dependent modified accelerogram $a_g^{(j)}$, $j = 1 \ldots N_s$. In this section, we propose a simplified formulation where only *one* mode-independent modified accelerogram is required, thus allowing a single dynamic analysis of the dry structure. The total displacements $\bar{u}^{(e)}(x, y, \omega)$ and $\bar{u}(x, y, \omega)$ within the dry and wet structures, respectively, can be written as

$$\bar{u}^{(e)}(x, y, \omega) = \ddot{u}_g(\omega) \sum_{j=1}^{N_s} \bar{Z}_j^{(e)}(\omega)\, \psi_j(x, y) \tag{6.16}$$

$$\bar{u}(x, y, \omega) = \ddot{u}_g(\omega) \sum_{j=1}^{N_s} \bar{Z}_j(\omega)\, \psi_j(x, y) \tag{6.17}$$

We next define a mode-independent accelerogram $\bar{a}_g$ so that

$$\bar{a}_g(x, y, \omega) \sum_{j=1}^{N_s} \bar{Z}_j^{(e)}(\omega)\, \psi_j(x, y) = \ddot{u}_g(\omega) \sum_{j=1}^{N_s} \bar{Z}_j(\omega)\, \psi_j(x, y) \tag{6.18}$$

yielding

$$\bar{a}_{\mathrm{g}}(x,y,\omega) = \ddot{u}_{\mathrm{g}}(\omega)\,\frac{\displaystyle\sum_{j=1}^{N_{\mathrm{s}}} \bar{Z}_j(\omega)\,\psi_j(x,y)}{\displaystyle\sum_{j=1}^{N_{\mathrm{s}}} \bar{Z}_j^{(\mathrm{e})}(\omega)\,\psi_j(x,y)} \tag{6.19}$$

Note that instead of depending on mode shape j as the accelerogram $a_{\mathrm{g}}^{(j)}$ defined previously in Eq. (6.14), the new accelerogram $\bar{a}_{\mathrm{g}}$ is a function of coordinates x and y where the mode shapes are evaluated. The displacements of the wet structure subjected to accelerogram $\bar{a}_{\mathrm{g}}$ can be expressed

$$\bar{u}(x,y,\omega) = \bar{a}_{\mathrm{g}}(x,y,\omega) \sum_{j=1}^{N_{\mathrm{s}}} \bar{Z}_j^{(\mathrm{e})}(\omega)\,\psi_j(x,y) \tag{6.20}$$

$$= \ddot{u}_{\mathrm{g}}(\omega)\,\frac{\displaystyle\sum_{j=1}^{N_{\mathrm{s}}} \bar{Z}_j(\omega)\,\psi_j(x,y)}{\displaystyle\sum_{j=1}^{N_{\mathrm{s}}} \bar{Z}_j^{(\mathrm{e})}(\omega)\,\psi_j(x,y)} \sum_{j=1}^{N_{\mathrm{s}}} \bar{Z}_j^{(\mathrm{e})}(\omega)\,\psi_j(x,y) \tag{6.21}$$

We show numerically that the following approximation yields excellent results

$$\bar{u}(x,y,\omega) \approx \ddot{u}_{\mathrm{g}}(\omega)\,\frac{\displaystyle\sum_{j=1}^{N_{\mathrm{s}}} \bar{Z}_j(\omega)}{\displaystyle\sum_{j=1}^{N_{\mathrm{s}}} \bar{Z}_j^{(\mathrm{e})}(\omega)} \sum_{j=1}^{N_{\mathrm{s}}} \bar{Z}_j^{(\mathrm{e})}(\omega)\,\psi_j(x,y) \tag{6.22}$$

The validity of this simplification will be illustrated later for various dam-reservoir systems. Accordingly, a simplified modified accelrogram $\tilde{a}_{\mathrm{g}}$ can be computed as follows

$$\tilde{a}_{\mathrm{g}}(\omega) = \ddot{u}_{\mathrm{g}}(\omega)\,\frac{\displaystyle\sum_{j=1}^{N_{\mathrm{s}}} \bar{Z}_j(\omega)}{\displaystyle\sum_{j=1}^{N_{\mathrm{s}}} \bar{Z}_j^{(\mathrm{e})}(\omega)} \tag{6.23}$$

Introducing this frequency-dependent and coordinate-independent acceleration into Eq. (6.15) yields the simplified mode- and coordinate-independent accelerogram $\tilde{a}_{\mathrm{g}}(t)$ that can be di-

rectly applied to the dry structure to obtain the corresponding dynamic response of the wet structure.

To simplify computations further, we propose a simplified method to obtain the generalized coordinates $\bar{Z}_j$, $j=1\ldots N_\mathrm{s}$, instead of solving Eq. (6.5) using a matrix analysis numerical solution scheme. In a fundamental mode analysis, i.e. $N_\mathrm{s}=1$, the only generalized coordinate $\bar{Z}_1$ is given by

$$\bar{Z}_1(\omega) = \frac{\bar{Q}_1(\omega)}{\bar{S}_{1,1}(\omega)} \tag{6.24}$$

When two structural modes are to be included, the generalized coordinates can be obtained as

$$\bar{Z}_1(\omega) = \frac{\bar{S}_{2,2}(\omega)\,\bar{Q}_1(\omega) - \bar{S}_{1,2}(\omega)\,\bar{Q}_2(\omega)}{\bar{S}_{1,1}(\omega)\bar{S}_{2,2}(\omega) - \bar{S}^2_{1,2}(\omega)} \tag{6.25}$$

$$\bar{Z}_2(\omega) = \frac{\bar{S}_{1,1}(\omega)\,\bar{Q}_2(\omega) - \bar{S}_{1,2}(\omega)\,\bar{Q}_1(\omega)}{\bar{S}_{1,1}(\omega)\bar{S}_{2,2}(\omega) - \bar{S}^2_{1,2}(\omega)} \tag{6.26}$$

Finally, if higher mode effects are to be included in the analysis, i.e. $N_\mathrm{s} \geqslant 3$, we show that the generalized coordinates can be approximated by decoupling the system of equations (6.5) as follows

$$\bar{Z}_1(\omega) \approx \frac{\bar{S}_{2,2}(\omega)\,\bar{Q}_1(\omega) - \bar{S}_{1,2}(\omega)\,\bar{Q}_2(\omega)}{\bar{S}_{1,1}(\omega)\bar{S}_{2,2}(\omega) - \bar{S}^2_{1,2}(\omega)} \tag{6.27}$$

$$\bar{Z}_j(\omega) \approx \frac{\bar{S}_{j-1,j-1}(\omega)\,\bar{Q}_j(\omega) - \bar{S}_{j-1,j}(\omega)\,\bar{Q}_{j-1}(\omega)}{\bar{S}_{j-1,j-1}(\omega)\bar{S}_{j,j}(\omega) - \bar{S}^2_{j-1,j}(\omega)} \qquad \text{for } j=2\ldots N_\mathrm{s} \tag{6.28}$$

The parameters $\bar{S}_{j,m}$ and $\bar{Q}_m$ in Eqs. (6.24) to (6.28) are given by Eqs. (6.6) and (6.7) for j, $m=1\ldots N_\mathrm{s}$. Using the above decoupling scheme, we show that only parameters $\vartheta_{j,j-1}$, $\vartheta_{j,j}$ and Γ_j from Eqs. (6.8) and (6.9) are required to determine $\bar{Z}_j$ for $j=1\ldots N_\mathrm{s}$. Simplified expressions are developed next to evaluate these terms. The technique used is based on the approach proposed by Bouaanani and Perrault (2010) consisting of approximating the x–component of mode shape $\boldsymbol{\psi}_j$ of the dry structure by a polynomial function of order $N_{\boldsymbol{\psi}_j}$ and coefficients $a_{j,k}$ as illustrated in Fig. 6.2

$$\psi_j^{(x)}(0,\bar{y}) \approx \sum_{k=0}^{N_{\boldsymbol{\psi}_j}} a_{j,k}\,\bar{y}^k \tag{6.29}$$

where $\bar{y}=y/H_\mathrm{s}$. When dam foundation flexibility is neglected, the mode shapes of the dam on a rigid foundation are considered and $a_{j,0}=0$, $j=1\ldots N_\mathrm{s}$, because there is no translation

at dam base. The dam foundation can also be assumed massless (Bayraktar et al., 2005), in which case, only soil flexibility is considered while inertia and radiation damping effects are neglected. When such an approximation is adopted, the mode shapes of the dam-foundation system are used and the non-null translation at dam base yields $a_{j,0} \neq 0$, $j = 1 \dots N_\mathrm{s}$ as illustrated in Fig. 6.2.

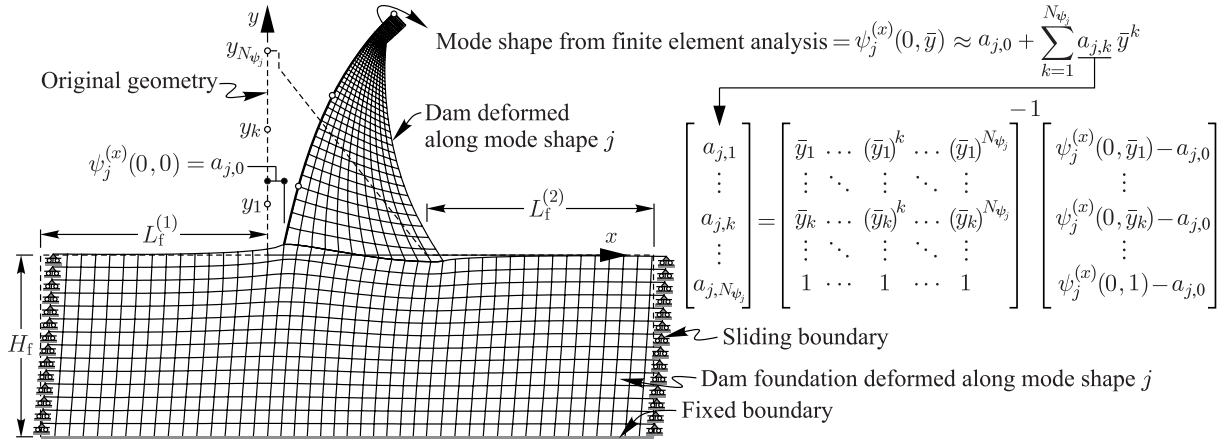

Figure 6.2 Approximation of the mode shapes of a gravity dam-foundation system.

Substituting Eq. (6.29) into Eqs. (6.8), (6.9), and (6.A.2), we show that the parameters Γ_j, $\vartheta_{j,j-1}$, and $\vartheta_{j,j}$, for $j = 1 \dots N_\mathrm{s}$, can be obtained as

$$\Gamma_j(\omega) = -2\rho_\mathrm{r} H_\mathrm{r}^2 \sum_{n=1}^{N_\mathrm{w}} \frac{\lambda_n^2(\omega)}{\beta_n(\omega)} \frac{I_{0,n}(\omega)}{\kappa_n(\omega)} S_{j,n}(\omega) \tag{6.30}$$

$$\vartheta_{j,j-1}(\omega) = 2\rho_\mathrm{r} H_\mathrm{r}^2 \sum_{n=1}^{N_\mathrm{w}} \frac{\lambda_n^2(\omega)}{\beta_n(\omega)\,\kappa_n(\omega)} \big[S_{j-1,n}(\omega)\big] \big[S_{j,n}(\omega)\big] \tag{6.31}$$

$$\vartheta_{j,j}(\omega) = 2\rho_\mathrm{r} H_\mathrm{r}^2 \sum_{n=1}^{N_\mathrm{w}} \frac{\lambda_n^2(\omega)}{\beta_n(\omega)\,\kappa_n(\omega)} \big[S_{j,n}(\omega)\big]^2 \tag{6.32}$$

in which N_w is the number of water modes included in the analysis, λ_n are eigenvalues to be determined by solving Eq. (6.A.3) numerically or by using the closed-form expression in Eq. (6.A.5) as proposed by Bouaanani and Perrault (2010), the parameters β_n, κ_n and $I_{0,n}$ are obtained from Eqs. (6.A.8) to (6.A.9), respectively, and $S_{j,n}$ is defined by

$$S_{j,n}(\omega) = F_{j,n}(\omega)\, I_{0,n}(\omega) + G_{j,n}(\omega) \tag{6.33}$$

where the functions $F_{j,n}$ and $G_{j,n}$ are given by Bouaanani and Perrault (2010) and recalled in Eqs. (6.A.11) and (6.A.12). We show that only the first term of the sums in Eqs. (6.30), (6.31) and (6.32) is highly frequency-dependent, while the others, i.e. $n=2\dots N_{\mathrm{w}}$, can be assumed frequency-independent. This approximation leads to the simplified expressions

$$\Gamma_j(\omega) = \gamma_j(\omega) + \gamma_j^* \tag{6.34}$$
$$\vartheta_{j,j-1}(\omega) = \theta_{j,j-1}(\omega) + \theta_{j,j-1}^* \tag{6.35}$$
$$\vartheta_{j,j}(\omega) = \theta_{j,j}(\omega) + \theta_{j,j}^* \tag{6.36}$$

The frequency-dependent parameters γ_j, $\theta_{j,j-1}$ and $\theta_{j,j}$ can be determined as

$$\gamma_j(\omega) = -2\rho_{\mathrm{r}} H_{\mathrm{r}}^2 \, \frac{\lambda_1^2(\omega)}{\beta_1(\omega)} \frac{I_{0,1}(\omega)}{\kappa_1(\omega)} \, S_{j,1}(\omega) \tag{6.37}$$

$$\theta_{j,j-1}(\omega) = 2\rho_{\mathrm{r}} H_{\mathrm{r}}^2 \, \frac{\lambda_1^2(\omega)}{\beta_1(\omega)\,\kappa_1(\omega)} \left[S_{j-1,1}(\omega)\right] \left[S_{j,1}(\omega)\right] \tag{6.38}$$

$$\theta_{j,j}(\omega) = 2\rho_{\mathrm{r}} H_{\mathrm{r}}^2 \, \frac{\lambda_1^2(\omega)}{\beta_1(\omega)\,\kappa_1(\omega)} \left[S_{j,1}(\omega)\right]^2 \tag{6.39}$$

where $I_{0,1}$ is given by Eq. (6.A.9), and $F_{j,1}$ and $G_{j,1}$ can be obtained from Eqs. (6.A.11) and (6.A.12). The frequency-independent parameters γ_j^*, $\theta_{j,j-1}^*$ and $\theta_{j,j}^*$ in Eqs. (6.34) to (6.36) are given by

$$\gamma_j^* = -2\rho_{\mathrm{r}} H_{\mathrm{r}}^2 \sum_{n=2}^{N_{\mathrm{w}}} \frac{\lambda_n^2(0)}{\beta_n(0)} \frac{I_{0,n}(0)}{\kappa_n(0)} \, S_{j,n}(0) \tag{6.40}$$

$$\theta_{j,j-1}^* = 2\rho_{\mathrm{r}} H_{\mathrm{r}}^2 \sum_{n=2}^{N_{\mathrm{w}}} \frac{\lambda_n^2(0)}{\beta_n(0)\,\kappa_n(0)} \left[S_{j-1,n}(0)\right] \left[S_{j,n}(0)\right] \tag{6.41}$$

$$\theta_{j,j}^* = 2\rho_{\mathrm{r}} H_{\mathrm{r}}^2 \sum_{n=2}^{N_{\mathrm{w}}} \frac{\lambda_n^2(0)}{\beta_n(0)\,\kappa_n(0)} \left[S_{j,n}(0)\right]^2 \tag{6.42}$$

and can be simplified further for practical evaluation to

$$\gamma_j^* = \frac{8\rho_\mathrm{r}}{\pi^2}\,\eta\,H_\mathrm{s}^2 \sum_{k=0}^{N_{\psi_j}} a_{j,k}\,\eta^k\,B_k \tag{6.43}$$

$$\theta_{j,j-1}^* = \frac{4\rho_\mathrm{r}}{\pi}\,\eta^2 H_\mathrm{s}^2 \sum_{k=0}^{N_{\psi_j}} \left\{ \sum_{s=k}^{N_{\psi_j}} \left[(a_{j,k}\,a_{j-1,s} + a_{j-1,k}\,a_{j,s})\,\eta^k\,\eta^s\,A_{k,s} \right] - a_{j,k}\,a_{j-1,k}\,\eta^{2k}\,A_{k,k} \right\} \tag{6.44}$$

$$\theta_{j,j}^* = \frac{4\rho_\mathrm{r}}{\pi}\,\eta^2 H_\mathrm{s}^2 \sum_{k=0}^{N_{\psi_j}} \left[2 \sum_{s=k}^{N_{\psi_j}} \left(a_{j,k}\,a_{j,s}\,A_{k,s}\,\eta^k\,\eta^s \right) - a_{j,k}^2\,A_{k,k}\,\eta^{2k} \right] \tag{6.45}$$

where $\eta = H_\mathrm{r}/H_\mathrm{s}$ and

$$A_{k,s} = \sum_{n=2}^{N_\mathrm{w}} \frac{f_k(n)\,f_s(n)}{(2n-1)}; \qquad B_k = \sum_{n=2}^{N_\mathrm{w}} \frac{(-1)^n\,f_k(n)}{(2n-1)^2} \tag{6.46}$$

with

$$f_k(n) = \frac{1}{\eta^{k+1}} \int_0^\eta \bar{y}^k \cos\left[\frac{(2n-1)\,\pi\,\bar{y}}{2\eta} \right] \mathrm{d}\bar{y} \tag{6.47}$$

For practical computations, the coefficients $A_{k,s}$ and B_k were determined with sufficient reservoir modes N_w to ensure convergence and are given in Table 6.A1 for $k = 0 \ldots 8$ and $s = 0 \ldots 8$.

6.3 Numerical examples

6.3.1 Frequency response of gravity dams on rigid foundations

We consider four typical concrete gravity dam sections D1, D2, D3, and D4, with heights H_s of 21 m, 35 m, 60 m and 90 m, respectively, as illustrated in Fig. 6.3. A mass density $\rho_\mathrm{s} = 2400$ kg/m^3, a Poisson's ratio $\nu = 0.2$ and a modulus of elasticity $E_\mathrm{s} = 25$ GPa are assumed as concrete material properties for each dam and a 5% structural viscous damping ratio is used. The mass density of water is taken as $\rho_\mathrm{r} = 1000$ kg/m^3 with a pressure wave velocity of $C_\mathrm{r} = 1440$ m/s. Reservoir heights H_r of 18 m, 32 m, 57 m and 86 m are considered for dams D1, D2, D3, and D4, respectively.

The dam monoliths are discretized into 9-node plane strain finite elements using the software ADINA (2010). For each dam-reservoir system, the displacement frequency response curves for a unit ground acceleration $\ddot{u}_\mathrm{g}(\omega) = 1$ are determined in two ways : (i) the exact

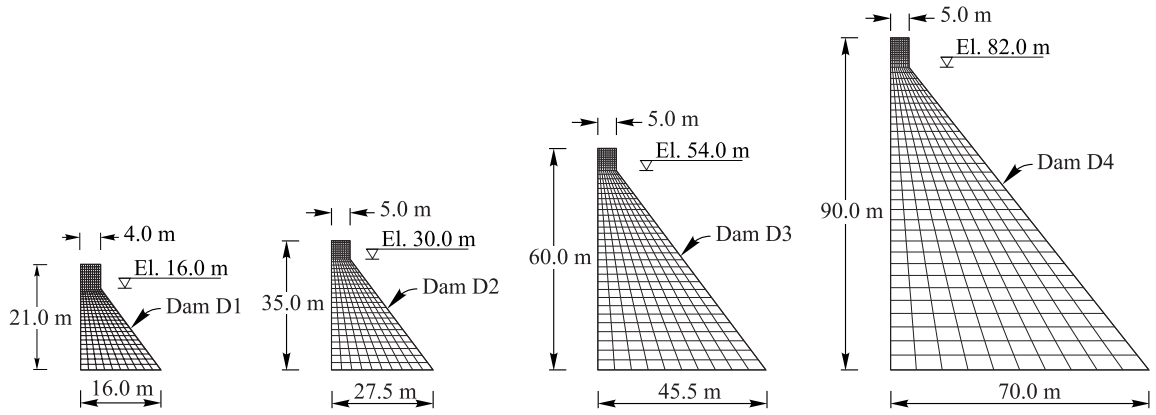

Figure 6.3 Dimensions of studied gravity dam monoliths.

MAM formulation using Eq. (6.21) with the generalized coordinates determined by applying Eqs. (6.6) to (6.9) and then solving Eq. (6.5) numerically ; and (ii) the simplified MAM formulation using Eq. (6.22) with the generalized coordinates determined by applying Eqs. (6.24) to (6.47). When Eq. (6.21) is used, the accelerogram is coordinate-dependent and thus the results are shown in Fig. 6.4 for four different heights $y = H_s$, $y = 3\,H_s/4$, $y = H_s/2$ and $y = H_s/4$ of points belonging to the dam-reservoir interface. The practically coincident curves confirm the validity of the approximation in Eq. (6.22), and show that neglecting coordinate dependency in the computation of the simplified modified acceleration $\tilde{a}_g$ does not affect considerably the results.

6.3.2 Time-history response of gravity dams on rigid foundations

In this example, we investigate the dynamic response of the four dam-reservoir systems described previously, subjected to a horizontal component ground motion $\ddot{u}_g$ from Imperial Valley earthquake (1940) recorded at El Centro. The results of the exact and simplified MAM formulations developed in sections 6.2.2 and 6.2.3 are compared to those from an advanced finite element solution taking account of fluid-structure interaction between the dam and the reservoir. In the latter case, the dam is modeled using 9-node solid finite elements as before, while the reservoir is discretized using ADINA potential-based fluid elements (Bouaanani and Lu, 2009, ADINA, 2010). A direct integration time-history dynamic analysis and Rayleigh damping are used.

The formulation of the exact MAM described in Section 6.2.2 is applied using $N_s = 5$ modified accelerograms $a_g^{(j)}$, $j = 1 \ldots N_s$, determined according to Eqs. (6.14) and (6.15). This number of modes is shown sufficient to obtain convergence for the four studied gravity dams.

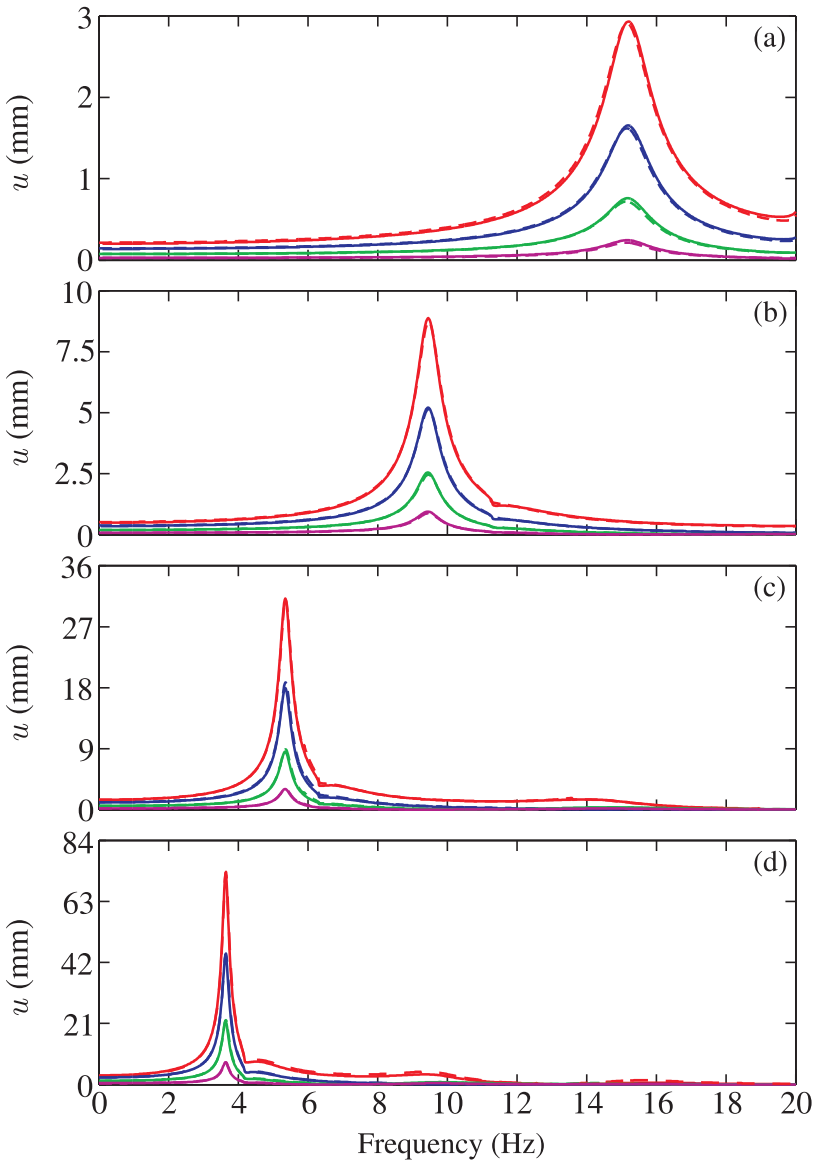

Figure 6.4 Displacement frequency response under unit harmonic ground motion computed at four different heights of points belonging to the dam-reservoir interface : (a) Dam D1 ; (b) Dam D2 ; (c) Dam D3 ; (d) Dam D4. — $y = H_s$; — $y = 3\,H_s/4$; — $y = H_s/2$; — $y = H_s/4$. Continuous lines : Results obtained using Eq. (6.21) ; Dotted lines : Results obtained using Eq. (6.22).

Each of the four dry structures is subjected to the 5 modified accelerations and a frequency shift is applied to isolate the effect of each mode and compute the corresponding modal eigenvalues and eigenvectors. Modal superposition is applied next to obtain the total time-history response of each dam-reservoir system. The same number $N_s = 5$ of modes is used to apply the formulation of the simplified MAM presented in Section 6.2.3. In this case, each of

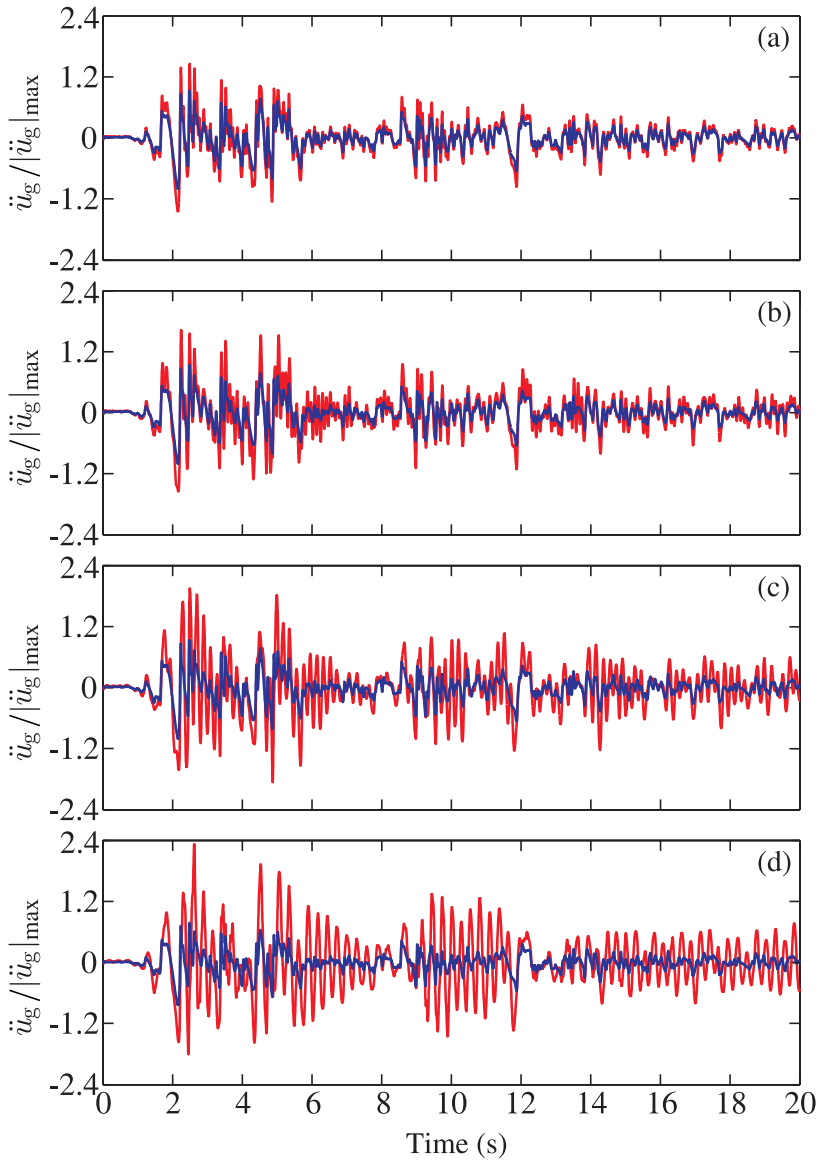

Figure 6.5 Input accelerograms : (a) Dam D1 ; (b) Dam D2 ; (c) Dam D3 ; (d) Dam D4. — Original accelrogram to be applied to dam-reservoir system ; — Simplified modified accelrogram to be applied to the dam without reservoir, i.e. Dry structure.

the four dry structures is subjected to a single modified mode-independent accelerogram $\tilde{a}_g$ determined according to Eq. (6.23). The original input accelorgram $\ddot{u}_g$ is compared to the modified accelerogram $\tilde{a}_g$ in Fig. 6.5. As can be seen, the modified accelerogram has higher amplitudes than the original one and that its frequency content is different.

Fig. 6.6 shows the crest displacements obtained using the proposed exact and simplified modified accelerogram methods, superposed to crest displacements from finite element ana-

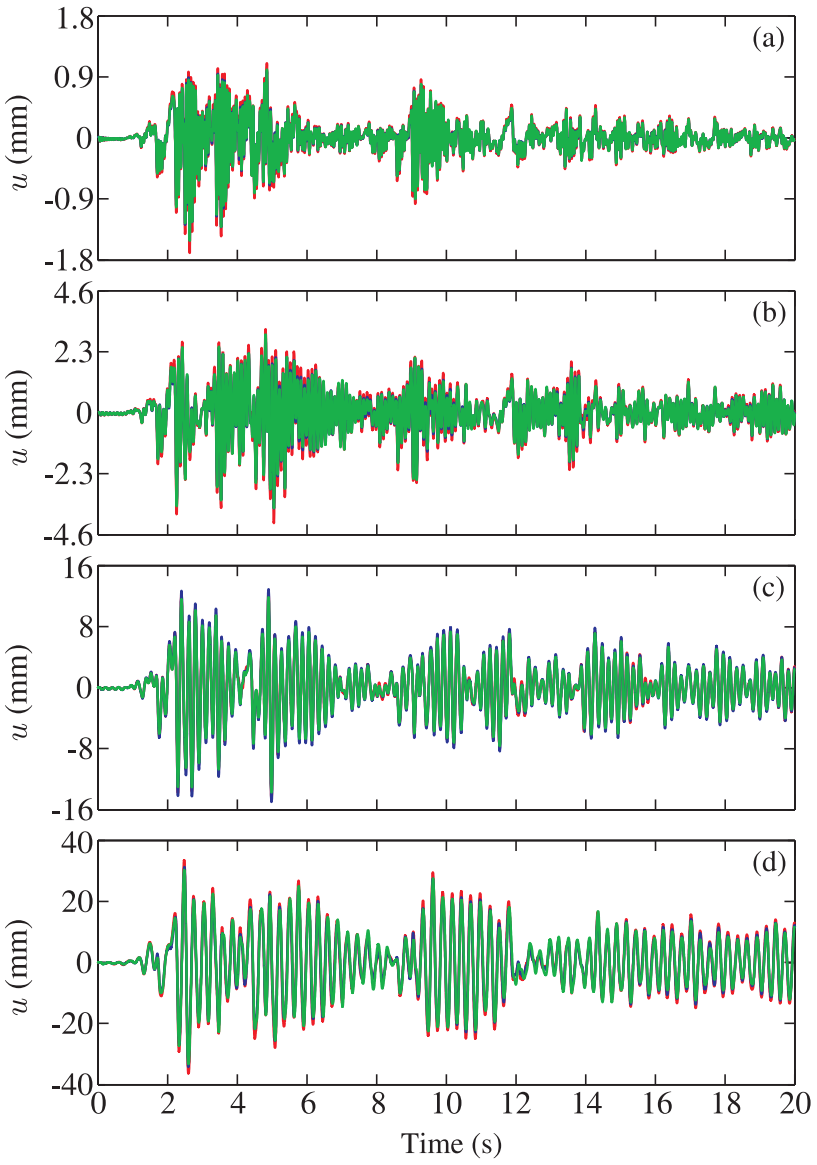

Figure 6.6 Crest displacements : (a) Dam D1 ; (b) Dam D2 ; (c) Dam D3 ; (d) Dam D4. — Proposed exact modified accelerogram method ; — Proposed simplified modified accelerogram method ; — Finite element analysis of dam-reservoir system.

lyses. We clearly see that the agreement between the three methods is excellent irrespective of the dam-reservoir geometrical properties. This figure also illustrates the effect of dam height and consequently the flexibility of the dam monolith on the dynamic response in terms of frequency content and amplitude. The ability of the proposed modified accelerogram method in predicting stress distributions within the studied dam monoliths is investigated next. Fig. 6.7 presents the maximum principal stress σ_I at maximum crest displacement for the

four studied dams obtained using the proposed exact and simplified modified accelerogram methods as well as finite element analyses. For clarity, all dam cross sections are scaled to have the same height. Fig. 6.7 shows that the three methods yield practically the same stress distributions for the four dam sections studied.

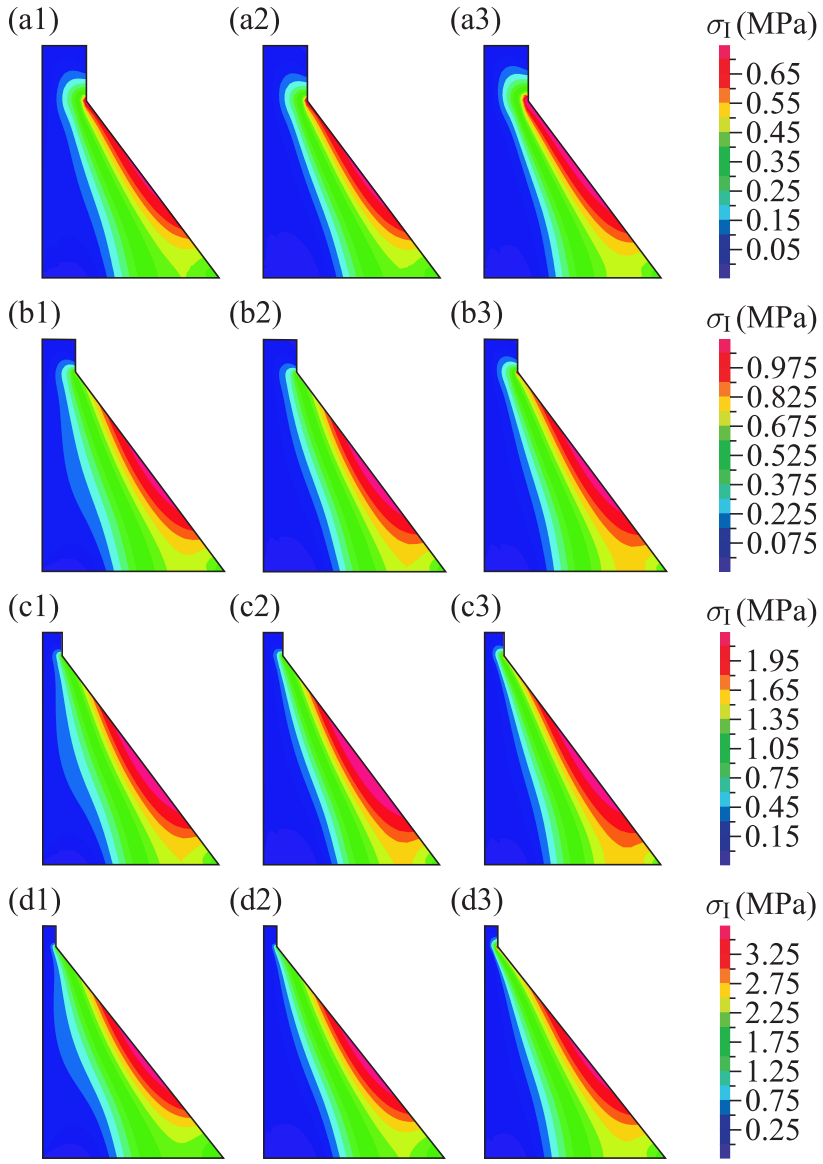

Figure 6.7 Maximum principal stress at maximum displacement : (a1) to (a3) Dam D1 ; (b1) to (b3) Dam D2 ; (c1) to (c3) Dam D3 ; (d1) to (d3) Dam D4. (a1) to (d1) Finite element analysis of dam-reservoir system ; (a2) to (d2) Proposed exact modified accelerogram method ; (a2) to (d2) Proposed simplified modified accelerogram method.

6.3.3 Time-history response of a gravity dam including the effects of foundation flexibility and reservoir bottom wave absorption

In this example, the proposed modified accelerogram methods are applied to determine the seismic response of the highest dam D4 described previously, while accounting for the effects of a flexible massless foundation and reservoir bottom wave absorption. For illustration purposes, a massless foundation with an elastic modulus $E_{\mathrm{f}}=2E_{\mathrm{s}}$ and a Poisson's ratio $\nu_{\mathrm{f}}=0.3$ is considered. The foundation domain is extended to $H_{\mathrm{f}} = 2H_{\mathrm{s}}$ in the vertical direction and $L_{\mathrm{f}}^{(1)}=L_{\mathrm{f}}^{(2)}=4H_{\mathrm{s}}$ in both upstream and downstream direction of the dam as illustrated in Fig. 6.2. Reservoir bottom wave absorption levels corresponding to $\alpha=1$, 0.85, 0.65 and 0.45 are included. The eigenvalues λ_n are determined by solving Eq. (6.A.3) numerically when applying the exact formulation of the modified accelerogram, while Eq. (6.A.5) is used when the simplified formulation of the modified accelerogram is applied. The crest displacements obtained using the proposed exact and simplified modified accelerogram methods are plotted in Fig. 6.8. For comparison purposes, the solution for a fully reflective reservoir bottom is superposed to those for absorptive reservoir bottoms. The results in Fig. 6.8 confirm the ability of the proposed simplified method to account for the effects of a massless flexible foundation and reservoir bottom wave absorption. As expected, reservoir bottom wave absorption damps out the dynamic response of the dam. We also note that for the studied dam, Eq. (6.A.5) gives satisfactory results even for the case $\alpha=0.45$.

6.4 Conclusions

A practical and efficient procedure to analyze earthquake-excited gravity dams was proposed. The developed formulation consists of including the effects of fluid-structure interaction into a new accelerogram obtained through modification of the original input ground acceleration. Using the modified accelerogram avoids the finite or boundary element discretization of the fluid domain and direct modeling of related fluid-structure interaction forces and boundary conditions. The modified accelerogram is to be applied to the dry structure, i.e. without the impounded reservoir, and can therefore be implemented in standard finite element software that includes only classical solid finite elements, and not necessarily fluid-structure interaction capabilities. The proposed procedure accounts for important seismic dam response parameters such as dam and foundation flexibility, water compressibility, and reservoir bottom wave absorption. The exact and simplified formulations of the method were developed, and their efficiency validated through examples of dam-reservoir systems with different geometries. Very satisfactory agreement is obtained when comparing the obtained results to more advanced finite element solutions including fluid-structure interaction capabilities. This

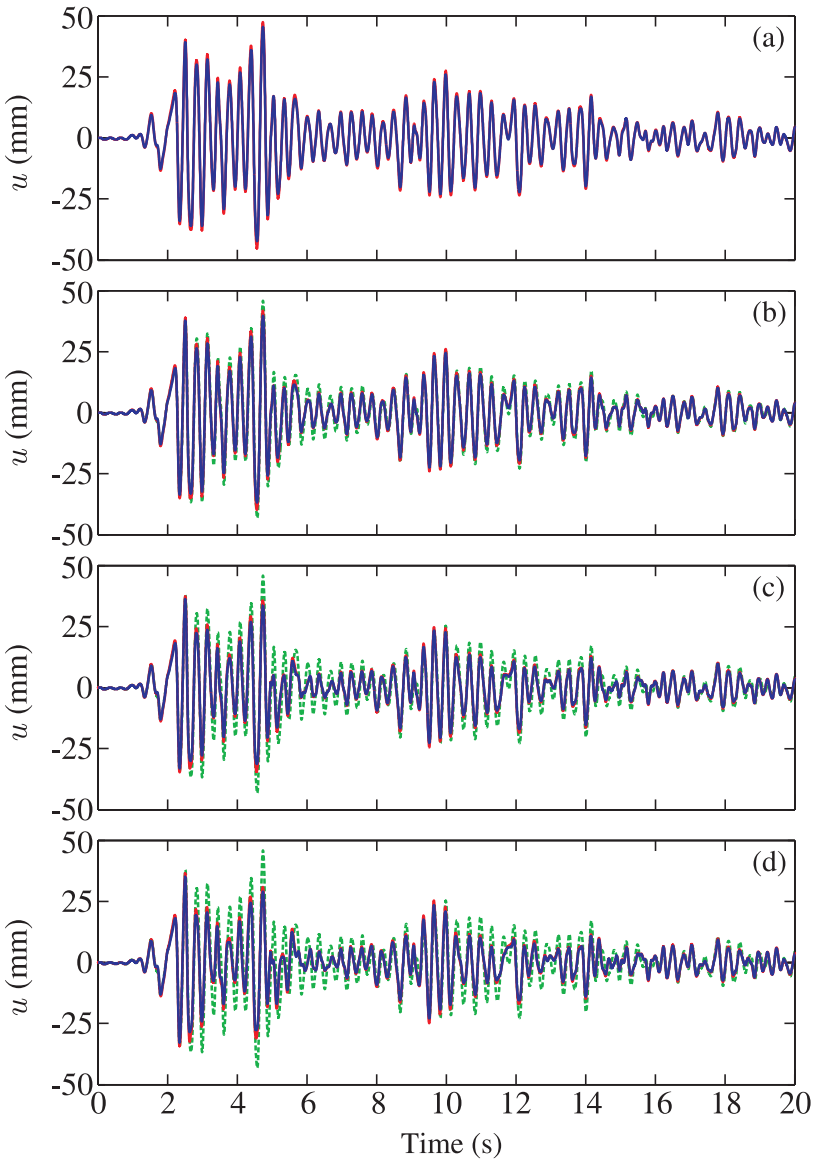

Figure 6.8 Crest displacement of dam D4 including the effects of foundation flexibility and reservoir bottom wave absorption : (a) $\alpha = 1$; (b) $\alpha = 0.85$; (c) $\alpha = 0.65$; (d) $\alpha = 0.45$. ___ Proposed exact modified accelerogram method ; ___ Proposed simplified modified accelerogram method ; _ _ Finite element analysis of dam-reservoir system with fully reflective reservoir bottom.

new procedure enhances the efficiency of seismic assessment of gravity dams by reducing the modeling and computational burden associated with reservoir discretization, while keeping the main advantages of conventional solid finite element software in conducting dynamic analyses and providing the resulting stresses, strains, or other dam response indicators.

Table 6.A1 Coefficients $A_{k,s} \times 10^3$ and $B_k \times 10^3$ evaluated for $k, s = 0 \ldots 8$.

$k =$	0	1	2	3	4	5	6	7	8
$B_k =$	-32.97427384	-37.45499915	-30.64003702	-24.67556090	-20.15164058	-16.74618429	-14.14344980	-12.11590236	-10.50697982
				$A_{k,s}$					
$s =$ 0	21.24170215	23.96908441	19.58885542	15.77091707	12.87840422	10.70209611	9.03919792	7.74396318	6.71622511
$s =$ 1	23.96908441	27.52291127	22.14548574	17.59759460	14.22526604	11.72801005	9.84309534	8.38910974	7.24446429
$s =$ 2	19.58885542	22.14548574	18.19497354	14.71696011	12.06490952	10.05935367	8.52043902	7.31745061	6.35992337
$s =$ 3	15.77091707	17.59759460	14.71696011	12.09861481	10.05323129	8.47641403	7.24730581	6.27381015	5.49028110
$s =$ 4	12.87840422	14.22526604	12.06490952	10.05323129	8.45106450	7.19601600	6.20446897	5.41006113	4.76430202
$s =$ 5	10.70209611	11.72801005	10.05935367	8.47641403	7.19601600	6.17969804	5.36758710	4.71048720	4.17170323
$s =$ 6	9.03919792	9.84309534	8.52043902	7.24730581	6.20446897	5.36758710	4.69239585	4.14142654	3.68624888
$s =$ 7	7.74396318	8.38910974	7.31745061	6.27381015	5.41006113	4.71048720	4.14142654	3.67364512	3.28464162
$s =$ 8	6.71622511	7.24446429	6.35992337	5.49028110	4.76430202	4.17170323	3.68624888	3.28464162	2.94873327

Acknowledgements

The authors would like to acknowledge the financial support of the Natural Sciences and Engineering Research Council of Canada (NSERC) and the Quebec Fund for Research on Nature and Technology (FQRNT).

References

ADINA (2010). "Theory and Modeling Guide." Report ARD 06-7. ADINA R & D, Inc.

Bayraktar, A., Hançer, E., Akköse, M. (2005). "Influence of base-rock characteristics on the stochastic dynamic response of dam–reservoir–foundation systems." *Engineering Structures*, 27, 1498-1508.

Bouaanani, N., Lu, F. Y. (2009). "Assessment of potential-based fluid finite elements for seismic analysis of dam–reservoir systems." *Journal of Computers and Structures*, 87, 206-224.

Bouaanani, N., Miquel, B. (2010). "A new formulation and error analysis for vibrating dam–reservoir systems with upstream transmitting boundary conditions." *Journal of Sound and Vibration*, 329, 1924–1953.

Bouaanani, N., Perrault, C. (2010). "Practical formulas for frequency domain analysis of earthquake-induced dam-reservoir interaction." *Journal of Engineering Mechanics*, 136, 107-119.

Chakrabarti, P., Chopra, A. K. (1973). "Earthquake analysis of gravity dams including hydrodynamic interaction." *Earthquake Engineering and Structural Dynamics*, 2, 143-160.

Chopra, A. K. (1970). "Earthquake response of concrete gravity dams." Report No. UCB/EERC-70/01, University of California, Berkeley.

Chopra, A. K. (1978). "Earthquake resistant design of concrete gravity dams." *Journal of the Structural Division* (ASCE), 104, 953-971.

Fenves, G., Chopra, A. K. (1984). "Earthquake analysis and response of concrete gravity dams." Report No. UCB/EERC-84/10, University of California, Berkeley, California.

Fenves, G., Chopra A. K. (1984). "EAGD-84, a computer program for earthquake analysis of concrete gravity dams." Report No. UCB/EERC-84/11, University of California, Berkeley, California.

Fenves, G., Chopra, A. K. (1987). "Simplified earthquake analysis of concrete gravity dams." *Journal of Structural Engineering*, 113(8), 1688-1708.

Fok, K. L., Hall, J. F., Chopra, A. K. (1986). "EACD-3D, a computer program for three-dimensional earthquake analysis of concrete dams." Report No. UCB/EERC-86/09, University of California, Berkeley, California.

Hall, J. F., Chopra, A. K. (1982). "Two-dimensional dynamic analysis of concrete gravity and embankment dams including hydrodynamic effects." *Earthquake Engineering and Structural Dynamics*, 10, 305-332.

Humar, J. L., Jablonski, A. M. (1988). "Boundary element reservoir model for seismic analysis of gravity dams." *Earthquake Engineering and Structural Dynamics*, 16, 1129-1156.

Liu, P. H., Cheng A., (1984). "Boundary solutions for fluid-structure interaction." *Journal of Hydraulic Engineering*(ASCE), 110 (1), 51-64.

Maeso, O., Aznarez, JJ., Dominguez, J. (2004) "Three-dimensional models of reservoir sediment and effects on the seismic response of arch dams." *Earthquake Engineering and Structural Dynamics*, 33, 1103-1123.

Maity, D. (2005). "A novel far-boundary condition for the finite element analysis of infinite reservoir." *Applied Mathematics and Computation*, 170, 1314-1328.

Miquel, B., Bouaanani, N. (2010). "Simplified evaluation of the vibration period and seismic response of gravity dam-water systems." *Journal of Engineering Structures*, 32, 2488-2502.

Saini, S. S., Bettess, P., Zienkiewicz, O. C. (1978). "Coupled hydrodynamic response of concrete gravity dams using finite and infinite elements." *Earthquake Engineering and Structural Dynamics*, 6, 363-374.

Sharan, S. K. (1985). "Finite element modelling of infinite reservoirs." *Journal of Engineering Mechanics*(ASCE), 111, 1457-1469.

Sommerfeld, A. (1949). "Partial differential equations in physics." Academic Press, New York.

Tsai, C. S., Lee, G. C. (1987). "Arch dam-fluid interactions : by FEM-BEM and substructure concept." *International Journal of Numerical Methods in Engineering*, 24, 2367-2388.

Zienkiewicz, O. C., Newton, R. E. (1969). "Coupled vibrations in a structure submerged in a compressible fluid." *International Symposium on Finite Element Techniques*, Stuttgart.

Appendix A

The frequency response function (FRF) for total hydrodynamic pressure exerted on the face of the dam subjected to unit horizontal harmonic ground acceleration $\ddot{u}_{\mathrm{g}}(t)=\mathrm{e}^{\mathrm{i}\omega t}$ can be decomposed as (Fenves and Chopra, 1984a)

$$\bar{p}(y,\omega) = \bar{p}_0(y,\omega) - \omega^2 \sum_{j=1}^{N_{\mathrm{s}}} \bar{Z}_j(\omega)\, \bar{p}_j(y,\omega) \tag{6.A.1}$$

where $\bar{p}_0$ is the FRF for hydrodynamic pressure due to rigid body motion of the dam, and where $\bar{p}_j$ is the FRF corresponding to hydrodynamic pressure due to horizontal acceleration $\psi_j^{(x)}(y)=\psi_j^{(x)}(0,y)$ of the dam upstream face along structural mode j. Using the boundary conditions translating free reservoir surface, compatibility at dam-reservoir interface, undisturbed pressure at infinite and wave reflection at reservoir bottom, FRFs $\bar{p}_0$ and $\bar{p}_j$ can be expressed at upstream face of the dam as (Fenves and Chopra, 1984a, Bouaanani and Miquel, 2010)

$$\bar{p}_0(y,\omega) = -2\rho_{\mathrm{r}} H_{\mathrm{r}} \sum_{n=1}^{N_{\mathrm{w}}} \frac{\lambda_n(\omega)^2\, I_{0,n}(\omega)}{\beta_n(\omega)\,\kappa_n(\omega)}\, Y_n(y,\omega)\,;\;\; \bar{p}_j(y,\omega) = -2\rho_{\mathrm{r}} H_{\mathrm{r}} \sum_{n=1}^{N_{\mathrm{w}}} \frac{\lambda_n(\omega)^2\, I_{j,n}(\omega)}{\beta_n(\omega)\,\kappa_n(\omega)}\, Y_n(y,\omega) \tag{6.A.2}$$

where N_{w} is the number of water modes included in the analysis, and λ_n and Y_n are complex-valued frequency-dependent eigenvalues and orthogonal eigenfunctions satisfying for each reservoir mode n

$$\mathrm{e}^{2\mathrm{i}\lambda_n(\omega)H_{\mathrm{r}}} = -\frac{\lambda_n(\omega)-\omega q}{\lambda_n(\omega)+\omega q}\,; \qquad Y_n(y,\omega) = \frac{\big[\lambda_n(\omega)-\omega q\big]\mathrm{e}^{-\mathrm{i}\lambda_n(\omega)\,y} + \big[\lambda_n(\omega)+\omega q\big]\mathrm{e}^{\mathrm{i}\lambda_n(\omega)\,y}}{2\lambda_n(\omega)} \tag{6.A.3}$$

in which q is a damping coefficient defined at the reservoir bottom as

$$q = \frac{\rho_{\mathrm{r}}}{\rho_{\mathrm{f}} C_{\mathrm{f}}} = \frac{1}{C_{\mathrm{r}}}\frac{1-\alpha}{1+\alpha} \tag{6.A.4}$$

where ρ_{f} and C_{f} denote the mass density and the compression wave velocity within the reservoir foundation, respectively, C_{r} is compression wave velocity within the reservoir, and α is the wave reflection coefficient representing the portion of the wave amplitude reflected back to the reservoir. The first relation in Eq. (6.A.3) is a transcendental equation to be solved numerically to obtain the eigenvalues λ_n. In the context of a simplified method, the following approximate closed-form expression developed by the second author in a previous work (Bouaanani and Perrault, 2010) can be used for highly to moderately reflective

reservoirs, i.e. $\alpha \geqslant 0.65$

$$\lambda_n(\omega) = \frac{(2n-1)\pi}{4H_\mathrm{r}} + \sqrt{\frac{(2n-1)^2\pi^2}{(4H_\mathrm{r})^2} + \mathrm{i}\,\frac{\omega q}{H_\mathrm{r}}} \tag{6.A.5}$$

If full wave reflection at reservoir bottom is assumed (i.e. $\alpha = 1$), the reservoir modes λ_n are frequency-independent and simplify to

$$\lambda_n = \frac{(2n-1)\,\pi}{2\,H_\mathrm{r}} \tag{6.A.6}$$

yielding to hydrodynamic pressure FRFs $\bar{p}_0$ and $\bar{p}_j$

$$\bar{p}_0(y,\omega) = \frac{-4\rho_\mathrm{r}}{\pi} \sum_{n=1}^{N_\mathrm{w}} \frac{(-1)^n}{(2n-1)} \frac{\cos(\lambda_n\, y)}{\sqrt{\lambda_n^2 - \dfrac{\omega^2}{C_\mathrm{r}^2}}}\,; \qquad \bar{p}_j(y,\omega) = 2\rho_\mathrm{r} \sum_{n=1}^{N_\mathrm{w}} \frac{I_{j,n}(\omega)}{\sqrt{\lambda_n^2 - \dfrac{\omega^2}{C_\mathrm{r}^2}}} \cos\left(\lambda_n\, y\right) \tag{6.A.7}$$

The parameters β_n, κ_n, $I_{0,n}$, and $I_{j,n}$ in Eq. (6.A.2) are given by

$$\beta_n(\omega) = H_\mathrm{r}\left[\lambda_n(\omega)^2 - \omega^2\, q^2\right] + \mathrm{i}\,\omega q\,; \qquad \kappa_n(\omega) = \sqrt{\lambda_n(\omega)^2 - \frac{\omega^2}{C_\mathrm{r}^2}} \tag{6.A.8}$$

$$I_{0,n}(\omega) = \frac{\mathrm{i}\mathrm{e}^{-\mathrm{i}\lambda_n(\omega)H_\mathrm{r}}}{\lambda_n(\omega)^2 H_\mathrm{r}}\left[\lambda_n(\omega) - \omega q + \omega q \mathrm{e}^{\mathrm{i}\lambda_n(\omega)H_\mathrm{r}}\right]; \qquad I_{j,n}(\omega) = \frac{1}{H_\mathrm{r}} \int_0^{H_\mathrm{r}} \psi_j^{(x)}(y)\, Y_n(y,\omega)\,\mathrm{d}y \tag{6.A.9}$$

For practical computations, the the x–component of mode shape $\boldsymbol{\psi}_j$, $j = 1 \ldots N_\mathrm{s}$, of the dry structure can be approximated by a polynomial function of order $N_{\boldsymbol{\psi}_j}$ and coefficients $a_{j,k}$ as given by Eq. (6.29) and illustrated in Fig. 6.2. Bouaanani and Perrault (2010) showed that the parameters $I_{0,n}$ and $I_{j,n}$ can then be related by

$$I_{j,n}(\omega) = F_{j,n}(\omega)\, I_{0,n}(\omega) + G_{j,n}(\omega) \tag{6.A.10}$$

where the coefficients $F_{j,n}$ and $G_{j,n}$ are developed by Bouaanani and Perrault (2010) as

$$F_{j,n}(\omega) = \sum_{k} \left\{ \left[\sum_{\ell=0}^{k} (-1)^{k-\ell} \frac{\Lambda_{2\ell}(\lambda_n H_\mathrm{r})}{\Lambda_{2k}(\lambda_n H_\mathrm{s})} \right] a_{j,2k} + \left[\sum_{\ell=0}^{k} (-1)^{k-\ell} \frac{\Lambda_{2\ell+1}(\lambda_n H_\mathrm{r})}{\Lambda_{2k+1}(\lambda_n H_\mathrm{s})} \right] a_{j,2k+1} \right\} \tag{6.A.11}$$

$$G_{j,n}(\omega) = -\frac{\mathrm{i}\,\omega q}{\lambda_n^2 H_\mathrm{r}} F_{j,n}(\omega) + \frac{1}{\lambda_n H_\mathrm{r}} \sum_{k} \left\{ \left[\frac{\mathrm{i}\,\omega q}{\lambda_n} \frac{(-1)^k}{\Lambda_{2k}(\lambda_n H_\mathrm{s})} \right] a_{j,2k} - \left[\frac{(-1)^k}{\Lambda_{2k+1}(\lambda_n H_\mathrm{s})} \right] a_{j,2k+1} \right\} \tag{6.A.12}$$

in which $\lambda_n(\omega)$ is noted as λ_n for clarity and the complex-valued function Λ_m is defined as

$$\Lambda_m(z) = \frac{z^m}{m!} \tag{6.A.13}$$

CHAPITRE 7

Discussion générale

7.1 Introduction

Bien que de nombreuses méthodes complexes existent dans la littérature et puissent tenir compte de nombreux paramètres ayant de l'influence sur la réponse dynamique des structures en contact avec de l'eau, ces méthodes ne sont que rarement utilisées dans la pratique routinière de l'ingénieur. Leur complexité ainsi que l'expertise requise pour les appliquer sont souvent un frein à leur utilisation. Par conséquent, et comme il a été mentionné précédemment, les méthodes simplifiées demeurent les plus courantes. Cependant, ces méthodes ont été développées en se basant sur de nombreuses hypothèses simplificatrices qui peuvent affecter l'estimation de la réponse dynamique des systèmes étudiés. Le but de ce chapitre est de comparer des méthodes simplifiées courantes à des techniques complexes afin d'identifier leur validité et leur robustesse. La réponse dynamique des systèmes eau-structures dépend de très nombreux paramètres rendant impossible l'isolation de l'effet de chacun d'entre eux. C'est pour cela que nous nous contenterons d'étudier la validité de ces méthodes pour plusieurs géométries données d'un système barrage-réservoir. On doit donc noter que les résultats obtenus ici ne permettent pas de généraliser les conclusions à tous les barrages. Néanmoins, nous cherchons dans ce chapitre à mettre en valeur les conséquences que peuvent avoir les hypothèses simplificatrices sur la réponse dynamique des structures en contact avec de l'eau. Par ailleurs, nous aborderons certaines difficultés liées à la modélisation de l'interaction fluide-structure.

7.2 Description des méthodes étudiées

Nous reprenons tout d'abord certaines méthodes présentées dans la revue de littérature et détaillées dans les chapitres précédents. De nouveaux développements liés à la méthode pseudo-dynamique développée au cours de ce doctorat seront décrits. À des fins de clarté, le même système et la même notation que ceux présentés dans la Figure 2.1 seront utilisés pour chacune des méthodes décrites ci-après. Nous considérons une fondation rigide et aucune absorption engendrée par le dépôt de sédiments au fond du réservoir.

7.2.1 Méthodes de références

La méthode analytique de Chopra et collaborateurs ainsi que la méthode numérique des éléments finis sont présentées ici et serviront de méthodes de références pour les comparaisons.

Méthode analytique de Fenves et Chopra (1984)

Cette méthode ayant été largement décrite dans les chapitres précédents, seules les équations nécessaires pour le calcul de la réponse dynamique d'un système barrage-réservoir y seront rappelées. L'équilibre dynamique du système barrage-réservoir peut s'exprimer dans le domaine fréquentiel par :

$$\left[-\omega^2\,\mathbf{M} + \mathrm{i}\,\omega\,\mathbf{C} + \mathbf{K}\right]\overline{\mathbf{U}}(\omega) = -\mathbf{M}\,\mathbf{1} + \bar{F}_{\mathrm{h}}(\omega) \tag{7.1}$$

où $\overline{\mathbf{U}}$ est un vecteur colonne contenant les fonctions de réponses en fréquences (FRF) des déplacements relatifs nodaux du barrage, $\mathbf{M}$, $\mathbf{C}$ et $\mathbf{K}$ sont respectivement les matrices de masses, d'amortissement, et de rigidité, $\bar{F}_{\mathrm{h}}$ est un vecteur colonne contenant les FRF des pressions hydrodynamiques, et $\mathbf{1}$ est un vecteur colonne de même dimension que celui des déplacements, et contenant des zéros sauf sur les degrés de liberté horizontaux qui correspondent à la direction de l'excitation sismique. En utilisant la superposition modale, les FRF des déplacements et accélérations aux coordonnées (x, y) sont donnés par

$$\bar{u}(x,y,\omega) = \ddot{u}_{\mathrm{g}}(\omega)\sum_{j=1}^{N_{\mathrm{s}}}\psi_j^{(x)}(x,y)\,\bar{Z}_j(\omega)\,; \qquad \bar{\ddot{u}}(x,y,\omega) = -\ddot{u}_{\mathrm{g}}(\omega)\,\omega^2\sum_{j=1}^{N_{\mathrm{s}}}\psi_j^{(x)}(x,y)\,\bar{Z}_j(\omega) \tag{7.2}$$

$$\bar{v}(x,y,\omega) = \ddot{u}_{\mathrm{g}}(\omega)\sum_{j=1}^{N_{\mathrm{s}}}\psi_j^{(y)}(x,y)\,\bar{Z}_j(\omega)\,; \qquad \bar{\ddot{v}}(x,y,\omega) = -\ddot{u}_{\mathrm{g}}(\omega)\,\omega^2\sum_{j=1}^{N_{\mathrm{s}}}\psi_j^{(y)}(x,y)\,\bar{Z}_j(\omega) \tag{7.3}$$

où $\bar{u}$ et $\bar{v}$ sont les déplacements horizontaux et verticaux relatifs, $\bar{\ddot{u}}$ et $\bar{\ddot{v}}$ les accélérations horizontales et verticales, $\psi_j^{(x)}$ et $\psi_j^{(y)}$ sont les composantes x– et y–du $j^{\text{ème}}$ mode du barrage, $\bar{Z}_j$ la coordonnée généralisée, N_{s} le nombre de modes structuraux inclut dans l'analyse et $\ddot{u}_{\mathrm{g}}(\omega)$ est l'amplitude de l'accélération du sol à la fréquence d'excitation ω. Fenves et Chopra (1984) ont démontré que la pression hydrodynamique totale peut se décomposer en une pression due au mouvement de corps rigide du barrage $\bar{p}_0$ et une pression du à sa flexibilité $\bar{p}_j$. La pression total $\bar{p}$ pour une accélération unitaire du sol se calcule en utilisant l'équation (3.2).
Afin de déterminer les déplacements dans la structure, les coordonnées généralisées doivent être déterminées au préalable. Pour cela, les équations (3.3) à (3.8) doivent être évaluées pour chaque fréquence et mode structural afin de calculer les pressions $\bar{p}_0$ et $\bar{p}_j$. Pour le

calcul des ces pressions, on note que les modes de vibrations structuraux sont nécessaires. Une analyse modale par éléments finis de la structure sèche (i.e. avec le réservoir vide) peut être réalisée. Ces pressions sont ensuite utilisées pour le calcul des termes de la matrice $\bar{\mathbf{S}}$ et du vecteur $\bar{\mathbf{Q}}$. Ils sont donnés respectivement par les équations (3.12) et (3.13). Dans ces équations, les propriétés dynamiques de la structure sèche sont aussi nécessaires. De même que précédemment, une analyse par éléments finis permettera de calculer les fréquences naturelles ω_n et les facteurs de participations modales L_n. Si les modes structuraux utilisés proviennent d'une analyse par éléments finis, ils sont généralement normalisés par rapport à la masse et donc $M_n = 1$. Finalement, la résolution du système (3.11) permet alors d'obtenir les coordonnées généralisées pour chacun des modes structuraux inclus dans l'analyse. Dans le cas ou un seul mode de vibration est pris en compte, la coordonnée généralisée peut directement être calculée par l'équation (3.17).

Une fois que les coordonnées généralisées sont calculées, les déplacements, vitesses, accélérations et pressions peuvent être déterminés par superposition modale. Dans ce qui suit, nous nous intéresserons aussi à la position de la résultante des forces hydrodynamiques y_{g} ainsi qu'à la force de cisaillement totale à la base de l'ouvrage $\mathcal{V}$. Ces deux résultats peuvent être calculés par :

$$y_{\mathrm{g}}(\omega) = \frac{\displaystyle\int_0^{H_{\mathrm{r}}} y\, \bar{p}(0, y, \omega)\, \mathrm{d}y}{\displaystyle\int_0^{H_{\mathrm{r}}} \bar{p}(0, y, \omega)\, \mathrm{d}y} \tag{7.4}$$

$$\mathcal{V}(\omega) = \ddot{u}_{\mathrm{g}}(\omega) \sum_{j=1}^{N_{\mathrm{s}}} \omega_j^2\, L_j\, \bar{Z}_j(\omega) \tag{7.5}$$

Méthode des éléments finis

Cette méthode a été décrite dans la revue de littérature ainsi que dans les chapitres précédants. Elle consiste à discrétiser le réservoir et la structure en éléments finis. Des éléments d'interfaces sont placés entre les deux domaines afin de tenir compte de l'interaction fluide-structure. Dans notre cas, la formulation Eulérienne pour les éléments finis fluides et le logiciel ADINA (2010) ont été choisis. En effet, les travaux de Bouaanani et Lu (2009) ont validé ces choix en montrant notamment que d'excellents résultats sont obtenus lorsque comparés à la méthode analytique de Fenves et Chopra (1984).

Deux types d'analyses sont possibles afin de déterminer les courbes de réponses en fré-

quences. La première consiste à utiliser une analyse modale. Pour celle-ci, un ratio d'amortissement modal est utilisé. L'autre solution, très coûteuse en temps de calcul, consiste à réaliser une analyse temporelle par intégration directe où un amortissement de Rayleigh (1877) est utilisé. Un signal sinusoïdal unitaire de fréquence ω est utilisé comme excitation. Suffisamment de pas de calcul sont pris en compte afin d'obtenir la magnitude maximale de la réponse permanente. Cette démarche est effectuée pour chaque fréquence d'intérêt.

Selon le type d'analyse effectuée, la compressibilité de l'eau peut ou non être incluse. En effet, l'interaction fluide-structure modifie les propriétés dynamiques de la structure. Lorsque la compressibilité de l'eau est négligée, l'effet de l'interaction fluide-structure peut être modélisé comme une masse ajoutée indépendante de la fréquence d'excitation. Cette masse modifie la période de vibration du système et ajoute une force additionnelle. Lorsque la compressibilité est incluse, cette masse ajoutée devient dépendante de la fréquence, et un amortissement additionnel est ajouté au système eau-structure. Afin d'expliquer ce phénomène, il faut se rappeler que l'incompressibilité signifie que les ondes de pressions se déplacent à une vitesse infinie dans le domaine d'eau. Par conséquent, quelle que soit la longueur du réservoir, une onde de pression peut instantanément se propager d'un bord à l'autre du domaine. Lorsque la compressibilité de l'eau est incluse, cette même onde met un certain temps pour se propager d'un côté à l'autre. Si le domaine est semi-infini, l'onde devrait se propager vers l'infini. Ceci a pour conséquence une perte d'énergie ou amortissement additionnel. La dépendance de la fréquence dans le cas d'une eau compressible provient du fait que, tout comme une structure, le réservoir a des périodes de vibrations. Selon si l'excitation est proche ou loin de ces périodes, l'amplification ne sera pas la même.

Pour l'eau considérée incompressible, ces observations justifient les résultats obtenus dans le chapitre 4. Nous avions conclu que le domaine d'eau peut être seulement modélisé sur une distance égale à trois fois sa hauteur, et un mur rigide peut-être utilisé comme condition aux frontières. En effet, étant donné que pour cette hypothèse il n'y a aucune perte d'énergie en raison de la géométrie infinie du domaine d'eau, une condition aux frontières transmettantes n'est pas requise. Avec ces observations, une analyse modale ou temporelle par intégration directe peut être réalisée.

Dans le cas où la compressibilité de l'eau est incluse dans l'analyse, un mur rigide n'est plus adéquat pour la modélisation du domaine d'eau, car on doit tenir compte de la dissipation d'énergie de propagation des ondes de compression à l'infini. Une condition aux frontières transmettantes (CFT) est alors nécessaire. Dans la première partie de cette thèse,

une attention particulière a été portée à l'utilisation de ces conditions aux frontières et leur comportement. Les résultats de cette recherche ont fait l'objet d'un article mis en annexe A de cette thèse. De par le grand nombre de CFT proposées dans la littérature, il a paru utile de proposer un test numérique permettant de valider leur performance et leur efficacité. Pour cela, nous avons commencé par développer une formulation analytique pour étudier un système barrage-réservoir où le réservoir est tronqué à une certaine distance et où l'on applique une CFT donnée. Cette formulation a conduit à l'expression exacte de la CFT requise pour obtenir une réponse dynamique identique à celle d'un réservoir infini. Afin de comprendre le fonctionnement de la CFT exacte développée ou d'autres conditions reportées dans la littérature, nous avons testé la sensibilité de la réponse d'un système barrage-réservoir à : (i) la distance de troncature du réservoir, (ii) la profondeur du réservoir, (iii) l'absorption d'énergie au fond du réservoir en raison de la sédimentation, (iv) la compressibilité de l'eau, et (v) la rigidité du barrage. Une des observations très importantes qui ressort de ces tests numériques est que contrairement à beaucoup de CFT proposées dans la littérature, la CFT exacte dépend de la fréquence d'excitation et varie verticalement selon la hauteur du réservoir. C'est pour ces raisons qu'une analyse modale d'un système où la compressibilité de l'eau est incluse ne peut pas être réalisée. Étant donné que l'amortissement est négligé lors de la résolution du problème aux valeurs propres dans une analyse modale, on obtient par ce type d'analyse une très bonne estimation des périodes naturelles du système barrage-réservoir. Lorsque l'on cherche à obtenir des courbes de réponses en fréquences, on doit donc utiliser une analyse temporelle par intégration directe décrite précédemment.

7.2.2 Description des méthodes simplifiées existantes

Méthode des masses ajoutées de Westergaard (1933)

En ce qui concerne le développement des masses de Westergaard (1933), nous avons vu que le barrage est considéré comme étant infiniment rigide. Cela signifie physiquement qu'il n'y a aucune amplification dynamique le long de la hauteur du barrage et donc que le déplacement de n'importe quel point de la structure est égal à celui du sol. Si on applique cette hypothèse à l'équation développée par Fenves et Chopra (1984) pour le calcul de la pression hydrodynamique totale, cela signifie aussi que

$$\bar{p}(x, y, \omega) = \bar{p}_0(x, y, \omega) \tag{7.6}$$

D'après l'équation (3.4) la pression totale peut alors être calculée par

$$\bar{p}_0(x,y,\omega) = \frac{4\rho_\mathrm{r}}{\pi}\sum_{n=1}^{N_\mathrm{r}} \frac{(-1)^n}{(2n-1)}\,\frac{\mathrm{e}^{\kappa_n(\omega)x}}{\kappa_n(\omega)}\,\cos\left(\lambda_n\,y\right) \tag{7.7}$$

Lorsque l'on néglige la compressibilité de l'eau, i.e. $C_\mathrm{r} \to +\infty$, cette pression hydrodynamique devient indépendante de la fréquence d'excitation soit

$$\bar{p}_0(x,y) = \frac{8\rho_\mathrm{r} H_\mathrm{r}}{\pi^2}\sum_{n=1}^{N_\mathrm{r}} \frac{(-1)^n}{(2n-1)^2}\,\mathrm{e}^{\lambda_n x}\,\cos\left(\lambda_n\,y\right) \tag{7.8}$$

En simplifiant cette dernière équation, Westergaard (1933) propose l'approximation donnée par l'équation (2.9) pour la pression hydrodynamique. L'effet de la pression est ensuite transformé en masses ajoutées telles que formulées dans l'équation (2.10)

Dans la revue de littérature, nous avons présenté un facteur de correction C_e à appliquer sur les masses ajoutées de Westergaard (1933) afin de tenir compte de la compressibilité de l'eau. Ce rapport est donc défini comme étant le ratio de la pression tenant compte de la compressibilité de l'eau (i.e. (7.7)) sur celle négligeant la compressibilité (i.e. (7.8)) et ce pour chaque mode acoustique du réservoir n . En utilisant les deux équations précédentes on montre alors que

$$C_{\mathrm{e},n}(\omega) = \left\{1 - \left[\frac{\omega}{(2n-1)\,\omega_0}\right]^2\right\}^{-0.5} \tag{7.9}$$

où $\omega_0 = \pi C_\mathrm{r}/(2H_\mathrm{r})$ est la fréquence fondamentale du réservoir. Cette expression peut être réécrite en terme de période T

$$C_{\mathrm{e},n}(T) = \left\{1 - \left[\frac{4\,H_\mathrm{r}}{(2n-1)\,T\,C_\mathrm{r}}\right]^2\right\}^{-0.5} \tag{7.10}$$

Si on se limite seulement au premier mode $n=1$, on retrouve le facteur de correction proposé par Westergaard (1933) :

$$C_{\mathrm{e},1}(T) = \left\{1 - \left[\frac{4\,H_\mathrm{r}}{T\,C_\mathrm{r}}\right]^2\right\}^{-0.5} \tag{7.11}$$

On remarque que selon la période d'excitation, ce facteur peut être réel ou imaginaire. Étant donné que la pression tenant compte de la compressibilité de l'eau est elle aussi purement réelle ou imaginaire, la valeur absolue de ce facteur peut être utilisée. Les courbes de contours donnant la valeur absolue de $C_{\mathrm{e},2}$ et $C_{\mathrm{e},2}$ pour les deux premiers modes sont présentées dans

la figure 7.1 en fonction de la hauteur du réservoir et de la période d'excitation.
On remarque que l'effet de la compressibilité sur le deuxième mode acoustique peut généralement être négligé. En effet, à part pour des périodes d'excitations très faibles, on a $C_{e,2} \simeq 1$. Par ailleurs, la contribution des modes acoustiques supérieurs sur la pression hydrodynamique étant bien moindre que celle du premier mode, cela justifie encore plus cette simplification. On remarque cependant que pour le premier mode acoustique, la valeur de ce coefficient de correction varie de façon très importante en fonction de la hauteur du réservoir et de la période d'excitation. Par exemple, pour un barrage de 75 m excité à une période de 0.2 s on obtient $C_{e,1} \geq 3$. Cela signifie que la pression hydrodynamique associée au mouvement de corps rigide du barrage et tenant compte de la compressibilité de l'eau est plus de 3 fois supérieure à celle négligeant la compressibilité de l'eau. Nous avions vu que dans la pratique, il est préférable de fixer la valeur de T afin d'obtenir des masses ajoutées indépendantes de la fréquence. La figure 7.1 montre clairement que la variation de C_e en fonction de la période d'excitation est très importante, et par conséquent une telle pratique ne semble pas être justifiée sachant que le contenu fréquentiel d'un tremblement de terre ne se limite pas à une seule fréquence.

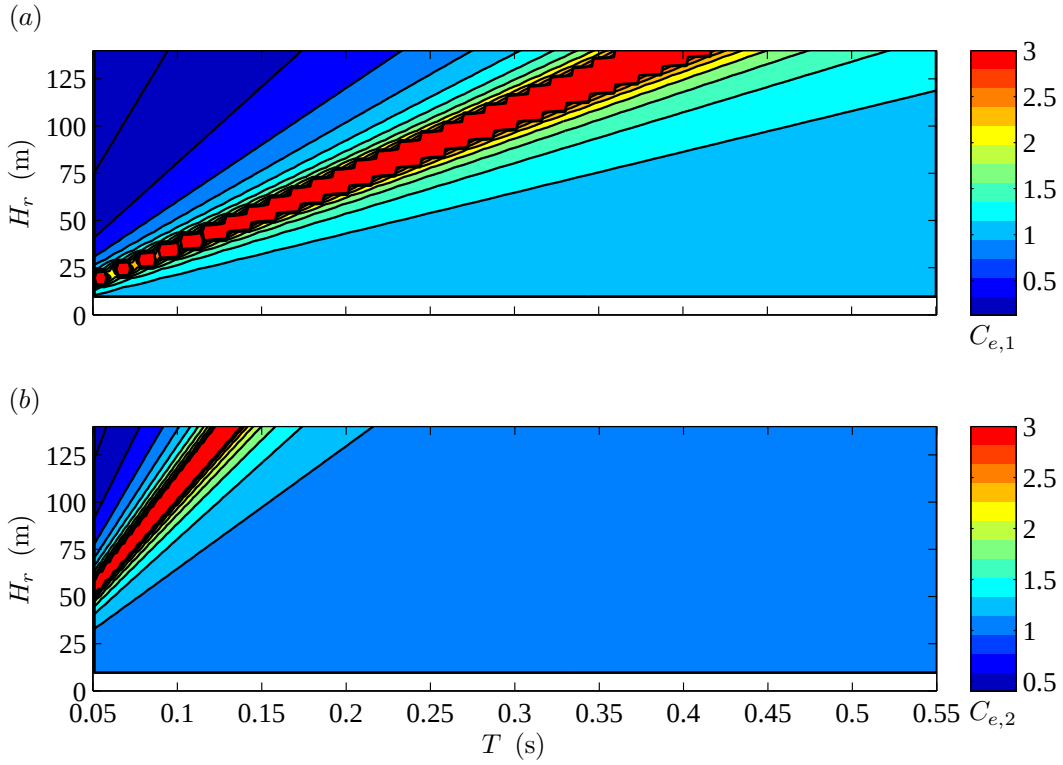

Figure 7.1 Valeur de $C_{e,n}$, $n=1,2$: (a) $n=1$; (b) $n=2$.

Dans ce qui suit, un coefficient de correction $C_{e,n} = 1$ sera utilisé pour cette méthode. Sous ces hypothèses et en utilisant le profil de pression simplifiée de Westergaard (1933), on montre que la position de la résultante des forces hydrodynamiques peut être calculée par

$$y_g = \frac{2}{5} H_r \tag{7.12}$$

et la force de cisaillement à la base est donnée par

$$\mathcal{V}(\omega) = \left[M_s + \frac{7}{12} \rho_r H^2 \right] \ddot{u}_g(\omega) \tag{7.13}$$

où M_s est la masse totale du barrage.
Nous nous intéresserons aussi aux réponses obtenues par l'utilisation des masses ajoutées de Westergaard (1933) sur une structure modélisée comme étant flexible dans un logiciel d'éléments finis. En effet, malgré les hypothèses de développement, cette façon de faire est très courante.

Méthode de Fenves et Chopra (1985)

Cette méthode a été décrite dans la section 2.3.2. La méthodologie pour l'appliquer a été décrite par Fenves et Chopra (1985). Dans ce qui suit, nous utiliserons seulement l'approximation du mode fondamental ψ_1 dont les valeurs sont données par Fenves et Chopra (1985) et de la période fondamentale du barrage donnée par

$$T_1 = \frac{0.38 H_s}{\sqrt{E_s}} \tag{7.14}$$

Ces deux paramètres seront alors introduits dans la méthode développée durant cette thèse et décrite au chapitre 3. On doit noter que d'autres approximations ont été réalisées lors du développement de leur méthode et peuvent affecter les résultats.

Méthode simplifiée de Miquel et Bouaanani (2010)

Cette méthode a été développée au cours de cette thèse de doctorat et a fait l'objet d'un article présenté dans le chapitre 3. Contrairement à la méthode de Fenves et Chopra (1985), cette méthode permet de calculer les courbes de réponses en fréquences des quantités d'intérêts. Les étapes pour calculer ces quantités sont présentées en annexe B.2 où certains nouveaux développements ont été ajoutés.

7.3 Description et discussion des propriétés utilisées pour l'analyse paramétrique

7.3.1 Description du modèle utilisé

La section du barrage-poids Pine Flat aux États-Unis, illustrée dans la figure 7.2.(b), est utilisée comme section de référence. Ce barrage a une hauteur de $H_{\mathrm{PF}} = 121.92\,\mathrm{m}$, et une base de largeur $B_{\mathrm{PF}} = 95.805\,\mathrm{m}$. Une masse volumique de $\rho_{\mathrm{s}} = 2400\ \mathrm{kg/m^3}$, un module d'élasticité de $E_{\mathrm{s}} = 25\,\mathrm{GPa}$ et un coefficient de Poisson de $\nu = 0.2$ sont adoptés comme propriétés pour l'ouvrage.

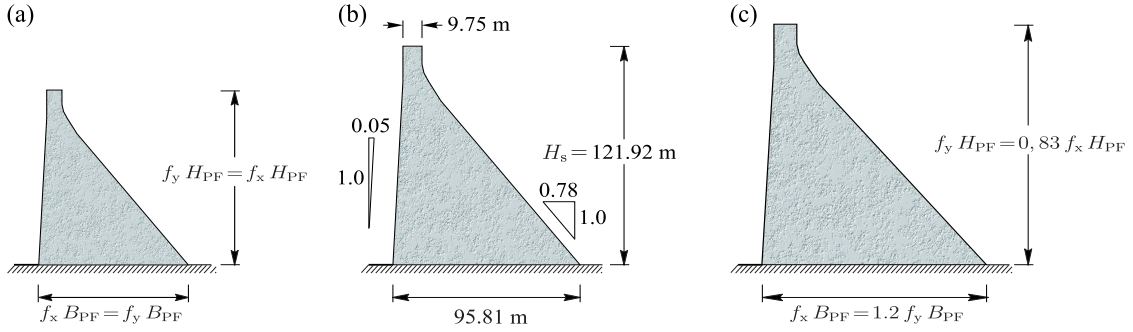

Figure 7.2 Dimension de la section du barrage-poids Pine Flat et transformations géométriques : (a) Transformation homothétique ; (b) Section de référence ; (c) Transformation non-homothétique.

Afin de permettre une analyse paramétrique, cette section est ensuite transformée linéairement en multipliant toutes les coordonnées géométriques de la structure selon les axes X et Y par les facteur $f_{\mathrm{x}} = B_{\mathrm{s}}/B_{\mathrm{PF}}$ et $f_{\mathrm{y}} = H_{\mathrm{s}}/H_{\mathrm{PF}}$, respectivement. B_{s} et H_{s} désignent la base et la hauteur de la section transformée, respectivement. Nous étudierons deux types de transformations : une transformation homothétique où $f_{\mathrm{x}} = f_{\mathrm{y}}$ illustrée dans la figure 7.2.(a) et une transformation non-homothétique où $f_{\mathrm{x}} = 1.2\,f_{\mathrm{y}}$ illustrée dans la figure 7.2.(c).
Le réservoir a une hauteur de H_{r} égale à celle de la structure $H_{\mathrm{r}} = H_{\mathrm{s}}$. L'eau de masse volumique de $\rho_{\mathrm{r}} = 1000\,\mathrm{kg/m^3}$ est considérée comme compressible ou incompressible. Dans le premier cas, une vitesse de propagation des ondes de compression $C_{\mathrm{r}} = 1440\,\mathrm{m/s}$ est choisie.

7.3.2 Type d'analyse effectuée

Le système barrage-réservoir est étudié en utilisant les analyses décrites précédemment. Afin de simplifier le texte, les analyses seront référées comme suit :

– Type I : Il s'agit de la méthode des éléments finis décrite dans la section 7.2.1. Le

programme ADINA (2010) est utilisé pour discrétiser le système barrage-réservoir et la compressibilité de l'eau est incluse.

- Type II : La même analyse que celle de type I est réalisée, mais la compressibilité de l'eau est ignorée.
- Type III : Il s'agit de la méthode analytique développée par Fenves et Chopra (1984) et décrite dans la section 7.2.1. La section du barrage est modélisée dans ADINA afin de calculer les propriétés dynamiques de la structure, et ici la compressibilité de l'eau est incluse.
- Type IV : La même analyse que celle de type III est réalisée, mais la compressibilité de l'eau est ignorée (i.e. $C_{\mathrm{r}} \to \infty$).
- Type V : La formulation des masses ajoutées de Westergaard (1933) décrite dans la section 7.2.2 est analysée. Dans ce cas, les masses ajoutées sont placées sur un barrage infiniment rigide, et les résultats d'intérêts peuvent être calculés analytiquement sans l'utilisation de programme d'éléments finis.
- Type VI : Les masses ajoutées de Westergaard (1933) sont appliquées à un modèle éléments finis de la section flexible du barrage.
- Type VII : La méthode simplifiée développée au cours de cette thèse et décrite sous la section 7.2.2 est analysée. Pour cela, les propriétés dynamiques sont obtenues par analyse modale de la section du barrage.
- Type VIII : Les propriétés dynamiques standards développées par Fenves et Chopra (1985) sont utilisées dans la méthode simplifiée développée au cours de cette thèse. Aucune analyse par éléments finis n'est requise.

7.3.3 Analyse paramétrique et programme développé

Afin d'effectuer l'analyse paramétrique pour les analyses de types I à IV ainsi que VI et VII, un programme a été réalisé sous Matlab ® (2007) nous permettant (i) de modifier automatiquement la géométrie du modèle éléments finis de la section du barrage ; (ii) d'effectuer une analyse modale ; (iii) de récupérer les propriétés dynamiques de la section du barrage transformée ; et (iv) de réaliser l'analyse dynamique et récupérer les résultats d'intérêts. Dans le cas de l'analyse type VI, les masses sont intégrées directement dans le modèle éléments finis grâce au programme développé.

Pour les analyses de types V et VIII, aucune propriété venant d'un modèle éléments finis n'est requise. Ces méthodes ont donc été programmées directement sous Matlab ® (2007).

Le choix de réaliser à la fois une transformation homothétique et non-homothétique vient du fait que lorsque l'on applique une homothétie de la section d'origine, la période de vibration est affectée mais pas le mode.

La réponse dynamique des systèmes barrage-réservoir dépend très fortement du contenu fréquentiel des tremblements de terre. Comme nous allons le voir plus tard, les méthodes simplifiées étudiées dans ce chapitre surestiment ou sous-estiment la période fondamentale des systèmes barrages-réservoir. Par conséquent, des valeurs supérieures d'amplification dynamique sont généralement obtenues avec la méthode qui estime une période fondamentale la plus proche du contenu fréquentiel du séisme. C'est pour cela que les résultats suivants seront normalisés par rapport à l'accélération du sol.

7.3.4 Discussion sur l'amortissement

Il est très difficile de déterminer la matrice d'amortissement d'une structure, car les propriétés d'amortissement des matériaux sont généralement méconnues. Par ailleurs, l'utilisation de matrices d'amortissement non diagonales entraîne des calculs très complexes qui nécessitent une très importante capacité de calcul. De ce fait, la détermination des matrices d'amortissement se limite généralement à l'utilisation des ratios d'amortissement modaux. Ces ratios peuvent être déterminés par des essais expérimentaux in-situ où la courbe de réponse en fréquence d'une certaine quantité (ex. déplacements) est obtenue, et où la méthode de la demi-bande est appliquée. Ici encore, les valeurs de ces amortissements sont discutables, car ces essais sont réalisés à très faibles amplitudes d'excitation ne permettant pas ainsi de développer tout l'amortissement matériel. Si ces ratios d'amortissement sont calculés à partir de résultats provenant de fortes excitations (lors d'un séisme), les valeurs obtenues pourraient être très différentes. En effet, ces ratio peuvent inclure la perte d'énergie dans le système en raison des déformations non linéaires. Par conséquent, les ratios d'amortissements modaux utilisés proviennent souvent de résultats obtenus sur des structures similaires et leurs valeurs peuvent donc être très arbitraires. Le but de cette partie n'est pas de proposer de nouvelles valeurs d'amortissement, mais plutôt de discuter de l'effet de l'implémentation de cet amortissement dans les équations de la dynamique.

Nous avons vu précédemment que l'interaction fluide-structure ajoute une masse, une force et un amortissement additionnel causé par la géométrie semi-infinie du réservoir et la compressibilité de l'eau. Réécrivons les équations (3.12) et (3.13) ainsi

$$\begin{aligned}\bar{S}_{j,n}(\omega) = \big[-\omega^2 \left(M_{j,j} + M_{j,j}^{(a)}(\omega) \right) + \mathrm{i}\,\omega \, \left(C_{j,j} + C_{j,j}^{(a)}(\omega) \right) + \omega_j^2 \, M_{j,j} \big] \delta_{j,n} \\ - \left[\omega^2 M_{j,n}^{(a)}(\omega) + \mathrm{i}\,\omega \, C_{j,n}^{(a)}(\omega) \right] (1 - \delta_{j,n})\end{aligned} \tag{7.15}$$

$$\bar{Q}_n(\omega) = -L_n - L_n^{(a)}(\omega) \tag{7.16}$$

pour $j, n = 1 \ldots N_\mathrm{s}$ et où $M_{j,n}^{(a)}$, $C_{j,n}^{(a)}$ et $L_n^{(a)}$ sont respectivement la masse, l'amortissement et la force ajoutée engendrés par l'interaction fluide-structure et définis par

$$M_{j,n}^{(a)}(\omega) = -\mathrm{Re}\left[\int_0^{H_\mathrm{r}} \bar{p}_j(0, y, \omega)\, \psi_n^{(x)}(y)\, \mathrm{d}y\right] \tag{7.17}$$

$$C_{j,n}^{(a)}(\omega) = \omega\, \mathrm{Im}\left[\int_0^{H_\mathrm{r}} \bar{p}_j(0, y, \omega)\, \psi_n^{(x)}(y)\, \mathrm{d}y\right] \tag{7.18}$$

$$L_n^{(a)}(\omega) = \int_0^{H_\mathrm{r}} \bar{p}_0(0, y, \omega)\, \psi_n^{(x)}(y)\, \mathrm{d}y \tag{7.19}$$

Lorsque la compressibilité de l'eau est négligée, il n'y a aucun amortissement ajouté provenant de la géométrie semi-infinie du réservoir et donc $C_{j,n}^{(a)} = 0$, $j, n = 1 \ldots N_\mathrm{s}$.

Les termes hors diagonales des matrices d'amortissement et de masses ajoutées font que les équations de la dynamique sont couplées. La matrice de rigidité est quant à elle non affectée par l'interaction fluide-structure. En utilisant cette observation, la condition suivante peut être écrite :

$$\omega_j^2\, M_{j,j} = \widetilde{\omega}_j^{\,2}\, \widetilde{M}_{j,j}(\widetilde{\omega}_j) \tag{7.20}$$

pour $j, n = 1 \ldots N_\mathrm{s}$ et où $\widetilde{\omega}_j$ est la période naturelle du système barrage-réservoir et $\widetilde{M}_{j,j}$ est la masse totale du système équivalent à un degré de liberté. Cette masse est donnée par l'équation (3.28) si seulement un mode structural est inclus. Si plusieurs modes sont pris en compte dans l'analyse, ces masses doivent exister, car les systèmes barrages-réservoirs ont des périodes naturelles réelles et positives.

Nous étudions maintenant l'implémentation de l'amortissement dans les méthodes numériques ou analytiques. Nous avons vu tout d'abord que deux types d'analyses peuvent être effectuées lors de l'utilisation des logiciels d'éléments finis : (i) Analyse modale ; (ii) Analyse temporelle par intégration directe où la valeur maximale de la réponse permanente est calculé, et ce, pour chaque fréquences d'intérêts.
Une analyse modale peut être utilisée dans le cas où une hypothèse d'eau incompressible a été faite. Tel que développé dans le chapitre 5, on peut se limiter à la modélisation du réservoir d'une longueur égale à trois fois sa hauteur. Dans ce cas, une condition de mur rigide peut être utilisée à la distance de troncature, car aucune radiation des ondes de pression n'est possible sous cette hypothèse. Pour ce type d'analyse, la masse généralisée calculée correspond

à celle du système barrage-réservoir et l'amortissement est introduit par

$$C_{j,j} = 2\,\xi_j\,\widetilde{\omega_j}\,\widetilde{M}_{j,j}(\widetilde{\omega_j}) \tag{7.21}$$

On remarque clairement que ce type d'analyse va amortir à la fois l'eau et la structure. Pour amortir seulement la structure, l'amortissement suivant doit être utilisé :

$$C_{j,j} = 2\,\xi_j\,\omega_j\,M_{j,j} \tag{7.22}$$

Par conséquent, si l'on choisi d'appliquer de l'amortissement seulement sur la structure, le ratio d'amortissement $\widetilde{\xi}$ doit être utilisé lors d'une analyse modale sous hypothèse d'eau incompressible :

$$\widetilde{\xi_j} = \frac{\omega_j\,M_{j,j}}{\widetilde{\omega_j}\,\widetilde{M}_{j,j}(\widetilde{\omega_j})}\xi_j \tag{7.23}$$

soit en utilisant l'équation (7.20) devient

$$\widetilde{\xi_j} = \frac{\widetilde{\omega_j}}{\omega_j}\xi_j \tag{7.24}$$

Si l'on utilise la méthode des masses ajoutées dans un modèle éléments finis pour une analyse modale, et que l'on cherche à appliquer seulement de l'amortissement sur la structure, on doit tout d'abord effectuer une analyse modale du barrage seul, puis du barrage avec masse ajoutée pour calculer le bon coefficient d'amortissement modal nécessaire pour l'analyse finale.

Lorsque la compressibilité de l'eau est incluse, de par la dépendance fréquentielle des CFT, ce type d'analyse n'est pas possible.

Une analyse temporelle par intégration directe peut être effectuée pour une hypothèse d'eau compressible ou bien incompressible. Dans le premier cas, des conditions aux frontières existent dans ADINA (2010) ou dans la littérature telles que largement décrites par Bouaanani et Miquel (2010). Lorsque la compressibilité de l'eau est négligée, en se basant encore sur les résultats du chapitre 5, le réservoir peut être tronqué à une distance égale à deux fois sa hauteur, et une condition de mur rigide peut alors être appliquée.

Dans ce type d'analyse, l'amortissement est inclus sous forme d'amortissement de Rayleigh :

$$\mathbf{C} = \alpha\,\mathbf{M} + \beta\,\mathbf{K} \tag{7.25}$$

En utilisant les propriétés d'othogonaliltés des modes de vibrations, et en supposant les modes

normalisés par rapport à la masse, cette équation peut s'écrire sous la forme suivante :

$$C_{j,j} = \alpha + \beta\,\omega_j^2 \tag{7.26}$$

Si on utilise les deux premiers modes de vibration pour calculer les coefficients α et β, on obtient

$$\alpha = 2\,\xi_1\,\omega_1 - \beta\,\omega_1^2 \tag{7.27}$$

$$\beta = \frac{2\,\xi_1\,\omega_1 - 2\,\xi_2\,\omega_2}{\omega_1^2 - \omega_2^2} \tag{7.28}$$

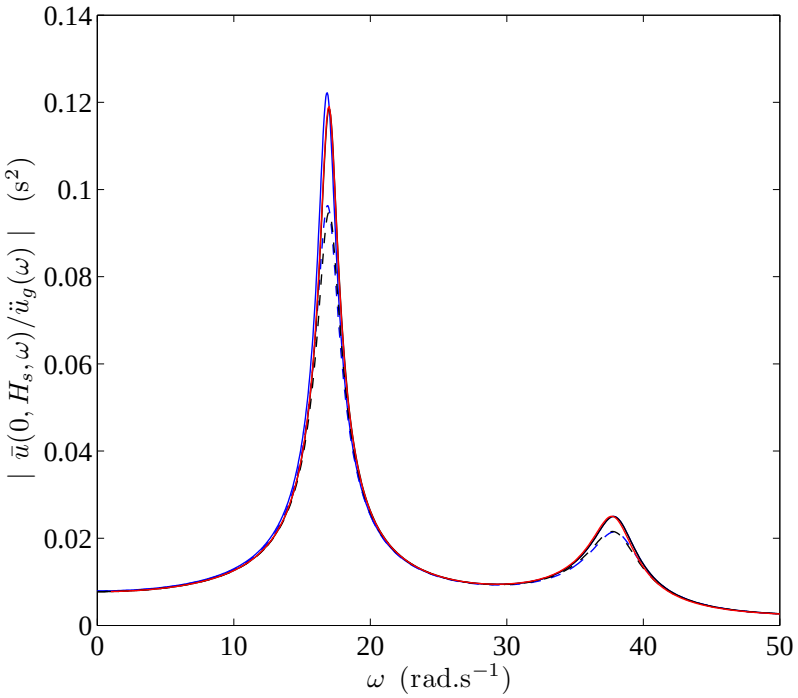

Figure 7.3 Effet de l'amortissement : eau incompressible. ___ Analyse modale type II avec amortissement donné par l'équation (7.24) ; _ _ Analyse modale type II avec amortissement donné par l'équation (7.21) ; ___ Analyse temporelle type II amortissement donné par l'équation (7.26) ; ___ Analyse modale type IV avec amortissement donné par l'équation (7.24) ; _ _ Analyse type IV avec amortissement hystérétique.

Pour les méthodes analytiques, l'amortissement peut directement être inclus sous la forme donnée dans l'équation (7.22) et entraîne une force d'amortissement de $\mathrm{i}\,\omega\,\omega_j\,\xi_j\,M_{j,j}$. Dans la littérature, il est courant d'utiliser une force d'amortissement indépendante de la fréquence et donnée par $\mathrm{i}\,\omega_j^2\,\eta_\mathrm{s}\,M_{j,j}$, où η_s est le facteur d'amortissement hystérétique. En se

référant à l'équation(7.20), à la résonance, la force d'amortissement est dans ce cas égale à $\mathrm{i}\,\widetilde{\omega_j}^2\,\eta_\mathrm{s}\,\widetilde{M}_{j,j}(\widetilde{\omega_j})$. Il est donc clair que l'utilisation d'amortissement hystérétique amortie à la fois le réservoir et le barrage telle que discutée pour les analyses modales.

Les discussions précédentes sont maintenant analysées numériquement pour la section du barrage Pine Flat et pour les analyses type I à IV. Les courbes de réponses en fréquences pour le déplacement en crête du barrage sont illustrées en figure 7.3 pour de l'eau incompressible, et figure 7.4 pour de l'eau compressible.

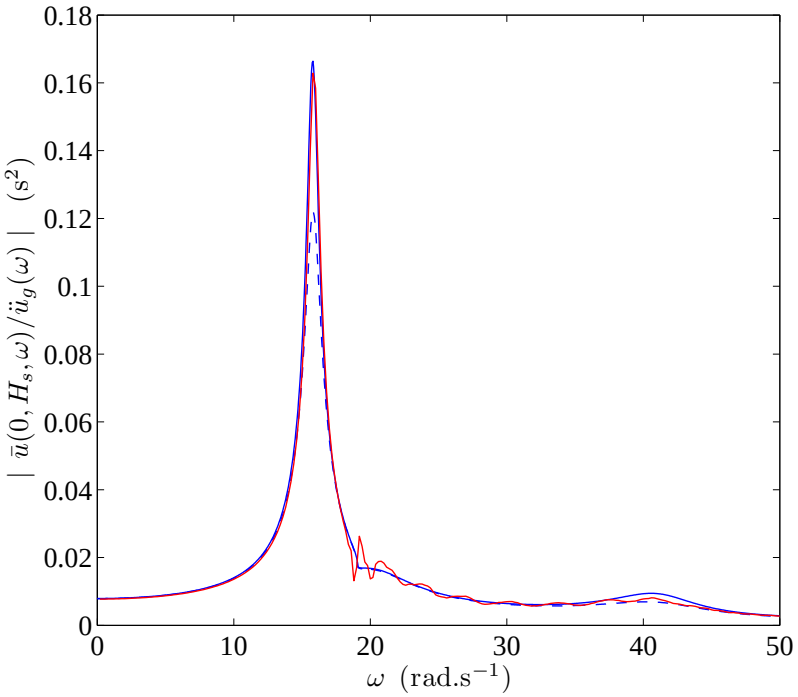

Figure 7.4 Effet de l'amortissement : eau compressible. — Analyse temporelle type I amortissement donné par l'équation (7.26) ; — Analyse modale type III avec amortissement donné par l'équation (7.24) ; – – Analyse type III avec amortissement hystérétique.

Tout d'abord, ces figures valident l'excellente concordance des résultats entre méthodes analytiques et méthodes numériques telle que confirmée par Bouaanani et Lu (2009). Dans le cas où une analyse temporelle est effectuée pour calculer la courbe de réponse en fréquence, on observe des oscillations dans le cas compressible et non dans le cas incompressible. Si l'on se rappelle qu'il n'y a aucune absorption des ondes dans le cas incompressible et que la condition de frontière à la distance de troncature peut être modélisée par un mur rigide, cela signifie que la condition aux frontières absorbante utilisée pour le cas compressible induit une erreur.

Elle n'absorbe pas toutes les ondes incidentes. Finalement, on remarque que le type d'amortissement utilisé à un effet important dans la zone de résonance du système barrage-réservoir.

Dans ce qui suit, nous choisissons un amortissement hystérétique de 0.1 et qui sera donc appliqué au système barrage-réservoir. Cela semble plus justifié, car les mesures d'amortissement pour ces structures proviennent de tests in-situ qui donne la valeur du système barrage-réservoir et non celle du barrage. Par ailleurs, l'analyse de type I ne sera pas effectuée, car les résultats obtenus seront très semblables à ceux de la méthode analytique de Chopra et collaborateurs.

7.4 Résultats

Nons avons décrit précédemment les méthodes les plus utilisées pour l'analyse dynamique des systèmes barrage-réservoir. Par la suite, nous analyserons la capacité des méthodes simplifiées à estimer le comportement dynamique de ces structures en contact avec de l'eau. Seule l'étude du mode fondamental sera effectuée dans un premier temps. Finalement, nous étudierons ensuite l'effet de la compressibilité et des modes supérieurs de vibrations.

7.4.1 Validité de la méthode des masses ajoutées de Westergaard (1933)

Nous étudions tout d'abord les résultats obtenus avec la méthode V et présentés en figures 7.5 et 7.6.

Comme prédit par l'équation (7.12) la position de la résultante calculée, estimée par l'analyse de type V, ne dépend que de la hauteur du réservoir. De même, la force de cisaillement à la base estimée par cette méthode et donnée par l'équation (7.13) est aussi indépendante de la fréquence d'excitation lorsque normalisée par rapport à l'accélération du sol. On remarque que pour l'analyse de type III, ces deux résultats dépendent fortement de la fréquence, et ce, surtout dans les zones de résonances. Il est à noter que les zones de résonances ne sont pas les mêmes entre la force de cisaillement et celle de la force hydrodynamique. Ceci s'explique par un déphasage entre le déplacement de la structure et l'orientation de la force hydrodynamique. Les résultats obtenus avec la méthode des masses de Westergaard (1933) sous-estiment fortement la position de la résultante hydrodynamique ainsi que la force de cisaillement à la base de l'ouvrage dans ces zones de résonances. Si le contenu fréquentiel du tremblement de terre est loin de la période de résonance, alors des résultats très proches seront obtenus avec les deux méthodes. Néanmoins, si le tremblement de terre excite la structure à des périodes proches ou égales à celles du système, une estimation des efforts non conservateurs peut être obtenue en utilisant la méthode V.

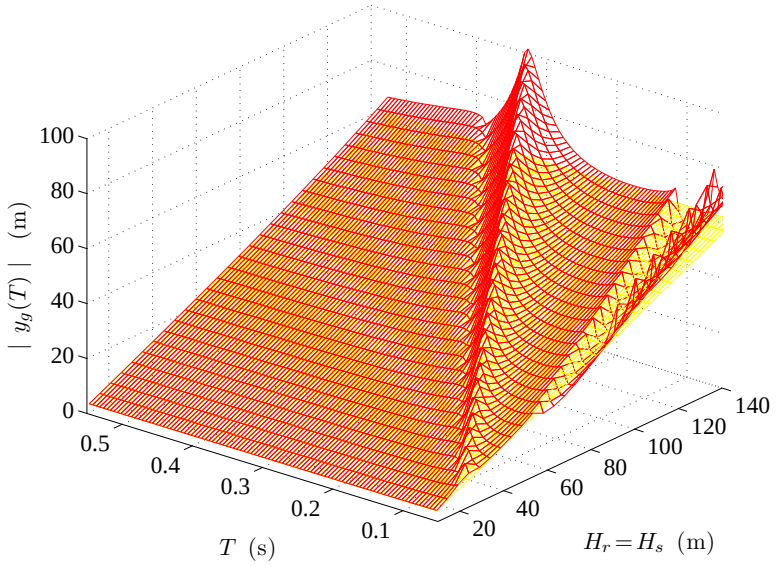

Figure 7.5 Hauteur de la résultante des forces hydrodynamiques y_g. Méthode des masses ajoutées de Westergaard (1933). $f_x = f_y$ avec $f_y = 0.08 \ldots 1.2$: — Analyse type III ; — Analyse type V.

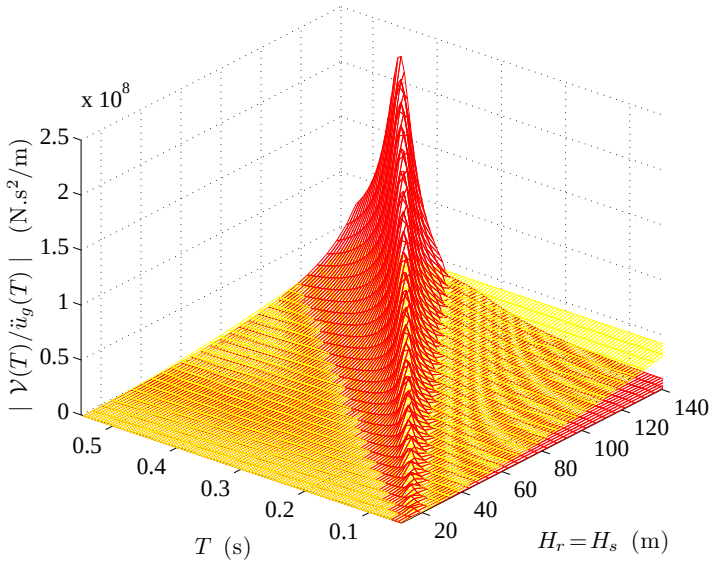

Figure 7.6 Force de cisaillement à la base du barrage $\mathcal{V}$ normalisée par rapport à l'accélération. Méthode des masses ajoutées de Westergaard (1933). $f_x = f_y$ avec $f_y = 0.08 \ldots 1.2$: — Analyse type III ; — Analyse type V.

On note que cette méthode est la plus utilisée dans la pratique. Afin de ne pas sous-estimer les forces que peuvent subir ces structures lors d'un tremblement de terre, il est indispensable

de réaliser des analyses plus avancées dans le but d'estimer l'effet de la flexibilité.

Nous incluons maintenant la flexibilité de l'ouvrage en évaluant l'analyse de type VI. La force de cisaillement à la base est cette fois obtenue directement des résultats fournis par le logiciel d'éléments finis et illustrée en figure 7.7.

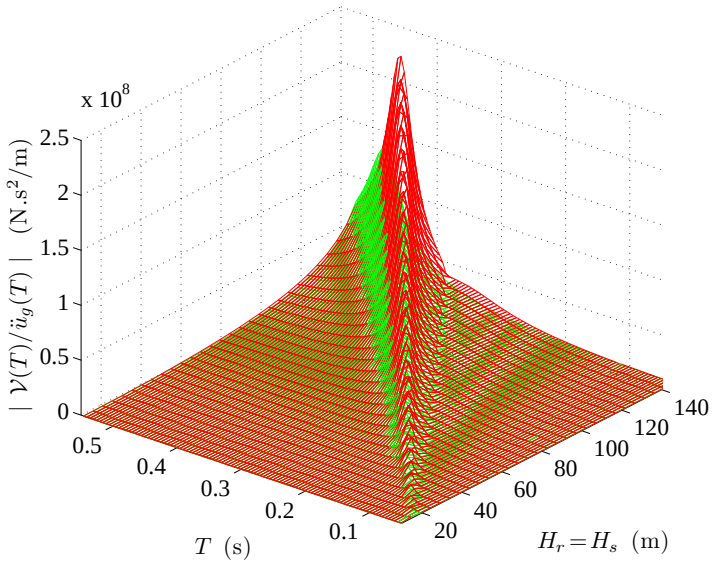

Figure 7.7 Force de cisaillement à la base du barrage $\mathcal{V}$ normalisée par rapport à l'accélération. Méthode des masses ajoutées de Westergaard (1933) incluant la flexibilité de la structure. $f_x = f_y$ avec $f_y = 0.08 \ldots 1.2$: — Analyse type III ; — Analyse type VI.

Inclure la flexibilité de l'ouvrage tout en modélisant les effets d'interaction fluide structure grâce aux masses ajoutées améliore nettement les résultats. On remarque, néanmoins, que la réponse estimée par l'analyse de type V sous-estime la force dans la zone de résonance et prédit une période fondamentale du système barrage-réservoir légèrement plus élevée que celle obtenue par l'analyse de référence de type III. Par ailleurs, comme discuté précédemment, cette méthode n'a pas été développée pour inclure la flexibilité. Selon la géométrie et les propriétés des matériaux de la structure, il est impossible de prédire l'erreur qu'induit l'utilisation de cette méthode à moins de réaliser une analyse plus avancée de type I ou III.

7.4.2 Validité de la méthode simplifiée de Fenves et Chopra (1985)

Nous étudions ici la capacité de la méthode de type VIII à prédire la réponse dynamique du système barrage-réservoir. La position de la résultante hydrodynamique ainsi que la force de cisaillement à la base de l'ouvrage sont comparées à celles obtenues par la méthode de référence III en figures 7.8 et 7.9.

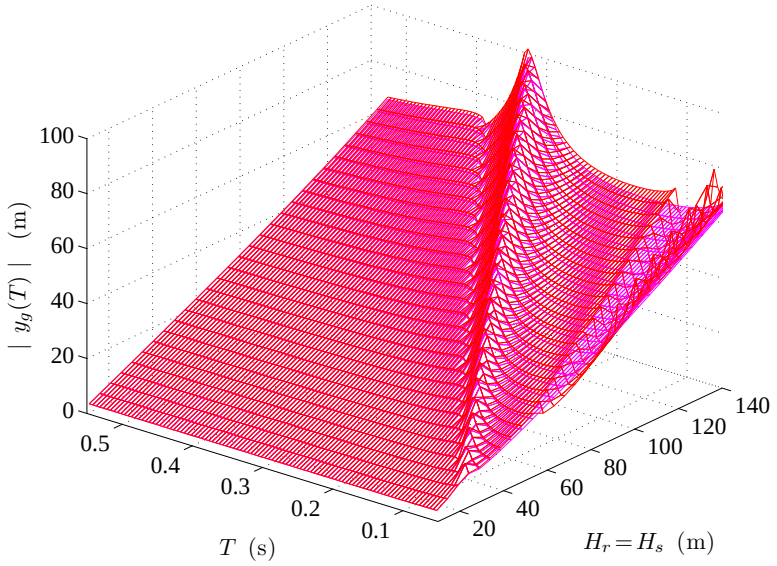

Figure 7.8 Hauteur de la résultante des forces hydrodynamiques y_g. Méthode simplifiée de Fenves et Chopra (1985). $f_x = f_y$ avec $f_y = 0.08 \ldots 1.2$: — Analyse type III ; — Analyse type VIII.

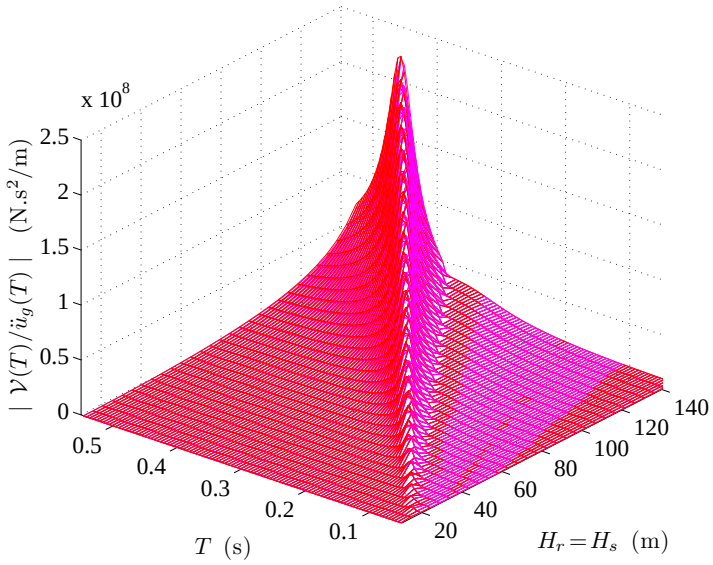

Figure 7.9 Force de cisaillement à la base du barrage $\mathcal{V}$ normalisée par rapport à l'accélération. Méthode simplifiée de Fenves et Chopra (1985). $f_x = f_y$ avec $f_y = 0.08 \ldots 1.2$: — Analyse type III ; — Analyse type VIII.

On observe que cette méthode permet une très bonne prédiction de la réponse dynamique pour cette analyse. Nous augmentons maintenant la base de la section de référence. Les ré-

sultats sont présentés dans les figures 7.10 et 7.11.

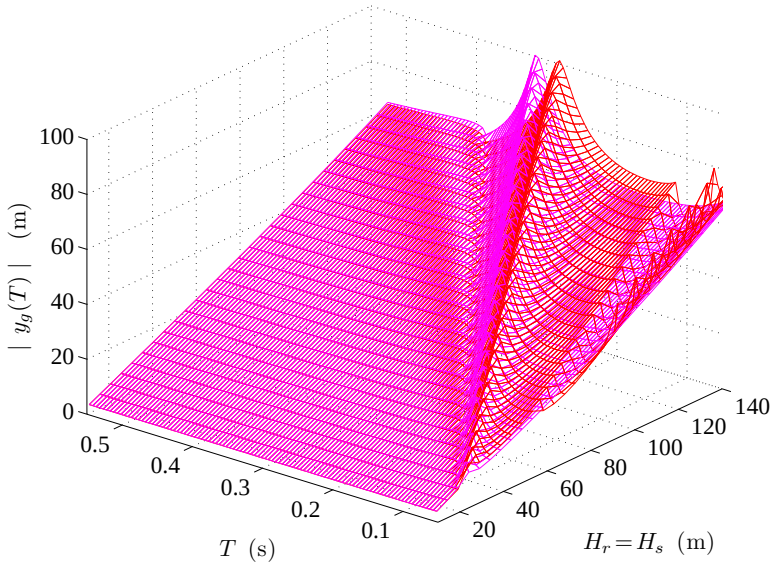

Figure 7.10 Hauteur de la résultante des forces hydrodynamiques y_g. Méthode simplifiée de Fenves et Chopra (1985). $f_x = 1.2\, f_y$ avec $f_y = 0.08 \ldots 1.2$: — Analyse type III ; — Analyse type VIII.

En comparant ces nouveaux résultats aux précédents, on remarque qu'en modifiant légèrement la section de référence une erreur est introduite dans l'estimation de la réponse dynamique en utilisant la méthode VIII. Afin de développer leur méthode simplifiée, Fenves et Chopra (1985) ont déterminé un mode et une période fondamentale basés sur une section typique d'un ouvrage. D'après les résultats des figures 7.8 et 7.9, on déduit que cette section typique correspond à celle du barrage Pine Flat. Nous avons vu précédemment qu'une homothétie d'une section ne modifie pas le mode de vibration, mais seulement la période. Il est donc probable que l'équation (7.14) ait été obtenue en effectuant la même démarche qu'ici et que le mode de vibration est celui de Pine Flat. Lorsque l'on fait varier légèrement la géométrie, les propriétés dynamiques standards proposées par Fenves et Chopra (1985) deviennent une approximation et donc introduisent une erreur dans les résultats. On en conclut donc que si une section à l'étude ressemble fortement à celle de Pine Flat, une bonne estimation de son comportement sera obtenue avec cette méthode. Dans la pratique, cela est rarement le cas. On peut donc s'attendre à des erreurs bien plus importantes que celles montrées ici. Par ailleurs, tels que précisés précédemment, seulement le mode type et la période de vibration sont utilisés ici. Lorsque la méthode simplifiée de Fenves et Chopra (1985) est entièrement utilisée, d'autre simplification tels que le calcul des masses, forces et profils de pressions

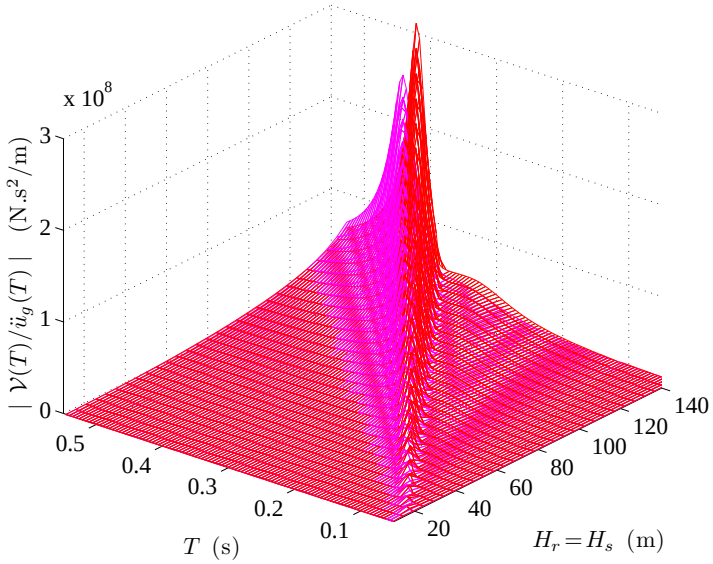

Figure 7.11 Force de cisaillement à la base du barrage $\mathcal{V}$ normalisée par rapport à l'accélération. Méthode simplifiée de Fenves et Chopra (1985). $f_{\mathrm{x}} = 1.2\, f_{\mathrm{y}}$ avec $f_{\mathrm{y}} = 0.08 \ldots 1.2$: — Analyse type III ; — Analyse type VIII.

peuvent induire une erreur supplémentaire.

7.4.3 Validité de la méthode simplifiée développée au cours de cette thèse

On analyse finalement la capacité de la méthode développée au cours de cette thèse à prédire le comportement dynamique. Les figures 7.12 à 7.15 illustrent les résultats obtenus pour les deux cas : (i) $f_{\mathrm{x}} = f_{\mathrm{y}}$ et (ii) $f_{\mathrm{x}} = 1.2\, f_{\mathrm{y}}$.

On démontre clairement ici que cette nouvelle méthode permet de tenir compte de la géométrie de l'ouvrage étudiée de manière plus précise et prédit mieux les termes hydrodynamiques nécessaires aux calculs des résultats d'intérêt. Si une analyse spectrale doit être réalisée, cette méthode permet de s'assurer de la qualité de la réponse obtenue de part sa robustesse. Ceci n'est pas le cas avec l'utilisation des masses de Westergaard (1933) ou de la méthode simplifiée de Fenves et Chopra (1985). L'erreur induite par les simplifications incluses dans le développement ne peut pas être quantifiée qu'en réalisant une analyse plus avancée.

7.4.4 Exemple

Les méthodes décrites précédemment sont testées numériquement pour un tremblement de terre donné et pour $f_{\mathrm{y}} = 0.56$ et $f_{\mathrm{x}} = 1.2 f_{\mathrm{y}}$, soit un barrage de hauteur de 68.27 m.

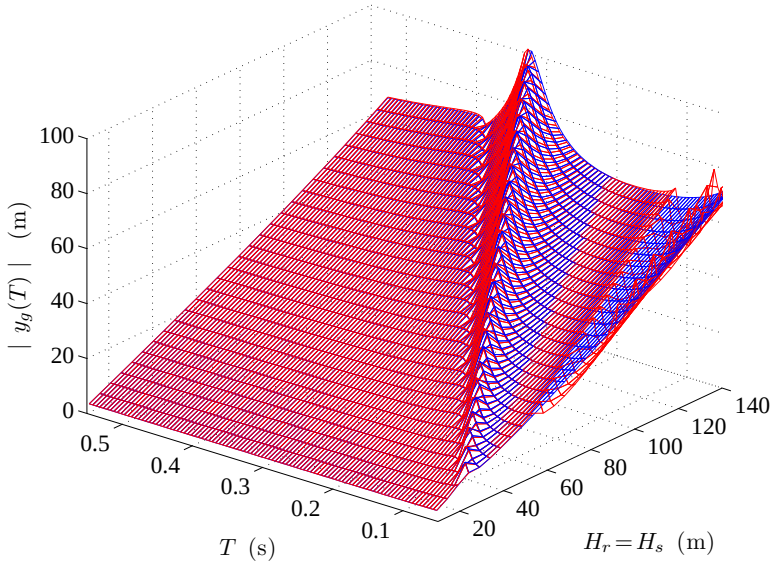

Figure 7.12 Hauteur de la résultante des forces hydrodynamiques y_g. Méthode développée dans cette thèse. $f_x = f_y$ avec $f_y = 0.08 \ldots 1.2$: — Analyse type III ; — Analyse type VII.

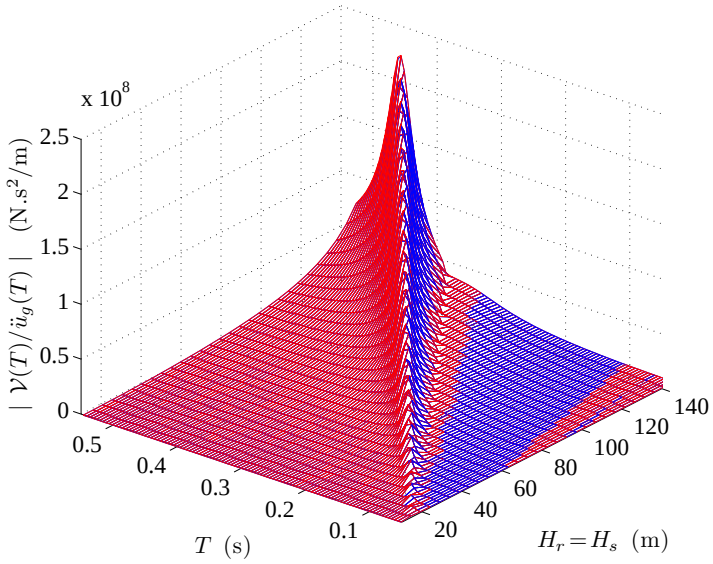

Figure 7.13 Force de cisaillement à la base du barrage $\mathcal{V}$ normalisée par rapport à l'accélération. Méthode développée dans cette thèse. $f_x = f_y$ avec $f_y = 0.08 \ldots 1.2$: — Analyse type III ; — Analyse type VII.

Le système barrage-réservoir est soumis au tremblement de terre d'Imperial Valley dont l'accélérogramme et l'amplitude de la transformée de Fourier, sont illustrés en figure 7.16.

En comparant les différentes méthodes simplifiées, on remarque dans la figure 7.17 que

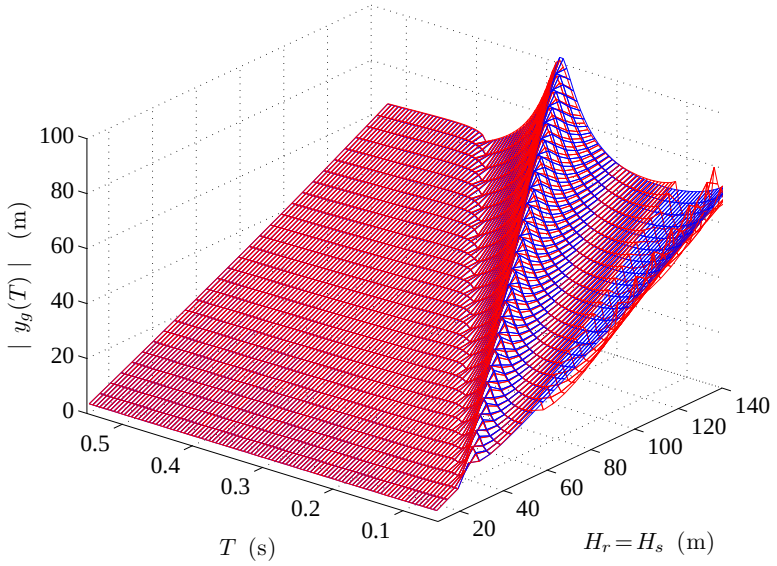

Figure 7.14 Hauteur de la résultante des forces hydrodynamiques y_g. Méthode développée dans cette thèse. $f_x = 1.2\, f_y$ avec $f_y = 0.08 \ldots 1.2$: — Analyse type III ; — Analyse type VII.

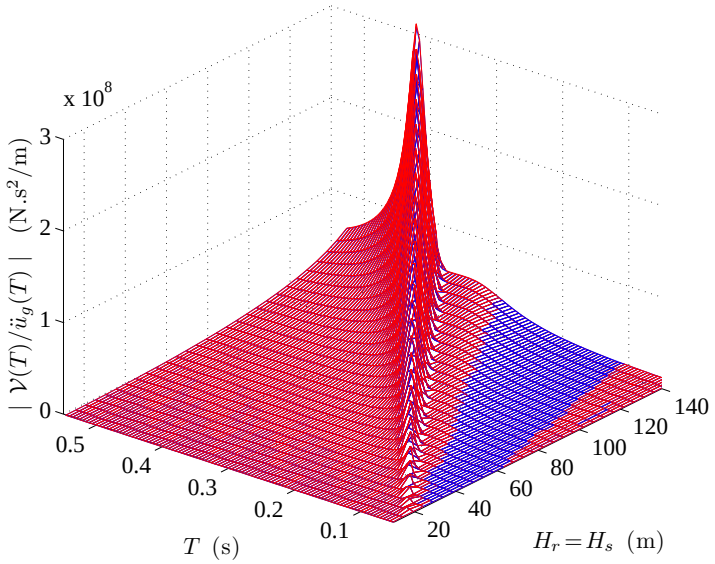

Figure 7.15 Force de cisaillement à la base du barrage $\mathcal{V}$ normalisée par rapport à l'accélération. Méthode développée dans cette thèse. $f_x = 1.2\, f_y$ avec $f_y = 0.08 \ldots 1.2$: — Analyse type III ; — Analyse type VII.

les méthodes V, VI, et VIII introduisent une erreur importante et ce, malgré le fait que les courbes de réponses précédentes aient montré une erreur plutôt faible. Il est à noter que dans la pratique l'analyse de type V reste la plus utilisée, et comme le montre cette figure, des

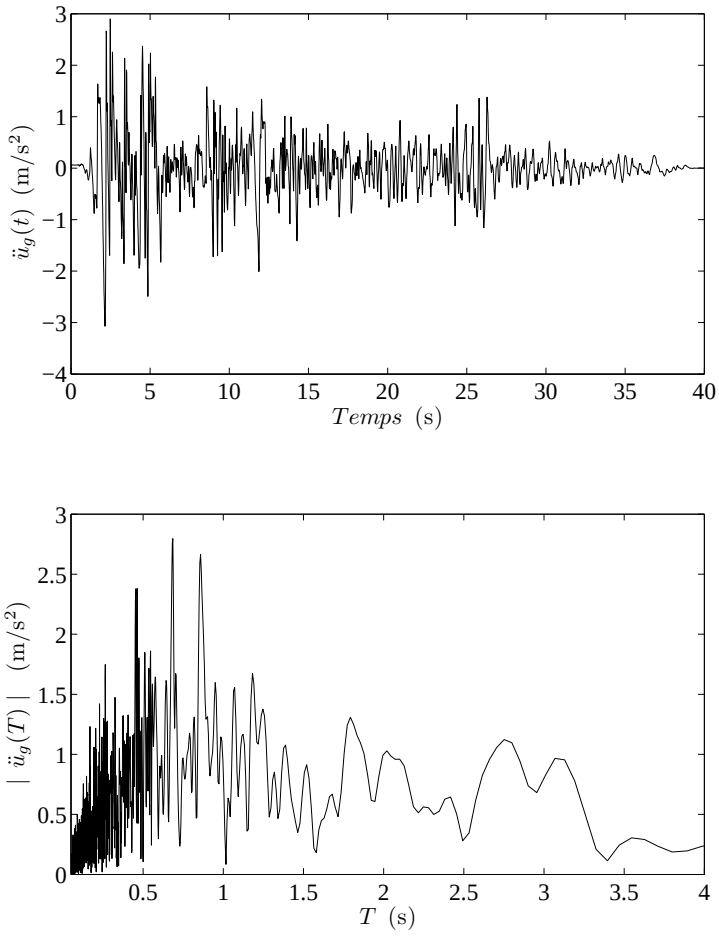

Figure 7.16 Enregistrement d'Imperial Valley

résultats non conservateurs peuvent être obtenus.

7.4.5 Effet de la compressibilité

Nous étudions l'effet de la compressibilité sur la réponse dynamique des systèmes barrages réservoir. Dans cette partie, seules les méthodes de références II, III, IV seront analysées. La méthode par éléments finis de type I n'est pas incluse dans les résultats pour les raisons qui ont été décrites précédemment. Dans le cas de l'analyse de type II, nous avons vu qu'une analyse modale reste possible et que le réservoir peut être modélisé sur une longueur seulement égale à trois fois sa hauteur. Les résultats pour la force de cisaillement à la base sont présentés en figure 7.18 pour le cas $f_{\mathrm{x}} = f_{\mathrm{y}}$.

Encore une fois, l'excellente concordance des résultats entre méthodes de type II et IV

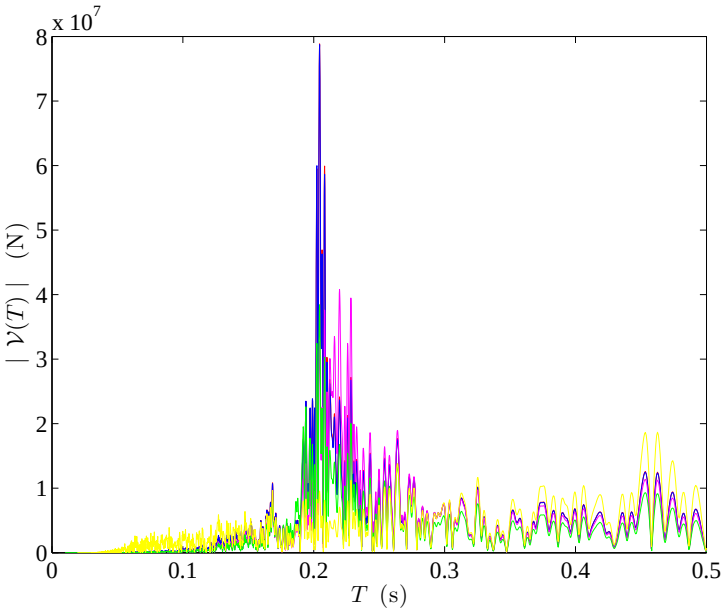

Figure 7.17 Force de cisaillement à la base du barrage $\mathcal{V}$ obtenue pour le tremblement de terre Imperial valley : — Analyse type III ; — Analyse type V ; — Analyse type VI ; — Analyse type VII ; — Analyse type VIII

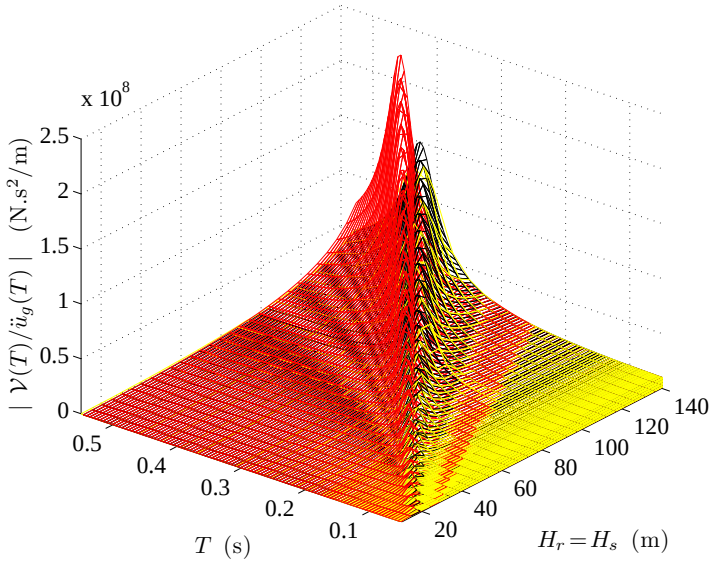

Figure 7.18 Force de cisaillement à la base du barrage $\mathcal{V}$. Effet de la compressibilité $f_x = f_y$ avec $f_y = 0.08 \ldots 1.2$: — Analyse type II ; — Analyse type III ; — Analyse type IV.

valide l'utilisation de la méthode de Fenves et Chopra (1985) comme référence. Cette figure montre aussi clairement que la compressibilité a un effet considérable sur la réponse

dynamique des systèmes barrage-réservoir, et celle-ci doit être incluse.

7.4.6 Effet des modes supérieurs

Les méthodes VII et VIII ont été développées en considérant seulement le mode fondamental de vibration et en effectuant une correction statique pour les modes supérieurs. Dans cette partie, nous étudions la validité de cette correction statique et la comparons aux résultats obtenus lorsque les modes supérieurs sont inclus dans les analyses.

Lorsque N_s modes de vibrations sont inclus dans l'analyse, la force de cisaillement à la base peut être calculée par l'équation (7.5). Cette équation peut être réécrite sous la forme

$$\mathcal{V}(\omega) = \mathcal{V}_1(\omega) + \mathcal{V}_\mathrm{s}(\omega) \tag{7.29}$$

où $\mathcal{V}_1$ est la force de cisaillement à la base due au premier mode et $\mathcal{V}_\mathrm{s}$ est celle due aux modes supérieurs de vibration :

$$\mathcal{V}_1 = \ddot{u}_\mathrm{g}(\omega)\, \omega_1^2\, L_1\, \bar{Z}_1(\omega) \tag{7.30}$$

$$\mathcal{V}_\mathrm{s} = \ddot{u}_\mathrm{g}(\omega) \sum_{j=2}^{N_\mathrm{s}} \omega_j^2\, L_j\, \bar{Z}_j(\omega) \tag{7.31}$$

On note ici que $\bar{Z}_1$ est différent de celui donné par l'équation (3.17). En effet, dû au couplage des coordonnées généralisées, celui-ci doit être calculé en résolvant le système (3.11). Fenves et Chopra (1985) ont montré qu'en effectuant une correction statique, l'effet des modes supérieurs peut être pris en compte par

$$\begin{aligned} \mathcal{V}_\mathrm{st} = \ddot{u}_\mathrm{g}(\omega) \int_0^{H_\mathrm{s}} \Bigg\{ & \mu_\mathrm{s}(y) \left[1 - \frac{L_1}{M_1}\, \psi_1^{(x)}(0,y) \right] \\ & + \left[\widehat{\bar{p}}_0(0,y) - \frac{\mu_\mathrm{s}(y)}{M_1}\, \psi_1^{(x)}(0,y) \int_0^{H_\mathrm{r}} \widehat{\bar{p}}_0(0,y)\, \psi_1^{(x)}(0,y)\, \mathrm{d}y \right] \Bigg\}\, \mathrm{d}y \end{aligned} \tag{7.32}$$

On note que l'équation (7.32) est différente que l'équation (2.16), car $\ddot{u}_\mathrm{g}(\omega)$ est ici utilisé et non $\ddot{x}_\mathrm{g}^{(\max)}$. En faisant ainsi, $\mathcal{V}_\mathrm{st}$ et $\mathcal{V}_\mathrm{s}$ peuvent être normalisées par l'accélération. Ceci est illustré dans la figure 7.19. Dans cette figure, on compare la force due aux modes supérieurs obtenue par correction statique $\mathcal{V}_\mathrm{st}$ à celle obtenue par l'équation (7.31) en utilisant la méthode type III. On montre aussi l'estimation de ces forces dues aux modes supérieurs obtenues avec la méthode VI.

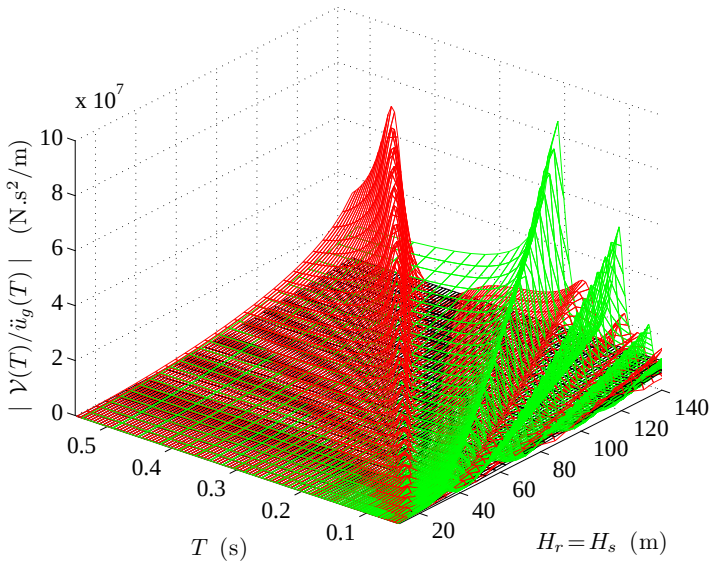

Figure 7.19 Effet des modes supérieurs sur la force de cisaillement à la base du barrage $\mathcal{V}$ normalisé par rapport à l'accélération. $f_{\mathrm{x}} = f_{\mathrm{y}}$ avec $f_{\mathrm{y}} = 0.08 \ldots 1.2$: — f_{s} calculée avec l'analyse type III ; — f_{st} calculée avec l'analyse type III ; — f_{s} calculée avec l'analyse type VI ;

Si on compare les valeurs calculées avec celles des figures précédentes, on remarque clairement que l'effet des modes supérieurs est bien moindre que celui du mode fondamental de vibration. Néanmoins, on remarque aussi que la correction statique est non conservatrice et par conséquent une analyse par superposition modale ou intégration directe peut s'avérer nécessaire. Finalement, la solution des masses ajoutées de Westergaard (1933) induit une importante erreur dans les périodes de vibration des modes supérieurs.

7.5 Conclusion

Nous avons analysé à travers cette partie différents types d'analyses qui peuvent être réalisés pour estimer le comportement dynamique des systèmes barrage-réservoir. Nous avons mis en valeurs les différentes hypothèses simplificatrices utilisées pour le développement des méthodes simplifiées existantes et analysé l'effet qu'elles ont sur la réponse dynamique. Nous avons par ailleurs montré certaines difficultés à l'utilisation de méthodes complexes telle que celle des éléments finis. De cette section nous pouvons conclure que si le contenu fréquentiel d'un séisme était parfaitement prédictible, de nombreuses simplifications pourraient être réalisées. Néanmoins, cela n'est pas le cas, et par conséquent le comportement dynamique des

systèmes barrages-réservoir doit être correctement prédit sur une large gamme de fréquences. La seule méthode simplifiée permettant une excellente estimation de ce comportement est celle développée au cours de cette thèse. Finalement, nous avons montré que l'effet des modes supérieurs peut dans certains cas être non négligeable, et une correction statique s'avère insuffisante. Afin de tenir compte de l'effet de ces modes, les autres méthodes développées au cours de cette thèse permettent de réaliser une analyse dynamique intégrant les modes supérieurs. Ces méthodes sont nécessaires dans la pratique pour plusieurs raisons qui ont été revues dans la section 2.3.3.

RÉFÉRENCES

ADINA Theory and Modeling Guide. Report ARD 10-7. ADINA R & D, Inc., 2010.

Bouaanani N, Lu F.Y. Assessment of potential-based fluid finite elements for seismic analysis of dam-reservoir systems. *Journal of Computers and Structures* 2009 ; **87** : 206-224.

Bouaanani N, Miquel B. A new formulation and error analysis for vibrating dam-reservoir systems with upstream transmitting boundary conditions.*Journal of Sound and Vibration* 2010 ; **329** : 1924-1953.

Fenves G, Chopra A.K. Earthquake analysis and response of concrete gravity dams. Report No. UCB/EERC-84/10, University of California, Berkeley, California, 1984.

Fenves G, Chopra AK. Simplified analysis for earthquake resistant design of concrete gravity dams. Report No. UCB/EERC-85/10, University of California, Berkeley, 1985.

MATLAB ®. The Mathworks, Inc., Natick, MA, USA, 2007.

Miquel B, Bouaanani N. Simplified evaluation of the vibration period and seismic response of gravity dam-water systems.*Engineering structures* 2010 ; **32** : 2488-2502.

Rayleigh, Lord (1877), Theory of Sound (two volumes), Dover Publications, New York, reissued 1945, second edition.

Westergaard HM. Water pressures on dams during earthquakes. *Transactions*(ASCE) 1933 ; **98** : 418-472.

CHAPITRE 8

Conclusions et recommandations

8.1 Conclusions

Cette thèse de doctorat avait pour objectif de développer des approches pratiques pour le calcul dynamique des structures en contact avec de l'eau. Il existe de nombreuses techniques pour assurer un comportement adéquat des structures conventionnelles (bâtiments, ponts, etc.) sous l'effet d'un tremblement de terre. Dans le cas des structures en contact avec de l'eau, l'interaction fluide-structure complexifie grandement les calculs. Les méthodes simplifiées couramment utilisées actuellement étant basées sur de nombreuses approximations, nous avons développé des techniques plus robustes tout en gardant une grande simplicité d'implémentation. Cela a conduit à plusieurs nouveaux développements notamment pour le calcul des paramètres hydrodynamiques. Les contributions suivantes ont été réalisées au cours de cette thèse de doctorat :

- Développer une formulation simplifiée pour le calcul de la période fondamentale d'un système eau-structure, une information importante lors de l'évaluation du comportement dynamique.
- Développer une méthode analytique simplifiée pour l'étude dynamique d'un système eau-structure prenant en compte un maximum de phénomènes ayant une grande influence sur le comportement dynamique, tel que la géométrie de la structure, l'effet des modes supérieurs et la compressibilité de l'eau.
- Développer une méthode numérique pour effectuer l'analyse dynamique temporelle d'un système eau-structure en incluant directement l'effet de l'interaction fluide-structure au modèle éléments finis de la structure seule, i.e. sans eau.
- Développer un test numérique permettant d'estimer l'erreur introduite dans un modèle d'éléments finis incluant des conditions aux frontières transmettantes pour représenter le comportement dynamique d'une structure retenant un domaine d'eau quasi infini.

Pour chacune des ces contributions, nous rappelons les conclusions qui ont été mises en valeur :

8.1.1 Développement d'une formulation simplifiée pour le calcul de la période fondamentale d'un système eau-structure

Cette partie de la recherche a été présentée dans le chapitre 3 et a fait l'objet d'un article publié dans une revue scientifique. Nous avons développé une technique pour calculer la période fondamentale d'un système barrage-réservoir. Il s'agit du paramètre clef de toute analyse spectrale. Cette formulation tient compte de la flexibilité de la structure, et de la variation du niveau d'eau. Lorsque l'on néglige la compressibilité de l'eau, nous avons développé une expression simple pour calculer ce paramètre. Lorsque la compressibilité de l'eau est prise en compte, la période fondamentale du système peut être obtenue par la résolution d'une équation cubique. Les résultats obtenus ont été comparés à ceux de la méthode des éléments finis et à ceux d'une méthode analytique avancée, et cela, pour différentes géométries et propriétés des barrages-poids étudiés. On montre qu'une très bonne prédiction de cette période est obtenue en utilisant cette nouvelle technique, et cela, indépendamment de la géométrie de l'ouvrage.

8.1.2 Développement d'une méthode spectrale simplifiée pour l'étude d'un système eau-structure

En combinant les développements réalisés pour le calcul de la période fondamentale d'un système eau-structure avec de nouvelles expressions simplifiées élaborées pour le calcul de certains termes hydrodynamiques, une méthode spectrale simplifiée a été développée. Celle-ci fait aussi partie de l'article présentée dans le chapitre 3. Cette méthode donne d'excellents résultats lorsqu'elle est comparée à des techniques avancées et nécessitant une grande expertise. Le chapitre 7 met en valeur les avantages à l'utilisation de cette nouvelle méthode robuste en la comparant aux autres méthodes classiques. À travers cette discussion, nous montrons clairement l'effet que peut engendrer une hypothèse de structure rigide sur les efforts sismiques. Cette hypothèse est encore courante dans la pratique et peut entrainer une sous-estimation des efforts sismiques. La méthode pseudo-dynamique classique considère l'effet de la flexibilité, mais tient compte de façon partielle de la géométrie de l'ouvrage. Cette simplification peut entrainer une erreur dans les résultats. La fiabilité de la méthode développée au cours de cette thèse répond au besoin de techniques simplifiées, mais avant tout précises.

8.1.3 Développement de méthodes numériques pour l'analyse dynamique des structures en contact avec de l'eau

Les analyses spectrales ne tiennent pas compte de la nature oscillatoire et transitoire des vibrations. Lorsqu'une analyse spectrale démontre que des zones de l'ouvrage excèdent

les contraintes admissibles, il est nécessaire de réaliser une analyse dynamique pour juger de la durée et de l'étendue de ces zones. De par la formulation des analyses spectrales, une combinaison modale est nécessaire pour calculer la réponse totale de la structure. Ce type de combinaison peut engendrer une erreur conservatrice ou non dans les résultats. Par ailleurs, la méthode spectrale proposée et celle existante effectuent une correction statique pour la prise en compte des modes supérieurs. Nous avons montré dans le chapitre 7 que ces modes supérieurs ont un effet non négligeable sur la réponse dynamique des systèmes barrage-réservoir et qu'une correction statique peut s'avérer non suffisante. Pour les structures plus flexibles, on peut s'attendre à un effet encore plus prononcé des modes supérieurs.

Pour cela, différentes méthodes ont été mises au point pour tenir compte de l'effet de l'interaction fluide-structure et de la flexibilité du sol. La première permet l'étude de structure vibrant en contact avec de l'eau d'un ou des deux côtés et a fait l'objet d'un article présenté dans le chapitre 4. Cette nouvelle technique permet de tenir compte de la flexibilité de la structure et du sol, des modes de vibrations supérieurs, des niveaux d'eau de hauteurs variables, et de différentes conditions aux frontières pour le ou les domaines d'eau. Une méthodologie a été développée pour calculer les fréquences naturelles de chaque mode de vibration du système eau-structure. Cette nouvelle technique a ensuite été étendue pour le calcul de poutres en contact avec de l'eau et la méthode a été soumise à une revue scientifique et présentée dans le chapitre 5. Cette méthode étend les solutions analytiques existantes pour le calcul des modes de vibrations et période naturelle des poutres à une solution intégrant l'effet d'interaction fluide-structure. Elle permet de tenir compte de différentes conditions d'appuis de la poutre (encastrée, libre, rotulée, etc.) et permet une très bonne estimation dynamique du comportement d'une poutre ou bien d'une structure ayant un comportement de poutre.

Ces méthodes donnent d'excellents résultats lorsqu'elles sont comparées à des techniques avancées. Dans la pratique, la technique simplifiée la plus courante pour la réalisation d'une analyse dynamique temporelle est l'utilisation de masses ajoutées pour simuler l'effet de l'interaction fluide-structure. Nous avons montré dans le chapitre 7 que ces masses peuvent introduire une erreur plus ou moins importante dans l'estimation du comportement dynamique lorsqu'utilisées sur un modèle flexible de l'ouvrage. Dans la pratique, la plupart des guides ou codes existants proposent une évolution progressive dans la complexité des analyses dynamiques à réaliser pour assurer la sécurité d'un ouvrage hydraulique. L'analyse dynamique temporelle d'une structure correspond généralement à l'analyse la plus avancée demandée par ces guides ou codes. Il est donc primordial que la prédiction du comportement dynamique de l'ouvrage soit précise, ce que ne peut pas assurer la méthode des masses ajoutées. Les techniques développées au cours de cette thèse de doctorat répondent à ce besoin de méthodes

précises et robustes.

8.1.4 Développement de la méthode de l'accélérogramme modifiée

La prise en compte numériquement de l'effet de l'interaction fluide-structure sur le comportement des ouvrages en contact avec de l'eau est limité à l'utilisation de certain logiciel d'éléments finis qui offrent cette capacité. Par ailleurs, la modélisation de ce phénomène requiert une grande expertise et une capacité de calcul importante. Les méthodes analytiques, lorsque programmées, peuvent tenir compte de cette interaction en nécessitant d'une expertise et d'un temps de calcul moindre. Néanmoins, contrairement aux logiciels d'éléments finis, il est difficile avec les méthodes analytiques d'obtenir une vue globale du comportement de la structure étudiée ainsi que les efforts internes primordiaux pour statuer sur la sécurité de l'ouvrage lors d'un tremblement de terre. Dans la pratique, les masses ajoutées peuvent être utilisées, mais ne garantissent pas la validité des résultats obtenus telle que discutée précédemment. Une autre technique consiste à calculer les forces dynamiques analytiquement et les placer sur le modèle éléments finis. Cette dernière reste complexe et est longue à appliquée.

Afin de combiner les avantages des méthodes numériques et analytiques, une méthode d'accélérogramme modifiée (MAM) a été développée et a fait l'objet d'un article présenté dans le chapitre 6. Celle-ci consiste à transformer l'accélérogramme de dimensionnement en un nouveau accélérogramme intégrant l'effet d'interaction fluide-structure. Ce dernier peut alors être appliqué directement à la structure sèche afin d'obtenir la réponse dynamique de la structure en contact avec de l'eau. Elle intègre dans sa formulation de nombreux paramètres ayant de l'influence sur le comportement dynamique et permet de traiter analytiquement l'effet d'interaction fluide-structure tout en gardant les avantages de la modélisation par éléments finis de la structure. Deux formulations sont proposées : (i) une formulation exacte et (ii) une formulation simplifiée. Nous montrons que les deux formulations donnent d'excellents résultats lorsque comparées à la méthode des éléments finis. La formulation simplifiée est quasiment instantanée en temps de calcul et s'avère très intéressante pour la pratique et éventuellement pour la recherche telle qu'il sera discuté plus bas. L'utilisation de la méthode exacte reste aussi très intéressante, mais son utilisation est plus complexe de part la façon dont sont programmés les logiciels d'éléments finis commerciaux.

8.1.5 Développement d'un test d'erreur associée à l'utilisation de conditions aux frontières transmettantes

Lorsque la méthode des éléments finis est utilisée pour la modélisation de systèmes barrages-réservoir, elle nécessite de tronquer virtuellement le réservoir et d'appliquer une

condition aux frontières pour simuler l'infinité de celui-ci. L'emplacement et la formulation de celle-ci sont très importants, car si un mauvais choix est fait, cela pourrait entraîner une erreur considérable dans les résultats. De nombreuses différentes conditions aux frontières ont été développées, mais il n'existe aucune technique pour évaluer l'erreur qu'elles introduisent dans le modèle éléments finis.

À travers l'article présenté en annexe A, une nouvelle formulation analytique exacte des conditions aux frontières transmettantes (CFT) a été développée. Cette formulation a ensuite permis de comprendre le fonctionnement des CFT mais aussi de développer un test afin vérifier la validité des nombreuses conditions aux frontières existantes dans la littérature et/ou programmées dans les logiciels d'éléments finis. L'extension de la formulation développée peut permettre l'étude de systèmes telles que des réservoirs à parois flexibles. Ceci a été réalisé dans un article accepté pour publication et présenté en annexe C de ce document.

8.1.6 Conclusions générales

Afin de développer ces méthodes simplifiées, une partie de cette recherche a été dévouée à s'assurer de la fiabilité des résultats obtenus avec les méthodes complexes existantes dans la littérature. Ces méthodes ayant servi de références pour la comparaison des résultats obtenus avec les méthodes pratiques développées, plusieurs développements et discussions ont été réalisés pour s'assurer de la fiabilité de nos références. Nous avons par ailleurs mis en valeur de nombreuses difficultés qu'engendre l'utilisation de ces méthodes telles que l'implémentation de l'amortissement. De plus, les développements des méthodes pratiques ont permis certaines simplifications possibles lors de l'utilisation des éléments finis comme se contenter de modéliser les domaines d'eau sur une longueur égale à trois fois leurs hauteurs lorsque la compressibilité de l'eau est négligée.

Généralement, en statique, l'utilisation de méthodes simplifiées entraîne la surestimation d'une quantité d'intérêt et donc, ces méthodes sont considérées comme étant conservatrices. Des méthodes plus complexes sont alors utilisées pour raffiner les résultats si nécessaire. En dynamique, et comme il a été mentionné dans cette thèse, la méthode la plus simple peut entraîner une sous-estimation des quantités d'intérêts. Il est donc important de ne pas se limiter à une analyse pseudo-statique lorsqu'un ouvrage est dans une zone de haute et moyenne sismicité. Les méthodes qui ont été proposées à travers cette thèse de doctorat permettent d'obtenir rapidement une très bonne estimation du comportement de l'ouvrage en contact avec de l'eau étudié. Programmées dans un logiciel spécialisé, elle permettront aux ingénieurs civil praticiens de réaliser des analyses dynamiques de niveau de complexité différents et ce sans nécessiter d'une grande expertise.

8.2 Recommandations

En vue des nombreux développements, ce projet de recherche a permis de simplifier et démystifier les analyses dynamiques des structures en contact avec de l'eau et ouvre la porte à de nombreux axes de recherches. Certains de ces futurs axes de recherches sont mis en valeurs dans ce qui suit et triés par ordre de complexité.

8.2.1 Accélération verticale

Les méthodes développées se sont concentrées sur la prise en compte de l'effet de l'interaction fluide-structure pour une accélération horizontale. Cette accélération est en effet plus critique pour les barrages et surtout plus complexe à tenir compte. De par les développements analytiques existant dans la littérature pour une accélération verticale, il serait intéressant de rajouter ce type d'accélération dans toutes les méthodes développées. Ces développements ne devraient pas être complexes en vue des développements déjà réalisés.

8.2.2 Généralisation de ces méthodes à d'autres systèmes

En se basant sur les simplifications réalisées pour le développement des méthodes présentées dans cette thèse, les méthodes simplifiées peuvent être généralisées pour d'autres types de structures. Par exemple, en annexe C, une méthode analytique est présentée pour l'étude de structure contenant de l'eau. L'utilisation de la méthode présentée en chapitre 5 serait très adéquate pour traiter ce problème de façon simplifiée.

8.2.3 Analyse non-linéaire

Il serait très intéressant de confronter la méthode de l'accélérogramme modifiée à l'analyse d'une structure ayant un comportement non linéaire. Pour cela, les propriétés dynamiques linéaires de la structure seraient utilisées pour calculer les propriétés nécessaires au calcul de l'accélérogramme modifié. Cet accélérogramme serait alors utilisé sur la même structure ayant un comportement non linéaire. De par la formulation de cet accélérogramme, une partie de l'effet de la non-linéarité devrait être prise en compte dans l'analyse. Un test de sensibilité permettra alors de voir jusqu'à quelle limite on peut utiliser cette formulation. Le but de cette vérification est surtout pour l'utilisation de cet accélérogramme sur une table vibrante afin de réaliser une simulation hybride. Pour ce type expérimentation, l'effet de l'eau est pris en compte dans l'accélérogramme, et la structure quant à elle est installée sur la table vibrante.

8.2.4 Prise en compte de l'effet de l'interaction sol-structure

Les méthodes qui ont été développées au cours de cette thèse de doctorat peuvent toutes tenir compte de l'effet de la flexibilité du sol. Néanmoins, en négligeant la masse du sol, on ignore l'effet inertiel de celui-ci. Ceci à l'avantage de ne pas avoir à réaliser une déconvolution du tremblement de terre de dimensionnement, mais peut introduire une erreur dans le comportement dynamique de l'ouvrage. Par ailleurs, le sol permet d'augmenter l'amortissement global du système, il est donc avantageux d'en tenir compte. Le sol a un comportement très non-linéaire. Il serait intéressant d'étudier l'effet qu'a celui-ci sur le comportement, mais avant tout de s'assurer d'une modélisation adéquate de celui-ci.

8.2.5 Étude des systèmes tridimensionnels

Tel que démontré lors de test in situ, l'effet tridimensionnel est non négligeable. Une telle étude va être réalisée suite à une analyse pseudo-statique, pseudo-dynamique et dynamique temporelle d'une section de l'ouvrage. Elle correspond donc à une analyse dynamique raffinée. Il est fort probable que les développements de la Méthode de l'Accélérogramme Modifiée puissent être étendus à l'analyse d'un modèle tridimensionnel. Nous avions vu que deux formulations existent pour cette méthode, l'une dite exacte, et l'autre dite simplifiée. L'extension de la méthode exacte devrait permettre d'excellents résultats. Pour celle simplifiée, une analyse de sensibilité devra être effectuée. Dans tous les cas, en se contentant de la méthode exacte, elle devrait offrir un énorme gain de temps et de diminution de la complexité du modèle éléments finis.

BIBLIOGRAPHIE

- ADINA Theory and Modeling Guide. Report ARD 06-7. ADINA R & D, Inc., 2006.
- ADINA Theory and Modeling Guide. Report ARD 10-7. ADINA R & D, Inc., 2010.
- Balendra T., Ang K. K., Paramasivam P., and Lee S. V. Seismic design of flexible cylindrical liquid storage tanks. *Earthquake Engineering and Structural Dynamics* 1982 ; **10**(3) : 477–496.
- Bathe KJ, Hahn W. On transient analysis of fluid–structure systems. *Journal of Computers and Structures* 1979 ; **10** : 383–91.
- Bayraktar A., Hançer E., Akköse M. Influence of base-rock characteristics on the stochastic dynamic response of dam–reservoir–foundation systems. *Engineering Structures* 2005 ; **27** : 1498-1508.
- Blevins, R.D. Formulas for natural frequency and mode shape, Kriger publishing Company, Florida, 1984.
- Bouaanani N, Lu F.Y. Assessment of potential-based fluid finite elements for seismic analysis of dam-reservoir systems. *Journal of Computers and Structures* 2009 ; **87** : 206-224.
- Bouaanani N, Miquel B. A new formulation and error analysis for vibrating dam-reservoir systems with upstream transmitting boundary conditions.*Journal of Sound and Vibration* 2010 ; **329** : 1924-1953.
- Bouaanani N, Paultre P, Proulx J. Two-dimensional modelling of ice-cover effects for the dynamic analysis of concrete gravity dams. *Earthquake Engineering and Structural Dynamics* 2002 ; **31** : 2083–2102.
- Bouaanani N, Paultre P, Proulx J. A closed-form formulation for earthquake-induced hydrodynamic pressure on gravity dams. *Journal of Sound and Vibration* 2003 ; **261** : 573-582.
- Bouaanani N, Paultre P. A new boundary condition for energy radiation in covered reservoirs using BEM, *Engineering analysis with boundary elements* 2005 ; **29** : 903–911.
- Bouaanani N, Perrault C. Practical Formulas for Frequency Domain Analysis of Earthquake-Induced Dam-Reservoir Interaction.*Journal of Engineering Mechanics*(ASCE) 2010 ; **136** : 107-119.
- Bustamante J.I, Rosenblueth E, Herrera I, Flores A, Presión hydrodinámica en presas y depósitos. *Boletin Sociedad Mexicana de Ingeneria Sismica* 1963 ; **1** :37–54.
- Canadian Dam Association (CDA). Dam safety guidelines. Edmonton, Alberta ; 1999.

- ACB/CDA. Dam Safety Guidelines, Canadian Dam Association, Edmonton ; 2007 ;
- Celep Z, Bazant P. Spurious reflection of elastic waves due to gradually changing finite element size. *International Journal of Numerical Methods in Engineering* 1983 ; **19** : 631–646.
- Çetin M, Mengi Y. Transmitting boundary conditions suitable for analysis of dam-reservoir interaction and wave load problems. *Applied Mathematical Modelling* 2003 ; **23** : 451–470.
- Chakrabarti P, Chopra AK. Earthquake analysis of gravity dams including hydrodynamic interaction. *Earthquake Engineering and Structural Dynamics* 1973 ; **2** : 143-160.
- Chardrasekaran A.R, Saini S.S, Malhotra M.M. Hydrodynamic pressure on circular cylindrical cantilever structures surrounded by water. Fourth Symposium on Earthquake Engineering, Roorkee, India, 1970, pp. 161–171.
- Chang J.Y., Liu W.H. Some studies on the natural frequencies of immersed restrained column. *Journal of Sound and Vibration* 1989 ; **13** : 516–524.
- Chen B.F. The significance of earthquake-induced dynamic forces in coastal structures design, *Ocean Engineering* 1995 ; **22** : 47–65.
- Chen B.F. Dynamic responses of coastal structures during earthquakes including sediment-sea-structure interaction.*Soil Dynamics and Earthquake Engineering* 2000 ; **20** : 445–467.
- Christopoulos C., Léger P., Filliatraut A. Sliding response of gravity dams including vertical seismic accelerations.*Earthquake Engineering and Engineering vibration* 2003 ; **2** : 89-200.
- Chopra A.K. Hydrodynamic pressures on dams during earthquakes. *Journal of the Engineering Mechanics Division* (ASCE) 1967 ; **93** : 205–223.
- Chopra A. K. Earthquake behavior of reservoir-dam systems. *Journal of the Engineering Mechanics Division* (ASCE) 1968 ; No. EM6 : 1475–1500.
- Chopra AK. Earthquake response of concrete gravity dams. Report No. UCB/EERC-70/01, University of California, Berkeley, 1970.
- Chopra AK. Earthquake resistant design of concrete gravity dams. *Journal of the Structural Division*(ASCE) 1978 ; **104** : 953-971.
- Chopra A.K, Chakrabarti P, Gupta S. Earthquake response of concrete gravity dams including hydrodynamic and foundation interaction effects. Report No. UCB/EERC-80/01, University of California, Berkeley, California, 1980.
- Clough RW, Penzien J. Dynamics of Structures, McGraw-Hill, Inc., New York, 1975.
- Corns C.F, Schrader E.K, Tarbox G.S. Gravity dam design and analysis. Advanced Dam Engineering For Design, Construction and Rehabilitation. Chapter 16, edited by

R.B Jansen, Van Nostrand Reinhold, 1988.
– Coté, M. Revue critique sur la nouvelle Loi sur la securite des barrages L.R.Q., chapitre S-3.1.01. Mémoire. Université de Sherbrooke, 2008, 330 pages.
– Dasgupta G, Chopra A.K. Dynamic stifness Matrices for viscoelastic half planes. *Journal of the engineering mechanics division* 1979 ; **105** : 729-745.
– De Souza S.M, Pedroso L.J. Study of flexible wall acoustic cavities using Beam Finite Element. Mechanics of Solids in Brazil, Brazilian Society of Mechanical Sciences and Engineering, H.S. da Costa Mattos & Marcílio Alves (Editors), 2009, pp. 223–237.
– Duron Z, Hall J. Experimental and finite element studies of the forced vibration response of Morrow Point Dam. *Earthquake Engineering and Structural Dynamics* 1988 ; **16** : 1021—1039.
– Everstine G. C. A symmetric potential formulation for fluid-structure interaction. *Journal of Sound and Vibration* 1981 ; **79**(1) : 157–160.
– Fenves G, Chopra A.K. Earthquake analysis and response of concrete gravity dams. Report No. UCB/EERC-84/10, University of California, Berkeley, California, 1984.
– Fenves G, Chopra AK. EAGD-84, a computer program for earthquake analysis of concrete gravity dams. Report No UCB/EERC-84/11, University of California, Berkeley, California, 1984.
– Fenves G, Chopra AK. Simplified analysis for earthquake resistant design of concrete gravity dams. Report No. UCB/EERC-85/10, University of California, Berkeley, 1985.
– Fenves G, Chopra AK. Simplified earthquake analysis of concrete gravity dams. *Journal of Structural Engineering* 1987 ; **113**(8) : 1688-1708.
– Fenves G, Luis M. V. Nonlinear Dynamic Analysis of Fluid-Structure Systems *J. Eng. Mech* 1988 ; **114** : 219-241.
– Feltrin G. Absorbing Boundaries for the Time-Domain Analysis of Dam-Reservoir-Foundation Systems. Institute of Structural Engineering Swiss Federal Institute of Technology Zurich 1997.
– Federal Guidelines for Dam Safety, U.S. Department of Homeland Security, Federal Emergency Management Agency, United States, 50 p ; 2004.
– FERC (Federal Energy Regulatory Commission). Engineering guidelines for evaluation of hydropower projects – Draft Chapter III Gravity Dams. Federal Energy Regulatory Commission, Office of Energy Projects, Division of Dam Safety and Inspections, Washington DC, USA ; 2000.
– S.R. Finch, Mathematical constants. Cambridge University Press, 2003.
– Fok K.L, Hall J.F, Chopra A.K. EACD-3D, a computer program for three-dimensional earthquake analysis of concrete dams. Report No. UCB/EERC-86/09, University of

California, Berkeley, California, 1986.

– Gogoi I, Maity D. A non-reflecting boundary condition for the finite element modeling of infinite reservoir with layered sediment. *Advances in Water Resources* 2006 ; **29** : 1515-1527.
– Goto H, Toki K. Vibrational characteristics and aseismic design of submerged bridge piers. Proceedings of the Third World Conference on Earthguake Engineering, Vol. II, New Zealand, 1965 pp. 107–122.
– Graham E. W, Rodriguez A. M. Characteristics of fuel motion which affect airplane dynamics. *Journal of Applied Mechanics* 1952 ; **19** :381–388.
– Han R.P.S, Xu H. Simple and accurate added mass model for hydrodynamic fluid-structure interaction analysis. *Journal of the Franklin Institute* 1996 ; 333B, no. 6, 929–945.
– Hall, J. F. (ed.). Northridge earthquake of January 17, 1994 : Reconnaissance report. *Earthquake Spectra*, Supplement C to Volume 11, Vol. 1, Earthquake Engineering Research Institute, Oakland, CA. 1995.
– Hall J.F, Chopra A.K. Two-dimensional dynamic analysis of concrete gravity and embankment dams including hydrodynamic effects. *Earthquake Engineering and Structural Dynamics* 1982 ; **10** : 305–332.
– CSB (Comite Suisse des Barrages). Methods of analysis for the prediction and the verification of dam behaviour, Wasser Energie Luft, Baden, Suisse, p. 74-110 ; 2003.
– Hanson R. D. Behavior of storage tanks, the Great Alaska earthquake of 1964. *Proc., National Academy of Science*, Washington, D.C., 7, 331–339. 1973.
– Haroun, M. A. Dynamic analyses of liquid storage tanks. *Report No. EERL 80-04, California Institute of Technology*, Pasedenas, CA. 1980.
– Haroun M. A. and Housner G. W. Seismic design of liquid storage tanks. *Journal of Technical Councils of ASCE* 1981 ; **107** : 191–207.
– Haroun M. A. and Housner G. W. Earthquake response of deformable liquid storage tanks. *Journal of Applied Mechanics* 1981 ; **48**(2) : 411–418.
– Haroun M. A. and Housner G. W. Complications in free vibration analysis of tanks. *Proc., ASCE Engineering Mechanics Division* 1982 ; **108**(5) : 801–818.
– Haroun M. A. Vibration studies and tests of liquid storage tanks. *Earthquake Engineering and Structural Dynamics* 1983 ; **11**(2) : 179–206.
– Hatanaka M. Study on the earthquake-resistant design of gravity type dams. *Proceedings of the Second World Conference on Earthquake Engineering*, Tokyo and Kyoto, Japan, 1960 ; **II** : 82.1–82.16.
– Higham N. J. Accuracy and stability of numerical algorithms (second ed.) SIAM, 2002.

– Hoskins, L. M. and Jacobsen, L. S. Water pressure in a tank caused by a simulated earthquake. *Bulletin of the Seismological Society of America* 1934 ; **24** : 1–32.
– Housner G. W. "Dynamic pressures on accelerated fluid containers." *Bulletin of the Seismological Society of America* 1957 ; **47** : 15–35.
– Housner G. W. Nuclear reactors and earthquakes. *Report No. TID-7024 - United States Atomic Energy Commission*, Washington, D.C. 1963.
– Humar J, Roufaiel M. Finite element analysis of reservoir vibration. *Journal of Engineering Mechanics*(ASCE) 1983 ; **109** : 215-230.
– Humar J.L, Jablonski A.M. Boundary element reservoir model for seismic analysis of gravity dams. *Earthquake Engineering and Structural Dynamics* 1988 ; **16** : 1129–1156.
– Hydro-Québec. Guide devaluation de la securite sismique des barrages, Hydro-Québec, Québec ; 2000.
– Jacobsen L.S. Impulsive hydrodynamics of fluid inside a cylindrical tank and of fluid surrounding a cylindrical pier. Bulletin of the Seismological Society of America 1949 ; 39 189–1949.
– Jacobson L. S. and Ayre R. S. Hydrodynamic experiments with rigid cylindrical tanks subjected to transient motions. *Bulletin of the Seismological Society of America* 1951 ; **41** : 313–346.
– Jablonski A.M. Effect of location of transmitting boundary on seismic hydrodynamic pressures on gravity dams. Proceedings of the Fourth U.S. National Conference on Earthquake Engineering, Palm Springs, California, 1990 ; 95–103.
– Javanmardi F., Léger P. Tinawi R. Seismic Water Pressure in Cracked Concrete Gravity Dams : Experimental Study and Theoretical Modeling. *Journal of Structural Engineering* 2005 ; **131** : 139-150.
– Kana D. D. Seismic response of flexible cylindrical liquid storage tanks. *Nuclear Engineering and Design* 1979 ; **52**(1) : 185–199.
– Kotsubo S. Seismic force effect on submerged bridge piers with elliptic cross-sections. Proceedings of the Third World Conference on Earthguake Engineering, Vol. II, New Zealand, 1965 pp. 342–356.
– Küçükarslan S. An exact truncation boundary condition for incompressible–unbounded infinite fluid domains, *Applied Mathematics and Computation* 2005 ; **163** : 61—69.
– Lamb, H. Hydrodynamics. 6th ed. New York : Dover ; 1945.
– Leclerc, M., Léger, P., Tinawi, R.Computer Aided Stability Analysis of Gravity Dams - CADAM. *International Journal Advances in Engineering Software* 2003 ; **34** : 403-420.
– Léger, P., Javanmardi, F., Tinawi, R. (2005). Variations des sous-pressions dans les fissures sismiques des barrages en béton - modélisation numérique. 7iemes Colloque

National de calcul en structures, v. 2, p. 507-512.

- Liaw C.Y, Chopra A.K. Dynamics of towers surrounded by water. *International Journal Earthquake Engineering and Structural Dynamics* 1974 ; **3**(1) : 33—49.
- Liu Ph, Cheng A. Boundary solutions for fluid-structure interaction. *Journal of Hydraulic Engineering*(ASCE) 1984 ; **110** : 51–64.
- Lysmer J, Kuhlemeyer RL. Finite dynamic model for infinite media. *J Eng Mech Div* (ASCE) 1969 ; **95** :859–77.
- Maeso O, Aznarez J.J, Dominguez J. Three-dimensional models of reservoir sediment and effects on the seismic response of arch dams. *Earthquake Engineering and Structural Dynamics* 2004 ; **33** :1103–1123.
- Maity D. A novel far-boundary condition for the finite element analysis of infinite reservoir. *Applied Mathematics and Computation* 2005 ; **170** :1314–1328.
- Maity D, Bhattacharyya S.K. Time-domain analysis of infinite reservoir by finite element method using a novel far-boundary condition. *Finite Elements in Analysis and Design* 1999 ; **32** : 85-96.
- Malhotra, P. K., Norwood, M. A. and Wieland, M. Simple procedure for seismic analysis of liquid-storage tanks. *IABSE Structural Engineering International* 2000 ; **3** : 197–201.
- MATLAB ®. The Mathworks, Inc., Natick, MA, USA, 2007.
- MATLAB ®. The Mathworks, Inc., Natick, MA, USA, 2011.
- Maeso O, Aznarez JJ, Dominguez J. Three-dimensional models of reservoir sediment and effects on the seismic response of arch dams. *Earthquake Engineering and Structural Dynamics* 2004 ; **33** : 1103-1123.
- Miquel B, Bouaanani N. Simplified evaluation of the vibration period and seismic response of gravity dam-water systems.*Engineering structures* 2010 ; **32** : 2488-2502.
- Nagaya K. Transient response in flexure to general uni-directional loads of variable cross-section beam with concentrated tip inertias immersed in a fluid. *Journal of Sound and Vibration* 1985 ; **99**(3) : 361-–378.
- Nagaya K., Hai, Y. Seismic response of underwater members of variable cross section. *Journal of Sound Vibration* 1985 ; **103** :119–138.
- Nasserzare J, Lei Y, Eskandari-Shiri S. Computation of natural frequencies and mode shapes of arch dams as an inverse problem. *Advances in Engineering Software* 2000 ; **31**(11) : 827–836
- Newmark N.M, Rosenblueth E. Fundamental of Earthquake Engineering, Edited by N.M Newmark and W.J HallR, 1971.
- Noble, CR. Finite element techniques for realistically simulating the seismic response of concrete dams. Ph.D. Thesis, University of California, Davis, 2007, 231 pages.

– Okamoto S. *Introduction to earthquake engineering*. 2nd edition, University of Tokyo Press : Tokyo, 1984.
– Oz H.R. Natural frequenciesof an immersed beam carrying a tip mass with rotatory inertia. *Journal of Sound and Vibration* 2003 ; **266** : 1099-–1108.
– Proulx J, Paultre P. Experimental and numerical investigation of dam-reservoir-foundation for a large gravity dam. *Canadian Journal of Civil Engineering* 1997 ; **24** : 90-105.
– Proulx J, Paultre P, Rheault J, Robert Y. An experimental investigation of water level effects on the dynamic behaviour of a large arch dam. *Earthquake Engineering and Structural Dynamics* 2001 ; **30** : 1147–1166.
– Rayleigh, Lord (1877), Theory of Sound (two volumes), Dover Publications, New York, reissued 1945, second edition.
– Rao P.V. Calculation of added mass of circular and rectangular piers oscillating in water. Proceedingd of the Fifth Symposium of Earthquake Engineering 1974 ; 97.
– Rea D, Liaw CY, Chopra, AK. Dynamic properties of Pine Flat dam. Report UCB/EERC-72/07, University of California, Berkeley, California, 1972.
– Reinhardt F, Soeder H. *dtv-Atlas zur Mathematik*. Deutscher Taschenbuch Verlag : Munich, 2001.
– Saini S.S. Coupled hydrodynamic response of a gravity dam using finite and infinite elements. Proceeding of the Seventh Symposium on Earthquake Engineering, Vol. 2 (Roorkee, India, 1982) 45–50.
– Saini S.S, Bettess P, Zienkiewicz O.C. Coupled hydrodynamic response of concrete gravity dams using finite and infinite elements. *Earthquake Engineering and Structural Dynamics* 1978 ; **6** : 363–374.
– Sharan S.K. Finite element analysis of unbounded and incompressible fluid domains. *International Journal of Numerical Methods in Engineering* 1985 ; **21** : 1659-1669.
– Sharan S.K. Finite element modelling of infinite reservoirs. *Journal of Engineering Mechanics*(ASCE) 1985 ; **111** : 1457-1469.
– Sharan S.K. A non-reflecting boundary in fluid-structure interaction. *Journal of Computers and Structures* 1987 ; **26** : 841-846.
– Sharan S.K. Efficient finite element analysis of hydrodynamic pressure on dams. *Journal of Computers and Structures* 1992 ; **42** : 713-723.
– Sommerfeld A. Partial differential equations in physics. Academic Press, New York, 1949.
– Steinbrugge K. V. and Flores R. The Chilean earthquakes of May, 1960 : A structural engineering viewpoint. *Bulletin of the Seismological Society of America* 1963 ; **53**(2) : 225–307.

– Steinberg L. J and Cruz, A. M. When natural and technological disasters collide : Lessons from the Turkey earthquake of August 17, 1999. *Natural Hazards Review* 2004 ; **3**(5) : 121–130.
– Stefan C. L. Modèle constitutif hydromécanique tridimensionnel pour l'analyse de stabilité des piliers d'évacuateur de crues. Thèse de doctorat, École Polytechnique de Montréal, Montréal, 2011, 199 pages.
– Tanaka Y, Hudspeth R. T. Restoring forces on vertical circular cylinders forced by earthquakes. *International Journal Earthquake Engineering and Structural Dynamics* 1988 ; **16**(1) : 99—119.
– Tinawi R., Léger P., Leclerc M., Cipolla G. Seismic Response of Concrete Gravity Dams - Correlations Between Shake Table Tests and Numerical Analyses. 12th World Congress on Earthquake Engineering, 2000.
– Tsai C.S, Lee G.C. Arch dam-fluid interactions : by FEM-BEM and substructure concept. *International Journal of Numerical Methods in Engineering* 1987 ; **24** : 2367–2388.
– US Army corps of Engineers. Engineering and Design - Gravity Dam Design. Report No. EM 1110-2-2200, 1995.
– US Army corps of Engineers. Engineering and Design - Time-History Dynamic Analysis of Concrete Hydraulic Structures. Report No. EM 1110-2-6051, 2003.
– USBR (United States Bureau of Reclamation). Design of small dams. Denver, Colorado ; 1987.
– Uscilowska A, Kolodziej J.A. Free vibration of immersed column carrying a tip mass. *Journal of Sound and Vibration* 1998 ; **216** : 147-–157.
– Veletsos, A. S. Seismic effects in flexible liquid storage tank. *Proc., 5th World Conference on Earthquake Engineering* 1974 ; 630–639.
– Veletsos A. S. and Yang J. Y. Dynamics of fixed-base liquid storage tanks. *US-Japan Seminar for Earthquake Engineering Research*, Tokyo, Japan 1976, 317–341.
– Veletsos A. S. and Yang J. Y. Earthquake response of liquid storage tanks. *Proc., Second EMD Specialty Conference*, ASCE, Raleigh, NC, 1977, 1–24.
– Werner P. W. and Sundquist K. J. On hydrodynamic earthquake effects. *Transactions of the American Geophysical Union* 1949 ; **30**(5) : 636–657.
– USBR (United States Bureau of Reclamation). Design of small dams. Denver, Colorado ; 1987.
– Westergaard HM. Water pressures on dams during earthquakes. *Transactions*(ASCE) 1933 ; **98** : 418-472.
– Wilson EL, Khalvati M. Finite elements for the dynamics analysis of fluid–solid systems.

Int J Numer Methods Eng 1983 ; **19** : 1657–68.

– Wu J.S, Chen K.-W. An alternative approach to the structural motion analysis of wedge-beam offshore structures supporting a load. *Ocean Engineering* 2003 ; **30**(14) : 1791–1806.
– Wu J.S, Chen C.T. An exact solution for the natural frequencies and mode shapes of an immersed elastically restrained wedge beam carrying an eccentric tip mass with mass moment of inertia. *Journal of Sound and Vibration* 2005 ; **286** : 549–568.
– Wu J.S, Hsu S.-H. A unified approach for the free vibration analysis of an elastically supported immersed uniform beam carrying an eccentric tip mass with rotary inertia. *Journal of Sound and Vibration* 2006 ; **291** : 1122–1147.
– Xing J.T. Natural vibration of two-dimensional slender structure-water interaction systems subject to Sommerfeld radiation condition. *Journal of Sound and Vibration* 2007 ; **308** : 67–79.
– Xing J.T, Price W.G, Pomfret M.J, Yam L.H. Natural vibration of a beam-water interaction system, *Journal of Sound and Vibration* 1997 ; **199** : 491–512.
– Zhao S, Xing J.T, Price W.G. Natural vibration of a flexible beam–water coupled system with a concentrated mass attached at the free end of the beam. Proceedings of the Institution of Mechanical Engineers, Part M : Journal of Engineering for the Maritime Environment, Vol. 216, no. 2, 2002, pp. 145–154.
– Zienkiewicz O.C, Kelly D.W, Bettes P. The Sommerfeld (radiation) condition on infinite domains and its modelling in numerical procedures. *Computing Methods in Applied Sciences and Engineering* 1977,**I** : 169–203.
– Zienkiewicz O.C, Newton R.E. Coupled vibrations in a structure submerged in a compressible fluid. International Symposium on Finite Element Techniques, (Stuttgart, 1969).

ANNEXE A

A new formulation and error analysis for vibrating dam-reservoir systems with upstream transmitting boundary conditions

Najib Bouaanani [1] **and Benjamin Miquel** [2]

Paper published in *Journal of Sound and Vibration*, Volume 329, Issue 10, 10 May 2010, Pages 1924-1953. Doi :10.1016/j.jsv.2009.12.005

Submitted 28 January 2009. Accepted 3 December 2009.

This paper proposes and validates a new formulation to investigate the dynamic response of dam-reservoir systems with upstream Transmitting Boundary Conditions (TBCs). The mathematical derivations are provided for the new formulation as well as for exact and various approximate TBCs. The developed analytical equations can be solved numerically to assess the accuracy of a given TBC and determine the associated error independently of FEM or BEM modeling of the reservoir. The method is first validated in the case of semi-infinite reservoirs and an excellent agreement is obtained against classical techniques. The paper presents a fundamental understanding of the behavior of various TBCs and a systematic identification of their influence on the system's dynamic response, considering : (i) dam flexibility, (ii) water compressibility, (iii) reservoir bottom wave absorption, (iv) reservoir truncation length, and (v) excitation frequency. The new method is used to obtain exact error estimators to evaluate the effects of various TBCs on the dam-reservoir first resonant frequency and hydrodynamic forces acting on the dam upstream face. The proposed formulation can be programmed easily and used efficiently for rigorous assessment of classical or newly-developed TBCs for vibrating dam-reservoir systems or similar fluid-structure problems.

1. Associate Professor, Department of Civil, Geological and Mining Engineering, École Polytechnique de Montréal, Montréal, QC H3C 3A7, Canada
Corresponding author. E-mail : najib.bouaanani@polymtl.ca

2. Graduate Research Assistant, Department of Civil, Geological and Mining Engineering, École Polytechnique de Montréal, Montréal, QC H3C 3A7, Canada.

A.1 Introduction

Accurate evaluation of reservoir loading on a dam upstream face is crucial for its seismic safety assessment. Significant research has been devoted to study this type of loading since the pioneering work of Westergaard [1] who used a heightwise added mass distribution to model hydrodynamic pressure on a dam upstream face. This concept has been widely used for several decades to design earthquake resistant gravity dams. More advanced analytical and numerical frequency-domain and time-domain approaches were proposed later to account for dam deformability, water compressibility and reservoir bottom wave absorption in the seismic response of dam-reservoir systems [2, 3, 4, 5, 6, 7, 8, 9, 10, 11, 12, 13]. Some of these procedures were validated against forced-vibration testing of concrete gravity and arch dams [14, 15, 16]. Among the numerical techniques used to study dam-reservoir systems, the Finite Element Method (FEM) and Boundary Element Method (BEM) have gained wide popularity. Due to the large extent of the reservoir, these methods require its virtual truncation at a finite distance from dam face and application of appropriate Transmitting Boundary Conditions (TBCs) at the upstream end of the reservoir. Here, we note that although BEM may intrinsically satisfy radiation conditions at infinity contrary to FEM, to reduce computational burden, it might be useful to split an infinite reservoir into : (i) a finite near field region to be discretized by BEM, and (ii) an infinite near field region, to be modeled as a infinite continuum domain or by infinite finite elements [11]. In this case, as for FEM, a TBC has to be applied at the boundary between the near field and the far field to ensure adequate energy radiation at infinity. These special boundary conditions and the truncation distance should be defined appropriately to prevent reflection of spurious waves back towards the dam. Otherwise, significant error may be introduced in the prediction of the dynamic response of the dam-reservoir system.

Among the many TBCs proposed in the literature, the Sommerfeld radiation boundary condition has been widely used [17, 18, 19, 20]. Although the method can be easily incorporated in a FEM or BEM program, it performs adequately only when placed at a large distance from dam face. Saini et al. [8] and Saini [21] studied the coupled response of dam-reservoir systems and developed infinite elements to model energy dissipation at the far upstream end of the reservoir. They concluded that the effect of radiation damping is significant at high frequencies of excitation. Hall and Chopra [5] developed a substructuring technique where the dam, reservoir and foundation are modeled using finite elements and their responses coupled through interface forces to obtain the global dynamic behavior. They considered a one-dimensional model to account for reflection of waves at reservoir bottom, and proposed a one-dimensional infinite boundary condition to simulate absorption of compression waves

outgoing from a seismically excited dam-reservoir towards its upstream end. Humar and Roufaiel [22] proposed a modified Sommerfeld boundary condition, implemented it into a finite element program and proved its efficiency to be superior to the classical Sommerfeld TBC for frequencies between the first and the second natural frequencies of the reservoir. They did not consider reservoir bottom wave absorption in their study. Neglecting water compressibility, Sharan [23] proposed a TBC based on the analytical solution for hydrodynamic pressure in a reservoir impounded by a rigid dam. He concluded that this TBC gives satisfactory results even for very short reservoir truncation lengths. Sharan [24] extended his TBC to include water compressibility, but still considered a complete reflective reservoir bottom and a rigid dam. He showed that the new TBC is a generalization of the Sommerfeld TBC and of that proposed by Humar and Roufaiel [22]. He also confirmed that the Sommerfeld TBC gives satisfactory results only when placed very far away from dam face and for excitation frequencies lower than the reservoir first natural frequency. Sharan [25] extended the use of his TBC to deformable dams by dividing the reservoir into a near-field domain with an arbitrary shape, and a far-field domain with a uniform rectangular geometry. He modeled the whole dam-reservoir system using finite elements and applied a TBC based on a rigid dam assumption to the upstream end of the far-field domain. The TBC was improved later by including the effects of reservoir bottom wave absorption [26]. Satisfactory results were obtained for short truncation lengths and a wide range of excitation frequencies except near the second and third natural frequencies of the reservoir [26]. Jablonski [27] developed a BEM program implementing the TBC proposed by Hall and Chopra [5]. He studied the effect of the location of this TBC on hydrodynamic pressures at dam upstream face, and concluded that the accuracy of the results is sensitive to the type and size of the boundary elements used, a result also previously reported for finite element models [28, 29].

All the TBCs described above were however developed considering a rigid dam assumption. Recently, Maity and Bhattacharyya [30] proposed a TBC that intrinsically takes account of dam flexibility and is therefore height-dependent. They considered a completely reflective reservoir bottom and implemented this TBC into a FEM program. They evidenced the effects of dam flexibility, and the TBC was shown efficient in time-domain analyses of dam-reservoir systems. Çetin and Mengi [31] developed a TBC based on spectral theory of waves propagating horizontally along a fluid reservoir with a completely reflective reservoir bottom. They assessed the TBC through BEM analysis of two benchmark problems of rigid dams subjected to harmonic and time dependent loadings. Bouaanani et al. [32] formulated a new TBC to account for energy radiation in ice-covered reservoirs, including the effects of reservoir bottom wave absorption and water compressibility. They implemented the proposed TBC into a BEM program and proved its effectiveness and accuracy through a parametric study of

a typical dam–reservoir system. Maity [33] and Küçükarslan [34] proposed TBCs to study earthquake-induced horizontal vibrations of incompressible–unbounded infinite fluid domains with completely reflective reservoir bottoms. They incorporated the TBCs into FEM programs and showed their performance to be superior to classical TBCs when placed near dam upstream face. Gogoi and Maity [35] extended the TBC proposed by Maity and Bhattacharyya [30] to include energy dissipation at reservoir bottom. They defined the new TBC based on a closed-form formulation of hydrodynamic pressure proposed by Bouaanani et al. [36]. The proposed TBC was implemented in a FEM code for frequency- and time-domain analyses of dam-reservoir systems and was found to perform efficiently on a wide frequency range of interest in dam seismic analyses.

TBCs are generally approximate, absorbing only a portion of impinging waves, and thus introducing some error into the solution. This error is usually to be minimized based on the experience and judgement of the analyst after some initial guess of the truncation boundary location. Successive trials are then performed to ensure numerical convergence of the FEM or BEM solutions as a function of truncation length and mesh refinement. It is important however to separate errors that can be attributed strictly to the type of TBC applied and its location from the discretization, convergence, or other numerical or modeling errors specific to the FEM or BEM packages used. Such a validation is generally conducted through comparison with the exact solution of the mathematical model describing dam-reservoirs with upstream TBCs. However, available analytical solutions can handle only heightwise constant TBCs and thus cannot be used to validate FEM or BEM models with height-dependent TBCs which include dam flexibility effects. The main objective of this work is to develop an original and rigorous analytical technique to reliably predict the accuracy of a given TBC in a vibrating dam-reservoir system and estimate the TBC effects and associated error independently of FEM or BEM modeling of the reservoir. This method would be also useful in testing, validating or developing either frequency-dependent TBCs or frequency-independent TBCs which are generally more suitable for time domain analyses of dam-reservoir systems. Another objective of this work is to use the proposed method to present a fundamental understanding of the behavior of various TBCs and provide a systematic identification of their influence on the dynamic response of a dam-reservoir system, considering the effects of : (i) dam flexibility, (ii) water compressibility, (iii) reservoir bottom wave absorption, (iv) reservoir truncation length, and (v) excitation frequency. To the authors' knowledge, such a thorough analysis has never been published.

This paper is organized as follows. In Section A.2, we briefly review the mathematical background of a classical analytical technique and we define some common TBCs. We then establish the mathematical formulation underlying the new analytical method proposed to

study dam-reservoir systems with upstream TBCs. In Section A.3, we examine the sensitivity of common TBCs to various key factors, and we illustrate the use of the proposed method to investigate the efficiency and accuracy of these TBCs. The last section contains some concluding remarks.

A.2 Mathematical formulations

A.2.1 Review of the formulation for a semi-infinite reservoir

Fig. A.1(a) illustrates a typical gravity dam of height H_s, impounding a rectangular semi-infinite reservoir of constant height H_r. The effects of sediments that may be deposited at reservoir bottom are also considered. A Cartesian coordinate system with axes x and y and origin at the heel of the structure is adopted as well as the following main assumptions : (i) the dam and the water are assumed to have a linear elastic behavior ; (ii) the water in the reservoir is compressible and inviscid, with its motion irrotational and limited to small amplitudes ; and (iii) gravity surface waves are neglected. Under these assumptions, the hydrodynamic pressure $p(x, y, t)$ in the reservoir obeys the wave equation

$$\nabla^2 p = \frac{1}{C_\mathrm{r}^2} \frac{\partial^2 p}{\partial t^2} \tag{A.1}$$

where ∇^2 is the Laplace differential operator, t the time variable, ρ_r the mass density of water and C_r the compression wave velocity given by

$$C_\mathrm{r} = \sqrt{\frac{\mu_\mathrm{r}}{\rho_\mathrm{r}}} \tag{A.2}$$

in which μ_r denotes the bulk modulus of water.
Considering horizontal harmonic ground accelerations $\ddot{u}_\mathrm{g}(t) = a_\mathrm{g}\, \mathrm{e}^{\mathrm{i}\omega t}$, the hydrodynamic pressure in the reservoir can be expressed in the frequency domain as $p(x, y, t) = \bar{p}(x, y, \omega)\, \mathrm{e}^{\mathrm{i}\omega t}$, where $\bar{p}(x, y, \omega)$ is a complex-valued Frequency Response Function (FRF). Introducing this transformation into Eq. (A.1) yields the classical Helmholtz equation

$$\nabla^2 \bar{p} + \frac{\omega^2}{C_\mathrm{r}^2}\, \bar{p} = 0 \tag{A.3}$$

The dam section can be modeled using finite elements and assuming that the system has a constant hysteretic damping, the dynamic equilibrium of the dam-reservoir system can be

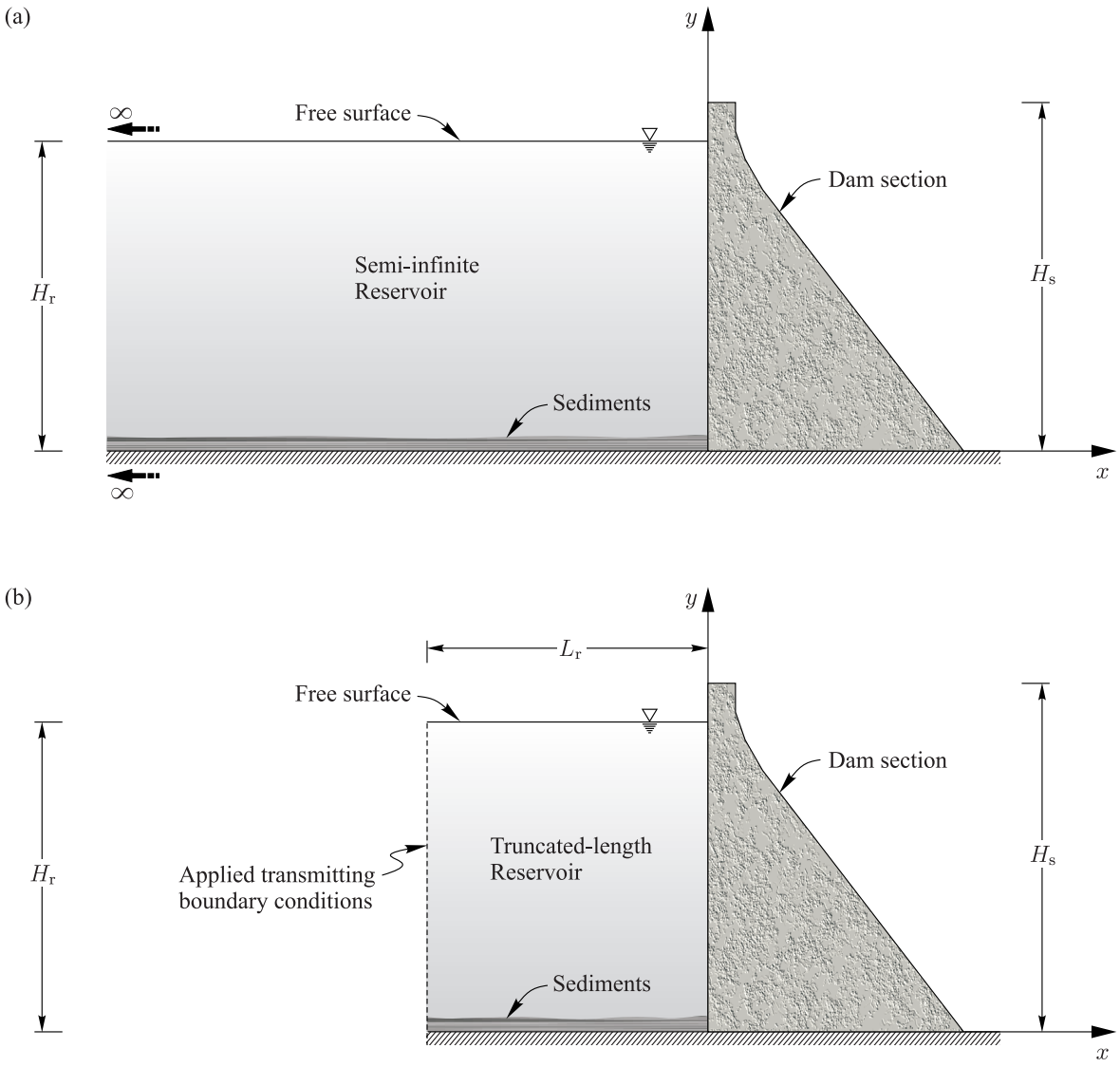

Figure A.1 Dam-reservoir systems considered for the analytical formulation : (a) Dam impounding a semi-infinite reservoir ; (b) Dam impounding a truncated-length reservoir.

expressed in the frequency domain as

$$\left[-\omega^2\,\mathbf{M} + (1 + \mathrm{i}\,\eta_\mathrm{s})\,\mathbf{K}\right]\vec{U}_b(\omega) = -a_\mathrm{g}\,\mathbf{M}\,\mathbf{1} + \bar{\mathbf{F}}_\mathrm{h}(\omega) \tag{A.4}$$

where $\vec{U}_b$ is a column-vector containing the FRFs of dam nodal displacements relative to the ground, $\mathbf{M}$ and $\mathbf{K}$ are the dam mass and stiffness matrices, respectively, η_s is the structural hysteretic damping factor, $\bar{\mathbf{F}}_\mathrm{h}$ is a column-vector containing the FRFs of hydrodynamic pres-

sure loads, and **1** is a column-vector with the same dimension as the vector of nodal relative displacements, containing zeros except along horizontal degrees of freedom which correspond to the direction of earthquake excitation. Using a modal superposition analysis, the FRFs of relative displacement and acceleration components at coordinate (x, y) can be expressed as

$$\bar{u}(x,y,\omega) = \sum_{j=1}^{m_\mathrm{s}} \psi_j^{(x)}(x,y)\,\bar{Z}_j(\omega)\,; \qquad \bar{\ddot{u}}(x,y,\omega) = -\omega^2 \sum_{j=1}^{m_\mathrm{s}} \psi_j^{(x)}(x,y)\,\bar{Z}_j(\omega) \tag{A.5}$$

$$\bar{v}(x,y,\omega) = \sum_{j=1}^{m_\mathrm{s}} \psi_j^{(y)}(x,y)\,\bar{Z}_j(\omega)\,; \qquad \bar{\ddot{v}}(x,y,\omega) = -\omega^2 \sum_{j=1}^{m_\mathrm{s}} \psi_j^{(y)}(x,y)\,\bar{Z}_j(\omega) \tag{A.6}$$

where $\bar{u}$ and $\bar{v}$ denote the horizontal and vertical relative displacements, respectively, $\bar{\ddot{u}}$ and $\bar{\ddot{v}}$ the horizontal and vertical accelerations, respectively, $\psi_j^{(x)}$ and $\psi_j^{(y)}$ the x– and y–components of the $j^{\,\mathrm{th}}$ dam mode shape, $\bar{Z}_j$ the generalized coordinate, and m_s the number of structural mode shapes included in the analysis. The hydrodynamic pressure FRF $\bar{p}$ can be decomposed as [6]

$$\bar{p}(x,y,\omega) = \bar{p}_0(x,y,\omega) - \omega^2 \sum_{j=1}^{m_\mathrm{s}} \bar{Z}_j(\omega)\,\bar{p}_j(x,y,\omega) \tag{A.7}$$

where $\bar{p}_0$ is the FRF for hydrodynamic pressure due to rigid body motion of the dam, and where $\bar{p}_j$ is the FRF corresponding to hydrodynamic pressure due to horizontal acceleration $\psi_j^{(x)}(y) = \psi_j^{(x)}(0,y)$ of the dam upstream face along structural mode j. The boundary conditions to be satisfied by FRFs $\bar{p}_0$ and $\bar{p}_j$ are detailed in this section.

– *At dam-reservoir interface*

  This boundary condition is based on compatibility between hydrodynamic pressures and normal displacements at dam-reservoir interface, yielding [6]

$$\frac{\partial \bar{p}_0}{\partial x}(0,y,\omega) = -\rho_\mathrm{r} a_\mathrm{g}\,; \qquad \frac{\partial \bar{p}_j}{\partial x}(0,y,\omega) = -\rho_\mathrm{r} \psi_j^{(x)}(y) \tag{A.8}$$

– *At reservoir free surface*

  Neglecting the effect of gravity waves at reservoir free surface [38, 39], hydrodynamic pressures at this location are assumed null

$$\bar{p}_0(x, H_\mathrm{r}, \omega) = \bar{p}_j(x, H_\mathrm{r}, \omega) = 0 \tag{A.9}$$

– *At reservoir bottom*

  This boundary condition was introduced by Hall and Chopra (1982) to approximately account for energy dissipation at reservoir bottom through one-dimensional partial

absorption of incident compression waves normal to the reservoir bottom boundary

$$\frac{\partial \bar{p}_0}{\partial y}(x,0,\omega) = \mathrm{i}\omega q\, \bar{p}_0(x,0,\omega)\,; \qquad \frac{\partial \bar{p}_j}{\partial y}(x,0,\omega) = \mathrm{i}\omega q\, \bar{p}_j(x,0,\omega) \tag{A.10}$$

where q is a damping coefficient defined at the reservoir bottom as

$$q = \frac{\rho_\mathrm{r}}{\rho_\mathrm{f}\, C_\mathrm{f}} \tag{A.11}$$

and where ρ_f and C_f denote the mass density and the compression wave velocity within the reservoir foundation, respectively. The portion of the wave amplitude reflected back to the reservoir is represented by the wave reflection coefficient α defined by

$$\alpha = \frac{1 - q\, C_\mathrm{r}}{1 + q\, C_\mathrm{r}} \tag{A.12}$$

where α may vary from 0 for full wave absorption, to 1 for full wave reflection.

– *At infinity upstream of the reservoir*

To obtain analytical expressions for the FRFs $\bar{p}_0$ and $\bar{p}_j$, Hall and Chopra (1982) and Fenves and Chopra (1984) considered an undisturbed pressure condition implying a null hydrodynamic pressure at infinity of the continuum fluid domain upstream, i.e. when $x \to -\infty$ according to the system of axes in Fig. A.1(a) :

$$\lim_{x \to -\infty} \bar{p}_0\,(x,y,\omega) = \lim_{x \to -\infty} \bar{p}_j\,(x,y,\omega) = 0 \tag{A.13}$$

In the rest of the paper, a superscript $^{(\infty)}$ will be used to denote hydrodynamic pressures, forces and other physical quantities determined using the aforementioned boundary conditions. These boundary conditions are coupled to Eq. (A.3) to determine classical expressions of hydrodynamic pressure [6]. The resulting FRFs $\bar{p}_0^{(\infty)}$ and $\bar{p}_j^{(\infty)}$ are written here as the summation of m_r functions $\bar{p}_{0n}^{(\infty)}$ and $\bar{p}_{jn}^{(\infty)}$ corresponding each to a reservoir mode n

$$\bar{p}_0^{(\infty)}(x,y,\omega) = \sum_{n=1}^{m_\mathrm{r}} \bar{p}_{0n}^{(\infty)}(x,y,\omega) \tag{A.14}$$

$$\bar{p}_j^{(\infty)}(x,y,\omega) = \sum_{n=1}^{m_\mathrm{r}} \bar{p}_{jn}^{(\infty)}(x,y,\omega) \tag{A.15}$$

in which

$$\bar{p}_{0n}^{(\infty)}(x,y,\omega) = -2\rho_{\mathrm{r}} a_{\mathrm{g}} H_{\mathrm{r}} \frac{\lambda_n^2(\omega)}{\beta_n(\omega)} \frac{I_{0n}(\omega)}{\kappa_n(\omega)} \, \mathrm{e}^{\kappa_n(\omega)\, x} \, Y_n(y,\omega) \tag{A.16}$$

$$\bar{p}_{jn}^{(\infty)}(x,y,\omega) = -2\rho_{\mathrm{r}} H_{\mathrm{r}} \frac{\lambda_n^2(\omega)}{\beta_n(\omega)} \frac{I_{jn}(\omega)}{\kappa_n(\omega)} \, \mathrm{e}^{\kappa_n(\omega)\, x} \, Y_n(y,\omega) \tag{A.17}$$

where λ_n and Y_n are complex-valued frequency dependent eigenvalues and orthogonal eigenfunctions satisfying for each reservoir mode n

$$\mathrm{e}^{2\mathrm{i}\lambda_n(\omega) H_{\mathrm{r}}} = -\frac{\lambda_n(\omega) - \omega q}{\lambda_n(\omega) + \omega q} \tag{A.18}$$

$$Y_n(y,\omega) = \frac{\big[\lambda_n(\omega) - \omega q\big] \mathrm{e}^{-\mathrm{i}\lambda_n(\omega)\, y} + \big[\lambda_n(\omega) + \omega q\big] \mathrm{e}^{\mathrm{i}\lambda_n(\omega)\, y}}{2\lambda_n(\omega)} \tag{A.19}$$

and where the terms β_n, κ_n, I_{0n}, I_{jn} are given by

$$\beta_n(\omega) = H_{\mathrm{r}} \big[\lambda_n^2(\omega) - \omega^2 q^2\big] + \mathrm{i}\,\omega q\,; \qquad \kappa_n(\omega) = \sqrt{\lambda_n^2(\omega) - \frac{\omega^2}{C_{\mathrm{r}}^2}} \tag{A.20}$$

$$I_{0n}(\omega) = \frac{1}{H_{\mathrm{r}}} \int_0^{H_{\mathrm{r}}} Y_n(y,\omega)\, \mathrm{d}y\,; \qquad I_{jn}(\omega) = \frac{1}{H_{\mathrm{r}}} \int_0^{H_{\mathrm{r}}} \psi_j^{(x)}(y)\, Y_n(y,\omega)\, \mathrm{d}y \tag{A.21}$$

Iterative techniques such as Newton–Raphson method can be used to solve Eq. (A.18) at each excitation frequency ω. We note that for a completely reflective reservoir bottom, i.e. $\alpha = 1$, $\kappa_n(\omega)$ is either : (i) a real positive number when exciting frequency ω is lower than the vibration frequency $\omega_{\mathrm{r}n}$ of the impounded reservoir, or (ii) a pure imaginary number otherwise [5, 6, 22]. In the first case, the sums in Eqs. (A.14) and (A.15) decay exponentially with increasing distance upstream, and in the second case, these sums contain a non-decaying part representing waves propagating in the upstream direction. When reservoir bottom absorption is included, κ_n is a complex number with a positive real part, and the series in Eqs. (A.14) and (A.15) decay with increasing distance upstream, although slowly for slightly absorptive reservoirs. The number of reservoir modes m_{r} to be included in the analysis should be selected based on the convergence of the sums in Eqs. (A.14) and (A.15). Through extensive numerical analyses of idealized dam sections, Fenves and Chopra (1984) proposed and validated a minimum value $m_{\mathrm{r}} > \omega_{\max}/(2\omega_0) + 5$ to ensure convergence, where $\omega_{\max}$ denotes the maximum excitation frequency considered in the analysis, and $\omega_0 = \pi\, C_{\mathrm{r}}/(2H_{\mathrm{r}})$ the natural frequency of the full semi-infinite reservoir.

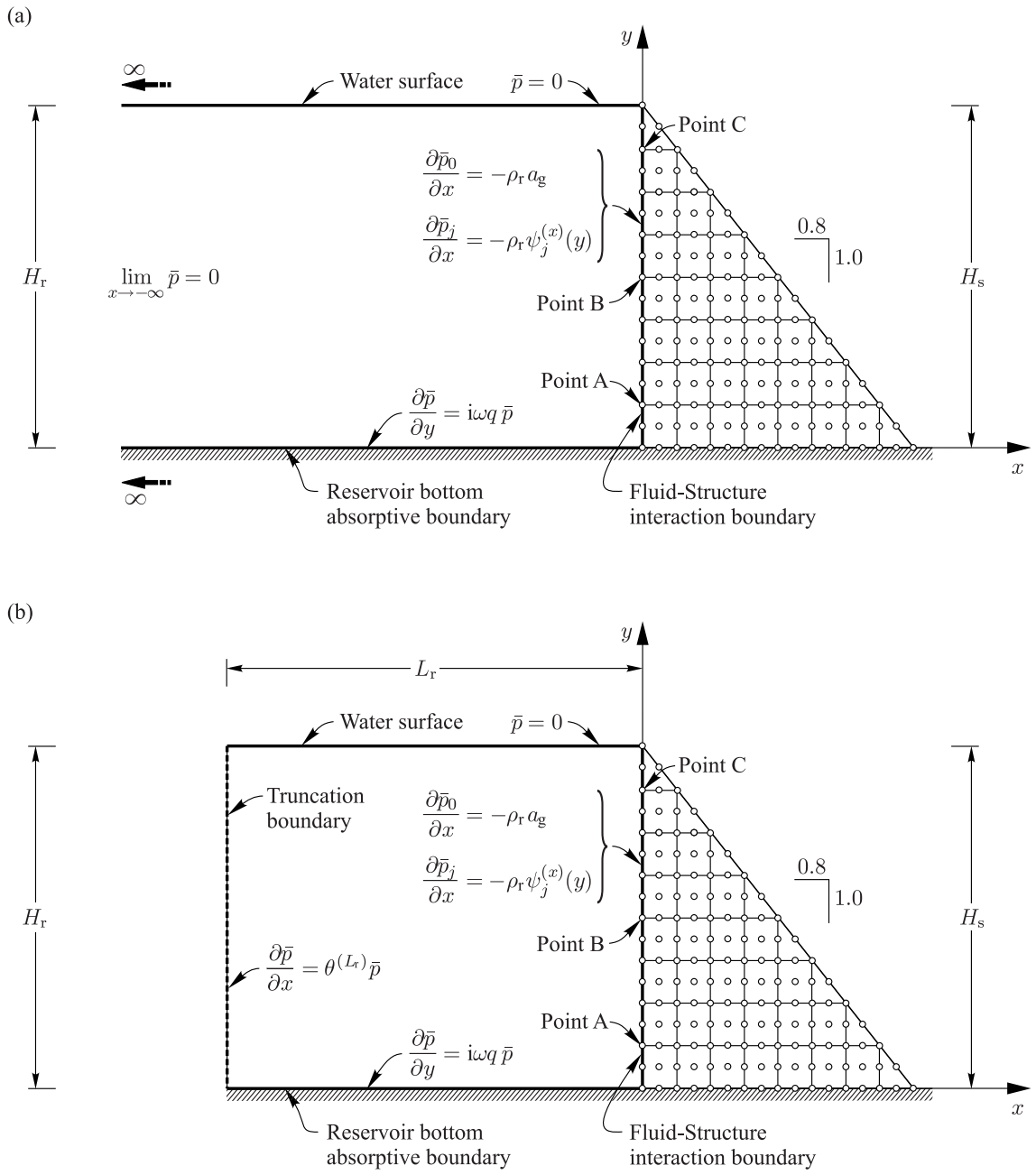

Figure A.2 Dam-reservoir systems studied and boundary conditions used : (a) Dam impounding a semi-infinite reservoir ; (b) Dam impounding a truncated-length reservoir.

If water compressibility is neglected, real-valued and frequency-independent eigenvectors λ_n and eigenvectors Y_n are given by

$$\lambda_n = \frac{(2n-1)\pi}{2H_\mathrm{r}}\,; \qquad\qquad Y_n(y) = \cos\left[\frac{(2n-1)\pi y}{2H_\mathrm{r}}\right] \tag{A.22}$$

and Eqs. (A.20) and (A.21) simplify to

$$\beta_n = \frac{(2n-1)^2\pi^2}{4H_\mathrm{r}}\,; \qquad\qquad \kappa_n = \frac{(2n-1)\pi}{2H_\mathrm{r}} \tag{A.23}$$

$$I_{0n} = 2\,\frac{(-1)^{n-1}}{(2n-1)\pi}\,; \qquad\qquad I_{jn} = \frac{1}{H_\mathrm{r}}\int_0^{H_\mathrm{r}} \psi_j^{(x)}(y)\,\cos\left[\frac{(2n-1)\pi y}{2H_\mathrm{r}}\right]\,\mathrm{d}y \tag{A.24}$$

yielding the hydrodynamic pressures

$$\bar{p}_{0n}^{(\infty)}(x,y) = -8\rho_\mathrm{r} a_\mathrm{g} H_\mathrm{r} \frac{(-1)^{n-1}\cos\left[\dfrac{(2n-1)\,\pi\,y}{2H_\mathrm{r}}\right]}{(2n-1)^2\,\pi^2}\,\mathrm{e}^{\kappa_n\,x} \tag{A.25}$$

$$\bar{p}_{jn}^{(\infty)}(x,y) = -4\rho_\mathrm{r} \frac{\cos\left[\dfrac{(2n-1)\,\pi\,y}{2H_\mathrm{r}}\right]}{(2n-1)\,\pi}\,\mathrm{e}^{\kappa_n\,x}\int_0^{H_\mathrm{r}} \psi_j^{(x)}(y)\,\cos\left[\frac{(2n-1)\pi y}{2H_\mathrm{r}}\right]\,\mathrm{d}y \tag{A.26}$$

Depending on whether water compressibility is included or not, Eqs. (A.16) and (A.17) or Eqs. (A.25) and (A.26) are used to obtain hydrodynamic pressures $\bar{p}_0^{(\infty)}$ and $\bar{p}_j^{(\infty)}$. The FRF for total hydrodynamic pressure is then given by [Eq. (A.7)]

$$\bar{p}(x,y,\omega) = \bar{p}_0(x,y,\omega) - \omega^2 \sum_{j=1}^{m_\mathrm{s}} \bar{Z}_j(\omega)\,\bar{p}_j(x,y,\omega) \tag{A.27}$$

where the vector $\bar{\mathbf{Z}}^{(\infty)}$ of generalized coordinates $\bar{Z}_j^{(\infty)}$, $j = 1 \ldots m_\mathrm{s}$, is obtained by solving the system of equations

$$\bar{\mathbf{S}}^{(\infty)}\,\bar{\mathbf{Z}}^{(\infty)} = \bar{\mathbf{Q}}^{(\infty)} \tag{A.28}$$

in which elements of matrices $\bar{\mathbf{S}}^{(\infty)}$ and $\bar{\mathbf{Q}}^{(\infty)}$ are obtained for $n = 1 \ldots m_\mathrm{s}$ and $j = 1 \ldots m_\mathrm{s}$ as

$$\bar{S}_{nj}^{(\infty)}(\omega) = \Big[-\omega^2 + \big(1 + \mathrm{i}\,\eta_\mathrm{s}\big)\,\omega_n^2 \Big]\delta_{nj} + \omega^2 \int_0^{H_\mathrm{r}} \bar{p}_j^{(\infty)}(0,y,\omega)\,\psi_n^{(x)}(y)\,\mathrm{d}y \tag{A.29}$$

$$\bar{Q}_n^{(\infty)}(\omega) = -a_\mathrm{g}\boldsymbol{\psi}_n^\mathrm{T}\,\mathbf{M}\,\mathbf{1} + \int_0^{H_\mathrm{r}} \bar{p}_0^{(\infty)}(0,y,\omega)\,\psi_n^{(x)}(y)\,\mathrm{d}y \tag{A.30}$$

where δ denotes the Kronecker symbol and ω_n is the vibration frequency corresponding to structural mode shape ψ_n. A convergence study is conducted to determine the sufficient numbers m_s and m_r of structural and reservoir mode shapes to be included into each specific analysis. We can also define the FRFs for hydrodynamic forces applied on dam upstream face, i.e. at $x = 0$ according to the system of axes in Fig. A.1

$$\bar{F}_0^{(\infty)}(\omega) = \int_0^{H_\mathrm{r}} \bar{p}_0^{(\infty)}(0, y, \omega)\,\mathrm{d}y\,; \qquad \bar{F}^{(\infty)}(\omega) = \int_0^{H_\mathrm{r}} \bar{p}^{(\infty)}(0, y, \omega)\,\mathrm{d}y \tag{A.31}$$

The formulation described in this section was originally developed by Fenves and Chopra (1984) to investigate earthquake excited gravity dams impounding semi-infinite reservoirs. The method is based on a sub-structuring technique, where the dam is modeled using finite elements and where reservoir effects are accounted for analytically through hydrodynamic loads applied at dam upstream face and determined using mode shapes of the dam with an empty reservoir. Bouaanani and Lu (2009) showed that this procedure to include dam-reservoir interaction yields excellent results when compared to techniques where the reservoir is modeled numerically using potential-based fluid finite elements. This analytical method will be referred to as the *classical* formulation in the rest of the paper and will serve as our reference solution.

A.2.2 New formulation considering transmitting boundary conditions

As mentioned previously, appropriate TBCs are required for efficient finite element or boundary element modeling of dam-reservoir systems. In this case, exact radiation boundary conditions at the far dam upstream face [Eq.(A.13)] are replaced by TBCs to be applied at a finite distance L_r from dam upstream face as shown in Fig. A.1(b). TBCs are used to prevent or reduce reflection of waves impinging a fictitious truncation boundary of an infinite reservoir. They can be generally defined by the relationship between the hydrodynamic pressure and its normal gradient both determined at the truncation boundary. According to the system of axes in Fig. A.1(b), we consider TBCs that can be expressed as

$$\frac{\partial \bar{p}_0^{(\infty)}}{\partial x}(-L_\mathrm{r}, y, \omega) = \theta_0^{(L_\mathrm{r})}(y, \omega)\,\bar{p}_0^{(\infty)}(-L_\mathrm{r}, y, \omega) \tag{A.32}$$

$$\frac{\partial \bar{p}_j^{(\infty)}}{\partial x}(-L_\mathrm{r}, y, \omega) = \theta_j^{(L_\mathrm{r})}(y, \omega)\,\bar{p}_j^{(\infty)}(-L_\mathrm{r}, y, \omega) \tag{A.33}$$

where the functions $\theta_0^{(L_\mathrm{r})}$ and $\theta_j^{(L_\mathrm{r})}$ are generally height- and frequency-dependent. We note that the TBC in Eq. (A.32) accounts for rigid body motion of the dam, while that in Eq. (A.33)

accounts for dam elastic deformation along structural mode shape $\psi_j^{(x)}$. In the rest of the paper, a superscript $^{(L_\mathrm{r})}$ will be used to denote hydrodynamic pressures obtained using TBCs placed at a distance L_r from dam upstream face. Differentiating Eq. (A.27) with respect to x gives

$$\frac{\partial \bar{p}^{(\infty)}}{\partial x}(x,y,\omega) = \frac{\partial \bar{p}_0^{(\infty)}}{\partial x}(x,y,\omega) - \omega^2 \sum_{j=1}^{m_\mathrm{s}} \bar{Z}_j(\omega)\, \frac{\partial \bar{p}_j^{(\infty)}}{\partial x}(x,y,\omega) \tag{A.34}$$

Taking $x=-L_\mathrm{r}$ and substituting Eqs. (A.32) and (A.33) into Eq. (A.34) yields

$$\frac{\partial \bar{p}^{(\infty)}}{\partial x}(-L_\mathrm{r},y,\omega) = \theta_0^{(L_\mathrm{r})}(y,\omega)\, \bar{p}_0^{(\infty)}(-L_\mathrm{r},y,\omega) - \omega^2 \sum_{j=1}^{m_\mathrm{s}} \bar{Z}_j(\omega)\, \theta_j^{(L_\mathrm{r})}(y,\omega)\, \bar{p}_j^{(\infty)}(-L_\mathrm{r},y,\omega) \tag{A.35}$$

Using Eqs. (A.27) and (A.35), we can define a TBC expressed in terms of total hydrodynamic pressure $\bar{p}^{(\infty)}$ as

$$\frac{\partial \bar{p}^{(\infty)}}{\partial x}(-L_\mathrm{r},y,\omega) = \theta^{(L_\mathrm{r})}(y,\omega)\, \bar{p}^{(\infty)}(-L_\mathrm{r},y,\omega) \tag{A.36}$$

in which the height- and frequency-dependent function $\theta^{(L_\mathrm{r})}$ is given by

$$\theta^{(L_\mathrm{r})}(y,\omega) = \frac{\theta_0^{(L_\mathrm{r})}(y,\omega)\, \bar{p}_0^{(\infty)}(-L_\mathrm{r},y,\omega) - \omega^2 \sum_{j=1}^{m_\mathrm{s}} \bar{Z}_j(\omega)\, \theta_j^{(L_\mathrm{r})}(y,\omega)\, \bar{p}_j^{(\infty)}(-L_\mathrm{r},y,\omega)}{\bar{p}_0^{(\infty)}(-L_\mathrm{r},y,\omega) - \omega^2 \sum_{j=1}^{m_\mathrm{s}} \bar{Z}_j(\omega)\, \bar{p}_j^{(\infty)}(-L_\mathrm{r},y,\omega)} \tag{A.37}$$

The TBCs defined by Eqs. (A.32) to (A.37) will be referred to as *analytical* TBCs in the rest of the paper. Using Eqs. (A.14) and (A.15), the functions $\theta_\ell^{(L_\mathrm{r})}\,;\ell=0,j\,;$ can be expressed as

$$\theta_\ell^{(L_\mathrm{r})}(y,\omega) = \frac{\sum_{n=1}^{m_\mathrm{r}} \kappa_n(\omega)\, \bar{p}_{\ell n}^{(\infty)}(-L_\mathrm{r},y,\omega)}{\sum_{n=1}^{m_\mathrm{r}} \bar{p}_{\ell n}^{(\infty)}(-L_\mathrm{r},y,\omega)} \tag{A.38}$$

We will also examine the effectiveness of truncated TBCs, where the sum in Eq. (A.38) is truncated at a given number $\widetilde{m}_\mathrm{r}$ less than the number of reservoir modes m_r ensuring convergence, yielding the function $\tilde{\theta}_\ell^{(L_\mathrm{r})}$

$$\tilde{\theta}_\ell^{(L_\mathrm{r})}(y,\omega) = \frac{\sum_{n=1}^{\widetilde{m}_\mathrm{r}} \kappa_n(\omega)\, \bar{p}_{\ell n}^{(\infty)}(-L_\mathrm{r},y,\omega)}{\sum_{n=1}^{\widetilde{m}_\mathrm{r}} \bar{p}_{\ell n}^{(\infty)}(-L_\mathrm{r},y,\omega)} \tag{A.39}$$

When water compressibility is neglected, Eq. (A.38) transforms to

$$\theta_\ell^{(L_\mathrm{r})}(y) = H_\mathrm{r}\,\frac{\displaystyle\sum_{n=1}^{m_\mathrm{r}} \lambda_n I_{\ell n}\cos(\lambda_n\,y)\,\mathrm{e}^{-\lambda_n L_\mathrm{r}}}{\displaystyle\sum_{n=1}^{m_\mathrm{r}} \frac{I_{\ell n}}{\lambda_n}\cos(\lambda_n\,y)\,\mathrm{e}^{-\lambda_n L_\mathrm{r}}} \tag{A.40}$$

where λ_n and $I_{\ell n}$ are determined according to Eqs. (A.22) and (A.24), respectively. We note that Eq. (A.40) also corresponds to very low frequencies, i.e. $\omega \to 0$, when water compressibility is included. In the rest of the paper, analytical TBCs will be distinguished as compressibility- or incompressibility-based depending on whether compressible or incompressible water assumptions are adopted.

When a TBC is applied at a finite length L_r, Eqs. (A.14) to (A.17) of the classical formulation are no longer valid to determine hydrodynamic pressure within the reservoir. To get a rigorous assessment of the accuracy and effectiveness of a given TBC, a new formulation is developed in this work. To alleviate the text, the detailed mathematical derivations of the formulation are presented in Appendix A. When TBCs in (A.32) and (A.33) are imposed at a distance L_r from dam upstream face, we show in Appendix A that hydrodynamic pressures $\bar{p}_0^{(L_\mathrm{r})}$ and $\bar{p}_j^{(L_\mathrm{r})}$ can be expressed as

$$\bar{p}_0^{(L_\mathrm{r})}(x,y,\omega) = \sum_{n=1}^{m_\mathrm{r}} \bar{p}_{0n}^{(L_\mathrm{r})}(x,y,\omega) \tag{A.41}$$

$$\bar{p}_j^{(L_\mathrm{r})}(x,y,\omega) = \sum_{n=1}^{m_\mathrm{r}} \bar{p}_{jn}^{(L_\mathrm{r})}(x,y,\omega) \tag{A.42}$$

where FRFs $\bar{p}_{0n}^{(L_\mathrm{r})}$ and $\bar{p}_{jn}^{(L_\mathrm{r})}$ are given by

$$\begin{aligned}\bar{p}_{0n}^{(L_\mathrm{r})}(x,y,\omega) &= \left\{\left[\mathrm{e}^{-\kappa_n(\omega)\,x} + \mathrm{e}^{\kappa_n(\omega)\,x}\right]\Gamma_n^{(0)}(\omega) - 2\rho_\mathrm{r} a_\mathrm{g} H_\mathrm{r}\frac{\lambda_n^2(\omega)}{\beta_n(\omega)}\frac{I_{0n}(\omega)}{\kappa_n(\omega)}\,\mathrm{e}^{\kappa_n(\omega)\,x}\right\} Y_n(y,\omega)\\ &= \left[\mathrm{e}^{-\kappa_n(\omega)\,x} + \mathrm{e}^{\kappa_n(\omega)\,x}\right]\Gamma_n^{(0)}(\omega)\,Y_n(y,\omega) + \bar{p}_{0n}^{(\infty)}(x,y,\omega)\end{aligned} \tag{A.43}$$

$$\begin{aligned}\bar{p}_{jn}^{(L_\mathrm{r})}(x,y,\omega) &= \left\{\left[\mathrm{e}^{-\kappa_n(\omega)\,x} + \mathrm{e}^{\kappa_n(\omega)\,x}\right]\Gamma_n^{(j)}(\omega) - 2\rho_\mathrm{r} H_\mathrm{r}\frac{\lambda_n^2(\omega)}{\beta_n(\omega)}\frac{I_{jn}(\omega)}{\kappa_n(\omega)}\,\mathrm{e}^{\kappa_n(\omega)\,x}\right\} Y_n(y,\omega)\\ &= \left[\mathrm{e}^{-\kappa_n(\omega)\,x} + \mathrm{e}^{\kappa_n(\omega)\,x}\right]\Gamma_n^{(j)}(\omega)\,Y_n(y,\omega) + \bar{p}_{jn}^{(\infty)}(x,y,\omega)\end{aligned} \tag{A.44}$$

in which $\Gamma_n^{(0)}(\omega)$ and $\Gamma_n^{(j)}(\omega)$ are elements of vectors $\mathbf{\Gamma}^{(0)}$ and $\mathbf{\Gamma}^{(j)}$, obtained by solving the

systems of linear equations

$$\mathbf{A}^{(0)}(\omega)\ \mathbf{\Gamma}^{(0)}(\omega) = \mathbf{B}^{(0)}(\omega)\,; \qquad\qquad \mathbf{A}^{(j)}(\omega)\ \mathbf{\Gamma}^{(j)}(\omega) = \mathbf{B}^{(j)}(\omega) \tag{A.45}$$

where the elements of matrix $\mathbf{A}^{(\ell)}$ and vector $\mathbf{B}^{(\ell)}$ are given for $\ell = 0, j$ by Eqs. (A.A.24) and (A.A.25) of Appendix A. Eqs. (A.A.24) and (A.A.25) will be used later to assess the efficiency of various TBCs and evaluate the associated errors. One important aspect of this formulation is that it takes account of the variations of the functions $\theta_0^{(L_\mathrm{r})}$ and $\theta_j^{(L_\mathrm{r})}$ over reservoir height. This dependence is investigated next. Using Eq. (A.38) the derivatives of the functions $\theta_\ell^{(L_\mathrm{r})}\,; \ell = 0, j\,;$ with respect to coordinate y can obtained as

$$\frac{\partial \theta_\ell^{(L_\mathrm{r})}}{\partial y}(y,\omega) = \frac{\displaystyle\sum_{s=1}^{m_\mathrm{r}}\sum_{n=1}^{m_\mathrm{r}} \Big[\kappa_s(\omega) - \kappa_n(\omega)\Big]\, \bar{p}_{\ell\, s}^{(\infty)}(-L_\mathrm{r}, y, \omega)\, \bar{p}_{\ell\, n}^{(\infty)}(-L_\mathrm{r}, y, \omega) \dfrac{\overline{Y}_n(y,\omega)}{Y_n(y,\omega)}}{\displaystyle\sum_{s=1}^{m_\mathrm{r}}\sum_{n=1}^{m_\mathrm{r}} \bar{p}_{\ell\, s}^{(\infty)}(-L_\mathrm{r}, y, \omega)\, \bar{p}_{\ell\, n}^{(\infty)}(-L_\mathrm{r}, y, \omega)} \tag{A.46}$$

where

$$\overline{Y}_n(y,\omega) = \frac{\partial Y_n}{\partial y}(y,\omega) = \frac{1}{2}\Big\{ \big[\lambda_n(\omega) - \omega q\big] \mathrm{e}^{-\mathrm{i}\lambda_n(\omega)\, y} - \big[\lambda_n(\omega) + \omega q\big] \mathrm{e}^{\mathrm{i}\lambda_n(\omega)\, y} \Big\} \tag{A.47}$$

Eq. (A.46) shows that the derivatives of the functions $\theta_0^{(L_\mathrm{r})}$ and $\theta_j^{(L_\mathrm{r})}$ with respect to coordinate y are generally not null. Consequently, these functions as well as the function $\theta^{(L_\mathrm{r})}$ [Eq. (A.37)] are generally not constant over reservoir height. This behavior will be investigated numerically later as well as the implications of heightwise variations of TBCs on the frequency response curves of hydrodynamic pressures and forces applied at dam upstream face.

As proven in Appendix A, if functions $\theta_\ell^{(L_\mathrm{r})}$ were assumed constant over reservoir height, i.e. independent of the y coordinate, Eqs. (A.43) and (A.44) simplify to

$$\bar{p}_{0n}^{(L_\mathrm{r})}(x,y,\omega) = -2\rho_\mathrm{r} a_\mathrm{g} H_\mathrm{r} \frac{\lambda_n^2(\omega)}{\beta_n(\omega)} \frac{I_{0n}(\omega)}{\kappa_n(\omega)}\, X_{0n}^{(L_\mathrm{r})}(x,\omega)\, Y_n(y,\omega) \tag{A.48}$$

$$\bar{p}_{jn}^{(L_\mathrm{r})}(x,y,\omega) = -2\rho_\mathrm{r} H_\mathrm{r} \frac{\lambda_n^2(\omega)}{\beta_n(\omega)} \frac{I_{jn}(\omega)}{\kappa_n(\omega)}\, X_{jn}^{(L_\mathrm{r})}(x,\omega)\, Y_n(y,\omega) \tag{A.49}$$

where $X_{\ell\, n}^{(L_\mathrm{r})}$ and $\zeta_{\ell\, n}^{(L_\mathrm{r})}$ are given for $\ell = 0, j$ by Eqs. (A.A.32) and (A.A.33) of Appendix A.

For illustration purposes, Eqs. (A.48), (A.49), and then Eqs. (A.41) and (A.42) will be used later to investigate the following height-independent TBCs :

– Sommerfeld radiation boundary condition [17, 18], corresponding to

$$\theta_0^{(L_\mathrm{r})}(\omega) = \theta_j^{(L_\mathrm{r})}(\omega) = \frac{\mathrm{i}\,\omega}{C_\mathrm{r}} \tag{A.50}$$

– Sharan boundary condition [25, 26], corresponding to

$$\theta_0^{(L_\mathrm{r})}(\omega) = \theta_j^{(L_\mathrm{r})}(\omega) = \kappa_1(\omega) \tag{A.51}$$

We note that the Sharan boundary condition is a special case of Eq. (A.39) with $\widetilde{m}_\mathrm{r} = 1$.

Once hydrodynamic pressures are determined for each reservoir mode n, Eqs. (A.41) and (A.42) are used to sum up the contributions of the $\widetilde{m}_\mathrm{r}$ reservoir modes included in the analysis. The FRF for total hydrodynamic pressure is given by

$$\bar{p}^{\,(L_\mathrm{r})}(x,y,\omega) = \bar{p}_0^{(L_\mathrm{r})}(x,y,\omega) - \omega^2 \sum_{j=1}^{m_\mathrm{s}} \bar{Z}_j^{(L_\mathrm{r})}(\omega)\, \bar{p}_j^{(L_\mathrm{r})}(x,y,\omega) \tag{A.52}$$

where the vector $\bar{\mathbf{Z}}^{(L_\mathrm{r})}$ of generalized coordinates $\bar{Z}_j^{(L_\mathrm{r})}$, $j = 1 \ldots m_\mathrm{s}$, is obtained by solving the system of equations

$$\bar{\mathbf{S}}^{(L_\mathrm{r})}\, \bar{\mathbf{Z}}^{(L_\mathrm{r})} = \bar{\mathbf{Q}}^{(L_\mathrm{r})} \tag{A.53}$$

in which elements of matrices $\bar{\mathbf{S}}^{(L_\mathrm{r})}$ and $\bar{\mathbf{Q}}^{(L_\mathrm{r})}$ are now defined for $n = 1 \ldots m_\mathrm{s}$ and $j = 1 \ldots m_\mathrm{s}$ by

$$\bar{S}_{nj}^{(L_\mathrm{r})}(\omega) = \Big[-\omega^2 + \big(1 + \mathrm{i}\,\eta_\mathrm{s}\big)\,\omega_n^2 \Big]\delta_{nj} + \omega^2 \int_0^{H_\mathrm{r}} \bar{p}_j^{(L_\mathrm{r})}(0,y,\omega)\, \psi_n^{(x)}(y)\, \mathrm{d}y \tag{A.54}$$

$$\bar{Q}_n^{(L_\mathrm{r})}(\omega) = -a_\mathrm{g} \boldsymbol{\psi}_n^\mathrm{T}\, \mathbf{M}\, \mathbf{1} + \int_0^{H_\mathrm{r}} \bar{p}_0^{(L_\mathrm{r})}(0,y,\omega)\, \psi_n^{(x)}(y)\, \mathrm{d}y \tag{A.55}$$

Hydrodynamic forces at dam upstream face corresponding to hydrodynamic pressures $\bar{p}_0^{(L_\mathrm{r})}$ and $\bar{p}^{\,(L_\mathrm{r})}$ can then be obtained as

$$\bar{F}_0^{(L_\mathrm{r})}(\omega) = \int_0^{H_\mathrm{r}} \bar{p}_0^{(L_\mathrm{r})}(0,y,\omega)\, \mathrm{d}y\,; \qquad \bar{F}^{\,(L_\mathrm{r})}(\omega) = \int_0^{H_\mathrm{r}} \bar{p}^{\,(L_\mathrm{r})}(0,y,\omega)\, \mathrm{d}y \tag{A.56}$$

A.3 Numerical results

A.3.1 Dam-reservoir system studied

For purpose of illustration, the new formulation presented previously is applied to analyse the dam-reservoir system shown in Fig. A.2, subjected to a unit horizontal harmonic ground

acceleration $\ddot{u}_{\mathrm{g}}(t) = \mathrm{e}^{\mathrm{i}\omega t}$. A simplified triangular dam cross-section with dimensions inspired from the tallest non-overflow monolith of Pine Flat dam is considered. This standard dam section was shown appropriate for a preliminary design and safety evaluation of concrete gravity dams and was introduced to develop and illustrate simplified earthquake analysis procedures proposed by Chopra et al. [2, 6, 41]. The dam cross-section has a height $H_{\mathrm{s}} = 121.92\,\mathrm{m}\,(400\,\mathrm{ft})$, a downstream slope of 0.8 and a vertical upstream face. A full reservoir is assumed, i.e. $H_{\mathrm{r}} = H_{\mathrm{s}}$, and different reservoir truncation lengths L_{r} are considered as will be discussed later. Fig. A.2 illustrates the boundary conditions used. A dam Poisson's ratio $\nu_{\mathrm{s}} = 0.2$ and mass density $\rho_{\mathrm{s}} = 2400\,\mathrm{kg/m^3}$ are adopted. To assess the influence of dam stiffness, two modulus of elasticity $E_{\mathrm{s}} = 25\,\mathrm{GPa}$ and $E_{\mathrm{s}} = 35\,\mathrm{GPa}$ are considered. A constant structural hysteretic damping factor $\eta_{\mathrm{s}} = 0.1$ is adopted. The water is assumed compressible, with a velocity of pressure waves $C_{\mathrm{r}} = 1440\,\mathrm{m/s}$ and a mass density $\rho_{\mathrm{r}} = 1000\,\mathrm{kg/m^3}$. To obtain the mode shapes ψ_j, $j = 1 \ldots m_{\mathrm{s}}$, the dam section is modeled using quadrilateral 9-node and triangular 6-node plane stress finite elements as illustrated in Fig. A.2.

A.3.2 Investigation of the response mechanisms of various TBCs

Before investigating the effects of various TBCs on reservoir hydrodynamic response, we first examine the dependency of the absolute values of functions $\theta_0^{(L_{\mathrm{r}})}$ and $\theta^{(L_{\mathrm{r}})}$ to frequency and reservoir depth. Fig. A.3 shows the values of the dimensionless parameter $H_{\mathrm{r}}\left|\theta_0^{(L_{\mathrm{r}})}\right|$ determined at three reservoir depths corresponding to points A, B and C belonging to dam-reservoir interface. Points A, B and C are located at heights $y_{\mathrm{A}} = 0.1H_{\mathrm{r}}$, $y_{\mathrm{B}} = 0.5H_{\mathrm{r}}$ and $y_{\mathrm{C}} = 0.9H_{\mathrm{r}}$ as shown in Fig. A.2. Both compressible and incompressible water assumptions as well as Sommerfeld and Sharan boundary conditions are included. Results are determined for frequency ratios ω/ω_0 varying from 0 to 6. Three truncation lengths $L_{\mathrm{r}} = 0.5H_{\mathrm{r}}$, $L_{\mathrm{r}} = H_{\mathrm{r}}$ and $L_{\mathrm{r}} = 2H_{\mathrm{r}}$ and five reflection coefficients $\alpha = 1.0$, $\alpha = 0.8$, $\alpha = 0.6$, $\alpha = 0.4$, and $\alpha = 0.2$ are considered. First, it is clearly seen that the parameter $H_{\mathrm{r}}\left|\theta_0^{(L_{\mathrm{r}})}\right|$ is not constant over reservoir height as usually assumed in previous research. In fact, Fig. A.3 shows that this assumption holds only over a lower frequency range up to a characteristic frequency $\omega^{(L_{\mathrm{r}})}$ depending on truncation length L_{r}. We note that $\omega^{(L_{\mathrm{r}})}$ becomes larger as truncation length increases. We also observe that the variations of $H_{\mathrm{r}}\left|\theta_0^{(L_{\mathrm{r}})}\right|$ become generally smoother with increasing reservoir bottom wave absorption and truncation length, suggesting a smaller error when a TBC assumed constant over reservoir height is used in these ranges.

The results corresponding to an incompressible water assumption are obtained using Eq. (A.40). As expected, Fig. A.3 shows that the dimensionless parameter $H_{\mathrm{r}}\left|\theta_0^{(L_{\mathrm{r}})}\right|$ is not sensitive to frequency variations and reservoir bottom wave absorption. The curves are almost constant over reservoir height, namely as truncation length increases.

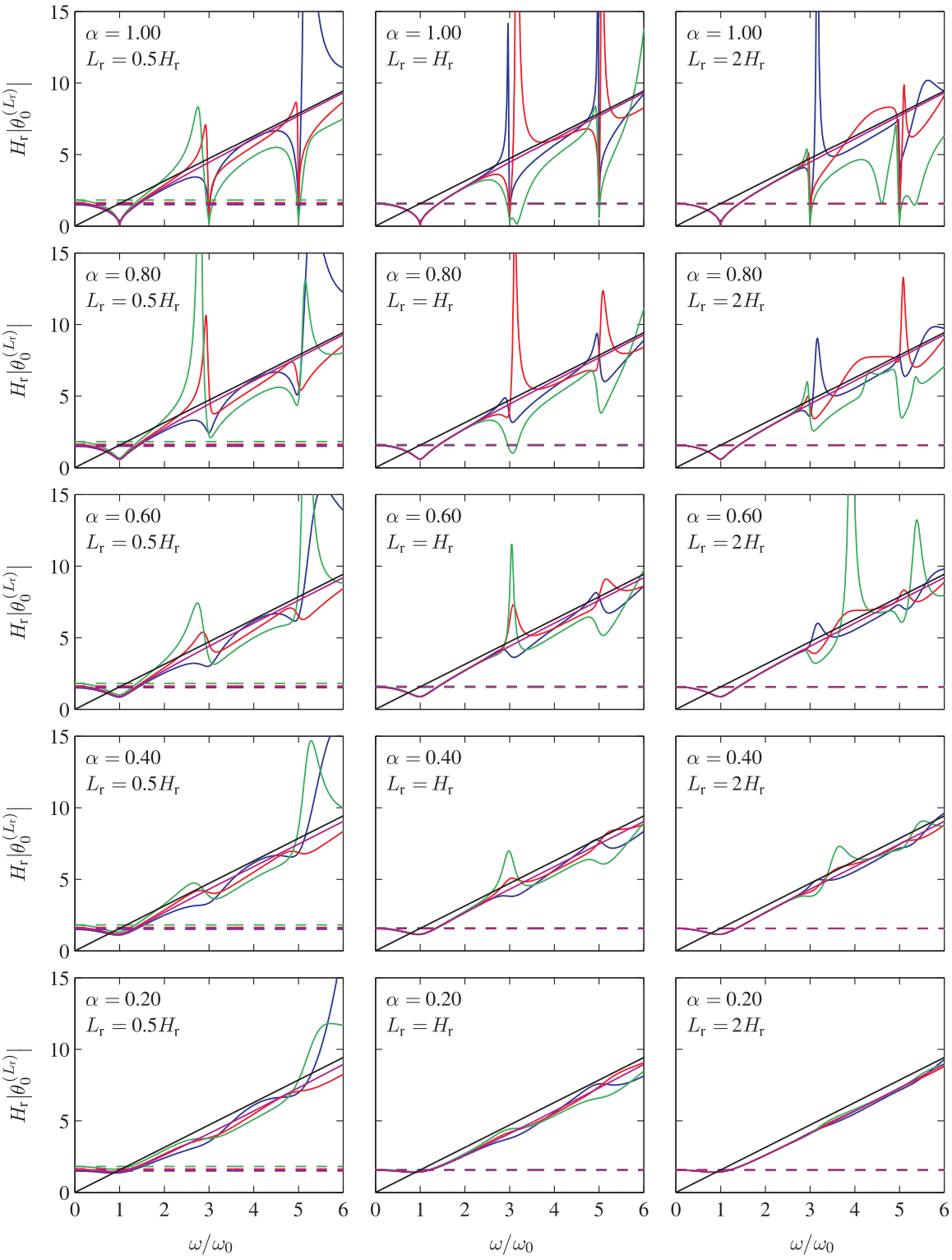

Figure A.3 Variation of the parameter $H_r\left|\theta_0^{(L_r)}\right|$ for a rigid dam as a function of frequency ratio ω/ω_0, height y, wave reflection coefficient α and truncation length L_r. — $y_A = 0.1H_r$; — $y_B = 0.5H_r$; — $y_C = 0.9H_r$; — Sommerfeld BC ; — Sharan BC. Continuous lines : compressible water ; dotted lines : incompressible water.

According to Eq. (A.50), the Sommerfeld radiation boundary condition varies linearly with frequency ratio. For lower frequencies, i.e. in this case $\omega \leqslant \omega_0$, the difference between the curves representing the Sommerfeld and analytical TBC are very different, getting closer as frequency ratio increases. Fig. A.3 confirms that the effectiveness of the Sommerfeld boundary condition is least for very low frequencies, and that it increases with higher frequencies, larger truncation length and more energy dissipation at reservoir bottom. The curves representing Sharan boundary condition coincide with those of the exact boundary condition up to frequency $\omega^{(L_\mathrm{r})}$. This behavior explains the efficiency of Sharan boundary condition in the lower frequency range as will be discussed later. We also note that the curves corresponding to Sommerfeld and Sharan boundary conditions are different at lower frequencies, while getting closer with approximately parallel curves in the higher frequency range. The effects of dam flexibility are included next. Figs. A.4 and A.5 illustrate the variations of dimensionless parameter $H_\mathrm{r}\left|\theta^{(L_\mathrm{r})}\right|$ considering two dam concrete modulus of elasticity $E_\mathrm{s} = 35\,\mathrm{GPa}$ and $E_\mathrm{s} = 25\,\mathrm{GPa}$, respectively. By comparing Figs. A.3 to A.5, it can be concluded that the analytical TBC is very sensitive to dam stiffness. The curves show that the amplitudes of $H_\mathrm{r}\left|\theta^{(L_\mathrm{r})}\right|$ become generally sharper as dam flexibility increases. Closer examination of the curves obtained for $L_\mathrm{r} = 0.5H_\mathrm{r}$ shows that dam flexibility causes larger variations of the parameter $H_\mathrm{r}\left|\theta^{(L_\mathrm{r})}\right|$ over reservoir height at the lower frequency range. This effect vanishes as truncation length increases. We also observe that reservoir bottom wave absorption and dam flexibility have very little effect on the maximum frequency $\omega^{(L_\mathrm{r})}$ below which $H_\mathrm{r}\left|\theta_0^{(L_\mathrm{r})}\right|$ and $H_\mathrm{r}\left|\theta_0^{(L_\mathrm{r})}\right|$ can be considered constant over reservoir height. At high frequencies, some curves exhibit sharp peaks corresponding to values of coordinate y and frequency ω that make the absolute value of the denominator in Eq. (A.38) very small for a given truncation distance L_r. As observed for $H_\mathrm{r}\left|\theta_0^{(L_\mathrm{r})}\right|$, increasing reservoir bottom wave absorption and truncation length cause the variations of $H_\mathrm{r}\left|\theta^{(L_\mathrm{r})}\right|$ to become generally smoother. Figs. A.3 to A.5 show that the difference between the curves obtained under compressible and incompressible water assumptions is significant except for highly absorptive reservoirs at a very low frequency range. It is seen that incompressibility-based boundary conditions determined at different heights get closer as truncation length increases. We also conclude that Sharan boundary condition is in excellent agreement with the compressibility-based analytical TBC between 0 and $\omega^{(L_\mathrm{r})}$, and for a wider frequency range as reservoir bottom wave absorption increases.

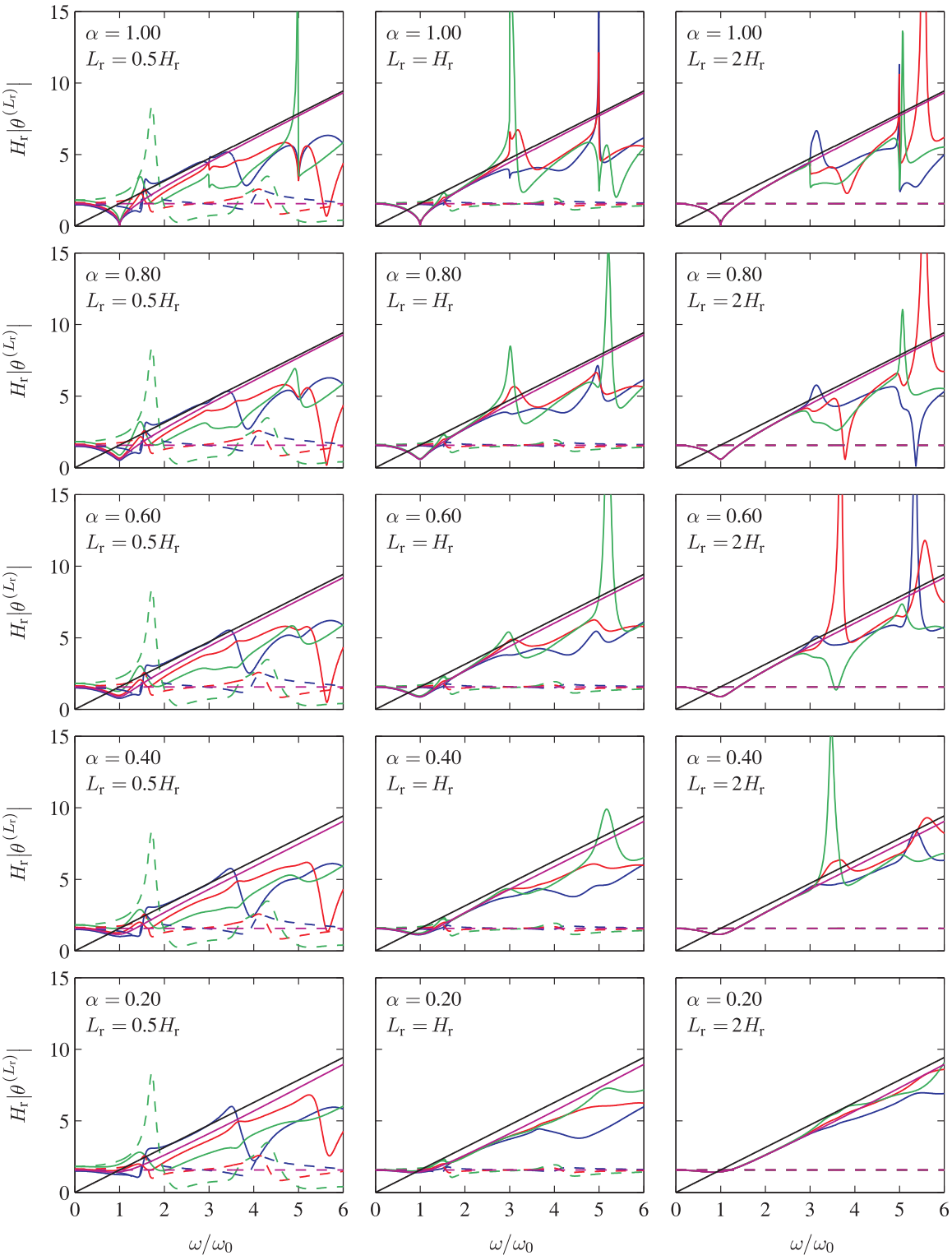

Figure A.4 Variation of the parameter $H_r\left|\theta^{(L_r)}\right|$ for a flexible dam $E_s = 35\,\text{GPa}$ as a function of frequency ratio ω/ω_0, height y, wave reflection coefficient α and truncation length L_r. — $y_A = 0.1H_r$; — $y_B = 0.5H_r$; — $y_C = 0.9H_r$; — Sommerfeld BC ; — Sharan BC. Continuous lines : compressible water ; dotted lines : incompressible water.

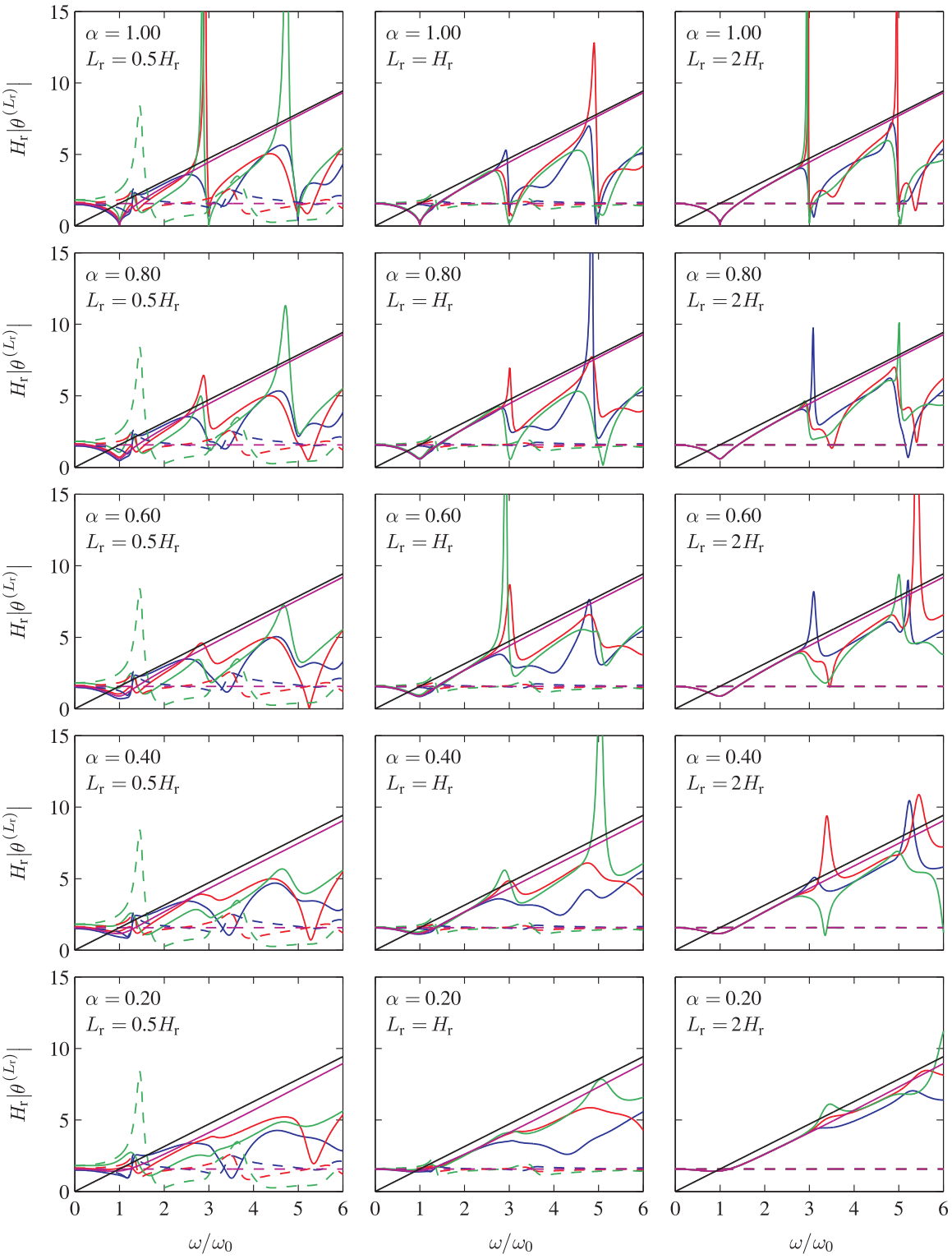

Figure A.5 Variation of the parameter $H_{\mathrm{r}}\left|\theta^{(L_{\mathrm{r}})}\right|$ for a flexible dam $E_{\mathrm{s}} = 25\,\mathrm{GPa}$ as a function of frequency ratio ω/ω_0, height y, wave reflection coefficient α and truncation length L_{r}. — $y_{\mathrm{A}} = 0.1H_{\mathrm{r}}$; — $y_{\mathrm{B}} = 0.5H_{\mathrm{r}}$; — $y_{\mathrm{C}} = 0.9H_{\mathrm{r}}$; — Sommerfeld BC ; — Sharan BC. Continuous lines : compressible water ; dotted lines : incompressible water.

To further investigate the variations of $H_{\mathrm{r}}\left|\theta_0^{(L_{\mathrm{r}})}\right|$ and $H_{\mathrm{r}}\left|\theta^{(L_{\mathrm{r}})}\right|$ over reservoir height, the heightwise profiles of these functions are determined at three reservoir truncation lengths $L_{\mathrm{r}} = 0.5H_{\mathrm{r}}$, $L_{\mathrm{r}} = H_{\mathrm{r}}$ and $L_{\mathrm{r}} = 2H_{\mathrm{r}}$ and for frequencies ranging from 0 to $6\omega_0$. For brevity, only results obtained at frequency ratios $\omega/\omega_0 = 0.8$, $\omega/\omega_0 = 1.2$, $\omega/\omega_0 = 2.0$ and $\omega/\omega_0 = 4.0$ are illustrated in Figs. A.6 to A.9, respectively. Profiles corresponding to both compressible and incompressible water assumptions as well as the constant profiles representing Sommerfeld and Sharan boundary conditions are shown. We first observe that the profiles are sensitive to dam stiffness, reservoir bottom wave absorption and frequency ratio and that they tend to become constant over reservoir height as truncation length increases. At the lower frequency ratios $\omega/\omega_0 = 0.8$ and $\omega/\omega_0 = 1.2$, we observe that the compressiblity-based profiles converge towards incompressibility-based ones as reservoir bottom wave absorption increases. This implies that the error associated with the use of an incompressibility-based TBC condition increases for highly reflective reservoirs. Figs. A.6 and A.7 also show that the three incompressibility-based profiles have each an inflexion point that is almost common. The same applies to the compressibility-based profiles. We note that the inflexion point is approximately located at the same reservoir height for all the profiles. Incompressibility- and compressibility-based Sharan boundary conditions also approximately pass through this inflexion point. A closer look at curves shows that the maximum variation of $H_{\mathrm{r}}\left|\theta_0^{(L_{\mathrm{r}})}\right|$ and $H_{\mathrm{r}}\left|\theta^{(L_{\mathrm{r}})}\right|$ over height increases with reservoir bottom wave absorption and dam flexibility. This behavior can be used to evaluate the error resulting from the use an incompressibility- or compressibility-based Sharan boundary condition. Figs. A.8 and A.9 show that, at higher frequency ratios $\omega/\omega_0 = 2.0$ and $\omega/\omega_0 = 4.0$, convergence between compressibility- and incompressibility-based profiles with increasing reservoir bottom wave absorption and truncation length is not as obvious as for lower frequency ratios. Some profiles have now more that one inflexion point, i.e. the case $\alpha = 1$, $E_{\mathrm{s}} = 35\,\mathrm{GPa}$ and $L_{\mathrm{r}} = 2H_{\mathrm{r}}$, and some show sharp peaks corresponding to a very small absolute value of the denominator in Eq. (A.38), i.e. the case $\alpha = 0.8$, $E_{\mathrm{s}} = 25\,\mathrm{GPa}$ and $L_{\mathrm{r}} = H_{\mathrm{r}}$.

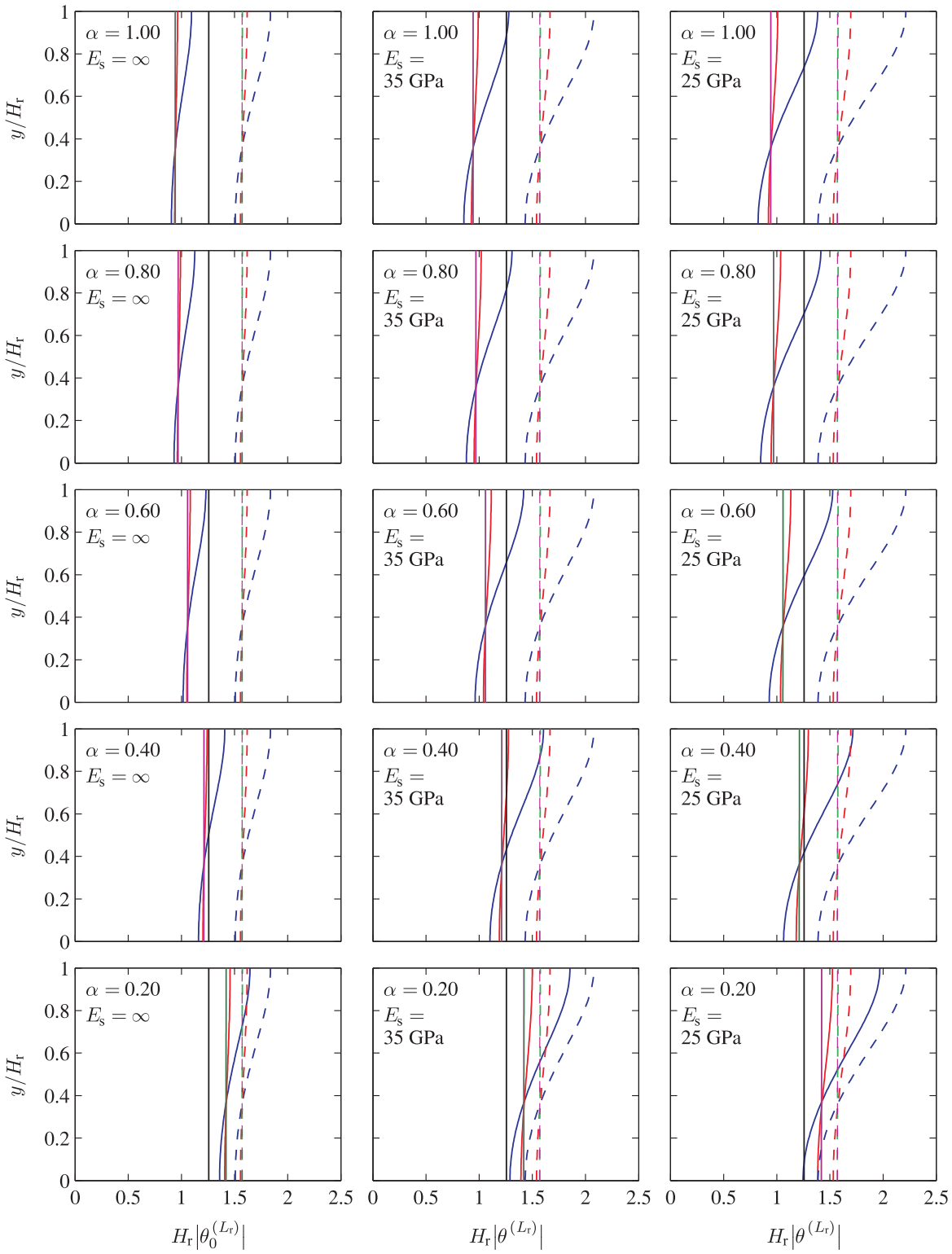

Figure A.6 Variation of the parameter $H_r\left|\theta^{(L_r)}\right|$ for $\omega = 0.8\omega_0$ as a function of height y, wave reflection coefficient α and truncation length L_r. — $L_r = 0.5H_r$; — $L_r = H_r$; — $L_r = 2H_r$. — Sommerfeld BC ; — Sharan BC. Continuous lines : compressible water ; dotted lines : incompressible water.

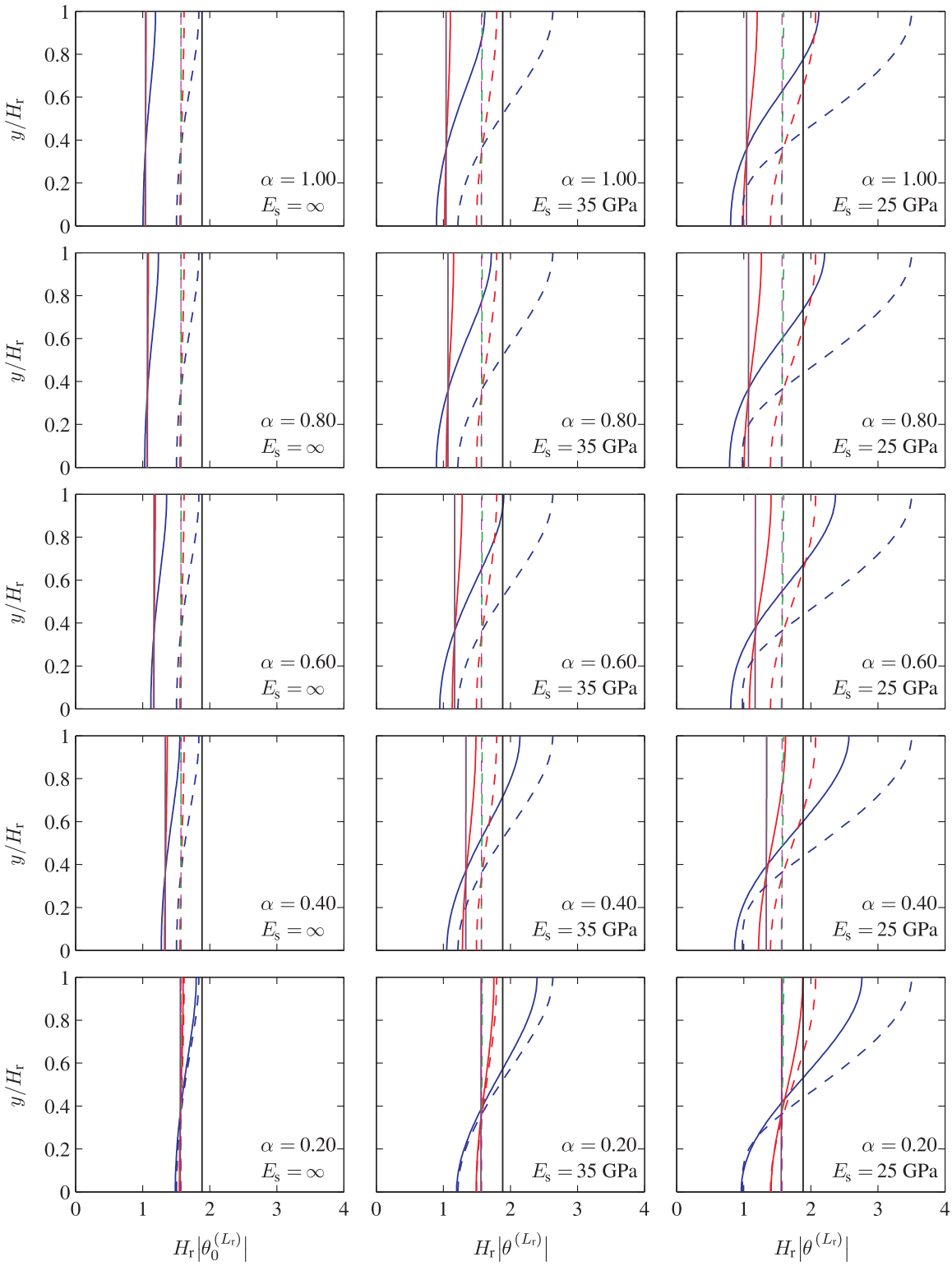

Figure A.7 Variation of the parameter $H_r\left|\theta^{(L_r)}\right|$ for $\omega = 1.2\omega_0$ as a function of height y, wave reflection coefficient α and truncation length L_r. — $L_r = 0.5H_r$; — $L_r = H_r$; — $L_r = 2H_r$. — Sommerfeld BC ; — Sharan BC. Continuous lines : compressible water ; dotted lines : incompressible water.

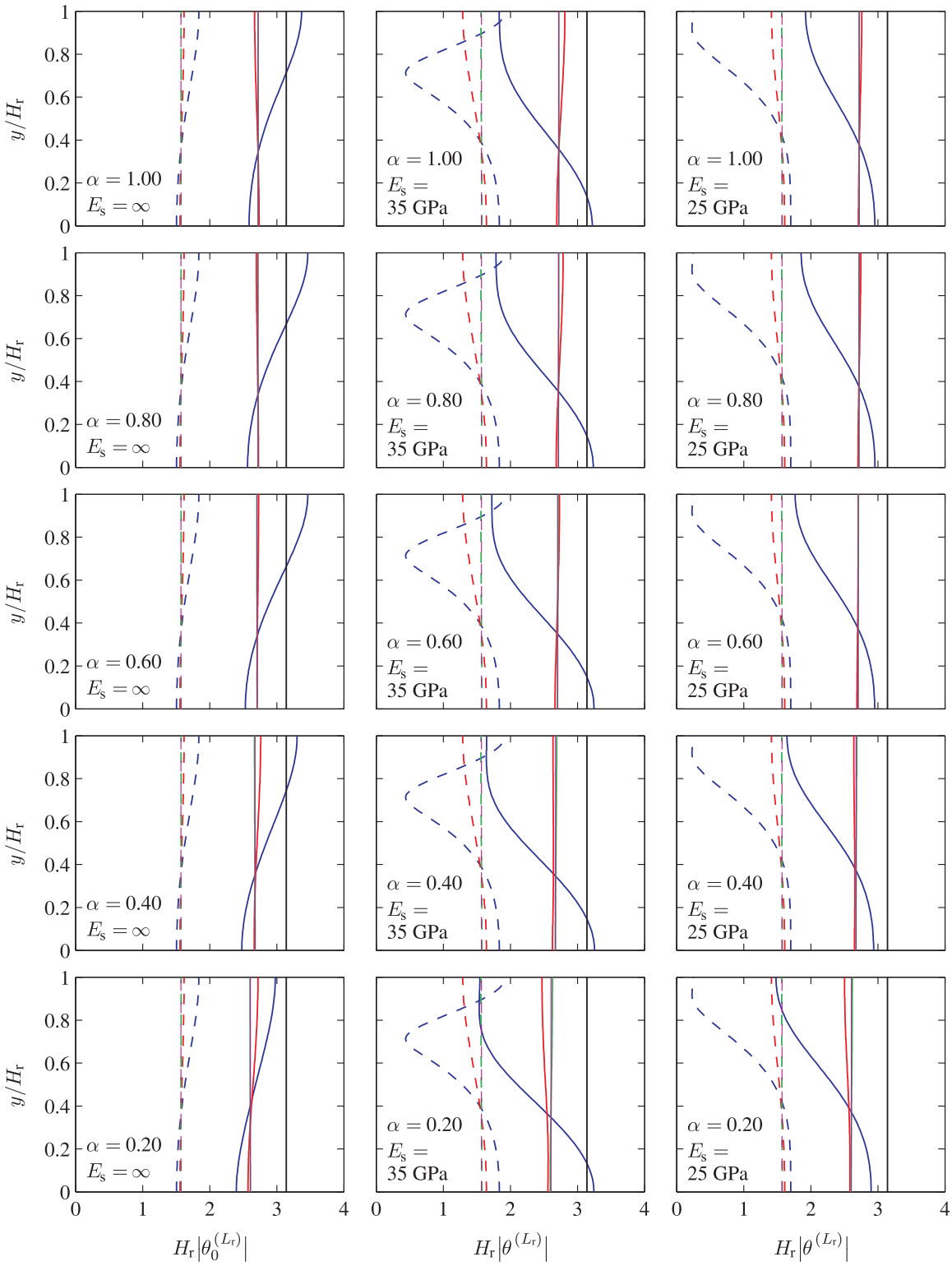

Figure A.8 Variation of the parameter $H_r\left|\theta^{(L_r)}\right|$ for $\omega = 2\omega_0$ as a function of height y, wave reflection coefficient α and truncation length L_r. — $L_r = 0.5H_r$; — $L_r = H_r$; — $L_r = 2H_r$. — Sommerfeld BC ; — Sharan BC. Continuous lines : compressible water ; dotted lines : incompressible water.

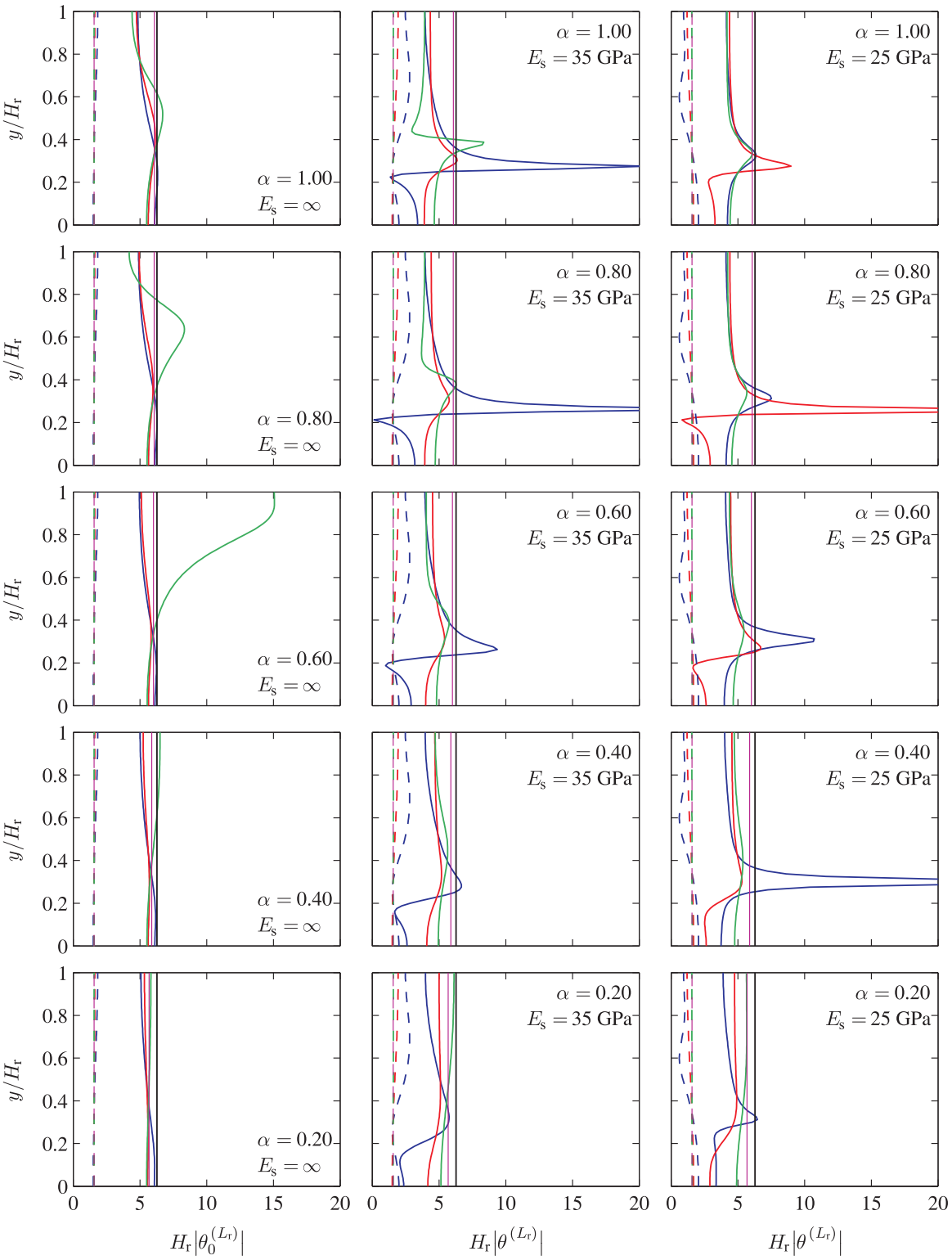

Figure A.9 Variation of the parameter $H_r\left|\theta^{(L_r)}\right|$ for $\omega = 4\omega_0$ as a function of height y, wave reflection coefficient α and truncation length L_r. — $L_r = 0.5H_r$; — $L_r = H_r$; — $L_r = 2H_r$. — Sommerfeld BC ; — Sharan BC. Continuous lines : compressible water ; dotted lines : incompressible water.

A.3.3 Error analyses

The formulations presented previously were fully programmed using MATLAB® [37]. To first validate the new formulation, it is used to determine hydrodynamic forces and pressures acting on the upstream face of the dam when applying the analytical TBC at a reservoir truncation length as small as $L_r = 0.1H_r$. Rigid and flexible dams with $E_s = 35\,\text{GPa}$ and $E_s = 25\,\text{GPa}$ are considered. In each case, five reflection coefficients $\alpha = 1.0$, $\alpha = 0.8$, $\alpha = 0.6$, $\alpha = 0.4$, and $\alpha = 0.2$ are investigated. Fig. A.10 compares the hydrodynamic force FRFs obtained to those determined using the classical solution presented in Section A.2.1, while Fig. A.11 illustrates the heightwise distributions of hydrodynamic pressure determined at different frequencies using both methods. Hydrodynamic forces and pressures are normalized by hydrostatic force $F_{stat} = \rho_r g H_r^2/2$ and hydrostatic pressure $p_{stat} = \rho_r g H_r$, respectively. As can be seen, the new formulation yields a prefect agreement, irrespective of the level of reservoir bottom wave absorption and dam stiffness.

The validated new formulation is applied next to assess the effectiveness of various TBCs and determine the error associated with their use. The effect of an incompressibility-based TBC at three truncation lengths $L_r = 0.5H_r$, $L_r = H_r$ and $L_r = 2H_r$ of a compressible reservoir is investigated first. Rigid and flexible dams as well as different reservoir bottom wave absorption levels are considered. Fig. A.13 shows the obtained frequency response curves of hydrodynamic forces as well as the classical solutions. The large discrepancies in the results show that incompressibility-based TBCs may induce significant errors, although better agreement is found in the lower frequency range for reservoirs with a highly absorptive bottom. The Sommerfeld radiation boundary condition presented in Eq. (A.50) is studied next. Using Eqs. (A.48), (A.49), and then Eqs. (A.41) and (A.42), hydrodynamic pressure FRFs of hydrodynamic forces are determined considering three reservoir truncation lengths $L_r = 0.5H_r$, $L_r = H_r$ and $L_r = 2H_r$. Fig. A.12 shows the results obtained as well as the classical solutions for a semi-infinite reservoir. It is seen that the frequency response curves are very sensitive to reservoir truncation length. In the low frequency range, the Sommerfeld radiation boundary condition is indeed effective only for relatively high reservoir truncation lengths, of the order of $L_r = 2H_r$ in the present case. However, even when using such an important truncation length, some discrepancies are persistent at the higher frequency range, namely for reservoirs with a highly absorptive bottom. Frequency response curves of hydrodynamic forces obtained using Sharan boundary condition [Eq. (A.51)] at three reservoir truncation lengths $L_r = 0.1H_r$, $L_r = 0.5H_r$ and $L_r = H_r$ are then examined. To allow clear reading of the curves, Fig. A.14 illustrates the results for a low frequency range from 0 to $3\omega_0$, and Fig. A.15 for a high frequency range from $3\omega_0$ to $6\omega_0$.

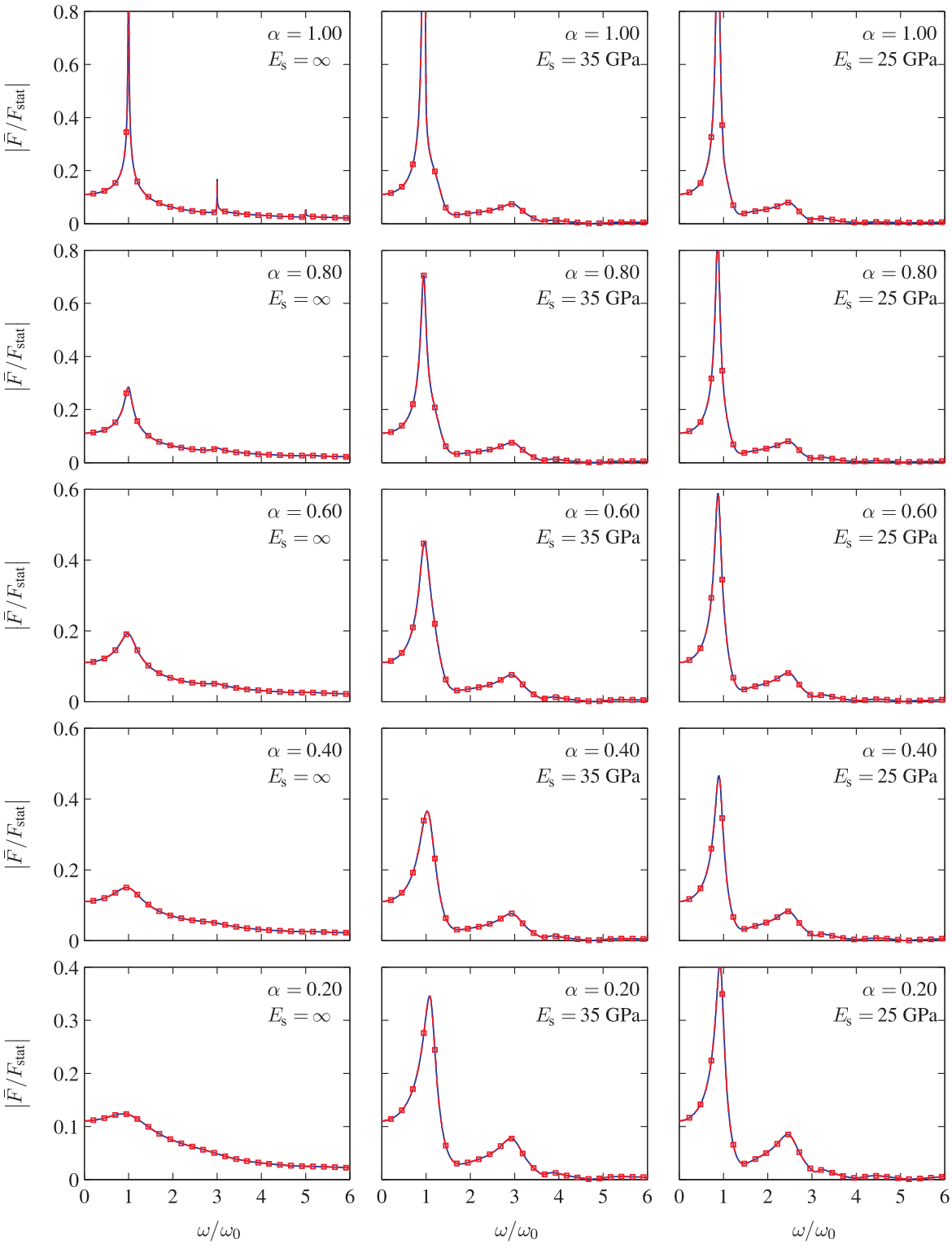

Figure A.10 FRFs for normalized hydrodynamic forces determined using : (i) the new formulation for a truncated reservoir ($L_r = 0.1H_r$), and (ii) the classical solution considering a semi-infinite reservoir. ▬□▬ New analytical solution ; ▬▬ Classical solution.

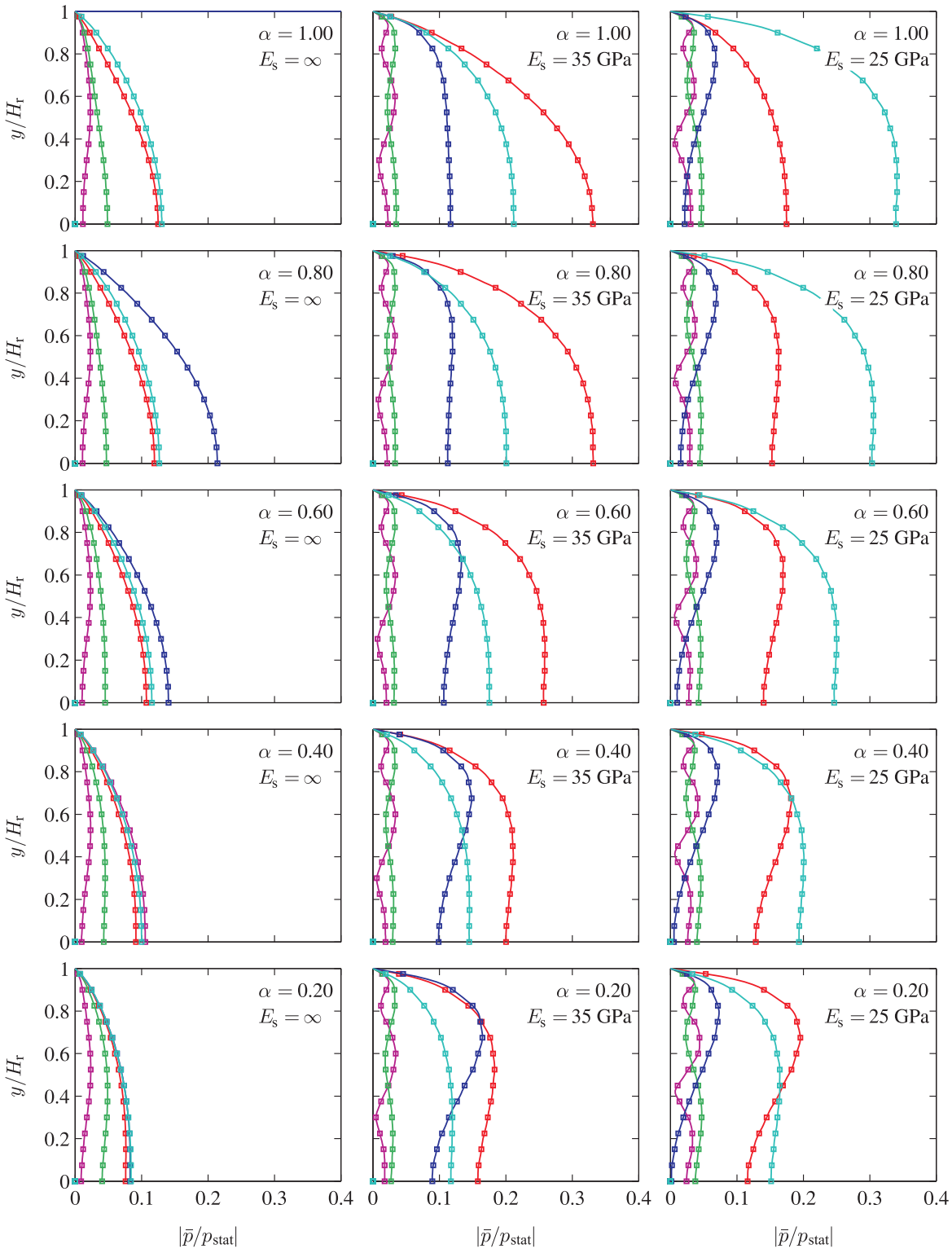

Figure A.11 Heightwise distributions of normalized hydrodynamic pressures on dam upstream face determined using : (i) the new formulation for a truncated reservoir ($L_r = 0.1H_r$), and (ii) the classical solution considering a semi-infinite reservoir. – □ – New analytical solution ; — Classical solution : — $\omega = 0.8\omega_0$; — $\omega = \omega_0$; — $\omega = 1.2\omega_0$; — $\omega = 2\omega_0$; — $\omega = 4\omega_0$.

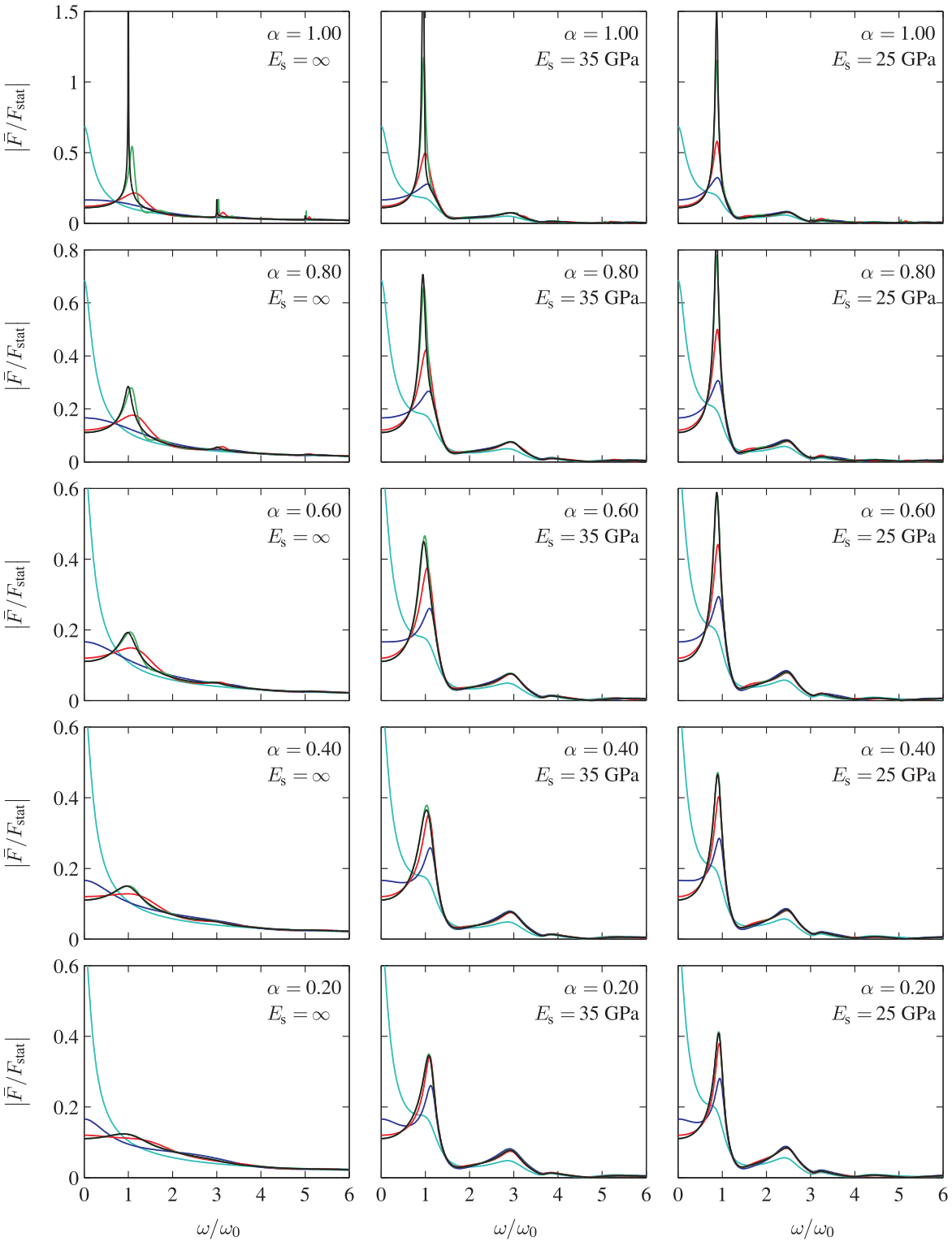

Figure A.12 FRFs for normalized hydrodynamic forces determined using : (i) the new analytical formulation considering Sommerfeld boundary condition, and (ii) the classical solution considering a semi-infinite reservoir. — $L_r = 0.1H_r$; — $L_r = 0.5H_r$; — $L_r = H_r$; — $L_r = 2H_r$; — Classical solution.

We observe that Sharan boundary condition yields excellent results in the low frequency range for truncation lengths as small as $L_r = 0.1H_r$ for the rigid dam case. When dam flexibility is included, this truncation length yields some discrepancies with the classical solution, and a larger truncation length $L_r = 0.5H_r$ is required to reach an excellent agreement. In the higher frequency range, Fig. A.15 reveals that discrepancies are induced even for truncation lengths as high as $L_r = H_r$. Accurate evaluation of hydrodynamic forces acting on a dam upstream face is of practical value for its design or safety evaluation. To get more insight into the sensitivity of hydrodynamic forces to a given TBC, the following error estimators are proposed

$$\eta_{|\bar{F}_0|}^{(L_r)}(\omega) = \frac{\left|\bar{F}_0^{(L_r)}(\omega)\right| - \left|\bar{F}_0^{(\infty)}(\omega)\right|}{\left|\bar{F}_0^{(\infty)}(\omega)\right|}; \qquad \eta_{|\bar{F}|}^{(L_r)}(\omega) = \frac{\left|\bar{F}^{(L_r)}(\omega)\right| - \left|\bar{F}^{(\infty)}(\omega)\right|}{\left|\bar{F}^{(\infty)}(\omega)\right|} \tag{A.57}$$

Figs. A.16 to A.19 illustrate error estimators $\eta_{|\bar{F}_0|}^{(L_r)}$ and $\eta_{|\bar{F}|}^{(L_r)}$ for hydrodynamic forces determined using Sommerfeld, Sharan and truncated analytical TBCs [Eq. (A.39)] considering $\widetilde{m}_r = 2$ to m_r. Results are shown for four reservoir truncation lengths $L_r = 0.1H_r$, $L_r = 0.5H_r$, $L_r = H_r$ and $L_r = 2H_r$. Error estimators are given in % and are presented as bar charts equally spaced at frequency increments of $\Delta\omega = 0.08\omega_0$ over a frequency ratio range from 0 to 6. For each truncation length, rigid and flexible dams with $E_s = 35\,\text{GPa}$ and $E_s = 25\,\text{GPa}$ are investigated, as well as five reflection coefficients $\alpha = 1.0$, $\alpha = 0.8$, $\alpha = 0.6$, $\alpha = 0.4$, and $\alpha = 0.2$. The bar charts in Fig. A.16 clearly indicate that the error associated with the Sommerfeld boundary condition is the highest for most of the frequency range of interest. It is seen that the Sharan boundary condition yields satisfactory results only for very low frequencies. The error associated with the Sharan boundary condition varies significantly as a function of frequency ratio and dam flexibility, but we note that this error globally increases with dam stiffness. Sharan and Sommerfeld boundary conditions yield similar error estimators in the higher frequency range. We also observe that error estimators are less sensitive to reservoir bottom wave absorbtion. More reservoir modes need to be included to match hydrodynamic pressures in the higher frequency range. The number of reservoir modes required for convergence in a rigid dam case, i.e. $\widetilde{m}_r \approx 3$, is less than that required in the case of a flexible dam, i.e. $\widetilde{m}_r \approx 10$. It is important to note however that an increase in the number of reservoir modes does not necessarily reduce the error estimators over the whole frequency range, but rather enlarges the lower frequency range over which error is minimum. No definite trend could be identified regarding the sign of the error estimators. For example, Sharan boundary condition is shown to be alternatively conservative or nonconservative depending on the frequency ratio. As truncation length increases, Fig. A.17 shows that error estimators generally diminish over the whole frequency range. For low frequencies, Sommerfeld boun-

dary condition still yields unsatisfactory results, while the error due to Sharan boundary condition is nearly null. Fewer reservoir modes are now required to obtain convergence over all the frequency range, i.e. $\widetilde{m}_{\mathrm{r}} \approx 3$. The effect of energy dissipation at reservoir bottom is slightly more important than for truncation length $L_{\mathrm{r}} = 0.1H_{\mathrm{r}}$. It is seen that reservoir bottom wave absorption causes error estimators to slightly diminish. As previously, Sharan and Sommerfeld yield approximately similar error estimators in the higher frequency range. The same conclusions apply to Figs. A.18 and A.19. We namely observe that the error reduction due to reservoir bottom wave absorption becomes more predominant with increasing truncation length. For a truncation length $L_{\mathrm{r}} = 2H_{\mathrm{r}}$, two reservoir modes are sufficient to obtain convergence over a wide frequency range up to $\omega \approx 5\omega_0$, and three are required for higher frequencies.

Finally, predicting the first resonant frequency of a dam-reservoir system plays an important role in the assessment of the seismic response of dams. Error estimators for the first resonant frequency of a dam-reservoir system can be defined as

$$\eta_{\omega_{\mathrm{r}}}^{(L_{\mathrm{r}})} = \frac{\omega_{\mathrm{r}}^{(L_{\mathrm{r}})} - \omega_{\mathrm{r}}^{(\infty)}}{\omega_{\mathrm{r}}^{(\infty)}} \tag{A.58}$$

where $\omega_{\mathrm{r}}^{(L_{\mathrm{r}})}$ denotes the dam-reservoir resonant frequency obtained using a truncation length L_{r}, and $\omega_{\mathrm{r}}^{(\infty)}$ the resonant frequency corresponding to a semi-infinite reservoir. We may also examine error estimators for hydrodynamic force coefficients at dam upstream face

$$\eta_{c_{\mathrm{h}}}^{(L_{\mathrm{r}})} = \frac{c_{\mathrm{h}}^{(L_{\mathrm{r}})} - c_{\mathrm{h}}^{(\infty)}}{c_{\mathrm{h}}^{(\infty)}} \tag{A.59}$$

where hydrodynamic force coefficients $c_{\mathrm{h}}^{(\infty)}$ and $c_{\mathrm{h}}^{(L_{\mathrm{r}})}$ are defined by

$$c_{\mathrm{h}}^{(\infty)} = \frac{\left|\bar{F}^{(\infty)}(\omega)\right|_{\max}}{F_{\mathrm{stat}}}\,; \qquad\qquad c_{\mathrm{h}}^{(L_{\mathrm{r}})} = \frac{\left|\bar{F}^{(L_{\mathrm{r}})}(\omega)\right|_{\max}}{F_{\mathrm{stat}}} \tag{A.60}$$

For purpose of illustration, error estimators determined according to Eqs. (A.58) to (A.60) are presented in Table A1 for a gravity dam with modulus of elasticity $E_{\mathrm{s}} = 25\,\mathrm{GPa}$. As can be seen in this case, Sommerfeld boundary condition cannot be used to determine the first resonant frequency of the dam-reservoir system, neither the corresponding hydrodynamic force coefficient for a short truncation length $L_{\mathrm{r}} = 0.1H_{\mathrm{r}}$. As truncation length increases, Sommerfeld boundary condition becomes more accurate to predict the first resonant frequency. Predictions of corresponding resonant amplitudes are however generally less accurate, but are improved for reservoirs with a highly absorptive bottom. Sharan boundary condition yields

satisfactory predictions of both first resonant frequency and corresponding amplitude, except for the short truncation length $L_r = 0.1H_r$. We also note that including additional reservoir modes, i.e. $\widetilde{m}_r = 2$ to $\widetilde{m}_r = 3$, yields an excellent agreement with the classical solution even for short truncation lengths and irrespective of reservoir bottom wave absorption levels.

A.4 Concluding remarks

This paper presented and validated an original formulation to study dynamically excited dam-reservoir systems with upstream TBCs. First, a review of main developments related to the application of TBCs in dam engineering was presented. Then, the detailed mathematical derivations were provided for various TBCs and their sensitivity to : (i) truncation length, (ii) reservoir depth, (iii) reservoir bottom wave absorption, (v) water compressibility, and (iv) dam stiffness was thoroughly investigated over a wide frequency range of interest in dam engineering applications. The systems of equations resulting from the analytical formulation were solved numerically to assess the accuracy and effectiveness of some classical approximate TBCs and determine the exact error associated with their use independently of FEM or BEM modeling of the reservoir. Exact analytical TBCs were also developed for comparison purposes. The effects of reservoir truncation length, reservoir bottom wave absorption, water compressibility and dam stiffness on the frequency response of hydrodynamic pressures and forces applied at a dam upstream face were identified and discussed. We showed that the widely used assumption that TBCs are height-independent holds only over a low frequency range up to a characteristic frequency which increases with truncation length. This height-dependence was observed to generally increase with higher reservoir bottom wave reflection and dam flexibility. We also concluded that the effect of water compressibility is significant except for highly absorptive reservoirs at a very low frequency range. Using the new formulation, error estimators were determined to provide guidelines for selecting TBCs to be implemented in Finite Element or Boundary Element models of dam-reservoir systems. For that purpose, the sensitivity of hydrodynamic forces acting on dam upstream face and that of the first resonant frequency of the dam-reservoir system to the various aforementioned parameters were systematically investigated. The following main trends could be identified especially when short reservoir truncation lengths are required to reduce computational burden : (i) incompressibility-based TBCs generally induce significant errors and should not be used, (ii) Sommerfeld TBC fails in predicting the first resonant frequency of the dam-reservoir system as well as hydrodynamic forces on most of the frequency range of interest, (iii) Improved results can be obtained by using the Sharan TBC or the truncated analytical TBCs introduced in the paper, and applying the error estimators proposed to control the quality of

Table A1 Error estimation of hydrodynamic force coefficients for a gravity dam with modulus of elasticity $E_{\mathrm{s}}=25\,\mathrm{GPa}$.

Truncation length	Boundary condition	Reservoir bottom wave absorption levels									
		$\alpha=1.0$		$\alpha=0.8$		$\alpha=0.6$		$\alpha=0.4$		$\alpha=0.2$	
		$\eta_{\omega_{\mathrm{r}}}^{(L_{\mathrm{r}})}$	$\eta_{c_{\mathrm{h}}}^{(L_{\mathrm{r}})}$	$\eta_{\omega_{\mathrm{r}}}^{(L_{\mathrm{r}})}$	$\eta_{c_{\mathrm{h}}}^{(L_{\mathrm{r}})}$	$\eta_{\omega_{\mathrm{r}}}^{(L_{\mathrm{r}})}$	$\eta_{c_{\mathrm{h}}}^{(L_{\mathrm{r}})}$	$\eta_{\omega_{\mathrm{r}}}^{(L_{\mathrm{r}})}$	$\eta_{c_{\mathrm{h}}}^{(L_{\mathrm{r}})}$	$\eta_{\omega_{\mathrm{r}}}^{(L_{\mathrm{r}})}$	$\eta_{c_{\mathrm{h}}}^{(L_{\mathrm{r}})}$
$L_{\mathrm{r}}=0.1H_{\mathrm{r}}$	Sommerfeld TBC	–	–	–	–	–	–	–	–	–	–
	Sharan TBC	-3.773	-10.764	-2.857	-2.181	-3.773	-1.037	-4.587	-4.055	-4.504	-9.642
	Analytical TBC, $\widetilde{m}_{\mathrm{r}}=2$	-0.943	-0.263	0.000	2.185	0.000	2.402	-0.917	2.735	0.000	2.798
	Analytical TBC, $\widetilde{m}_{\mathrm{r}}=3$	0.000	-0.998	0.000	-0.902	0.000	0.211	-0.917	0.484	0.000	0.527
$L_{\mathrm{r}}=0.5H_{\mathrm{r}}$	Sommerfeld TBC	1.886	-78.810	3.809	-64.121	4.716	-50.075	3.669	-38.720	2.702	-31.226
	Sharan TBC	0.000	-0.341	0.000	0.034	0.000	-0.005	-0.917	-0.103	0.000	-0.301
	Analytical TBC, $\widetilde{m}_{\mathrm{r}}=2$	0.000	-0.001	0.000	0.005	0.000	0.006	0.000	0.006	0.000	0.006
	Analytical TBC, $\widetilde{m}_{\mathrm{r}}=3$	0.000	0.000	0.000	0.000	0.000	0.001	0.000	0.001	0.000	0.001
$L_{\mathrm{r}}=1.0H_{\mathrm{r}}$	Sommerfeld TBC	0.943	-61.924	2.857	-41.524	2.830	-25.015	1.834	-13.482	1.801	-7.019
	Sharan TBC	0.000	-0.003	0.000	0.000	0.000	0.000	0.000	-0.002	0.000	-0.004
	Analytical TBC, $\widetilde{m}_{\mathrm{r}}=2$	0.000	0.000	0.000	0.000	0.000	0.000	0.000	0.000	0.000	0.000
	Analytical TBC, $\widetilde{m}_{\mathrm{r}}=3$	0.000	0.000	0.000	0.000	0.000	0.000	0.000	0.000	0.000	0.000
$L_{\mathrm{r}}=2.0H_{\mathrm{r}}$	Sommerfeld TBC	0.000	-24.349	0.952	-8.878	0.943	-1.276	0.000	1.285	0.900	1.052
	Sharan TBC	0.000	0.000	0.000	0.000	0.000	0.000	0.000	0.000	0.000	0.000
	Analytical TBC, $\widetilde{m}_{\mathrm{r}}=2$	0.000	0.000	0.000	0.000	0.000	0.000	0.000	0.000	0.000	0.000
	Analytical TBC, $\widetilde{m}_{\mathrm{r}}=3$	0.000	0.000	0.000	0.000	0.000	0.000	0.000	0.000	0.000	0.000

the solution as a function of frequency ratio, dam flexibility and wave absorption at reservoir bottom. The in-depth parametric studies presented illustrate how the proposed formulation and error estimators can be used efficiently for a rigorous assessment of the accuracy and effectiveness of classical or newly-developed TBCs, namely by defining reservoir length to depth ratios and frequency ranges for which the application of these TBCs would be recommended. We note that the proposed method, which can be easily programmed, is valuable in testing, validating or developing TBCs that are either height-dependent or independent, and frequency-dependent or independent, with the latter case being generally more suited for time domain analyses. Finally, although the paper provided the formulation and fundamental mechanisms involved in vibrating dam-reservoir systems with upstream TBCs, the methodology and findings described can be extended to other similar fluid-structure problems.

Acknowledgements

The authors would like to acknowledge the financial support of the Natural Sciences and Engineering Research Council of Canada (NSERC).

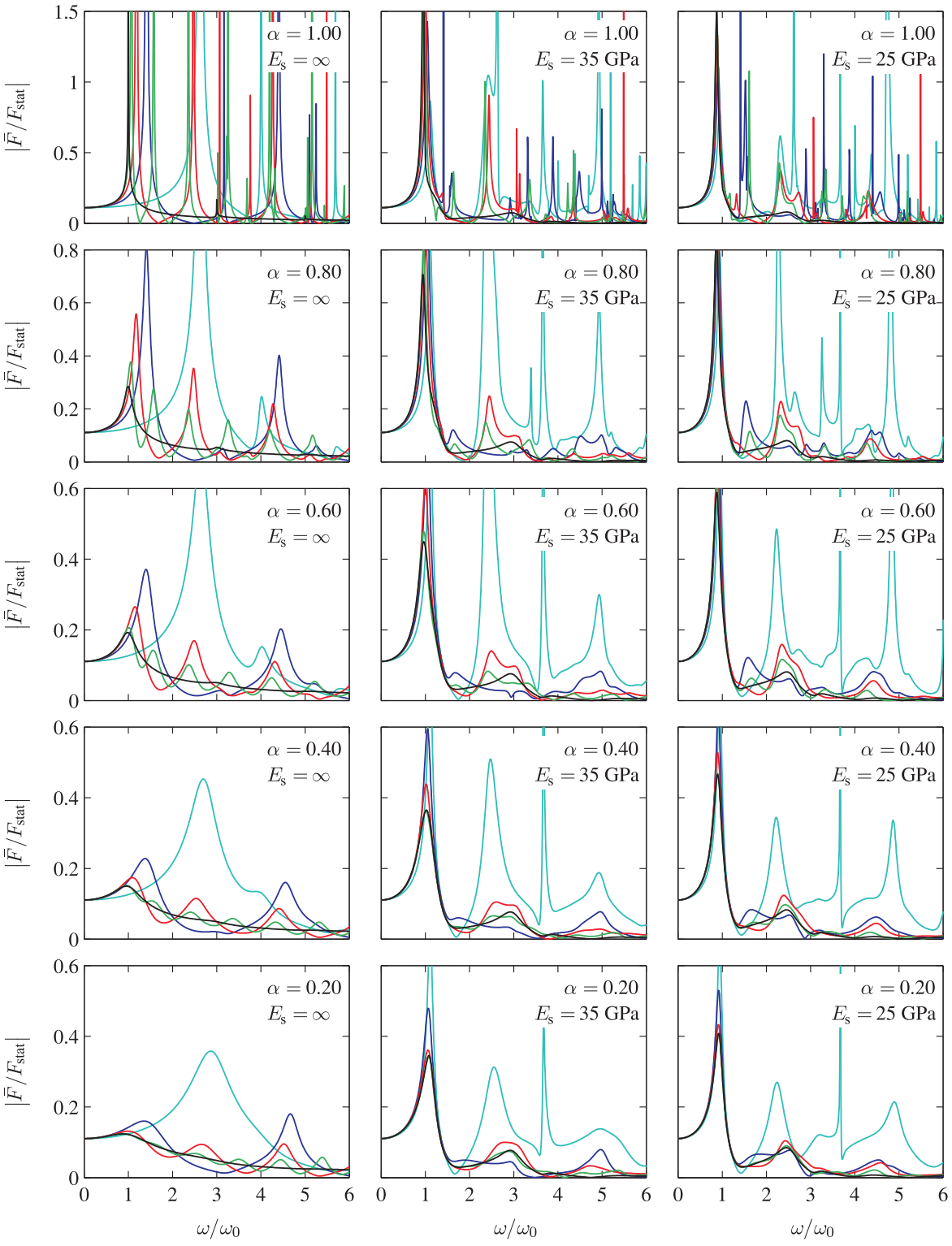

Figure A.13 FRFs for normalized hydrodynamic forces determined using : (i) the new analytical formulation considering an incompressibility-based analytical boundary condition, and (ii) the classical solution considering a semi-infinite reservoir. — $L_r = 0.1H_r$; — $L_r = 0.5H_r$; — $L_r = H_r$; — $L_r = 2H_r$; — Classical solution ;.

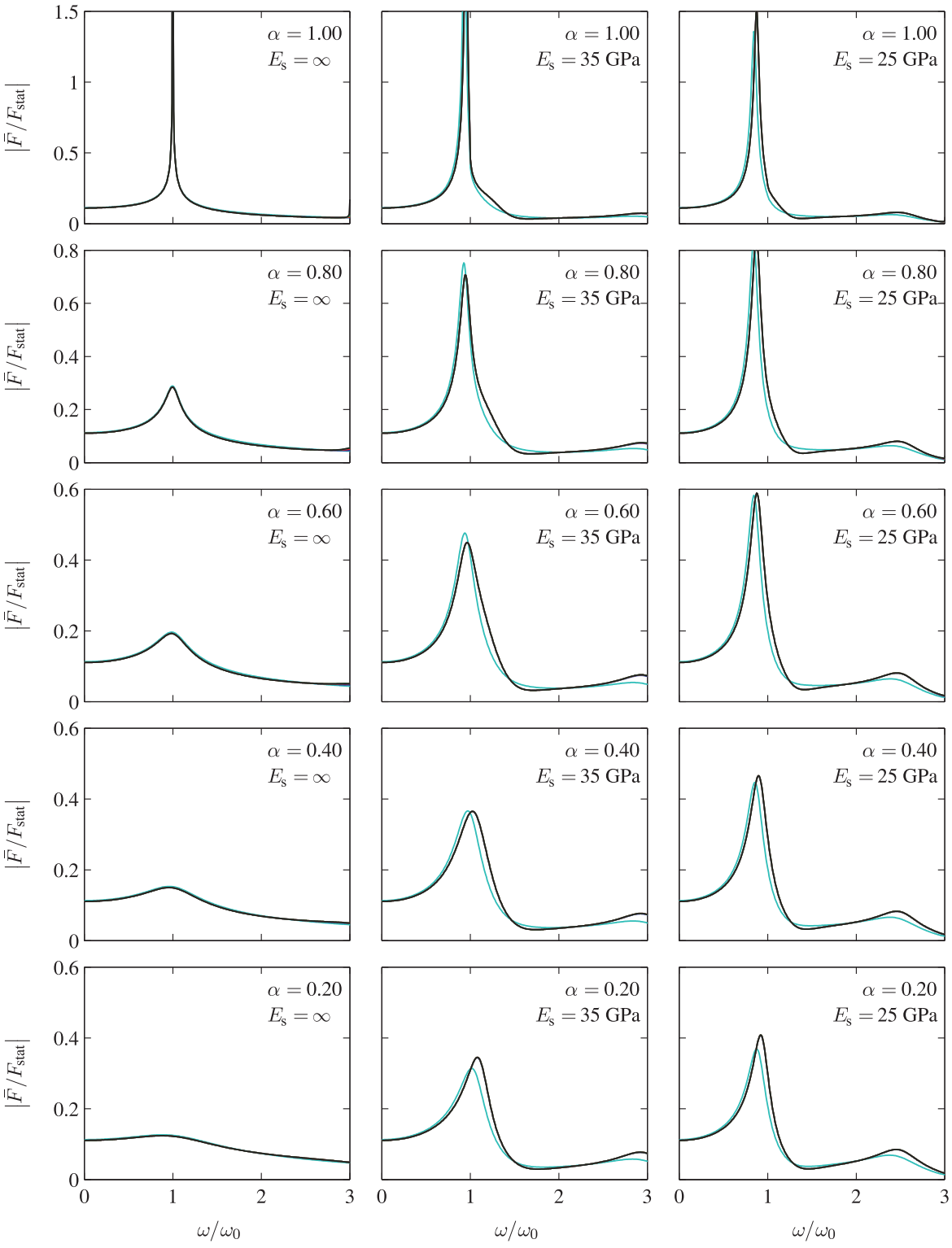

Figure A.14 FRFs for normalized hydrodynamic forces determined for low frequencies using : (i) the new analytical formulation considering Sharan boundary condition, and (ii) the classical solution considering a semi-infinite reservoir. — $L_r = 0.1H_r$; — $L_r = 0.5H_r$; — $L_r = H_r$; — Classical solution.

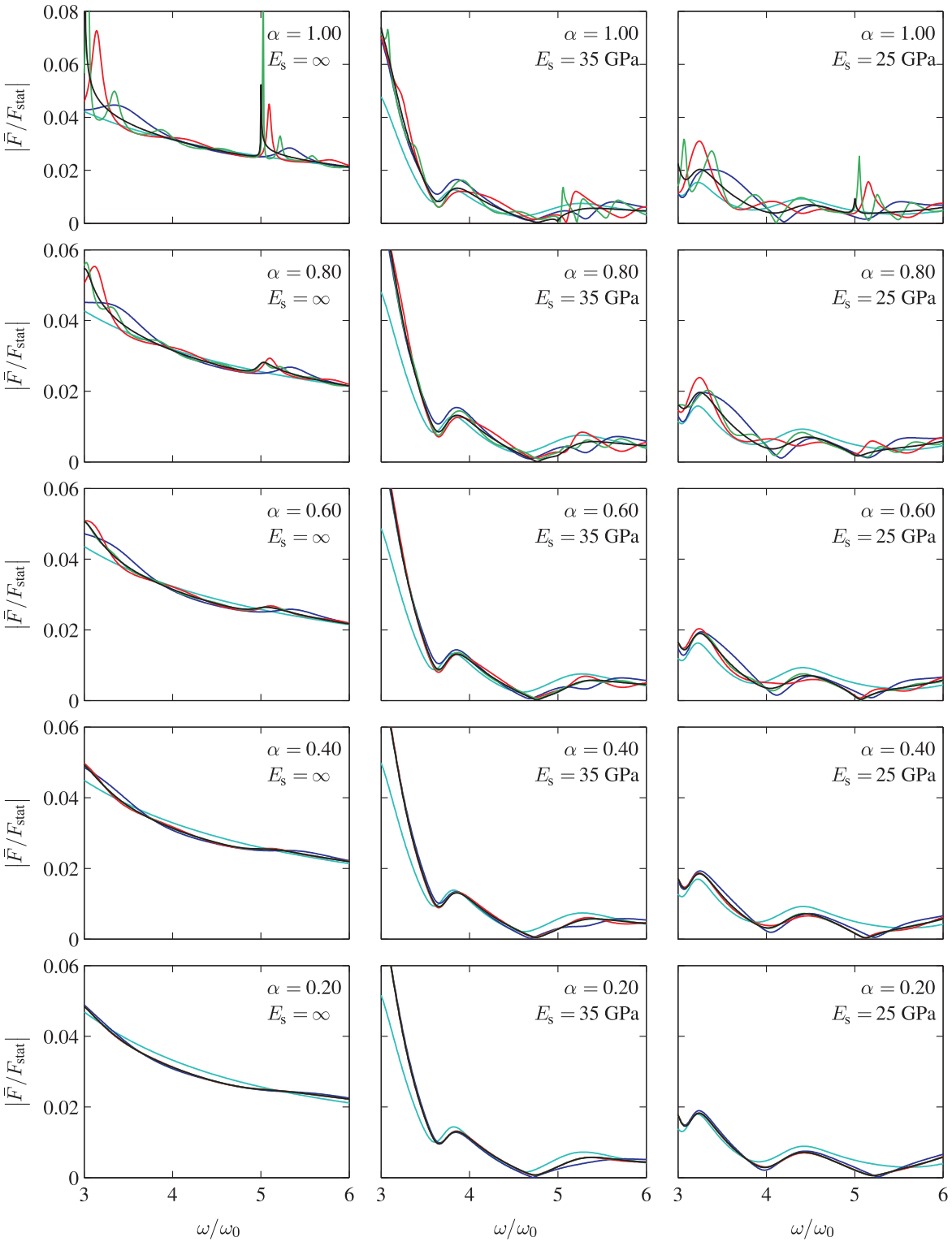

Figure A.15 FRFs for normalized hydrodynamic forces determined for high frequencies using : (i) the new analytical formulation considering Sharan boundary condition, and (ii) the classical solution considering a semi-infinite reservoir. — $L_r = 0.1H_r$; — $L_r = 0.5H_r$; — $L_r = H_r$; — Classical solution.

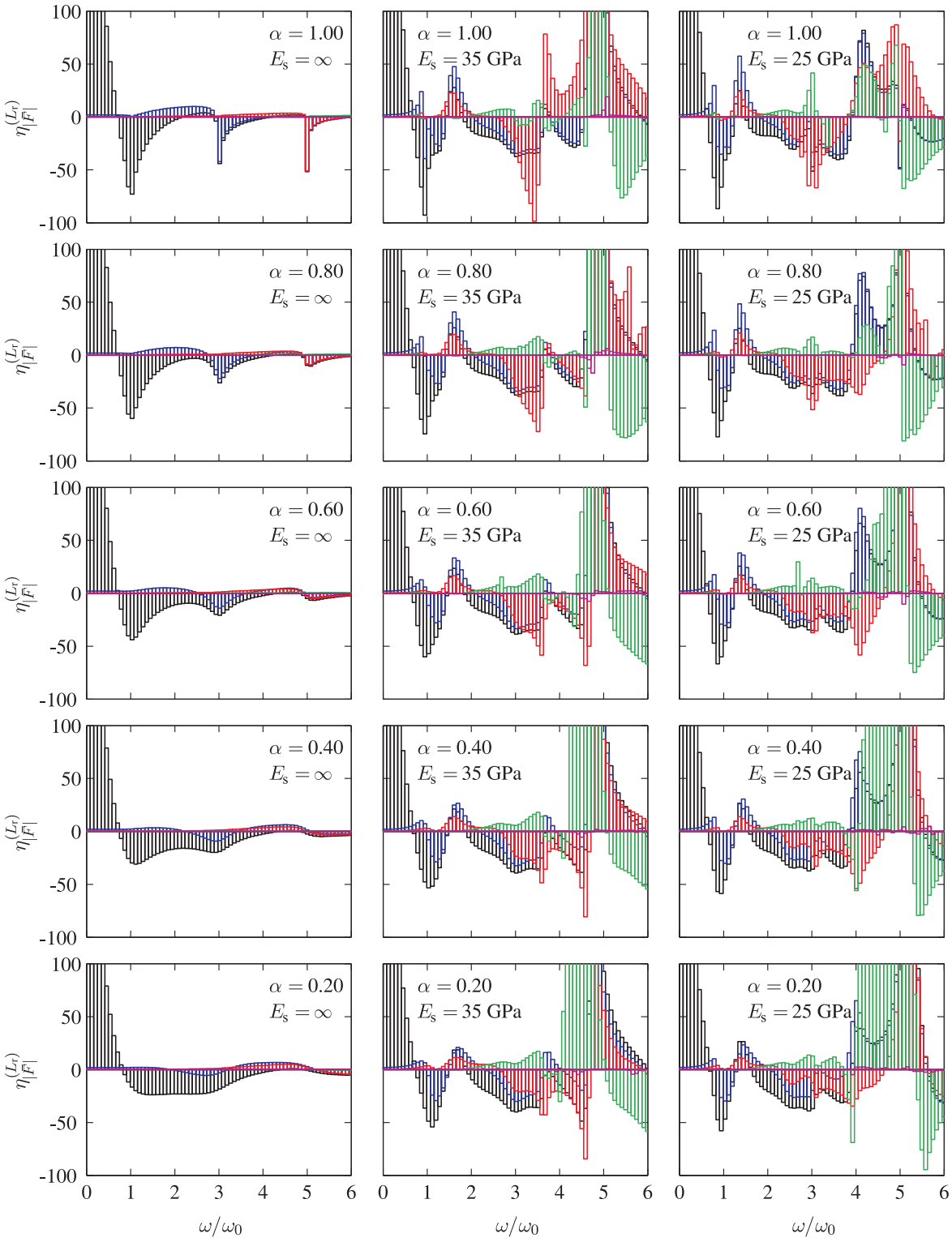

Figure A.16 Hydrodynamic force error estimators for a truncation length $L_r = 0.1H_r$. — Sommerfeld BC ; — Sharan BC ; — Analytical BC with $\widetilde{m}_r = 2$; — Analytical BC with $\widetilde{m}_r = 3$; — Analytical BC with $\widetilde{m}_r = 10$.

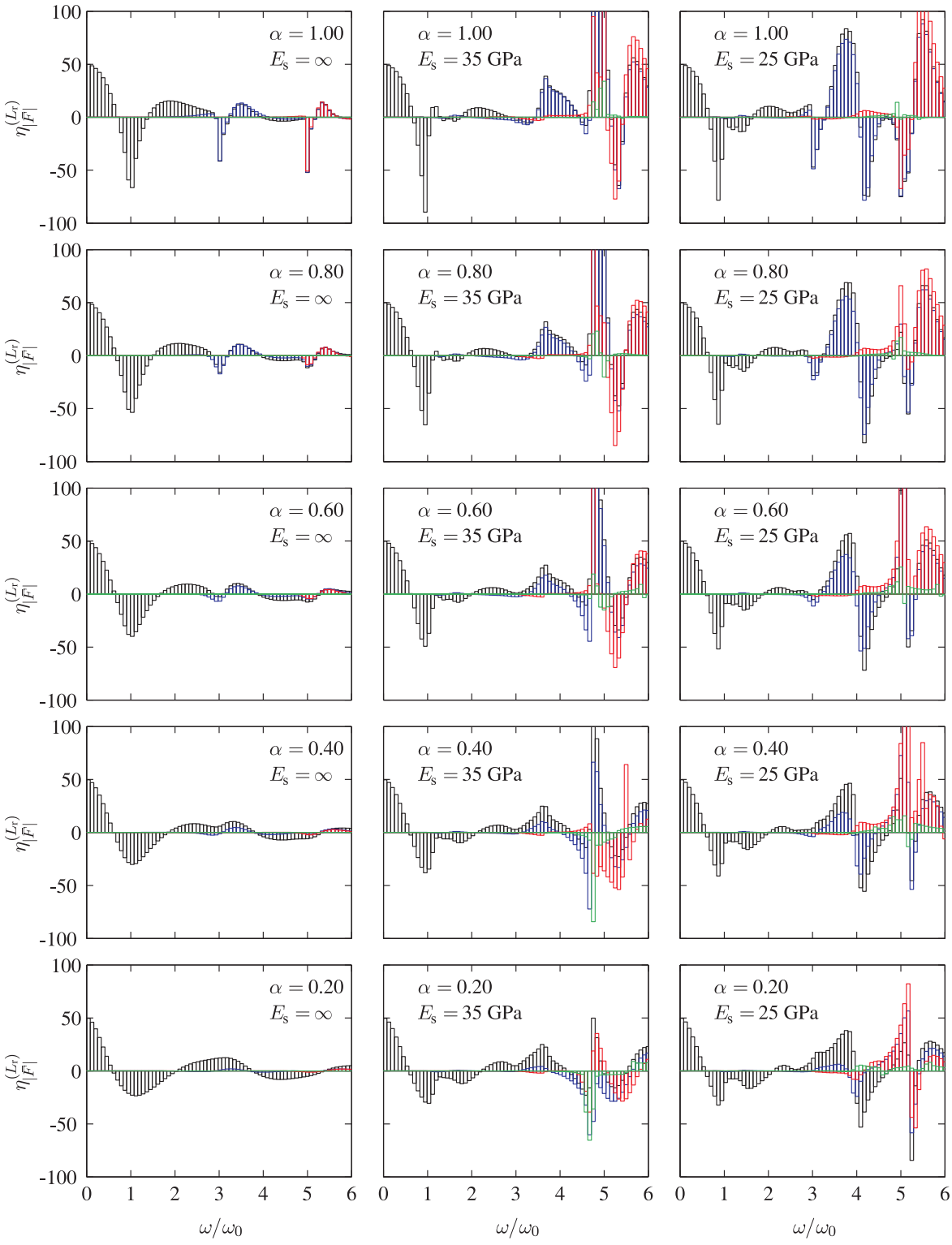

Figure A.17 Hydrodynamic force error estimators for a truncation length $L_r = 0.5H_r$. — Sommerfeld BC ; — Sharan BC ; — Analytical BC with $\widetilde{m}_r = 2$; — Analytical BC with $\widetilde{m}_r = 3$.

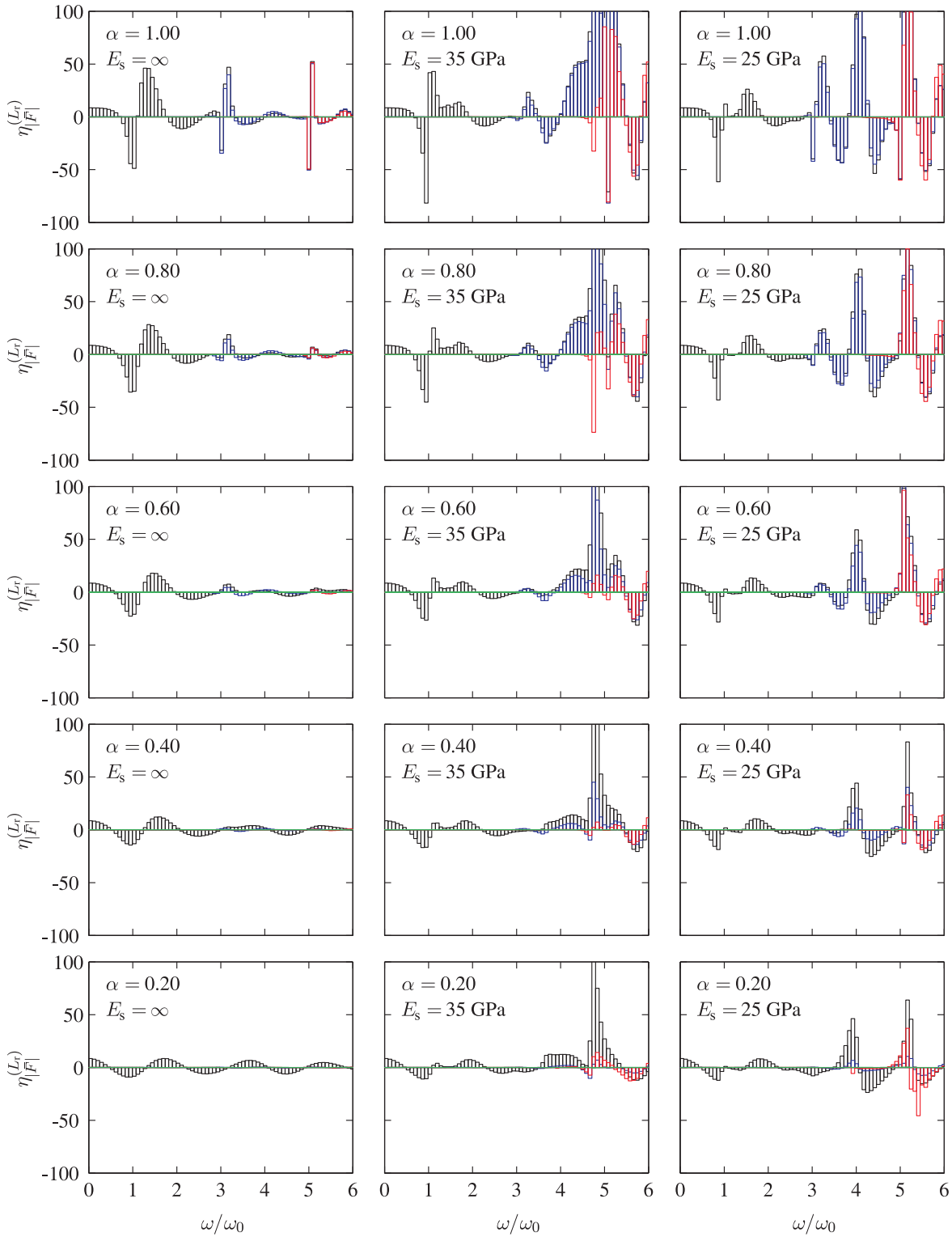

Figure A.18 Hydrodynamic force error estimators for a truncation length $L_\mathrm{r} = H_\mathrm{r}$. — Sommerfeld BC ; — Sharan BC ; — Analytical BC with $\widetilde{m}_\mathrm{r} = 2$; — Analytical BC with $\widetilde{m}_\mathrm{r} = 3$.

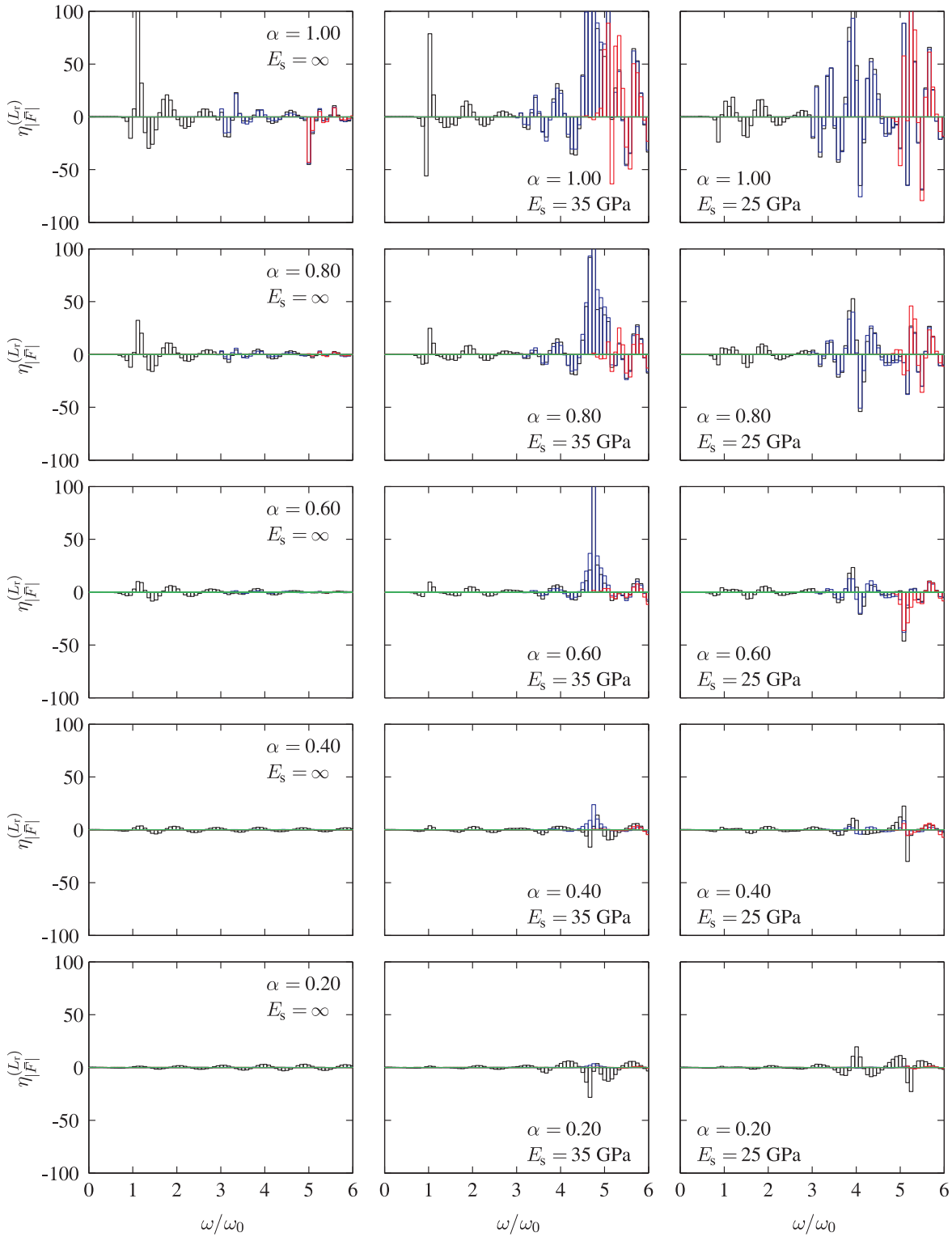

Figure A.19 Hydrodynamic force error estimators for a truncation length $L_r = 2H_r$. — Sommerfeld BC ; — Sharan BC ; — Analytical BC with $\widetilde{m}_r = 2$; — Analytical BC with $\widetilde{m}_r = 3$.

References

[1] H.M. Westergaard, Water pressures on dams during earthquakes, Transactions, ASCE 98 (1933) 418–472.

[2] A.K. Chopra, Earthquake response of concrete gravity dams. Report No. UCB/EERC-70/01, University of California, Berkeley, California, 1970.

[3] P. Chakrabarti, A.K. Chopra, Earthquake analysis of gravity dams including hydrodynamic interaction, Earthquake Engineering and Structural Dynamics 2 (1973) 143-–160.

[4] A.K. Chopra, Earthquake resistant design of concrete gravity dams, Journal of the Structural Division, ASCE 104 (1978) 953–971.

[5] J.F. Hall, A.K. Chopra, Two-dimensional dynamic analysis of concrete gravity and embankment dams including hydrodynamic effects, Earthquake Engineering and Structural Dynamics 10 (1982) 305–332.

[6] G. Fenves, A.K. Chopra, Earthquake analysis and response of concrete gravity dams. Report No. UCB/EERC-84/10, University of California, Berkeley, California, 1984.

[7] K.L. Fok, J.F. Hall, A.K. Chopra, EACD-3D, a computer program for three-dimensional earthquake analysis of concrete dams. Report No. UCB/EERC-86/09, University of California, Berkeley, California, 1986.

[8] S.S. Saini, P. Bettess, O.C. Zienkiewicz, Coupled hydrodynamic response of concrete gravity dams using finite and infinite elements, Earthquake Engineering and Structural Dynamics 6 (1978) 363–374.

[9] Ph. Liu, A. Cheng, Boundary solutions for fluid-structure interaction, Journal of Hydraulic Engineering, ASCE 110 (1984) 51–64.

[10] C.S. Tsai, G.C. Lee, Arch dam-fluid interactions : by FEM-BEM and substructure concept, International Journal of Numerical Methods in Engineering 24 (1987) 2367–2388.

[11] J.L. Humar, A.M. Jablonski, Boundary element reservoir model for seismic analysis of gravity dams, Earthquake Engineering and Structural Dynamics 16 (1988) 1129–1156.

[12] J.T. Xing, W.G. Price, M.J. Pomfret, L.H. Yam, Natural vibration of a beam-water interaction system, Journal of Sound and Vibration, 199 (1997) 491–512.

[13] O. Maeso, J.J. Aznarez, J. Dominguez, Three-dimensional models of reservoir sediment and effects on the seismic response of arch dams, Earthquake Engineering and Structural Dynamics 33 (2004) 1103–1123.

[14] Z. Duron, J. Hall, Experimental and finite element studies of the forced vibration response of Morrow Point Dam, Earthquake Engineering and Structural Dynamics 16 (1988) 1021—1039.

[15] J. Proulx, P. Paultre, J. Rheault, Y. Robert, An experimental investigation of water level effects on the dynamic behaviour of a large arch dam, Earthquake Engineering and Structural Dynamics 30 (2001) 1147–1166.

[16] N. Bouaanani, P. Paultre, J. Proulx, Two-dimensional modelling of ice-cover effects for the dynamic analysis of concrete gravity dams, Earthquake Engineering and Structural Dynamics 31 (2002) 2083–2102.

[17] A. Sommerfeld, Partial differential equations in physics. Academic Press, New York, 1949.

[18] O.C. Zienkiewicz, R.E. Newton, Coupled vibrations in a structure submerged in a compressible fluid, in : International Symposium on Finite Element Techniques, (Stuttgart, 1969).

[19] O.C. Zienkiewicz, D.W. Kelly, P. Bettes, The Sommerfeld (radiation) condition on infinite domains and its modelling in numerical procedures, in : Computing Methods in Applied Sciences and Engineering, Vol. I (1977) 169–203.

[20] J.T. Xing, Natural vibration of two-dimensional slender structure-water interaction systems subject to Sommerfeld radiation condition, Journal of Sound and Vibration, 308 (2007) 67–79.

[21] S.S. Saini, Coupled hydrodynamic response of a gravity dam using finite and infinite elements, in : Proceeding of the Seventh Symposium on Earthquake Engineering, Vol. 2 (Roorkee, India, 1982) 45–50.

[22] J. Humar, M. Roufaiel, Finite element analysis of reservoir vibration, Journal of Engineering Mechanics, ASCE 109 (1983) 215–230.

[23] S.K. Sharan, Finite element analysis of unbounded and incompressible fluid domains. International Journal of Numerical Methods in Engineering 21 (1985) 1659–1669.

[24] S.K. Sharan, Finite element modelling of infinite reservoirs, Journal of Engineering Mechanics, ASCE 111 (1985) 1457–1469.

[25] S.K. Sharan, A non-reflecting boundary in fluid-structure interaction, Journal of Computers and Structures 26 (1987) 841–846.

[26] S.K. Sharan, Efficient finite element analysis of hydrodynamic pressure on dams, Journal of Computers and Structures 42 (1992) 713–723.

[27] A.M. Jablonski, Effect of location of transmitting boundary on seismic hydrodynamic pressures on gravity dams, in : Proceedings of the Fourth U.S. National Conference on Earthquake Engineering (Palm Springs, California, 1990) 95–103.

[28] J. Lysmer, R.L. Kuhlemeyer, Finite dynamic model for infinite media, Journal of the Engineering Mechanics Division 95 (1969) 859-–877.

[29] Z. Celep, P. Bazant, Spurious reflection of elastic waves due to gradually changing finite element size, International Journal of Numerical Methods in Engineering 19 (1983) 631–646.

[30] D. Maity, S.K. Bhattacharyya, Time-domain analysis of infinite reservoir by finite element method using a novel far-boundary condition, Finite Elements in Analysis and Design 32 (1999) 85–96.

[31] M. Çetin, Y. Mengi, Transmitting boundary conditions suitable for analysis of dam-reservoir interaction and wave load problems, Applied Mathematical Modelling 27 (2003) 451–470.

[32] N. Bouaanani, P. Paultre, A new boundary condition for energy radiation in covered reservoirs using BEM, Engineering analysis with boundary elements 29 (2005) 903–911.

[33] D. Maity, A novel far-boundary condition for the finite element analysis of infinite reservoir, Applied Mathematics and Computation 170 (2005) 1314–1328.

[34] S. Küçükarslan, An exact truncation boundary condition for incompressible–unbounded infinite fluid domains, Applied Mathematics and Computation 163 (2005) 61—69.

[35] I. Gogoi, D. Maity, A non-reflecting boundary condition for the finite element modeling of infinite reservoir with layered sediment, Advances in Water Resources 29 (2006) 1515–1527.

[36] N. Bouaanani, P. Paultre, J. Proulx, A closed-form formulation for earthquake-induced hydrodynamic pressure on gravity dams, Journal of Sound and Vibration, 261 (2003) 573–582.

[37] MATLAB ®. The Mathworks, Inc., Natick, MA, USA, 2007.

[38] J.I. Bustamante, E. Rosenblueth, I. Herrera, A. Flores, Presión hydrodinámica en presas y depósitos. Boletin Sociedad Mexicana de Ingeneria Sismica, 1 (1963) 37–54.

[39] A.K. Chopra, Hydrodynamic pressures on dams during earthquakes. Journal of the Engineering Mechanics Division, ASCE 93 (1967) 205–223.

[40] N. Bouaanani, F.Y. Lu, Assessment of potential-based fluid finite elements for seismic analysis of dam–reservoir systems, Journal of Computers and Structures 87 (2009) 206–224.

[41] G. Fenves, A.K. Chopra, Simplified earthquake analysis of concrete gravity dams, Journal of Structural Engineering, ASCE 113 (1987) 1688–1708.

Appendix

The hydrodynamic pressure frequency response fonctions $\bar{p}_0^{(L_\mathrm{r})}$ and $\bar{p}_j^{(L_\mathrm{r})}$ are determined in this appendix for the TBCs given by Eqs. (A.32) and (A.33). For clarity and brevity, the following notation is used in this appendix

$$\bar{p}_\ell^{(L_\mathrm{r})}(x,y,\omega) = \begin{cases} \bar{p}_0^{(L_\mathrm{r})}(x,y,\omega) & \text{if} \quad \ell = 0 \qquad \text{(A.A.1)} \\ \bar{p}_j^{(L_\mathrm{r})}(x,y,\omega) & \text{if} \quad \ell = j \qquad \text{(A.A.2)} \end{cases}$$

and

$$f_0(y) = a_\mathrm{g}\,; \qquad \eta_0 = a_\mathrm{g} \qquad \text{(A.A.3)}$$

$$f_1(y) = \psi_j^{(x)}(y)\,; \qquad \eta_1 = 1 \qquad \text{(A.A.4)}$$

Throughout the appendix, subscript ℓ can take the values 0 or j.

Using the technique of separation of variables, hydrodynamic pressures can be expressed as

$$\bar{p}_\ell^{(L_\mathrm{r})}(x,y,\omega) = \bar{p}_{\ell x}^{(L_\mathrm{r})}(x,\omega)\,\bar{p}_{\ell y}^{(L_\mathrm{r})}(y,\omega) \qquad \text{(A.A.5)}$$

Substitution into Eq. (A.3) yields the two differential equations

$$\frac{\mathrm{d}^2\bar{p}_{\ell x}^{(L_\mathrm{r})}}{\mathrm{d}x^2} - \kappa^2\bar{p}_{\ell x}^{(L_\mathrm{r})} = 0 \tag{A.A.6}$$

$$\frac{\mathrm{d}^2\bar{p}_{\ell y}^{(L_\mathrm{r})}}{\mathrm{d}y^2} + \lambda^2\bar{p}_{\ell y}^{(L_\mathrm{r})} = 0 \tag{A.A.7}$$

where λ and κ are complex constants related by

$$\kappa^2 = \lambda^2 - \frac{\omega^2}{C^2} \tag{A.A.8}$$

The general solutions of Eqs. (A.A.7) and (A.A.6) can be written respectively as

$$\bar{p}_{\ell x}^{(L_\mathrm{r})}(x,\omega) = \gamma_1^{(\ell)}(\omega)\, e^{-\kappa x} + \gamma_2^{(\ell)}(\omega)\, e^{\kappa x} \tag{A.A.9}$$

$$\bar{p}_{\ell y}^{(L_\mathrm{r})}(y,\omega) = \gamma_3^{(\ell)}(\omega)\, \mathrm{e}^{-\mathrm{i}\lambda y} + \gamma_4^{(\ell)}(\omega)\, \mathrm{e}^{\mathrm{i}\lambda y} \tag{A.A.10}$$

where the coefficients $\gamma_1^{(\ell)}(\omega)$, $\gamma_2^{(\ell)}(\omega)$, $\gamma_3^{(\ell)}(\omega)$ and $\gamma_4^{(\ell)}(\omega)$ are to be determined by imposing the boundary conditions.

Using the transformations of Eq. (C.A.5) into Eqs. (A.9) and (A.10), we obtain the boundary conditions to be satisfied by $\bar{p}_{\ell y}^{(L_\mathrm{r})}$

$$\frac{\mathrm{d}\bar{p}_{\ell y}^{(L_\mathrm{r})}}{\mathrm{d}y}(0,\omega) = \mathrm{i}\omega q\bar{p}_{\ell y}^{(L_\mathrm{r})}(0,\omega) \tag{A.A.11}$$

$$\bar{p}_{\ell y}^{(L_\mathrm{r})}(H_\mathrm{r},\omega) = 0 \tag{A.A.12}$$

Substituting $\bar{p}_{\ell y}^{(L_\mathrm{r})}(y,\omega)$ by its expression in Eq. (C.A.7) into Eqs. (C.A.9) and (C.A.10) yields Eq. (A.18) to be satisfied by the eigenvalues $\lambda_n(\omega)$. The associated eigenvectors Y_n, $n = 1 \ldots m_\mathrm{r}$ are given by Eq. (C.A.12) and they satisfy the orthogonality relations

$$\int_0^{H_\mathrm{r}} Y_s(y,\omega)\, Y_n(y,\omega)\, \mathrm{d}y = \begin{cases} 0 & \text{if} \quad s \neq n \qquad \text{(A.A.13)} \\ \dfrac{\beta_n(\omega)}{2\lambda_n^2(\omega)} & \text{if} \quad s = n \qquad \text{(A.A.14)} \end{cases}$$

Using Eq. (C.A.6), the hydrodynamic pressure can be expressed as the summation

$$\begin{aligned}\bar{p}_\ell^{(L_\mathrm{r})}(x,y,\omega) &= \sum_{n=1}^{\infty}\Big[\gamma_{1,n}^{(\ell)}(\omega)\,\mathrm{e}^{-\kappa_n(\omega)x}+\gamma_{2,n}^{(\ell)}(\omega)\,\mathrm{e}^{\kappa_n(\omega)x}\Big]Y_n(y,\omega)\\ &\approx \sum_{n=1}^{m_\mathrm{r}}\Big[\gamma_{1,n}^{(\ell)}(\omega)\,\mathrm{e}^{-\kappa_n(\omega)x}+\gamma_{2,n}^{(\ell)}(\omega)\,\mathrm{e}^{\kappa_n(\omega)x}\Big]Y_n(y,\omega)\end{aligned} \tag{A.A.15}$$

where the complex coefficients $\kappa_n(\omega)$ are given by Eq. (A.20) and m_r is the number of reservoir modes.

Coefficients $\gamma_{1,n}^{(\ell)}(\omega)$ and $\gamma_{2,n}^{(\ell)}(\omega)$ are to be determined by imposing the boundary conditions at dam upstream face [Eqs. (A.8)] and at the reservoir truncation boundary [Eqs. (A.32) and (A.33)]

$$\frac{\partial\bar{p}_\ell^{(L_\mathrm{r})}}{\partial x}(0,y,\omega) = -\rho_\mathrm{r} f_\ell(y) \tag{A.A.16}$$

$$\frac{\partial\bar{p}_\ell^{(L_\mathrm{r})}}{\partial x}(-L_\mathrm{r},y,\omega) = \theta_\ell^{(L_\mathrm{r})}(y,\omega)\,\bar{p}_\ell^{(L_\mathrm{r})}(-L_\mathrm{r},y,\omega) \tag{A.A.17}$$

which yields after substitution of Eq. (C.A.18)

$$\sum_{n=1}^{m_\mathrm{r}}\kappa_n(\omega)\Big[\gamma_{1,n}^{(\ell)}(\omega)-\gamma_{2,n}^{(\ell)}(\omega)\Big]Y_n(y,\omega) = \rho_\mathrm{r} f_\ell(y) \tag{A.A.18}$$

$$\begin{aligned}\sum_{n=1}^{m_\mathrm{r}}\Big\{&\gamma_{1,n}^{(\ell)}(\omega)\Big[\kappa_n(\omega)+\theta_\ell^{(L_\mathrm{r})}(y,\omega)\Big]\mathrm{e}^{\kappa_n(\omega)L_\mathrm{r}}\\ &-\gamma_{2,n}^{(\ell)}(\omega)\Big[\kappa_n(\omega)-\theta_\ell^{(L_\mathrm{r})}(y,\omega)\Big]\mathrm{e}^{-\kappa_n(\omega)L_\mathrm{r}}\Big\}Y_n(y,\omega)=0\end{aligned} \tag{A.A.19}$$

Multiplying Eq. (A.A.18) by eigenvectors $Y_s(y,\omega),\ s=1\ldots m_\mathrm{r}$, integrating over reservoir height H_r and using the orthogonality relationships in Eqs. (A.A.13) and (A.A.14) gives

$$\gamma_{2,n}^{(\ell)}(\omega) = \gamma_{1,n}^{(\ell)}(\omega) - 2\rho_\mathrm{r}\eta_\ell H_\mathrm{r}\frac{\lambda_n^2(\omega)}{\beta_n(\omega)}\frac{I_{\ell\,n}(\omega)}{\kappa_n(\omega)} \tag{A.A.20}$$

Replacing into Eq. (A.A.19) yields

$$\begin{aligned}\sum_{n=1}^{m_\mathrm{r}}\Big\{\kappa_n\Big[\mathrm{e}^{-\kappa_n(\omega)L_\mathrm{r}}-\mathrm{e}^{\kappa_n(\omega)L_\mathrm{r}}\Big]-\Big[\mathrm{e}^{-\kappa_n(\omega)L_\mathrm{r}}+\mathrm{e}^{\kappa_n(\omega)L_\mathrm{r}}\Big]\theta_\ell^{(L_\mathrm{r})}(y,\omega)\Big\}Y_n(y,\omega)\,\gamma_{1,n}^{(\ell)}(\omega)\\ = 2\rho_\mathrm{r}\eta_\ell H_\mathrm{r}\sum_{n=1}^{m_\mathrm{r}}\frac{\lambda_n^2(\omega)}{\beta_n(\omega)}\frac{I_{\ell\,n}(\omega)}{\kappa_n(\omega)}\mathrm{e}^{-\kappa_n(\omega)L_\mathrm{r}}\Big[\kappa_n(\omega)-\theta_\ell^{(L_\mathrm{r})}(y,\omega)\Big]Y_n(y,\omega)\end{aligned} \tag{A.A.21}$$

Both sides of this equation can then be multiplied by eigenvectors $Y_s(y,\omega),\ s = 1 \dots m_\mathrm{r}$, and integrated over reservoir height H_r to obtain the system of linear equations

$$\mathbf{A}^{(\ell)}\,\mathbf{\Gamma}^{(\ell)} = \mathbf{B}^{(\ell)} \tag{A.A.22}$$

in which the elements of matrix $\mathbf{A}^{(\ell)}$ and vectors $\mathbf{\Gamma}^{(\ell)}$ and $\mathbf{B}^{(\ell)}$ are defined for $n = 1 \dots m_\mathrm{r}$ and $s = 1 \dots m_\mathrm{r}$ as

$$\Gamma_n^{(\ell)} = \gamma_{1,n}^{(\ell)}(\omega)\,; \tag{A.A.23}$$

$$\begin{aligned} A_{sn}^{(\ell)}(\omega) = {} & \frac{\kappa_n(\omega)\,\beta_n(\omega)}{2\lambda_n^2(\omega)}\Big[\mathrm{e}^{-\kappa_n(\omega)L_\mathrm{r}} - \mathrm{e}^{\kappa_n(\omega)L_\mathrm{r}}\Big]\delta_{sn} \\ & - \Big[\mathrm{e}^{-\kappa_n(\omega)L_\mathrm{r}} + \mathrm{e}^{\kappa_n(\omega)L_\mathrm{r}}\Big]\int_0^{H_\mathrm{r}} \theta_\ell^{(L_\mathrm{r})}(y,\omega)\,Y_s(y,\omega)\,Y_n(y,\omega)\,\mathrm{d}y \end{aligned} \tag{A.A.24}$$

$$\begin{aligned} B_s^{(\ell)}(\omega) = 2\rho_\mathrm{r}\eta_\ell H_\mathrm{r}\sum_{n=1}^{m_\mathrm{r}} \frac{\lambda_n^2(\omega)}{\beta_n(\omega)}\frac{I_{\ell\,n}(\omega)}{\kappa_n(\omega)}\Bigg[& \frac{\kappa_n(\omega)\,\beta_n(\omega)}{2\lambda_n^2(\omega)}\,\delta_{sn} \\ & - \int_0^{H_\mathrm{r}} \theta_\ell^{(L_\mathrm{r})}(y,\omega)\,Y_s(y,\omega)\,Y_n(y,\omega)\,\mathrm{d}y\Bigg]\,\mathrm{e}^{-\kappa_n(\omega)L_\mathrm{r}} \end{aligned} \tag{A.A.25}$$

where δ is the Kronecker symbol. Eq. (C.A.18) transforms then to

$$\begin{aligned} \bar{p}_\ell^{\,(L_\mathrm{r})}(x,y,\omega) &= \sum_{n=1}^{m_\mathrm{r}} \left\{ \Big[\mathrm{e}^{-\kappa_n(\omega)\,x} + \mathrm{e}^{\kappa_n(\omega)\,x}\Big]\,\Gamma_n^{(\ell)}(\omega) - 2\rho_\mathrm{r}\eta_\ell H_\mathrm{r}\frac{\lambda_n^2(\omega)}{\beta_n(\omega)}\frac{I_{\ell n}(\omega)}{\kappa_n(\omega)}\,\mathrm{e}^{\kappa_n(\omega)\,x}\right\} Y_n(y,\omega) \\ &= \bar{p}_\ell^{\,(\infty)}(x,y,\omega) + \sum_{n=1}^{m_\mathrm{r}} \Big[\mathrm{e}^{-\kappa_n(\omega)\,x} + \mathrm{e}^{\kappa_n(\omega)\,x}\Big]\,\Gamma_n^{(\ell)}(\omega)\,Y_n(y,\omega) \end{aligned} \tag{A.A.26}$$

If the functions $\theta_\ell^{(L_\mathrm{r})}$ were assumed constant over reservoir height, i.e. independent of the y coordinate, the integrals in Eqs. (A.A.24) and (A.A.25) become by virtue of orthogonality relations of eigenvectors Y_n

$$\int_0^{H_\mathrm{r}} \theta_\ell^{(L_\mathrm{r})}(\omega)\,Y_s(y,\omega)\,Y_n(y,\omega)\,\mathrm{d}y = \frac{\beta_n(\omega)}{2\lambda_n^2(\omega)}\,\theta_\ell^{(L_\mathrm{r})}(\omega)\,\delta_{sn} \tag{A.A.27}$$

Replacing into Eq.(A.A.24) shows that matrix $\mathbf{A}^{(\ell)}$ is diagonal in this case, with elements

given by

$$A_{sn}^{(\ell)}(\omega) = \frac{\beta_n(\omega)}{2\lambda_n^2(\omega)} \left\{ \left[\mathrm{e}^{-\kappa_n(\omega)L_\mathrm{r}} - \mathrm{e}^{\kappa_n(\omega)L_\mathrm{r}} \right] \kappa_n(\omega) - \left[\mathrm{e}^{-\kappa_n(\omega)L_\mathrm{r}} + \mathrm{e}^{\kappa_n(\omega)L_\mathrm{r}} \right] \theta_\ell^{(L_\mathrm{r})}(\omega) \right\} \delta_{sn} \tag{A.A.28}$$

Replacing Eq.(A.A.27) into Eq.(A.A.25), the elements of vector $\mathbf{B}^{(\ell)}$ also simplify to

$$B_s^{(\ell)}(\omega) = \rho_\mathrm{r}\eta_\ell H_\mathrm{r} \frac{I_{\ell\, s}(\omega)}{\kappa_s(\omega)} \left[\kappa_s(\omega) - \theta_\ell^{(L_\mathrm{r})}(\omega) \right] \mathrm{e}^{-\kappa_s(\omega)L_\mathrm{r}} \tag{A.A.29}$$

The solution of the system of equations (A.A.22) is then obtained as

$$\begin{aligned} \gamma_{1,n}^{(\ell)}(\omega) &= \frac{B_n^{(\ell)}(\omega)}{A_{nn}^{(\ell)}(\omega)} \\ &= \frac{2\rho_\mathrm{r}\eta_\ell H_\mathrm{r}}{\beta_n(\omega)\,\kappa_n(\omega)} \frac{\lambda_n^2(\omega)\, I_{\ell\, n}(\omega) \left[\kappa_n(\omega) - \theta_\ell^{(L_\mathrm{r})}(\omega) \right] \mathrm{e}^{-\kappa_n(\omega)L_\mathrm{r}}}{\left\{ \left[\mathrm{e}^{-\kappa_n(\omega)L_\mathrm{r}} - \mathrm{e}^{\kappa_n(\omega)L_\mathrm{r}} \right] \kappa_n(\omega) - \left[\mathrm{e}^{-\kappa_n(\omega)L_\mathrm{r}} + \mathrm{e}^{\kappa_n(\omega)L_\mathrm{r}} \right] \theta_\ell^{(L_\mathrm{r})}(\omega) \right\}} \end{aligned} \tag{A.A.30}$$

Substituting into Eq. (A.A.20) and then Eq. (C.A.18), yields the hydrodynamic pressure

$$\bar{p}_\ell^{(L_\mathrm{r})}(x, y, \omega) = -2\rho_\mathrm{r}\eta_\ell H_\mathrm{r} \sum_{n=1}^{m_\mathrm{r}} \frac{\lambda_n^2(\omega)}{\beta_n(\omega)} \frac{I_{\ell\, n}(\omega)}{\kappa_n(\omega)} X_{\ell\, n}^{(L_\mathrm{r})}(x, \omega)\, Y_n(y, \omega) \tag{A.A.31}$$

where

$$X_{\ell\, n}^{(L_\mathrm{r})}(x, \omega) = \frac{\mathrm{e}^{\kappa_n(\omega)(x+L_\mathrm{r})} + \zeta_{\ell\, n}^{(L_\mathrm{r})}(\omega)\, \mathrm{e}^{-\kappa_n(\omega)(x+L_\mathrm{r})}}{\mathrm{e}^{\kappa_n(\omega)L_\mathrm{r}} - \zeta_{\ell\, n}^{(L_\mathrm{r})}(\omega)\, \mathrm{e}^{-\kappa_n(\omega)L_\mathrm{r}}} \tag{A.A.32}$$

and

$$\zeta_{\ell\, n}^{(L_\mathrm{r})}(\omega) = \frac{\kappa_n(\omega) - \theta_\ell^{(L_\mathrm{r})}(\omega)}{\kappa_n(\omega) + \theta_\ell^{(L_\mathrm{r})}(\omega)} \tag{A.A.33}$$

ANNEXE B

Étapes de calcul pour la méthode pseudo-dynamique

Dans cette annexes, nous décrivons les étapes de calculs pour l'utilisation de la méthode pseudo-dynamique développée au cours de cette thèse. Cette méthode peut être utilisée pour réaliser une analyse spectrale ou bien calculer les courbes de réponses en fréquence de quantité d'intérêts. Ces deux méthodes sont présentée.

B.1 Réponse spectrale

- Étape 1. Modéliser la section du barrage dans un logiciel d'éléments-finis. Insérer les propriétés dynamiques des matériaux (E_s, ρ_s, coefficient de poisson). Descritiser le barrage et choisir une hypothèse de contraintes ou déformations planes. Effectuer une analyse modale et récupérer les résultats suivant : L_1, $\psi_1^{(x)}(0,y)$ et ω_1. Si le mode fondamental est normalisé par rapport à la masse alors $M_1 = 1$, sinon récupérer M_1. Cette étape peut être omise si on utilise des propriétés dynamiques existantes dans la littérature telles que [5]
- Étape 2. Approximer le mode fondamental par une équation cubique :

$$\psi_1^{(x)}(0,y) = a_1 \frac{y}{H_\mathrm{s}} + a_2 \left(\frac{y}{H_\mathrm{s}}\right)^2 + a_3 \left(\frac{y}{H_\mathrm{s}}\right)^3$$

- Étape 3. Calculer :

$$\begin{aligned}
\omega_0 =& \frac{\pi\, C_\mathrm{r}}{2\, H_\mathrm{r}}\,; \quad \eta = \frac{H_\mathrm{r}}{H_\mathrm{s}} \\
F_1(\eta) =& \eta a_1 + \left(1 - \frac{8}{\pi^2}\right)\eta^2 a_2 + \left(1 - \frac{24}{\pi^2}\right)\eta^3 a_3 \\
G_1(\eta) =& -\frac{4\eta}{\pi^2}\left(a_1 - \frac{24\eta^2}{\pi^2}\, a_3\right) \\
\varphi(\eta) =& \eta^4 \Big[8.735 a_1^2 + 14.059 a_1 a_2 \eta + \left(5.776 a_2^2 + 11.172 a_1 a_3\right)\eta^2 \\
& + 9.343 a_2 a_3 \eta^3 + 3.840 a_3^2 \eta^4\Big] \times 10^{-3} \\
\theta(\eta) =& \eta^3 \left(3.795 a_1 + 3.105 a_2 \eta + 2.500 a_3 \eta^2\right) \times 10^{-3}
\end{aligned}$$

– Étape 4. Calculer $R_1 = \omega_1/\omega_0$ et les coefficients

$$A_0 = 1 + \frac{4\rho_{\mathrm{r}} H_{\mathrm{s}}^2\, \varphi(\eta)}{M_1}\,; \quad A_1 = A_0^2$$

$$A_2 = -\,A_0\left(A_0 + 2R_1^2\right) + \left\{\frac{4\rho_{\mathrm{r}}\eta^2 H_{\mathrm{s}}^2}{M_1\pi^3}\Big[2F_1(\eta) + \pi\, G_1(\eta)\Big]^2\right\}^2$$

$$A_3 = R_1^2\left(2A_0 + R_1^2\right)\,; \quad A_4 = -R_1^4$$

$$D_1 = \frac{A_3}{A_1} - \frac{1}{3}\left(\frac{A_2}{A_1}\right)^2\,; \quad D_2 = \frac{2}{27}\left(\frac{A_2}{A_1}\right)^3 - \frac{A_2 A_3}{3A_1^2} + \frac{A_4}{A_1}$$

$$\Delta = \left(\frac{D_1}{3}\right)^3 + \left(\frac{D_2}{2}\right)^2$$

$$U = \left(-\frac{D_2}{2} + \sqrt{\Delta}\right)^{1/3}\,; \quad V = -\frac{1}{3}\frac{D_1}{U}\,; \quad \tau = -\frac{1}{2} + \mathrm{i}\,\frac{\sqrt{3}}{2}$$

$$\Gamma_1 = U + V\,; \quad \Gamma_2 = \tau\, U + \tau^2\, V\,; \quad \Gamma_3 = \tau^2\, U + \tau\, V$$

– Étape 5. Déterminer Γ^* comme étant la seule solution réel parmis Γ_1, Γ_2 et Γ_3 qui satisfait

$$\frac{1}{3}\frac{A_2}{A_1} \leqslant \Gamma^* \leqslant R_1^2 + \frac{1}{3}\frac{A_2}{A_1}$$

– Étape 6. Calculer la fréquence ω_{r} et période $\widetilde{T}_{\mathrm{r}}$ fondamentales du système barrage-réservoir données par

$$\omega_{\mathrm{r}} = \omega_0\sqrt{\Gamma^* - \frac{1}{3}\frac{A_2}{A_1}}\,; \qquad \widetilde{T}_{\mathrm{r}} = \frac{2\pi}{\omega_0\sqrt{\Gamma^* - \dfrac{1}{3}\dfrac{A_2}{A_1}}}$$

– Étape 7. Calculer pour $\omega = 0$ et $\omega = \omega_{\mathrm{r}}$

$$B_{1,1}(\omega) = 4\rho_{\mathrm{r}}\eta^2 H_{\mathrm{s}}^2 \, \frac{\left[2F_1(\eta) + \pi\, G_1(\eta)\right]^2}{\pi^3 \sqrt{1 - \dfrac{\omega^2}{\omega_0^2}}} \, ; \quad B_{0,1}(\omega) = 8\rho_{\mathrm{r}}\eta^2 H_{\mathrm{s}}^2 \, \frac{\left[2F_1(\eta) + \pi\, G_1(\eta)\right]}{\pi^3 \sqrt{1 - \dfrac{\omega^2}{\omega_0^2}}}$$

$$B_1(\omega) = B_{1,1}(\omega) + 4\rho_{\mathrm{r}} H_{\mathrm{s}}^2 \, \varphi(\eta) \, ; \quad B_0(\omega) = B_{0,1}(\omega) + 8\rho_{\mathrm{r}} H_{\mathrm{s}}^2 \, \theta(\eta)$$

$$\widetilde{L}_1(\omega) = L_1 + B_0(\omega) \, ; \quad \widetilde{M_1}(\omega) = M_1 + \mathrm{Re}\big[B_1(\omega)\big]$$

$$\widetilde{\xi}_{\mathrm{r}}(\omega) = \frac{2\,\omega_1\,\xi\, M_1 - \omega\, \mathrm{Im}\big[B_1(\omega)\big]}{2\,\omega_{\mathrm{r}} \left\{M_1 + \mathrm{Re}\big[B_1(\omega)\big]\right\}}$$

– Étape 8. Calculer pour $\omega = 0$ et $\omega = \omega_{\mathrm{r}}$ et pour chaque hauteur des noeuds à la paroie amont du barrage :

$$D_0(y) = 2.8058 \left(\frac{y}{H_{\mathrm{r}}}\right)^5 - 5.3611 \left(\frac{y}{H_{\mathrm{r}}}\right)^4 + 4.2307 \left(\frac{y}{H_{\mathrm{r}}}\right)^3 - 1.9243 \left(\frac{y}{H_{\mathrm{r}}}\right)^2 + 0.1504 \left(\frac{y}{H_{\mathrm{r}}}\right) + 0.0803$$

$$\bar{p}_0(0, y, \omega) = \frac{8\,\rho_{\mathrm{r}}\,\eta\, H_{\mathrm{s}}}{\pi^2} \left[D_0(y) - \frac{\cos\left(\dfrac{\pi\, y}{2\, H_{\mathrm{r}}}\right)}{\sqrt{1 - \dfrac{\omega^2}{\omega_0^2}}} \right]$$

$$
\begin{aligned}
D_1(y) =& 3.0879\left(\frac{y}{H_\mathrm{r}}\right)^5 - 6.3542\left(\frac{y}{H_\mathrm{r}}\right)^4 + 5.4887\left(\frac{y}{H_\mathrm{r}}\right)^3 \\
& - 2.4592\left(\frac{y}{H_\mathrm{r}}\right)^2 + 0.1052\left(\frac{y}{H_\mathrm{r}}\right) + 0.1138 \\
D_2(y) =& 2.9376\left(\frac{y}{H_\mathrm{r}}\right)^5 - 5.6640\left(\frac{y}{H_\mathrm{r}}\right)^4 + 4.3598\left(\frac{y}{H_\mathrm{r}}\right)^3 \\
& - 1.8771\left(\frac{y}{H_\mathrm{r}}\right)^2 + 0.1544\left(\frac{y}{H_\mathrm{r}}\right) + 0.0713 \\
D_3(y) =& 3.1687\left(\frac{y}{H_\mathrm{r}}\right)^5 - 6.1118\left(\frac{y}{H_\mathrm{r}}\right)^4 + 4.3463\left(\frac{y}{H_\mathrm{r}}\right)^3 \\
& - 1.6242\left(\frac{y}{H_\mathrm{r}}\right)^2 + 0.1565\left(\frac{y}{H_\mathrm{r}}\right) + 0.0463 \\
\bar{p}_1(0,y,\omega) =& \frac{8\,\rho_\mathrm{r}\,\eta^2\,H_\mathrm{s}}{\pi^2}\big[a_1\,D_1(y) + a_2\,\eta\,D_2(y) + a_3\,\eta^2\,D_3(y) \\
& - \frac{2F_1(\eta) + \pi\,G_1(\eta)}{2\,\eta\sqrt{1-\dfrac{\omega^2}{\omega_0^2}}}\cos\left(\frac{\pi\,y}{2\,H_\mathrm{r}}\right)\big]
\end{aligned}
$$

– Étape 9. Calculer

$$
f_1(y) = \frac{\widetilde{L}_1(\omega_\mathrm{r})}{\widetilde{M}_1(\omega_\mathrm{r})}\,S_\mathrm{a}\big(\widetilde{T}_1,\widetilde{\xi}_1\big)\left\{\mu_\mathrm{s}(y)\left[a_1\frac{y}{H_\mathrm{s}} + a_2\left(\frac{y}{H_\mathrm{s}}\right)^2 + a_3\left(\frac{y}{H_\mathrm{s}}\right)^3\right] - \bar{p}_1(0,y,\omega_\mathrm{r})\right\}
$$

où $S_\mathrm{a}\big(\widetilde{T}_\mathrm{r},\widetilde{\xi}_1(\omega_\mathrm{r})\big)$ est la pseudo-accélération obtenue par le spectre de dimensionnement pour une période de $\widetilde{T}_\mathrm{r}=2\,\pi/\omega_\mathrm{r}$ et un ratio d'amortissement de $\widetilde{\xi}_1(\omega_\mathrm{r})$.

– Étape 10. Appliquer les forces sur la face amont du modèle éléments finis, et en réalisant une analyse statique, récupérer les résultats d'intéret r_1

– Étape 11. Calculer les forces statiques associées aux modes de vibrations supérieurs :

$$
\begin{aligned}
f_\mathrm{sc}(y) = \ddot{x}_\mathrm{g}^{(\max)}\Bigg\{&\mu_\mathrm{s}(y)\Bigg[1 - \frac{L_1}{M_1}\left(a_1\frac{y}{H_\mathrm{s}} + a_2\left(\frac{y}{H_\mathrm{s}}\right)^2 + a_3\left(\frac{y}{H_\mathrm{s}}\right)^3\right)\Bigg] \\
&- \left[\bar{p}_0(0,y,0) - \frac{\mu_\mathrm{s}(y)}{M_1}\left[a_1\frac{y}{H_\mathrm{s}} + a_2\left(\frac{y}{H_\mathrm{s}}\right)^2 + a_3\left(\frac{y}{H_\mathrm{s}}\right)^3\right]B_0(0)\right]\Bigg\}
\end{aligned}
$$

où $\ddot{x}_{\mathrm{g}}^{(\max)}$ est l'accélération maximale.

– Étape 12. Appliquer les forces sur la face amont du modèle éléments finis, et en réalisant une analyse statique, récupérer les résultats d'intéret r_{sc}
– Étape 13. Combiner les résultats précedent pour calculer la valeur total de la quantitée d'intéret $r_{\max}$ donnée par

$$r_{\max} = r_{\mathrm{st}} \pm \sqrt{r_1^2 + r_{\mathrm{sc}}^2}$$

où r_{st} est la valeur statique de la quantité d'interet.

B.2 Réponse fréquentielle

– Étape 1. Suivre les étapes 1 à 6 précédentes
– Étape 2. Calculer pour chaque ω d'intérêts les étapes 7 et 8 précédentes
– Étape 3. Calculer pour chaque ω d'intérêts :

$$\bar{Z}_1(\omega) = \frac{-\widetilde{L}_1(\omega)}{-\omega^2\,\widetilde{M}_1(\omega) + 2\,\mathrm{i}\,\omega\,\omega_{\mathrm{r}}\,\widetilde{\xi}_{\mathrm{r}}(\omega)\,\widetilde{M}_1(\omega) + \omega_1^2\,M_1}$$

– Étape 4. Calculer pour chaque ω d'intérêts la pressions, les déplacements, vitesses, accélérations ou forces.

ANNEXE C

Seismic response of asymmetric rectangular liquid containing structures

Najib Bouaanani [1], M.ASCE ; **Damien Goulmot** [2] and **Benjamin Miquel** [3]

Paper accepted in *Journal of Engineering Mechanics* (ASCE)

Submitted 30 October 2011. Accepted 22 February 2012.

A new formulation to investigate the seismic response of symmetric and asymmetric rectangular liquid-containing structures is developed and validated in this paper. The proposed method is based on a sub-structuring approach, where the flexible containing structure is modeled using finite elements, while the impulsive effects of the fluid domain are modeled analytically through interaction forces at the fluid-structure interfaces. The technique takes account of geometrical or material asymmetry of the containing structure, fluid compressibility, and energy dissipation through reservoir bottom absorption. The formulation is presented in such a way that it can be easily coded into a practical and computationally efficient program and is applied to illustrative examples highlighting the effects of geometrical and material asymmetry on the dynamic responses of liquid-containing structures. The obtained frequency- and time-domain results are successfully validated against advanced finite element analyses.

1. Associate Professor, Department of Civil, Geological and Mining Engineering, École Polytechnique de Montréal, Montréal, QC H3C 3A7, Canada
Corresponding author. E-mail : najib.bouaanani@polymtl.ca

2. Graduate Research Assistant, Department of Civil, Geological and Mining Engineering, École Polytechnique de Montréal, Montréal, QC H3C 3A7, Canada.

3. Graduate Research Assistant, Department of Civil, Geological and Mining Engineering, École Polytechnique de Montréal, Montréal, QC H3C 3A7, Canada.

C.1 Introduction

The dynamic response of liquid containing structures has been extensively investigated since the early works of Hoskins and Jacobsen (1934), Jacobsen (1949), Werner and Sundquist (1949), Jacobsen and Ayre (1951), Graham and Rodriguez (1952), and Housner (1957, 1963). The continuous impetus for more refined research on this topic has been sustained by severe damage to liquid containing structures caused by events such as the 1960 Chilean earthquakes (Steinbrugge, 1963), the 1964 Alaska earthquake (Hanson, 1973), the 1994 Northridge earthquake (Hall, 1995), and the 1999 Turkey earthquake (Steinberg and Cruz, 2004). During such events, liquid containing structures must be damage-proof to avoid spillage of hazardous materials such as toxic chemicals and highly inflammable products. Water storage tanks are also crucial post-earthquake lifeline structures, providing water to extinguish fires occurring in the aftermath of earthquakes, as well as safe supplies of drinking water.

The authors of the earlier studies (Jacobsen, 1949, Werner and Sundquist, 1949, Jacobsen and Ayre, 1951, Housner, 1957, Housner, 1963) developed analytical methods to evaluate the effects of dynamic fluid pressure assuming that the containers are rigid, and that the fluid is incompressible and inviscid, with its motion limited to small displacements. The work of Chopra (1967, 1968, 1970) on gravity dams showed that structural flexibility influences significantly the dam's interaction with the impounded reservoir, and consequently the overall seismic response. Subsequent studies on liquid containing structures also confirmed that the flexibility of container walls affects considerably the coupled dynamic response of the fluid-container system and should thus be included in such analyses (Veletsos, 1974, Veletsos and Yang, 1976, Veletsos and Yang, 1977, Haroun, 1980, Haroun, 1983, Haroun and Housner, 1981, Haroun and Housner, 1981, Balendra et al., 1982). The dynamic fluid pressures within liquid containing structures are generally decomposed into (i) a convective component generated by the sloshing of a portion of the fluid near the free surface, and (ii) an impulsive component generated by a portion of the fluid accelerating with the container. It has been shown that the coupling between liquid sloshing modes and container vibration modes is weak (Veletsos, 1974, Haroun, 1980, Haroun and Housner, 1982). Consequently, convective and impulsive pressures can first be determined separately and their effects combined later to obtain the total dynamic response (Kana, 1979, Malhotra et al., 2000). In practice, convective pressures are determined assuming that the container is rigid, and impulsive pressures are obtained by analyzing the interacting liquid-structure system while neglecting sloshing effects (Veletsos, 1974, Haroun and Housner, 1981).

Although significant work has been dedicated to the dynamics of liquid-containing structures, there is no available practical analytical technique to evaluate the dynamic and seismic

responses of asymmetric rectangular liquid-containing structures. The non-symmetry of a liquid-containing structure is common and may originate from various sources, such as different geometries of the lateral walls, i.e. *geometric asymmetry*, as illustrated in Fig. C.1, or their different constitutive materials, i.e. *material asymmetry*, due to intentional design, asymmetric damage or asymmetric retrofitting for example. In such cases, the two walls's flexibilities and consequently the fluid boundary conditions at the lateral walls are no longer symmetric as assumed in available analytical approaches.

In this paper, we propose an original analytical method to investigate the dynamic and seismic responses of symmetric and asymmetric rectangular liquid-containing structures. In addition to accounting for walls' flexibility, the developed frequency- and time-domain solutions will also include the effects of water compressibility as well as energy dissipation through wave absorption at the container's bottom, two parameters which did not receive much attention in the literature relating to liquid-containing structures.

C.2 Governing equations

C.2.1 Reservoir dynamics and boundary conditions

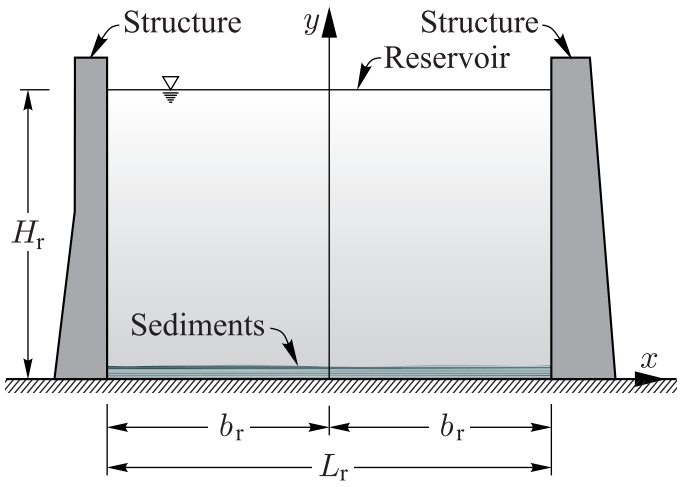

Figure C.1 General geometry of the studied geometrically or materially asymmetric liquid containing structures.

We consider an asymmetric liquid containing structure as illustrated in Fig. C.1. For clarity, the terms structure and reservoir are used in this paper to refer to the solid and fluid domains of the system, respectively. We assume that : (i) the longitudinal dimension of the structure is sufficiently large so that it can be modeled as a two-dimensional plane-

strain elasticity problem; (ii) all materials have a linear elastic behavior; (iii) the walls are flexible and have vertical faces at the interface with the reservoir; (iv) the contained liquid is compressible, inviscid, with its motion irrotational and limited to small amplitudes; (v) sediment deposits may accumulate at the reservoir bottom, (vi) gravity surface waves and convective effects are neglected. The reservoir is of length $L_\mathrm{r} = 2\,b_\mathrm{r}$ and height H_r as illustrated in Fig. C.1. We adopt a Cartesian coordinate system with origin at the reservoir bottom, a horizontal axis x and a vertical axis y coincident with the axis of symmetry of the reservoir as shown in Fig. C.1. We note that the structure can have a geometric and/or material asymmetry as described before.

Under the above-mentioned assumptions, the hydrodynamic pressure $p(x, y, t)$ is governed by the classical wave equation

$$\nabla^2 p = \frac{1}{C_\mathrm{r}^2}\,\frac{\partial^2 p}{\partial t^2} \tag{C.1}$$

where ∇^2 is the Laplace differential operator, t the time variable, and C_r the compression wave velocity. Considering a unit horizontal harmonic ground accelerations $\ddot{u}_\mathrm{g}(t) = \mathrm{e}^{\mathrm{i}\omega t}$, the hydrodynamic pressure in the reservoir can be expressed in the frequency domain as $p(x, y, t) = \bar{p}(x, y, \omega)\,\mathrm{e}^{\mathrm{i}\omega t}$, where $\bar{p}(x, y, \omega)$ is a complex-valued Frequency Response Function (FRF). Introducing this transformation into Eq. (C.1) yields the classical Helmholtz equation

$$\nabla^2 \bar{p} + \frac{\omega^2}{C_\mathrm{r}^2}\,\bar{p} = 0 \tag{C.2}$$

The empty structure is first modeled using finite elements. The dynamic equilibrium of the structure-reservoir system can then be expressed in the frequency domain as

$$\left[-\omega^2\,\mathbf{M} + (1 + \mathrm{i}\,\eta_\mathrm{s})\,\mathbf{K}\right]\vec{U}_b(\omega) = -\mathbf{M}\,\mathbf{1} + \bar{\mathbf{F}}_\mathrm{h}(\omega) \tag{C.3}$$

where $\vec{U}_b$ is a column-vector containing the FRFs of the structure's nodal displacements relative to the ground, $\mathbf{M}$ and $\mathbf{K}$ are the structure's mass and stiffness matrices, respectively, η_s is the structural hysteretic damping factor assumed constant, $\bar{\mathbf{F}}_\mathrm{h}$ is a column-vector containing the FRFs of hydrodynamic pressure loads exerted at lateral walls, and $\mathbf{1}$ is a column-vector with the same dimension as the vector of nodal relative displacements, containing zeros except along horizontal degrees of freedom which correspond to the direction of earthquake excitation. Using modal superposition, the FRFs of relative displacement and acceleration

components at coordinate (x, y) can be expressed as

$$\bar{u}(x,y,\omega) = \sum_{j=1}^{m_\mathrm{s}} \psi_j^{(x)}(x,y)\,\bar{Z}_j(\omega)\,; \qquad \bar{\ddot{u}}(x,y,\omega) = -\omega^2 \sum_{j=1}^{m_\mathrm{s}} \psi_j^{(x)}(x,y)\,\bar{Z}_j(\omega) \tag{C.4}$$

$$\bar{v}(x,y,\omega) = \sum_{j=1}^{m_\mathrm{s}} \psi_j^{(y)}(x,y)\,\bar{Z}_j(\omega)\,; \qquad \bar{\ddot{v}}(x,y,\omega) = -\omega^2 \sum_{j=1}^{m_\mathrm{s}} \psi_j^{(y)}(x,y)\,\bar{Z}_j(\omega) \tag{C.5}$$

where $\bar{u}$ and $\bar{v}$ denote the horizontal and vertical relative displacements of a given point of the structure, respectively, $\bar{\ddot{u}}$ and $\bar{\ddot{v}}$ the horizontal and vertical accelerations, respectively, $\psi_j^{(x)}$ and $\psi_j^{(y)}$ the x– and y–components of the $j^{\,\mathrm{th}}$ mode shape of the empty structure, $\bar{Z}_j$ the generalized coordinate, and m_s the number of structural mode shapes included in the analysis. The hydrodynamic pressure FRF $\bar{p}$ can be decomposed as (Fenves and Chopra, 1984, Bouaanani and Lu, 2009)

$$\bar{p}(x,y,\omega) = \bar{p}_0(x,y,\omega) - \omega^2 \sum_{j=1}^{m_\mathrm{s}} \bar{Z}_j(\omega)\,\bar{p}_j(x,y,\omega) \tag{C.6}$$

where $\bar{p}_0$ is the FRF for hydrodynamic pressure due to rigid body motion of the empty structure, and where $\bar{p}_j$ is the FRF corresponding to hydrodynamic pressure due to horizontal accelerations $\psi_j^{(x)}(-b_\mathrm{r}, y)$ and $\psi_j^{(x)}(b_\mathrm{r}, y)$ along structural mode shape j of the empty structure. The boundary conditions to be satisfied by FRFs $\bar{p}_0$ and $\bar{p}_j$ are as follows :

– *At the structure-reservoir vertical interfaces*
  These boundary conditions are based on compatibility between hydrodynamic pressures and displacements at the lateral walls located at $x = -b_\mathrm{r}$ and $x = b_\mathrm{r}$, yielding

$$\frac{\partial \bar{p}_0}{\partial x}(-b_\mathrm{r}, y, \omega) = -\rho_\mathrm{r}\,; \qquad \frac{\partial \bar{p}_j}{\partial x}(-b_\mathrm{r}, y, \omega) = -\rho_\mathrm{r}\,\psi_j^{(x)}(-b_\mathrm{r}, y) \tag{C.7}$$

$$\frac{\partial \bar{p}_0}{\partial x}(b_\mathrm{r}, y, \omega) = -\rho_\mathrm{r}\,; \qquad \frac{\partial \bar{p}_j}{\partial x}(b_\mathrm{r}, y, \omega) = -\rho_\mathrm{r}\,\psi_j^{(x)}(b_\mathrm{r}, y) \tag{C.8}$$

  where ρ_r is the mass density of water.

– *At reservoir free surface*
  Neglecting the effects of gravity waves at reservoir free surface, hydrodynamic pressures at this location are assumed null

$$\bar{p}_0(x, H_\mathrm{r}, \omega) = \bar{p}_j(x, H_\mathrm{r}, \omega) = 0 \tag{C.9}$$

– *At reservoir bottom*

An absorptive boundary condition introduced by Hall and Chopra (1982) to account for energy dissipation through one-dimensional partial absorption of incident compression waves normal to the reservoir boundary

$$\frac{\partial \bar{p}_0}{\partial y}(x,0,\omega) = \mathrm{i}\,\omega q\,\bar{p}_0(x,0,\omega)\,; \qquad \frac{\partial \bar{p}_j}{\partial y}(x,0,\omega) = \mathrm{i}\,\omega q\,\bar{p}_j(x,0,\omega) \tag{C.10}$$

where q is a damping coefficient defined at the reservoir bottom as

$$q = \frac{\rho_\mathrm{r}}{\rho_\mathrm{f}\,C_\mathrm{f}} \tag{C.11}$$

with ρ_f and C_f denoting the mass density and the compression wave velocity within the reservoir foundation, respectively. The portion of the wave amplitude reflected back to the reservoir is represented by the wave reflection coefficient α defined by

$$\alpha = \frac{1 - q\,C_\mathrm{r}}{1 + q\,C_\mathrm{r}} \tag{C.12}$$

where α may vary from 0 for full wave absorption, to 1 for full wave reflection. In the latter case, Eq. (C.10) simplifies to

$$\frac{\partial \bar{p}_0}{\partial y}(x,0,\omega) = \frac{\partial \bar{p}_j}{\partial y}(x,0,\omega) = 0 \tag{C.13}$$

C.2.2 New formulation for coupled vibrations of structure-reservoir systems

Using Eq. (C.2) and the above-mentioned boundary conditions, we show in Appendix A that FRFs $\bar{p}_0$ and $\bar{p}_j$ can be expressed as

$$\bar{p}_0(x,y,\omega) = \rho_\mathrm{r} H_\mathrm{r} \sum_{n=1}^{m_\mathrm{r}} \frac{\lambda_n^2(\omega)\big[I_{0\,n}^-(\omega)\,X_n^-(x,\omega) - I_{0\,n}^+(\omega)\,X_n^+(x,\omega)\big]}{\beta_n(\omega)\,\kappa_n(\omega)\,\sinh[b_\mathrm{r}\kappa_n(\omega)]\cosh[b_\mathrm{r}\kappa_n(\omega)]}\,Y_n(y,\omega) \tag{C.14}$$

$$\bar{p}_j(x,y,\omega) = \rho_\mathrm{r} H_\mathrm{r} \sum_{n=1}^{m_\mathrm{r}} \frac{\lambda_n^2(\omega)\big[I_{j\,n}^-(\omega)\,X_n^-(x,\omega) - I_{j\,n}^+(\omega)\,X_n^+(x,\omega)\big]}{\beta_n(\omega)\,\kappa_n(\omega)\,\sinh[b_\mathrm{r}\kappa_n(\omega)]\cosh[b_\mathrm{r}\kappa_n(\omega)]}\,Y_n(y,\omega) \tag{C.15}$$

in which the parameters $\beta_n(\omega)$, $\kappa_n(\omega)$, $X_n^-(x,\omega)$, and $X_n^+(x,\omega)$ are given by Eqs. (C.A.14), (C.A.16), (C.A.27) and (C.A.28) of Appendix A, respectively, and where the integrals $I_{0\,n}^-(\omega)$,

$I^{+}_{0\,n}(\omega)$, $I^{-}_{j\,n}(\omega)$ and $I^{+}_{j\,n}(\omega)$ are obtained from Eqs. (C.A.21) and (C.A.22) of Appendix A as

$$\begin{aligned} I^{-}_{0\,n}(\omega) = I^{+}_{0\,n}(\omega) &= \frac{1}{H_{\mathrm{r}}}\int_0^{H_{\mathrm{r}}} Y_n(y,\omega)\,\mathrm{d}y \\ &= \frac{\mathrm{i}\,\mathrm{e}^{-\mathrm{i}H_{\mathrm{r}}\lambda_n(\omega)}}{H_{\mathrm{r}}\lambda_n^2(\omega)}\Big[\lambda_n(\omega) - \omega q + \omega q \mathrm{e}^{\mathrm{i}H_{\mathrm{r}}\lambda_n(\omega)}\Big] \end{aligned} \tag{C.16}$$

$$I^{-}_{j\,n}(\omega) = \frac{1}{H_{\mathrm{r}}}\int_0^{H_{\mathrm{r}}} \psi_j^{(x)}(-b_{\mathrm{r}}, y)\, Y_n(y,\omega)\,\mathrm{d}y \tag{C.17}$$

$$I^{+}_{j\,n}(\omega) = \frac{1}{H_{\mathrm{r}}}\int_0^{H_{\mathrm{r}}} \psi_j^{(x)}(b_{\mathrm{r}}, y)\, Y_n(y,\omega)\,\mathrm{d}y \tag{C.18}$$

We note that

$$I^{-}_{j\,n}(\omega) = 0 \quad \text{when the wall at } x = -b_{\mathrm{r}} \text{ is rigid} \tag{C.19}$$

$$I^{+}_{j\,n}(\omega) = 0 \quad \text{when the wall at } x = b_{\mathrm{r}} \text{ is rigid} \tag{C.20}$$

Evaluating the FRFs $\bar{p}_0$ and $\bar{p}_j$ at the structure's vertical walls, i.e. $x = -b_{\mathrm{r}}$ and $x = b_{\mathrm{r}}$, gives

$$\bar{p}_0(-b_{\mathrm{r}}, y, \omega) = \rho_{\mathrm{r}} H_{\mathrm{r}} \sum_{n=1}^{m_{\mathrm{r}}} \frac{\lambda_n^2(\omega)\big\{\cosh[2\,b_{\mathrm{r}}\kappa_n(\omega)] - 1\big\}\, I_{0\,n}(\omega)}{\beta_n(\omega)\,\kappa_n(\omega)\,\sinh[b_{\mathrm{r}}\kappa_n(\omega)]\,\cosh[b_{\mathrm{r}}\kappa_n(\omega)]}\, Y_n(y,\omega) \tag{C.21}$$

$$\bar{p}_j(-b_{\mathrm{r}}, y, \omega) = \rho_{\mathrm{r}} H_{\mathrm{r}} \sum_{n=1}^{m_{\mathrm{r}}} \frac{\lambda_n^2(\omega)\,\big\{I^{-}_{j\,n}(\omega)\cosh[2\,b_{\mathrm{r}}\kappa_n(\omega)] - I^{+}_{j\,n}(\omega)\big\}}{\beta_n(\omega)\,\kappa_n(\omega)\,\sinh[b_{\mathrm{r}}\kappa_n(\omega)]\,\cosh[b_{\mathrm{r}}\kappa_n(\omega)]}\, Y_n(y,\omega) \tag{C.22}$$

and

$$\bar{p}_0(b_{\mathrm{r}}, y, \omega) = -\bar{p}_0(-b_{\mathrm{r}}, y, \omega) \tag{C.23}$$

$$\bar{p}_j(b_{\mathrm{r}}, y, \omega) = \rho_{\mathrm{r}} H_{\mathrm{r}} \sum_{n=1}^{m_{\mathrm{r}}} \frac{\lambda_n^2(\omega)\,\big\{I^{-}_{j\,n}(\omega) - I^{+}_{j\,n}(\omega)\,\cosh[2\,b_{\mathrm{r}}\kappa_n(\omega)]\big\}}{\beta_n(\omega)\,\kappa_n(\omega)\,\sinh[b_{\mathrm{r}}\kappa_n(\omega)]\cosh[b_{\mathrm{r}}\kappa_n(\omega)]}\, Y_n(y,\omega) \tag{C.24}$$

If water is assumed incompressible, Eq. (C.A.16) simplifies to

$$\kappa_n = \lambda_n = \frac{(2n-1)\,\pi}{2H_{\mathrm{r}}} \tag{C.25}$$

and hydrodynamic pressures $\bar{p}_0$ and $\bar{p}_j$ become

$$\bar{p}_0(-b_\mathrm{r}, y) = \frac{4\rho_\mathrm{r} H_\mathrm{r}}{\pi^2} \sum_{n=1}^{m_\mathrm{r}} \frac{(-1)^{n-1}\big[\cosh(2\,b_\mathrm{r}\kappa_n) - 1\big]}{(2n-1)^2\,\sinh(b_\mathrm{r}\kappa_n)\,\cosh(b_\mathrm{r}\kappa_n)}\,\cos(\lambda_n\,y) \tag{C.26}$$

$$\bar{p}_j(-b_\mathrm{r}, y) = \frac{2\rho_\mathrm{r} H_\mathrm{r}}{\pi} \sum_{n=1}^{m_\mathrm{r}} \frac{\big[I^-_{j\,n}\cosh(2\,b_\mathrm{r}\kappa_n) - I^+_{j\,n}\big]}{(2n-1)\,\sinh(b_\mathrm{r}\kappa_n)\,\cosh(b_\mathrm{r}\kappa_n)}\,\cos(\lambda_n\,y) \tag{C.27}$$

and

$$\bar{p}_0(b_\mathrm{r}, y) = -\bar{p}_0(-b_\mathrm{r}, y, \omega) \tag{C.28}$$

$$\bar{p}_j(b_\mathrm{r}, y) = \frac{2\rho_\mathrm{r} H_\mathrm{r}}{\pi} \sum_{n=1}^{m_\mathrm{r}} \frac{\big[I^-_{j\,n} - I^+_{j\,n}\,\cosh(2\,b_\mathrm{r}\kappa_n)\big]}{(2n-1)\,\sinh(b_\mathrm{r}\kappa_n)\cosh(b_\mathrm{r}\kappa_n)}\,\cos(\lambda_n\,y) \tag{C.29}$$

The FRF for total hydrodynamic pressure is given by Eq. (C.6) where the vector $\bar{\mathbf{Z}}$ of generalized coordinates $\bar{Z}_j$, $j=1\ldots m_\mathrm{s}$, is obtained by solving the system of equations

$$\bar{\mathbf{S}}\,\bar{\mathbf{Z}} = \bar{\mathbf{Q}} \tag{C.30}$$

in which elements of matrices $\bar{\mathbf{S}}$ and $\bar{\mathbf{Q}}$ are obtained for $n=1\ldots m_\mathrm{s}$ and $j=1\ldots m_\mathrm{s}$ as

$$\bar{S}_{nj}(\omega) = \Big[-\omega^2 + \big(1 + \mathrm{i}\,\eta_\mathrm{s}\big)\,\omega_n^2\Big]\delta_{nj} + \omega^2\left[\int_0^{H_\mathrm{r}} \bar{p}_j(b_\mathrm{r}, y, \omega)\,\psi_n^{(x)}(b_\mathrm{r}, y)\,\mathrm{d}y - \int_0^{H_\mathrm{r}} \bar{p}_j(-b_\mathrm{r}, y, \omega)\,\psi_n^{(x)}(-b_\mathrm{r}, y)\,\mathrm{d}y\right] \tag{C.31}$$

$$\bar{Q}_n(\omega) = -\,\boldsymbol{\psi}_n^\mathrm{T}\,\mathbf{M}\,\mathbf{1} + \int_0^{H_\mathrm{r}} \bar{p}_0(b_\mathrm{r}, y, \omega)\,\psi_n^{(x)}(b_\mathrm{r}, y)\,\mathrm{d}y - \int_0^{H_\mathrm{r}} \bar{p}_0(-b_\mathrm{r}, y, \omega)\,\psi_n^{(x)}(-b_\mathrm{r}, y)\,\mathrm{d}y \tag{C.32}$$

where δ denotes the Kronecker symbol and ω_n is the vibration frequency corresponding to structural mode shape $\boldsymbol{\psi}_n$ of the structure without water. A convergence study must be conducted to determine the sufficient numbers m_s and m_r of structural and reservoir mode shapes to be included into each specific analysis. We note that if the containing structure is

symmetric, Eqs. (C.31) and (C.32) simplify to

$$\bar{S}_{nj}(\omega) = \Big[-\omega^2 + \big(1 + \mathrm{i}\,\eta_\mathrm{s}\big)\,\omega_n^2 \Big]\delta_{nj} + 2\,\omega^2 \int_0^{H_\mathrm{r}} \bar{p}_j(b_\mathrm{r}, y, \omega)\,\psi_n^{(x)}(b_\mathrm{r}, y)\,\mathrm{d}y \tag{C.33}$$

$$\bar{Q}_n(\omega) = -\,\boldsymbol{\psi}_n^\mathrm{T}\,\mathbf{M}\,\mathbf{1} + 2\int_0^{H_\mathrm{r}} \bar{p}_0(b_\mathrm{r}, y, \omega)\,\psi_n^{(x)}(b_\mathrm{r}, y)\,\mathrm{d}y \tag{C.34}$$

The structural displacement and acceleration time-history responses to a ground acceleration $\ddot{u}_\mathrm{g}(t)$ can be obtained as

$$u(x,y,t) = \sum_{j=1}^{m_\mathrm{s}} \psi_j^{(x)}(x,y)\,Z_j(t)\,; \qquad \ddot{u}(x,y,t) = \sum_{j=1}^{m_\mathrm{s}} \psi_j^{(x)}(x,y)\,\ddot{Z}_j(t) \tag{C.35}$$

$$v(x,y,t) = \sum_{j=1}^{m_\mathrm{s}} \psi_j^{(y)}(x,y)\,Z_j(t)\,; \qquad \ddot{v}(x,y,t) = \sum_{j=1}^{m_\mathrm{s}} \psi_j^{(y)}(x,y)\,\ddot{Z}_j(t) \tag{C.36}$$

where the time-domain generalized coordinates Z_j are given by the Fourier integrals

$$Z_j(t) = \frac{1}{2\pi}\int_{-\infty}^{\infty} \bar{Z}_j(\omega)\,\bar{\ddot{u}}_\mathrm{g}(\omega)\,\mathrm{e}^{\mathrm{i}\omega t}\,\mathrm{d}\omega\,; \qquad \ddot{Z}_j(t) = -\frac{1}{2\pi}\int_{-\infty}^{\infty} \omega^2\,\bar{Z}_j(\omega)\,\bar{\ddot{u}}_\mathrm{g}(\omega)\,\mathrm{e}^{\mathrm{i}\omega t}\,\mathrm{d}\omega \tag{C.37}$$

in which $\bar{\ddot{u}}_\mathrm{g}(\omega)$ is the Fourier transform of the ground acceleration $\ddot{u}_\mathrm{g}(t)$

$$\bar{\ddot{u}}_\mathrm{g}(\omega) = \int_0^{t_a} \ddot{u}_\mathrm{g}(t)\,\mathrm{e}^{-\mathrm{i}\omega t}\,\mathrm{d}t \tag{C.38}$$

with t_a denoting the time duration of the applied accelerogram.

Based on these relations, other quantities of interest can also be determined. For example, the shear forces at a given horizontal cutting section at position y_A of each wall can also be obtained by expressing the dynamic equilibrium of the wall's portion above the cutting section, yielding

$$V^-(y_\mathrm{A}, t) = \int_{y_\mathrm{A}}^{H_\mathrm{r}} p(-b_\mathrm{r}, y, t)\,\mathrm{d}y - \iint_{\mathcal{A}^-(y_\mathrm{A})} \rho_\mathrm{s}(x,y)\Big[\ddot{u}_\mathrm{g}(t) + \ddot{u}(x,y,t)\Big]\,\mathrm{d}x\,\mathrm{d}y \tag{C.39}$$

$$V^+(y_\mathrm{A}, t) = \int_{y_\mathrm{A}}^{H_\mathrm{r}} p(b_\mathrm{r}, y, t)\,\mathrm{d}y - \iint_{\mathcal{A}^+(y_\mathrm{A})} \rho_\mathrm{s}(x,y)\Big[\ddot{u}_\mathrm{g}(t) + \ddot{u}(x,y,t)\Big]\,\mathrm{d}x\,\mathrm{d}y \tag{C.40}$$

where V^- and V^+ is the shear forces at the left and right walls of the liquid-container, respectively, $\mathcal{A}^-$ and $\mathcal{A}^+$ are the areas of the portions located above the cutting sections of the left and right walls, respectively, and ρ_s is the density of the constitutive material(s) of

the liquid container.

C.3 Validation examples

The dynamic response of symmetric and asymmetric liquid containing structures are investigated in this section to validate the proposed method and illustrate its application. The description as well as the frequency- and time-domain analyses of the studied systems are presented in the next two subsections.

C.3.1 Geometrically asymmetric wall-water system

In this section, we investigate the geometrically asymmetric wall-water system illustrated in Fig. C.2. The following properties are adopted for the structure's material : modulus of elasticity $E_s = 25\,\text{GPa}$, Poisson's ratio $\nu_s = 0.2$, and mass density $\rho_s = 2400\,\text{kg/m}^3$.

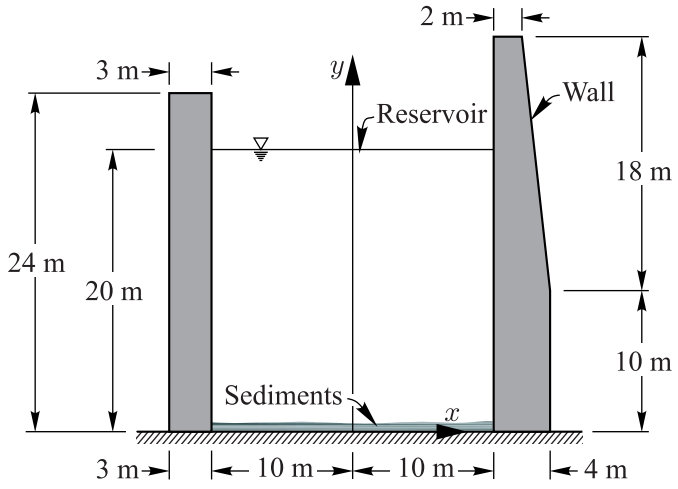

Figure C.2 Geometry of the studied geometrically asymmetric wall-water system.

The reservoir contains water of mass density $\rho_r = 1000\,\text{kg/m}^3$, and has a height $H_r = 20\,\text{m}$ and a length $L_r = 20\,\text{m}$. Water is considered compressible with a velocity of pressure waves $C_r = 1440\,\text{m/s}$. A constant structural hysteretic damping factor $\eta_s = 0.1$ is assumed. To obtain the mode shapes ψ_j, $j = 1 \ldots m_s$, of the walls without water and corresponding modal participation factors, the structures are discretized into 8-node plane-strain solid finite elements using the software ADINA (2010). Fig. C.3 (a) illustrates the finite element mesh used. Application of the proposed method described in Section C.2.2 reveals that frequency response convergence up to 20 Hz requires that the first eight modes of the empty structure be included in the analysis, i.e. $m_s = 8$. Fig. C.4 illustrates the first eight mode shapes given

by ADINA (2010) as well as the corresponding frequencies and horizontal effective modal masses expressed in percentage of total mass of the walls. As can be seen,mode 6 is a vertical mode, and can therefore be neglected in the analysis. We also note that a wide frequency range up to 20 Hz was studied for purpose of illustration although a lower cutting frequency could have been selected considering the usual frequency content of interest under seismic excitation. The same frequency range will be used in the next examples. To validate the results, we conduct a finite element analysis where both the walls and the reservoir are modeled using 8-node plane strain and 8-node potential-based finite elements programmed in ADINA (2010), respectively. Fig. C.3 (b) illustrates the finite element model used. In this case, dynamic interaction between the walls and the reservoir is achieved through fluid-structure interface elements and a potential-based formulation of the fluid domain (Everstine, 1981, Bouaanani and Lu, 2009).

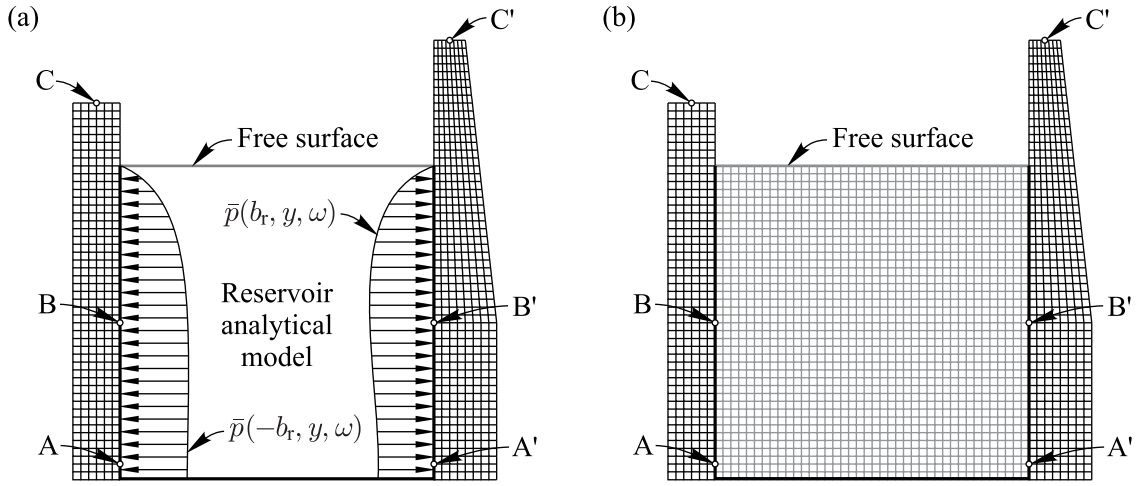

Figure C.3 Geometry of the studied geometrically asymmetric wall-water system.

Fig. C.5 shows the obtained FRFs of nondimensionalized scaled hydrodynamic pressures $|p/(\rho g H_r)|$ and scaled horizontal relative displacements $|u/u_{st}|$ where u_{st} is the lateral static displacement under the effect of hydrostatic pressure. The results are determined at points A, B, and C located on the left wall, and points A', B' and C' belonging to the right wall as indicated in Fig. C.3.

The vertical positions of the points are $y_A = y_{A'} = 1\,\text{m}$, $y_B = y_{B'} = 10\,\text{m}$, $y_C = 24\,\text{m}$ and $y_{C'} = 28\,\text{m}$. The FRFs in Fig. C.5 clearly show that the results of the proposed method are in excellent agreement with the finite element solutions over a wide frequency range up to 20 Hz. The proposed method is then used to determine the FRFs including a reflection

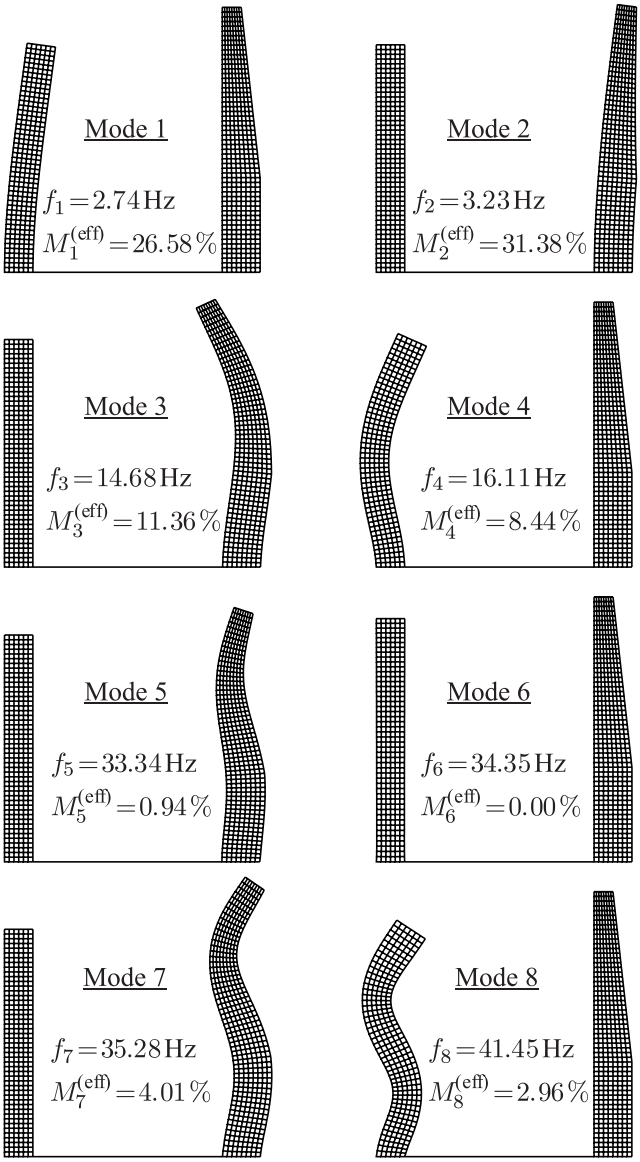

Figure C.4 Mode shapes, frequencies and effective modal masses of the walls.

wave coefficient $\alpha = 0.2$ at reservoir's bottom. The obtained FRFs are superposed to those in Fig. C.5 and show that, in this case, the influence of reservoir bottom absorption affects mainly hydrodynamic pressures at higher frequencies larger than 10 Hz. The techniques described previously are also applied next to determine hydrodynamic pressure profiles corresponding to frequencies $0.8\,\tilde{f}_1$ and $1.2\,\tilde{f}_1$, where $\tilde{f}_1$ denotes the coupled vibration frequency of the wall-water system. The obtained profiles presented in Fig. C.6 confirm that the proposed procedure yields excellent results when compared to advanced finite element formulations.

Next, we investigate the performance of the proposed method in assessing the seismic

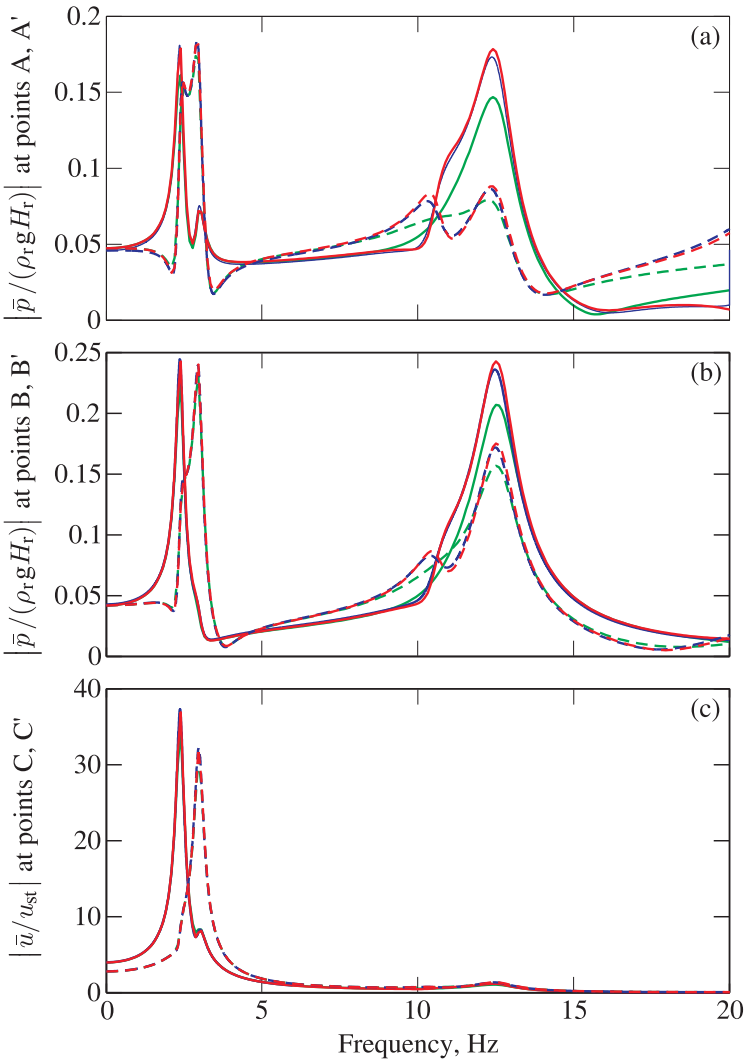

Figure C.5 Nondimensionalized hydrodynamic pressures and displacements for the geometrically asymmetric wall-water system : (a) and (b) hydrodynamic pressures, (c) displacements. Continuous lines : Points A, B and C. Dotted lines : Points A', B' and C'. — Finite element solution ; — Proposed solution with $\alpha = 1.0$; — Proposed solution with $\alpha = 0.2$.

response of the previously described wall-water system. Fig. C.7 illustrates the horizontal acceleration component of Imperial Valley earthquake (1940) at El Centro selected to conduct the analyses using the proposed and finite element techniques described above. The obtained time-histories of nondimensionalized horizontal relative displacements $|u/u_{st}|$ at points C and C' are shown in Fig. C.8 (a) and (b). Fig. C.8 (c) and (d) illustrate the nondimensionalized shear forces V/F_{stat} at sections A and A' where $F_{stat} = \rho_r g H_r^2/2$ denotes the hydrostatic force. Fig. C.8 clearly shows that the time-history responses predicted by the proposed method are almost identical to those from finite element analyses.

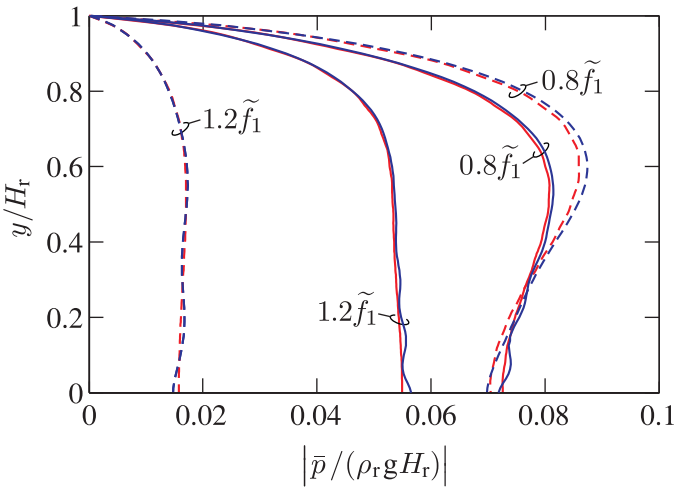

Figure C.6 Nondimensionalized hydrodynamic pressure profiles on the walls of the asymmetric wall-water system. Continuous lines : Left wall. Dotted lines : Right wall. — Finite element solution ; — Proposed solution.

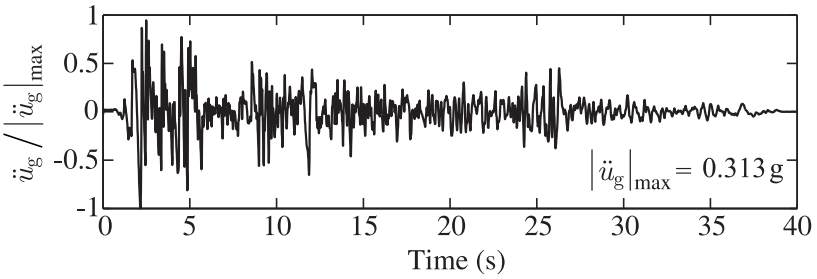

Figure C.7 Horizontal acceleration component of Imperial Valley earthquake (1940).

C.3.2 Materially asymmetric tank-reservoir system

We consider the tank-reservoir system illustrated in Fig. C.9. The tank has a material asymmetry due to the retrofitting of one of its damaged lateral walls using a high performance material.

The following properties are adopted for the structure's materials : moduli of elasticity of the original and reinforcing materials $E_s^{(1)} = 25\,\text{GPa}$ and $E_s^{(2)} = 55\,\text{GPa}$, respectively, Poisson's ratio $\nu_s = 0.2$, and mass density $\rho_s = 2400\,\text{kg/m}^3$. The tank is filled with water with a mass density $\rho_r = 1000\,\text{kg/m}^3$ up to a height $H_r = 10\,\text{m}$. The length of the reservoir is $L_r = 18\,\text{m}$. Water is considered compressible with a velocity of pressure waves $C_r = 1440\,\text{m/s}$. A constant structural hysteretic damping factor $\eta_s = 0.1$ is assumed. Fig. C.10 (a) illustrates the finite element model of the empty tank used to obtain the modal properties required for the proposed

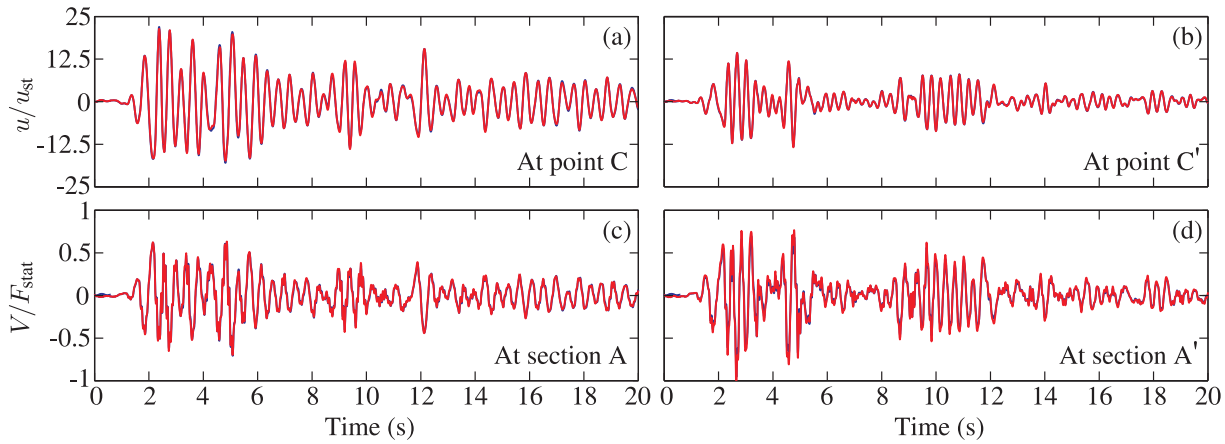

Figure C.8 Time-history response of the geometrically asymmetric wall-water system : (a) Nondimensionalized displacement at point C ; (b) Nondimensionalized displacement at point C' ; (c) Nondimensionalized shear force at section A ; (d) Nondimensionalized shear force at section A'. Finite element solution ; Proposed solution.

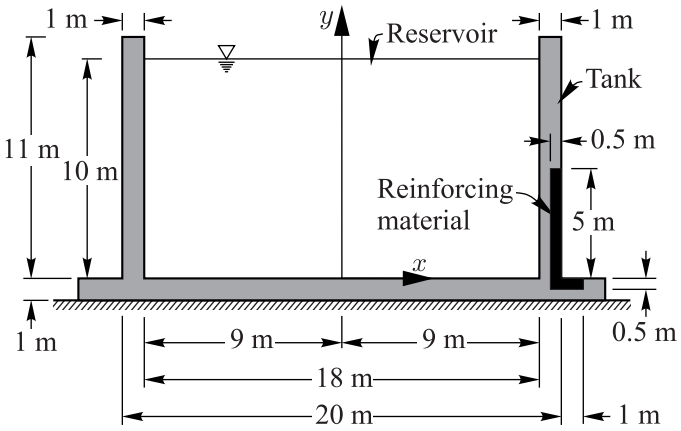

Figure C.9 Geometry of the studied materially asymmetric tank-reservoir system.

method, while Fig. C.3 (b) shows the tank-reservoir system's finite element model constructed for comparison purposes. 8-node solid and fluid finite elements programmed in ADINA (2010) are used as in the previous models.

In this case, we show that the first six modes of the empty reinforced tank are to be included in the analysis for convergence up to 20 Hz, i.e. $m_s = 6$. Fig. C.11 presents the six mode shapes of the empty reinforced tank obtained using ADINA (2010) as well as the corresponding frequencies and horizontal effective modal masses expressed in percentage of total mass of the empty tank. By comparing these modes to those of the original symmetric

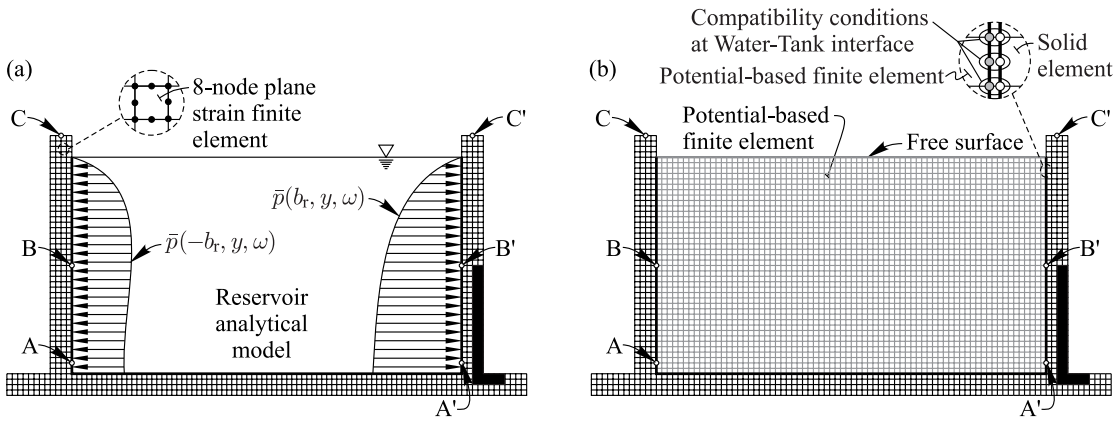

Figure C.10 Finite elements models : (a) Retrofitted tank and analytical model for hydrodynamic pressure ; (b) Retrofitted tank-water system.

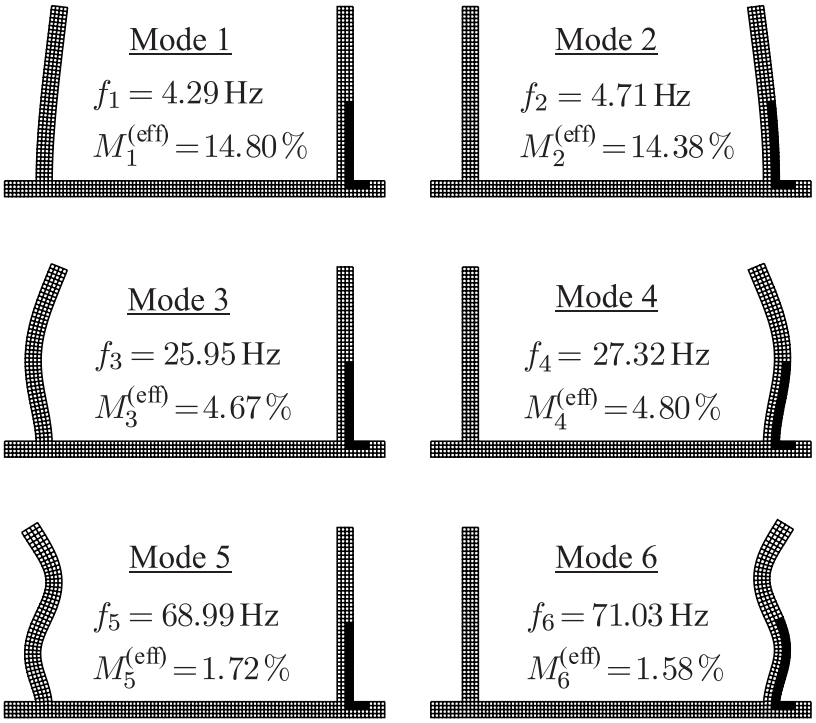

Figure C.11 First six mode shapes and corresponding frequencies and effective modal masses of the asymmetrical tank.

tank, we observe that asymmetry affects the frequencies of modes 2, 4 and 6, as well as the corresponding modal masses which are now non-null.

The dynamic response of the reinforced tank-reservoir system is then studied using the previously described analytical and finite element models shown in Figs. C.10 (a) and (b).

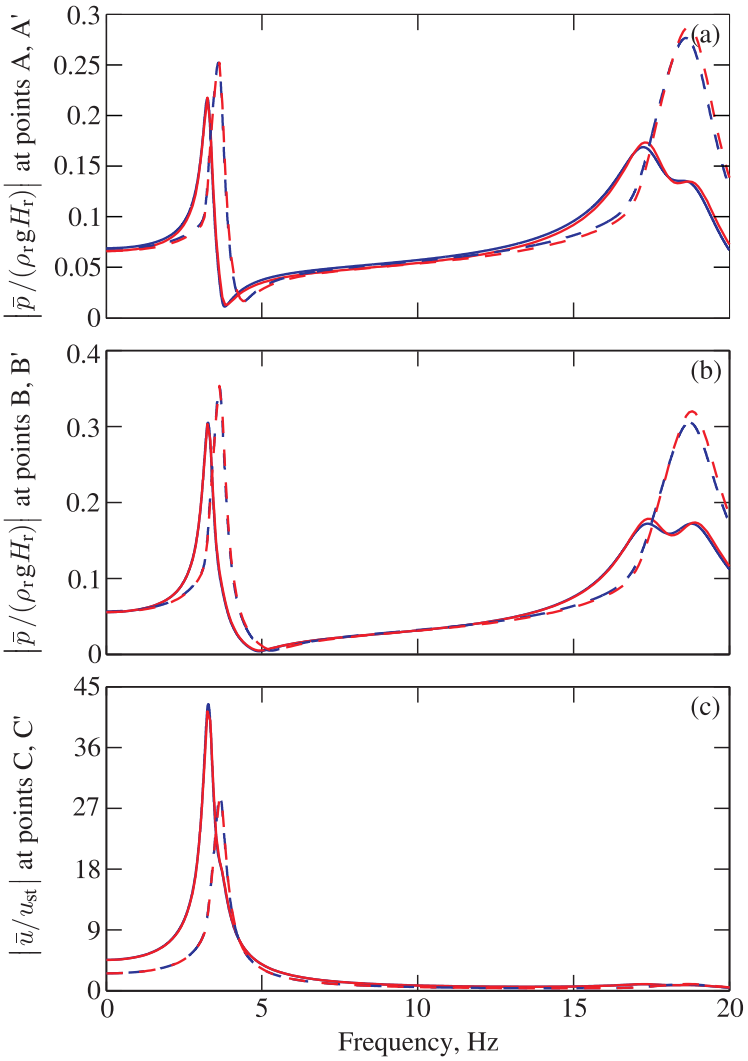

Figure C.12 Nondimensionalized hydrodynamic pressures and displacements for the materially asymmetric tank-reservoir system : (a) and (b) hydrodynamic pressures, (c) displacements. Continuous lines : Points A, B and C. Dotted lines : Points A', B' and C'. ___ Finite element solution ; ___ Proposed solution.

Fig. C.12 presents the resulting FRFs of nondimensionalized hydrodynamic pressures $|p/(\rho g H_r)|$ obtained at points A, B, A' and B', as well as the nondimensionalized horizontal relative displacements $|u/u_{st}|$ at points C and C'. The positions of the points are illustrated in Fig. C.10 and are located at $y_A = y_{A'} = 0.5\,\text{m}$, $y_B = y_{B'} = 5\,\text{m}$, and $y_C = y_{C'} = 11\,\text{m}$.

Fig. C.12 shows that the agreement between the proposed method and the finite element solution is excellent over the wide frequency range studied. The hydrodynamic pressure profiles are also determined using the proposed and finite element methods. Fig. C.13 illustrates the profiles corresponding to frequencies $0.8\,\tilde{f}_1$ and $1.2\,\tilde{f}_1$, where $\tilde{f}_1$ denotes the coupled vibra-

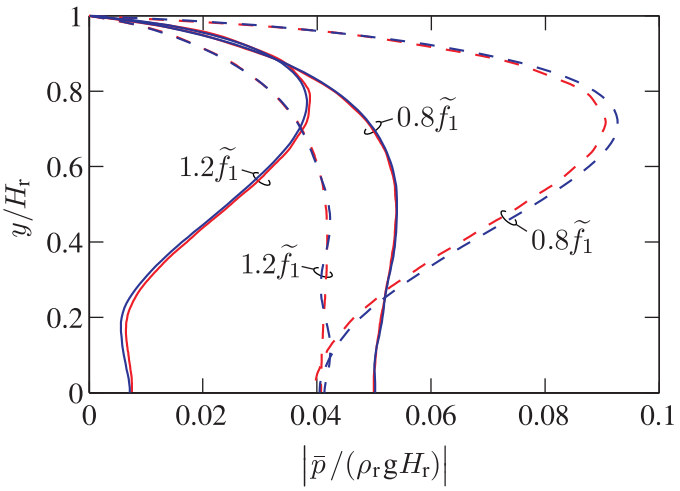

Figure C.13 Nondimensionalized hydrodynamic pressure profiles on the walls of the materially asymmetric tank-reservoir system. Continuous lines : Left wall. Dotted lines : Right wall. — Finite element solution ; — Proposed solution.

tion frequency of the tank-reservoir system. These results confirm that the proposed method and advanced finite element modeling yield almost identical hydrodynamic profiles.

The seismic response of the tank-reservoir system is investigated next using the proposed and finite element techniques described above. The tank-reservoir is subjected to the horizontal component of the El Centro ground motion from Imperial Valley earthquake (1940) shown in Fig. C.7. Fig. C.8 illustrates the obtained nondimensionalized horizontal relative displacements $|u/u_{st}|$ at points C and C' as well as the shear forces V/F_{stat} at sections A and A', where $F_{stat} = \rho_r g H_r^2/2$ denotes the hydrostatic force as previously. Again, the time-history results confirm that the proposed procedure yields excellent results when compared to advanced finite element formulations.

C.4 Conclusions

This paper presented and validated an original formulation to study horizontally accelerated symmetrical and asymmetrical liquid-containing structures. The new formulation is based on a sub-structuring approach, where the flexible containing structure is modeled using finite elements, while the impulsive effects of the fluid domain are modeled analytically through interaction forces at the fluid-structure interfaces. The detailed mathematical derivations accounting for geometrical or material asymmetry of the containing structure are developed, considering both incompressible or compressible water assumptions. The proposed formulation also includes the effects of energy dissipation through reservoir bottom absorption. The

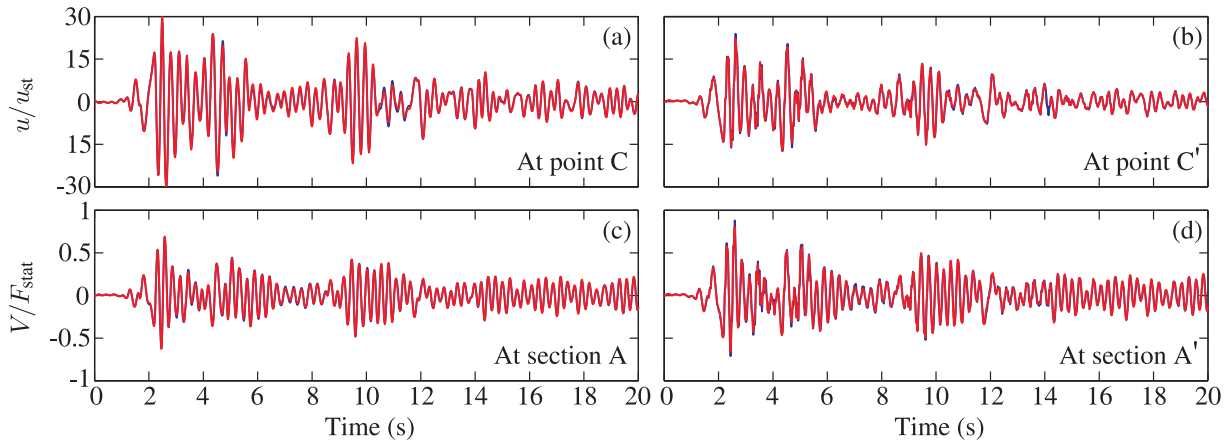

Figure C.14 Time-history response of the materially asymmetric tank-reservoir system : (a) Nondimensionalized displacement at point C ; (b) Nondimensionalized displacement at point C' ; (c) Nondimensionalized shear force at section A ; (d) Nondimensionalized shear force at section A'. — Finite element solution ; — Proposed solution.

technique was programmed and its application illustrated through examples highlighting the effects of geometrical and material asymmetry on the frequency- and time-domain dynamic responses of liquid-containing structures. It is seen that geometrical or material asymmetry affects the dynamic behavior of liquid containing structures, namely in terms of frequency response functions and time history responses of various quantities of interest. The obtained impulsive hydrodynamic pressures, displacements and shear forces were illustrated and successfully validated against advanced finite element analyses. The proposed technique is formulated in such a way that it can be easily coded into a practical and computationally efficient program.

Acknowledgements

The authors would like to acknowledge the financial support of the Natural Sciences and Engineering Research Council of Canada (NSERC) and the Quebec Fund for Research on Nature and Technology (FQRNT).

References

ADINA (2010). "Theory and modeling guide." Report ARD 10-7, ADINA R& D, Inc., Watertown, MA.

Balendra, T., Ang, K. K., Paramasivam, P., and Lee, S. V. (1982). "Seismic design of flexible cylindrical liquid storage tanks." *Earthquake Engineering and Structural Dynamics*, 10(3), 477–496.

Bouaanani, N. and Lu, F. Y. (2009). "Assessment of potential-based fluid finite elements for seismic analysis of dam–reservoir systems." *Journal of Computers and Structures*, 87(3-4), 206–224.

Chopra, A. K. (1967). "Reservoir-dam interaction during earthquakes." *Bulletin of the Seismological Society of America*, 57(4), 675–687.

Chopra, A. K. (1968). "Earthquake behavior of reservoir-dam systems." *ASCE Journal of the Engineering Mechanics Division*, 94(EM6), 1475–1500.

Chopra, A. K. (1970). "Earthquake response of concrete gravity dams." *ASCE Journal of the Engineering Mechanics Division*, 96(EM4), 443–454.

Everstine, G. C. (1981). "A symmetric potential formulation for fluid-structure interaction." *Journal of Sound and Vibration*, 79(1), 157–160.

Fenves, G. and Chopra, A. K. 1984. "Earthquake analysis and response of concrete gravity dams." *Report No. UCB/EERC-84/10, University of California*, Berkeley, California.

Graham, E. W., Rodriguez A. M. (1952). "Characteristics of fuel motion which affect airplane dynamics." *Journal of Applied Mechanics*, 19, 381–388.

Hall, J. F. (ed.). (1995). "Northridge earthquake of January 17, 1994 : Reconnaissance report." *Earthquake Spectra*, Supplement C to Volume 11, Vol. 1, Earthquake Engineering Research Institute, Oakland, CA.

Hanson, R. D. (1973). "Behavior of storage tanks, the Great Alaska earthquake of 1964." *Proc., National Academy of Science*, Washington, D.C., 7, 331–339.

Haroun, M. A. (1980). "Dynamic analyses of liquid storage tanks." *Report No. EERL 80-04, California Institute of Technology*, Pasedenas, CA.

Haroun, M. A. and Housner, G. W. (1981). "Seismic design of liquid storage tanks." *Journal of Technical Councils of ASCE*, 107, 191–207.

Haroun, M. A. and Housner, G. W. (1981). "Earthquake response of deformable liquid storage tanks." *Journal of Applied Mechanics*, 48(2), 411–418.

Haroun, M. A. and Housner, G. W. (1982). "Complications in free vibration analysis of tanks." *Proc., ASCE Engineering Mechanics Division*, 108(5), 801–818.

Haroun, M. A. (1983). "Vibration studies and tests of liquid storage tanks." *Earthquake Engineering and Structural Dynamics*, 11(2), 179–206.

Hoskins, L. M. and Jacobsen, L. S. (1934). "Water pressure in a tank caused by a simulated earthquake." *Bulletin of the Seismological Society of America*, 24, 1–32.

Housner, G. W. (1957). "Dynamic pressures on accelerated fluid containers." *Bulletin of the Seismological Society of America*, 47, 15–35.

Housner, G. W. (1963). "Nuclear reactors and earthquakes." *Report No. TID-7024 - United States Atomic Energy Commission*, Washington, D.C.

Jacobsen, L. S. (1949). "Impulsive hydrodynamics of fluid inside a cylindrical tank and of fluid surrounding a cylindrical pier." *Bulletin of the Seismological Society of America*, 39(3), 189–204.

Jacobson, L. S. and Ayre, R. S. (1951). "Hydrodynamic experiments with rigid cylindrical tanks subjected to transient motions." *Bulletin of the Seismological Society of America*, 41, 313–346.

Kana, D. D. (1979). "Seismic response of flexible cylindrical liquid storage tanks." *Nuclear Engineering and Design*, 52(1), 185–199.

Malhotra, P. K., Norwood, M. A. and Wieland, M. (2000). "Simple procedure for seismic analysis of liquid-storage tanks." *IABSE Structural Engineering International*, 3, 197–201.

Steinbrugge, K. V. and Flores, R. (1963). "The Chilean earthquakes of May, 1960 : A structural engineering viewpoint." *Bulletin of the Seismological Society of America*, 53(2), 225–307.

Steinberg, L. J. and Cruz, A. M. (2004). "When natural and technological disasters collide : Lessons from the Turkey earthquake of August 17, 1999." *Natural Hazards Review*, (3)5, 121–130.

Veletsos, A. S. (1974). "Seismic effects in flexible liquid storage tank." *Proc., 5th World Conference on Earthquake Engineering*, 630–639.

Veletsos, A. S. and Yang, J. Y. (1976). "Dynamics of fixed-base liquid storage tanks." *US-Japan Seminar for Earthquake Engineering Research*, Tokyo, Japan, 317–341.

Veletsos, A. S. and Yang, J. Y. (1977). "Earthquake response of liquid storage tanks." *Proc., Second EMD Specialty Conference*, ASCE, Raleigh, NC, 1–24.

Werner, P. W. and Sundquist, K. J. (1949). "On hydrodynamic earthquake effects." *Transactions of the American Geophysical Union*, 30(5), 636–657.

Appendix A

For clarity and brevity, the following notation is used

$$\bar{p}_\ell(x,y,\omega) = \begin{cases} \bar{p}_0(x,y,\omega) & \text{if} \quad \ell = 0 \qquad \text{(C.A.1)} \\ \bar{p}_j(x,y,\omega) & \text{if} \quad \ell = j \qquad \text{(C.A.2)} \end{cases}$$

and

$$f_0^-(y) = 1\,; \qquad f_0^+(y) = 1 \qquad \text{(C.A.3)}$$

$$f_j^-(y) = \psi_j^{(x)}(-b_\mathrm{r}, y)\,; \qquad f_j^+(y) = \psi_j^{(x)}(+b_\mathrm{r}, y) \qquad \text{(C.A.4)}$$

Throughout this appendix, subscript ℓ can take the values 0 or j.

Using the technique of separation of variables, we can show that hydrodynamic pressure can be expressed as

$$\bar{p}_\ell(x,y,\omega) = \bar{p}_{\ell\,x}(x,\omega)\,\bar{p}_{\ell\,y}(y,\omega) \qquad \text{(C.A.5)}$$

where the pressures $\bar{p}_{\ell\,x}$ and $\bar{p}_{\ell\,y}$ are given by

$$\bar{p}_{\ell\,x}(x,\omega) = \gamma_1^{(\ell)}(\omega)\,\mathrm{e}^{-\kappa(\omega)\,x} + \gamma_2^{(\ell)}(\omega)\,\mathrm{e}^{\kappa(\omega)\,x} \qquad \text{(C.A.6)}$$

$$\bar{p}_{\ell\,y}(y,\omega) = \gamma_3^{(\ell)}(\omega)\,\mathrm{e}^{-\mathrm{i}\,\lambda(\omega)\,y} + \gamma_4^{(\ell)}(\omega)\,\mathrm{e}^{\mathrm{i}\,\lambda(\omega)\,y} \qquad \text{(C.A.7)}$$

in which λ and κ are complex constants related by

$$\kappa(\omega)^2 = \lambda(\omega)^2 - \frac{\omega^2}{C^2} \qquad \text{(C.A.8)}$$

and the coefficients $\gamma_1^{(\ell)}(\omega)$, $\gamma_2^{(\ell)}(\omega)$, $\gamma_3^{(\ell)}(\omega)$ and $\gamma_4^{(\ell)}(\omega)$ are to be determined by imposing appropriate boundary conditions.

Using the transformation of Eq. (C.A.5) into Eqs. (C.9) and (C.13), we obtain the boundary conditions to be satisfied by function $\bar{p}_{\ell\, y}$ as

$$\frac{\mathrm{d}\bar{p}_{\ell\, y}}{\mathrm{d}y}(0,\omega) - \mathrm{i}\omega q\, \bar{p}_{\ell\, y}(0,\omega) = 0 \tag{C.A.9}$$

$$\bar{p}_{\ell\, y}(H_\mathrm{r},\omega) = 0 \tag{C.A.10}$$

Substituting $\bar{p}_{\ell\, y}(y,\omega)$ by its expression in Eq. (C.A.7) into Eqs. (C.A.9) and (C.A.10) yields to a Sturm-Liouville problem with complex-valued frequency-dependent eigenvalues $\lambda_n(\omega)$ to be obtained by solving the characteristic equation

$$\mathrm{e}^{2\mathrm{i}\lambda_n(\omega)H_\mathrm{r}} = -\frac{\lambda_n(\omega) - \omega q}{\lambda_n(\omega) + \omega q} \tag{C.A.11}$$

and eigenvectors

$$Y_n(y,\omega) = \frac{\big[\lambda_n(\omega) - \omega q\big]\mathrm{e}^{-\mathrm{i}\lambda_n(\omega)\, y} + \big[\lambda_n(\omega) + \omega q\big]\mathrm{e}^{\mathrm{i}\lambda_n(\omega)\, y}}{2\lambda_n(\omega)} \tag{C.A.12}$$

satisfying the orthogonality relations for $n = 1 \ldots m_\mathrm{r}$ and $s = 1 \ldots m_\mathrm{r}$

$$\int_0^{H_\mathrm{r}} Y_s(y,\omega)\, Y_n(y,\omega)\, \mathrm{d}y = \frac{\beta_n(\omega)}{2\lambda_n^2(\omega)}\, \delta_{sn} \tag{C.A.13}$$

where δ denotes the Kronecker symbol and where the parameter β_n is given by

$$\beta_n(\omega) = H_\mathrm{r}\big[\lambda_n^2(\omega) - \omega^2 q^2\big] + \mathrm{i}\,\omega q \tag{C.A.14}$$

Using Eqs. (C.A.5) and (C.A.6) and the eigenvectors in Eq. (C.A.12), we show that hydrodynamic pressure can be expressed as

$$\begin{aligned} \bar{p}_\ell(x,y,\omega) &= \sum_{n=1}^{\infty} \Big[\gamma_{1,n}^{(\ell)}(\omega)\, \mathrm{e}^{-\kappa_n(\omega)\, x} + \gamma_{2,n}^{(\ell)}(\omega)\, \mathrm{e}^{\kappa_n(\omega)\, x}\Big]\, Y_n(y,\omega) \\ &\approx \sum_{n=1}^{m_\mathrm{r}} \Big[\gamma_{1,n}^{(\ell)}(\omega)\, \mathrm{e}^{-\kappa_n(\omega)\, x} + \gamma_{2,n}^{(\ell)}(\omega)\, \mathrm{e}^{\kappa_n(\omega)\, x}\Big]\, Y_n(y,\omega) \end{aligned} \tag{C.A.15}$$

in which the sum is truncated to include only the first m_r reservoir modes, and where the

frequency-dependent parameter κ_n is given by Eq. (C.A.8) as

$$\kappa_n(\omega) = \sqrt{\lambda_n^2(\omega) - \frac{\omega^2}{C_\mathrm{r}^2}} \tag{C.A.16}$$

The coefficients $\gamma_{1,n}(\omega)$ and $\gamma_{2,n}(\omega)$ are obtained by substituting Eq. (C.A.15) into Eqs. (C.A.6) and (C.A.7), yielding

$$\sum_{n=1}^{m_\mathrm{r}} \kappa_n(\omega) \left[\gamma_{1,n}^{(\ell)}(\omega)\, \mathrm{e}^{\kappa_n(\omega)\, b_\mathrm{r}} - \gamma_{2,n}^{(\ell)}(\omega)\, \mathrm{e}^{-\kappa_n(\omega)\, b_\mathrm{r}}\right] Y_n(y,\omega) = \rho_\mathrm{r} f_\ell^-(y) \tag{C.A.17}$$

$$\sum_{n=1}^{m_\mathrm{r}} \kappa_n(\omega) \left[\gamma_{1,n}^{(\ell)}(\omega)\, \mathrm{e}^{-\kappa_n(\omega)\, b_\mathrm{r}} - \gamma_{2,n}^{(\ell)}(\omega)\, \mathrm{e}^{\kappa_n(\omega)\, b_\mathrm{r}}\right] Y_n(y,\omega) = \rho_\mathrm{r} f_\ell^+(y) \tag{C.A.18}$$

Adding Eqs. (C.A.17) to (C.A.18) gives

$$\sum_{n=1}^{m_\mathrm{r}} 2\left[\gamma_{1,n}^{(\ell)}(\omega) - \gamma_{2,n}^{(\ell)}(\omega)\right] \kappa_n(\omega) \cosh[b_\mathrm{r}\kappa_n(\omega)]\, Y_n(y,\omega) = \rho_\mathrm{r}\left[f_\ell^-(y) + f_\ell^+(y)\right] \tag{C.A.19}$$

Multiplying Eq.(C.A.19) by eigenvectors $Y_n(y,\omega)$, $s = 1 \ldots m_\mathrm{r}$, integrating over reservoir height H_r and using trigonometric orthogonality relationships yields for each reservoir mode n

$$\gamma_{2,n}^{(\ell)}(\omega) = \gamma_{1,n}^{(\ell)}(\omega) - \frac{\rho_\mathrm{r} H_\mathrm{r} \lambda_n^2(\omega)\left[I_{\ell n}^+(\omega) + I_{\ell n}^-(\omega)\right]}{\beta_n(\omega)\, \kappa_n(\omega) \cosh[b_\mathrm{r}\kappa_n(\omega)]} \tag{C.A.20}$$

where the parameters $I_{\ell n}^-(\omega)$ and $I_{\ell n}^+(\omega)$ are given by

$$I_{\ell n}^-(\omega) = \frac{1}{H_\mathrm{r}} \int_0^{H_\mathrm{r}} f_\ell^-(y)\, Y_n(y,\omega)\, \mathrm{d}y \tag{C.A.21}$$

$$I_{\ell n}^+(\omega) = \frac{1}{H_\mathrm{r}} \int_0^{H_\mathrm{r}} f_\ell^+(y)\, Y_n(y,\omega)\, \mathrm{d}y \tag{C.A.22}$$

Substituting Eq. (C.A.20) into Eq. (C.A.18) yields

$$\begin{aligned} \sum_{n=1}^{m_\mathrm{r}} \kappa_n(\omega) \Bigg\{ & -2\,\gamma_{1,n}^{(\ell)}(\omega) \sinh[b_\mathrm{r}\kappa_n(\omega)] \\ & + \frac{\rho_\mathrm{r} H_\mathrm{r} \lambda_n^2(\omega)\left[I_{\ell n}^+(\omega) + I_{\ell n}^-(\omega)\right]}{\beta_n(\omega)\, \kappa_n(\omega) \cosh[b_\mathrm{r}\kappa_n(\omega)]}\, \mathrm{e}^{b_\mathrm{r}\kappa_n(\omega)} \Bigg\} Y_n(y,\omega) = \rho_\mathrm{r} f_\ell^+(y) \end{aligned} \tag{C.A.23}$$

Multiplying Eq.(C.A.23) by eigenvectors $Y_n(y,\omega)$, $s = 1 \ldots m_\mathrm{r}$, integrating over reservoir

height H_{r} and using trigonometric orthogonality relationships, gives for each reservoir mode n

$$\gamma_{1,n}^{(\ell)}(\omega) = \frac{\rho_{\mathrm{r}} H_{\mathrm{r}} \lambda_n^2(\omega) \left[I_{\ell n}^{-}(\omega)\, \mathrm{e}^{b_{\mathrm{r}}\kappa_n(\omega)} - I_{\ell n}^{+}(\omega)\, \mathrm{e}^{-b_{\mathrm{r}}\kappa_n(\omega)} \right]}{2\, \beta_n(\omega)\, \kappa_n(\omega) \sinh[b_{\mathrm{r}}\kappa_n(\omega)] \cosh[b_{\mathrm{r}}\kappa_n(\omega)]} \tag{C.A.24}$$

and using Eq. (C.A.20)

$$\gamma_{2,n}^{(\ell)}(\omega) = \frac{\rho_{\mathrm{r}} H_{\mathrm{r}} \lambda_n^2(\omega) \left[I_{\ell n}^{-}(\omega)\, \mathrm{e}^{-b_{\mathrm{r}}\kappa_n(\omega)} - I_{\ell n}^{+}(\omega)\, \mathrm{e}^{b_{\mathrm{r}}\kappa_n(\omega)} \right]}{2\, \beta_n(\omega)\, \kappa_n(\omega) \sinh[b_{\mathrm{r}}\kappa_n(\omega)] \cosh[b_{\mathrm{r}}\kappa_n(\omega)]} \tag{C.A.25}$$

Substituting Eqs. (C.A.24) and (C.A.25) into Eq. (C.A.15) leads to the following expressions of hydrodynamic pressures within the vibrating reservoir

$$\bar{p}_\ell(x, y, \omega) = \rho_{\mathrm{r}}\, H_{\mathrm{r}} \sum_{n=1}^{m_{\mathrm{r}}} \frac{\lambda_n^2(\omega) \left[I_{\ell n}^{-}(\omega)\, X_n^{-}(x, \omega) - I_{\ell n}^{+}(\omega)\, X_n^{+}(x, \omega) \right]}{\beta_n(\omega)\, \kappa_n(\omega)\, \sinh[b_{\mathrm{r}}\kappa_n(\omega)] \cosh[b_{\mathrm{r}}\kappa_n(\omega)]}\, Y_n(y, \omega) \tag{C.A.26}$$

in which

$$X_n^{-}(x, \omega) = \cosh\left[(x - b_{\mathrm{r}})\, \kappa_n(\omega) \right] \tag{C.A.27}$$

$$X_n^{+}(x, \omega) = \cosh\left[(x + b_{\mathrm{r}})\, \kappa_n(\omega) \right] \tag{C.A.28}$$